ARCTEC CANADA LIMITED

[redacted]

ARCTEC CANADA LIMITED 1957C

TP 8797E

INVESTIGATION OF THE ADDED MASS PHENOMENON WITH A FLEXIBLE MODEL OF THE M.V. ARCTIC: VOLUME 1 - REVIEW OF EXISTING METHODS, AVAILABLE DATA AND SUMMARY OF EXPERIMENTAL RESULTS

PREPARED FOR: TRANSPORTATION DEVELOPMENT CENTRE

by:

B.C. Menon
D.J. Howard
L.D. Phillips

MARCH 1987

PREPARED BY:

ARCTEC CANADA LIMITED
311 Legget Drive,
Kanata, Ontario.
K2K 1Z8

PROJECT TEAM:

Balji Menon, Project Manager
Claude Daley, In-house Consultant
David Howard, (Project Engineer - Task 3)
Loyd Phillips, (Project Engineer - Task 2)
Michael Steele, (Systems Analyst)

DISCLAIMER: The contents of this report reflect the views of the authors and not necessarily the official view or opinions of the Transportation Development Centre of Transport Canada.

Un sommaire en français de ce rapport est inclus avant la table des matières.

Approved by: ______________________

Transport Canada Transports Canada

Development Développement

REPORT DOCUMENTATION FORM

1. Transport Canada Report No. **TP 8797E**	2. TDC Project No. 6637/6639	3. Recipient's Catalogue No.

4. Title and Subtitle **INVESTIGATION OF THE ADDED MASS PHENOMENON WITH A FLEXIBLE MODEL OF THE M.V. ARCTIC: VOLUME 1 - REVIEW OF EXISTING METHODS, AVAILABLE DATA AND SUMMARY OF EXPERIMENTAL RESULTS**	5. Report Date March 1987 6. Performing Organization Report No. 1957C
7. Author(s) **B.C. Menon, D.J. Howard, L.D. Phillips**	8. Transport Canada File No. D1460-231
9. Performing Organization Name and Address Arctec Canada Limited 311 Legget Drive Kanata, Ontario K2K 1Z8	10. DSS File No. 11SD.T8200-5-5595 11. DSS or Transport Canada Contract No 11SD.T8200-5-5595/01-SD
12. Sponsoring Agency Name and Address Transportation Development Centre (TDC) 200 Dorchester Blvd. West Suite 601, West Tower Montreal, Quebec H2Z 1X4	13. Type of Report and Period Covered Final 14. Sponsoring Agency Code
15. Supplementary Notes See also: Volume 2: Time Domain Analysis of Hull Response During Ramming. Volume 3: Model Experiments in Open Water and in Ice.	16. TDC Project Officer **C. Nowicki, I.M. Bayly**

17. Abstract

A state-of-the-art review of the methods currently used in the estimates of hydrodynamic added mass and damping in ship hull response calculations is carried out. Application of selected methods to the MV ARCTIC hull form is made and numerical values are presented. It is seen that most methods of computing the added mass distributions result in numerical values of the same order of magnitude. On the other hand, damping calculation methods do not provide consistent values appropriate for quantitative prediction purposes. A review of the mathematical basis of hull response prediction models is made and methods of isolating hydrodynamic forces are identified. Results from experimental studies (reported in vol. 2 and 3) are summarized.

18. Key Words Hydrodynamic Added Mass, Damping, MV ARCTIC, Segmented Model, Flexural Modes, Level Ice, Impulse Tests, Oscillation Tests.	19. Distribution Statement A limited number of copies are available from the Transportation Development Centre.

20. Security Classification (of this report) Unclassified	21. Security Classification (of this page) Unclassified	22. No. of Pages 90	23. Price ---

Transports Canada Transport Canada
Développement Development

FORMULE DOCUMENTAIRE DU RAPPORT

1. N° du rapport Transports Canada
TP 8797E

2. N° de l'étude — CDT
6637/6639

3. N° de catalogue du destinataire

4. Titre et sous-titre
INVESTIGATION OF THE ADDED MASS PHENOMENON WITH A FLEXIBLE MODEL OF THE M.V. ARCTIC: VOLUME 1 - REVIEW OF EXISTING METHODS, AVAILABLE DATA AND SUMMARY OF EXPERIMENTAL RESULTS

5. Date du rapport
mars 1987

6. N° du rapport de l'organisme exécutant
1957C

7. Auteur(s)
B.C. Menon, D.J. Howard, L.D. Phillips

8. N° de dossier Transports Canada
D1460-231

9. Nom et adresse de l'organisme exécutant
Arctec Canada Limited
311 Legget Drive
Kanata (Ontario)
K2K 1Z8

10. N° de dossier — ASC
11SD.T8200-5-5595

11. N° de contrat — ASC ou Transports Canada
11SD.T8200-5-5595/01-SD

12. Nom et adresse de l'organisme parrain
Centre de développement des transports (CDT)
200 ouest, boul. Dorchester
Suite 601, tour ouest
Montréal (Québec) H2Z 1X4

13. Genre de rapport et période visée
Final

14. Code de l'organisme parrain

15. Remarques additionnelles
Voir également:
Volume 2: Time Domain Analysis of Hull Response During Ramming. Volume 3: Model Experiments in Open Water and in Ice.

16. Agent de projet — CDT
C. Nowicki, I.M. Bayly

17. Résumé

Une revue de l'état actuel de la technique est réalisée en ce qui a trait aux méthodes actuelles d'estimation de la masse hydrodynamique ajoutée et de l'amortissement dans les calculs touchant le comportement de la coque. Certaines méthodes choisies sont appliquées à la configuration de la coque de l'ARCTIC et les valeurs numériques sont exposées. Il est démontré que la plupart des méthodes de calcul des répartitions de la masse ajoutée se traduisent par des valeurs numériques du même ordre de grandeur. Par contre, les méthodes de calcul de l'amortissement n'offrent pas une cohérence de valeurs permettant des prédictions quantitatives. Le document comporte un compte rendu de la base mathématique des modèles de prédiction du comportement de la coque, et identifie des méthodes permettant d'isoler les forces hydrodynamiques. Les résultats d'études expérimentales (indiquées dans les volumes 2 et 3) sont résumés.

18. Mots-clés
Masse hydrodynamique ajoutée, amortissement, M.V. ARCTIC, modèle segmenté, modes de flexion, glace plane, essais d'impulsion, essais d'oscillation.

19. Diffusion
Le Centre de développement des transports dispose d'un nombre limité d'exemplaires.

20. Classification de sécurité (de ce rapport)
non classifié

21. Classification de sécurité (de cette page)
non classifiée

22. Nombre de pages
90

23. Prix
—

Canada

SUMMARY

The purpose of the work reported in this and associated volumes was to investigate the hydrodynamic added mass phenomenon as it occurs during ship-ice interaction, to enable effective analysis and future calculation of global impact loads from experimental data.

This volume summarizes a review of currently used theoretical methods and available data for estimating the hydrodynamic added mass and damping that may be used in the calculations of ship hull flexural response. The review starts with a discussion of 'mode' shapes, as an understanding of this term is germane to the results presented in Volumes 2 and 3. The so-called mode shapes are convenient mathematical concepts that act as "building blocks" in the synthesis of hull response to any general external forcing function. It is pointed out that response calculations taking into account the 'wet' modes require prior knowledge of the fluid properties and the availability of a suitable method of estimating the fluid inertial reactions on the hull. The review part of the report is divided into two logical sections - methods of determining hydrodynamic added mass, and those used for estimating damping.

A close look at theoretical methods now used in the calculations of hydrodynamic added mass applied to the computations of transient hull response due to ice impact showed that the methods are suitable for the MV ARCTIC hull form if free-surface effects are ignored. At sufficiently high frequencies of motions, the method is accurate and gives simultaneously the heave added mass and the pitch added moment of inertia. Modifications of the added mass properties in shallow and confined waters have not been investigated thoroughly to provide reliable methods of estimating them. Works related to the influence of ice cover on the hydrodynamic added mass and damping are almost non-existent.

A brief overview of theoretical methods currently used in determining hydrodynamic added mass applicable to rigid hull vertical response calculations showed that these methods are well established. Experimental data required to validate the theoretical predictions have been identified. Published methods available for evaluating hydrodynamic added mass for applications to ship hull vibrations are discussed and are shown to be fairly simple to execute. The use of J-factors in the calculation of total heave added mass is illustrated and methods of extending this to the case of added mass distributions are discussed. Examples of added mass calculations using various methods, specifically for the MV ARCTIC hull form, are given and compared with experimentally derived results from Volumes 2 and 3. Use of detailed fluid-structure interaction modelling methods is reviewed and applications to the MV ARCTIC hull are discussed.

In the third section, ship vibration damping is reviewed. It is shown that available data for ship vibration damping calculations are sparse and widely scattered. Various investigators use entirely different values of the damping coefficient. Most experimental data refer to tests carried out with the ship stationary. Forward-speed effects on damping are poorly documented in the literature. The conventional approach of splitting the total damping into hydrodynamic and structural (internal) damping is discussed and available experimental data are presented. In the fourth section, a review of computational methods widely used for ship hull response prediction is given.

A summary of hydrodynamic added mass data determined from experiments with the 40:1 flexible scale model of the MV ARCTIC is given in section five. Mean segmental added mass distribution determined from model ridge ramming tests are presented, which show that the added mass for the first (bow) segment assumes large negative values and is dependent on the impact speed. Results from shaker tests also indicate that large added mass is to be expected at the nodes where the accelerations approach zero.

SOMMAIRE

L'objet des travaux exposés dans le présent document et dans les volumes connexes consiste à étudier le phénomène de la masse hydrodynamique ajoutée, tel qu'il survient lors de l'interaction navire-glaces, afin de permettre une analyse sérieuse et des calculs ultérieurs des charges d'impact globales à partir de données expérimentales.

Le présent volume présente une synthèse de la revue des méthodes théoriques actuelles et des données disponibles pour l'évaluation de la masse hydrodynamique ajoutée et de l'amortissement pouvant être utilisées lors du calcul du comportement de la coque d'un navire à la flexion. La revue comporte en premier lieu un exposé sur les formes du "mode", car la compréhension de ce terme est liée aux résultats présentés dans les volumes 2 et 3. Ces formes du mode sont des notions mathématiques pratiques qui agissent comme des "blocs de construction" dans la synthèse du comportement d'une coque à l'égard de toute fonction générale de force externe. Il est souligné que les calculs de comportement qui tiennent compte des formes de mode "mouillé" exigent à la fois une connaissance préalable des propriétés du fluide et la possibilité d'utiliser une méthode convenable d'estimer les réactions inertielles du fluide sur la coque. La partie revue du rapport est divisée en deux parties logiques, soit les méthodes permettant d'établir la masse hydrodynamique ajoutée et les méthodes permettant d'évaluer l'amortissement.

Un sérieux examen des méthodes théoriques actuelles utilisées dans la détermination de la masse hydrodynamique ajoutée, appliquée aux calculs du comportement transitoire de la coque découlant de l'impact des glaces, démontre que les méthodes conviennent à la configuration de la coque de l'ARCTIC si l'on ne tient pas compte des effets de surface libre. Dans le cas de fréquences de mouvements suffisamment élevées, la méthode est précise et indique simultanément la masse ajoutée en pilonnement et le moment d'inertie de tangage ajouté. Les modifications des propriétés de la masse ajoutée en eau peu profonde et en eau captive n'ont pas été étudiées suffisamment pour élaborer des méthodes sûres permettant de les évaluer. Les travaux touchant l'influence de la couverture de glace sur la masse hydrodynamique ajoutée et sur l'amortissement sont pratiquement inexistants.

Un rapide survol des méthodes théoriques actuelles permettant d'établir la masse hydrodynamique ajoutée applicable aux calculs de comportement vertical des coques rigides démontre que ces méthodes sont bien implantées. Les données expérimentales exigées pour la validation des prédictions théoriques ont été identifiées. Les méthodes publiées dont on dispose pour évaluer la masse hydrodynamique ajoutée, destinée à l'étude des vibrations des coques de navires, sont exposées et s'avèrent d'une exécution passablement facile. L'utilisation de facteurs J pour le calcul de la masse ajoutée totale en pilonnement est illustrée, et les méthodes permettant de l'appliquer aux répartitions de la masse ajoutée sont exposées. Le document offre des exemples de calculs de masse ajoutée selon diverses méthodes, plus précisément pour la configuration de la coque de l'ARCTIC, et ils sont comparés aux résultats obtenus expérimentalement dans les volumes 2 et 3. L'emploi de méthodes de modélisation d'interaction fluide-structure est étudié et leurs applications à la coque de l'ARCTIC font l'objet d'un exposé.

La troisième partie du document revoit la question de l'amortissement des vibrations du navire. On se rend compte que les données dont on dispose pour le calcul de l'amortissement des vibrations sont peu abondantes et fort clairsemées. Certains spécialistes utilisent des valeurs complètement différentes en ce qui a trait au coefficient d'amortissement. La majeure partie des données expérimentales font état d'essais réalisés lorsque le navire est stationnaire. Les effets de la marche avant sur l'amortissement sont mal documentés dans les ouvrages spécialisés. La technique classique consistant à séparer l'amortissement total en amortissement hydrodynamique et structural (interne), est exposée et les données expérimentales disponibles sont présentées. La quatrième partie présente une revue des méthodes de calcul communément utilisées pour la prédiction du comportement de la coque des navires.

Un résumé des données de la masse hydrodynamique ajoutée, obtenues à partir d'expériences performées avec le modèle (40:1) flexible de l'ARCTIC, est contenue dans la section cinq. Les distributions de la masse ajoutée moyenne en sections, recuelli des tests à l'échelle reduite d'impactes sur des faîtes de glaçes, sont présentées. Ceux-ci démontres que la masse ajoutée de la section de l'étrave prends des valeures hautement négatives et est directement lié à la vitesse d'impact. Les résultats de tests d'agitation forcé indique aussi qu'une masse ajoutée de forte ampleur est prévue aux points nodales où les accélérations approchent zéro.

ACKNOWLEDGEMENTS

The authors would like to acknowledge the support of Mr. Sydney Mathews of Coldstream Maritime Incorporated, who as technical liaison officer to TDC provided guidance and encouragement through close participation in all phases of this project. In addition, we would also like to thank Mr. Chris Novicki for his assistance in the contractual and administrative aspects of this work.

TABLE OF CONTENTS

1. INTRODUCTION....................1

1.1 Background....................1
1.2 Concept of Mode Shapes....................1

2. OVERVIEW OF METHODS-ADDED MASS AND DAMPING COMPUTATIONS.......4

2.1 Present Method of Determining Hydrodynamic Added Mass.........4
2.2 Effects of Water Depth....................12
2.3 Influence of Ice Cover....................17
2.4 Other General Theoretical Methods and Experimental Data....................17
2.5 Added Mass Computations in Ship Vibrations....................26
    2.5.1 Background....................26
2.6 Fluid-Structure Interaction Modelling Methods....................30
    2.6.1 Background....................30
    2.6.2 Natural Frequencies and Modes....................30
    2.6.3 Discussion of VTT Results....................35
2.7 Some General Observations....................37

3. SHIP VIBRATION DAMPING....................38

3.1 Background....................38
3.2 Review of Available Data for Ship Vibration Damping..........38
    3.2.1 Hydrodynamic Damping....................39
3.3 Other General Shortcomings of Past Damping Experiments.......41
3.4 Methods of Calculating Hull Damping....................42

4. REVIEW OF COMPUTATIONAL METHODS IN SHIP HULL RESPONSE........47

4.1 Governing Equations of Hull Elastic Response....................47
4.2 Solution of the Ship Response Problem....................50
    4.2.1 Free Vibration and Mode Shapes....................50
    4.2.2 Forced Vibration, Steady State....................51
    4.2.3 Transient and Non-Periodic Response....................53

5. RESULTS FROM EXPERIMENTS WITH MV ARCTIC SEGMENTED MODEL......57

5.1 Impact Tests....................57
5.2 Hammer and Shaker Tests....................60

REFERENCES....................65

APPENDIX A - EQUATIONS OF RIGID BODY MOTION

APPENDIX B - FORMULAE FOR EVALUATING THE Q_n DERIVATIVES

LIST OF FIGURES

1.1 Dry and Wet Vibratory Modes of Ship Hull....................2
2.1 Vessel at Free Surface and Its Double Body at Depth..........5
2.2 Sectional Added Mass Correction Factors for Fullness of Section Shape [1]..................................7
2.3 Dependence of Heave Added Mass on Frequency [1]............11
2.4 Comparison of Actual Water Line with Parabolic Approximation..13
2.5 Acceleration Records from Ramming of Pressure Ridges........14
2.6 Typical Model Test Data, M.V. ARCTIC Multi-year Ridge Ramming..15
2.7 Effect of Water Depth on the Natural Frequencies of Ship Model (7)..16
2.8 Sectional Added Mass and Damping Comparison Between Theory and Experiment..................................19
2.9 Heave Hydrodynamic Added Mass..............................21
2.10 Influence of Forward Speed on Pitch-Heave Coupled Added Mass..21
2.11 Sectional Added Mass Coefficients for High Frequencies......24
2.12 Sectional Added Mass Coefficients for High Frequencies......25
2.13 Sectional Added Mass Coefficients for High Frequencies......25
2.14 Lewis Sections and Inertia Coefficients (Cv)................27
2.15 FE Model of M.V. Arctic (a) and the Corresponding Fluid Finite Element Mesh (b)..................................31
2.16 Natural Frequencies of M.V. Arctic as a Function of the Mode Number..33
2.17 Three Lowest Flexural Mode Shapes of the MV ARCTIC..........34
2.18 Ratio of Wet and Dry Frequencies Using Three-Dimensional F.E. Method..36
3.1 Damping Coefficients Used by Various Investigators..........40
3.2 Damping For Submerged Spheroids and "Thin" Surface Ships....44
3.3 Hydrodynamic Added Mass for Circular, Rectangular and Ship-Shaped Sections....................................44
4.1 Free Body Diagram of a Segment of Scale Model...............48
5.1 Segmented Distribution of Non-Dimensional Added Mass........59
5.2 Variation of the "J" Factor Along Model....................61
5.3 Variation of the "J" Factor with Velocity..................63
5.4 Variation of the "J" Factor due to the Presence of Ice......64

LIST OF TABLES

2.1 Natural Frequencies of M.V. ARCTIC [30]....................32
5.1 Segmental Distribution of Non-Dimensional Added Mass........58

NOMENCLATURE

A	Shear Area
A	Amplification factor
A_{22}, A_{33}, A_{44}, A_{55}, A_{66}	= Hydrodynamic Added Masses and Added Moments of Inertia
b	Beam at water line
B	Breadth of spheroid
B_{22}, B_{33}, B_{44}, B_{55}, B_{66}	= Hydrodynamic Damping Forces and Moments
C_y', C_z', C_ϕ'	= Dimensionless coefficients
$C/\mu w$	Equivalent linear damping coefficient
C/C_c	Critical damping
E	Modulus of elasticity
$F(v,\eta,x,t)$	= Total vertical hydrodynamic force
G	Modulus of rigidity (shear modulus)
g	Acceleration due to gravity
I	Sectional Moment of Inertia
I_o	Mass rotary moment of inertia per unit length
J	Non-dimensional, mode-dependent added mass factor commonly referred to as J-factor
L	Length of spheroid
M	Response parameter, bending moment
M'	Mass of fluid displaced by a unit length of the cylinder
m_s	Rigid body mass per unit length
m_a	Added mass/unit length
n	Coefficient of waterline fullness
N	Hydrodynamic damping coefficient
q	Added mass for semi-elliptical section
Q	Magnification factor

$Q(x,t)$	Vertical excitation force
s	Beam/2 x draft
U	Forward speed of model
V	Response parameter, shear force
w	Vertical response of model
W_d	Work done by damping force
W_w	Energy dissipated in outgoing waves
y	Ordinates of flotation line
x	Position variable along longitudinal axis of ship
γ	Specific weight of water = ρg
θ	Response parameter, slope
π	3.14159265....
∂	Partial derivative symbol
β	Represents the midship section coefficient $\equiv C_m$
α	Waterplane coefficient $\equiv C_{wp}$
ξ_L	Dimensionless frequency parameter based on Length
ξ_B	Dimensionless frequency parameter based on Beam
ρ	Mass density of water
η	Dissipation factor, water surface height relative to still water
$\zeta_{1,2}$	Correction factors for sectional added mass
ω	Circular frequency of vibration
ω_n	Natural frequency of the model
μ	Mass per unit length of circular frequency of vibration

1. INTRODUCTION

1.1 Background

Ship hull vibratory response has historically been a problem to the maritime community. Operation of ships in ice-covered waters has further raised the significance of the influence of vibrations and hull response in ship design. The trend toward larger ships in the arctic with increased propulsive power has aggravated the problem and the requirements for the stiffness of the hulls are coming under more close scrutiny.

1.2 Concept of Mode Shapes

Consider a ship moving with constant forward speed through a broken ice field with a set of accompanying 'equilibrium axes' (Figure 1.1(a)). These axes move with the steady speed of the ship, but do not perform any other motion so that the ship deflects and distorts about them, so to speak. The actual departures from the mean position within the axes, then, are close to being periodic in time but of some complex shape which depends not only on the form of the ship structure, but also on the characteristics of the ice field it is passing through. For a purely symmetric motion of the ship hull (such as longitudinal vertical plane response) as a result of impact at the bow in otherwise calm water, the motion would quickly subside due to the presence of damping within the hull structure and due to the damping action of the water and the surrounding ice. In the case where one could suppress all forms of damping, the free vibration would continue indefinitely. These free, undamped vibrations could be performed in one or more specific and unchanging shapes (or 'modes'), each shape being identified with a specific natural frequency. Figure 1.1 shows the lowest mode shapes for an imaginary ship, (b) being those for the ship in vacuum and (c) being those for the ship in water. In (c) the water contributes to the mass distribution of the vessel and to the stiffness distribution. Of course the modes will become less and less like those of a non-uniform free-free beam as the order of the mode increases because of the influence of the super structure and the response of the local structure such as the panels, frames, bulkheads, grillages, etc.

The modal shapes of either set are all essentially 'different'. In mathematical terms, the differences of identity between any two modes within either set are expressed by their 'orthogonality'. Modal analysis is only made possible by the possession of orthogonality relations between the modes of the set employed. Theoretically all modes of vibration participate in the response of a ship hull to environmental excitation. Response to ice impact is dominated by the first few lower modes, but response to cyclic disturbances such as rotating machinery and wave-induced motions are dominated by modes with frequencies which couple with frequencies of excitation.

Figure 1.1 COORDINATE SYSTEMS

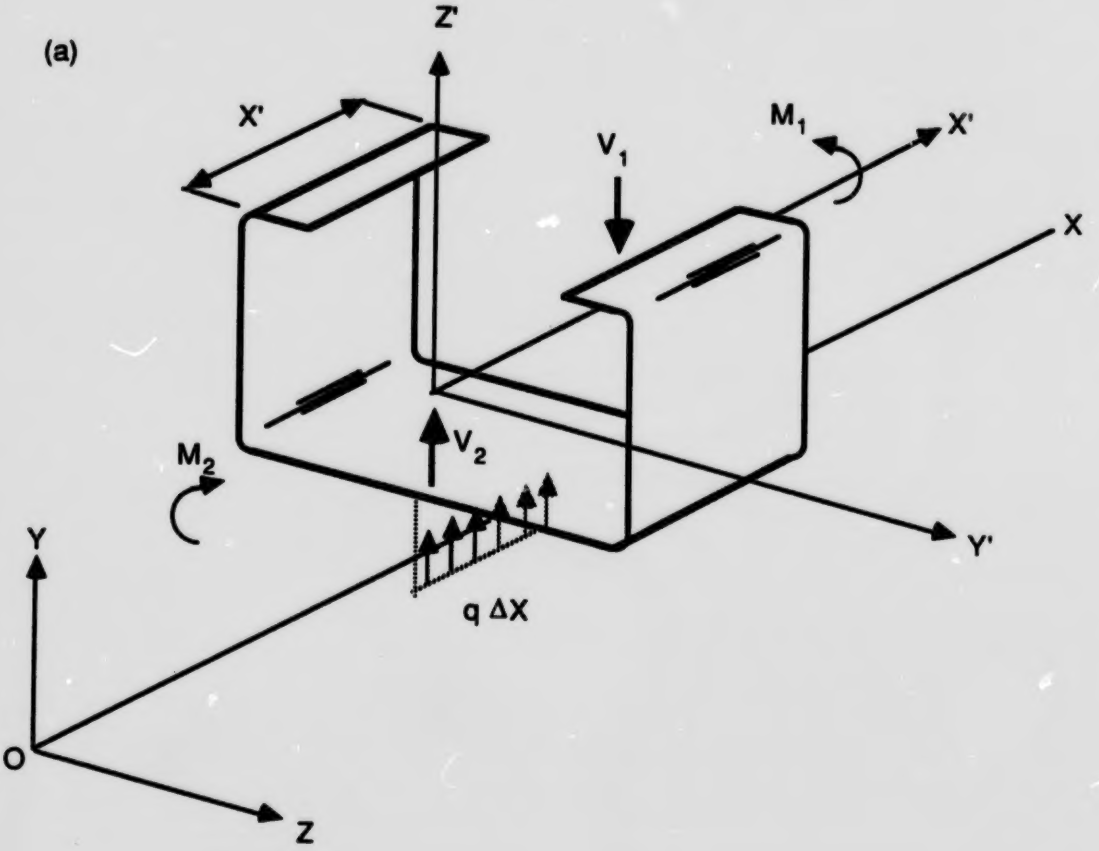

DRY AND WET VIBRATORY MODES OF SHIP HULL

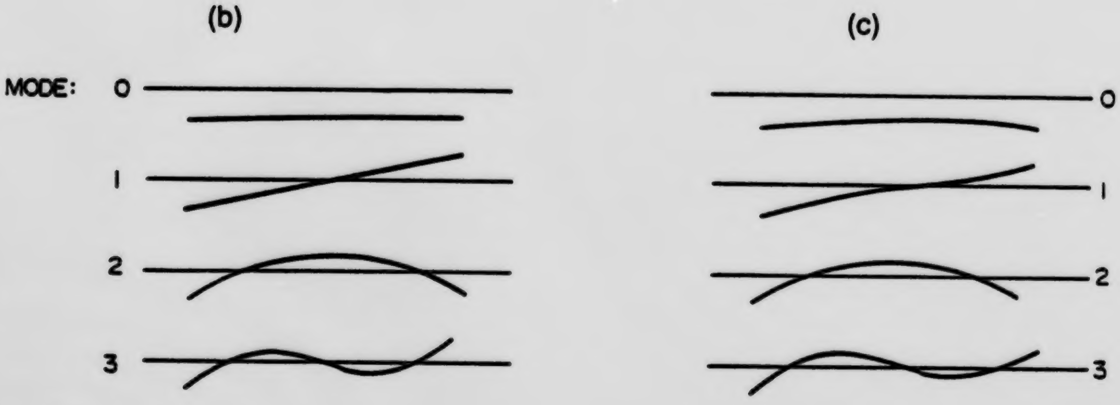

In Figure 1.1 set (b) does not possess a drawback that is inherent in set (c). To determine wet modes accurately one has to have prior knowledge of the fluid's properties, and one has also to adopt some suitable hydrodynamic theory to find the fluid actions; it might be 'strip theory' for instance. This hydrodynamic theory must necessarily be empirical. The wet mode shapes are to this extent empirical and the empiricism is reflected in the orthogonality relations between them. Again, the shapes of the wet modes, and hence the orthogonality relations, are to some extent dependent on ship speed. In the present study, an empirical or semi-empirical basis is sought that will provide a means of computing the hydrodynamic added mass.

As a first step in the study of the hydrodynamic added mass and damping, a state-of-the-art review of the literature on the subject was carried out, which covered methods of computing these coefficients, experimental determination as well as application to ship hull response calculations. Findings from this task are summarized here. As a continuation and conclusion of this effort, results from the experimental work carried out under other tasks (and reported in Volume 2 - Time Domain Analysis of Hull Response During Ramming and Volume 3 - Model Experiments in Open Water and In Ice) are summarized here and compared with other available data.

2. OVERVIEW OF METHODS - ADDED MASS AND DAMPING COMPUTATIONS

2.1 Present Method of Determining Hydrodynamic Added Mass

The evaluation of the hydrodynamic added masses and moments of inertias in a number of current mathematical models is based on expressions given in reference [1] which are based on the early works of Pavlenko [2] and Haskind [3]. As a basis for the scheme of computations of the added masses and inertias, four assumptions were invoked.

i) The added mass for a vessel floating on the surface of water equals half that for a body entirely submerged in a fluid medium of infinite extent, and having the shape of the submerged portion of the vessel doubled. (Figure 2.1).

ii) The flow over the sides of the vessel is two-dimensional, i.e. the sections are "wall-sided".

iii) The added masses and added moments of inertia are independent of the frequency of motion.

iv) The added masses and inertias are independent of the forward speed.

The above-mentioned expressions are based on specific mean distributions of the added mass and are only applicable to special water-plane forms; it is not known whether conventional icebreaker hull forms are well represented by these expressions. In order to assess the range of applicability of the added masses and inertias in ice impact situations to the M.V. ARCTIC hull form, numerical computations were made and the results are presented.

According to the above assumptions computation of the added mass in heave per unit length of the vessel may be performed for each section as for an infinitely long cylinder moving in a direction perpendicular to its axis and having the same cross-sectional shape as the doubled frame. The results of these computations, performed for each frame, independent of its neighbour, are integrated over the length of the vessel (Figure 2.1(c)). The theoretical arguments and the analytical details of the added mass calculations are discussed below.

The hypothesis of plane flow conforms closer to reality as the ratio of the length of the vessel to its transverse dimensions increases. The use of the hypothesis results in an excessive value for the added mass since it restricts the trajectories of the fluid particles. The shortest flow paths around the vessel will not lie in the planes of the frames, but will diverge from them more and more as the frame in question approaches the ends of the vessel.

FIGURE 2.1

VESSEL AT FREE SURFACE AND ITS DOUBLE BODY AT DEPTH

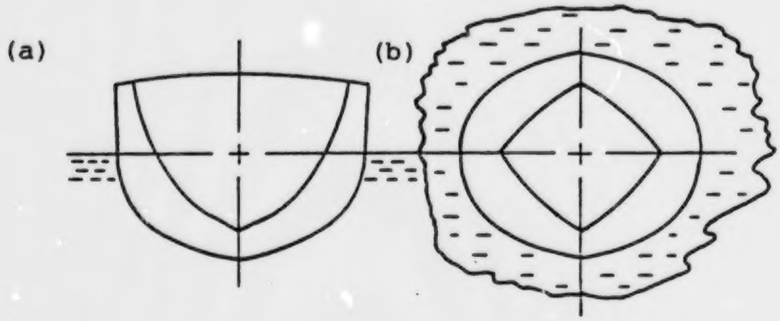

(c) ESTIMATED ADDED MASS DISTRIBUTION FOR MV ARCTIC

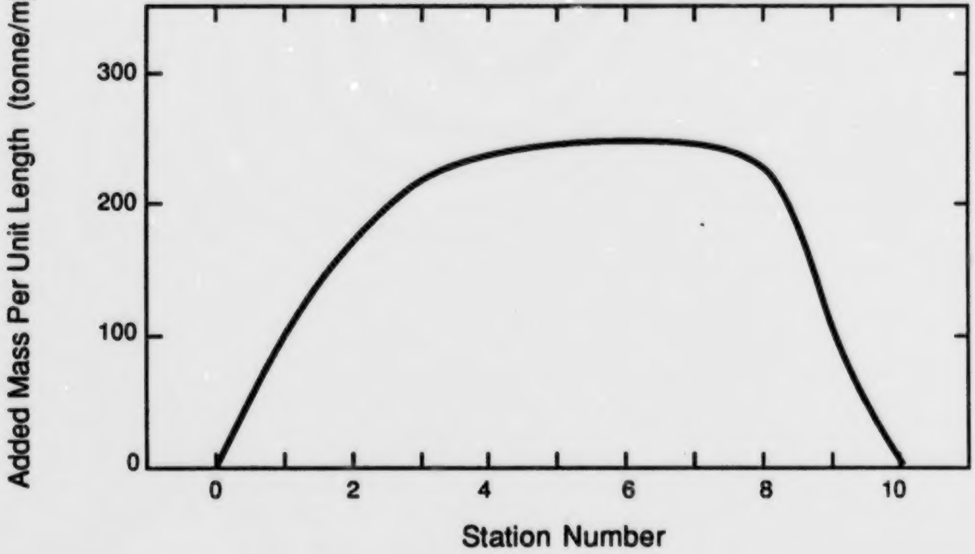

By adopting the assumption of plane flow we over estimate the kinetic energy of the water and hence the added mass. Therefore the results of the computation for the added mass, based upon the hypothesis of plane flow, should be multiplied by a correction coefficient ζ_1, less than unity.

To the above two assumptions there should be added a third, stating in effect that the oscillations of the vessel undergoing motions are so small that the volume and shape of the submerged part of the hull may be considered constant.

The added mass per unit length of an elliptical cylinder oscillating along its vertical axis is given by the following expression:

$$q_o = \frac{\gamma}{g} \frac{\pi}{4} b^2 \qquad (2.1)$$

where γ = specific weight of water

b = beam at water line

On the basis of the first hypothesis we can obtain the added mass for a frame of semi-elliptic shape

$$q = \frac{1}{2} q_o = \frac{\gamma}{g} \frac{\pi}{8} b^2 \qquad (2.2)$$

For other shapes the magnitudes of the added masses may be obtained by multiplying the values computed from Formula (2.1) by a correction factor, ζ_2. Also a correction coefficient ζ_1 must be used in equation (2.2) to account for the effect of longitudinal flow.

Figure 2.2 gives curves of correction factors ζ_2 determined as a function of the draft-to-breadth ratio and of the fullness coefficient of a section. On the same figure the shapes of the sections are shown for which the curves have been determined, for a ratio T/B = 0.5 and for various C_{sx}. Curves 1 and 2 both refer to sections with fullness coefficient C_{sx} = 1, but curve 1 refers to a rectangular section, and 2 to one with a rounded bilge.

FIGURE 2.2

SECTIONAL ADDED MASS CORRECTION FACTORS FOR FULLNESS OF SECTION SHAPE [1]

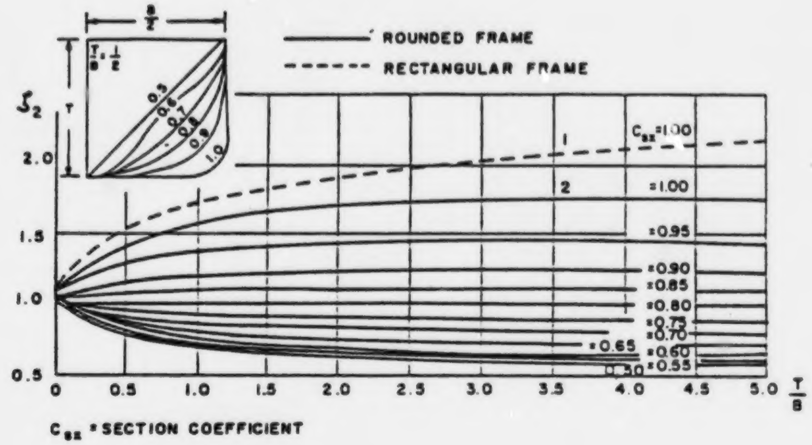

The total added mass is given by:

$$\Delta M = \zeta_1 \int_o^L q dx \tag{2.3}$$

Introducing formula (2.2) and noting that b = 2y, where y are the ordinates of the flotation line, we find

$$\Delta M = \zeta_1 \frac{\gamma}{g} \frac{\pi}{2} \int_o^L \zeta_2 y^2 dx = 0,160 \zeta_1 \gamma \int_o^L \zeta_2 y^2 dx \tag{2.4}$$

and the added moment of inertia in pitch

$$\Delta J = \zeta_1 \int_o^L qx \, dx = 0,160 \zeta_1 \gamma \int_o^L \zeta_2 x^2 y^2 dx \tag{2.5}$$

For approximate computations one may exploit the fact that, for various frames, the coefficients ζ_2 have values both greater and less than unity. Therefore, on the average, they may be set equal to unity. Furthermore, the actual shape of the water line may be approximately replaced by a parabola of the nth degree.

$$y = \frac{B}{2} \left[1 - \left(\frac{x}{\frac{L}{2}} \right)^n \right] \tag{2.6}$$

when n is related to the coefficient of waterline fullness by:

$$n = \frac{\alpha}{1 - \alpha} \tag{2.7}$$

where α = waterplane coefficient

Substituting into (2.4) $\zeta_2 = 1$, substituting y from equation (2.6), and also changing the limits of integration we find:

$$\Delta M = 0.160\zeta_1 \gamma \frac{B^2}{4} \int_{-L/2}^{L/2} \left[1 - \left(\frac{x}{\frac{L}{2}}\right)^n \right]^2 dx$$

With the new variable $z = 2x/L$ the integral becomes

$$\Delta M = 0.160\zeta_1 \frac{B^2 L}{4} \gamma \int_{-1}^{+1} (1 - z^n)^2 dz$$

performing the integration, we find

$$\Delta M = 0.160\zeta_1 \gamma \frac{LB^2}{4} \left(1 - \frac{2}{n+1} + \frac{1}{2n+1}\right)$$

and substituting for n from (2.7), we obtain finally

$$\Delta M = 0.080\zeta_1 \gamma L B^2 \frac{\alpha^2}{1+\alpha} \qquad (2.8)$$

Similarly we find for the added moment of inertia

$$\Delta J = 0.160\zeta_1 \gamma \frac{B^2}{4} \int_{-L/2}^{L/2} \left[1 - \left(\frac{x}{\frac{L}{2}}\right)^n \right]^2 dx$$

$$= 0.0066\zeta_1 \gamma B^2 L^3 \frac{\alpha^2}{(3 - 2\alpha)(3 - \alpha)} \qquad (2.9)$$

Equation 2.9 is less exact than equation 2.5 since the magnitude of the moment of inertia is significantly affected by the elements of added mass pertaining to the end sections for which $\zeta_2 \neq 1$.

The method described above is of little value in computing first moments of added mass because parabolic water lines are symmetrical about the middle frame.

The correction coefficient ζ_1 may be determined from the approximate formula [4]:

$$\zeta_1 = \frac{1}{1 + 0.8\ B/L} \qquad (2.10)$$

or from the empirical formula [4]:

$$\zeta_1 = \frac{L/B}{\sqrt{1+(L/B)^2}} \left[1 - 0{,}045 \frac{L/B}{1+(L/B)^2} \right] \qquad (2.11)$$

A more detailed study of the question of the added masses in ship motions discloses that the effect of the free surface is significantly more complex than was taken into account by the assumptions introduced earlier. The presence of the free surface of the water supporting a pitching and heaving ship results in the formation of waves, the effect of which is to change the character of flow about the vessel, and hence the added mass of the water. The characteristics of the waves so generated depend essentially upon their period, which equals the period of motions of the ship. Therefore, the added masses also depend on the periods of the ship motions. The nature of the dependence of the added masses upon the frequency of the heaving oscillations and pitching motions, determined for one particular case, is graphically shown in Figure 2.3. The value of the added mass, computed for this case by the approximate equation (2.8), is $\Delta M \approx 5$ kg. sec.^{2} m^{-1}.

A study of Figure 2.3 shows that equations of the type (2.8) or (2.9) give satisfactory results only for sufficiently high frequencies of motions and hence correspondingly small periods. As the frequency of the motions decrease beyond a certain value, the added masses begin to grow rapidly and their values greatly exceed those computed by Equations of the types (2.8) and (2.9). Lower frequency components of motion are associated with rigid body modes of motion, while frequencies in the vibratory mode are sufficiently high to justify the assumptions used in deriving equations (2.8) and (2.9).

FIGURE 2.3

DEPENDENCE OF HEAVE ADDED MASS ON FREQUENCY [1]

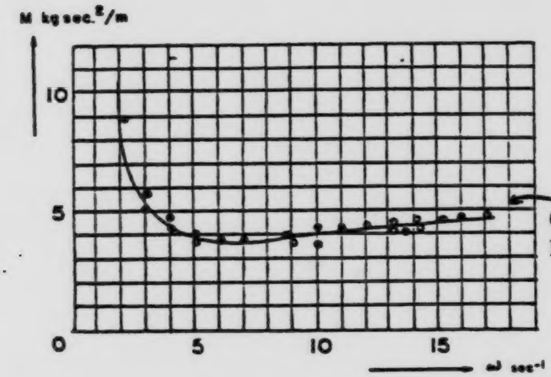

Calculated using
Eqn. (2.8)

The curve presented in Figure 2.3 was obtained from model tests [5], but the model particulars are not available to non-dimensionalize the data so that applicability to full scale hull forms cannot be considered. The curve refers to a particular case of motion (heave) only. Isolated computations and experiments performed (as shown subsequently) indicate the same qualitative relationships for other modes of motion. It may be concluded that equations of the type (2.8) and (2.9) give sufficiently accurate results for the limited case of high frequencies where the accelerations of the fluid particles are large in comparison with acceleration due to gravity.

It is now necessary to determine if the water plane shape and frequencies of motion represented by the above expressions for added mass apply to icebreaker hull forms. As a first step in this direction, half breadth plans were drawn for the LOUIS, RADISSON and the MV ARCTIC hull forms. Figure 2.4 (a), (b) and (c) show the waterlines of the three ships respectively along with the parabolic approximation to the waterlines as discussed above. It is seen that the approximation is fair in the case of the LOUIS and the RADISSON, while it is very close in the case of the MV ARCTIC. Therefore, the estimation of added mass in heave and the added moment of inertia (in pitch) may be accurate to the first order of magnitude. Moreover, the actual waterline shows that the distribution of the water-plane area about midship is approximately the same so that the first moment of the added mass (cross-coupling between heave and pitch) may be considered second order.

The ramming operation of an icebreaker will result in a series of consecutive discrete impacts, each of which may be individually simulated by the math model. Figure 2.5 and 2.6 show typical acceleration records obtained during ramming runs (these cases were extracted from LOUIS full scale data and MV ARCTIC model tests data [6]). It can be seen that a typical impact is of 1.0 sec. duration or less (frequency $\geq$ 1.0Hz).

2.2 Effects of Water Depth

Most of the present methods used in the determination of hydrodynamic added mass for hull flexural response calculations are based on the assumption of infinite water depth. The real situation in the model experiments is one of finite water depth. The necessity to investigate the influence of the bottom boundary on the hydrodynamic forces has been demonstrated in [7], where the effect of water depth on the natural frequencies of hull response were experimentally determined. Figure 2.7 depicts some of the results from [7].

In an experimental plan the effect of water depth should be investigated by conducting the tests initially in a water depth roughly equal to 1.5 times the draft of the model, and then repeating the tests in water depth equal to two times the draft. In a complete model experimental program, the effect of the width of the towing tank should also be taken into consideration. The added mass and damping forces associated with outgoing waves from an oscillating model will be influenced by the tank width, especially in the case of a stationary model.

FIGURE 2.4

COMPARISON OF ACTUAL WATER LINE WITH PARABOLIC APPROXIMATION

a) LOUIS ST.LAURENT

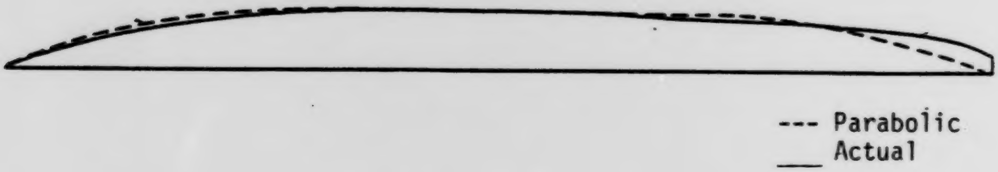

b) PIERRE RADISSON

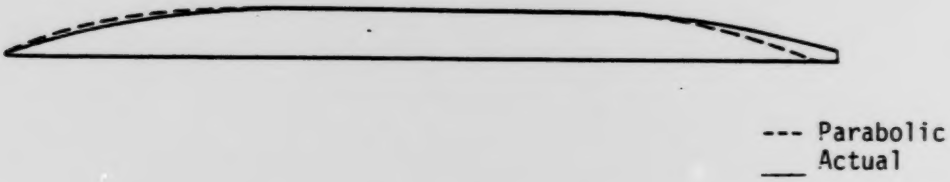

c) M.V. ARCTIC

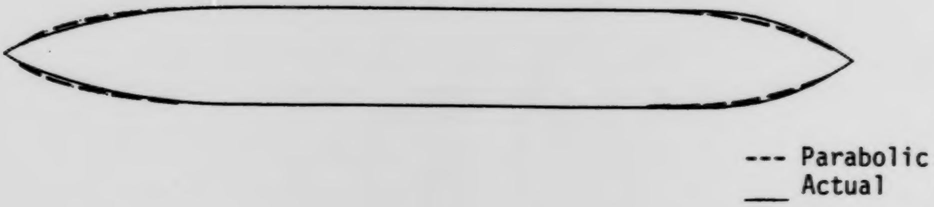

FIGURE 2.5

TYPICAL ACCELERATION RECORDS FROM RAMMING OF PRESSURE RIDGES
(FULL SCALE TESTS OF LOUIS ST. LAURENT)

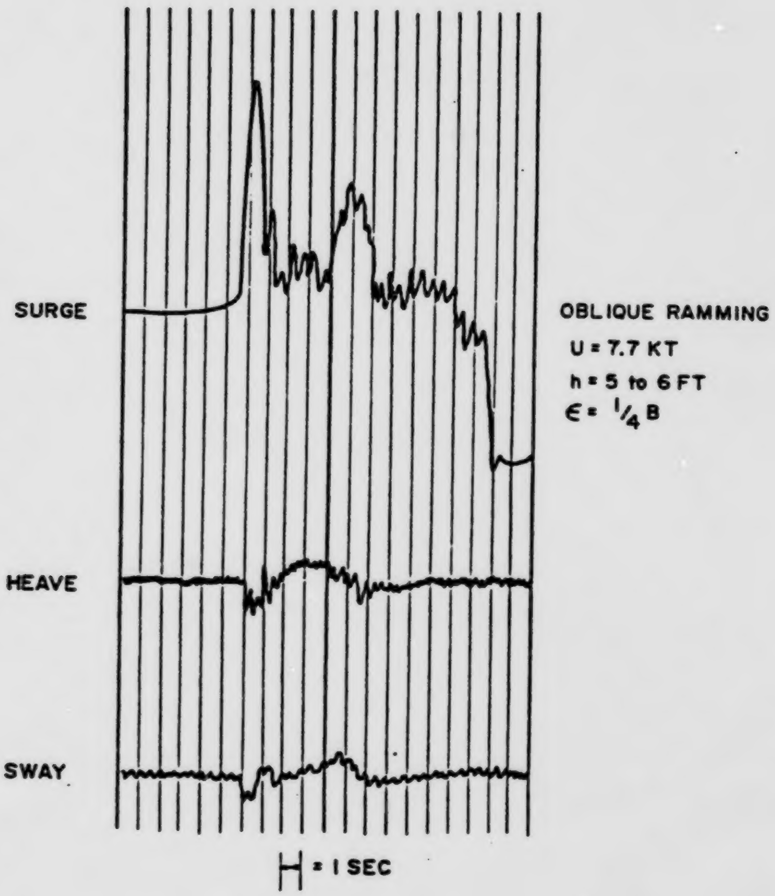

Figure 2.6 TYPICAL MODEL TEST DATA, M.V. ARCTIC MULTI-YEAR RIDGE RAMMING

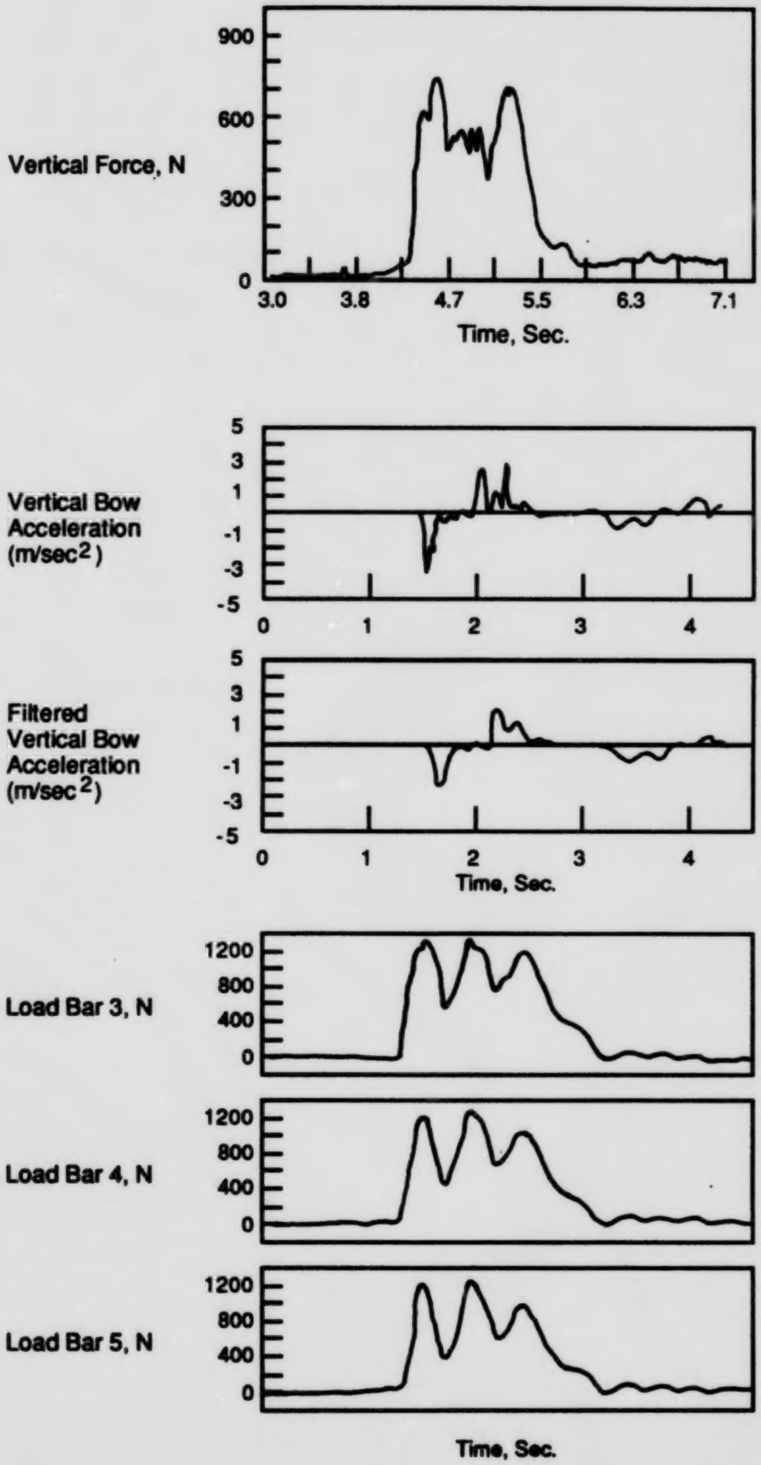

Figure 2.7

EFFECT OF WATER DEPTH ON THE NATURAL FREQUENCIES OF SHIP MODEL [7]

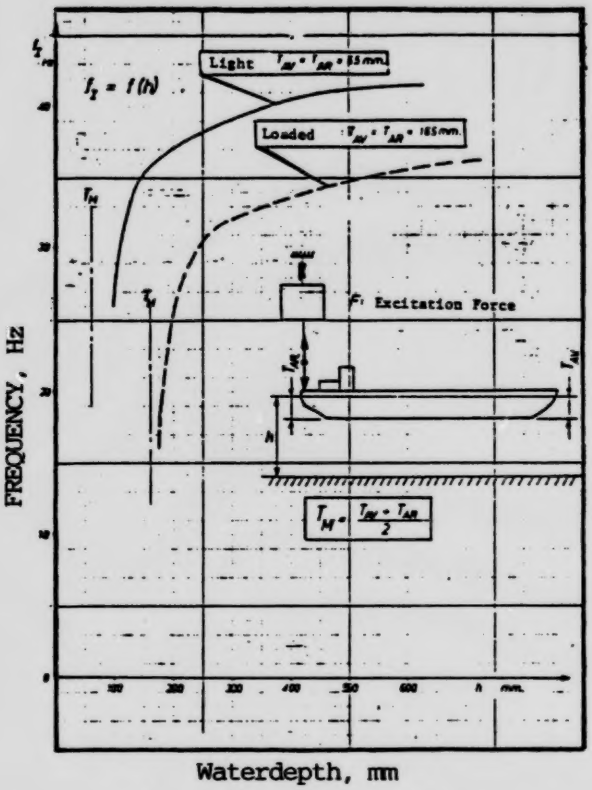

a) FIRST FLEXURAL MODE

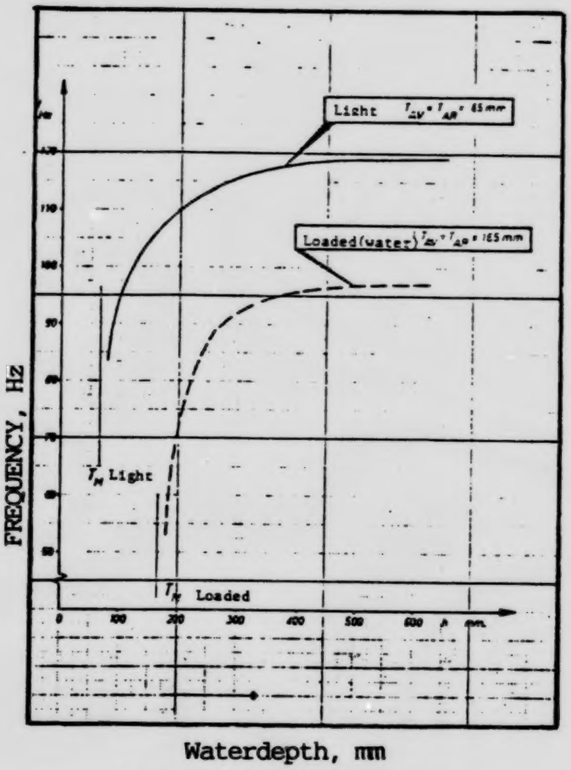

b) SECOND FLEXURAL MODE

2.3 Influence of Ice Cover

The hydrodynamic inertia and damping for an oscillating surface vessel are associated with a standing wave in the vicinity of the hull and an outgoing (progressive) wave far away from the hull. These are computed by solving the hydrodynamic wave radiation problem with appropriate free-surface and bottom boundary conditions as well as the radiation condition at infinity. In the case where the oscillations take place in the presence of floating ice on the free surface, the characteristics of the radiated waves will be altered. The modification of the 'open-water' values of the hydrodynamic added mass and damping will depend on the thickness and elasticity of the ice cover. No published material is available to quantify these effects at present.

In an experimental program, the effect of the ice cover on the hydrodynamic forces on the hull should be investigated by carrying out the tests with a sheet of synthetic ice of uniform thickness and strength in the tank. The test is to be initially conducted with the unbroken ice cover and then repeated with 95% coverage of broken floes.

2.4 Other General Theoretical Methods and Experimental Data

The first step in computing the ship motions due to ice impacts is to determine the hydrodynamic added mass and damping for each of the ship sections. Since accurate estimates for these sectional quantities are absolutely necessary in order to obtain useful final results, a discussion is presented in this section of available methods for solving the two-dimensional problem together with a comparison between theory and experiments.

More specifically, the hydrodynamic coefficients in the equations of hull rigid body motion, A_{jk} and B_{jk}, are all expressed in terms of two-dimensional sectional added-mass and damping coefficients for sway (a_{22}, b_{22}), heave (a_{33}, b_{33}), roll (a_{44}, b_{44}), and coupled sway-roll (a_{24}, b_{24}). Appendix A gives a complete description of the equations of rigid body motion defining the variables A_{jk} and B_{jk}.

There are three methods commonly in use for computing these two-dimensional sectional hydrodynamic quantities:

- The Lewis-form method
- The Tasai-Porter close-fit mapping method
- The Frank close-fit source-distribution method

In all three methods the viscous effects are ignored and linear water-wave theory is applied. The problem then consists of determining the velocity potential for a cylinder oscillating in the otherwise undisturbed free surface in the three modes: sway, heave, and roll. Having determined the velocity potential, the added mass, damping and excitation can be obtained by integrating the pressures given by the Bernoulli equation. The essential difference between these three methods is in the way the cylinder-wall condition is satisfied.

In the first method, the geometrical shape of the section is mathematically represented by the Lewis form [8] which has the same beam, draft, and area as the given section. This method is fast and quite accurate for many common ship-section forms, however, it cannot be applied, for example, to sections with large bulbs or to sections with very small sectional area. In the Tasai-Porter close-fit mapping method [9], [10], the ship sections are conformally mapped into a circle by applying a mapping function with as many coefficients as necessary in order to get the desired close-fit accuracy. In the last method, the Frank close-fit source distribution method [11], the shape of the section is represented by a given number of offset points (about eight to twelve points) with straight-line segments between the points. The velocity potential is obtained by distributing pulsating source singularities with constant strength over each of the straight segments.

Generally speaking, it can be stated that both close-fit methods apply with very satisfactory accuracy to practically any section shape and seem to be equally suited for ship-motion computations. One should note, on the other hand, that both close-fit methods require much more computing time than the Lewis-form method. Moreover, the Lewis-form method is quite suited for motions at high frequency.

At present the hydrodynamic coefficients for a particular hull form are determined by either one of the following methods:

- Calculation of the added mass and damping coefficients using one of the above theoretical methods.

- Experimental determination of the coefficients using a scale model of the hull form.

Turning now to the comparison between theory and experiments, it may be said that reliable comparisons for the high frequency limits of the coefficients are not available in the literature. Tests carried out for determining the added mass and mass moment of inertia for the limiting case of $\omega \to \infty$ are not available in the literature. However, added mass 'factors' from tests with beams including ellipsoids and ship models have been reported by Townsin [16].

Figure 2.8 shows the sectional added mass and damping for sway, heave, roll and coupled sway-roll. The theoretical values shown have been computed using Frank close-fit method. The experiments have been reported by Vugts [13]. All the comparisons have been made for a cylinder with a rectangular cross section with rounded bilges and beam/draft ratio of two. In other words, the

FIGURE 2.8

SECTIONAL ADDED MASS AND DAMPING
COMPARISON BETWEEN THEORY AND EXPERIMENT

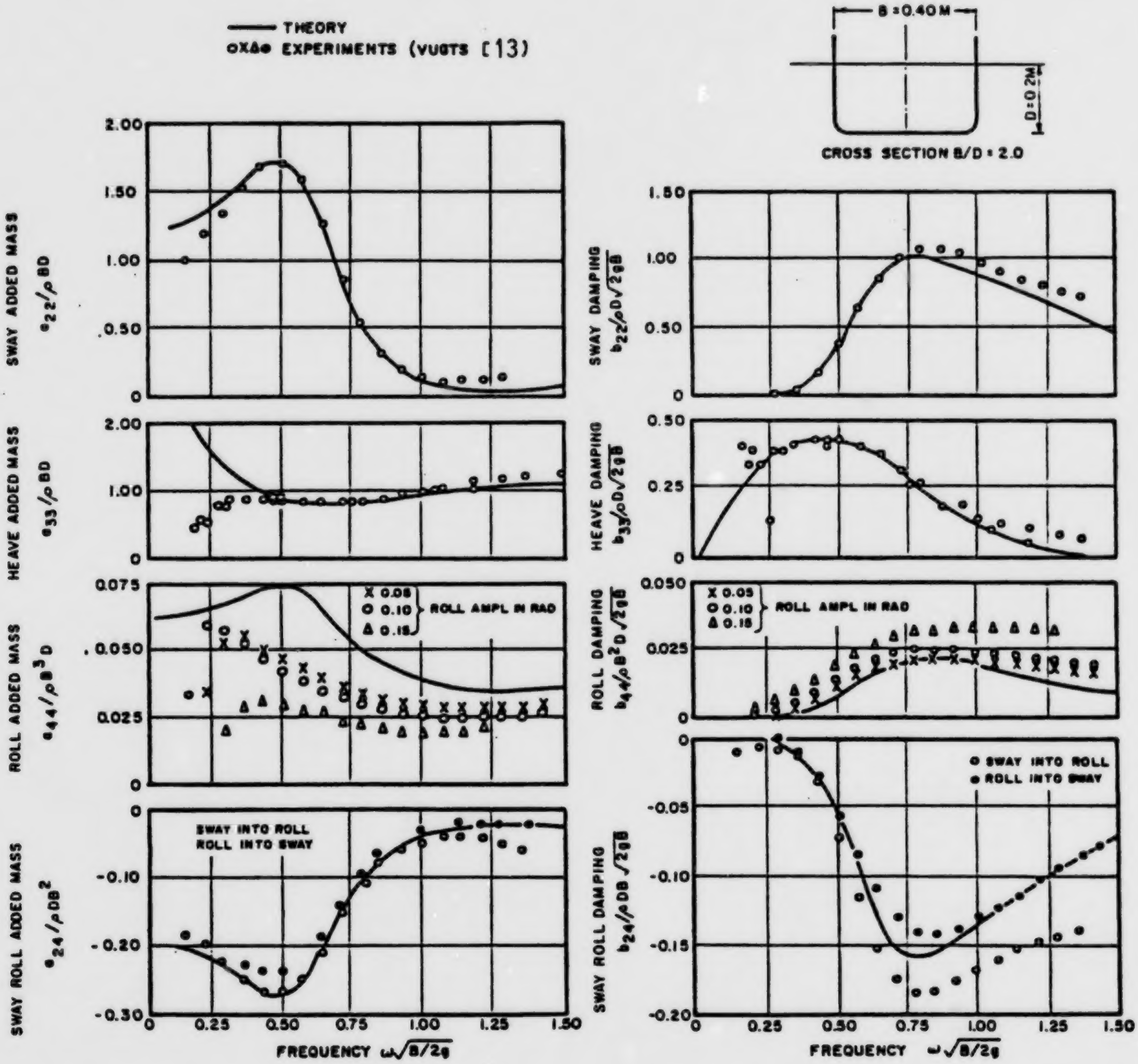

section shape is quite similar to the midship section for a large block coefficient ship. It is seen in Figure 2.8 that the agreement between theory and experiment is in general, very satisfactory at the high frequencies. However, the frequency parameter $\omega\sqrt{B/2g}$ does not extend to the values of 4 to 7 which are of interest in ice impacts. Large discrepancy between theory and experiment is seen for the roll added moment of inertia and damping in the entire frequency range. Vugts states that the lower measured roll added moment of inertia is due to experimental errors. The errors in damping are believed to be due to viscous effects. It is also seen in Figure 2.8 that the roll added inertia and damping are slightly nonlinear with the roll amplitude.

It is interesting to note in Figure 2.8 that the experimental values for added mass and damping for coupled sway-roll clearly show a difference between the case of "sway into roll" and the case of "roll into sway", while linear potential theory (Salvesen, et al [14]) predicts the hydrodynamic coefficients the same, i.e. $a_{24} = a_{42}$ and $b_{24} = b_{42}$. However, these coupled coefficients are small in magnitude at the high frequency limit.

Gerritsma [15] carried out forced oscillation tests on a ship model to determine the hydrodynamic added mass and damping coefficients as functions of frequency. The result of his experiments which were carried out at a forward speed corresponding to a Froude number of 0.3 are shown in Figure 2.9(a). It also shows the values calculated for $m_{33}(\omega)$ using a three-dimensional method of Haskind [3]. As a standard method of calculation, the results of a strip theory the same hull form for $\omega \to \infty$ are also shown in Figure 2.9(a) (denoted by "strip theory"). A correction to this to account for the influence of frequency using Ursell's results is also shown (denoted by "correction Ursell") [17]. It can be seen from the figure that the agreement between theory and experiment is reasonable. The measurements made at the higher frequencies are more reliable on account of the fact the shorter wave length disturbances travel slower thereby reducing wall effects. In Figure 2.9(b) a similar comparison is made between the calculations and the measurements for the added moment of inertia in pitching $m_{55}(\omega)$, which is non-dimensionalized using the mass moment of inertia of the model using a radius of gyration of 0.25L.

From Figure 2.9(a and b), it is seen that the added mass and added moment of inertia for heaving and pitching are of the same order of magnitude as the rigid body mass and inertia of the ship itself, and that these hydrodynamic coefficients corresponding to high frequencies are fairly accurately predicted by analytical methods.

FIGURE 2.9

a) HEAVE HYDRODYNAMIC ADDED MASS

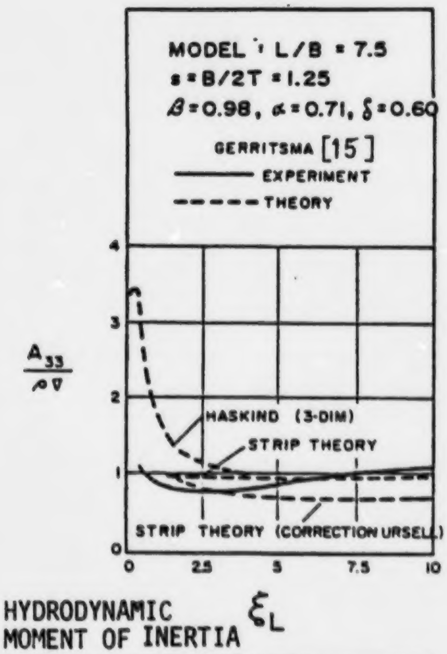

b) PITCH HYDRODYNAMIC
ADDED MOMENT OF INERTIA

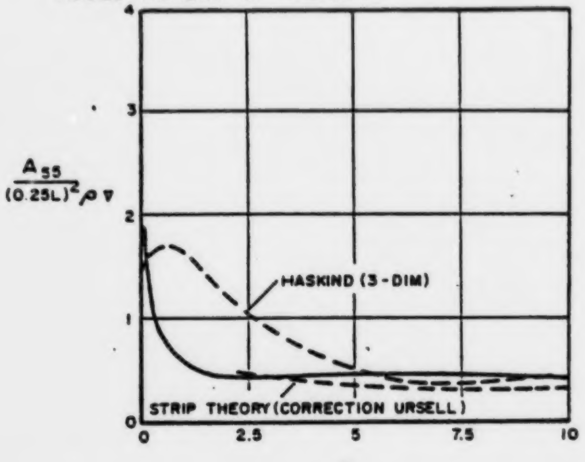

FIGURE 2.10

INFLUENCE OF FORWARD SPEED ON
PITCH-HEAVE COUPLED ADDED MASS

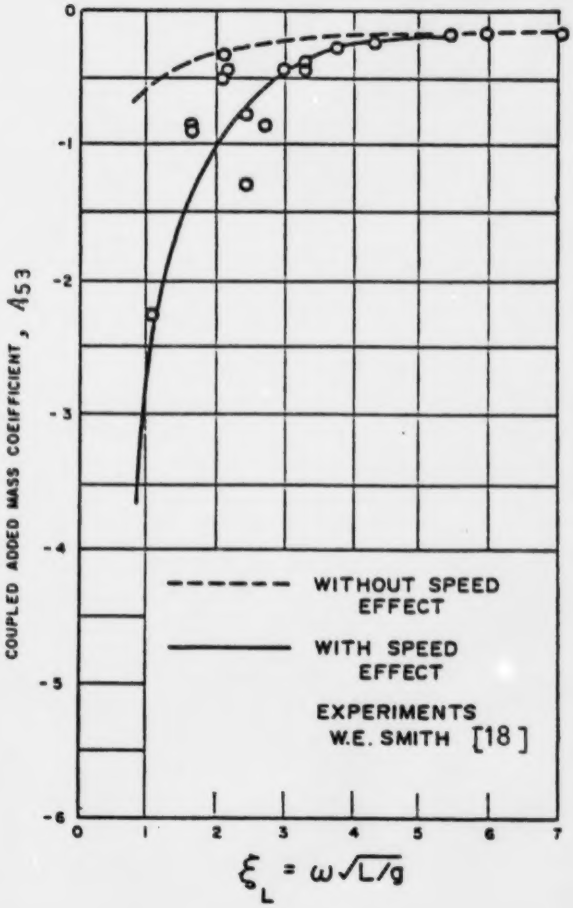

Experiments by Smith [18] gave results as shown in Figure 2.10 for the added mass cross-coupling coefficient A_{53}. Although the figure shows that A_{53} has a fairly strong speed dependence, the effect is almost negligible at high values of the frequency parameter. Note that the abscissa is defined in Figure 2.10 as is $\sqrt{L/g}$ so that if we calculate ξ_L, as defined earlier, its upper limit for the results shown is roughly 25. This is in the range of interest to the present study. It may be concluded that the forward speed effects on the hydrodynamic added mass is of second order.

Determination of Added Mass and Moment of Inertia Coefficients:

The following method of computation is adopted in the determination of the added mass and inertia coefficients. The method, based on strip theory, consists of first calculating the added mass for the different sections, two-dimensional flow being assumed and then integrating the results throughout the ship's length. The method, however, is not applicable for motion in the x-direction (i.e. surge).

Adopting the notations of Salvesen, et al [14], as shown in Appendix A, the following expressions may be written:

$$A_{22} = \int_{-L/2}^{L/2} a_{22}(x')\,dx' \tag{2.12}$$

$$A_{33} = \int a_{33}(x')\,dx' \tag{2.13}$$

$$A_{44} = \int a_{44}(x')\,dx' \tag{2.14}$$

$$A_{55} = \int a_{33}(x')\,x'^2\,dx' \tag{2.15}$$

$$A_{66} = \int a_{22}(x')\,x'^2\,dx' \tag{2.16}$$

In the above equations $a_{22}(x')$ represents the added mass per unit length of a section for 'horizontal' motion, $a_{33}(x')$ for 'vertical' motion and $a_{44}(x')$, the added moment of inertia per unit length of the section for rotation.

It is customary to introduce dimensionless coefficients C_y', C_z' and C_ϕ', for the two added masses and the added moment of inertia of a section.

$$a_{22}(x') = C_y' \ \pi/2 \ \rho \ T^2 \tag{2.17}$$

$$a_{33}(x') = C_z' \ \pi/2 \ \rho \ (b/2)^2 \tag{2.18}$$

$$a_{44}(x') = C_\phi' \ \pi/2 \ \rho \ (b/2)^4 \tag{2.19}$$

In the above expressions, b represents the water-plane breadth of the section concerned, which, for the midship section, is equal to B. The coefficients C_y', C_z' and C_ϕ' are as a rule, based on a circle, from which specific shapes of the body sections can be obtained by conformal transformation depending on the equations and constants used. In making these calculations, the frequency of motion appears to have a considerable effect on the magnitude of the coefficients, which is due to the presence of a free fluid surface. In close proximity to the body a standing wave pattern is also made to oscillate, which will influence the added mass.

A survey of the calculations of the added mass and mass moment of inertia for $\omega \to \infty$ concerning shapes of sections such as circles, ellipses, rectangles, polygons, etc. is given by Wendel [12].

Further extensions for other shapes of sections have been made by Landweber, and deMacagno [19] and by Dorofeyuk [20], who not only gives $C_z(\infty)$, but also $C_y(\infty)$.

In Figure 2.11 and 2.12 some results of the calculations have been summarized, from which $C_z(\infty)$ and $C_y(\infty)$ can be read as functions of β, the sectional area coefficient and s, the beam/2 x draft ratio. It will be evident that β and s are insufficient for characterizing the shapes of sections, so that, depending on the transformation used, a fairly large number of differences amongst them may occur. This will also clearly appear from the calculations of $C_z(\infty)$ for rotation. These were carried out by Kumai [21] and by Sebalov [22]; see Figure 2.13. In this figure a few of Wendel's values [12] have also been plotted for $\beta = 0.78$ and $s = 1.00$. The agreement between Wendel's and Kumai's calculations is reasonable; the calculations of Sebalov show a different behaviour.

In Figures 2.11, 2.12, and 2.13, β represents the midship section coefficient, Cm.

FIGURE 2.11

SECTIONAL ADDED MASS COEFFICIENTS FOR HIGH FREQUENCIES

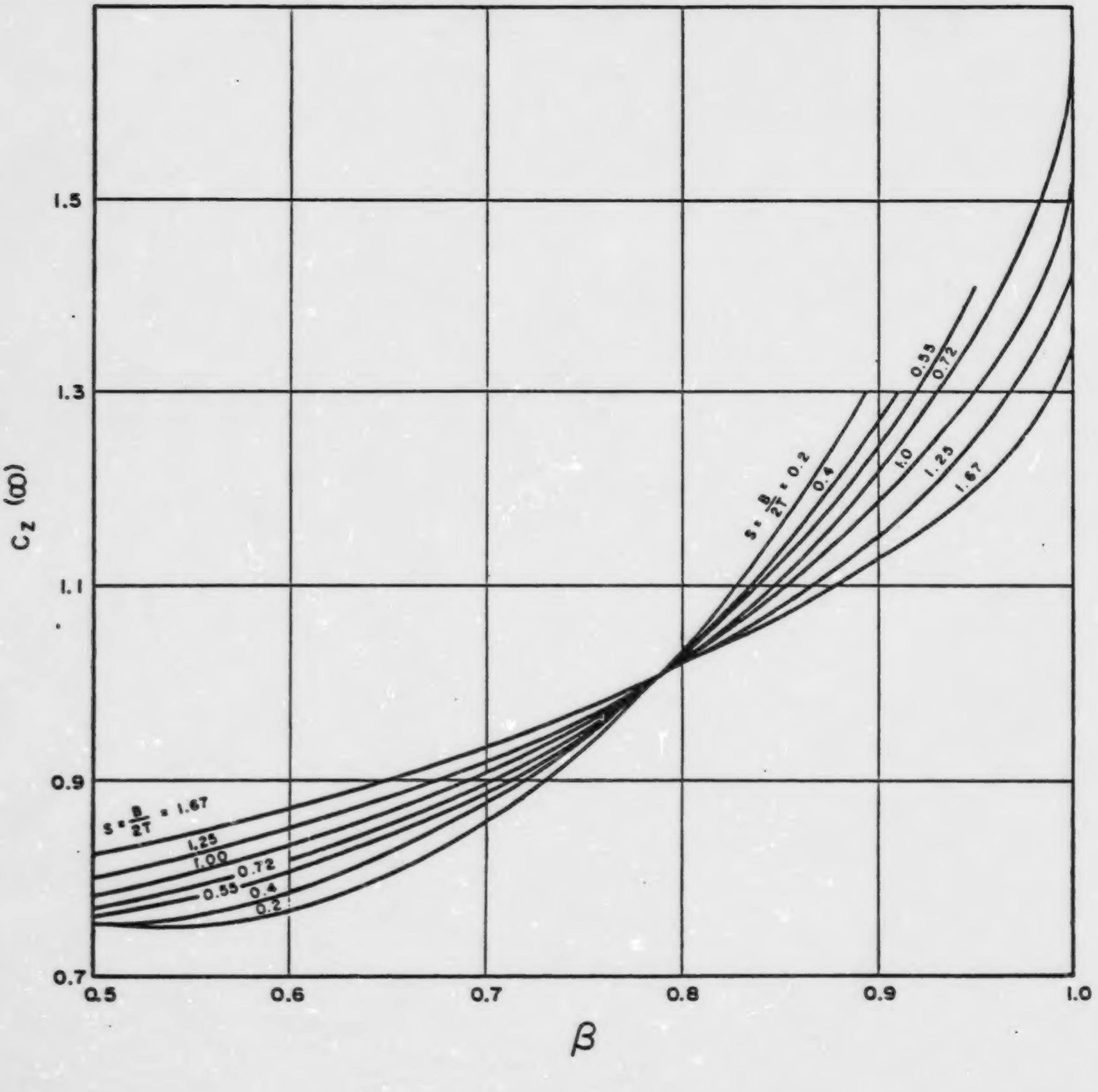

FIGURE 2.12
SECTIONAL ADDED MASS COEFFICIENTS FOR HIGH FREQUENCIES

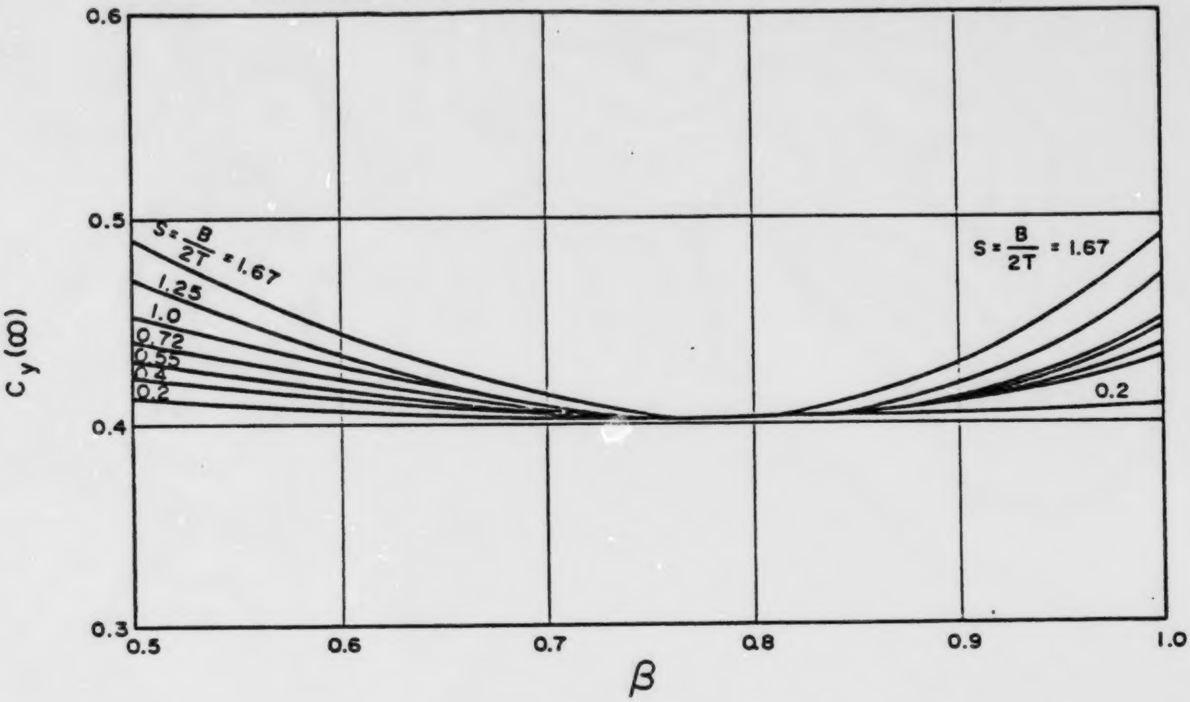

FIGURE 2.13
SECTIONAL ADDED MASS COEFFICIENTS FOR HIGH FREQUENCES

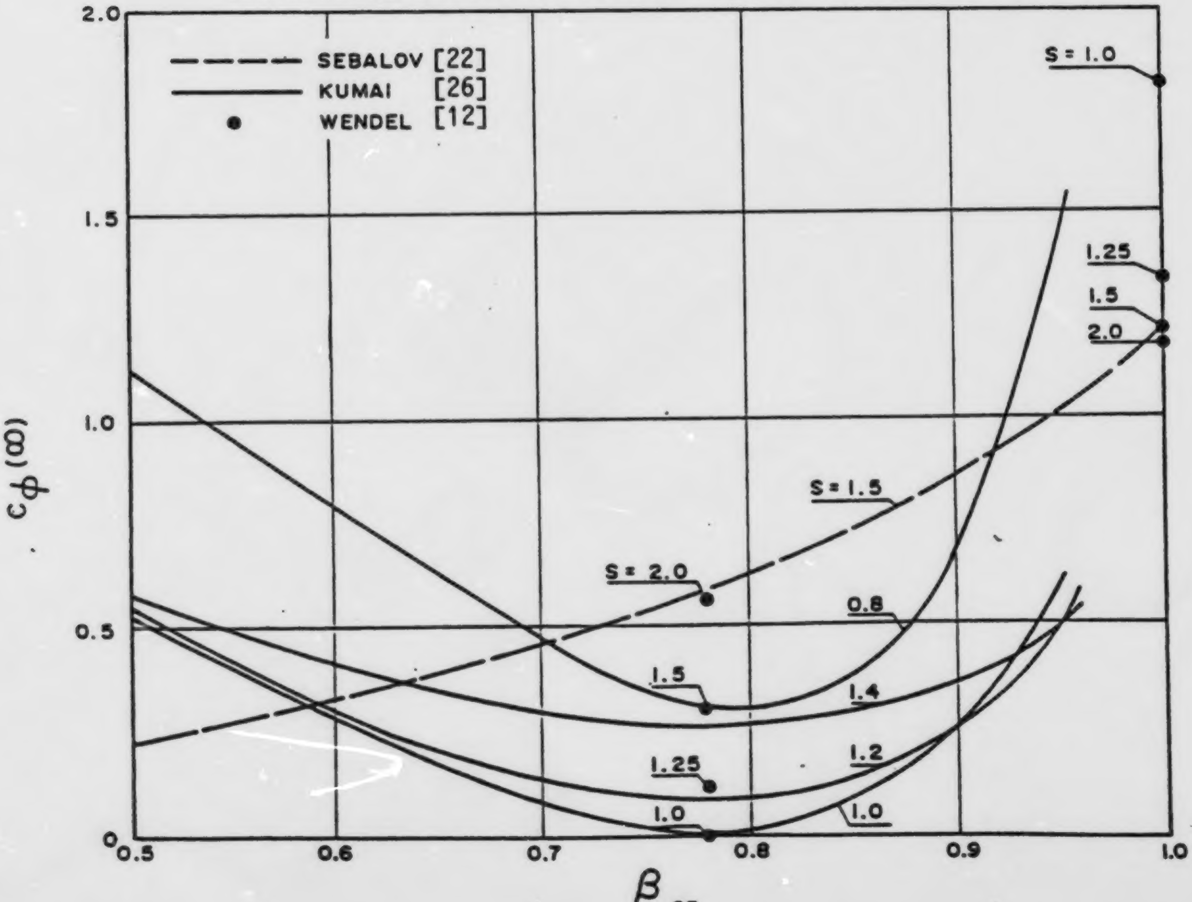

2.5 Added Mass Computations in Ship Vibrations

2.5.1 Background

Traditionally methods employed in the evaluation of hydrodynamic added mass were almost entirely based on Lewis's classical procedure [8] or its variations and extensions [23 - 26]. Lewis's method applies to a ship vibrating vertically as a one-dimensional beam where the added-mass distribution is evaluated using "strip theory". The added mass associated with each strip or segment is calculated using two-dimensional ideal fluid theory in the sectional planes of the respective strips. The variation of added mass from strip to strip then implies an added-mass distribution. The strip theory proposed by Lewis, which employs the conformal mapping technique, is simple to apply. However, its accuracy, which may be marginally acceptable for the zero-noded heave mode shape, deteriorates rapidly with modal order due to the increasing influence of three-dimensional hydrodynamic effects, which the strip theory ignores.

As an illustration of the procedure, which was briefly described in the Introduction, consider the case of an infinitely long rigid cylinder having circular cross section of radius R, moving perpendicular to its length with velocity U, in an infinite fluid of density ρ, at rest at infinity and without viscosity. It is possible to directly derive the two-dimensional (2-D) potential flow and to calculate the kinetic energy in the fluid. The latter is found to be:

$$KE = 1/2\rho\pi R^2U^2 \qquad \text{per unit length of cylinder} \qquad (2.20)$$

Setting $\rho\pi R^2 = M'$ it is seen that M' is the mass of fluid displaced by a unit length of the cylinder, and that

$$KE = 1/2M'U^2 \qquad (2.21)$$

The continuation of the procedure is then to correct this mass for the expected differences between the two-dimensional flow around a rigid cylinder and the three-dimensional flow around a flexible cylinder and add this corrected hydrodynamic mass or "added mass" to the mass per unit length of the cylinder itself.

Lewis extended the procedure described for the circular cylinder to those with cross sections resembling ship hull girders, Figure 2.14. He expressed the added mass as:

$$\text{2-D Added Mass} = C_V\rho\pi R^2 \qquad (2.22)$$

where C_V is the inertia coefficient for vertical vibration that is obtained by conformal transformation for a series of rigid cylinders

FIGURE 2.14

LEWIS SECTIONS AND INERTIA COEFFICIENTS (Cv)

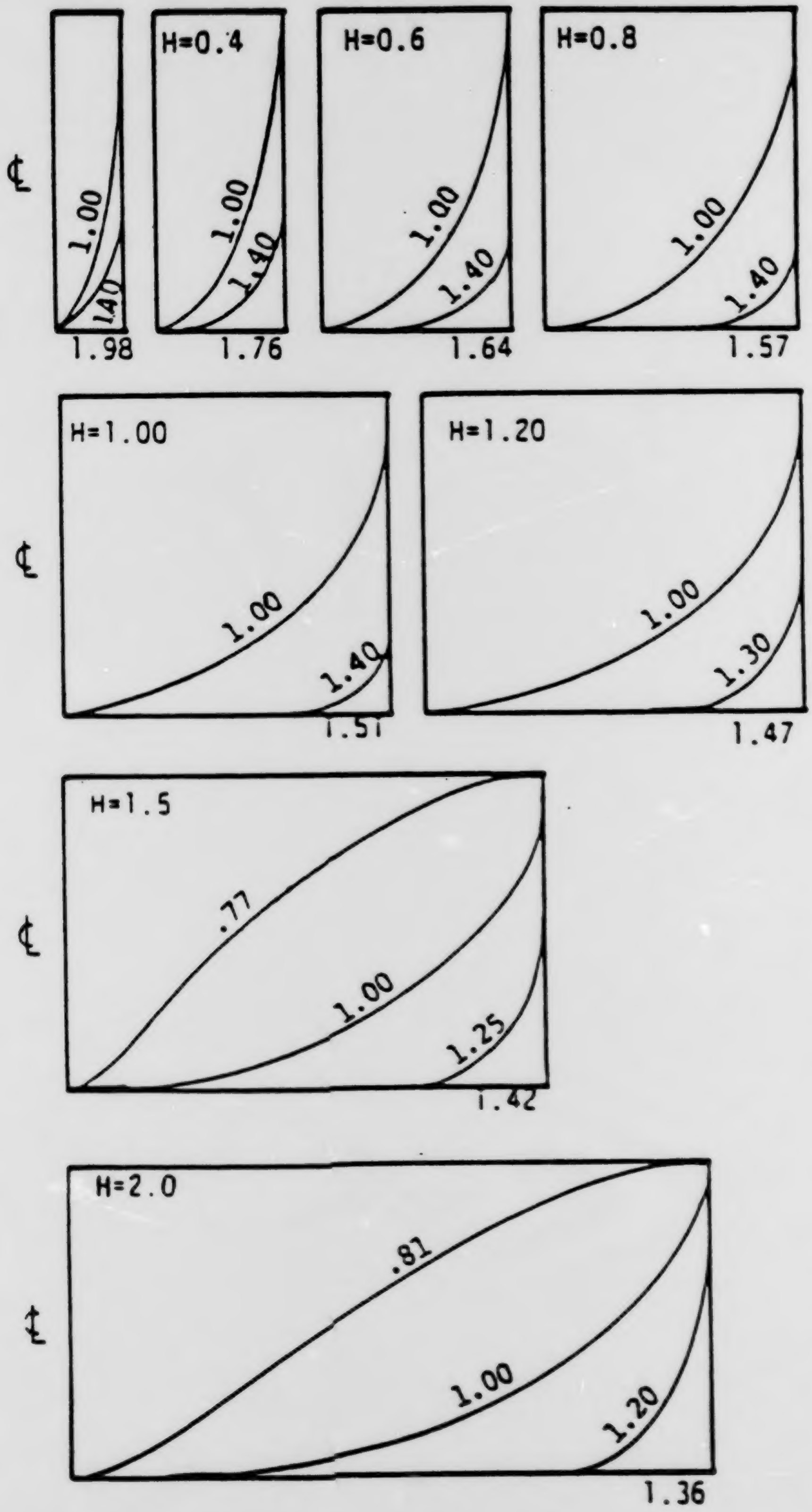

of an infinite length and various cross-sectional shapes as shown in Figure 2.14, for various beam-to-draft ratios, H (note Figure 2.14 only shows the right half of a section). To apply the results to the vertical vibration it is assumed that for a ship floating freely the added mass is one half of that for the underwater body of the ship in the lower half-plane combined with its image in the upper half-plane immersed in an infinite liquid and that the fluid motion is streamlined throughout. The validity of this image assumption was tested by Moullin [27, 28], who concluded by experiment that the added mass would be very nearly half that of the ship and its image in an infinite nonviscous fluid. The two-dimensional sectional added mass will then be 1/2 C_v times the added mass of the deeply submerged double body.

Lewis therefore developed approximate correction factors, called J-factors, to correct the overestimated strip-theory added-mass distribution for three-dimensionality. The Lewis J-factor is based on the ideal flow about a spheroid (ellipse of revolution); this flow can be calculated exactly, in closed form, for the vertical case. The spheroid is selected with the same beam-to-length ratio as that of the ship. The J-factor for some mode is then taken as the ratio of the fluid kinetic energy due to the spheroid vibrating with the specified one-dimensional mode shape, to the fluid kinetic energy of the same spheroid evaluated by strip theory. Lewis presented formulas in [8] for calculating the J-factors appropriate for correcting the strip-theory evaluations for vertical hull modes with two and three nodes. The accuracy of this correction obviously deteriorates on application to forms which deviate substantially from the spheroid. Wetted surfaces of conventional hull forms are not semi--spheroidal, particularly in the stern regions where accurate estimates of added-mass distributions are often most crucial if propeller induced hull response computations are of interest. In the case of icebreaking hull forms the bow region also deviates drastically from spheroidal geometries.

Lewis J-factors are essentially applicable only to the first two or three modes, as these are roughly the mode shapes calculable using the principles of Euler beam theory. Calculations of higher mode shapes require much more effort in order to account for the influence of local effects in the structure such as vibrations of hull bottom plating and those of the superstructure.

Vorus and Hylarides [29] present a comparison of the Lewis J-factors and "sectional" J-factors from their computations for a ship hull form utilizing a panel source distribution to derive the added mass matrix. Their sectional J-factor for the spheroid is

$$Jn(x) = - \left[\frac{\zeta Q_n{}'}{(\zeta-1)\ \bar{Q}_n{}' + \zeta Q_n{}'} \right] \tag{2.23}$$

where $$\zeta = \frac{I}{[1 - (B/L^2]^{1/2}}$$

B = breadth of spheroid

L = length of spheroid

$\dot{Q}_n^1$, $\bar{Q}_n^1$ = 1st and 2nd derivatives in ζ of Legendre functions of first degree and order n

Equation (2.23) above is the only expression based on the spheroid approximation in the literature that is applicable to the higher-order beam modes (of the order of six to ten). Formulae for evaluating the Q_n derivatives as derived in [29] are given in Appendix B. In Reference [29], the n in Equation (2.23) corresponds to modal order; that is n = 1 is heave, n = 2 is pitch, n = 3 is two-noded flexure, etc. The number of nodes in the mode shape is n - 1.

Formula (2.23) is valid only for the same set of special mode shapes that are recommended by Lewis in [8]. Although these special mode shapes are not identified specifically as such in [8], they are the Legendre polynomial derivatives

$$\frac{d}{d\mu} P_n(\mu) = P_n(\mu) \quad n = 1, 2, \ldots$$

where $\mu = 2x/L$. Lewis recognized that these mode shapes corresponded to a condition of minimum fluid kinetic energy. What he apparently did not realize was that the J-factors corresponding to the Pn mode shapes were the constant factors by which the three-dimensional and strip-theory (2-D) added-mass distributions differ point for point along the length of the spheroid. Lewis defined his J-factor as the ratio of 3-D to 2-D total fluid kinetic energy, thereby achieving reduction factors on total integrated added mass. By the formulation in [29] the same Jn is defined as the ratio of 3-D to 2-D added-mass distribution along the spheroid. By (2.23) this ratio is independent of the axial coordinate for the Pn(x) mode shapes assumed in its derivation.

2.6 Fluid-Structure Interaction Modelling Methods

2.6.1 Background

Applications of the finite element method to vibration analysis of MV ARCTIC hull was illustrated by Hakala [30]. A rather coarse structural finite element model was built (Figure 2.15a) which was capable of representing realistically only the lowest modes which were experimentally validated by an exciter test. The model consisted of 326 nodes, 873 degrees of freedom and 1260 elements most of which were simple 3- or 4- node flat membrane elements. The mass of the ship itself was lumped at the nodes. The added mass of the surrounding water was first taken into account using strip theory. The two-dimensional added masses for each cross section were determined by the Frank close-fit method [11]. The global mode-dependent J-factors and the local mode-independent correction factor were determined according to Andersson and Norrand [31] .

The fluid finite element model used in the three-dimensional interaction analysis is shown in Figure 2.15b. It contains 460 elements, 1030 nodes and 820 active degrees of freedom. The elements in the vicinity of the structure are 20-noded isoparametric ones. Further they are degraded into simpler elements with nodes at the corner points only.

The fluid mesh is extended around the ship four times the draught in the vertical direction, five times the half-breadth in the transverse direction and three times half-breadth in the longitudinal direction. The boundaries are assumed to be rigid walls except the free surface. According to the previous section, the fluid model is extended sufficiently far. The length-to-breadth ratio of the ship is $L/B = 8.6$ and the breadth-to-draught ratio $B/T = 2.1$.

2.6.2 Natural Frequencies and Modes

The seven lowest natural frequencies obtained by 2-D strip theory approaches as well as 3-D methods are given in Table 2.1. In addition, the frequencies of the dry ship and the frequencies, which could be determined in the exciter test performed by the VTT Ship Laboratory, are given for comparison. Figure 2.16 shows the same comparison graphically.

The three lowest measured and calculated natural modes are shown in Figure 2.17. The calculated modes were determined by the three-dimensional approach and were presented for the ship side. The experimental modes were measured on the main deck rather close to the side, but may be somewhat affected by the local deflections of the deck, which were not realistically modelled in the calculations. The modes were scaled similarly, i.e. the generalized mass is the same in both calculations and measurements.

FIGURE 2.15

FE MODEL OF THE MV ARCTIC (a) and the CORRESPONDING FLUID FINITE ELEMENT MESH (b) [30]

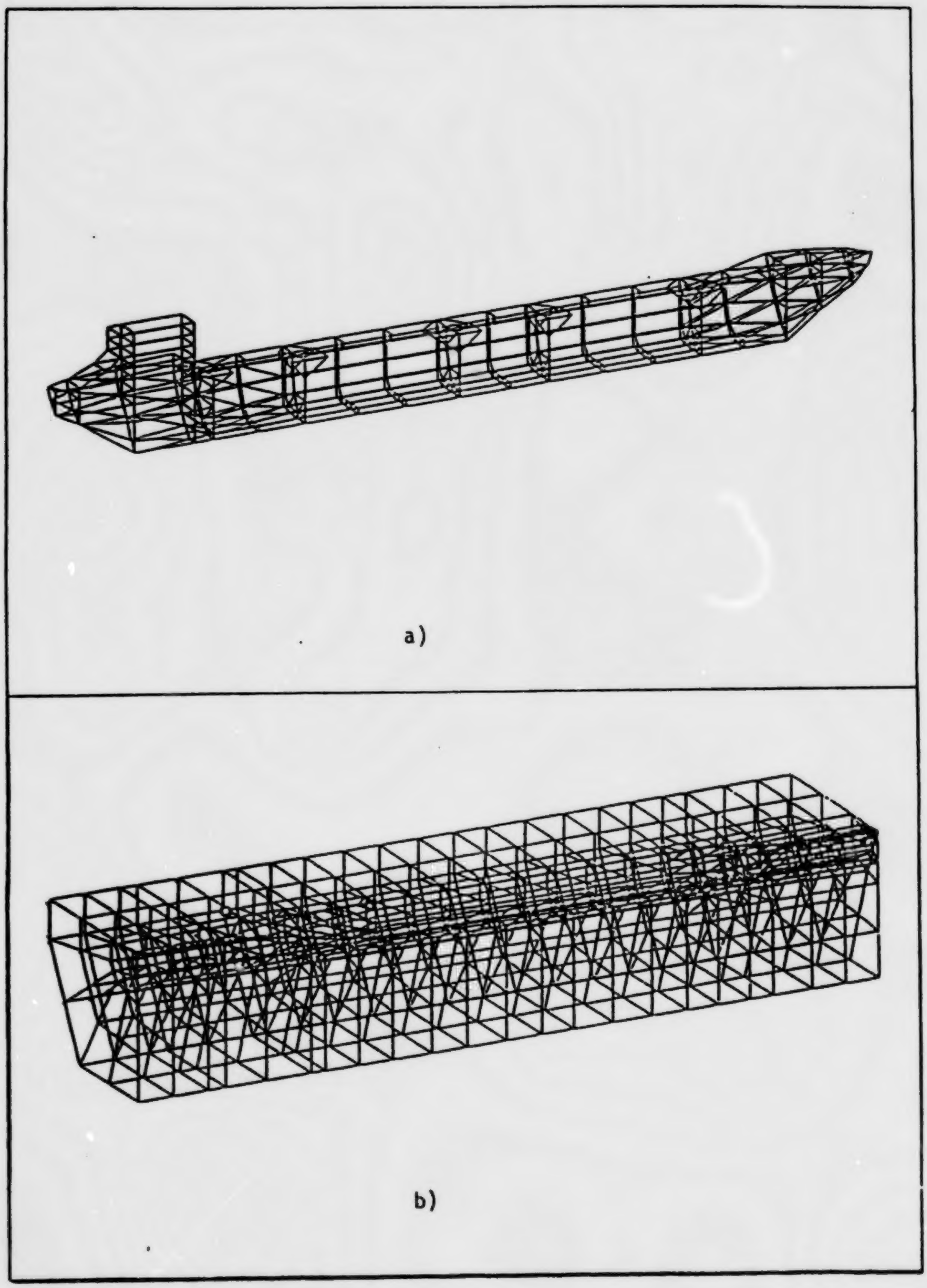

a)

b)

TABLE 2.1

NATURAL FREQUENCIES OF MV ARCTIC [30]

MODE NO.	DRY SHIP	STRIP THEORY	3-D ADDED MASS	MEASURED
1	1.26	0.98	1.00	0.93
2	2.63	1.97	2.09	1.98
3	4.05	2.80	3.24	3.12
4	4.47	3.27	3.75	3.98
5	5.58	3.84	4.87	4.86
6	5.85	4.06	5.18	5.26
7	6.46	4.65	5.80	5.80

FIGURE 2.16

NATURAL FREQUENCIES OF THE MV ARCTIC AS A FUNCTION OF THE MODE NUMBER [30]

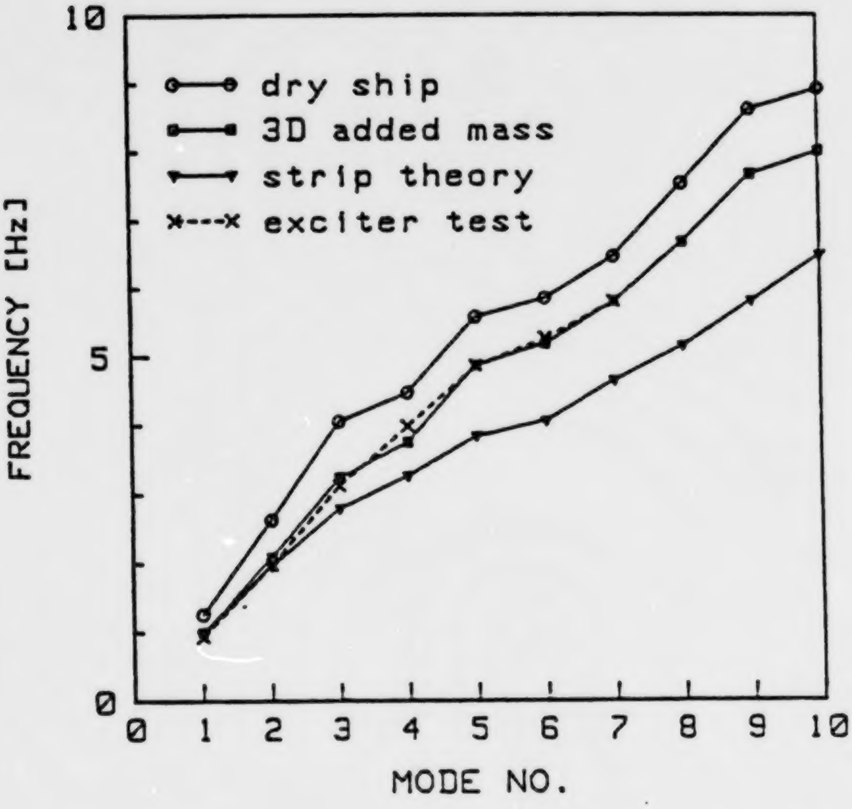

FIGURE 2.17

THREE LOWEST FLEXURAL MODE SHAPES OF MV ARCTIC [30]

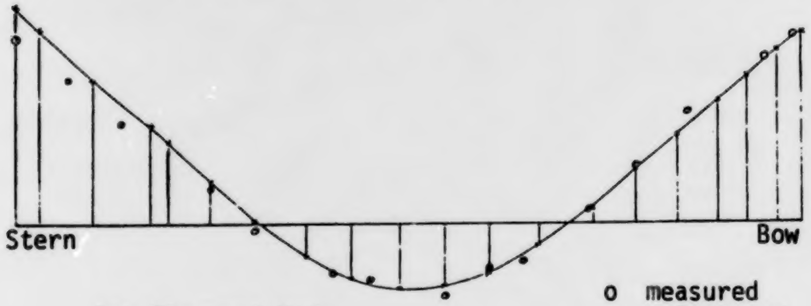

1st Flexural Mode

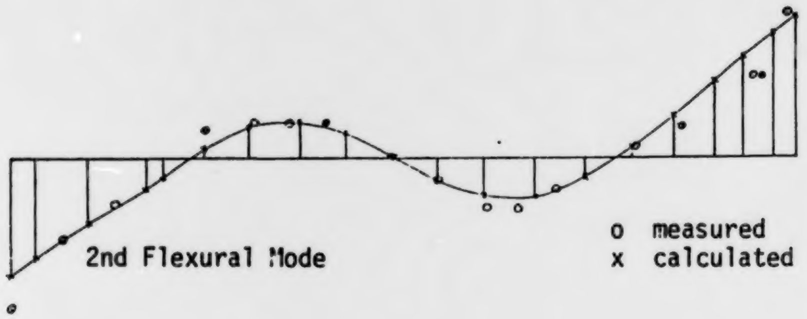

2nd Flexural Mode

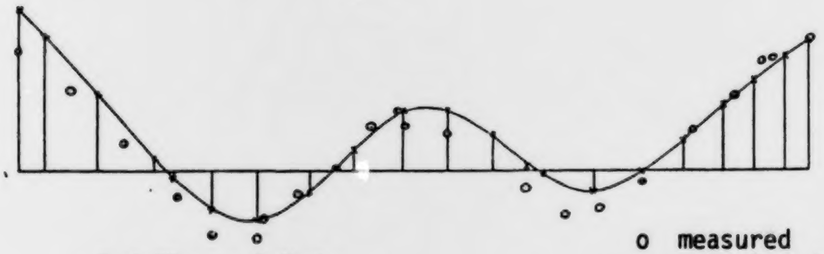

3rd Flexural Mode

2.6.3 Discussion of VTT Results

The structural model is so coarse that it cannot be assumed to give reliable results in higher modes. Especially this can be seen, when the strip theory approach is used. All masses are then directly lumped on the nodes, which leads to some overestimation of inertial effects and causes heavy deformation of the double bottom in the third mode. Correspondingly, higher calculated frequencies are increasingly lower than the measured ones and modes also differ substantially.

As can be seen in Figure 2.17 the three-dimensional treatment of added mass improves the situation quite radically. All seven lowest frequencies, which were identified in measurements, are given with reasonable accuracy. Also, the calculated and measured modes correspond to each other much better, although discrepancies are larger in the higher modes than for the lower modes shown in Figure 2.17. It seems that especially with coarse models the consistent treatment of mass with all coupling terms will considerably improve the behaviour of the model.

The ratio of wet and dry frequencies is graphically shown in Figure 2.18 as a function of the mode number. This ratio is nearly constant in the three lowest modes, which explains the rather good results obtained by strip theory. In higher modes, the ratio rapidly increases up to about 0.9. This kind of behaviour indicates that the vibration modes are not very beam-like, but that the structure behaves in a rather complicated manner. Also this phenomenon makes the use of strip theory somewhat doubtful in higher modes.

FIGURE 2.18

RATIO OF WET AND DRY FREQUENCIES USING THREE-DIRECTIONAL F.E. METHOD [30]

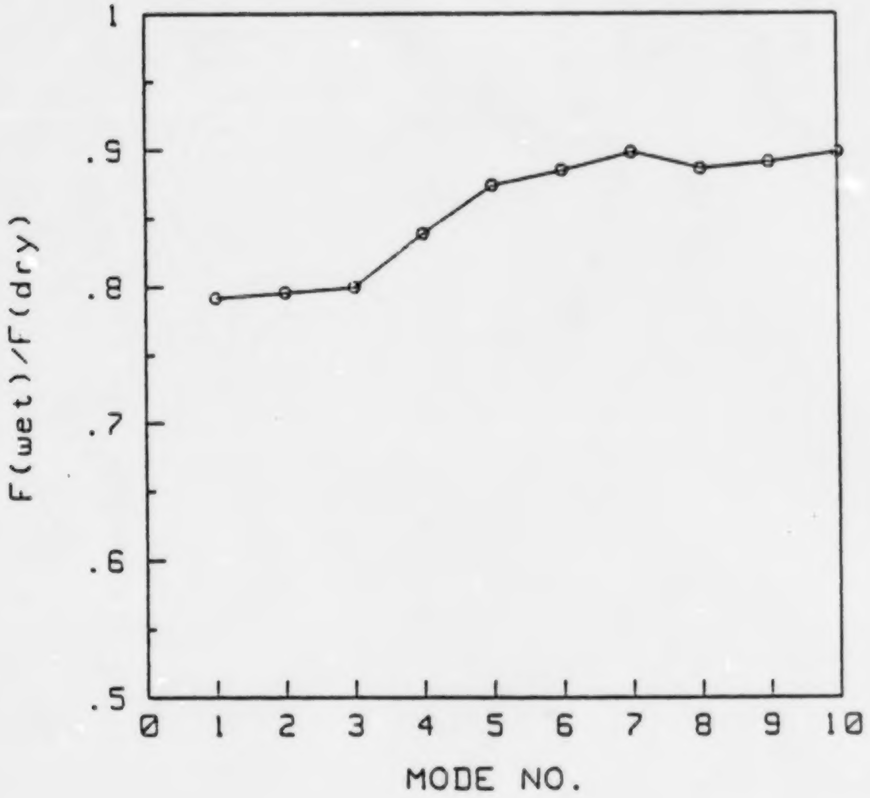

2.7 Some General Observations

The finite element method provides an efficient numerical tool for the solution of a true three-dimensional fluid-structure interaction problem. The fluid flow can be modelled with the same accuracy as the structural behaviour. Compared to the strip-theory approach, accuracy can be significantly improved at least in higher modes, or when the local behaviour is important, because all coupling terms are included and no artificial correction factors are needed.

In the present work, numerical procedures and corresponding computer programs are developed, which make the interaction analysis a highly automatic process. The key features are the use of dry modes of the ship and the corresponding modal added-mass matrix, which also make the solution economically feasible in practice. The most tedious phase is the construction of the fluid element mesh, but it can be automatically generated on the basis of the structural mesh, because the fluid domain is otherwise geometrically simple. The resulting three-dimensional fluid problem is normally an order of magnitude smaller than the structural problem, because there is only one unknown per node.

Numerical studies show, that especially in more complex modes, it is important to accurately model the fluid flow in the nearest vicinity of the structure. The infinity condition plays no role and thus the fluid finite element mesh need not be extended very far. However, the extent of the finite element mesh must be determined on the basis of the lowest modes, where the boundary effects are more significant but the fluid flow is otherwise simple. A balanced solution would then be a rather fine finite element mesh with high-order elements in the vicinity of the structure combined with infinite elements to model the infinity condition more realistically. The introduction of infinite elements requires no change in the developed interaction procedures, only the modelling of the fluid is somewhat changed.

For the same reason, the effect of restricted water is smaller in higher modes than in lower modes. A common rule of thumb regarding ship vibration tests says that the water depth should be at least five times the draught, in order to have results without shallow water effects. On the basis of the performed numerical studies it seems that this requirement can be much relaxed, when the modes corresponding to the blade frequency range of modern ships are investigated. This makes it reasonable to conduct an exciter test as early as the construction stage, because usually no corrections due to shallow water are needed.

3. SHIP VIBRATION DAMPING

3.1 Background

Ship damping dominates any attempts to make quantitative predictions of the vibratory response of hulls. Three basic components contribute to hull damping; structural damping, hydrodynamic damping and cargo damping. Ship damping data, adequate for making reliable vibration predictions, do not exist. Previous experiments aimed at evaluating ship damping have not produced the needed data. The distribution of the damping throughout the ship as well as the breakdown of the damping into its three basic components (structural, hydrodynamic and cargo) has not historically been addressed.

Theoretically, all modes of vibration participate in the response of a ship to excitation. Response to ice impact loading is dominated by the first few lower modes, but response to cyclic disturbances, such as rotating machinery and wave-induced motions, is typically dominated by modes with frequencies which couple with the frequencies of excitation. Damping characteristics are different for different modes, and therefore, damping coefficients for different modes are needed in order to make reliable vibration calculations.

3.2 Review of Available Data for Ship Vibration Damping

In the mid-1960's, Woolam [32] reviewed the state-of-the-art of vibration damping associated with ship hulls, and presented a categorized summary of available damping data based on ship class, type of hull framing, loading condition, mode number and method of excitation. In Reference [32], damping coefficients are presented for vertical modes of vibration for the first five modes of vibration and separate tables are presented for cargo ships, tankers, and miscellaneous ships. The damping coefficients given in [32] are presented in terms of the equivalent frequency-dependent linear-damping coefficient most common to the maritime industry. This representation was first used by McGoldrick [33] and assumes that $C/\mu\omega$ = constant, where C is the distributed linear damping force per unit velocity per unit length, μ is the mass per unit length of hull including the added mass of surrounding water, and ω is the circular frequency of vibration. A review of the tables in [32] shows that this factor is not a constant.

Past vibration tests have involved a wide variety of experimental techniques to measure hull damping, and a variety of expressions for defining damping coefficients have evolved. The most commonly used descriptions for damping are presented below.

- Equivalent linear damping coefficient ($C/\mu\omega$)
- Logarithmic decrement (δ)
- Magnification factor (Q)
- Amplification factor (A)
- Damping ratio ζ = C/critical damping = C/C_c
- Dissipation factor (η)

The following cross relationships and conversions exist among these quantities:

$$C/\mu\omega = \delta/\pi = 2\zeta = 2C/C_c = 1/Q = 1/A = \eta \qquad (3.1)$$

These relationships are based on linear single-degree-of-freedom systems.

Despite the apparent abundance of information presented in [33], the information is inadequate for predicting the response of ships at resonant conditions. The main inadequacies stem from:

- the lack of differentiation of the basic damping components (i.e. hydrodynamic, cargo and structural damping)
- the lack of information on the distribution of the damping along the ship.
- the frequency and mode dependency of damping coefficients are not being established, and
- most measuring and computing methods being based on single-degree-of-freedom methods.

The current indeterminate status of damping can be seen in Figure 3.1. Various investigators use entirely different values of the damping coefficient. Note that almost, if not all, of these experimental data were measured with the ships stationary.

To date, we have been unable to find experimental data which overcome all of these deficiencies, but several sources which address some aspects of the problem areas in hydrodynamic areas are discussed briefly below.

3.2.1 Hydrodynamic Damping

The relative importance of hydrodynamic damping is not clear in the literature and few experiments have been conducted to answer the questions. Sezawa and Watanabe [34] have divided hydrodynamic damping into three main sources:

- water friction,
- generation of pressure waves,
- generation of surface waves.

In the so-called rigid-body modes of a hull, hydrodynamic actions would seem to overwhelmingly predominate, but in hull-distortion modes, there seems to be a consensus among many researchers that hydrodynamic damping becomes less significant as structural and cargo damping come into play.

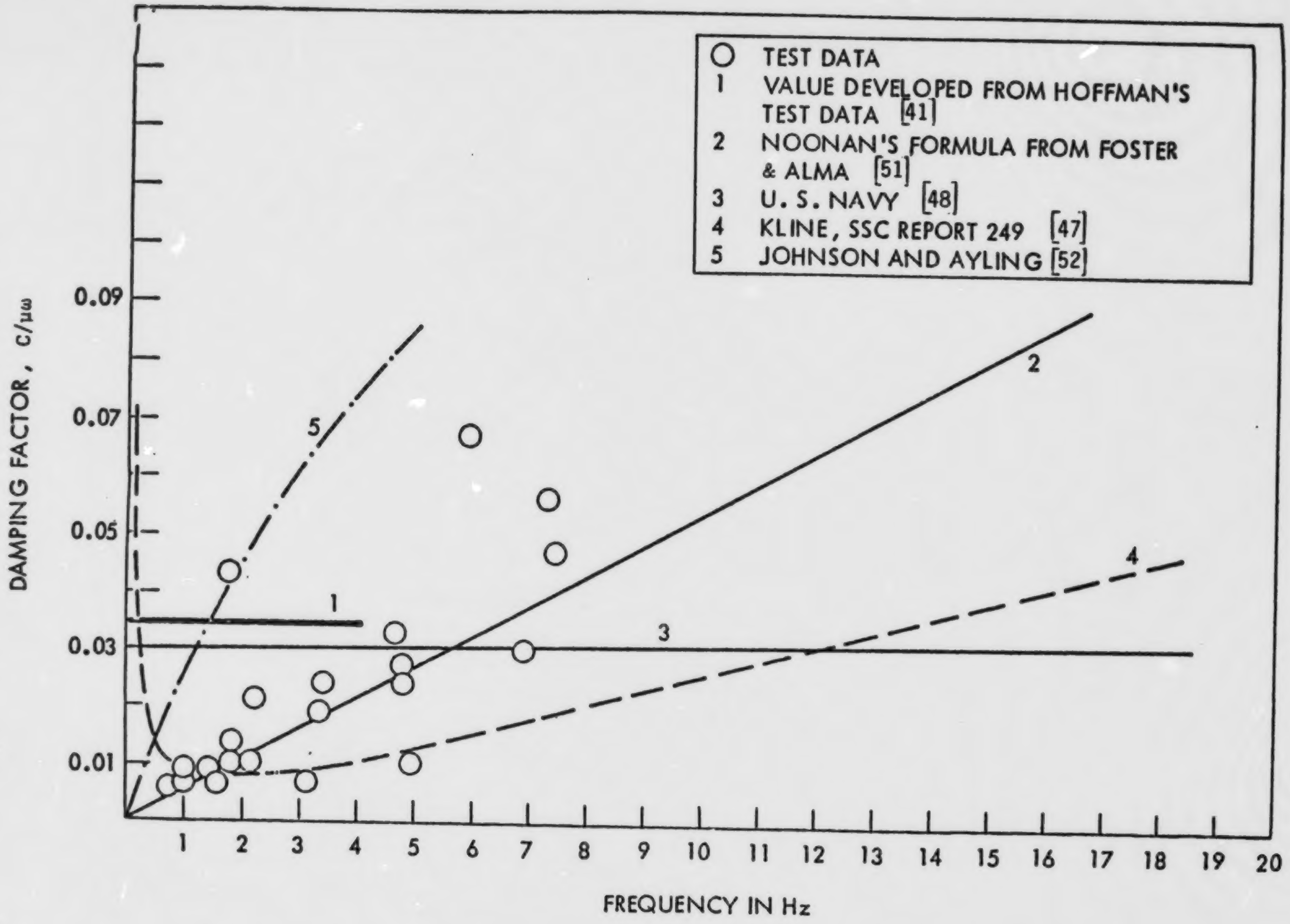

Figure 3.1 DAMPING COEFFICIENTS USED BY VARIOUS INVESTIGATORS

Betts [35] reviewed available theoretical and experimental evidence and concluded that "generally speaking, all forms of hydrodynamic damping are negligible in the higher modes of conventional ships". Robinson, [36], also states that "the least important source of damping at low hull frequencies appears to be that due to water". Kumai [37] also estimates that the total energy loss due to hydrodynamic damping is negligible compared with the loss due to structuraldamping. Borg [39] made energy calculations for a ship vibrating in the 2-node vertical mode following ship slamming, and concluded that the energy loss due to internal hull friction is many orders of magnitude greater than hydrodynamic energy absorption. Volcy [7] conducted tests on a 1/100 scale model of a tanker and measured damping for the model in air, and in water. He reported that there was not a significant variation of the damping coefficient for the model in air, and in water, for the model either empty or filled with water. (The model response was in the 2-node vertical mode).

In recent years, ships have been built with increasing hull flexibility, and hydrodynamic damping may play a more important role in hull vibrations than previously thought. The forward-speed effect on hull vibration has been recognized by Salvesen et al [14]. In the past, no damping experiments have been conducted to determine the effect of forward-speed on damping. In fact, Goodman has developed a method for studying wave-excited hull vibrations in large tankers and bulk carriers [40] and suggests that speed-dependent (hydrodynamic) damping is the predominant source of damping for a large tanker at service speed.

In light of the above discussion, it is apparent that more information is needed on the effects of hydrodynamic damping and forward-speed on the damping of hull vibrations.

3.3 Other General Shortcomings of Past Damping Experiments

Many measuring and computing methods treat the ship as a single damped mass-spring system. The results, even if accurate, provide the total damping of the ship. While such data are abundant and readily available, they are not adequate for ship vibration analysis.

The measurements obtained in damping experiments provide only the total response due to certain controlled excitations. It is generally understood that the total damping consists of at least three basic components, i.e. hydrodynamic, cargo and structural damping, and that for these components, and the effects of different frequencies, an experimental program must include methods for differentiating among these components. Little effort has been made in this direction in past experiments.

In order to make accurate and reliable ship vibration calculations, in addition to the magnitude, the distribution of the damping coefficients along the ship is required. None of the existing experimental data and computation methods can be used to determine the distribution of the damping.

The forward-speed effects have been recognized as being quite important [14]. In the past, no damping experiments have been conducted to determine the forward-speed effects on damping. Hoffman [41] has calculated the differences between the experimental results and the results in Goodman's method [40], and he indicated the importance of the forward-speed effects. However, he attributed these differences to the damping alone. Since Goodman's solutions also ignores the forward-speed effects on the hydrodynamic force and the stiffness of the hull, the actual forward-speed effects of damping are still unknown.

3.4 Methods of Calculating Hull Damping

As in the case in the calculation of the added mass coefficients, a strip theory representation is often made in the computation of the damping coefficients since damping, in principle, is only the in-phase component of the hydroforce. Therefore, analogous to equations (2.12) through (2.16), the following expressions can be written down for damping:

$$\text{SWAY:} \quad B_{22} = \int_{-L/2}^{L/2} b_{22} \, dx' \tag{3.2}$$

$$\text{HEAVE:} \quad B_{33} = \int_{-L/2}^{L/2} b_{33} \, dx' \tag{3.3}$$

$$\text{ROLL:} \quad B44 = \int_{-L/2}^{L/2} b44 \, dx' \tag{3.4}$$

$$\text{PITCH:} \quad B_{55} = \int_{-L/2}^{L/2} b_{33} \, x'^{2} \, dx' \tag{3.5}$$

$$\text{YAW:} \quad B_{66} = \int_{-L/2}^{L/2} b_{22} \, x'^{2} \, dx' \tag{3.6}$$

where b_{22} = damping coefficient per unit length of a section for horizontal motion
b_{33} = for vertical motion
b_{44} = for rotation

It is well known that in calculating the damping coefficient by means of a strip theory, errors arise because no allowance is made for the three-dimensional wave pattern around the ship. Owing to the ship motion waves are generated, moving amongst others, in a circular form from the fore and after parts of the ship, and these waves are disregarded in using a strip theory. Various calculations have been carried out by applying the strip theory to an idealized ship form, for which three-dimensional calculations are available. In this way the error made in using a strip theory, can be ascertained. As examples, Figure 3.2.a shows the result of calculations made by Havelock for a spheroid oscillating below the free surface and carrying out pitching and heaving motions. In this figure, the ratios B'33/B33 and B'_{55}/B_{55} are given as functions of the dimensionless frequency parameter $\xi_L = \omega^2/g\ L/2$ for a spheroid having a ratio L/B = 8. In the discussion on the results of similar calculations concerning a thin ship (Michell ship) with L/B = 6, 7 and 8 are given (Figure 3.2.b). A thin ship is a ship with the breadth dimension small compared to the length and the draft. The value of the frequency parameter ξ_L which is of practical importance for ships in ice, can be calculated based on the typical impact periods discussed earlier.

It may be said from the trend of the curves in Figure 3.2.b that at the range of values for ξ_L shown above, the 3-dimensional theory predicts damping coefficients which are almost of the same order as those predicted by a 2-dimensional theory. To what extent these calculations have general validity, is uncertain.

Presumably the discrepancies are too high for an icebreaking hull form with L/B between 4 and 5. It is, however, worthwhile pursuing the search for two-dimensional damping coefficients which at least give the correct order of magnitudes of the damping forces in an ice impact situation.

There is a direct connection between the damping coefficient per unit length for 2-dimensional motion and the amplitude of the waves emitted, since damping is exclusively due to the fact that waves are sent out which carry off energy.

From the differential equation of motion, it can be shown that the average energy expended per second in overcoming the damping force is given by:

$$W_d = 1/2\ \omega^2\ B_j\ \bar{x}^2_j \qquad (3.7)$$

where B_j = the damping coefficient in the jth mode of motion

$\bar{x}_j$ = amplitude of motion in the jth mode.

Assuming the amplitude of a wave emitted by the motion of the body in the jth mode to be $\bar{H}_j$, the amount of energy carried off by the waves on both sides every second is given by:

$$W_\omega = 1/2\omega\ \rho g^2\ \bar{H}^2_j$$

FIGURE 3.2

DAMPING FOR SUBMERGED SPHEROIDS AND "THIN" SURFACE SHIPS

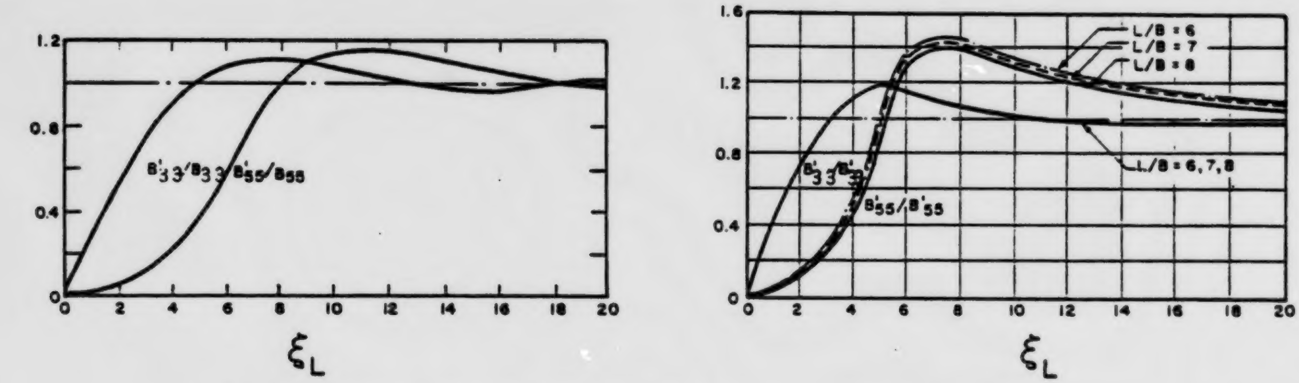

a) HEAVE AND PITCH DAMPING OF SUBMERGED SPHEROIDS

b) HEAVE AND PITCH DAMPING FOR THIN (Michell ships)

B'_{33}, B'_{55} = Three-dimensional damping in Heave and Pitch

FIGURE 3.3

HYDRODYNAMIC ADDED MASS FOR CIRCULAR, RECTANGULAR AND SHIP-SHAPED SECTIONS

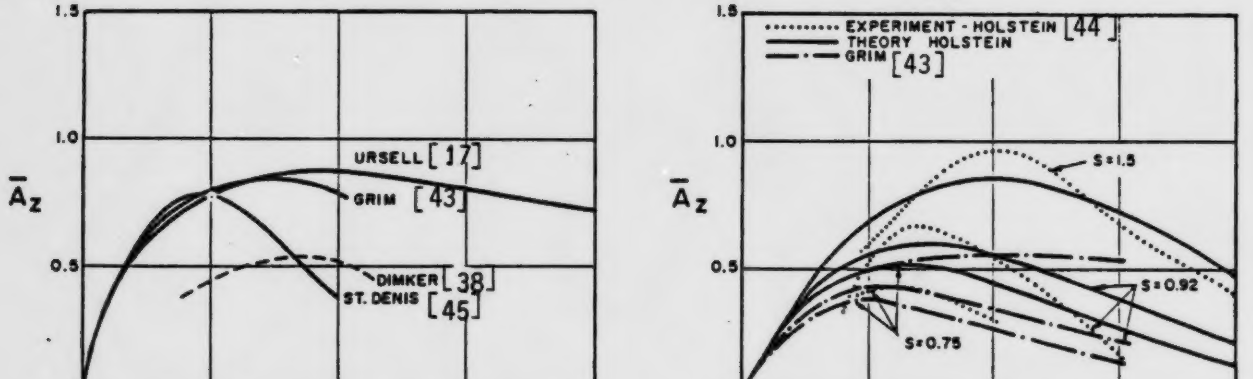

(a)

(b)

S=B/2T

Equating the two expressions yields for the damping coefficient:

$$B_j = \frac{\rho g^2}{\omega^3} \bar{A}^2_j \qquad (3.8)$$

where $\bar{A}_j = \bar{H}_j/\bar{X}_j$ represents the ratio of the amplitude of the wave emitted in the jth mode to the amplitude of motion in the jth mode. if, therefore, the amplitude ratio $\bar{A}_j$ is known, the damping coefficient per unit length can be calculated with the aid of (3.8). For heaving, swaying and rolling, the following formulae have been proposed [47].

$$b_{33} = \frac{\rho g^2}{\omega^3} \bar{A}^2_3; \ \bar{A}_3 = \bar{H}_3/\bar{X}_3 \quad \text{(heave)} \qquad (3.9)$$

$$b_{22} = \frac{\rho g^2}{\omega^3} \bar{A}^2_2; \ \bar{A}_2 = \bar{H}_2/\bar{X}_2 \quad \text{(sway)} \qquad (3.10)$$

$$b_{44} = \frac{\rho g^2}{\omega^3} (B/2)\, \bar{A}^2_4; \ \bar{A}_4 = \bar{H}/\bar{X}_4\ B/2 \quad \text{(roll)} \qquad (3.11)$$

For rolling, in equation (3.11) above, the ratio $\bar{A}_4$ has been non-dimensionalized using the vertical motion of the point on the section situated in the water plane.

The amplitude ratio $\bar{A}_3$ for heaving of a circular cylinder was calculated by Ursell [17]. The results of these calculations are given in Figure 3.3.a (see the curve marked "Ursell"). Ursell also calculated the amplitude ratio for higher frequencies than those given in Figure 3.3.a. It should be noted that the frequency parameter in Figure 3.3 is based on the beam of the hull so that the ξ_B values typical of icebreaking hull forms are 40 to 50. From this Figure it will be seen that for very high and very low frequencies, the amplitude ratio approaches zero, in which case the waves generated by the motion will be so small that they do not carry off any energy. For a specific frequency the curve shows a maximum.

For sections rather resembling those of a ship, Grim [43] carried out calculations concerning the amplitude ratio for heaving, $\bar{A}_3$. Grim's computations covered s = 0.4 to 1.4 and section coefficient β in the range of 0.6 to 1.0. The use of Grim's results in the case of a circle enables Grim's theory to be compared with that of Ursell (see the curve marked "Grim" in Figure 3.3.a). There is reasonable agreement. An approximate formula for A_3 for rectangular sections was suggested by Holstein [44] assuming that the vertical motion of a rectangle can be represented by a number of distributed pulsating sources.

$$\bar{A}_3 = \sin\xi_B \cdot \exp(-\xi_B/s) \tag{3.12}$$

The above expression is applicable only to low values of ξ_B.

St.Denis [45] suggested this formula also be used for other than rectangular sections. The use of this formula in the case of a circle enables St.Denis' theory to be compared with Grim's and Ursell's theories (see the curve marked "St.Denis") in Figure 3.3.a. It appears, therefore, that for large frequencies there will be a considerable difference between St.Denis' calculation and those made by Grim and Ursell.

The amplitude ratio for swaying and rolling available in [43] are only applicable to small values of the frequency parameter ξ_B (up to $\xi_B = 0.3$). For higher values of ξ_B (as high as 20) it is only known that the amplitude ratio and hence, the damping coefficients are small. As $\xi_B \to \infty$, the damping coefficient tends to zero.

It may, in general, be concluded that the hydrodynamic component of damping coefficients in all modes of motion can be assigned zero values in computations. This approximation should give sufficiently accurate results of accelerations for impact-type situations.

4. REVIEW OF COMPUTATIONAL METHODS IN SHIP HULL RESPONSE

4.1 Governing Equations of Hull Elastic Response

The theoretical basis of the experimental program for determining hull hydrodynamic coefficients is developed here. The basic equations of hull response are presented and examined in the light of the planned experiments. The source of these equations are [46, 47, 48, 49 and 50].

It is, in general, accepted that the vertical hull response can be treated as the flexural response of a non-uniform free-free Timoshenko beam. The governing differential equations of motion are:

$$w' = -\theta + \frac{V}{GA} \qquad \text{(Figure 4.1)}$$

$$\theta' = \frac{M}{EI} \qquad (4.1)$$

$$M' = V + I_o\,\theta + C_o\,\dot{\theta}$$

$$V' = m_s\ddot{w} + C\dot{w} - F(w, \eta, x, t) - Q(x,t)$$

where w, θ, M, V are the response parameters - deflection, slope, bending moment and shear force respectively,

I_o = mass rotary moment of inertia per unit length

I = moment of inertia of hull section

C_o, C = damping coefficients per unit length associated with the rotation and vertical motions of the hull

m_s = rigid body mass per unit length

A = shear area

$F(w, \eta, x,t)$ = total vertical hydrodynamic force

$Q(x,t)$ = Vertical excitation force

η = the water surface height relative to still water (the wave profile)

G = Modulus of rigidity (shear modulus)

E = Modulus of elasticity

x = position variable along the longitudinal axis of the ship

FIGURE 4.1

FREE-BODY DIAGRAM OF A SEGMENT OF SCALE MODEL

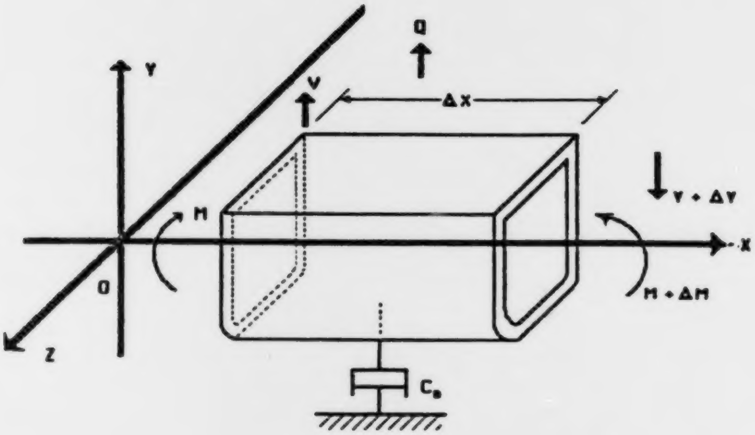

t = time

$'$ = (prime) denotes differentiation with respect to position x, $\frac{\partial}{\partial x}$

$\cdot$ = (dot) denotes differentiation with respect to time t, $\frac{\partial}{\partial t}$

The expression for the total vertical hydrodynamic force $F(w, \eta, x, t)$ involves certain hydrodynamic coefficients associated with added mass and damping. There are a number of methods available for the calculation of these coefficients. In summary, it has been proven that the two-dimensional conformal mapping method for added mass and damping coefficients is accurate for ship sections which are essentially "wall-sided" such as those in the "parallel" mid-body. However, towards the bow and stern of the ship, the accuracy of the method drops off because of deviation in section shape and three-dimensional effects. Since the variations of the hydrodynamic coefficients are greatest toward the bow and the stern, a more accurate method is required for determining these coefficients.

In general, the total hydrodynamic force (per unit length) of the surrounding water can be expressed as:

$$F(w,\eta,x,t) = - \frac{D}{Dt} m_a \cdot \frac{D}{Dt} (\dot{w}-\dot{\eta}) - \frac{N}{\omega_n^2} \frac{D}{Dt} (w-\eta) - \rho g B (w-\eta) \qquad (4.2)$$

where $\frac{D}{Dt} = \frac{\partial}{\partial t} - U \frac{\partial}{\partial x}$, substantial or total derivative

m_a = added mass/unit length

U = forward speed of model

N = hydrodynamic damping coefficient

w = vertical response of model

η = water surface elevation relative to MWL

B = beam of model

ρ = mass density of water

ω_n = natural frequency of the model

g = acceleration due to gravity

This expression simply states that the excitation consists of the inertia force, the damping force and the restoring force. All of these force components are functions of the relative position between the water surface and the hull section. If we consider calm-water test conditions, (i.e.: no wave) than $\eta = 0$. In general, equations (4.1) and (4.2) can be combined into the following matrix equation:

$$S' = KS + \overline{M}\ddot{S} + D\dot{S} + Q \qquad (4.3)$$

where $S \equiv w, \theta, M, V$ is the state variable vector

$$\dot{S} = \frac{\partial s}{\partial t}, \quad S' = \frac{\partial s}{\partial x}, \quad \ddot{S} = \frac{\partial^2 s}{\partial t^2}$$

$K, \overline{M}, D$ are stiffness, mass and damping matrices respectively

Q = the excitation vector

$= \{0, 0, b(x,t), f(x,t)\}$

where $b(x,t)$ is the moment load

$f(x,t)$ is the force load

In the frequency domain, they may be written as:

$$b(x,t) = b_c(x) \cos \omega t + b_s(x) \sin \omega t$$

$$f(x,t) = f_c(x) \cos \omega t + f_s(x) \sin \omega t$$

where ω is the excitation frequency.

4.2 Solution of the Ship Response Problem

4.2.1 Free Vibration and Mode Shapes

Omitting the damping and excitation terms in equation (4.3), the equation for the undamped response becomes:

$$S' = KS + \overline{M}\ddot{S} \qquad (4.4)$$

Assuming harmonic response of frequency ω such that

$$S = S_0 \sin \omega t$$

we have: $S_0' = (K - \overline{M}\omega^2)S_0$ (4.5)

Solution of (4.5) provides an infinite set of eigenvalues and eigenvectors ω_n and S_n, which satisfy the specified boundary conditions and the equation:

$$S_n' = (K - \overline{M}\omega_n^2)\, S_n \qquad (4.6)$$

where ω_n and $S_n(x)$ are the natural frequency and mode shape for the nth mode.

4.2.2 Forced Vibration, Steady State

Assuming a solution of the form

$$S(x,t) = \Sigma A_n S_n(x) \cos(\omega t - \phi_n) \tag{4.7}$$

where ϕ_n is the phase angle and substituting in (4. 3), and using the relation (4.6) yields

$$\Sigma A_n (\omega_n^2 - \omega^2) \overline{M}S_n \cos(\omega t - \phi_n) - \Sigma A_n \omega D S_n \sin(\omega t - \phi_n) = Q_c \cos \omega t + Q_s \sin \omega t \tag{4.8}$$

where $Q_c = \{0, 0, b_c, f_c\}$

$Q_s = \{0, 0, b_s, f_s\}$

Equations (4.8) represents a set of four simultaneous equations. Multiplying the third equation of (4.8) by θ_m and the fourth equation of (4.8) by w_m and integrating over the whole length of the ship yields:

$$\Sigma A_n[(\omega_n^2 - \omega^2) N_{mn} \cos(\omega t - \theta_n) - \omega D_{mn} \sin(\omega t - \theta_n)] = F_m \tag{4.9}$$

where $N_{mn} = \int_L [(I_o + I_a)\ \theta_n \theta_m + (m_s + m_a)\ w_n w_m]\, dz$

$D_{mn} = \int_L [C_o \theta_n \theta_m + C w_n w_m]\, dz$

$F_m = F_{cm} \cos \omega t + F_{sm} \sin \omega t$

$F_{cm} = \int_L (b_c \theta_m + f_c w_m)\, dz$

$F_{sm} = \int_L (b_s \theta_m + f_s w_m)\, dz$

where m_a and I_a are added mass and added moment of inertia, C_o and C are damping coefficients including all damping components. Unless the damping is everywhere proportional to mass, the coefficients A_n for various modes are coupled by the terms associated with the damping. If the damping coefficients are initially known this coupling poses no problem. Equation (4.9) can be solved explicitly for as many A_n as desired, taking into consideration all coupled terms.

In the present case, the damping coefficients are unknown, as are the added mass coefficients. As the coupling of the damping terms is an inherent problem, the solution is to excite the model in such a manner that the response can be controlled to be primarily in one particular mode (at a time). Then contributions from other modes become neglibible and the off-diagonal terms in the matrix D_{mn} can realistically be neglected. This concept is the basis for the proposed experimental program discussed in Section 1. The success of the experiments rests on the ability to devise an excitation method which closely achieves the "single-mode" response for each of the modes of interest. The theoretical basis for selecting the excitation which will generate this single-mode response needs to be developed. Since θ and w in equation (4.9) are eigenvectors, orthogonality implies that the matrix N with components N_{mn} is diagonal. Therefore, if all coupled terms can be neglected in equation (4.9), it reduces to:

$$A_n(\omega_n^2 - \omega^2)N_{nn}\cos(\omega t - \phi_n) - \omega D_{nn}\sin(\omega t - \phi_n) = F_{cn}\cos\omega t + F_{sn}\sin\omega t \tag{4.10}$$

Collecting the terms associated with $\cos\omega t$ and $\sin\omega t$ provides two equations with two unknowns, A_n and ϕ_n:

$$\phi_n = \arctan \frac{\mu_n\omega f_{nc} + (\omega_m^2 - \omega^2) f_{ns}}{(\omega_n^2 - \omega^2) + \mu_n \omega f_{ns}} \tag{4.11}$$

$$A_n = \frac{\sqrt{f_{nc}^2 + f_{ns}^2}}{\sqrt{(\omega_n^2 - \omega^2) + \mu_n^2 \omega^2}} \tag{4.12}$$

where $f_{nc} = \dfrac{F_{cn}}{N_{mn}}$, $f_{ns} = \dfrac{F_{sn}}{N_{nn}}$, $\mu_n = \dfrac{D_{nn}}{N_{nn}}$

Substituting (4.12) into equation (4.7),

$$S(x,t) = \Sigma \frac{\sqrt{f_{nc}^2 + f_{ns}}\cos(\omega t - \phi_n)}{\sqrt{(\omega_n^2 - \omega^2)^2 + \mu_n^2\omega^2}} S_n(x) \tag{4.13}$$

4.2.3 Transient and Non-Periodic Response

For non-period response which must be analyzed in the time domain, a more general non-harmonic mode shape must be used in the above procedure. Such a mode shape can be defined by:

$$S(x,t) = \Sigma A_n(t) \cdot S_n(x) \qquad (4.14)$$

Substituting this expression in (2.2) and using the relationship (4.6), we have:

$$\Sigma [M\omega_n^2 \; A_n(t) + D\omega \dot{A}_n(t) + \bar{M}\, \ddot{A}_n(t)] S_n(x) \; = F(x,t)$$

The above equation together with the result

$$F_n(t) = \frac{\int_0^L F(z,t)\, w_n(z)\, dz}{N_{nn}}$$

can be used to yield a solution for the modal response of the structure:

$$\ddot{A}_n(t) + \omega\mu_n \; \dot{A}_n(t) + \omega_n^2 \; A_n(t) \; = F_n(t) \qquad (4.15)$$

Equation (4.15) can be solved explicitly to give $A_n(t)$ in general form as:

$$A_n(t) = \exp(-\zeta_n \omega_n t)\, [\cos \alpha_n t + \frac{\zeta_n \omega_n}{\alpha_n} \; \sin \alpha_n t]\, A_n(0) +$$

$$\exp(-\zeta_n \omega_n t)\, \frac{\sin \alpha_n t}{\alpha_n} \dot{A}_n(0) + \qquad (4.16)$$

$$\int_0^t F_n(\gamma) \cdot \exp[\zeta_n \omega_n (t-\gamma)] \; \frac{\sin \alpha_n (t-\gamma)}{\alpha_n} \; d\gamma$$

where $\zeta_n = \frac{\mu_n}{2\omega_n}$, $\alpha_n = \omega_n \sqrt{1 - \zeta_n^2}$

If (4.16) is substituted in (4.14), we have the solution for the transient response of the hull.

From equation (4.16), if the model is excited to a certain response with initial displacement and/or velocity, the responses will gradually reduce to zero. If the response can be measured at a suitable point on the model, and if it is possible to 'filter' the contribution of the different modes and stored separately, then the damping factor ζ_n can be calculated.

Let t_o, t_m be two instances in time when the response reaches the maximum values $w_n(x,t_o)$, $w(x,t_m)$ and t_m is m periods after t_o. Then from (A-16)

$$\frac{w_n(x,t_o)}{w_n(x,t_m)} = \exp\left[\mu_n m \Pi / \alpha_n\right] \quad (4.17)$$

so that,

$$\frac{\mu_n}{\alpha_n} = \frac{1}{m\Pi} \ln\left[\frac{w_n(x, t_o)}{w_n(x, t_m)}\right] \quad (4.18)$$

The above ratio is the well-known "logarithmic decrement" in free, damped oscillation problems. For convenience in discussion, the parameter μ_n is called te 'total damping coefficient'. The coordinate variable x indicates that the response can be measured at any point along the length of the model, at which there is sufficient (measurable) response.

Once the value of μ_m is determined, we have from equation (4.12),

$$N_{nn} = D_{nn}/\mu_{nn}$$

or,

$$\int_o^L [(I_o + I_a)\,\theta_n^2 + (m_s + m_a)w_n^2]dx = D_{nn}/\mu_{nn} \quad (4.19)$$

where θ_n and w_n are the mode shapes of the n^{th} mode.

Theoretical Basis for the Magnification Damping Tests

Letting $W_n(x)$ be the measured peak of a steady-state vibration associated with the nth mode, we have:

$$W_n(x) = \frac{\sqrt{f_{nc}^2 + f_{ns}^2} \cdot w_n(x)}{\sqrt{(\omega_n^2 - \omega^2)^2 + \mu_n^2 \omega^2}} \qquad (4.20)$$

From equation (4.13), if the excitation force is given and the contribution of different mode shapes can be separated, the damping can be calculated as follows:

$$\mu_n = \left\{ \frac{f_{nc}^2 + f_{ns}^2}{\omega^2} \left[\frac{w_n(x)}{W_n(x)} \right]^2 - \frac{(\omega_n^2 - \omega^2)^2}{\omega^2} \right\}^{1/2} \qquad (4.21)$$

The above reasoning is based on the principle of the magnification tests in vibration analysis. In order to obtain the maximum responses with limited excitation capacity, the excitation frequency is chosen so that resonant conditions $(\omega - \omega_n)$ can be reached.

Distribution of Hydrodynamic Coefficients

In principle, the distribution of the hydrodynamic coefficients can be calculated as follows:

a. The total hydrodynamic coefficient μ_n associated with different modes are determined according to the measurements as shown in equations (4.17) or (4.21).

b. Let the distribution of the total or effective inertia I_e and the total or effective mass m_e be represented by m discrete points such as $I_e(x_1), \ldots\ldots I_e(x_m)$ and $m_e(x_1) \ldots\ldots m_e(x_m)$. Then equation (4.19) can be evaluated numerically in terms of the unknowns $I_e(x_i)$, $m_e(x_i)$, $i = 1, \ldots\ldots m$ as follows:

$$\int_0^L \left[\sum_{i=1}^{m} I_e(x_i)\, \theta_n^2 + \sum_{i=1}^{m} m_e(x_i)\, w_n^2 \right] dx = D_{nn}/\mu_{nn} \qquad (4.22)$$

The above expression is used to represent the integration scheme for two curves with m ordinates. Any numerical method such as Simpson's rule can be used. The results will be a set of simultaneous equations as follows:

$$\sum_{j=1}^{m} A_{ij}\, I_e(x_j) + \sum_{j=1}^{m} B_{ij}\, m_e(x_j) = D_{nn}/\mu_{nn} \qquad (4.23)$$

where $I_e(x_j)$ and $m_e(x_j)$ are the effective inertia and mass to be determined.

$$A_{ij} = \int_{\alpha}^{\beta} \theta_i^2(x)\, dx$$

$$B_{ij} = \int_{\alpha}^{\beta} w_i^2(x)\, dx \qquad (4.24)$$

where,

$$\alpha = \frac{x_i + x_{i-1}}{2}, \quad \beta = \frac{X_{i+1} + x_i}{2}$$

5. RESULTS FROM EXPERIMENTS WITH MV ARCTIC SEGMENTED MODEL

5.1 Impact Tests

Investigation of the hydrodynamic added mass phenomenon in ship-ice interaction carried out under this project is documented in Volume 2 of this report. Ship-ice interaction in ramming differs significantly from conventional hull response problems in open water, in that it is transient in nature and the ship is brought to rest in a relatively short period of time. In such situations the hydrodynamic inertial reaction, especially at the bow, is governed by a number of factors such as the presence of the ice feature as well as confinement by the bow notch in the ice, large bow motions during ride-up and the flexibility of the ship. Towards the stern, the influences of the ice features will diminish and the added mass may be expected to assume numerical values familiar in the open water context.

In keeping with the transient nature of the problem, the added mass distributions along the hull were extracted using time domain calculation methods. The method consists of applying D'Alembert's principle to the instantaneous vertical forces acting on the hull, which include ice forces on the bow, gravitational and buoyancy forces on each segment, the shear difference forces between segments and the total hydrodynamic force. The hydrodynamic force is the only unknown in the force balance process and therefore it can be calculated at every instant for each segment. In the analysis the total hydrodynamic force was not resolved into separate hydrodynamic added mass and fluid damping terms. The gross added mass time history is determined by dividing the hydrodynamic force by the corresponding segment accelerations.

The time histories of the segmental added mass are expressed in non-dimensional form using the segment mass displacement as the normalizing factor. The time histories are characterized by abrupt reversals of sign at acceleration zero crossings. At these singularity points the calculated added mass assumed very large values, as a result of division of total hydrodynamic force by accelerations approaching zero. The assignment of a mean value to any segment or portion of a segment was rendered difficult by the sign reversals and the singularities. However, it was generally observed that the average magnitudes of the added mass were highest at the bow and decreased with distance aft. The large values of hydrodynamic added mass for segment 1 are attributable to proximity effects (confinement and shallow water effects).

The principal results of the computational process are summarized in the order of increasing velocity (Figure 5.1). Table 5.1 lists the non-dimensional mean added mass for each segment. The added mass at the bow segment is significantly larger, but is followed by a substantial reduction in magnitude as well as a reversal in the sign at the second segment.

TABLE 5.1

SEGMENTAL DISTRIBUTION OF NON-DIMENSIONAL ADDED MASS

VEL. (m/s)	.24	.37	1.14	.37	.58	.67	.86
SEGMENT/ TEST	TS-6	TS-2	TS-1	TR-8	TR-10	TR-11	TR-9
1	-86.5	-81.9	-2.1	-114.9	-94.7	-54.7	-18.7
2	9.0	7.6	-11.7	9.0	7.8	3.8	2.7
3	5.0	6.2	5.7	5.8	5.4	2.2	1.7
4	4.9	5.2	2.9	3.8	4.2	2.6	1.3
5	4.0	2.3	2.1	2.5	3.9	3.0	2.0
6	3.3	-0.4	2.7	1.9	2.6	1.9	2.4
7	2.3	-12.7	4.1	1.3	4.4	-1.0	1.6
8	11.7	-23.7	5.1	3.1	8.8	-2.9	-1.3
9	12.1	4.5	7.0	3.3	6.4	-7.1	-1.1
10	-1.1	10.9	3.4	6.1	10.9	-5.0	-1.4
11	4.8	10.9	6.2	7.4	10.8	-6.8	0.3
12	24.7	23.0	21.7	11.3	27.2	-15.0	1.8

Note: Non-Dimensional added mass = segment added mass/mass displacement.

Figure 5.1

Segmented Distribution of Non-Dimensional Added Mass

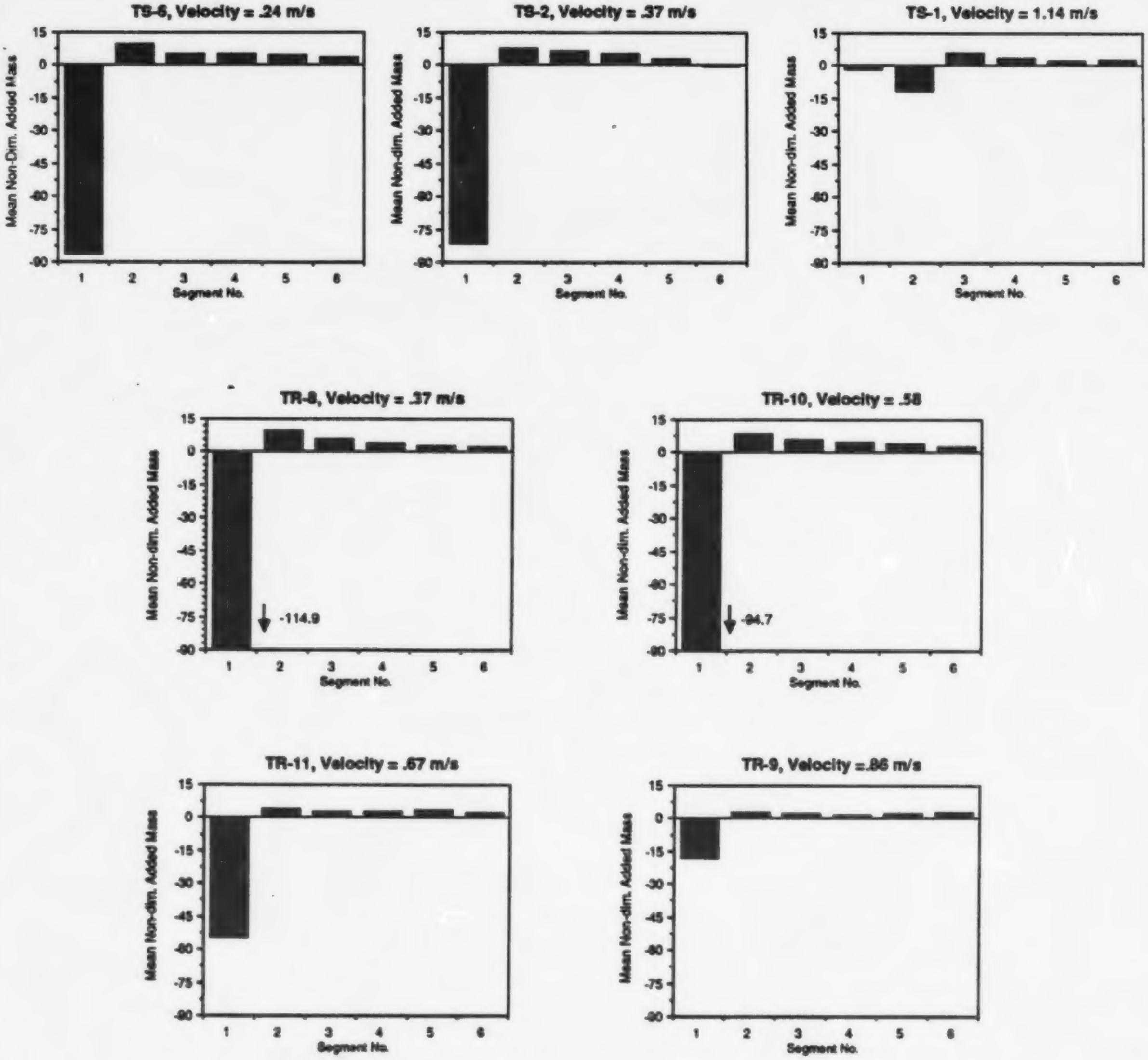

The mean added mass distribution shows a gradual decrease in magnitude around midship and through to segments 6 and 7. Towards the stern, one would realistically expect the non-dimensional added mass to approach the open water values as the influence of the ice features decreases with distance from the bow segment. It can also be seen from the results in Table 5.1 that the added mass at the bow segment is highest at the lowest impact speed and decreases as the speed increases. This shows that the dynamic effects are associated with the initial forward speed at impact. The results are only preliminary and further tests will be required to confirm this speed dependence.

5.2 Hammer and Shaker Tests

Model experiments were undertaken to quantify the hydrodynamic added mass and damping associated with longitudinal hull response in calm, ice-free water and in level unbroken ice, the results of which were reported in Volume 3. These experiments are distinct from those referred to in Section 5.1, in that the present series falls into the category of steady-state, constant frequency, constant amplitude oscillation tests, wherein the model is excited at one point on the forward segment of the hull and the responses of all the segments are measured. The experiments included impulse (hammer) tests as well as oscillation (shaker) tests in the wet and dry modes.

Both hammer and shaker tests were conducted in the dry mode. The wet tests were conducted in the towing tank with the model restrained in roll, surge, sway and yaw. Again, hammer and shaker tests were conducted both in the stationary mode as well as at forward speed. The wet tests were conducted in water with depth to draft ratio of 5.2. In order to assess the influence of water depth on hull response, the hammer tests were repeated in shallower water (depth to draft ratio 1.5). A limited series of ice tests was performed with the model stationary in level unbroken ice cover with uniform thickness (1.1 m full scale).

Examination of the transfer functions from the zero-speed dry, wet and ice cover tests depicted substantial differences in modal frequencies resulting from the hydrodynamic added mass effects. Forward speed effects were found to be significant at second and higher flexural modes of response.

From the dry hammer tests, it is seen that the structural (internal) hull damping increases with the mode number up to the third mode and at the fourth mode drops below that at the third mode. From the dry shaker tests, on the other hand, it is clearly observed that internal hull damping is a function of the frequency of oscillation. Further, significant variation of damping along the hull is observed only in the first mode. Once again, the magnitude of damping, increases with the mode number up to the third mode, beyond which it drops slightly.

Figure 5.2 VARIATION OF THE "J" FACTOR ALONG MODEL

a) First Flexural Mode

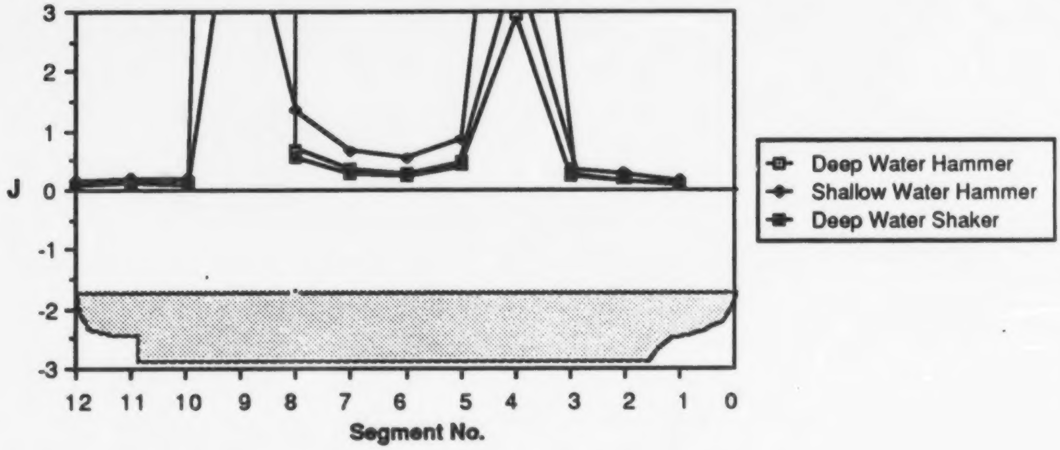

b) Second Flexural Mode

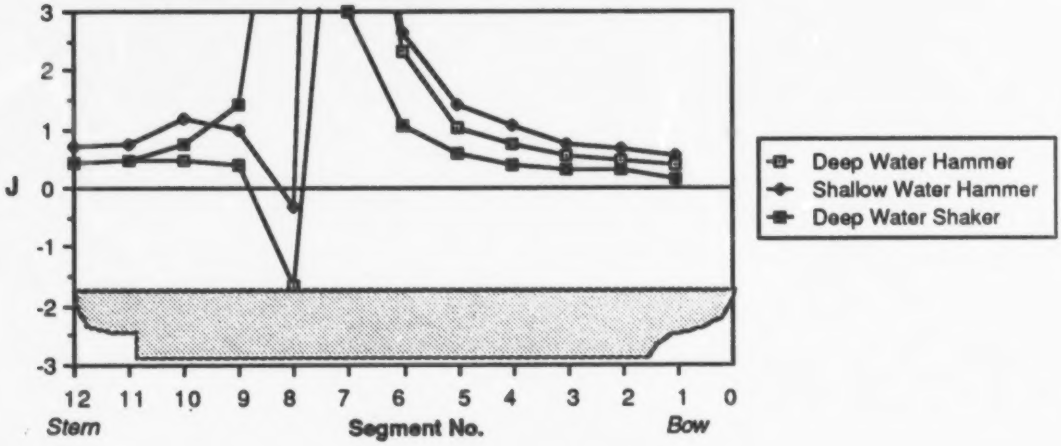

Hydrodynamic added mass from zero-speed hammer tests in deep water (Figure 5.2), expressed as J-factors, varies along the length of the hull attaining large values near the nodes. In general, positive values are obtained for J-factors. However, in the second flexural mode negative values are registered locally at segments where accelerations are very low (i.e. near the nodal points). Damping factor is nearly constant at 10% for the forward and aft segment of the hull, while for the intermediate segments the damping drops to roughly 4%. It is also seen that the damping is mode dependent, roughly 50% lower for the second mode. The hydrodynamic added mass from zero-speed hammer tests in shallow water (Figure 5.2) is roughly 40% higher at the bow and the forward segments, while at the stern segments it is 55 to 65% higher than those determined from the deep water tests.

In general, considerably lower added mass values (J-factors) were obtained from the zero-speed shaker tests. As shaker tests are inherently more accurate than the hammer tests, it is concluded that these numbers are appropriate for all application purposes. The hydrodynamic added mass from the shaker tests with forward speed (Figure 5.3) dropped as much as 30% at a moderate speed of 3 knots. Towards higher speeds (6 knots), this trend is reversed and the added mass shows fairly large fluctuations with associated local negative J-factors. Figure 5.4 shows preliminary results of the effect of ice cover on the J-values. For the first flexural mode, the ice does not appear to affect the added mass appreciably, the increase being typically 10% above that in open water. For the second flexural mode the added mass in ice tends to be lower than that in open water except those at the second and third nodal points. Further tests will be necessary to confirm these findings.

Figure 5.3 VARIATION OF THE "J" FACTOR WITH VELOCITY

a) First Flexural Mode

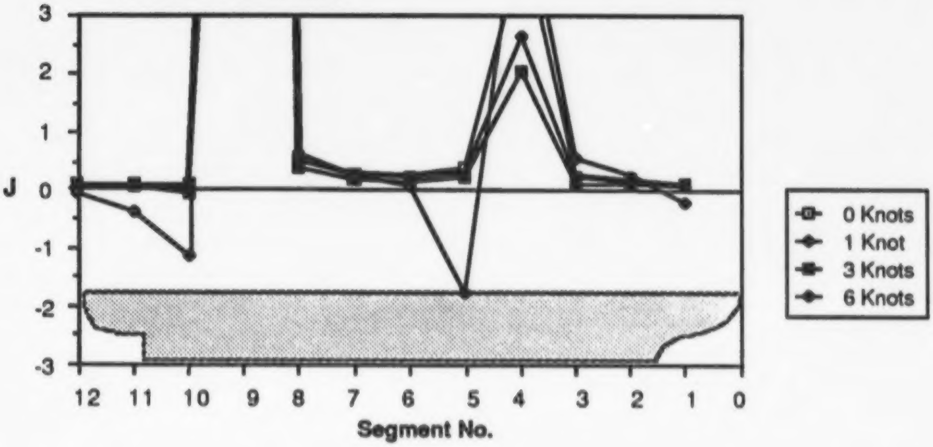

b) Second Flexural Mode

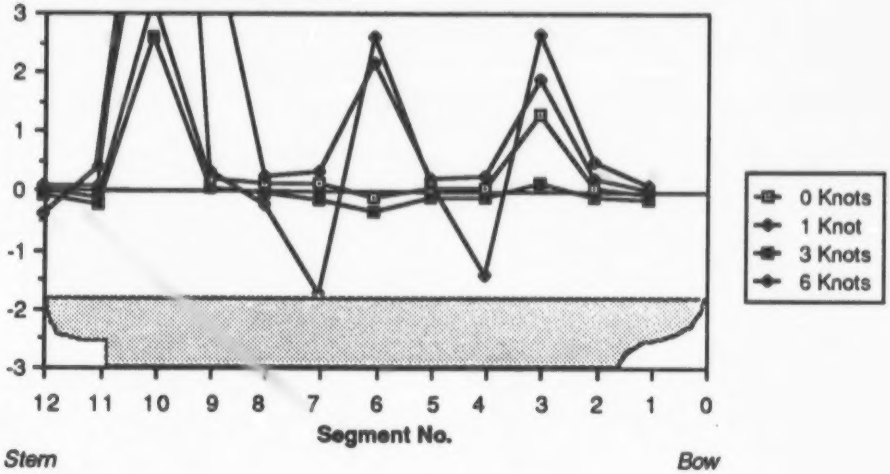

Figure 5.4 VARIATION OF THE "J" FACTOR DUE TO THE PRESENCE OF ICE

a) First Flexural Mode

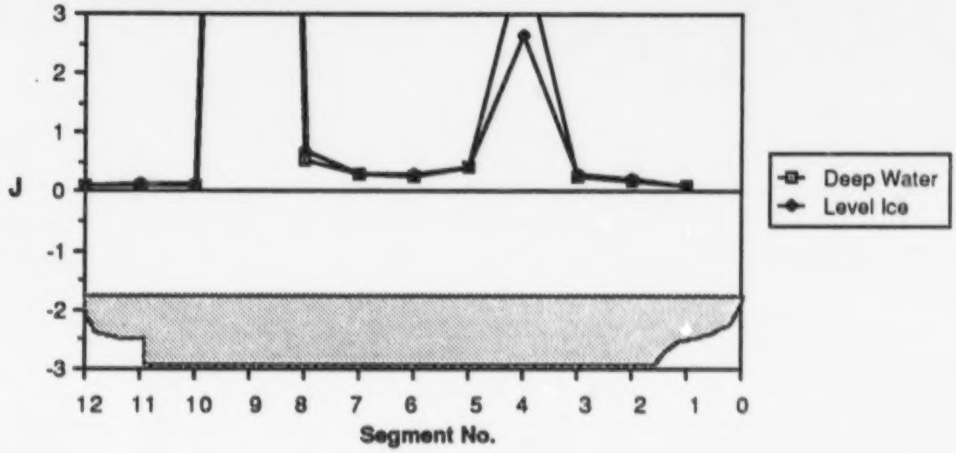

b) Second Flexural Mode

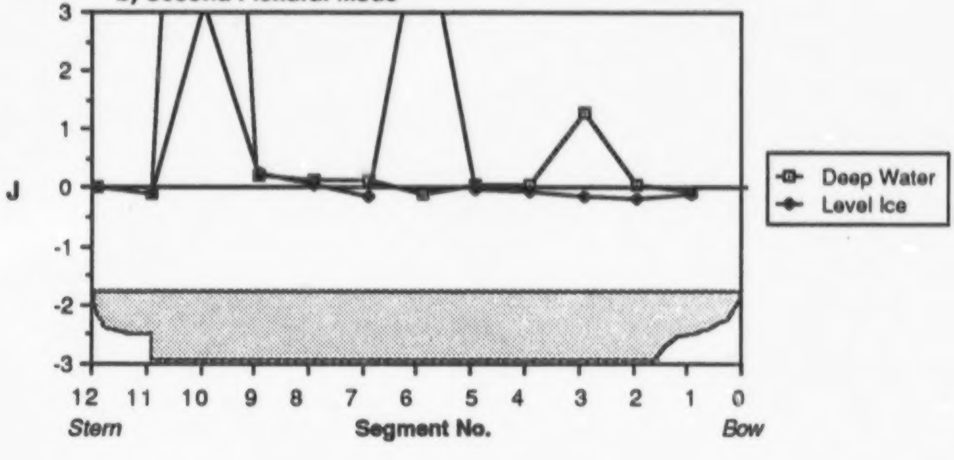

REFERENCES

[1] Blagoveshchensky, S.N., "Theory of Ship Motions", Vol. I and II, Dover Publications, New York, 1962.

[2] Pavlenko, G.E., "Ship Motions",Grostransizdat, 1935.

[3] Haskind, M.D., "Hydrodynamic Theory of Ship Motions in Waves, Prikladnaya Mathematika i Mechanika, Vol. X, No. 1, 1946.

[4] Povitsky, A.S., Sudostronoenie, Vol. 12, 1952.

[5] Voitkunsky, I.I. and A.N. Shebalov, "Experiments of River and Seagoing Vessels".

[6] Daley, C.G., and L.P. Phillips, Parametric Model Study of M.V. ARCTIC Hydroelastic Response During Multi-Year Ice Impacts, Transport Canada Report #TP6536E, 1985.

[7] Volcy, G.C., "L'amortissement dans le vibrations des Navires", Bulletin Technique due Bureau Veritas, p. 282-291, November 1979.

[8] Levis, F.M., "The Inertia of the Water Surrounding a Vibrating Ship", Trans. SNAME, Vol. 37, 1979.

[9] Tasai, F., "On the Damping Force and Added Mass of Ship Heaving and Pitching", Report of Research Institute for Applied Mechanics, Kyuchu University, 1960.

[10] Porter, W.R., "Pressure Distributions. Added Mass and Damping Coefficients for Cylinders Oscillating in a Free Surface", Institute of Engineering Research, University of California Report 1960.

[11] Frank, W., "Oscillation of Cylinders In or Below the Free Surface of Deep Fluids", NSRDC, Washington, DC, Report 2375, 1967.

[12] Wendel, K., "Hydrodynamic Masses and Hydrodynamic Moments of Inertia" (in German) Jahrb d. STG., Vol. 44, 1950.

[13] Vugts, J.H., "The Hydrodynamic Coefficients for Swaying, Heaving and Rolling Cylinders in a Free Surface", Laboratory for Ship Research Delft Technical School, Report #194, 1968.

[14] Salvesen, N., E. O. Tuck and O. Faltinsen, "Ship Motions and Sea Loads", Transactions, SNAME, 1970.

[15] Gerritsma, J., "Experimental Determination of Damping, Added Mass and Added Mass Moment of Inertia of a Ship Model, ISP, 4, 1957, p. 505-519.

[16] Townsin, R.L., "Virtual Mass Reduction Factors for Ship Vibration Calculations", Transactions, RINA, Vol. III, 1969.

[17] Ursell, F., "On the Heaving Motion of a Circular Cylinder on the Surface of a Fluid", Quart. Journal of Mechanical and applied Math., 2, 1949, p. 335-353.

[18] Smith, W.E., "Computation of Pitch and Heaving Motions for Arbitrary Ship Forms", Int. Shipbuilding Progress, Vol. 14, No. 155, 1967.

[19] Landweber, L. and de Macagno, M.C., "Added Mass of Two-Dimensional Forms Oscillating in a Free Surface", J. of Ship Research, November 1957.

[20] Dorofeyuk, S.K., "Investigation on the Added Mass with Ship Vibrations", Trudy Center Nautical Inst. A.N.K., Vypusk, 84, 1954, p.3-73.

[21] Kumai, T., "Added Mass Moment of Inertia by Torsional Vibration of Ships", European Shipbuilding, 7, 1958, p. 147-153.

[22] Sebalov, A.N., "The Problem of the Determination of the Added Mass Coefficient", Trudy Leningrad Korable, Inst. Vypusk, 12, 1954, p. 41-52.

[23] Taylor, J.L., "Some Hydrodynamic Inertia Coefficients", Philosophical Magazine, Vol. 9, No. 55, Jan. 1933.

[24] Landweber, L. and Macagno, M., "Irrotational Motion of the Liquid Surrounding a Vibrating Ellipsoid of Revolution", Journal of Ship Research, Vol. 2, No. 1, June 1958.

[25] Landweber, L. and Macagno, M., "Added Mass of a Rigid Prolate Spheroid Oscillating Horizontally in a Free Surface", Journal of Ship Research, Vol. 3, No. 4, March 1960.

[26] Kumai, T., "On the Three Dimensional Correction Factor for the Virtual Inertia Coefficient in the Vertical Vibrations of Ships", selected paper from the Journal of the Society of Naval Architects of Japan, Vol. 1, 1968.

[27] Todd, F.H., "Ship Hull Vibration", Arnold, N.Y., 1961.

[28] Moullin, E.B., et al, "The Added Mass of Prism Floating in Water", Proceedings, Cambridge Philosophical Society, 1930.

[29] Vorus, W.S. and S. Hylarides, "Hydrodynamic Added-Mass Matrix of Vibrating Ship Based on a Distribution of Hull Surface Sources", SNAME, Nov. 1981.

[30] Hakala, M.K., "Application of the Finite Element Method to Fluid-Structure Interaction in Ship Vibration", VTT Report #433, Espoo, Finland, 1986.

[31] Andersson, G. and Norrand, K., "A Method for the Calculation of Vertical Vibration with Several Nodes and Some Other Aspects of Ship Vibration", Transactions of RINA III, pp. 367-383, 1969.

[32] Woolam, W.E., "Research on Ship-Hull Damping Coefficients for Low-Freqency Vertical Flexural Modes of Vibration", Naval Ship Research and Development Center, Report 2323, May 1967.

[33] McGoldrick, R.T., "Comparison Between Theoretically and Experimentally Determined Natural Frequencies and Modes of Vibration of Ships", DTMB Report 906, August 1954.

[34] Sezawa, K. and W. Watanabe, "Damping Forces in Vibration of a Ship", Journal of Society of Naval Architects, Japan, No. 59, 1936.

[35] Betts, C.V., "On the Damping of Ship Hulls", M. Phil. Thesis, London University, 1975.

[36] Robinson, D.C., "Damping Characteristics of Ships in Vertical Flexure and Considerations in Hull Damping Investigation", DTMB Report 1876, December 1964.

[37] Kumai, T., "Damping Factors in the Higher Modes of Ship Vibration", European Shipbuilding, Vol. VII, No. 1, 1968.

[38] Dimpker, A., "Uber schwingende Korper an der Oberflache des Wassers", WRII, 15, 1934, p. 15-19.

[39] Borg, S.F., "The Analysis of Ship Structures Subjected to Slamming Loads", Journal of Ship Research, 4, No.3, pp. 11-27, 1960.

[40] Goodman, R.A., "Wave-Excited Main Hull Vibration in Large Tankers and Bulk Carriers", RINA, 1971.

[41] Hoffman, D., et al, "Experimental and Theoretical Evaluation of Springing on a Great Lakes Bulk Carrier", AD-776861, July 1973.

[42] Vossers, G., "Fundamentals of the Behaviour of Ships in Waves", Intl. Shipbuilding Prog., Vol. 6, No. 63, November 1959.

[43] Grim, O., "Berechnung der durch Schwingungen eines Schiffskorpers erzeugten hydrodynamischen Krafte", J.S.T.G., 47, 1953, p. 277-299.

[44] Holstein, H., Untersuchungen en einem Tauchwingen ausfuhrenden Quader", WRII 17, 1936, p. 385-389.

[45] St.Denis, M., "On Sustained Sea Speed", Trans. SNAME, 59, 1951, p. 745-792.

[46] Noonan, E.F., "Design Considerations for Shipboard Vibration", presented at the Feb.17, 1970 meeting of the New York Section of SNAME.

[47] Kline, R., "Springing and Hydroelastic Problems of Large Ships", August 26-29, 1975, SNAME.

[48] McGoldrick R.T., "Ship Vibration", DTNSRDC Report 1451, December 1960.

[49] Stiansen, S.G., A. Mansour and Y.N. Chen, "Dynamic Response of Large Great Lakes Bulk Carriers to Wave-Excited Loads", Transactions of SNAME, 1977.

[50] Chang, P.Y. "Structural Analysis of Cold Water Pipes for Ocean Thermal Energy Conversion Power Plants, "Hydronautics, Inc., TR No. 7676, May 1977.

[51] Foster, W.P. and H.F. Alma, "Damping Values of Naval Ships Obtained from Impulsive Loadings", Shock and Vibration Bulletin #40, December 1969.

[52] Johnson, A.J., "Vibration Tests of an all-welded and all-riveted 10,000 ton Dry Cargo Ship", Trans. NECIES, Vol.67, 1951, pp.205-276.

[53] Schmitke, R.T. and Whitten, B.W.: "SHIPMO - A FORTRAN Program to Predict Ship Motions in Waves". DREA Technical Memorandum 81/C, October 1981.

APPENDIX A

EQUATIONS OF RIGID BODY MOTION

REFERENCE [53]

It is assumed that the ship is symmetric about its longitudinal centerplane. Hence, the longitudinal motions (surge, heave, pitch) are uncoupled from the lateral motions (sway, roll, yaw), and the following two sets of equations result [53].

Longitudinal Motions

Surge: $$(A_{11} + m)\ddot{\eta}_1 + B_{11}\dot{\eta}_1 = F_1 e^{i\omega t} \qquad (A.1)$$

Heave: $$(A_{33} + m)\ddot{\eta}_3 + B_{33}\dot{\eta}_3 + C_{33}\eta_3$$

$$+ A_{35}\ddot{\eta}_5 + B_{35}\dot{\eta}_5 + C_{35}\eta_5 = F_3 e^{i\omega t} \qquad (A.2)$$

Pitch: $$(A_{53}\ddot{\eta}_3 + B_{53}\dot{\eta}_3 + C_{53}\eta_3$$

$$+ (A_{55} + I_5)\ddot{\eta}_5 + B_{55}\dot{\eta}_5 + C_{55}\eta_5 = F_5 e^{i\omega t} \qquad (A.3)$$

Lateral Motions

Sway: $$(A_{22} + m)\ddot{\eta}'_2 + B_{22}\dot{\eta}'_2 + A_{24}\ddot{\eta}_4 + B_{24}\dot{\eta}_4$$

$$+ A_{26}\ddot{\eta}_6 + (B_{26} + mU)\dot{\eta}_6 = F_2 e^{i\omega t} \qquad (A.4)$$

Roll: $$A_{24}\ddot{\eta}'_2 + B_{24}\dot{\eta}'_2 + (A_{44} + I_4)\ddot{\eta}_4 + B_{44}\dot{\eta}_4 + C_{44}\eta_4$$

$$+ A_{46}\ddot{\eta}_6 + B_{46}\dot{\eta}_6 = F_4 e^{i\omega t} \qquad (A.5)$$

Yaw: $$A_{62}\ddot{\eta}'_2 + B_{62}\dot{\eta}'_2 + A_{64}\ddot{\eta}_4 + B_{64}\dot{\eta}_4$$

$$+ (A_{66} + I_6)\ddot{\eta}_6 + B_{66}\dot{\eta}_6 = F_6 e^{i\omega t} \qquad (A.6)$$

where m is ship mass, and I_4, I_5 and I_6 are the moments of inertia for roll, pitch and yaw, respectively.

Detailed expressions for A_{jk}, B_{jk}, C_{jk} and F_j are given below:

Added Mass and Damping Coefficients

Longitudinal

$$A_{11} = k_1 m \tag{A.7}$$

$$B_{11} = \rho S_W C_{DT} U \tag{A.8}$$

$$A_{33} = \int_L a_{33} d\xi \tag{A.9}$$

$$B_{33} = \int_L b_{33} d\xi \tag{A.10}$$

$$A_{35} = -\int_L a_{33} \xi d\xi - \frac{U}{\omega^2} B_{33} \tag{A.11}$$

$$B_{35} = -\int_L b_{33} \xi d\xi + U A_{33} \tag{A.12}$$

$$A_{53} = -\int_L a_{33} \xi d\xi + \frac{U}{\omega^2} B_{33} \tag{A.13}$$

$$B_{53} = -\int_L b_{33} \xi d\xi - U A_{33} \tag{A.14}$$

$$A_{55} = \int_L a_{33}\xi^2 d\xi + \frac{U^2}{\omega^2}A_{33} \tag{A.15}$$

$$B_{55} = \int_L b_{33}\xi^2 d\xi + \frac{U^2}{\omega^2}B_{33} \tag{A.16}$$

Lateral

$$A_{22} = \int_L a_{22} d\xi + \Sigma a_p \sin^2\Gamma \tag{A.17}$$

$$B_{22} = \int_L b_{22} d\xi + \frac{1}{2}\rho U \Sigma S C_{L\alpha} C(k) \sin^2\Gamma + \frac{\pi}{2}\rho U T^2 \tag{A.18}$$

$$A_{24} = \int_L a_{24} d\xi - \Sigma a_p \sin\Gamma\vartheta \tag{A.19}$$

$$B_{24} = \int_L b_{24} d\xi - \frac{1}{2}\rho U \Sigma S C_{L\alpha} C(k) \sin\Gamma\vartheta \tag{A.20}$$

$$A_{26} = \int_L a_{22}\xi d\xi + \Sigma a_p s \sin^2\Gamma \tag{A.21}$$

$$B_{26} = \int_L b_{22}\xi d\xi + \frac{1}{2}\rho U \Sigma S C_{L\alpha} C(k)(s - c/4)\sin^2\Gamma + \frac{\pi}{2}\rho U T^2 x_p \tag{A.22}$$

$$A_{44} = \int_L a_{44} d\xi + \Sigma a_p \vartheta^2 \tag{A.23}$$

$$B_{44} = \int_L b_{44} d\xi + \frac{1}{2}\rho U \Sigma S C_{L\alpha} C(k)\vartheta^2 + \pi\rho U b_k^2 r^2 + B_V \tag{A.24}$$

$$A_{46} = \int_L a_{24}\xi d\xi - \Sigma a_p s \sin\Gamma\vartheta \tag{A.25}$$

$$B_{46} = \int_L b_{24}\xi d\xi - \frac{1}{2}\rho U \Sigma S C_{L\alpha} C(k) \sin\Gamma(s - c/4)\vartheta \tag{A.26}$$

$$A_{62} = \int_L a_{22}\xi d\xi - (U/\omega^2)\int_L b_{22} d\xi + \Sigma a_p s \sin^2\Gamma \tag{A.27}$$

$$B_{62} = \int_L b_{22}\xi d\xi + U\int_L a_{22} d\xi + \frac{1}{2}\rho U \Sigma x S C_{L\alpha} C(k) \sin^2\Gamma \\ + \frac{\pi}{2}\rho U T^2 x_p \tag{A.28}$$

$$A_{64} = \int_L a_{24}\xi d\xi - (U/\omega^2)\int_L b_{24} d\xi - \Sigma a_p s \sin\Gamma y \tag{A.29}$$

$$B_{64} = \int_L b_{24}\xi d\xi + U\int_L a_{24} d\xi - \frac{1}{2}\rho U \Sigma x S C_{L\alpha} C(k) \sin\Gamma \vartheta \tag{A.30}$$

$$A_{66} = \int_L a_{22}\xi^2 d\xi + \Sigma a_p s^2 \sin^2\Gamma \tag{A.31}$$

$$B_{66} = \int_L b_{22}\xi^2 d\xi + \frac{1}{2}\rho U \Sigma S C_{L\alpha} C(k)(s - c/4)x \sin^2\Gamma \tag{A.32}$$

$$+ \frac{\pi}{2}\rho U T^2 (C_p L/2)^2 + U\int_L a_{22}\xi d\xi$$

The integrations are over the length of the ship. In practice, the hull length is divided into approximately 20 sections and the two-dimensional added mass (a_{jk}) and wave-making damping (b_{jk}) are computed for each section.

APPENDIX B

FORMULAE FOR EVALUATING THE Q_n DERIVATIVES

REFERENCE [29]

J_n in terms of the regular Legendre functions is:

$$J_n = -\left[\frac{\zeta\dot{Q}_n}{(\zeta^2-1)\ddot{Q}_n + \zeta\dot{Q}_n}\right] \tag{B1}$$

The $\dot{Q}_n(\zeta)$ and $\ddot{Q}_n(\zeta)$ in (B1) are given by the following formulas,

$$\dot{Q}_n(\zeta) = \tfrac{1}{2}\dot{P}_n \ln\frac{\zeta+1}{\zeta-1} - \frac{P_n}{\zeta^2-1} - \dot{w}_{n-1}(\zeta) \tag{B2}$$

and, by differentiation

$$\ddot{Q}_n(\zeta) = \tfrac{1}{2}\ddot{P}_n \ln\frac{\zeta+1}{\zeta-1} - \frac{2\dot{P}_n}{\zeta^2-1} + \frac{2P_n\zeta}{(\zeta^2-1)^2} - \ddot{w}_{n-1}(\zeta)$$

where

$$\begin{aligned} w_{n-1}(\zeta) = {} & \frac{2n-1}{n}P_{n-1}(\zeta) + \frac{2n-5}{3(n-1)}P_{n-3}(\zeta) \\ & + \frac{2n-9}{5(n-2)}P_{n-5}(\zeta) + \frac{2n-13}{7(n-3)}P_{n-7}(\zeta) \\ & + \ldots \end{aligned} \tag{B3}$$

The summation in (B3) ceases when negative orders of P_m appear.

The Legendre polynomials appearing in (B3) are easily computed using the following formulas:

$$\begin{aligned} P_{2n}(\zeta) = (-1)^n \frac{(2n-1)!!}{2^n n!}\Bigg[1 & - \frac{2n(2n+1)}{2!}\zeta^2 \\ & + \frac{2n(2n-2)(2n+1)(2n+3)}{4!}\zeta^4 \\ & - \frac{2n(2n-2)(2n-4)(2n+1)(2n+3)(2n+5)}{6!}\zeta^6 \\ & + \ldots\Bigg] \end{aligned} \tag{B4}$$

and

$$\begin{aligned} P_{2n+1}(\zeta) = (-1)^n \frac{(2n+1)!!}{2^n n!}\Bigg[\zeta & - \frac{2n(2n+3)}{3!}\zeta^3 \\ & + \frac{2n(2n-2)(2n+3)(2n+5)}{5!}\zeta^5 \\ & - \frac{2n(2n-2)(2n-4)(2n+3)(2n+5)(2n+7)}{7!}\zeta^7 + \ldots\Bigg] \end{aligned}$$

Here the summations cease when the coefficient multiplying the ζ^m becomes negative.

The mode shapes,

$$\psi_n(x) = \dot{P}_n(\mu)$$

are easily evaluated from (B4) by replacing ζ by $\mu = 2x/L$ and differentiating the resulting polynomial with respect to μ. It can then be confirmed that the node number in the $\dot{P}_n$ mode shape is $n-1$; that is, $\dot{P}_1$ is the heave mode shape, $\dot{P}_2$ corresponds to pitch, etc.

Volume

2

ARCTEC CANADA LIMITED

ARCTEC CANADA LIMITED 1957C

TP 8797E

INVESTIGATION OF THE ADDED MASS PHENOMENON WITH A FLEXIBLE MODEL OF THE M.V. ARCTIC: VOLUME 2 - TIME DOMAIN ANALYSIS OF HULL RESPONSE DURING RAMMING

PREPARED FOR: TRANSPORTATION DEVELOPMENT CENTRE

by:

L.D. Phillips
B.C. Menon

MARCH 1987

PREPARED BY:

ARCTEC CANADA LIMITED
311 Legget Drive,
Kanata, Ontario.
K2K 1Z8

PROJECT TEAM:

Balji Menon, Project Manager
Claude Daley, In-house Consultant
Loyd Phillips, (Project Engineer - Task 2)
David Howard, (Project Engineer - Task 3)
Michael Steele, (Systems Analyst)

DISCLAIMER: The contents of this report reflect the views of the authors and not necessarily the official view or opinions of the Transportation Development Centre of Transport Canada.

Un sommaire en français est inclus avant la table des matières.

Approved by: ______________________________

Transport Canada Transports Canada

Development Developpement

REPORT DOCUMENTATION FORM

1. Transport Canada Report No.
TP 8797E

2. TDC Project No.
6637/6639

3. Recipient's Catalogue No.

4. Title and Subtitle
INVESTIGATION OF THE ADDED MASS PHENOMENON WITH A FLEXIBLE MODEL OF THE M.V. ARCTIC: VOLUME 2 - TIME DOMAIN ANALYSIS OF HULL RESPONSE DURING RAMMING

5. Report Date
March 1987

6. Performing Organization Report No.
1957C

7. Author(s)
L.D. Phillips, B.C. Menon

8. Transport Canada File No.
D1460-231

9. Performing Organization Name and Address
Arctec Canada Limited
311 Legget Drive
Kanata, Ontario
K2K 1Z8

10. DSS File No.
11SD.T8200-5-5595

11. DSS or Transport Canada Contract No
11SD.T8200-5-5595/01-SD

12. Sponsoring Agency Name and Address
Transportation Development Centre (TDC)
200 Dorchester Blvd. West
Suite 601, West Tower
Montreal, Quebec H2Z 1X4

13. Type of Report and Period Covered
Final

14. Sponsoring Agency Code

15. Supplementary Notes See also:
Volume 1: Review of Existing Methods, Available Data and Summary of Experimental Results. Volume 3: Model Experiments in Open Water and in Ice.

16. TDC Project Officer
C. Nowicki, I.M. Bayly

17. Abstract

In an earlier project, hull response and ice force data were obtained from tests with a segmented flexible model of the MV ARCTIC. These tests consisted of transient head-on ramming impacts at various speeds against simulated multi-year ice flues. This report contains a description of the mathodology and results of a time domaine analysis of the data collected from these experiments. The results consisted of time histories of the distribution of the total hydrodynamic force on the hull and gross added mass coefficients for each segment. Mean values of the segmental added mass have been determined for a range of impact velocities, concludies have been drawn on the accuracy of the results, and applicability of the results discussed. Recommendations are made for similar treatment of additional available data to confirm trends and to quantify hydrodynamic added mass and damping independently.

18. Key Words
Added Mass, MV ARCTIC Segmented Model
Ice Ramming.

19. Distribution Statement
A limited number of copies are available from the Transportation Development Centre.

20. Security Classification (of this report)
Unclassified

21. Security Classification (of this page)
Unclassified

22. No. of Pages
287

23. Price

Canada

Transports Canada Transport Canada
Développement Development

FORMULE DOCUMENTAIRE DU RAPPORT

1. Nº du rapport Transports Canada
TP 8797E

2. Nº de l'étude — CDT
6637/6639

3. Nº de catalogue du destinataire

4. Titre et sous-titre
INVESTIGATION OF THE ADDED MASS PHENOMENON WITH A FLEXIBLE MODEL OF THE M.V. ARCTIC: VOLUME 2 - TIME DOMAIN ANALYSIS OF HULL RESPONSE DURING RAMMING

5. Date du rapport
mars 1987

6. Nº du rapport de l'organisme exécutant
1957C

7. Auteur(s)
L.D. Phillips, B.C. Menon

8. Nº de dossier Transports Canada
D1460-231

9. Nom et adresse de l'organisme exécutant
Arctec Canada Limited
311 Legget Drive
Kanata (Ontario)
K2K 1Z8

10. Nº de dossier — ASC
11SD.T8200-5-5595

11. Nº de contrat — ASC ou Transports Canada
11SD.T8200-5-5595/01-SD

12. Nom et adresse de l'organisme parrain
Centre de développement des transports (CDT)
200 ouest, boul. Dorchester
Suite 601, tour ouest
Montréal (Québec) H2Z 1X4

13. Genre de rapport et période visée
Final

14. Code de l'organisme parrain

15. Remarques additionnelles
Voir également:
Volume 1: Review of Existing Methods, Available Data and Summary of Experimental Results. Volume 3: Model Experiments in Open Water and in Ice.

16. Agent de projet — CDT
C. Nowicki, I.M. Bayly

17. Résumé

À l'occasion d'un projet antérieur, les données touchant le comportement de la coque et la force des glaces ont été obtenues à partir d'essais réalisés sur un modèle flexible segmenté du N.M. ARCTIC. Ces essais comportaient des impacts d'éperonnage frontaux transitoires à diverses vitesses contre des floes de glace de plusieurs années. Le présent rapport contient une description de la méthodologie et des résultats d'une analyse par domaine temporel des données recueillies lors de ces travaux. Les résultats se traduisent par des valeurs en fonction du temps touchant la répartition de l'ensemble des forces hydrodynamiques sur la coque et les coefficients de la masse ajoutée brute pour chaque segment. Les valeurs moyennes de la masse ajoutée segmentaire ont été établies pour une plage de vitesses d'impact, des conclusions ont été tirées quant à la précision des résultats, et l'applicabilité des résultats est examinée. Des recommandations sont formulées à l'égard d'un traitement analogue des données disponible pour confirmer les tendances et pour quantifier individuellement la masse hydrodynamique ajoutée à l'amortissement.

18. Mots-clés
Masse ajoutée, modèle segmenté de l'ARCTIC, éperonnage des glaces.

19. Diffusion
Le Centre de développement des transports dispose d'un nombre limité d'exemplaires.

20. Classification de sécurité (de ce rapport)
non classifié

21. Classification de sécurité (de cette page)
non classifiée

22. Nombre de pages
287

23. Prix
—

CDT TDC 79-005
Rev 86

Canada

ACKNOWLEDGEMENTS

The authors would like to acknowledge the support of Mr. Sydney Mathews of Coldstream Maritime Incorporated, who as technical liaison officer to TDC provided guidance and encouragement through close participation in all phases of this project. In addition, we would also like to thank Mr. Chris Novicki for his assistance in the contractual and administrative aspects of this work.

SUMMARY

The purpose of the work reported in this and associated volumes was to investigate the hydrodynamic added mass phenomenon as it occurs during ship-ice interaction, to enable effective analysis and future calculation of global impact loads from experimental data. The project focussed on data from recent ship ramming tests performed at model scale using a flexible model of the MV ARCTIC.

This study attempts to solve the hydrodynamic added mass problem encountered in the calculation of the transient overall hull response to multi-year ice ramming forces. Ship-ice interaction in ramming differs significantly from conventional hull response problems in open water, in that it is transient in nature and the ship is brought to rest in a relatively short period of time. In such situations the hydrodynamic inertial reaction, especially at the bow, is governed by a number of factors such as the presence of the ice feature as well as confinement by the bow notch in the ice, large bow motions during ride-up and the flexibility of the ship. Towards the stern, the influences of the ice features will diminish and added mass may be expected to assume numerical values familiar in the open water context.

The data used in this exercise were taken from an archive of scale model test data available from a previous experimental program carried out by Arctec Canada Limited for Canadian Coast Guard Northern. In keeping with the transient nature of the problem, the added mass distributions along the hull have been extracted using time domain calculation methods. The method consists of applying D'Alembert's principle to the instantaneous vertical forces acting on the hull, which include ice forces on the bow, gravitational and buoyancy forces on each segment, the shear difference forces between segments and the total hydrodynamic force.

Based on the above assumption, the dynamic force balance on a segment can be written in mathematical form as:

$$\left[F_{ice}(t) + F_g(t) + F_B(t) + F_I(t) + F_{\Delta V}(t) + F_{Hyd}(t)\right]_{\text{segment } i} = 0$$

where F_{ice} = ice forces,

F_g = weight,

F_B = buoyancy (hydrostatic) forces,

F_I = inertia forces,

$F_{\Delta V}$ = shear difference forces, and

F_{Hyd} = hydrodynamic forces.

In the above formulation, it has been assumed that each force is concentrated at the centroid of the segment. The shear difference force is derived from the measured vertical bending moment distribution along the model. The inertial force is derived from the known segment body masses and the corresponding measured accelerations.

A number of simplifications have been invoked in the numerical modelling process in order to estimate the time varying magnitudes of the different forces acting on individual segments. For example, the wave profile is ignored and only the rigid body and flexural motions of the model are used to calculate the buoyancy force. The ice force at the bow is distributed over the first two segments on the basis of the penetration of the bow into the ice. The shear difference force is corrected to account for changes in the bending moment distribution caused by the longitudinal component of the ice force acting at the bow. The varying location of the ice force is also approximated and used to modify the moment acting on the bow segment.

The hydrodynamic force is the only unknown in the force balance process and therefore it can be calculated at every instant for each segment. In the present analysis the total hydrodynamic force has not been resolved into separate hydrodynamic added mass and fluid damping terms, although a methodology has been recommended for use in future work. The gross added mass time history is determined by dividing the hydrodynamic force by the corresponding segment accelerations. Test data covering a range of impact velocities are presented using twelve selected data sets from the experimental data base. In eleven cases, the original bow forefoot geometry was modified by removal of the ice knife resulting in a simpler configuration to analyze.

Figure 1 shows diagramatically the model hull segmentation scheme as well as the measurement parameters of the impact tests. Figures 2, 3, and 4 depict respectively the vertical segment accelerations, the total vertical hydrodynamic force derived and the gross added mass extracted from the above two. The time histories of the segmental added mass are expressed in non-dimensional form using the segment mass displacement as the normalizing factor. Note that the scale of the vertical axis is necessarily different from segment to segment since the magnitude of added mass varies drastically from the bow towards the stern. The time histories are characterized by abrupt reversals of sign at acceleration zero crossings. At these singularity points the calculated added mass assumed very large values, as a result of division of total hydrodynamic force by accelerations approaching zero.

The assignment of a mean value to any segment or portion of a segment was rendered difficult by the sign reversals and the singularities. The results were also sensitive to changes in the acceleration threshold, which was set at 0.05 m/s^2 in the analysis. Data points with acceleration values below this threshold were not included in the time history. However, it was generally observed that the average magnitudes of the added mass were highest at the bow and decreased with distance aft. The smallest values were seen on segments 9 and 10.

FIGURE 1

LOCATION OF INSTRUMENTATION

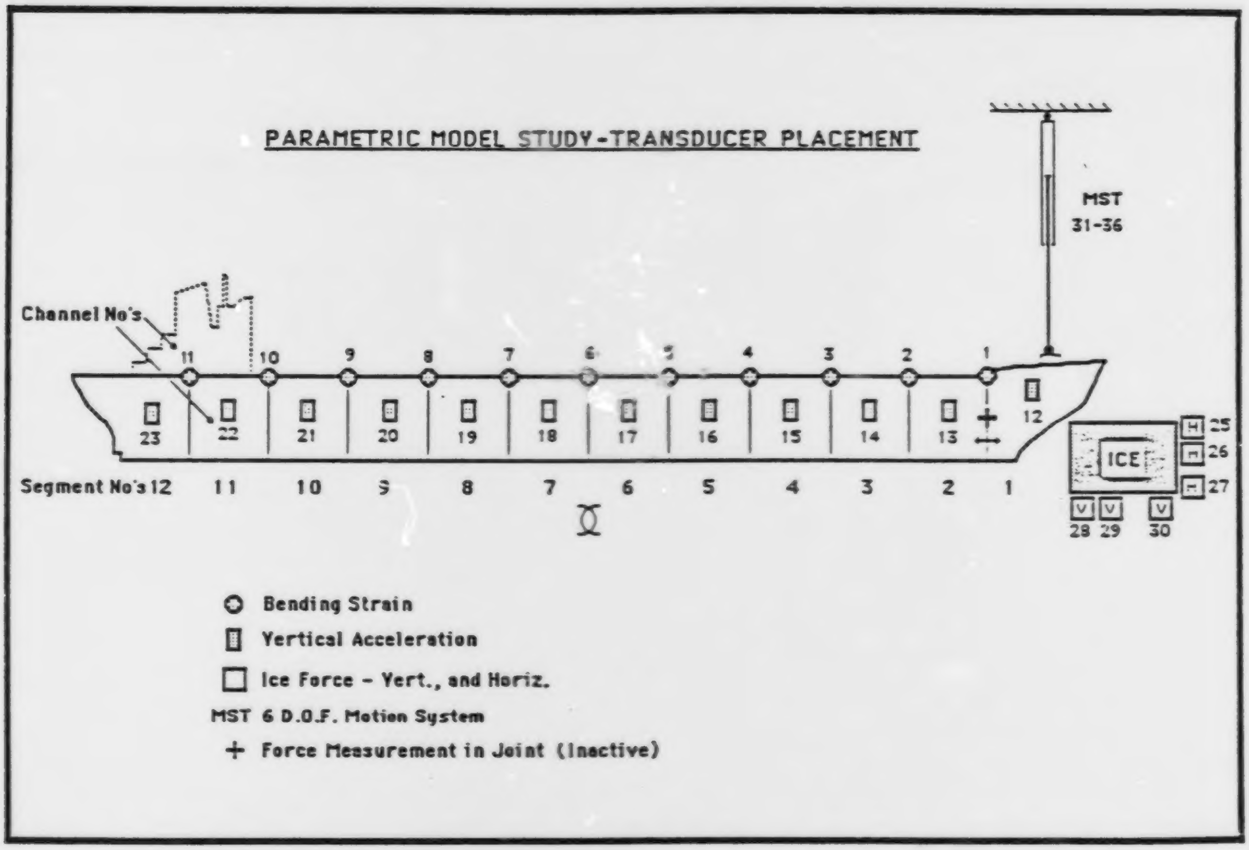

FIGURE 2

TEST TU-11 RESULTS:
SEGMENT ACCELERATIONS

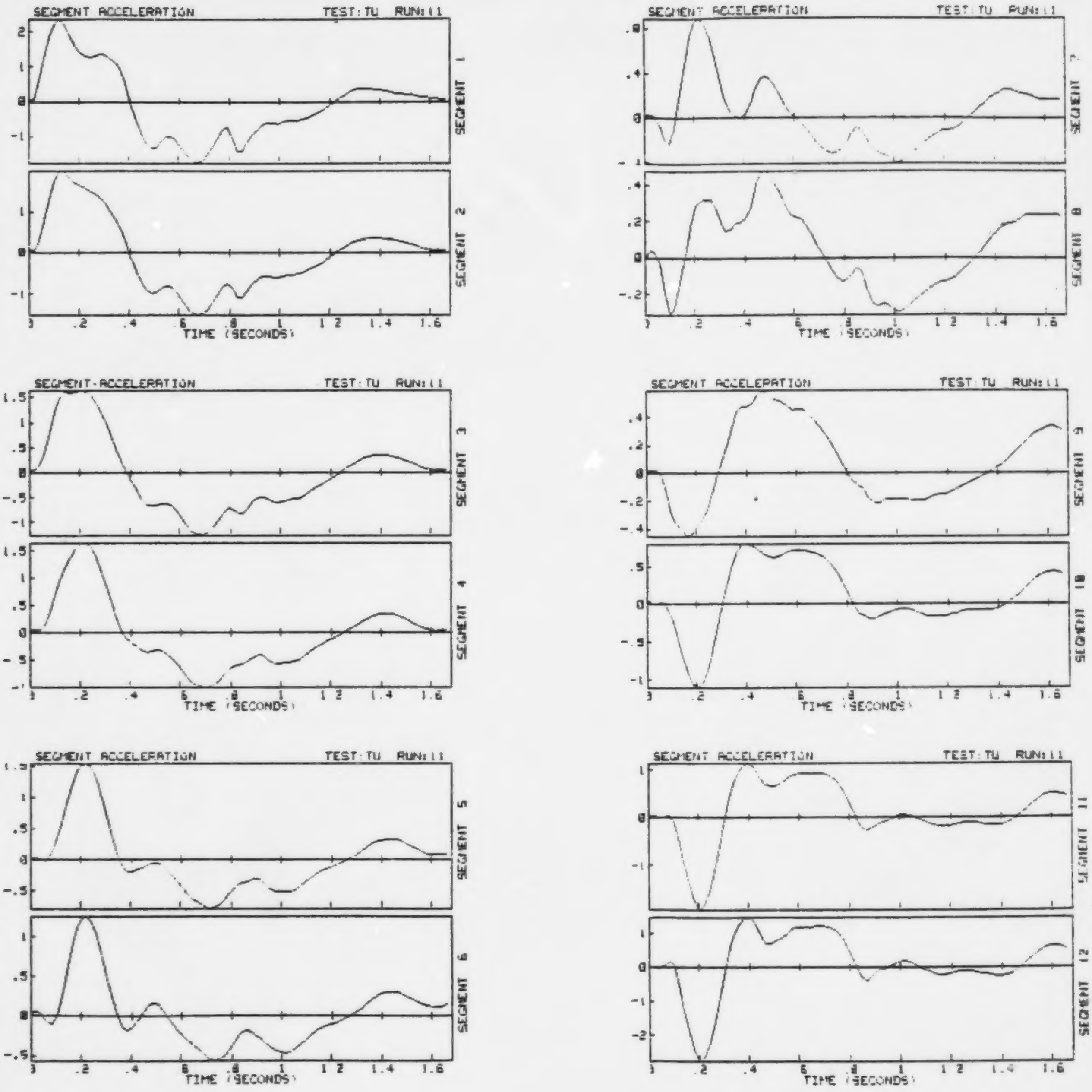

FIGURE 3

TEST TU-11 RESULTS:
HYDRODYNAMIC FORCE (INCLUDING ADDED MASS AND FLUID DAMPING EFFECTS)

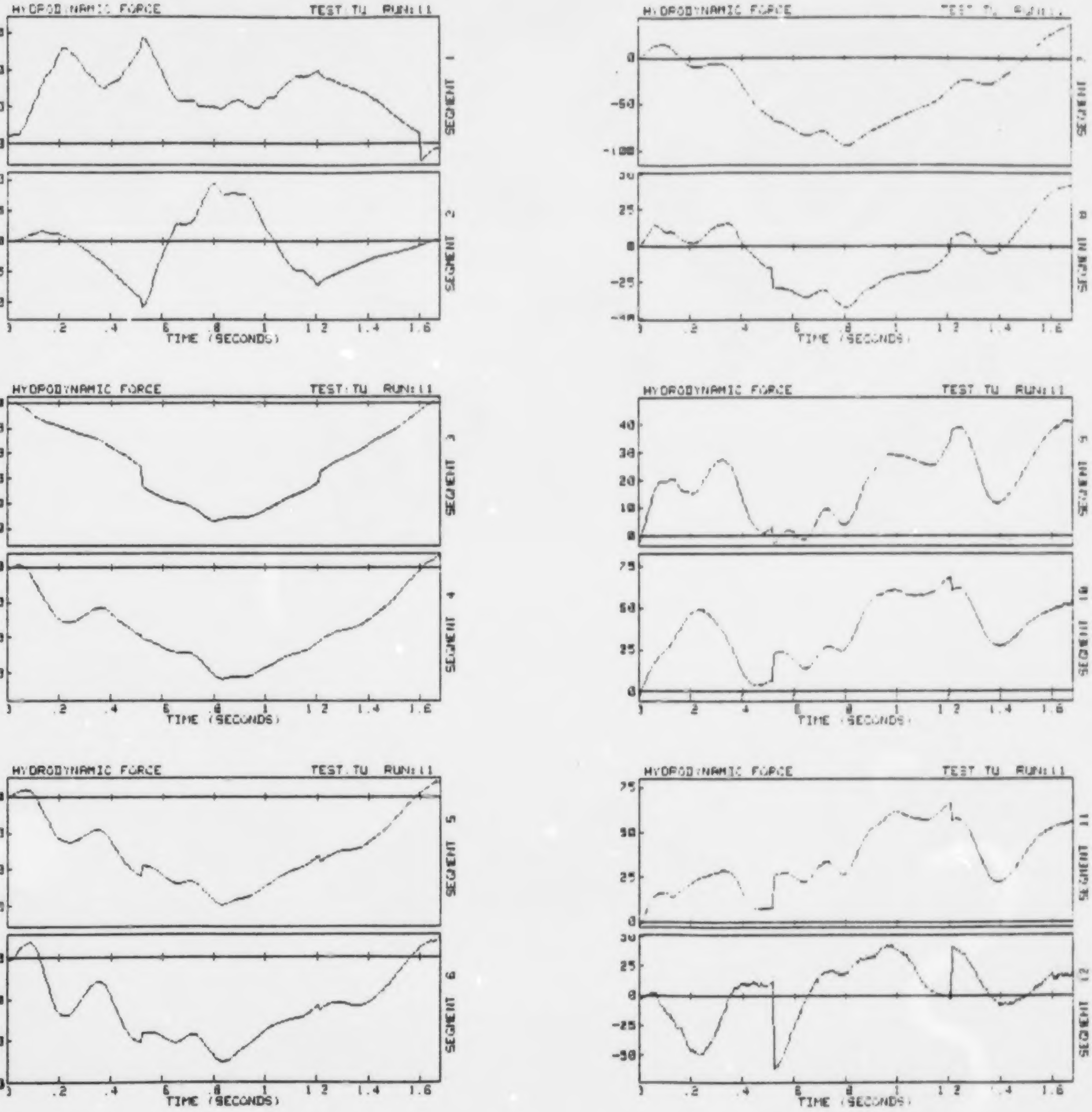

FIGURE 4

TEST TU-11 RESULTS:
NON-DIMENSIONAL ADDED MASS RATIO

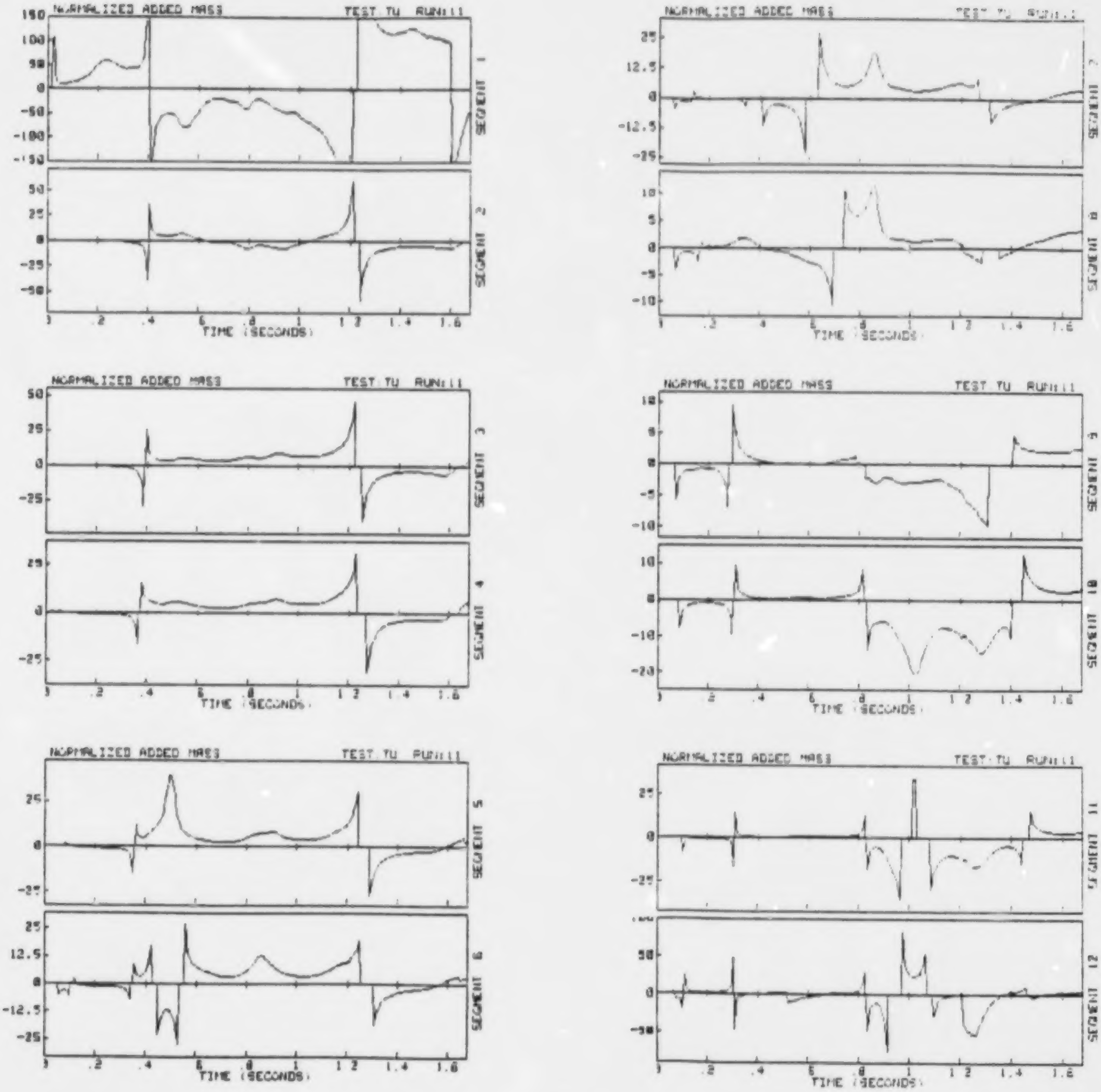

The large values of hydrodynamic added mass for segment 1 are attributable to proximity effects (confinement and shallow water effects). The vertical ice force appeared to be the dominant influence on the bow segment. A partial influence of the ice force was also seen on segment 2, where it causes a gradual change in the magnitude and the sign of the added mass during the slide-off phase of the interaction.

Examination of the added mass distribution along the length of the hull at various instances in time showed that, in addition to that at the bow segment, the added mass frequently assumed large negative values around the first node of the second flexural mode shape (between segments 2 and 3). At this point where accelerations approach zero, the hydrodynamic forces will vanish even if the added masses may be large.

The principal results of the computational process are summarized in the order of increasing velocity. Table 1 lists the non-dimensional mean added mass for each segment. The added mass at the bow segment is significantly larger, but is followed by a substantial reduction in magnitude as well as a reversal in the sign at the second segment. The mean added mass distribution shows a gradual decrease in magnitude around midship and through to segments 8 and 9. It is believed that the derived added mass is accurate only up to this location. The sources of the errors further aft are the inaccuracies in the estimate of segment positions from the measured model motions at the bow. Towards the stern, one would realistically expect the non-dimensional added mass to approach the open water values as the influence of the ice features decreases with distance from the bow segment.

The analysis provided an insight into the complexity of the hydrodynamic inertia phenomenon during transient ice/ship interaction. Local added mass effects in the area of the impact have mean values several times greater than the displacement mass and may be of opposite sign. In addition, there is significant time variation. Thus traditional calculation methods, which assume constant added mass, need to be modified to incorporate the time varying hydrodynamic inertia.

While the results indicate the above trends clearly, a number of deficiencies in the experimental program on which the analysis is based render some uncertainty concerning the values obtained. Recommendations for continuing the work, based on the value of the work in contributing to the understanding, include proposals for improvements to the experimental program.

TABLE 1

SEGMENTAL DISTRIBUTION OF NON-DIMENSIONAL ADDED MASS

TEST VEL. (m/s) SEGMENT	TS-6 .24 MEAN	TS-2 .37 MEAN	TR-8 .37 MEAN	TR-10 .58 MEAN	TR-11 .67 MEAN	TU-12 .73 MEAN	TR-9 .86 MEAN	TU-11 .98 MEAN	TT-10 1.03 MEAN	TS-1 1.14 MEAN	TG-2* 1.12 MEAN
1	-86.5	-81.9	-114.9	-94.7	-54.7	5.6	-18.7	4.9	-25.8	-2.1	-21.4
2	9.0	7.6	9.0	7.8	3.8	2.3	2.7	-1.4	-2.7	-11.7	-7.4
3	5.0	6.2	5.8	5.4	2.2	1.4	1.7	1.7	3.6	5.7	2.9
4	4.9	5.2	3.8	4.2	2.6	1.8	1.3	1.7	2.2	2.9	2.2
5	4.0	2.3	2.5	3.9	3.0	2.8	2.0	3.8	2.3	2.1	2.5
6	3.3	-.4	1.9	2.6	1.9	1.6	2.4	1.8	0.9	2.7	2.0
7	2.3	-12.7	1.3	4.4	-1.0	2.8	1.6	2.1	1.5	4.1	9.5
8	11.7	-23.7	3.1	8.8	-2.9	0.6	-1.3	1.0	1.1	5.1	7.5
9	12.1	4.5	3.3	6.4	-7.1	-.5	-1.1	-.8	0.3	7.0	4.3
10	-1.1	10.9	6.1	10.9	-5.0	-.2	-1.4	-3.3	2.0	3.4	0.7
11	4.8	10.9	7.4	10.8	-6.8	1.3	0.3	-2.6	2.6	6.2	2.5
12	24.7	23.0	11.3	27.2	-15.0	5.1	1.8	-1.2	5.3	21.7	17.5

Note: Non-Dimensional added mass with respect to segment mass displacement.
* Original MV ARCTIC Bow Geometry.

SOMMAIRE

L'objet des travaux exposés dans le présent document et dans les volumes connexes consiste à étudier le phénomène de la masse hydrodynamique ajoutée, tel qu'il survient lors de l'interaction navire-glaces, afin de permettre une analyse sérieuse et des calculs ultérieurs des charges d'impact globales à partir de données expérimentales. Le projet s'est appuyé sur les données de récents essais d'éperonnage réalisés à l'échelle à l'aide d'un modèle flexible du navire ARCTIC.

La présente étude tente de résoudre le problème de la masse hydrodynamique ajoutée lors du calcul du comportement transitoire global de la coque soumise à des forces d'éperonnage contre des floes de glace de plusieurs années. L'interaction navire-glaces lors de l'éperonnage diffère de façon marquée des problèmes de comportement de la coque en eau libre, du fait qu'elle est de nature transitoire et que le navire est mis en panne dans un laps de temps relativement court. Dans de telles situations, la réaction hydrodynamique inertielle, notamment à la proue, est déterminée par un certain nombre de facteurs tels que la présence de divers genres de glaces, l'encastrement de la proue dans les glaces, les grands mouvements de la proue lors de la montée et la flexibilité du navire. Vers la poupe, l'influence des glaces diminue et on peut s'attendre à ce que les valeurs numériques de la masse ajoutée s'apparentent à celles notées en eau libre.

Les données utilisées pour l'étude ont eté tirées du dossier des données d'essai sur modèle à l'échelle provenant d'un programme expérimental antérieur réalisé par Arctic Canada Limited, pour le compte de la Garde côtière canadienne (Nord canadien). En tenant compte de la nature transitoire du problème, les répartitions de la masse ajoutée le long de la coque ont été obtenues à l'aide de la méthode de calcul par domaine temporel. Cette méthode consiste à appliquer le principe d'Alembert aux forces verticales instantanées qui agissent sur la coque, incluant la force des glaces sur la coque, les forces gravitationnelles et ascensionnelles sur chaque segment, les forces de cisaillement distinctes entre les segments et la force hydrodynamique totale.

En fonctions de l'hypothèse susmentionnée, l'équilibre de force dynamique sur un segment peut avoir la représentation mathématique suivante:

$$F_{glace}(t) + F_g(t) + F_B(t) + F_I(t) \quad F_V(t) + F_{hyd}(t) = 0_{\text{segment } i}$$

où F_{glace} = forces des glaces
F_g = poids
F_B = forces ascensionnelles (hydrostatiques)
F_I = forces d'inertie
F_V = forces de cisaillement distinctes
F_{hyd} = forces hydrodynamiques

Dans cette formulation, on suppose que chaque force est concentrée au centre de masse du segment. La force de cisaillement distincte découle de la répartition mesurée du moment de flexion verticale le long du modèle. La force d'inertie découle des masses connues des segments et des accélérations mesurées correspondantes.

Un certain nombre de simplifications ont été utilisées dans le traitement numérique de modélisation afin d'évaluer l'ampleur des variations de temps des différentes forces agissant sur les segments distincts. Par exemple, le profil des vagues n'est pas pris en ligne de compte, et seuls les mouvements du corps rigide et les mouvements de flexion du modèle servent au calcul de la force ascensionnelle. La force des glaces à la proue est répartie sur les deux premiers segments en fonction de la pénétration de la proue dans les glaces. La force de cisaillement distincte est corrigée pour tenir compte des changements de répartition du moment de flexion, entraînés par la composante longitudinale de la force des glaces agissant en proue. L'emplacement variable de la force des glaces est également approché et utilisé pour modifier le moment exercé sur le segment de proue.

La force hydrodynamique est la seule inconnue dans le processus d'équilibre des forces et elle peut donc être calculée à chaque instant pour chaque segment. Dans la présente analyse, la force hydrodynamique totale n'a pas été décomposée en termes distincts de masse hydrodynamique ajoutée et d'amortissement hydraulique, bien qu'une méthodologie ait fait l'objet d'une recommandation pour utilisation dans des travaux ultérieurs. La valeur en fonction du temps de la masse ajoutée brute est établie en divisant la force hydrodynamique par les accélérations correspondantes des segments. Les données d'essais comportant une gamme de vitesses d'impact sont présentées par le biais de douze ensembles de données choisies provenant de la base de données expérimentales. Dans onze cas, la géométrie originale du brion de proue a été modifiée en enlevant l'éperon à glace, ce qui simplifie la configuration à analyser.

La figure 1 illustre sous forme de diagrammes la segmentation de la coque du modèle ainsi que les paramètres de mesure des essais d'impact. Les figures 2, 3 et 4 indiquent respectivement les accélérations verticales des segments, la force hydrodynamique verticale totale dérivée et la masse ajoutée brute découlant des deux susnommées. Les valeurs en fonction du temps de la masse ajoutée segmentaire sont exprimées sous forme non dimensionnelle, en utilisant le déplacement de la masse de segment comme facteur de normalisation. Il est à remarquer que l'échelle de l'axe vertical est nécessairement d'un segment à l'autre étant donné que l'ampleur de la masse ajoutée varie considérablement de la proue vers la poupe. Les valeurs en fonction du temps sont caractérisées par de brusques inversions de signe lorsque l'accélération passe de positif à négatif et vice versa. À ces points singuliers, la masse ajoutée calculée indique des valeurs considérables à la suite de la division de la force hydrodynamique totale par des accélérations à proximité de zéro.

Figure 1 EMPLACEMENT DES INSTRUMENTS

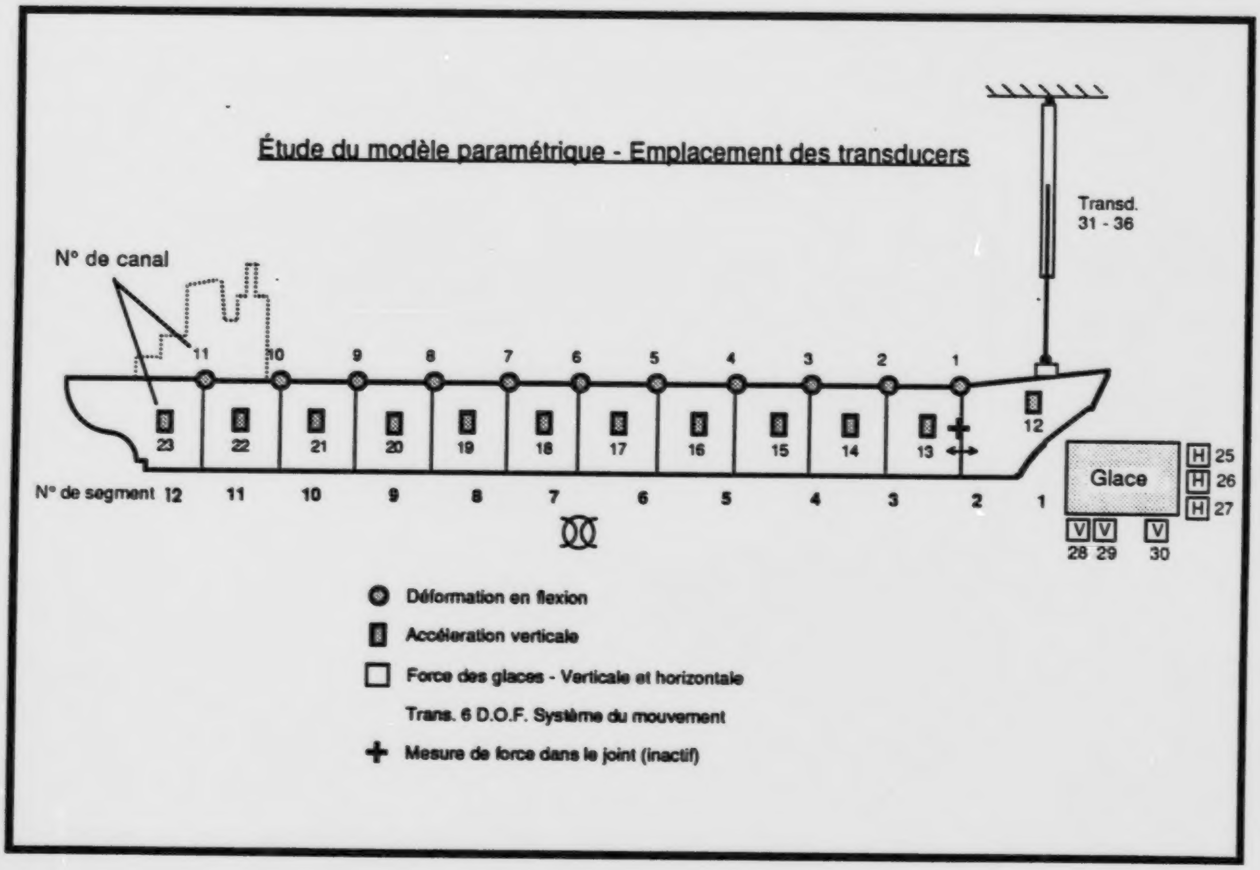
Étude du modèle paramétrique - Emplacement des transducers
Transd. 31 - 36
N° de canal
11
10
9
8
7
6
5
4
3
2
1
23
22
21
20
19
18
17
16
15
14
13
12
N° de segment 12
11
10
9
8
7
6
5
4
3
2
1
Glace
H 25
H 26
H 27
V 28
V 29
V 30
● Déformation en flexion
▨ Accélération verticale
☐ Force des glaces - Verticale et horizontale
Trans. 6 D.O.F. Système du mouvement
+ Mesure de force dans le joint (inactif)

FIGURE 2

RÉSULTATS ESSAI TU 11
Accélérations des segments

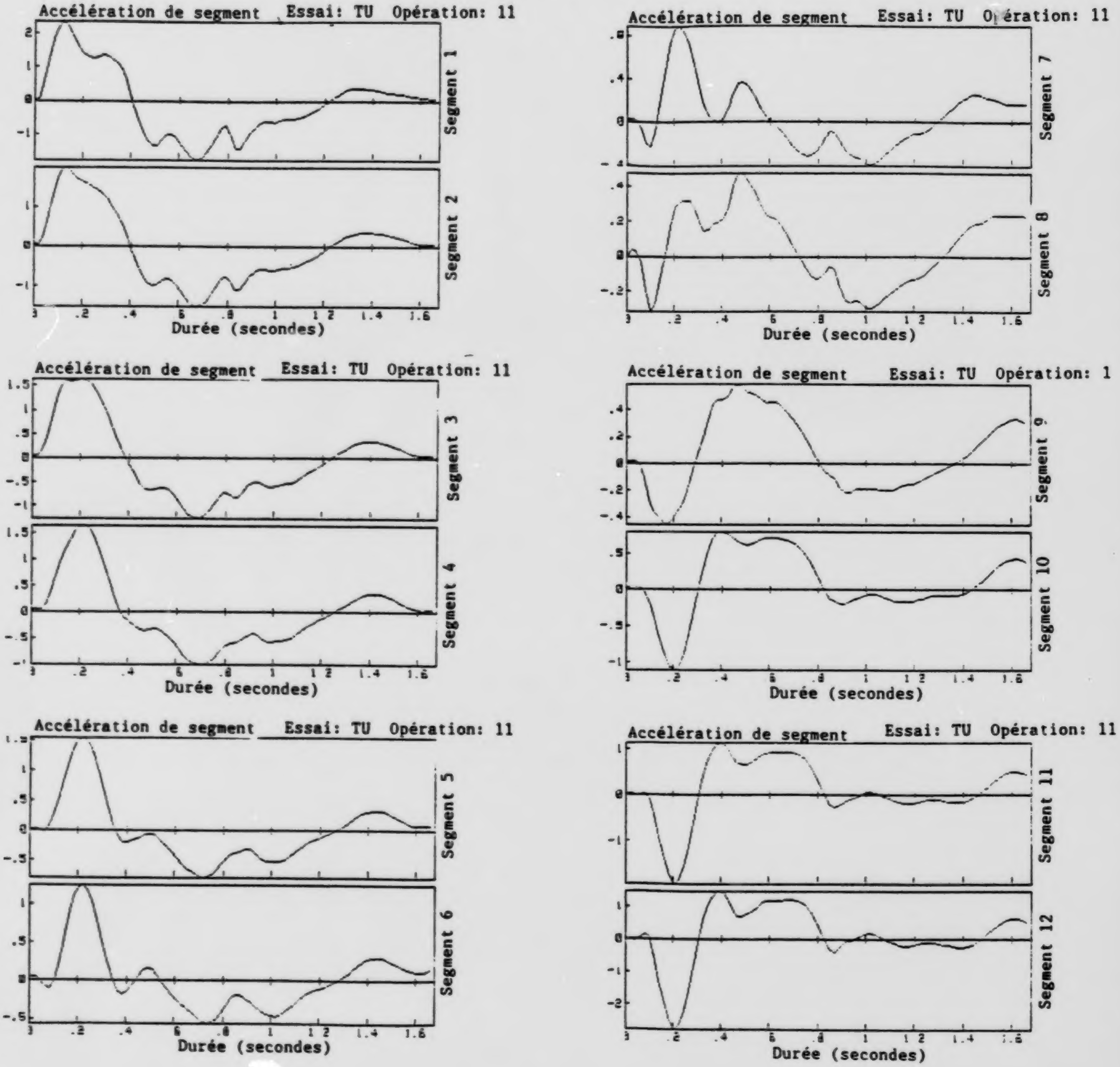

FIGURE 3

RÉSULTATS ESSAI TU-11
Force hydrodynamique (incluant effets de masse ajoutée
et amortissement hydraulique)

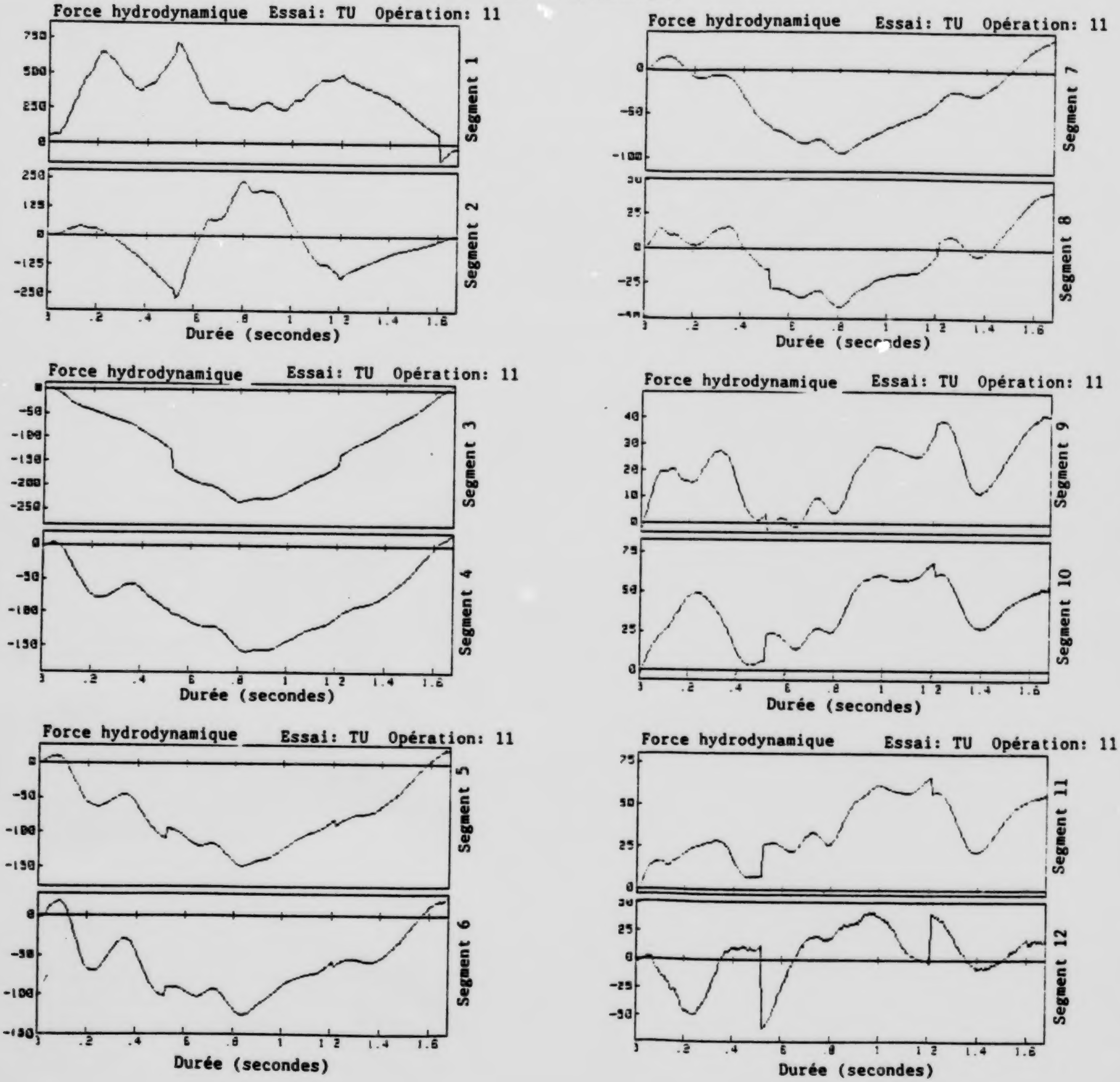

FIGURE 4

RÉSULTATS ESSAI TU-11
Rapport de la masse ajoutée non dimensionnelle

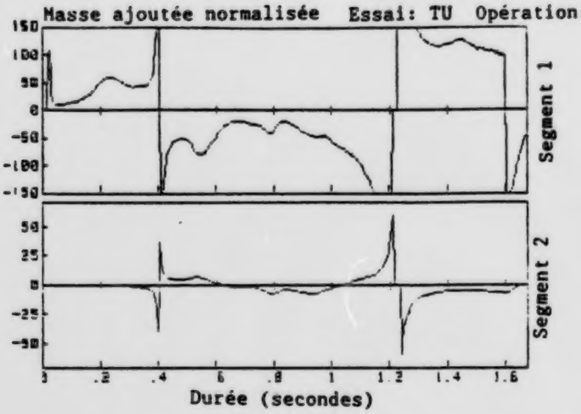
Masse ajoutée normalisée Essai: TU Opération: 11

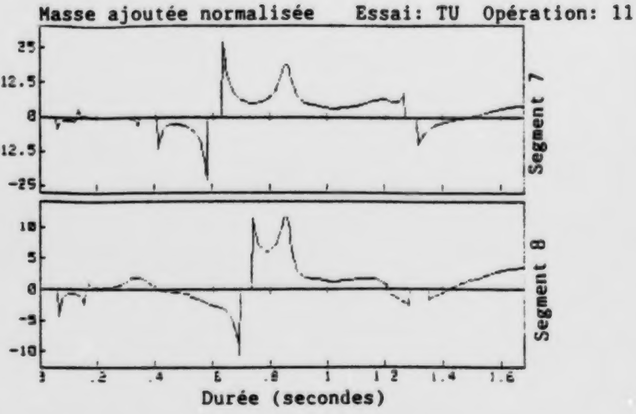
Masse ajoutée normalisée Essai: TU Opération: 11

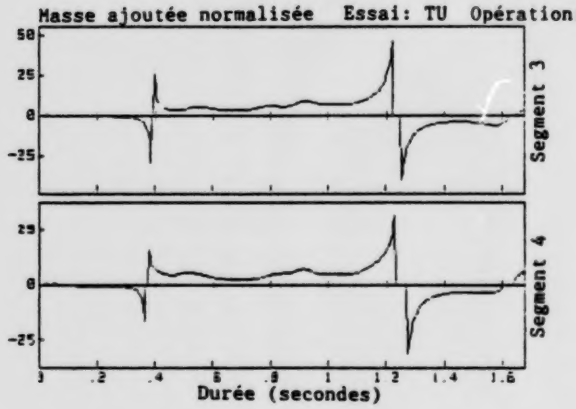
Masse ajoutée normalisée Essai: TU Opération: 11

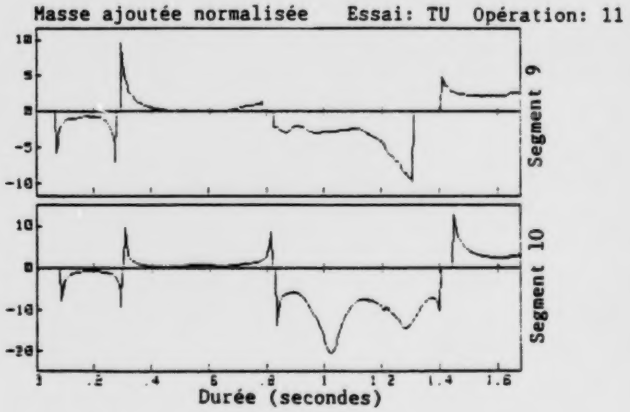
Masse ajoutée normalisée Essai: TU Opération: 11

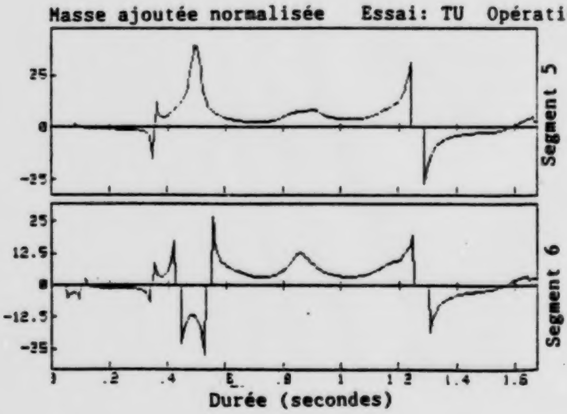
Masse ajoutée normalisée Essai: TU Opération: 11

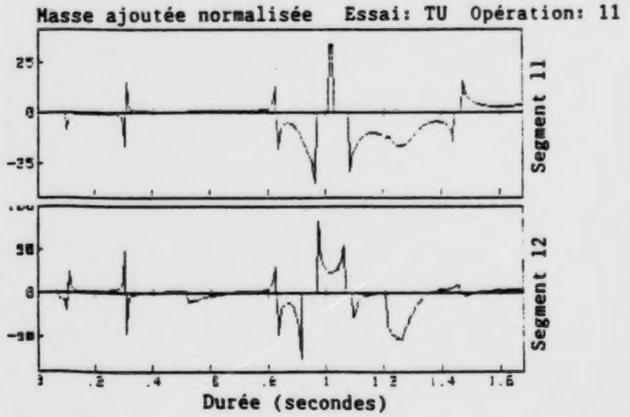
Masse ajoutée normalisée Essai: TU Opération: 11

L'attribution d'une valeur moyenne à un segment ou une partie quelconque d'un segment a été rendue difficile par les inversions des signes et les singularités. Les résultats ont été également sensibles aux changements du seuil d'accélération, établi à 0,05 m/s^2 dans l'analyse. Les points de données dont les valeurs d'accélération étaient inférieures à ce seuil n'ont pas été inclus dans les valeurs en fonction du temps. Cependant, on a généralement observé que les grandeurs moyennes de la masse ajoutée étaient plus élevées à la proue pour diminuer avec la distance vers la poupe. Les plus faibles valeurs ont été notées sur les segments 9 et 10. Les grandes valeurs de masse hydrodynamique ajoutée du segment 1 découlent des effets de proximité (effets d'encastrement et d'eau peu profonde). La force des glaces verticales semble être le facteur dominant quant au segment de proue. Un effet partiel de la force des glaces a été également noté sur le segment 2, alors qu'il provoque un changement graduel dans l'ampleur et le signe de la masse ajoutée durant la phase de glissement de l'interaction.

Une étude de la répartition de la masse ajoutée sur la longueur de la coque à divers points dans le temps indique que la masse ajoutée, outre celle au segment de proue, présente souvent de fortes valeurs négatives autour du premier noeud de la deuxième forme du mode de flexion (entre les segments 2 et 3). À ce point où les accélérations sont voisines de zéro, les forces hydrodynamiques disparaîtront même si les masses ajoutées sont importantes.

Les principaux résultats des calculs sont résumés selon l'ordre de l'accroissement de vitesse. Le tableau 1 indique la masse ajoutée non dimensionnelle moyenne de chaque segment. La masse ajoutée du segment de proue est nettement plus importante, mais elle est suivie par une diminution de grandeur marquée et par une inversion de signe au deuxième segment. La répartition de la masse ajoutée moyenne démontre une diminution de grandeur graduelle vers le milieu du navire et jusqu'aux segments 8 et 9. On présume que la masse ajoutée dérivée n'est précise que jusqu'à ce point. Les sources d'erreurs en s'éloignant vers la poupe représentent les imprécisions dans l'estimation de la position des segments à partir des mouvements mesurés du modèle à la proue. Vers l'arrière, on peut s'attendre à ce que la masse ajoutée non dimensionnelle approche des valeurs de l'eau libre étant donné que l'influence des glaces diminue avec l'éloignement du segment de proue.

L'analyse a offert un aperçu de la complexité du phénomène de l'inertie hydrodynamique lors de l'interaction transitoire glaces-navire. Les effets locaux de la masse ajoutée dans le secteur d'impact ont des valeurs moyennes de plusieurs fois supérieures à la masse de déplacement et peuvent être de signe opposé. En outre, il existe une importante variante de temps. C'est ainsi que les méthodes classiques de calcul, qui supposent une masse ajoutée constante, doivent être modifiées pour inclure l'inertie hydrodynamique à temps variable.

TABLEAU 1

RÉPARTITION SEGMENTAIRE DE LA MASSE AJOUTÉE NON DIMENSIONNELLE

ESSAI	TS-6	TS-2	TR-8	TR-10	TR-11	TU-12	TR-9	TU-11	TT-10	TS-1	TG-2*
VITESSE (m/s)	.24	.37	.37	.58	.67	.73	.86	.98	1.03	1.14	1.12
SEGMENT	MOYENNE	MOYENNE	MOYENNE	MOYENNE	MOYENNE	MOYENNE	MOYENNE	MOYENNE	MOYENNE	MOYENNE	MOYENNE
1	-86.5	-81.9	-114.9	-94.7	-54.7	5.6	-18.7	4.9	-25.8	-2.1	-21.4
2	9.0	7.6	9.0	7.8	3.8	2.3	2.7	-1.4	-2.7	-11.7	-7.4
3	5.0	6.2	5.8	5.4	2.2	1.4	1.7	1.7	3.6	5.7	2.9
4	4.9	5.2	3.8	4.2	2.6	1.8	1.3	1.7	2.2	2.9	2.2
5	4.0	2.3	2.5	3.9	3.0	2.8	2.0	3.8	2.3	2.1	2.5
6	3.3	-.4	1.9	2.6	1.9	1.6	2.4	1.8	0.9	2.7	2.0
7	2.3	-12.7	1.3	4.4	-1.0	2.8	1.6	2.1	1.5	4.1	9.5
8	11.7	-23.7	3.1	8.8	-2.9	0.6	-1.3	1.0	1.1	5.1	7.5
9	12.1	4.5	3.3	6.4	-7.1	-.5	-1.1	-.8	0.3	7.0	4.3
10	-1.1	10.9	6.1	10.9	-5.0	-.2	-1.4	-3.3	2.0	3.4	0.7
11	4.8	10.9	7.4	10.8	-6.8	1.3	0.3	-2.6	2.6	6.2	2.5
12	24.7	23.0	11.3	27.2	-15.0	5.1	1.8	-1.2	5.3	21.7	17.5

Note: Masse ajoutée non dimensionnelle en fonction du déplacement de masse due segment.
* Géométrie originale de la proue du N.M. Arctic.

Bien que les résultats reflètent nettement les tendances susmentionnées, un certain nombre d'insuffisances dans le programme expérimental sur lequel l'analyse est fondée entraînent certains doutes à l'égard des valeurs obtenues. Au nombre des recommandations formulées pour la poursuite des travaux, fondées sur la valeur du travail en faveur d'une meilleure compréhension, on note certaines propositions touchant l'amélioration du programme expérimental.

TABLE OF CONTENTS

1. INTRODUCTION.....1

2. BASIS OF EXPERIMENTAL DATA.....3
   2.1 Background.....3

3. METHODOLOGY OF EXTRACTING HYDRODYNAMIC ADDED MASS.....12
   3.1 Stages in the Extraction of Added Mass.....12
   3.2 Pre-processing of the MV ARCTIC Model Test Data.....12
   3.3 Time-Step Computations.....14
   3.4 Computing Shear Difference Forces.....18
   3.5 Computing Buoyancy Forces.....20
   3.6 Computing Hydrodynamic Added Mass.....24

4. IMPLEMENTATION OF ANALYSIS METHODS.....27
   4.1 Shear Difference Force.....27
   4.2 Corrections to the Shear Difference Force.....27
   4.3 Location of Ice Forces.....36
   4.4 Magnitude of Force Components.....38
   4.5 Segment Buoyancy Force.....40

5. RESULTS OF COMPUTATION.....42

6. DISCUSSION OF RESULTS.....54
   6.1 Hydrodynamic Added Mass Time Histories.....54
   6.2 Segmental Distribution of Added Mass.....58
   6.3 Velocity Dependence of Results.....58
   6.4 Observations.....65

7. CONCLUSIONS.....68
   7.1 Overview.....68
   7.2 Inference from Results.....68
   7.3 Observed Weaknesses and Possible Improvements.....69

REFERENCES.....71

APPENDIX A - TEST DATA AND RESULTS

LIST OF FIGURES

2.1 LINES AND PARTICULARS OF MV ARCTIC....4
2.2 LOCATION OF INSTRUMENTATION....8

3.1 STAGES IN THE EXTRACTION OF ADDED MASS....13
3.2 FREE BODY DIAGRAM OF SEGMENT....17
3.3 STEPWISE COMPUTATION OF SHEAR DIFFERENCE....19
3.4a RESOLVING RIGID BODY MOTIONS....21
3.4b FLEXIBLE MODEL SEGMENT HEAVE....21
3.5 SAMPLE OF MOTIONS DATA TEST TU-11....23
3.6 SAMPLE OF ACCELERATION DATA TEST TU-11....25

4.1 FORCE TRANSMITTED BETWEEN SEGMENTS AND CONTRIBUTING TO BENDING MOMENTS TEST TU-11....28
4.2 FITTING POLYNOMIALS TO BENDING MOMENT DISTRIBUTION AND CALCULATING SHEAR DISTRIBUTION TEST TU-11....29
4.3 LOCATION OF CENTROID OF MASS FORWARD OF ICE FORCE....33
4.4 BENDING MOMENT CORRECTION FOR LONGITUDINAL COMPONENT OF ICE FORCE....35
4.5 LOCATION OF ICE FORCES....37
4.6 ASSUMED DISTRIBUTION OF FORCE ALONG CONTACT REGION....39

5.1 TEST TU-11 RESULTS: SURGE, SURGE ACCELERATION AND VERTICAL ICE FORCES....44
5.2 TEST TU-11 RESULTS: SEGMENT ACCELERATIONS....46
5.3 TEST TU-11 RESULTS: INERTIA FORCES....47
5.4 TEST TU-11 RESULTS: BUOYANCY FORCES (WITH RESPECT TO THE STILL WATER DRAFT CONDITION)....48
5.5 TEST TU-11 RESULTS: SHEAR FORCES....50
5.6 TEST TU-11 RESULTS: SHEAR DIFFERENCE FORCES....52
5.7 TEST TU-11 RESULTS: HYDRODYNAMIC FORCE (INCLUDING ADDED MASS AND FLUID DAMPING EFFECTS)....53

6.1 TEST TU-11 RESULTS: NON-DIMENSIONAL VERTICAL ADDED MASS RATIO....55
6.2 TIME VARIATION OF MEAN ADDED MASS DISTRIBUTION....57
6.3 MEAN NON-DIMENSIONAL ADDED MASS....59
6.4 SEGMENTAL DISTRIBUTION OF MEAN ADDED MASS....60

LIST OF TABLES

2.1 MV ARCTIC MODAL PROPERTIES: MODEL AND FULL SCALE....6
2.2 SUMMARY OF MODEL TEST MATRIX....10

3.1 MODEL TESTS ASSESSED IN PRESENT STUDY....15

5.1 TYPICAL SUMMARY PAGE....43
6.1 SEGMENTAL DISTRIBUTION OF TOTAL HYDRODYNAMIC FORCE....63
6.2 SEGMENTAL DISTRIBUTION OF NON-DIMENSIONAL ADDED MASS....64

NOMENCLATURE

a_i	Segment acceleration
A	Designation of Original MV ARCTIC Bow Configuration
A_i	Waterplane area
$\bar{A}$	Section area coefficient
B	Designation of MV ARCTIC model with extended forefoot knife
BM	Bending moment (abbreviation)
b_n	Damping force coefficient
C_1	Designation of MV ARCTIC model with forefoot knife removed
c_d	Damping coefficient
E	Young's Modulus
f	Frequency
F	Force
F_B	Buoyancy Force (or change with respect to still water draft)
F_d	Damping Force
F_g	Gravitational Force
F_H	Horizontal ice force (measured)
F_{HI}	Hydrodynamic inertial force
F_I	Inertial force
F_{ICE}	Ice force
$F_{ICE-LONG}$	Longitudinal Component of Ice force
$F_{ICE-VERT}$	Ice Force Component normal to model longitudinal axis
F_{ma}	Added mass component of hydrodynamic inertial force
$F_{\Delta V}$	Shear difference loading
F_V	Vertical ice force (measured)
g	Gravitational constant: $9.807\ m/s^2$
h_{CG}	Heave at CG

I	Moment of Inertia; Notch Indentation length
I_A	Active notch indentation
k_i	Constants
L_i	Segment length
m	Total body mass of model
m_i	Segment body mass
m_{33}	Added mass
M	Bending moment
MST	6 degrees of freedom Motion Sensing Transducer
M_{CORR}	Correction of bending moment for longitudinal ice force
s	Seconds (abbreviation)
S	Surge distance from ice contact
t	Time
T	Time period; segment draft
T_A, T_B, etc.	Designation for series of tests
v	Velocity of impact
V	Shear force
X	Surge direction in absolute frame of reference
x'	Longitudinal axis in model based reference system
x_i	Segment centroid distance from LCG
x_{CG}	Distance of MST from model CG
Y	Lateral direction in absolute frame of reference
Z	Vertical direction in absolute frame of reference
Z_o	Spring bar distance to neutral axis
Z_i	Apparent segment heave

z'	Upward direction in model based reference system
Z_{BOW}	Apparent heave at bow (from MST)
Z_N	Distance between ice force and neutral axis
Z_{NB}	Constant distance between segment neutral axis and baseline

α	Model stem angle (averaged)
β	Section deadrise angle
Δ	Weight displacement
θ	Pitch angle
θ_{DEFL}	Model deflection angle with respect to the bow
ρ	density of water
∇	Volume displacement
ψ	Angle of Ice force with respect to surge axis

1. INTRODUCTION

This volume documents analysis work which was carried out to improve understanding of hydrodynamic added mass as it applies to ships ramming multi-year ice floes. Although added mass had not previously been studied in this context, it was believed that the ramming interaction differed significantly from the open water condition. The majority of research in the literature has involved periodic ship response; whereas the ship-ice interaction is transient in nature. The ship is brought to a standstill over a relatively short time span as a result of the ice forces acting on the bow. In this situation the added mass may be governed by a number of complicated flow factors, such as: confinement by the bow footprint, large bow motions during ride-up and the flexibility of the ship. Since there was no direct precedent for deriving added mass distributions, a number of approaches have been examined. It is believed that the time domain methods developed in this task represent a unique approach to deriving the added mass distribution for a flexible ship or model.

The added mass values that have been extracted here are taken from model test data available from a previous experimental program [1] carried out at Arctec Canada Limited for Canadian Coast Guard Northern. The present analysis task is independent of (but complementary to) a concurrent physical model investigation of added mass in open water and level ice, which is reported in Volume 3 - Model Experiments in Open Water and In Ice. Another difference between the two tasks is that the results of the physical model program in Volume 3 - Model Experiments in Open Water and In Ice, have been expressed in terms of frequency domain values, rather than as time series. Volume 1 - Review of Existing Methods, Available Data and Summary of Experimental Results, provides a background to the subject of hydrodynamic added mass and damping by reviewing the state-of-the art theoretical methods and available experimental data.

The same ship model has been used in both parts of the study. The prototype was the MV ARCTIC, a 28,000 tonne deadweight cargo vessel. Although this vessel has subsequently been substantially modified and converted to an OBO, the hull form tested was originally designated as Arctic Class 2 under the Canadian Arctic Shipping and Pollution Prevention Regulations (ASPPR). Particulars of this ship and the model are given in Section 2.1.

The scale model was fabricated in 1984 as part of the first phase [2] of work defined by a joint research agreement (JRPA #3) between Canada and Finland. In Canada, the study of the ship-ice ramming interaction has been sponsored by Canadian Coast Guard Northern, and supported by Energy Research and Development Funds administered by Transport Canada. The aim of that work was to develop general force and stress equations for ships impacting multi-year ice floes. Progress in that research at VTT in Finland and Arctec Canada Limited has recently been jointly reported [3].

For studying the stress distribution it was necessary to physically model the ship's modal properties. Therefore the MV ARCTIC model was segmented to permit flexural response. Improvements to the internal structure of the model were carried out during 1985 and a second phase of ramming tests followed in 1986. The measurements obtained from this latter series of tests has formed the basis for the present analysis.

A full scale reference for the model scale ramming tests was provided by results from a program of dedicated ramming trials for the MV ARCTIC which were carried out in June 1984. These trials were administered by Canadian Coast Guard Northern and involved a group of participating agencies [4].

Information on the dynamic properties of the MV ARCTIC was available from dynamic exciter tests [5] which were obtained in 1982 with the vessel in a grain loaded condition. These tests defined the natural frequency, generalized damping and generalized mass for the seven lowest flexural modes. In addition the analysis of the ramming trials data [6] included three dimensional finite element modelling of the ship structure and fluid coupling as a means of determining the ship's modal properties in the dedicated trials ballast condition.

The added mass extraction methodology is described in detail in Section 3. It involves a calculation of the hydrodynamic forces acting on each model segment using the measured ice forces, bending moments and motions data which were available from the model ramming tests. The procedure is illustrated in Section 5 by an example showing the step-by-step development of each of the component forces. Test data spanning a range of impact velocities has been studied. The principal results from each of the tests are summarized and interpreted in Section 6.

Although the numerical results from this task apply specifically to a particular set of model scale ramming tests, the conceptual development may be viewed in a broader context. Since the methodology is similar to that used for estimating global ice loads in full scale trials [7], it may be possible to use the model analysis results to verify the full scale measurement procedures. In addition, it has been commonly reported in ship-ice interaction studies [eg. 8, 9, 10] that the accuracy of motions prediction in ice is limited by a lack of knowledge about hydrodynamic added mass and its variation throughout the interaction period. For larger commercial vessels operating in multi-year ice zones there is a greater potential for significant hull girder stresses during ramming and therefore the concern about the reliability of hull response predictions has increased. Since incorporation of precise estimates of added mass is a key element in the successful development of hull response computing capability, the need for obtaining experimentally derived added mass data has been recognized. Hence this volume is devoted to exploring a method of applying experimentally derived hull response and ice force data to transient ship response in ice ramming and it is hoped that the present approach will pave the way for a better understanding and more precise estimates of the added mass phenomenon.

2. BASIS OF EXPERIMENTAL DATA

2.1 Background

The present task was made possible by the existence of data from a model test program performed for Canadian Coast Guard (Northern) during 1986. That program was carried out in the Kanata, Ontario ice basin of Arctec Canada Limited and involved model scale ramming trials of the MV ARCTIC in simulated multi-year ice floes. A detailed account of that work has been presented in [1] and [2]. A brief summary of that test program and its experimental set-up is provided here; including descriptions of all the features which are believed pertinent to the derivation of hydrodynamic added mass from the test data.

- MV ARCTIC

The prototype vessel was the 28,000 DWT ice strengthened bulk carrier, MV ARCTIC which is operated by Canarctic Shipping Limited. This ship was built as a prototype design for large commercial carriers operating extensively in Arctic waters. Its lines and general particulars are given in Figure 2.1. Since being commissioned in 1979, it has been the subject of a large number of model tests and full scale trials. However, the majority of the testing has investigated resistance in level ice. Full scale bending stresses during ramming of multi-year ice floes were measured during dedicated trials [6] near Coburg Island in 1984. Those dedicated trials were administered by Canadian Coast Guard Northern and carried out by a group of participating agencies.

The ship was tested over a range of speeds up to four knots; a limit imposed by safety concerns. Strain readings in the deck and bottom of the MV ARCTIC together with a finite element algorithm provided a measure of the bending moment and stress distribution along the ship during the impacts. Vertical bow force time histories were derived by a theoretical transfer function methodology using the strain readings.

Information on the dynamic properties of the MV ARCTIC has been accumulated from a combination of experimental testing and analysis methods. Dynamic exciter tests [5] using a hydraulic shaker were carried out in 1982 with the vessel in a grain loaded condition. These shaker tests defined the natural frequency, generalized damping and generalized mass for the seven lowest flexural modes. Since the ballast condition during dedicated trials in 1984 differed from the grain loaded condition, a finite element model of the ship structure and surrounding fluid was used in the stress measurement and force prediction algorithms.

FIGURE 2.1

LINES AND PARTICULARS OF MV ARCTIC

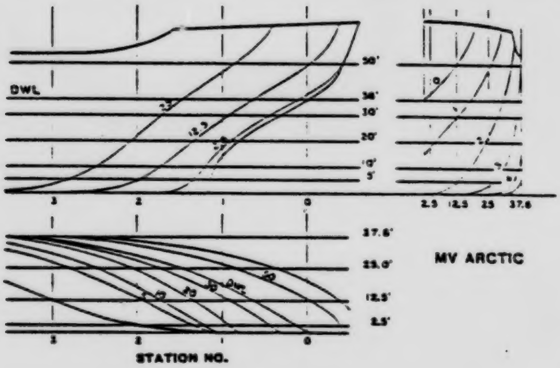

Bow Lines of the M.V.Arctic

SHIP NAME: M.V.ARCTIC	SCALE: 40:1
DIMENSIONAL PARAMETERS F.S. M.S. Loa = 209.5 5.24 (m) Lbp = 196.6 4.91 (m) B = 22.9 0.57 (m) d = 10.9 0.27 (m) D = 38,104 0.595 (T)	DIMENSIONLESS PARAMETERS Cb =.76 β_5 = 0 deg Cbf =.80 Cp =.76 f = 0.1 Cw =.88 γ =30 deg

STATION	0	1/2	1	2	3	4	5
α	32.8	30.8	27.2	15.2	6.3	0	0
β	55.4	44.1	35.0	19.6	6.3	0	0

Ship Hull Data Sheet

° Ship Model

A model of the MV ARCTIC was designed at Arctec Canada Limited in 1984 at a geometric scale of 40, giving a model about five meters in length. It was intended that this model would replicate the dynamic properties of the MV ARCTIC, and therefore the shell of the model was cut into 12 individual segments. The segments were linked along the neutral axis by self-aligning aircraft bearing joints. Each segment was separately ballasted to simulate the mass distribution of the corresponding length of the prototype ship during the 1984 dedicated trials. The stiffness distribution along the model was obtained by connecting adjacent segments with simply-support spring bars at known distances above the neutral axis bearings. The stiffness of these individual moment springs was varied by adjusting the spring bar end clamps; thereby allowing for change in the natural frequency of the model.

The nominal first flexural mode of the MV ARCTIC at model scale was 5.88 Hz. During the model tests relevant to the present added mass study, the model's first flexural mode was 5.4 Hz, in good agreement with the expected value. It was observed from hammer tests that the first mode damping was 5.5 percent, also in good agreement with the expected value of 5.87 percent. Table 2.1 lists additional information which has been extracted from the model test report [1].

° Multi-year Ice Floe Modelling

During the full scale dedicated trials there was a concerted attempt made to accurately measure the dimensions of the notches formed by the impacts. These dimensions were found to be a valuable reference in determining the corresponding model ice strengths; even though it was believed that the measurements were distorted by the breaking away of the ice edge and ship lateral motions.

Arctec's synthetic ice modelling material, MOD-ICE, was used to represent the multi-year ice floes. By adjusting the relative amounts of the different components of MOD-ICE, it was possible to obtain model notch dimensions which were geometrically equivalent to the full scale dimensions at corresponding speeds. It was found that a MOD-ICE uniaxial crushing strength of 17 kPa (at a strain rate of 10-1) was required to simulate the multi-year floes which were assumed to be about 4.8 MPa. It was subsequently observed that the stress results and bow force predictions obtained when using this model ice were in good agreement with the dedicated trials results for the ramming speeds tested. Hence it was believed that the ice scaling was reasonable and that its use at higher impact speeds was an acceptable extrapolation.

TABLE 2.1

MV ARCTIC MODAL PROPERTIES: MODEL AND FULL SCALE

FLEXURAL MODES	NOMINAL FREQUENCY		MEASURED FREQUENCY TESTS 1 (Hz) [1]	MEASURED FREQUENCY TESTS 2 (Hz) [1]
	FULL SCALE [4]	TARGET SCALE (Hz)		
1	0.93	5.88	3.9	5.4
2	1.94	12.3	8.5	12.0
3	2.77	17.5	15.8	20.9
4	3.70	23.4	22.5	29.3
1st MODE DAMPING	5.87%	5.87%	11.7%	5.5%

PHYSICAL MODEL PROPERTIES

SEGMENT	BODY MASS (kg)	SPRING BAR DISTANCE TO NEUTRAL AXIS Z_o (m)	CENTROID DISTANCE FROM LCG x_i (m) (m)
BOW 1	27.0	0.230	2.195
2	16.8	0.240	1.844
3	57.1	0.250	1.434
4	77.6	0.258	1.024
5	73.1	0.260	.615
6	88.9	0.265	.205
7	44.2	0.268	-.205
8	33.4	0.288	-.615
9	56.8	0.288	-1.024
10	64.7	0.246	-1.431
11	37.2	0.220	-1.833
STERN 12	18.7		-2.236
	595.5		

PRINCIPAL PARTICULARS

LENGTH B.P. = 4.916 meters
DRAFT (molded) = 0.275 meters
BREADTH (molded) = .572 meters
SEGMENTS 2-11 Length = 0.412 meters
SEGMENTS 1, 2 Length = 0.40 meters

MOD-ICE is a wax-like material which is poured while hot into appropriate molds and allowed to set as ice blocks. This feature of the MOD-ICE permitted the testing to be carried out at room temperature. The molds for the simulated ice floes were approximately one meter square and filled to a depth of 0.5 meters. During the ramming tests the ice blocks were fixed to a force balance. The support framework, ice block and force balance were analyzed to ensure that forced response at its natural frequencies would not distort the model test results. It was found that the first rotational frequency of this structure was about 28 Hz. Since this frequency was above the fourth mode of the model, it appeared that the force measurements would not be affected, and that digital filtering would be feasible if higher frequency structural response was noted.

° Instrumentation and Model Test Data

The available data from the dynamically scaled impact tests of the MV ARCTIC into model ice blocks includes time history records from:

- ° 12 ship-fixed and vertically sensing accelerometers at the centroids of the segments.
- ° 11 bending moment sensors recording the force transmitted through the inter-segment spring bars.
- ° 6 motion channels measuring the position of the model bow.
- ° 6 force balance channels recording vertical and horizontal components of the force acting on the ice.

Figure 2.2 illustrates the locations of the instrumentation on the model. Appendix A contains time histories of all the channels from the tests which were examined.

During testing the raw data signals were stored on 28 channel FM tapes and on an 8 channel recorder. At that time it was only possible to digitally sample 32 channels directly. This information was filtered, digitized and stored on Hewlett Packard diskettes as part of an earlier analysis. A typical record from one sensor included approximately 25 seconds of data. An initial interval of "zeros" in calm water was included at the start of each record, followed by a forward acceleration interval wherein the model is towed to the desired impact speed. The ship-ice interaction occupied about 2 to 3 seconds in the complete record. The final portion of the record showed the model response after it has slid off the ice.

FIGURE 2.2

LOCATION OF INSTRUMENTATION

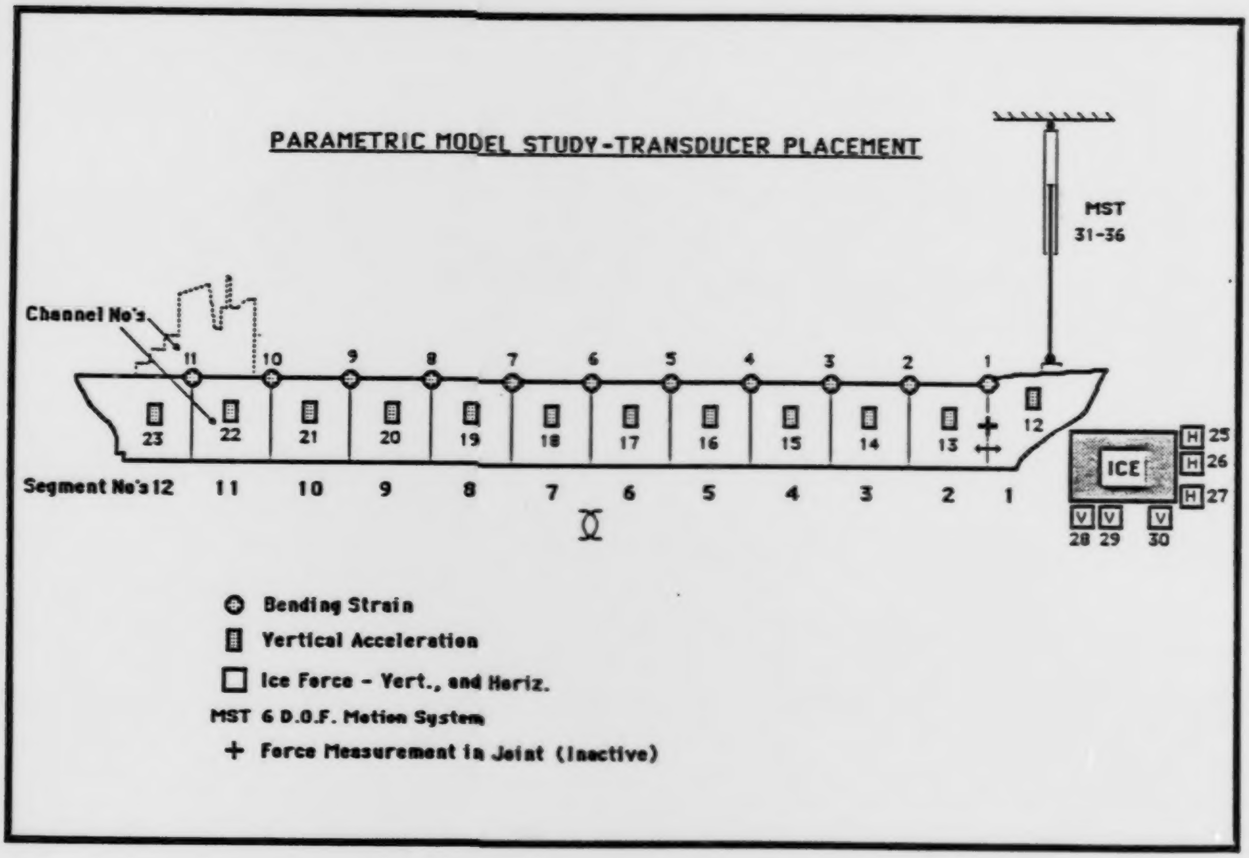

The data acquisition software sampled the data at 248 Hz. To limit the amount of unnecessary data stored in each record a window around the ship-ice interaction involving about 12 seconds has been accumulated. Calibration data for each of the channels was also stored on diskette. Pertinent details of the data channels are as follows:

i) The acceleration sensors were calibrated to plus or minus one gravity (9.807 m/s^2) by means of rotating the instrument through 90 degrees in the vertical plane. With this type of calibration a correction was required to account for the model's pitch and roll angles.

ii) The bending moments at the inter-segment spring bars have been measured in terms of bending loads transmitted through the spring bars. The bending moments were derived by multiplying the loads by their respective distances from the rotational joint at the neutral axis. These sensors have been calibrated by means of static loads applied at the bow.

iii) The motions of the bow are measured using a motions sensing transducer system (MST). Six potentiometer signals were monitored, reflecting the rotations and extension of this mechanical arm. The 6 channels were uncoupled to produce the heave, pitch, roll, yaw, sway and surge at the bow. Additional corrections were required to compute the usual heave at the centre of gravity.

iv) There were 3 vertical and 3 horizontal force sensing channels. The sum of each set of channels gave the total force in each direction as measured in the ice.

° Matrix of Conditions During MV ARCTIC Experiments

Table 2.2 summarizes the program of testing carried out in 1986. Data from approximately 160 ramming trials was obtained using 19 model ice blocks. The uniaxial model ice compression strength was varied during these tests from 7.4 kPa to 179 kPa, as a means of studying the effect of ice strength on the longitudinal stress distribution induced in the ship model. However, the majority of testing was at 30 kPa, which was slightly stronger than the nominal multi-year ice strength. The influence of model stiffness was also assessed in a number of tests by adjusting the first mode frequency. In addition there was a comparison between three forefoot configurations, which involved changes in the size of the ice knife. The forefoot configurations included the original MV ARCTIC bow form, an extended forefoot knife, and a "no forefoot knife" geometry.

Extension and removal of the ice knife involved a ±10cm (model scale) longitudinal change in the baseline length. In addition a minor amount of fairing to the forefoot was required in each case.

TABLE 2.2

SUMMARY OF MODEL TEST MATRIX

NO.	TEST SERIES	*NOTED STIFFNESS	UNIAXIAL ICE STRENGTH (kPa)	**BOW CONFIGURATION
1	TA	1	179.0	A
2	TB	1	30.7	A
3	TC	1	27.2	A
4	TD	1	21.0	A
5	TE	1	7.4	A
6	TF	1	120.6	A
7	TG	1	√ 30.0	A
8	TH	1	√ 30.0	A
9	TI	1	√ 30.0	A
10	TJ	1	29.6	A
11	TK	2	35.3	A
12	TL	3	√ 30.0	B
13	TM	3	26.7	B
14	TN	3	30.2	B
15	TP	3	28.1	B
16	TR	3	21.1	C
17	TS	3	28.0	C
18	TT	3	37.0	C
19	TU	3	34.7	C
20	TV	3	No Contact	C

√ No samples available: use average of corresponding remix ice strengths.

* Stiffness: Case 1, 1st Mode = 5.4 Hz
Case 2, 1st Mode = 4.2 Hz
Case 3 = Case 1 Reset

** Bow Configuration: A - MV ARCTIC Old Bow
B - Extended Forefoot Knife
C - No Forefoot Knife

A subset of the existing MV ARCTIC model test data was found amenable to extraction of added mass time histories by means of the present procedures. The ramming tests of the physical model in the configuration with the forefoot knife removed were found to have the most complete set of information. The 'old bow' configuration and 'extended forefoot' configuration data sets were missing roll and yaw motions and therefore it was not considered advisable to use these tests.

3. METHODOLOGY OF EXTRACTING HYDRODYNAMIC ADDED MASS

3.1 Stages in the Extraction of Added Mass

The methodology for deriving added mass coefficients from the model test data above is discussed in this section. On the basis of the results obtained here it is hoped a better understanding of the role played by hydrodynamic added mass will be gained. It will also allow an assessment of the applicability of conventional added mass values in representing the transient impact case. The present approach has been carried out in three stages:

- Pre-processing; involving the preparation of the time histories into a common format and the selection of representative tests for case studies.
- Time Step Computations; involving the calculation of sectional added mass time histories for each test.
- Post Processing; involving the analysis of the derived added mass records. It also includes the assessment of trends and a comparison with calculated results based on theoretical methods in the literature.

The relationship between each stage is shown in Figure 3.1 and outlined in the following sections.

3.2 Pre-processing of the MV ARCTIC Model Test Data

The computation phase was preceded by several organizational steps. The first was to select a set of test runs from amongst the 168 available for analysis. The selection process was limited by the following conditions:

- Ice strength was expected to be constant throughout the set and approximately 30 kPa. This value was representative of multi-year ice and was slightly stronger than that observed in dedicated full scale trials.
- The tests in the set are all required to have the same forefoot knife configuration.
- The first flexural mode of the model was required to be 5.4 Hz; the closest match during testing to the scaled ship value of 5.84 Hz.
- The time histories for all of the required sensor channels was expected to be available and usable.

Figure 3.1 STAGES IN THE EXTRACTION OF ADDED MASS

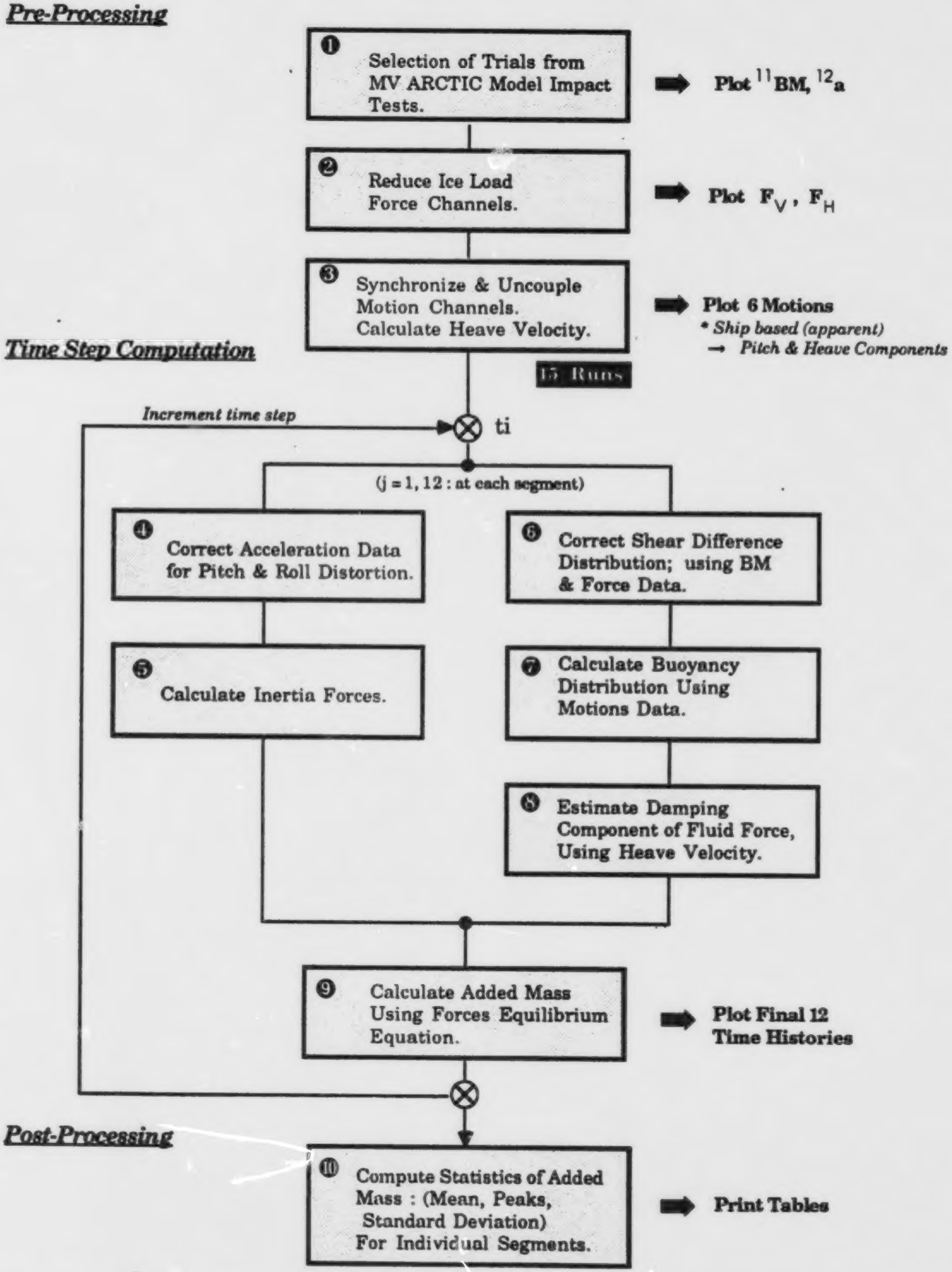
Pre-Processing
❶ Selection of Trials from MV ARCTIC Model Impact Tests.
Plot 11BM, 12a
❷ Reduce Ice Load Force Channels.
Plot F_V, F_H
❸ Synchronize & Uncouple Motion Channels. Calculate Heave Velocity.
Plot 6 Motions
* Ship based (apparent)
→ Pitch & Heave Components
Time Step Computation
15 Runs
Increment time step
ti
(j = 1, 12 : at each segment)
❹ Correct Acceleration Data for Pitch & Roll Distortion.
❺ Calculate Inertia Forces.
❻ Correct Shear Difference Distribution; using BM & Force Data.
❼ Calculate Buoyancy Distribution Using Motions Data.
❽ Estimate Damping Component of Fluid Force, Using Heave Velocity.
❾ Calculate Added Mass Using Forces Equilibrium Equation.
Plot Final 12 Time Histories
Post-Processing
❿ Compute Statistics of Added Mass : (Mean, Peaks, Standard Deviation) For Individual Segments.
Print Tables

It was desired that the model impact velocities cover a range up to 1.0 m/s, allowing a systematic examination of the influence of impact velocity on the added mass. Table 2.2 from [1] describes the physical model properties and give the test matrix for the different series of tests.

A preliminary set of tests was selected from ice block series TB, TC, TD, TG, TH, TI and TJ which correspond to the old bow form. TB has a large number of low and medium speed impacts while TI has a number of higher speed runs. However assessment of time histories showed that the roll and yaw motions were missing from these tests. Therefore, after a further screening of the available test data it was decided to use tests from series TR, TS, TT and TU. For these tests the forefoot knife had been removed from the model. Table 3.1 lists the specific tests examined in the present study.

The vertical and horizontal force acting on the ice during the impact had been measured using six force sensors. The first step in the pre-processing phase was to view the summed time histories as a means of checking that these data were reasonable.

The MST sensors provided six channels of motions data, allowing resolution of the pitch, heave, surge, roll, sway and yaw of the model. However, these six raw data channels were measured as rotational potentiometer signals, not as conventional ship motions. It was therefore necessary to uncouple these signals and convert them into usual cartesian coordinates. In addition, only three of the MST channels were digitized during the execution of the test program. The remaining three channels were stored in analogue form on magnetic tape. It was necessary to digitize these channels and synchronize them with the other information. Only then was it possible to resolve the MST data into motions in an absolute reference frame.

After assessing the time histories corresponding to each channel of the candidate test runs, a total of 14 tests were chosen for further study. Three tests with the original MV ARCTIC bow geometry were included to allow comparison between results obtained for the different forefoot configurations.

3.3 Time Step Computations

The added mass coefficients were derived using a time domain approach which is based on the force equilibrium at each of the 12 segments. It has been assumed that all of the body forces and surface forces act through the centre of mass of each segment, except at the bow and stern segments which are discussed at a later point in this text. In particular the ice force was considered separately.

TABLE 3.1

MODEL TESTS ASSESSED IN PRESENT STUDY

TEST	IMPACT VELOCITY (m/s)
TR-8	0.37
TR-9	0.86
TR-10	0.58
TR-11	0.67
TS-1	1.14
TS-2	0.37
TS-6	0.24
°TT-6	0.62
TT-10	1.03
TU-11	0.98
TU-12	0.73
*TG-2	1.12
°*TH-3	1.13
°*TI-2	1.02

Note: ° Assessed, but not used in final computations

* Original MV ARCTIC bow geometry

Figure 3.2 shows a free body diagram of the vertical forces acting on each segment. The force dynamics in the vertical plane (ship based) can be expressed as:

$$F_{ICE-VERT}(t) + F_g(t) + F_B(t) + F_I(t) + F_{\Delta V}(t) + F_{ma}(t) + F_d(t) = 0 \qquad (1)$$

where $F_{ICE-VERT}$ = ice force (vertical component)

F_I = inertia (body) force

F_g = gravitational force

F_B = buoyancy force

$F_{\Delta V}$ = shear difference force

F_d = fluid damping force

F_{ma} = Added mass component of hydrodynamic force

It is assumed that the structural damping is included in the shear difference term. It must be pointed out that the vertical ice force acts only on the first and second segments, i.e: $F_{ICE-VERT} = 0$ for $i = 3$ to 12.

For the model stationary in the still water the inertia force is zero. Gravity, buoyancy and shear difference cancel each other at every segment. This means that the following constraint is valid for the still water condition:

$$F_g(t) + F_B(t) + F_{\Delta V} = 0 , \qquad F_I(t) = 0 \qquad (2)$$

The bending moment time histories prior to impact do not show any change from the stationary condition due to forward speed (and the consequent bow wave). Hence equation 2 may be used as a zero reference condition for the time preceding the ice interaction. The still water bending moment is not introduced into the subsequent added mass calculations since the strain gauges measuring the bending moments are set to zero prior to each test. As a result, only differences from the still water conditions are considered in the force equilibria. Since the gravitational force is a constant in time, its difference from buoyancy force will be zero and therefore it need not be considered further.

Figure 3.2 FREE BODY DIAGRAM OF SEGMENT

Vertical Forces:

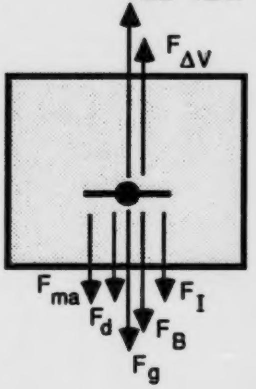

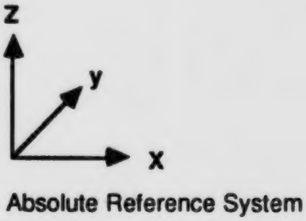

QUASI-STATIC EQUILIBRIA ON SEGMENTS

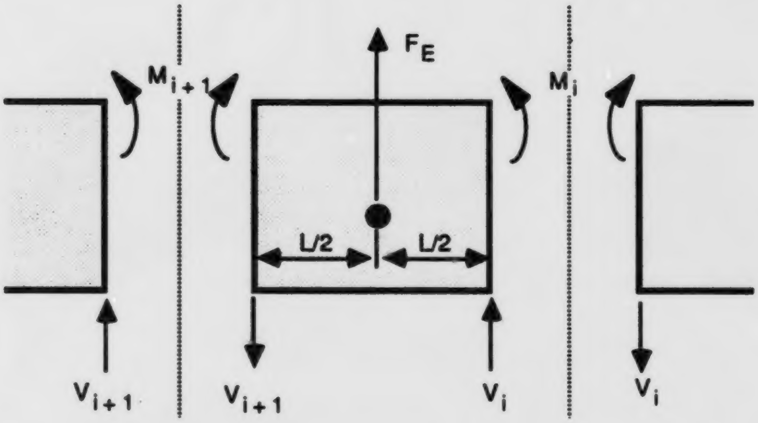

3.4 Computing Shear Difference Forces

The shear difference is the force acting on a segment as a result of the bending moment distribution in the model. Figure 3.2 also shows the forces and moments acting on one segment due to its interactions with its neighbours. If the body and surface forces act through the centre of the segment, the interaction can be described by two simple equations:

$$\Sigma \text{ Moments} = 0 \quad , \Sigma \text{ Forces (vertical)} = 0 \qquad (3)$$

If the subscript "i" refers to the sequence of inter-segment joint locations starting from the forward perpendicular, then the two equations can be written as:

$$-V_{i+1} + V_i + F_E = 0 \text{ , and} \qquad (4a)$$

$$V_i \cdot L_i + F_E \cdot L_i/2 = (M_{i+1} - M_i) \qquad (4b)$$

where F_E is a short-hand notation for the sum of all body and surface forces in equation (1) which are assumed acting at the centroid of the segment. It includes the inertia force, F_I; the hydrodynamic inertia force, F_{ma}; the damping reaction, F_d; and the buoyancy force, F_B, with respect to the free floating condition. The total bending moment $(M_{i+1} - M_i)$ at any instant is known from the measured load which is transmitted through the spring bars on either side of the segment. There is only one moment at the stern and at the bow segment. The shear, V_i, is introduced from the previous segment. The moment equation may equivalently be expressed as:

$$F_E = 2(M_{i+1} - M_i - V_i L_i)/L_i \qquad (5)$$

In Figure 3.3 it can be seen that V_o is defined as the ice force acting vertically at a distance L_1 from the first rotational joint. This distance will vary with time being maximum at the instant of contact and a minimum at the point of maximum forward surge. The change in L_1 may be estimated using the difference between surge and ice indentation. The exact determination of this distance is described in section 4.3.

The ice force normal to the ship longitudinal axis is calculated from the measured vertical force, F_V and horizontal force, F_H:

$$F_{ICE\text{-}VERT} = \{F_V^2 + F_H^2\}^{1/2} \sin(\theta + \psi) \qquad (6a)$$

where θ is the measured pitch angle and

$$\psi = \arctan(F_V/F_H) \qquad (6b)$$

In addition there will be a component of the ice force along the longitudinal axis of the ship given by:

$$F_{ICE\text{-}LONG} = \{F_V^2 + F_H^2\}^{1/2} \cos(\theta + \psi) \qquad (7)$$

Figure 3.3 STEPWISE COMPUTATION OF SHEAR DIFFERENCE

M.V. Arctic Model

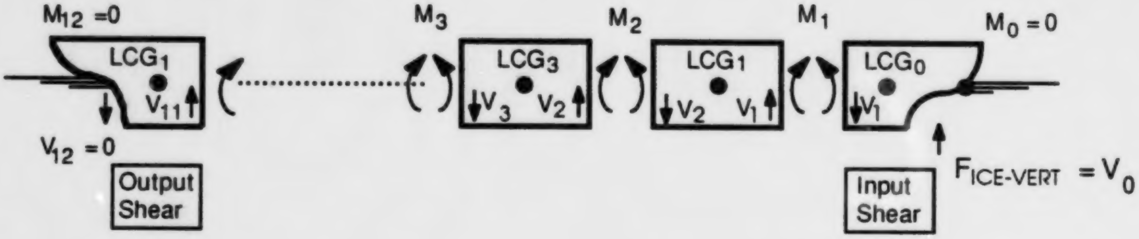

DIFFERENTATION METHOD

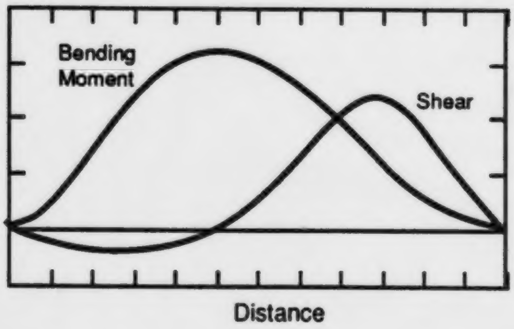

Equation 6a and 7 define the ice force components in the vertical and longitudinal planes in a ship based reference frame. The longitudinal force component has for convenience not been included in the above discussion of the theory. This was a reasonable first approximation because the proximity of the longitudinal force vector to the neutral axis was expected to reduce its affect. However, the effect of the longitudinal force on the moment balance was subsequently considered in the numerical implementation of the computational procedures and has been described in Section 4.2.

In equation 4a the next shear value, V_{i+1}, may be derived by eliminating F_E from equation 4a and 4b; in this manner progressing from the bow to the stern segment. This stepwise progression is given by:

$$V_{i+1} = V_i + 2(M_{i+1} - M_i)/L_i \qquad (8)$$

The shear difference force acting on each segment at its centroid is found by subtracting the shear at adjacent segment joints, on the same segment.

$$\Delta V_i = V_i - V_{i+1} = -2(M_{i+1} - M_i)/L_i \qquad (9)$$

The values of shear, V_i, may be verified by carrying out the stepwise calculation in equation 7 and checking that the use of measured ice force at the bow leads to a zero shear at the stern.

3.5 Computing Buoyancy Forces

The buoyancy force acting on a segment of the model is defined as the difference in weight displacement from the still water condition. It is dependent on the geometry of the segment and its vertical motions. The distribution of buoyancy force along the model is determined from the motions data which is measured at the bow. This is an approximate method of estimating the buoyancy force and is used in the absence of accurate motion measurements at each segment. The pitch angle and the bow heave are used to calculate the corresponding apparent heave at each segment.

For the case of the rigid model illustrated in Figure 3.4a, the total vertical motion at a segment is given by:

$$Z_i(t) = Z_{CG}(t) + x_i' \cdot \sin \theta \qquad (10)$$

where Z_{CG}, is the heave at the CG,

Z_{BOW}, is the bow rise due to pitch and heave,

x_{CG}, is the distance from the MST (on the bow) to the model CG

x_i', is the distance from the CG to the centroid of each segment in the body-fixed reference frame.

Figure 3.4a RESOLVING RIGID BODY MOTIONS

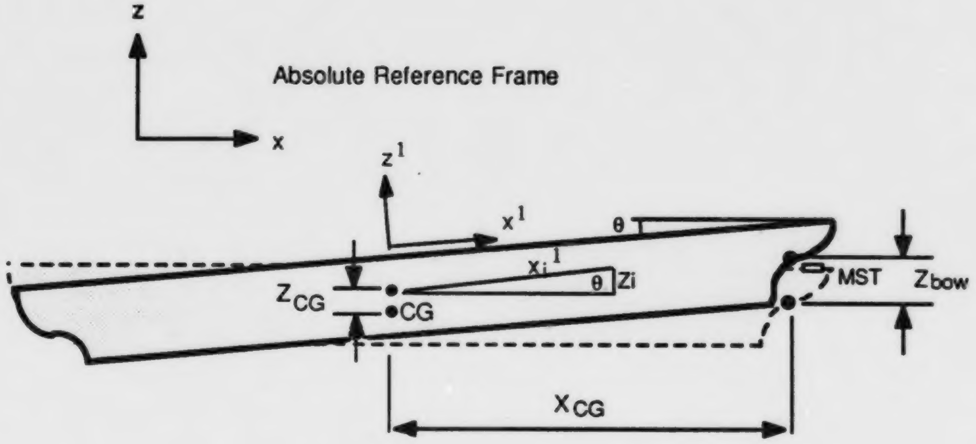

Figure 3.4b FLEXIBLE MODEL SEGMENT HEAVE

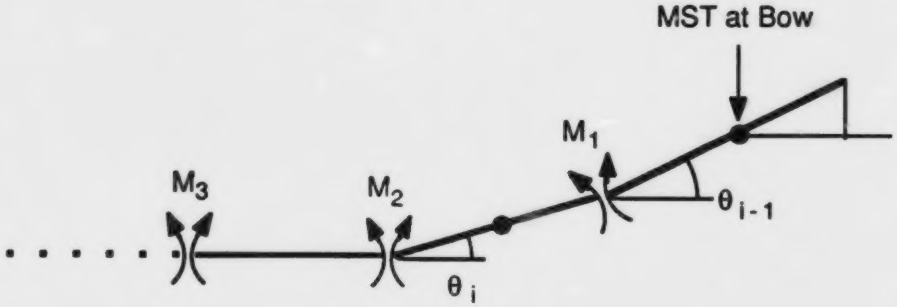

The motions data gives the total bow rise and therefore a simple geometric approximation is proposed for determining Z_{CG} from Z_{BOW}. This results in a pitch angle dependent expression for the rise of the CG which neglects the curvature induced into the model.

$$Z_{CG} = Z_{BOW} - x_{CG} \sin \theta \tag{11}$$

Combining equations (8) and (9) gives the apparent heave at each segment:

$$Z_i(t) = Z_{BOW} - (x_{CG} - x_i') \sin \theta(t) \tag{12}$$

However it was observed that the rigid body approximation resulted in heave values at the stern which were well in excess of the motions recorded on video. Therefore an equation was introduced to account for the influence of ship model flexure on the segment heave:

$$Z_i(t) = Z_{i-1}(t) - (L_i/2)\,[\sin\theta_{i-1}(t) + \sin\theta_i(t)] \tag{13}$$

where L_i is the distance between segment midpoints. Equation 13 expresses the segment heave in terms of the pitch angle distribution along the model. Figure 3.4b illustrates the localized bending between segments and the consequent changes of pitch. The initial values of $Z(t)$ and $\theta(t)$ are the measured bow rise and pitch respectively. (A representative set of motions data is shown in Figure 3.5). The pitch as a function of length along the model is determined by a spatial integration of the bending moment distribution.

$$\int_o^{x_i} \left(\frac{M}{EI}\right) dx = \tan \theta = \theta_{DEFL} \tag{14}$$

The integration constant is zero if the integration starts from the bow. Hence, the pitch at any segment is given in terms of the measured pitch at the bow and the calculated angle of deflection, θ_{DEFL}, for that distance aft of the bow:

$$\theta_i(t) = \theta_{BOW}(t) + \theta_{DEFL}(x_i) \tag{15}$$

The heave is calculated in an absolute frame of reference, rather than a ship based frame of reference. The corresponding heave in a model based reference system is:

$$Z_i'(t) = Z_i(t) \sec \theta(t) \tag{16}$$

FIGURE 3.5

SAMPLE OF MOTIONS DATA, TEST TU-11

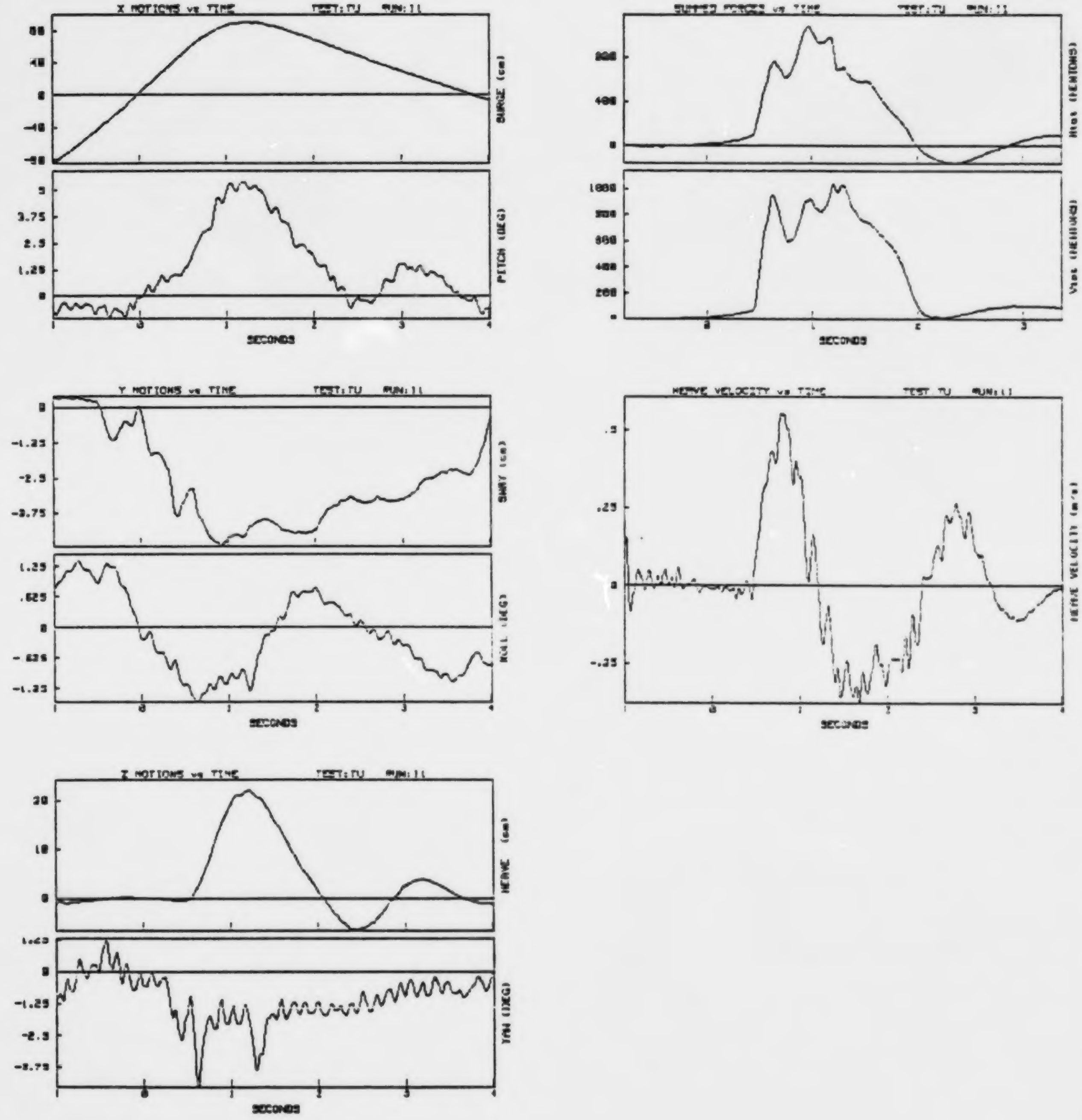

The static buoyancy force associated with this change in water level at each segment was calculated using the known segment waterplane areas; so that:

$$F_{Bi}(t) = Z_i(t) \cdot \rho g A_i(Z_i(t), \theta(t)) \qquad (17)$$

The water density ρ, and gravitational constant g, were assumed to be constant. The waterplane area is a time varying function of $Z_i(t)$ and is affected by the detailed geometry of the sections along model length. Hence A_i was defined in terms of regression equations based on section area curves of the MV ARCTIC at different drafts. However the MV ARCTIC model has a long parallel mid-body and wall sides, and therefore many of the segments have the same waterplane areas.

The bow wave is another hydrodynamic effect which may influence the buoyancy force distribution along the model and therefore the bending moments. When the model stops abruptly on striking the ice block, its bow wave is reflected from the ice. This is believed to induce a small horizontal force which is observed immediately prior to impact and a corresponding vertical force. It is believed that this is a second order effect and one which may be ignored in the preliminary calculation of added mass dealt with here.

3.6 Computing Hydrodynamic Added Mass

The vertical force terms in equation 1 can be rewritten in a form which includes the shear difference and the buoyancy force expressions which have been derived in the above equations, and then divided by the segment acceleration to give the time dependent mass components:

$$\frac{\Delta V_i}{a_i(t)} + \frac{\rho g \, Z_i A_i}{a_i(t)} + m_i + m_{33} + \frac{F_{ICE-VERT}}{a_i(t)} = 0 \qquad (18)$$

The heave added mass is denoted by m_{33}. The acceleration time histories measured at each segment must be corrected for time varying pitch and roll motions. The accelerometer correction in terms of pitch $\theta(t)$ and roll $\phi(t)$ is given by:

$$a_i(t) = a'_i(t) + 9.807(1-\cos\{\arcsin[\sin^2\theta + \sin^2\phi - \sin^2\phi \sin^2\theta]^{1/2}\}) \qquad (19)$$

where a'_i denotes measured acceleration

Figure 3.6 presents a typical series of acceleration time histories from test TU-11. Appendix A contains acceleration time histories for a number of tests, showing both corrected and original data.

FIGURE 3.6

SAMPLE OF ACCELERATION DATA, TEST TU-11

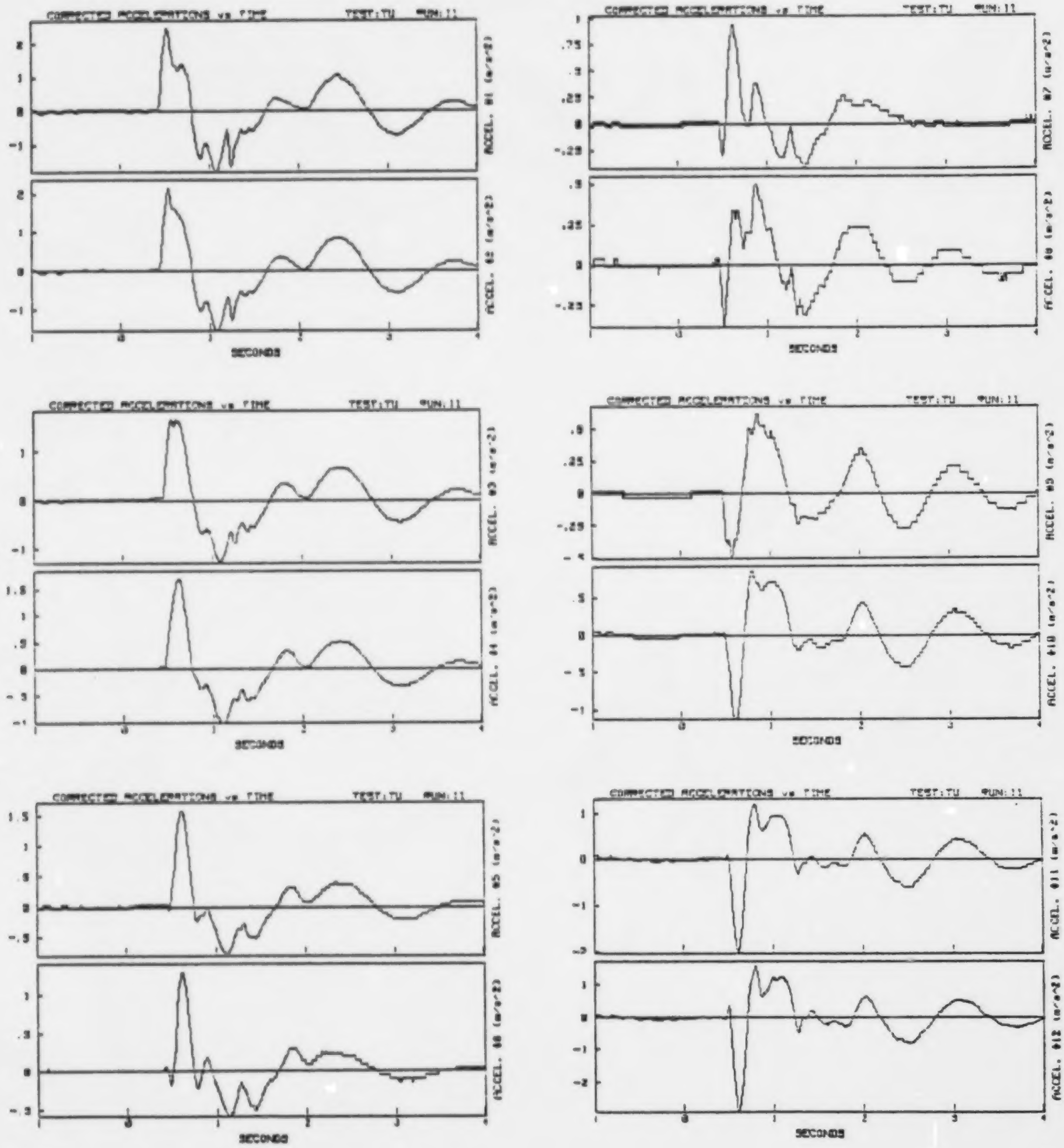

Based on the above equations and the known distribution of segment mass it was possible to assign values to all of the variables in equation 18, except added mass and damping. For the transient impact there was no direct method for resolving these two hydrodynamic effects. In consequence, numerical results for added mass were obtained by assuming that the damping component of the hydrodynamic force would always be small compared to the added mass effect. In the frequency domain the damping coefficient (as a percentage of critical) is given by the ratio of the mode width at its RMS value to the frequency of that mode:

$$C_k = \Delta f_k / f_k \quad \text{, at } k^{th} \text{ mode} \qquad (20)$$

The total damping of the model was estimated during the model test program as 5.5 percent for the first flexural mode. The structural damping of the model has been shown in Volume 3 to be less than 1 percent. This component is included within the calculated shear difference. The remainder of the total is fluid damping which is mainly divided between the bow and stern regions. At the bow the ice constrains the motions and therefore little fluid damping can occur. Hence, it was believed that assuming damping effects to be small would be reasonable along the parallel midbody of the ship model, but uncertain at the stern where whipping was observed to dissipate energy through wave formation. The final step in the time domain computation of the added mass time history involved the division of the force by the segment accelerations:

$$m_{33_i}(t) = - m_i - \frac{\rho g Z_i(t) A_i(t)}{a_i(t)} - \frac{\Delta V_i}{a_i(t)} - \frac{F_{ICE-VERT}}{a_i(t)} \qquad (21)$$

The terms in equation (17) with the exception of the shear difference are in an absolute frame of reference. Angular corrections to the forces are strictly required to express the added mass in a consistent model based reference frame. However the pitch time histories compiled in Appendix A typically have maximum values less than five degrees, and therefore it was decided to neglect the transformation since the error introduced was less than one percent.

4. IMPLEMENTATION OF ANALYSIS METHODS

4.1 Shear Difference Force

The equations of motion governing the derivation of added mass have been implemented on a Hewlett Packard 9816 computer system. It was not possible to calculate the shear difference force by means of the segment by segment procedure outlined in Section 3.4, since numerical oscillations in the shear were introduced. An modified solution procedure was instigated whereby the shear distribution was determined from the numerical derivative of the bending moment distribution. At each time step, the 11 measured bending moments were fitted to a seventh order polynomial by means of a least squares regression routine.

$$M(x) = k_o + kx + k_2x^2 + \ldots\ldots + k_7x^7 \qquad (22)$$

The moments at either extremity of the model were constrained to be zero. The shear distribution was then derived by numerically differentiating to give a corresponding sixth order polynomial.

$$V(x) = k_1 + 2\,k_2x + 3k_3x^2 + \ldots\ldots + 7k_7x^6 \qquad (23)$$

The shear difference across any segment was defined as the shear at its forward end minus the shear at its aft end. At the bow extremity and the aft extremity the shear values were constrained to be zero.

$$\Delta V = V_{i-1} - V_i \quad , \; i = 1, 2 \ldots , 12 \qquad (24)$$

Figure 4.1 shows the original bending moment time histories expressed as shear forces transmitted between segments. Figure 4.2 illustrates a sequence of time step calculations from Test TU-11 using every tenth data point. The data points are marked with an "x" and the bending moment polynomial and its corresponding shear polynomial are shown as solid lines.

4.2 Corrections to the Shear Difference Force

There were three principal corrections to the shear difference force which were included to improve the accuracy in the calculated values.

(i) A simple approximation for the detailed bending moment distribution over the bow segment was introduced to give more resolution in the derivature shear curve. This involved estimating the model mass forward of the centre of application of the ice force. The procedure for calculating the mass contributing to a moment at the bow is illustrated in Figure 4.3. The bending moment was negative by convention since the segment joint was in tension.

FIGURE 4.1

FORCE TRANSMITTED BETWEEN SEGMENTS AND CONTRIBUTING TO BENDING MOMENTS, TEST TU-11

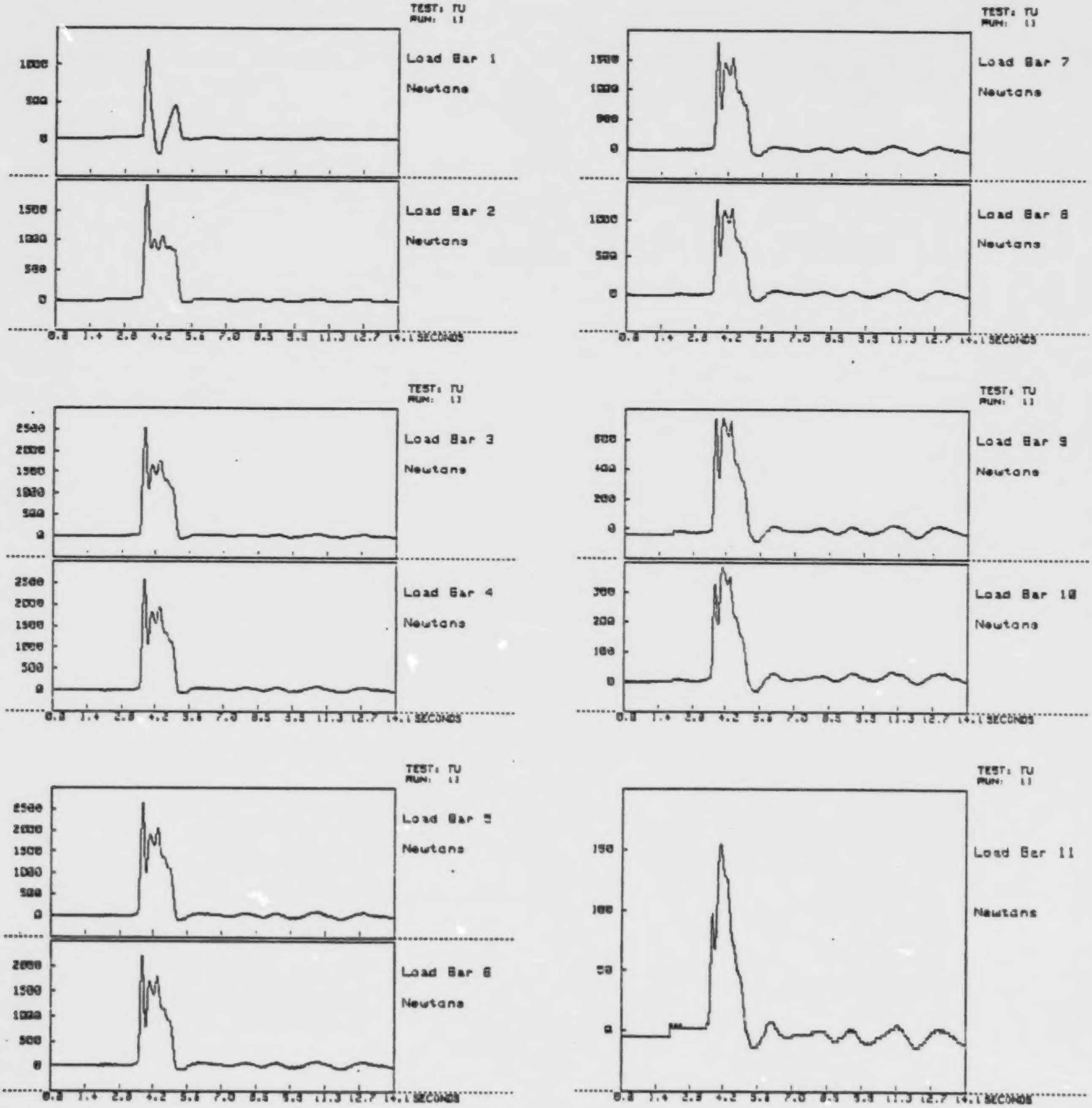

FIGURE 4.2

FITTING POLYNOMIALS TO BENDING MOMENT DISTRIBUTION AND CALCULATING SHEAR DISTRIBUTION. TEST TU-11

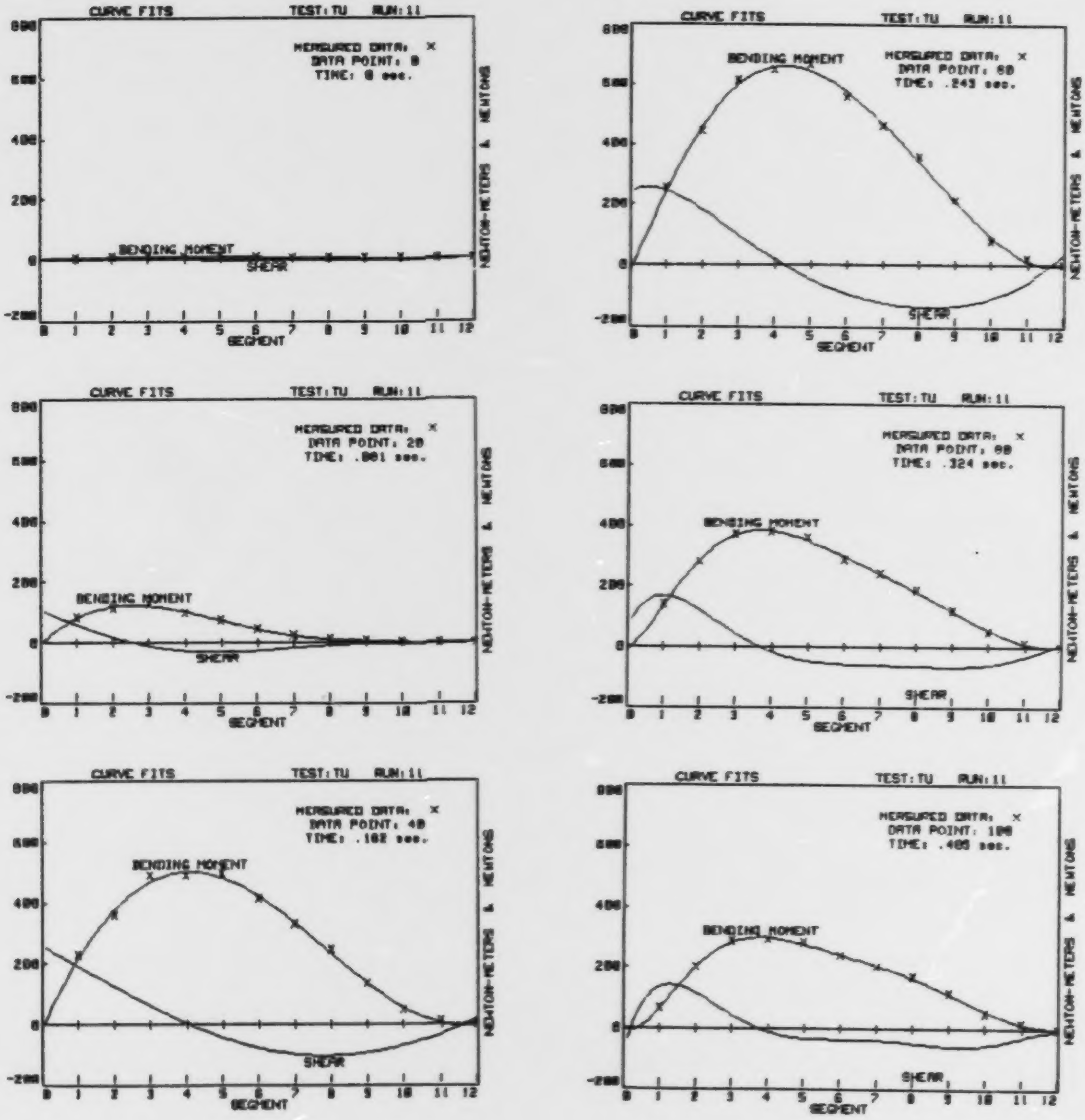

FIGURE 4.2 (continued)

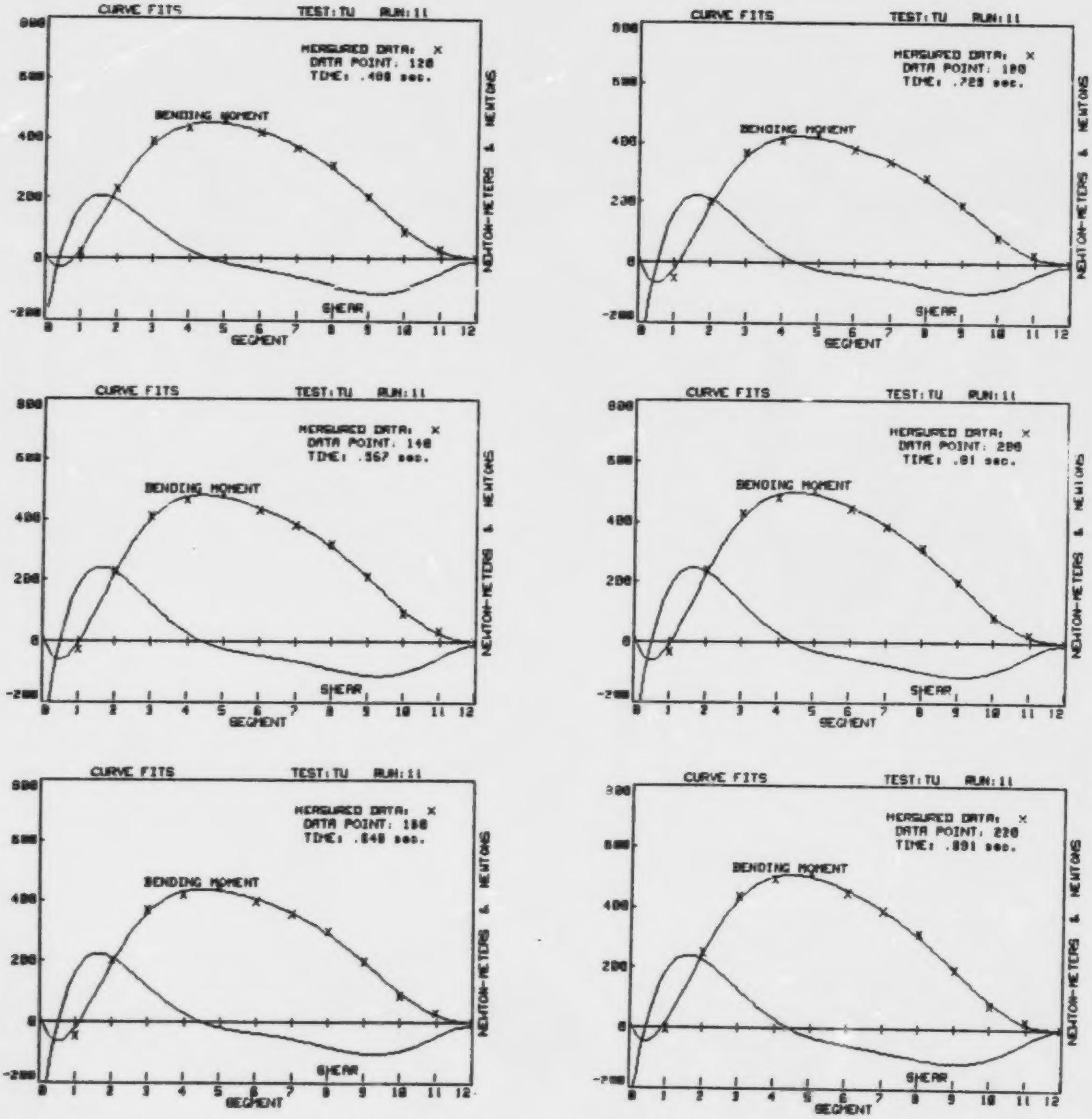

FIGURE 4.2 (continued)

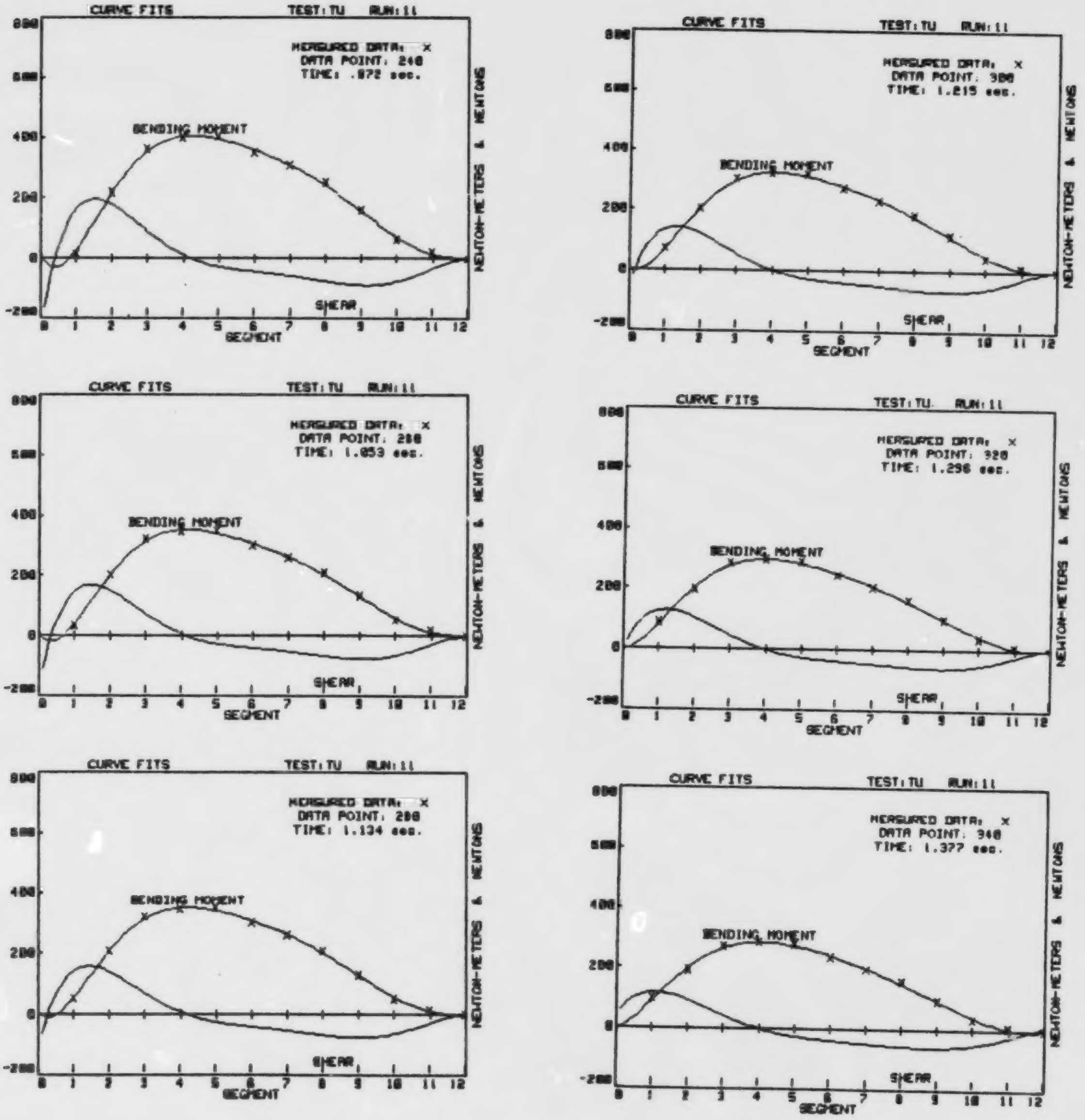

FIGURE 4.2 (continued)

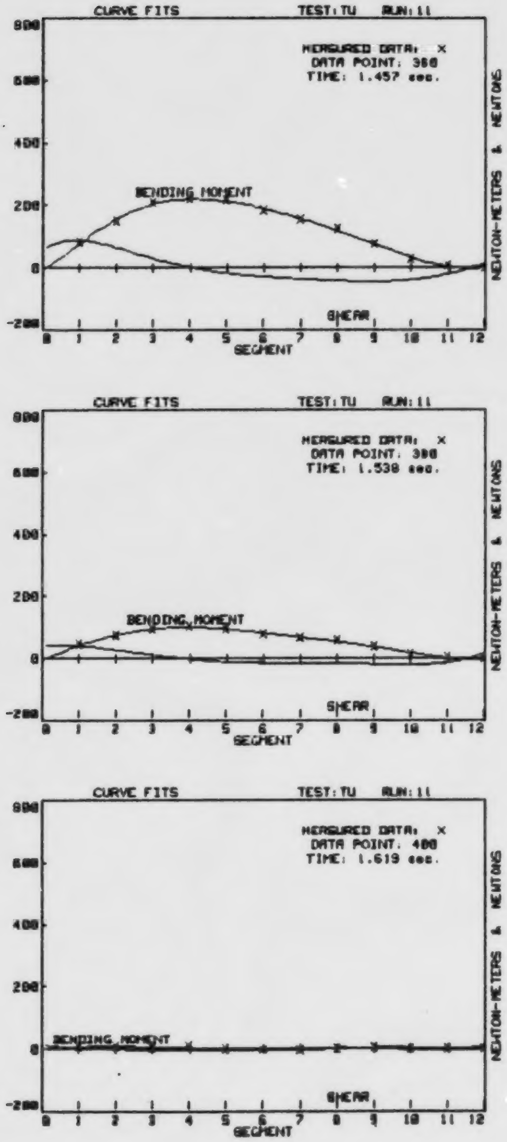

Figure 4.3
LOCATION OF CENTROID OF MASS FORWARD OF ICE FORCE

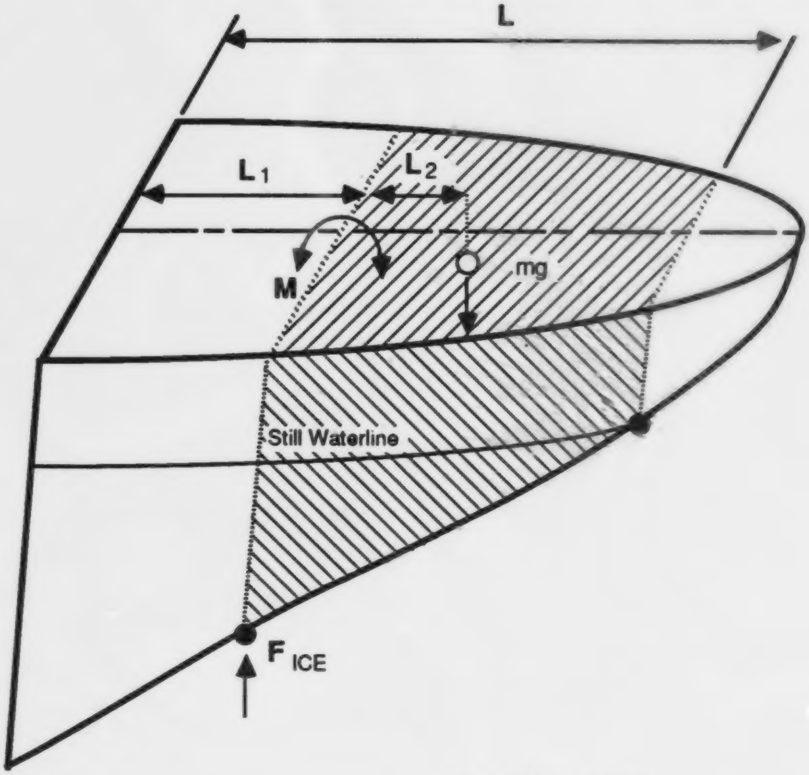

By Definition:

$$L_2 = (L-L_1)/3$$

Approximation:

$$M = -0.042\ L_2\ \rho g\ (L-L_1)^3$$

Hence the polynomial fit to the data was forced to follow this trend, giving rise to a modified shear at the first joint. In general, only this shear value and therefore only the first segment shear difference was affected.

(ii) The shear was constrained to be zero at both extremities of the model. However the polynomial fit process produced non-zero values. The value at the extremity was considered an error which was used to correct the shear difference. In each time step the shear difference value at each segment was adjusted by a simple factor which expressed the error at the aft extremity as a fraction of the vertical ice force. The error was defined as the value of the calculated shear at segment 12, ie. V_{12}.

$$\text{Factor} = \frac{F_{ICE-VERT}(t) - V_{12}(t)}{F_{ICE-VERT}(t)} \tag{25}$$

(iii) The longitudinal component of the ice force affects the moment balance on the model segments described by equation (4b). Longitudinal forces are transmitted through the spring bars and rotational joints as bending moments with respect to the neutral axis. The difficulty is that the measured bending moments include this influence from the longitudinal ice force; whereas the shear difference equation presumes that only vertical force components are present. The measured bending moments have therefore been corrected in the following manner, as illustrated in Figure 4.4.

° If the point of application of the ice force is below the neutral axis, a bending moment is calculated and added to the measured moment. If the force acts above the neutral axis, no calculation is performed and the correction is neglected. For the former case:

$$M_{CORR} = F_{ICE-LONG} \cdot Z_N \tag{26}$$

where Z_N is the moment arm between the neutral axis and the force vector.

° It is assumed that the bending moment is transmitted along the model and its magnitude attenuated in proportion to the body mass of each segment. Hence each measured moment is adjusted accordingly by an amount:

$$M_{CORR}(t)_i = M_{CORR}(t)_1 \cdot \left[1 - \sum_{j=1}^{i-1} m_j/m\right] \tag{27}$$

where m is total body mass.

Figure 4.4
BENDING MOMENT CORRECTION FOR LONGITUDINAL COMPONENT OF ICE FORCE

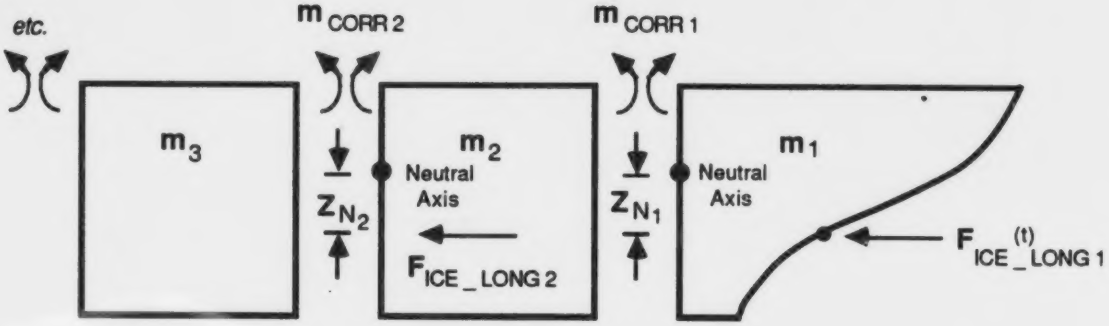

$$M_{CORR} = F_{ICE-LONG} \cdot Z_N$$

FOR ICE FORCE ON SEGMENT 1:

$$M_{CORR}(t)_i = M_{CORR}(t)_1 \cdot [1 - \sum_{j=1}^{i-1} m_j/m]$$

FOR ICE FORCE ON SEGMENT 1 and SEGMENT 2:

$$M_{CORR}(t)_i = M_{CORR}(t)_1 \cdot [1 - \sum_{j=1}^{i-1} m_j/m] + M_{CORR}(t)_2 \cdot [1 - \sum_{j=2}^{i-1} m_j/(m - m_1)]$$

- The ice load may be distributed over the first and second segment, in which case two bending moments are calculated. The correction for the subsequent segments is determined by a linear superposition of the influence of the two moments.

$$M_{CORR}(t)_i = M_{CORR}(t)_1 \cdot [1 - \sum_{j=1}^{i-1} m_j/m] \qquad (28)$$

$$+ M_{CORR}(t)_2 \cdot [1 - \sum_{j=2}^{i-1} m_j/(m - m_1)]$$

The longitudinal force causes a tensile stress in the upper deck which is opposite in sign to the bending stresses associated with the vertical force. Therefore the corrections at each inter-segment joint are added to the measured moments. Corrected shear and shear difference distributions at each time step are calculated on the basis of the revised bending moments. It is observed that the principal effect of the bending moment correction is on the added mass of the first two segments and on the aft segment.

4.3 Location of Ice Forces

The ice force at any instant in time is distributed over a small area of the model's surface. Since neither the centre of action nor the spread of the force is precisely known from the experimental data, it has been necessary to approximate these parameters. A reasonable assumption is that the centre of action of the force lies at the centroid of the notch area formed by the bow indentation into the ice. The centroid is one-third of the distance from the base towards the apex of a triangle.

The indentation length is calculated from the measured values of bow rise, $Z(t)$; pitch angle $\theta(t)$; and surge $X(t)$:

$$I(t) = X(t) - Z(t) \cot(\alpha + \theta(t)) \qquad (29)$$

where α is the mean stem angle in these tests, 34 degrees. Figure 4.5 illustrates this procedure. The instantaneous distance of the centre of force forward of the first segment joint is expressed in terms of the waterline length of the first segment, L_o; the surge, $X(t)$; and the indentation into the ice, $I(t)$:

$$L_1(t) = L_0 - [X(t) - I(t)] - 2/3\, I(t) \qquad (30)$$

The final term represents a shift from the apex to the centroid of the notch.

Figure 4.5
LOCATION OF ICE FORCES

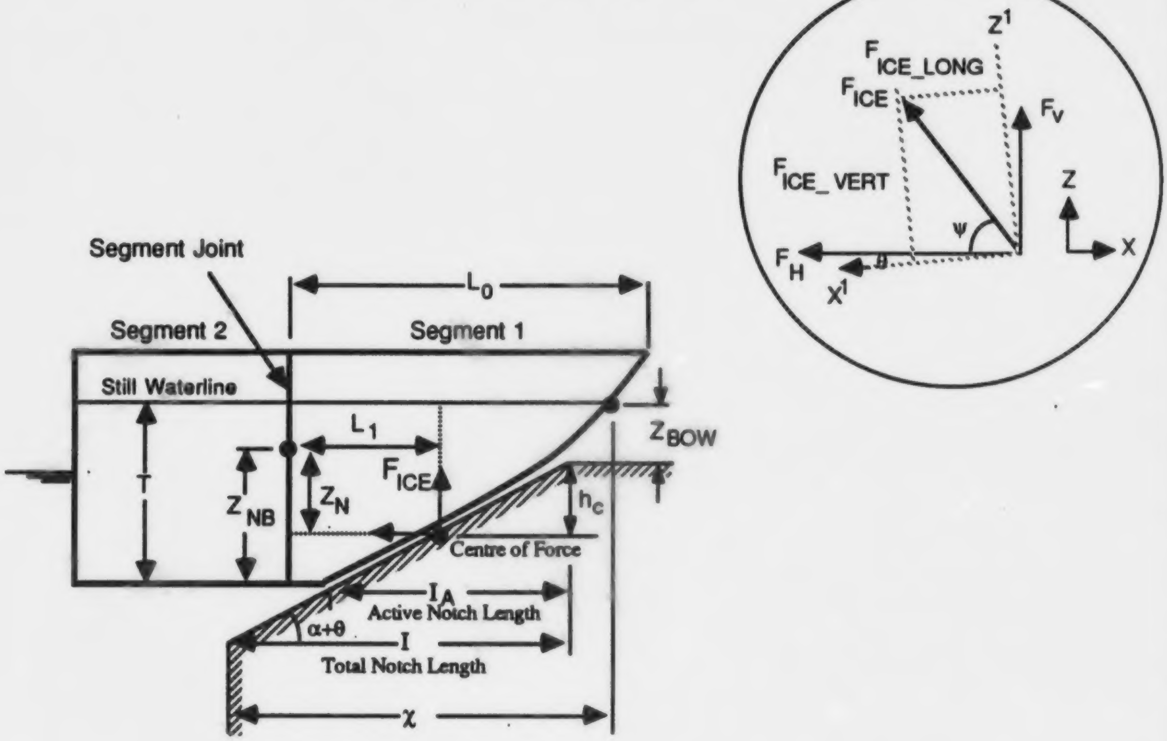

$$L_1(t) = L_0 - [X(t) - I(t)] - 2/3\ I(t)$$

where

$$I(t) = X(t) - Z(t)\cot(\alpha + \theta(t))$$

The lower part of the notch may not contribute to the distributed ice force as the bow rises above the ice surface. If the actual vertical depth of the notch exceeds the maximum defined by the draft, T, and the bow heave, Z(t);

$$[T - Z(t)] \leq I(t) \cdot \tan(34° + \theta(t)) \qquad (31)$$

then equation 30 takes the form:

$$L_1(t) = L_0 - [X(t) - I(t)] - 2/3\ [I_A(t)] \qquad (32)$$

where an active length of ice indentation is defined by:

$$I_A(t) = [T - Z(t)] \cdot \cot\ (34° + \theta(t)) \qquad (33)$$

It is assumed that the corresponding longitudinal component of the ice force will act at two-thirds of the depth of the notch. The amount of the notch actively involved in the ice interaction is again determined by the constraint equation 31. Since at any time the bow will have risen by an amount Z(t), the longitudinal force can be assumed to be concentrated at a distance Z_N below the neutral axis, given by:

$$Z_N(t) = [(Z(t) + h_A(t)) - (T - Z_{NB})] \qquad (34)$$

where $h_A(t) = (2/3)I_A\tan(34°)$ (35)

and Z_{NB} is the constant distance from the neutral axis to the ship model baseline.

The distance $Z_N(t)$ is the moment arm for the longitudinal ice force component. It will have a slightly different value at the second segment joint than at the first joint.

4.4 Magnitude of Force Components

It is assumed that the ice force is distributed over a region of the bow corresponding to the active portion of the notch, as described above. This means that a component of the vertical force (i.e. normal to the ship's longitudinal axis) will be assigned to segment one and the remainder assigned to segment two. Similarly the longitudinal force is divided between these two segments. The division of the ice force over the first two segments has been accounted for as explained below.

A simple force distribution was chosen to represent the ice force at any time. This is illustrated in Figure 4.6. Half of the force is linearly spread between the apex and the centroid; while the remainder is assumed to be linearly spread between the centroid and the base of the notch. The instantaneous location of the ice force, L_1, with respect to the first joint was previously determined and therefore the fraction of the total distribution falling into segments one and two can be estimated.

Figure 4.6

ASSUMED DISTRIBUTION OF FORCE ALONG CONTACT REGION

(a)

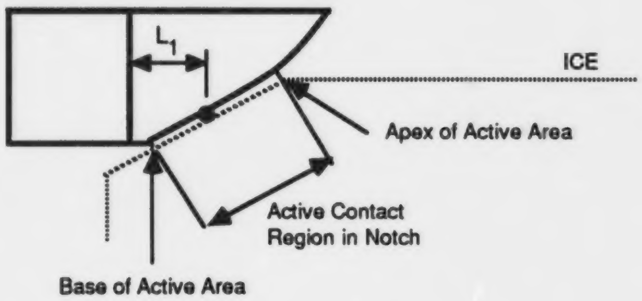

(Both vertical and longitudinal components)

(b)

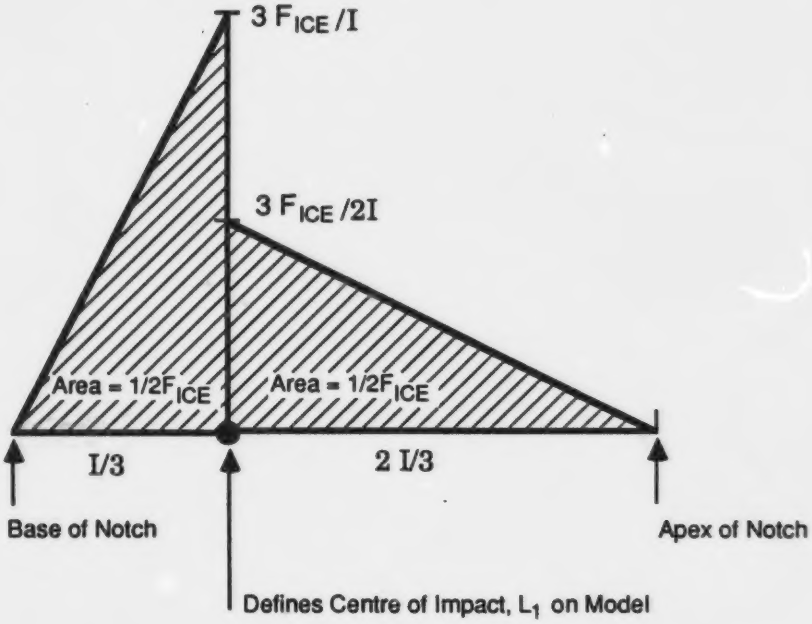

If $L_1 \geq I/3$, then all distribution on segment 1.
If $L_1 < I/3$, then part of force on segment 2.

The program checks the following constraint equations and thereby computes the forces on each segment at every time step.

Case 1: If $L_1(t) > 0$ and $(L_1(t) - I(t)/3) < 0$

In this case the centre of the force is on segment 1, but the tail of the distribution extends onto segment 2. Hence on segment 1 the vertical force is:

$$F_{ICE-VERT1} = F_{ICE-VERT} - F_{ICE-VERT2}$$

and on Segment 2:

$$F_{ICE-VERT2} = \frac{(-L_1(t) + I(t)/3)}{I(t)/3} \cdot \frac{F_{ICE-VERT}}{2} \qquad (36)$$

Case 2: If $L_1(t) < 0$

(that is the centre of the force is on segment Z), then on Segment 1:

$$FICE\text{-}VERT1 = \frac{2/3I(t) + L_1(t)}{2/3I(t)} \cdot \frac{F_{ICE-VERT}}{2}$$

and on Segment 2:

$$F_{ICE-VERT2} = F_{ICE-VERT} - F_{ICE-VERT1} \qquad (37)$$

The two longitudinal force components on segment 1 and segment 2 are given in an identical manner by the above two cases.

4.5 Segment Buoyancy Force

The buoyancy force for each segment was calculated at each time step using the apparent heave. This was expressed in terms of a reference volume displacement, ∇, at the still-water draft, T_i.

$$F_B(t) = \rho g[\nabla(Z_i(t)) - \nabla(T)] \qquad (38)$$

The volume displacement of each segment as a function of heave, $Z_i(t)$, was extracted from the MV ARCTIC section area curves. These curves were digitized from an available body plan. Hydrostatics for eight waterlines were plotted and a corresponding range of model displacements calculated for each section. A third order polynomial regression equation was fitted to this data.

For the three forward segments and the three aft segments the displacements were then calculated in terms of the polynomial coefficients.

$$\nabla(Z_i) = k_o + k_1\ Z_i(t) + k_1 Z_i{}^2(t) + k_3 Z_i{}^3(t)$$

and

$$\nabla(T_i) = k_i \qquad \text{(constants)} \tag{39}$$

Along the parallel midbody a simpler approximation could be used:

$$\nabla(Z_i(t)) = A_i \cdot Z_i(t)$$

$$\nabla(T_i) = A_i \cdot\ T_i \tag{40}$$

where A_i is the segment waterplane area. A_i varied between 0.212m^2 and 0.230m^2 over these segments.

The apparent heave, $Z_i(t)$, was based on the MST measurements of the bow heave and the measured pitch. The heave motions at subsequent segments along the model were evaluated using a bending moment correction which was described in Section 4.2. Hence the accuracy of the buoyancy difference force is limited by its sensitivity to the reliability of the MST motion measurements, as well as to the stiffness distribution assigned to the model. In equation 14 it was shown that the angular deflection of the model at a distance L along the model is given by:

$$\int_o^L (B/EI)\ dx = \theta_{DEFL} \qquad \text{(radians)} \tag{41}$$

An approximate value for the model flexural rigidity was arrived at from results of Finite Element analysis carried out concurrently (and reported in Volume 3 [12]). EI is taken as $2.0 \times 10^5\ \text{N/m}^2$ for the present calculations which gave the best approximation to the deflected shape of the model hull consistent with measurements. Integration in equation 41 made use of the 7th order polynomial fit from the shear calculation:

$$\frac{1}{EI}\left(\sum_{n=0}^{7} \frac{k_n}{n+1}\, x^{\,n+1}\right) = \theta_{DEFL}(x) \qquad \text{(radians)} \tag{42}$$

The predicted change in pitch due to model deflections calculated from equation 42 allowed computation of absolute pitch and segment heave in equation 13.

5. RESULTS OF COMPUTATION

A series of figures from Test TU-11 are presented in this section to illustrate the intermediate steps and the output from the computational process. Additional results from the selected tests are compiled in Appendix A. A typical summary page is shown in Table 5.1 listing the basic data for a test, TU-11. The nominal impact velocity in this test was 0.98 m/s, which corresponds to a ship speed of 12 knots. The ice freeboard was 0.025 meters. All of the data channels were sampled at 248 Hz, and therefore the time increment in the analysis was 0.004 seconds. The accelerometer threshold was set at 0.05 m/s^2. Results corresponding to smaller values of acceleration have not been presented in the added mass time series althouth they are included in all other computational steps. The total time of the ship-ice interaction from initial contact until back-off was 1.676 seconds. The time from initial contact until the point of maximum forward surge was 0.814 second.

Figure 5.1 shows the surge velocity and surge acceleration which were determined by successive numerical differentiations of the MST surge motion data. The ship speed was reduced from a maximum of 0.98 m/s at initial contact to zero at the point of maximum surge. Subsequently the model attained a negative terminal velocity as it slid off the ice. The corresponding surge accelerations were negative throughout the interaction; with a peak value of $-1.5 m/s^2$ at about 0.55 seconds into the impact. This means that the remainder of the impact period until maximum surge lasted about 0.26 seconds at model scale. Slide-off occupied 0.86 seconds, representing approximately one-half of the total interaction time.

Figure 5.1 also shows the division of the measured ice force into two bow forces (both normal to the longitudinal axis of the model at the bow). The two forces are applied to segment 1 and segment 2 respectively. The corresponding longitudinal force components are not shown. It was observed in this test that the force acted entirely on the first segment for the initial 0.5 seconds. Prominent peaks are observed at 0.22 second, 0.50 seconds and 0.80 seconds into the impact. This represents a ship-ice interaction force with a response mode at 3.3 Hz, although the first natural flexural mode of the model was 5.4 Hz.

The maximum peak force occurred at the instant of maximum forward surge or slide-up, and is divided between the first and second segments. However the relative magnitudes of the peaks have been shown [1] to depend on the size of the forefoot knife, and therefore the maximum force and the maximum forward surge would not necessarily coincide for other bow configurations.

TABLE 5.1

TYPICAL SUMMARY PAGE

```
MV  ARCTIC MODEL TESTS
ADDED MASS CALCULATION




TEST:          TU
RUN NUMBER:    11



NOMINAL IMPACT VELOCITY:         .98       m/s
NOMINAL SHIP SPEED:              12        kt
TIME TO MAXIMUM SURGE:           .814      s
TIME FROM IMPACT TO BACKOFF:     1.676     s



TIME INCREMENT:                   .004     s
ACCELEROMETER THRESHOLD:          .05      m/s^2



MODEL MASS:                        596     kg
WATER DEPTH:                       1.85    m
MODEL DRAFT:                       0.275   m
ICE FREEBOARD:                     0.025   m
```

FIGURE 5.1

TEST TU-11 RESULTS:

SURGE VELOCITY AND ACCELERATION TIME HISTORIES,
VERTICAL ICE FORCES ON SEGMENTS

IMPACT VELOCITY= .98 m/s
SHIP SPEED= 12.06 kt

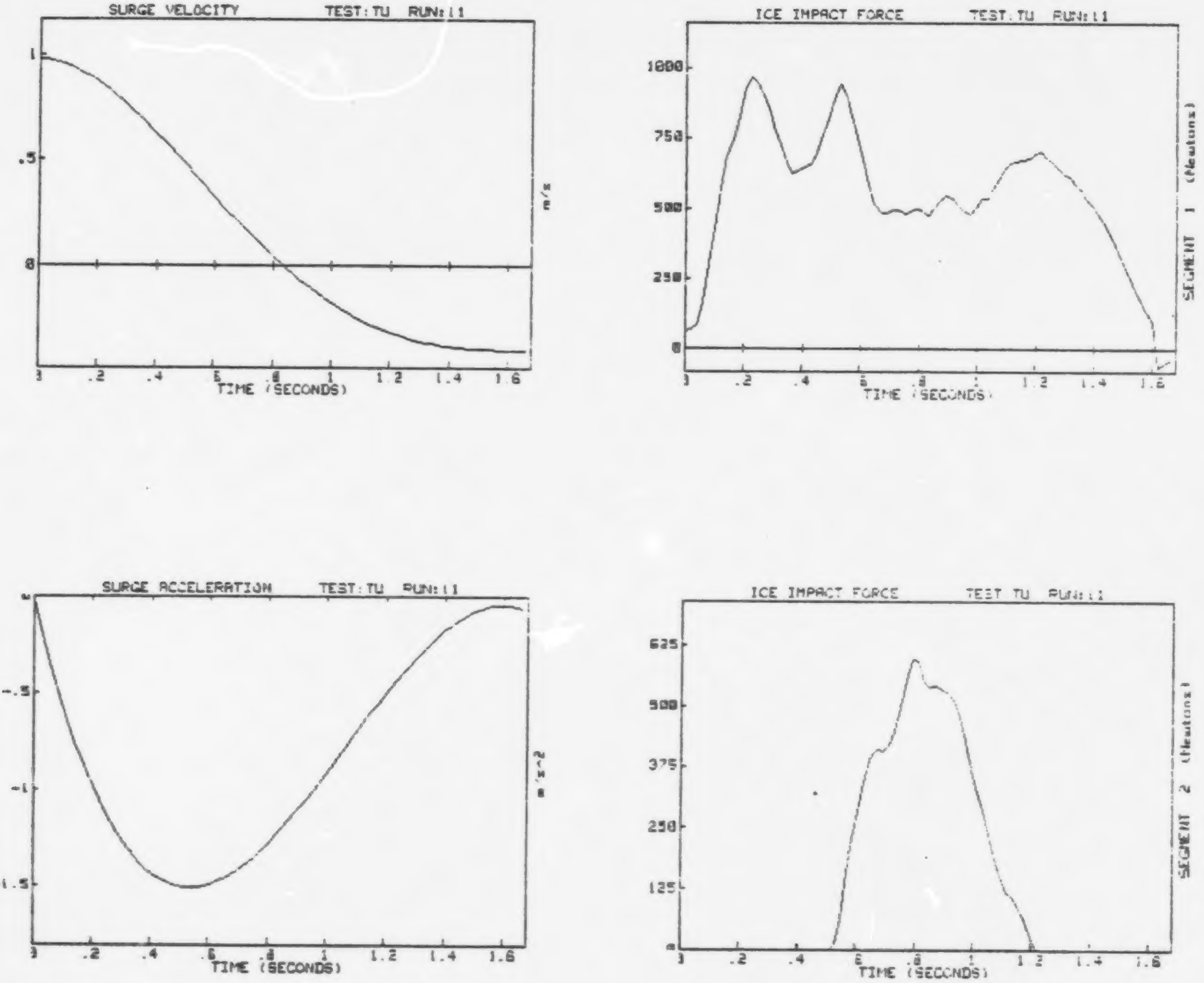

Figure 5.2 shows the acceleration time histories of each of the model segments. These accelerations are corrected for pitch and roll and referenced to a direction normal to the ship longitudinal axis. For small pitch angles they approximate the vertical accelerations. The acceleration is zero prior to the impact. It was observed that the forward segments exhibit large positive accelerations immediately after contact with the ice. This is followed by a negative acceleration peak between 0.4 seconds and 0.8 seconds, the latter time being at maximum surge. Generally smaller accelerations occurred during the slide-off phase of the interaction. A visual examination of the acceleration time history appeared to demonstrate a shift in periodicity to a frequency lower than the natural first mode frequency, similar to the shift observed in the force spectra.

The reverse trend was found for the aft segments. The initial peaks are negative due to the downward rigid body rotation and the superimposed flexural response. It should be noted that the measured acceleration was a combination of heave, rotational, forward velocity, and flexural components. The spatial change of acceleration may be viewed as a travelling wave, propagating along the model and decaying in time. Its peak magnitude decreased from a positive maximum of 2.5 m/s^2 at the bow segment to a minimum of 0.45 m/s^2 at segment 8 and then increased to an overall maximum of -3.8 m/s at the stern.

Test TU-11 had a relatively large impact velocity and therefore the measured accelerations were also large. In tests where the impact velocity was low, the accelerations were substantially reduced. For example Test TS-2 has a ship speed of 0.37 m/s. In this case a great many of the acceleration data points fell into the "noise" level, below the acceptable threshold. This problem was most acute for the middle segments which experienced the smallest accelerations.

Inertia (Body) Forces

The inertial force on each segment acts in the opposite direction to the forces causing motion normal to the model's longitudinal axis. The inertial force is given by the product of the body mass and the acceleration. Since body mass remains constant for each segment, the inertial forces in Figure 5.3 are scaled versions of the corresponding acceleration time histories, but with the sign reversed. The inertial forces were found to vary in magnitude between 15 Newtons and 120 Newtons.

Figure 5.4 shows the buoyancy forces expressed as a difference from the still water condition. Each of the time histories appeared roughly symmetric about the time of maximum surge. The seven forwardmost segments showed a monotonic decrease toward a minimum value at the maximum surge point. Segments 7 and 8 have smaller minima, and also a more noticeable positive force immediately after contact. The buoyancy force in the stern region was positive, as a consequence of rigid body rotations. In general, buoyancy force was governed by the rigid body motion, although the flexural effects were significant in the ride-up phase of the interaction.

FIGURE 5.2

TEST TU-11 RESULTS: SEGMENT ACCELERATIONS

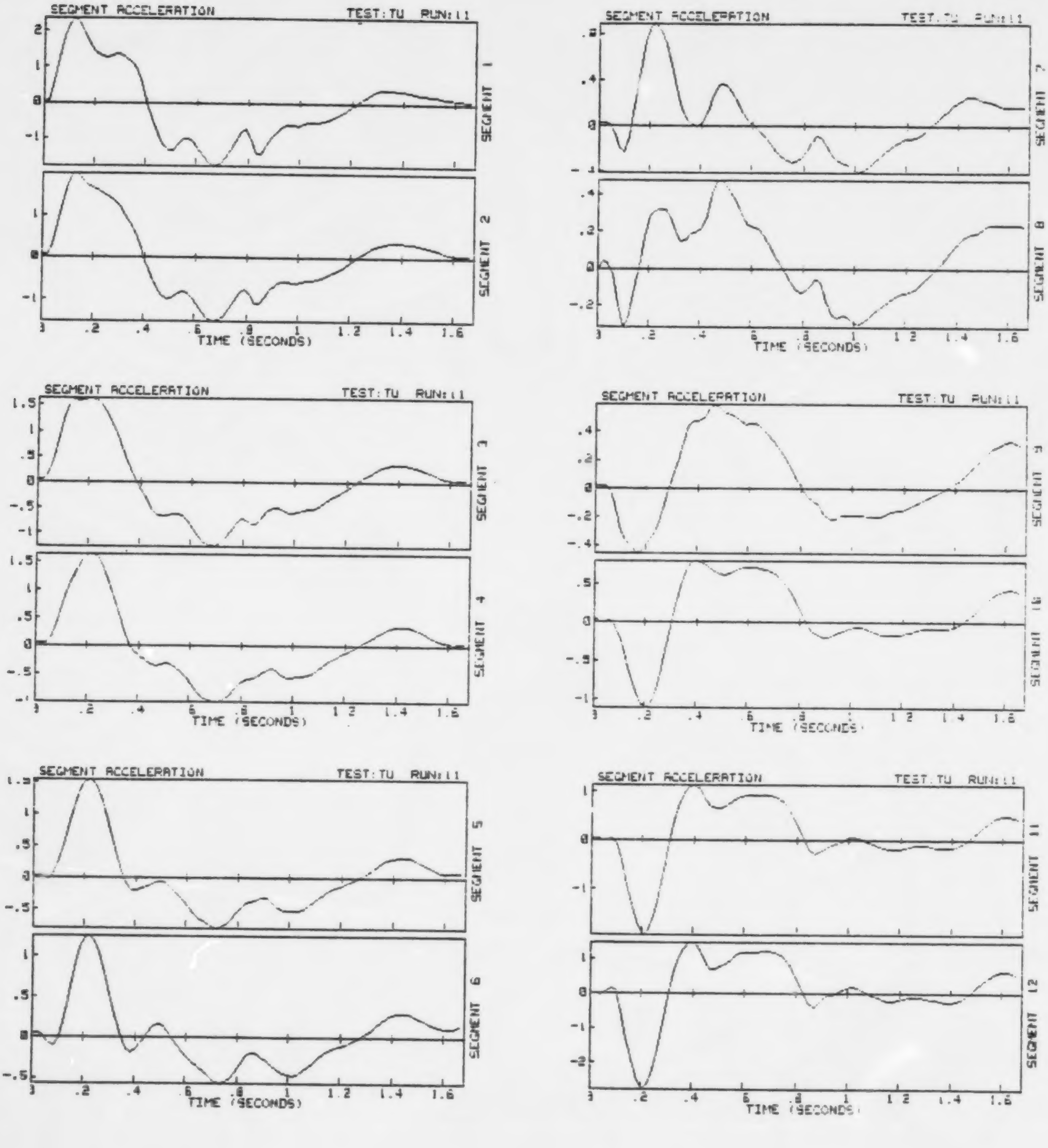

FIGURE 5.3

TEST TU-11 RESULTS:
INERTIA FORCES

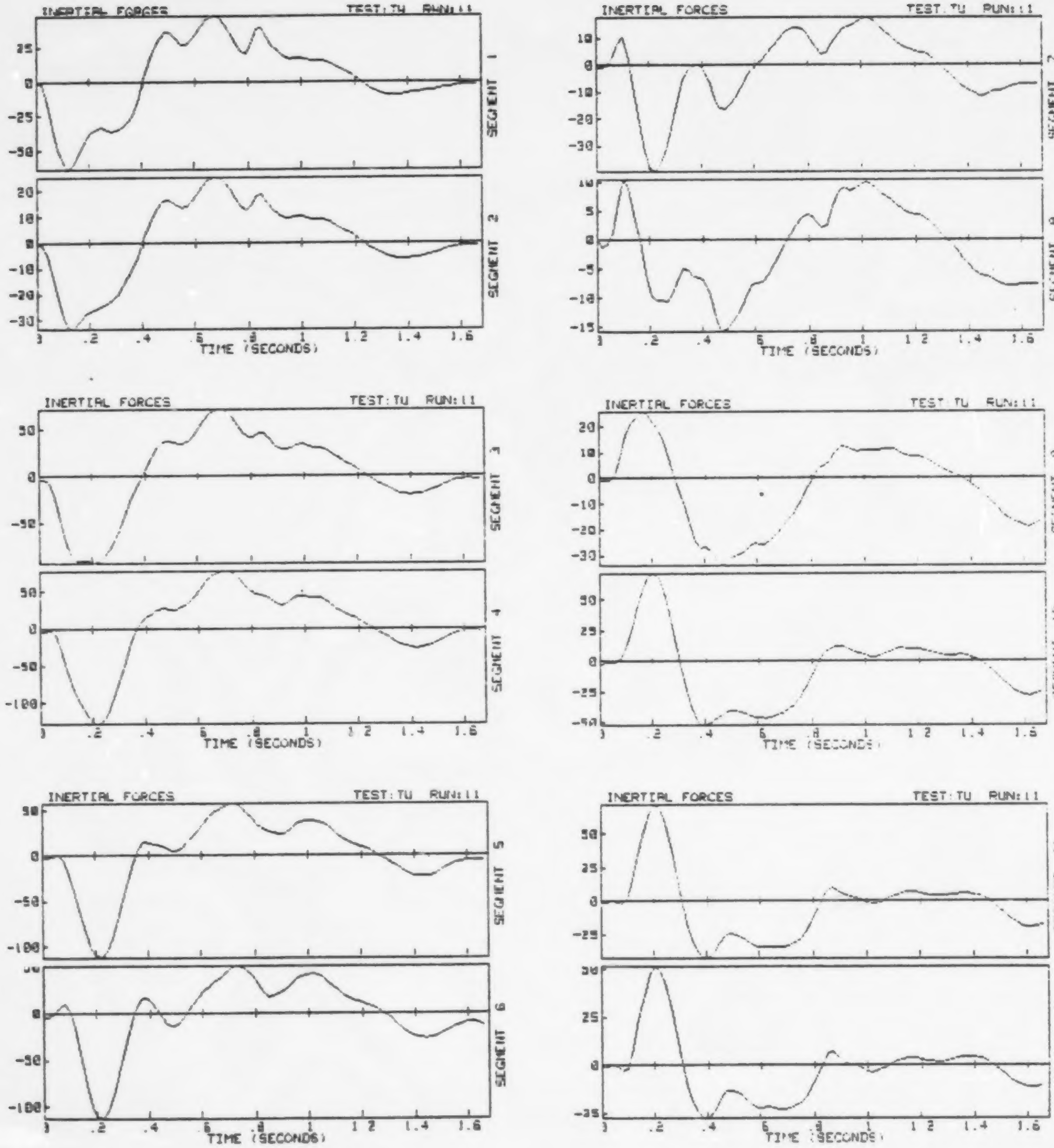

FIGURE 5.4

TEST TU-11 RESULTS:
BUOYANCY FORCES (WITH RESPECT TO THE STILL WATER DRAFT CONDITION)

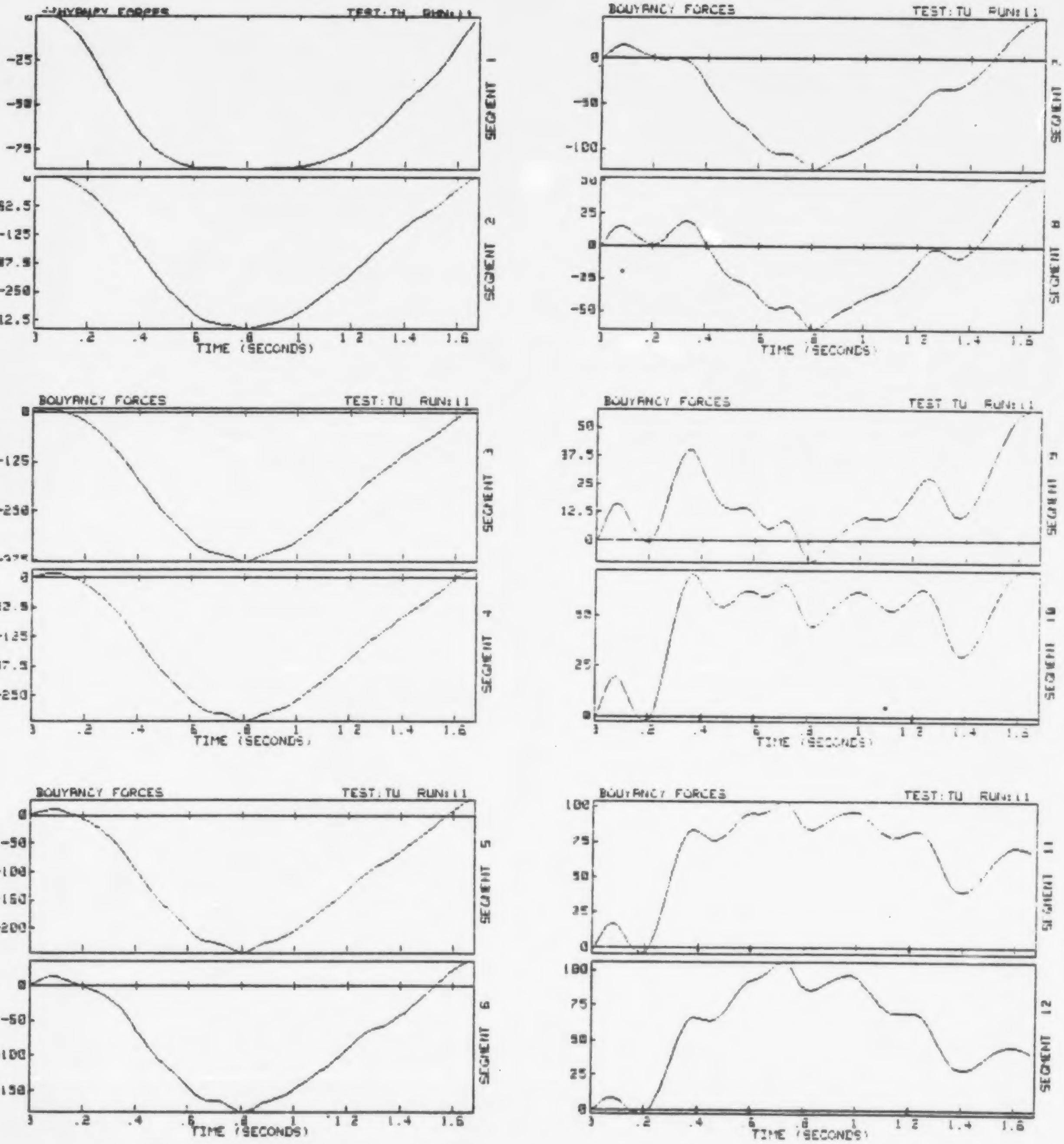

Considerable dynamic "whipping" response was noticed towards the aft segments. In part this was a natural phenomena arising from the flexibility of the structure. The ice constrained motions at the bow, whereas the stern was relatively free. However calculation of the segment heave, using pitch and heave measurements at the bow may have introduced some errors in the aft segment response time histories. The maximum amplitude of buoyancy force occurred on segment 3 and had a value of -375 Newtons. Segments 1 and 2 exhibited larger heave, but their finer section shapes mitigate in the force calculation. The smallest amplitudes are observed on segments 8 and 9. A maximum positive buoyancy force of 100 Newtons was found on segments 11 and 12.

A positive buoyancy force in the order of 50 Newtons was found to remain at the back-off point in the after segments. This was reasonable since the bow heave was zero, but the pitch had a small positive value and the heave velocities were negative. Hence, overall the model was still backing downward into the water at that time.

Shear Force

In the absence of independent shear force measurements, the segment shear force at any time is the longitudinal derivative of the bending moment distribution. Figure 5.4 shows the shear force time histories at each of the segments during Test TU-11. For all cases the segment shear was located at the aft end of the segment listed; that is, at the inter-segment joint.

The maximum amplitude of shear occurred at the bow segment. A peak value of 250 Newtons was observed at 0.2 seconds. A smaller second peak was found about 0.5 seconds and a third peak near the point of maximum surge. The trend was similar over the first four segments, but with the magnitude gradually attenuated. The remaining segments, except segment 12, showed a reversed trend. An initial maximum negative peak at 0.2 seconds was followed by a relatively steady shear level until 1.4 seconds; which then dropped to zero. The peak negative magnitudes increased from -50 Newtons at segment 5; remaining at approximately -130 Newtons from segment 7 through 10; and then was reduced at segment 11.

At segment 12 the derived shear peaks were positive, but smaller in magnitude. In fact the segment 12 shear values were located at the extreme aft end of the instantaneous waterplane. By definition the shear is zero at this point and the calculated data points were therefore considered as error values. They were subsequently compared to the corresponding ice forces and used as a correction on the shear difference forces.

FIGURE 5.5

TEST TU-11 RESULTS:
SHEAR FORCES

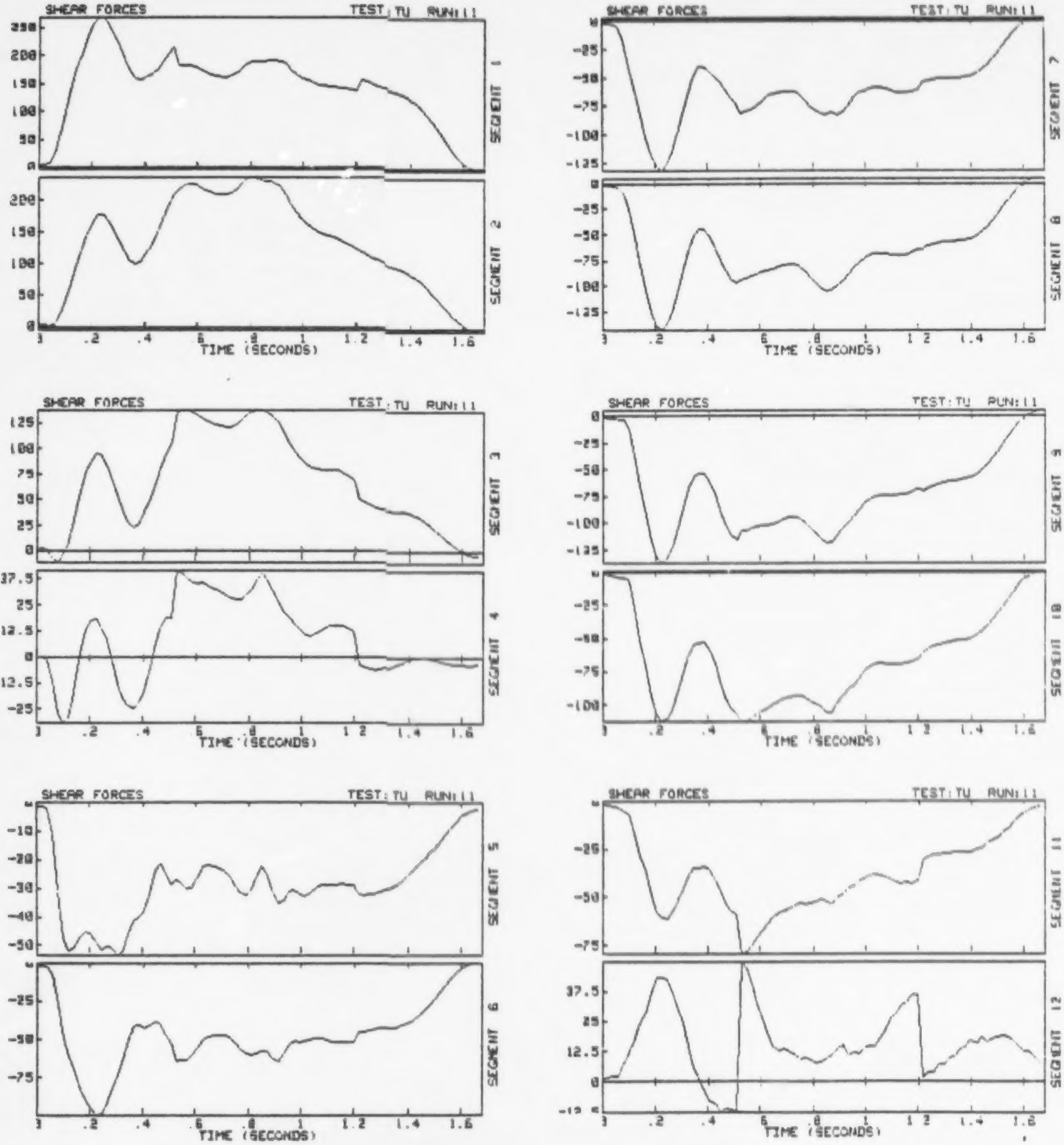

Shear Difference Forces

The shear difference across each of the segments is shown in Figure 5.6. It was assumed to act at the centre of mass of the segment numbered. The bow segment exhibited the largest magnitudes with a peak of -250 Newtons. For this segment the shear difference was simply the negative of the shear, since the forward extremity of the bow has a zero shear value. Similarly the shear difference at segment 12 was the shear at segment 11. The shear difference force at the bow segment and the aft 3 segments were negative. The remainder were predominantly positive. A similar variation was observed in all of these time histories. They showed a reduction in oscillations with time towards the end of the interaction.

Hydrodynamic Force

The summation of the inertial force, buoyancy force and shear difference (and where appropriate, the ice force) by means of D'Alembert's relation gives the negative of the net hydrodynamic force. The hydrodynamic force represents the total fluid force acting on the model segments and accounts for the effects of both added mass and damping. In the present treatment of the data, the net hydrodynamic force is taken to be associated with the hydrodynamic inertial reaction. Figure 5.7 shows these results for test TU-11.

Amplitudes in excess of 600 Newtons were observed for the bow segment. The trend parallels that of the ice force. Similarly, the positive peak at the time of maximum surge (0.8 seconds) for segment 2 reflected the ice force acting on that segment.

It is believed that this simple interpretation might conceal a number of physical interaction mechanisms. It might also reflect a failure of the extraction method to adequately resolve the shear over the bow region. This latter concern has arisen because the shear is not directly measured, but derived from the slope of the bending moment distribution. Answers to these questions will only become available if there is further experimental work with a physical model instrumented for shear.

Over the parallel midbody of the model between segments 3 and 8, the hydrodynamic force time histories appeared to be governed by the magnitude of the buoyancy force term. The trends were similar, with the former magnitudes slightly attenuated by the shear difference loading. The maximum negative peak typically occurred at the maximum surge time. Segment 3 had the largest magnitude at about -225 Newtons. The peak gradually reduced to -40 Newtons at segment 8. The trend appears to indicate that segment 2 would have had the largest peak in the absence of the ice force. The aft four segments were generally positive and smaller in value. The buoyancy force again appeared to be the most dominant effect, especially during the slide-off phase.

FIGURE 5.6

TEST TU-11 RESULTS
SHEAR DIFFERENCE FORCES

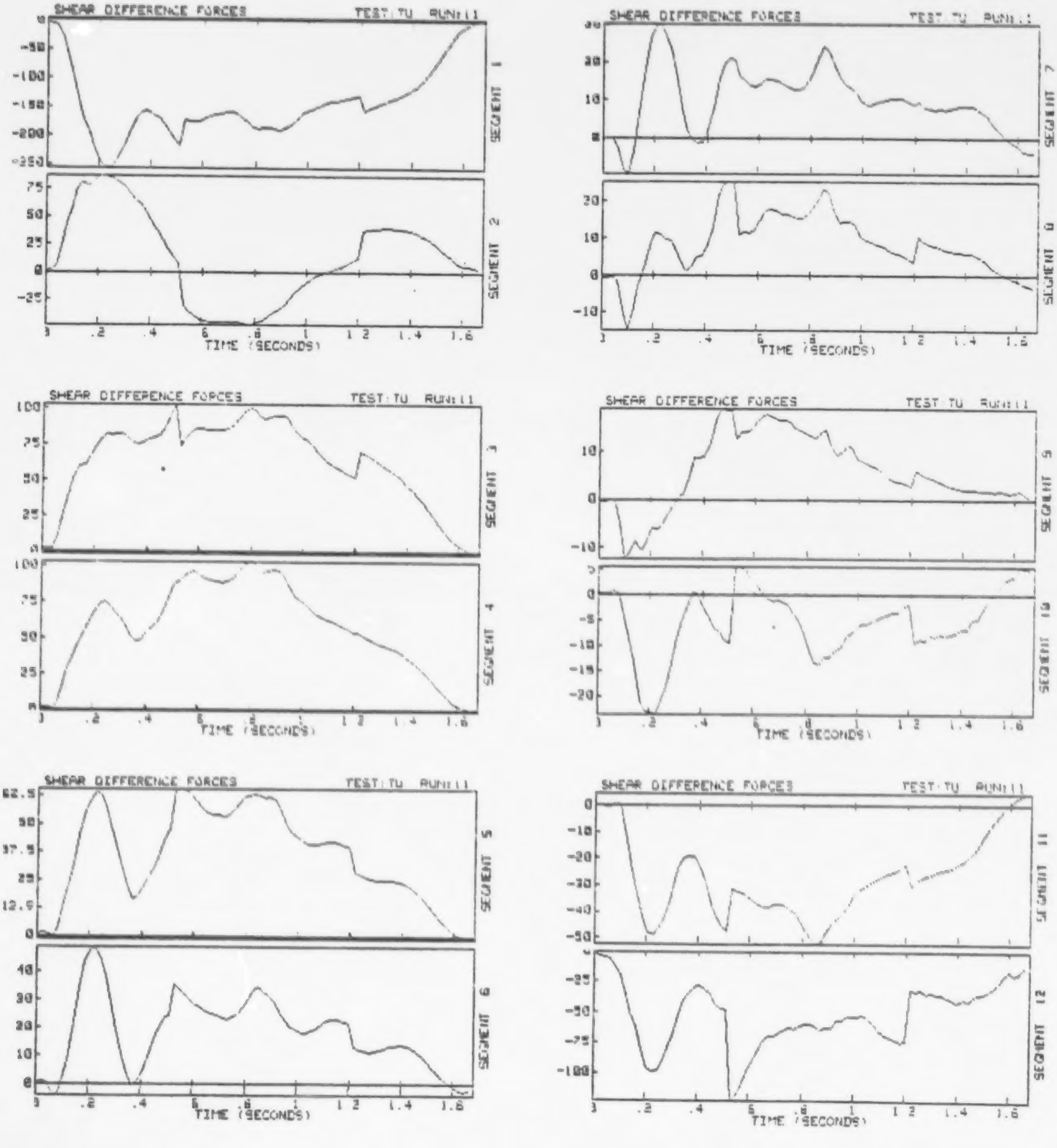

FIGURE 5.7

TEST TU-11 RESULTS:
HYDRODYNAMIC FORCE (INCLUDING ADDED MASS AND FLUID DAMPING EFFECTS)

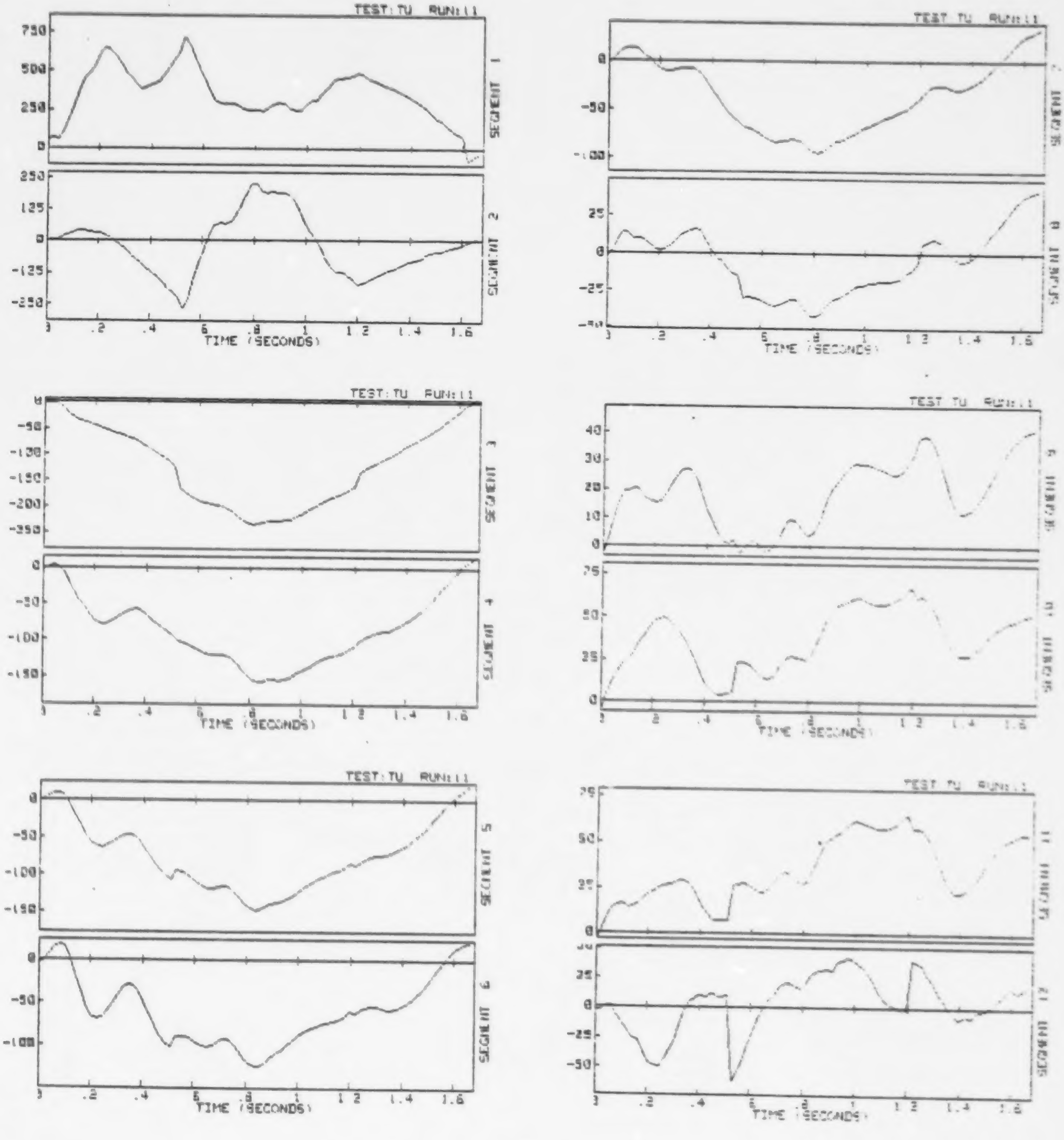

6. DISCUSSION OF RESULTS

6.1 Hydrodynamic Added Mass Time Histories

The previous section has used test TU-11 as an example in demonstrating the steps leading up to the extraction of segment hydrodynamic force time histories. Figure 6.1 presents the corresponding gross hydrodynamic added mass normalized by segment mass displacement. This is arrived at by simply dividing the total hydrodynamic force on each segment by the segment acceleration. Note that the scale of the vertical axis is necessarily different from segment to segment since the magnitude of added mass varies drastically from the bow towards the stern. The time histories are characterized by abrupt reversals of sign at acceleration zero crossings. At these singularity points the calculated added mass assumed very large values as a result of division of total hydrodynamic force by accelerations approaching zero.

One shift in sign for the forward four segments was observed at about 0.4 seconds. A second reversal occurred at 1.25 seconds. Throughout the ride-up phase and one half of the slide-off phase (0.4 - 1.2 sec.), the sign remained unchanged. Over this region the magnitude was relatively stable and showed the influence of flexural response. The four mid-segments also exhibited two major reversals of sign but with added mass magnitudes much lower than those for the forward segments. The trend was less well defined for the aft four segments, but generally similar. One apparent difference was more than two sign reversals - three for segments 9 and 10 and five or more for 11 and 12. (See time histories for segments 9, 10, 11 and 12). It is also seen that the magnitudes of added mass are the lowest for segments 9 and 10 and there is a gradual reduction in the stable range towards segment 10. For segments 11 and 12, the added mass time history is completely oscillatory and do not exhibit any discernible trend.

The assignment of a mean value to any segment or portion of a segment was rendered difficult by the sign reversals and the singularities. The results were also sensitive to changes in the acceleration threshold which was set at 0.05 m/s^2 in the analysis. Data points with acceleration values below this threshold were not included in the time history. However, it was generally observed that the magnitudes of the added mass were largest at the bow and decreased with distance aft. The smallest values were seen on segments 9 and 10. The stern showed an intermediate value.

The large values of hydrodynamic added mass for segment 1 are attributable to proximity effects (confinement and shallow water effects). The vertical ice force appeared to be the dominant influence on the bow segment, which also has the opposite trend to that of subsequent segments. A partial influence of the ice was also seen on segment 2, where it causes a gradual change in the magnitude and the sign of the added mass during the slide-off phase of the interaction. Similar trends in added mass time histories are seen in other cases studied and are included in Appendix A.

FIGURE 6.1

TEST TU-11 RESULTS:
NON-DIMENSIONAL VERTICAL ADDED MASS RATIO

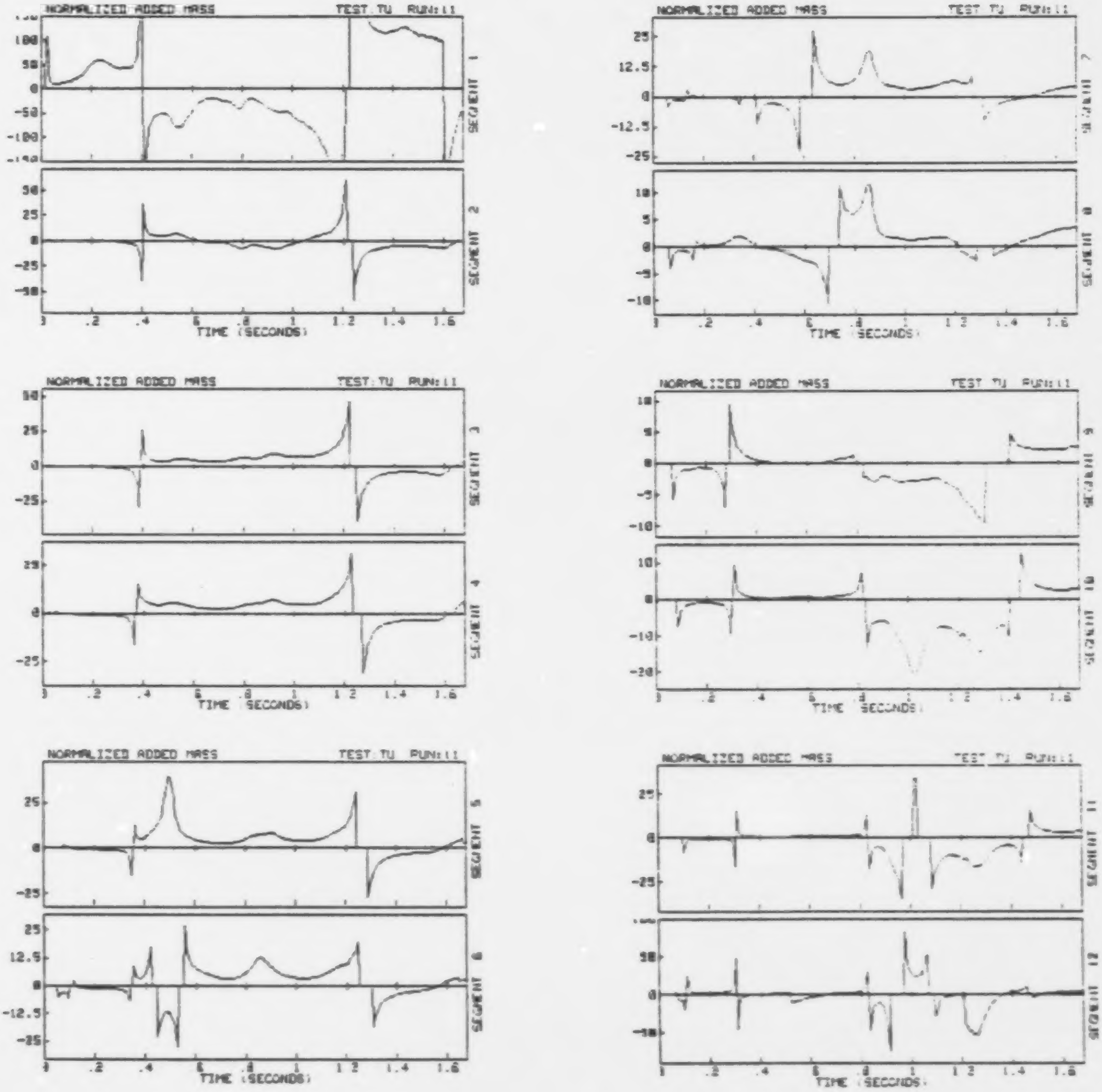

It must be noted that the non-dimensional added mass presented are computed based on a number of assumptions:

- Fluid damping is lumped together with the hydrodynamic inertia. This essentially results in large estimates for added mass coefficients.
- Each segment includes a combination of added mass effects associated with motions from various modes which are not resolved separately. For example, heave added mass should strictly be based on pure heave acceleration corrected for the effects of rotational acceleration and surge velocity:

  $$\ddot{Z}_i(t) = a_i(t) - x_i\ddot{\theta}_i(t) - \dot{x}(t)\dot{\theta}(t)$$

  However, individual segment rotations were not accurately known from the measured data.
- Three dimensional effects and the bow wave reflected off the ice feature may be important but ignored, since detailed wave profile data in a suitable form was not available for analysis.
- The hydrodynamic pressures in the impact notch governed by confinement and proximity effects are time dependent and hence the added mass due to the bow segment can be expected to dominate the fluid effects in the interaction.

The added mass distributions along the length of the hull at various instances in time are shown in Figure 6.2 for the case of test TS-6 (impact velocity = 0.24 m/s). For conciseness, only distributions 0.2 seconds apart are plotted and only non-dimensional added mass below 10 (typically at the bow segment) are shown. It is seen that initially at time t = 0.2 seconds, the added mass distribution exhibits nominal values except at the bow, where a large added mass is registered as a result of the initial indentation of the bow and the consequent reaction forces from the ice. The large magnitude of added mass is believed to be caused by the proximity effects (shallow and confined water effects). It is seen during subsequent time steps that this large peak propagates aft during which time the added mass at the bow oscillates between large positive and negative values. It is also seen that the added mass tend to assume large negative values between segments 2 and 3 (closer to 2) at a number of instances in time. This location coincides with the nodal point, where the accelerations will be zero. These large values of added mass near the node should not be extremely consequential since the hydrodynamic forces nearly vanish at the nodes.

Figure 6.2 TIME VARIATION OF MEAN ADDED MASS DISTRIBUTION

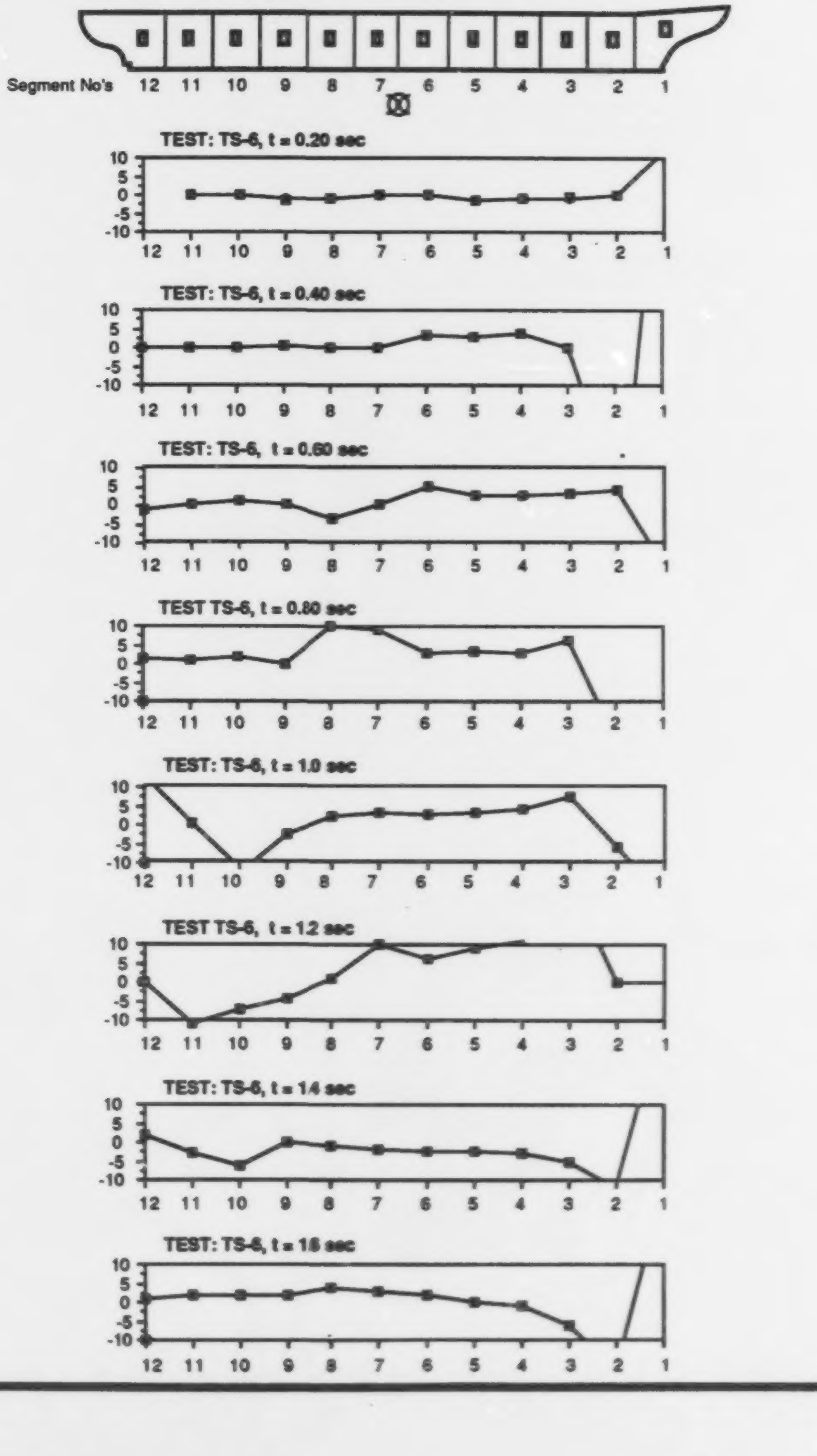

6.2 Segmental Distribution of Added Mass

Accurate measurements of bow accelerations are essential at all impact speeds. Figure 6.3 (a) lists the non-dimensional mean added mass for each segment from Test TU-11. The histogram illustrates the spatial distribution of added mass along the model. (As mentioned above (section 6.1), the added mass at the bow segment was significantly larger but was followed by a substantial reduction in magnitude as well as a reversal in the sign at the second segment. The mean added mass distribution assumed large values at segment 5 and showed a further reversal in sign between segments 8 and 9. It is believed that the calculated added mass is accurate only up to about midship. The sources of the errors further aft are the inaccuracies in the estimate of segment motions from the measured model motions at the bow. Towards the stern one would realistically expect the non-dimensional added mass to approach the open-water values as the influence of the ice feature decreases with distance from the bow segment. The first mode (two-noded flexural mode) of hull response is superimposed on the distribution. The corresponding second mode shape (three-noded flexural mode) is shown by the broken line. On comparing the added mass distribution with the first and second mode shapes, it is seen that there is a sign reversal of added mass in the neighborhood of the first node of the second mode shape. Figure 6.3(b) shows a slightly different distribution of the mean segmental added mass. Although the magnitudes are somewhat different, the trends with zero-crossing tendencies appear to be similar. Between segments 2 and 3 complete sign reversal did not occur, but a substantial reduction in the magnitude is indicated. Further aft, around segment 8 added mass decreases substantially and results in a sign reversal. This trend in the added mass distribution is exhibited in a number of other cases studied.

The distribution of the mean segmental non-dimensional added mass from all the ten tests are shown in Figure 6.4. Note that test TG2 involved a modified bow, and hence is not directly comparable with the other ten. In almost all these cases with the exception of Tests TU11 and TU12, (which were depicted earlier in Figure 6.3 (a) and (b), the added mass at the bow segment registered large negative values.

6.3 Velocity Dependence of Results

The principal results of the computational process are presented in the form of a set of time histories. In each case the hydrodynamic forces and the corresponding added mass ratios on the segments are given. The results are summarized in order of increasing speed although Tests TR-8 and TT-10 have velocities very similar to TS-2 and TU-11 respectively. (Table 6.1 and 6.2).

FIGURE 6.3

MEAN NON-DIMENSIONAL ADDED MASS

a) TEST: Tu 11

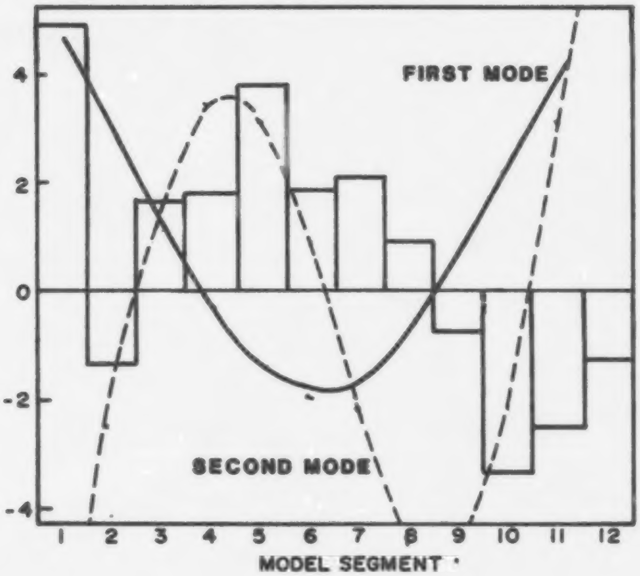

b) TEST: Tu 12

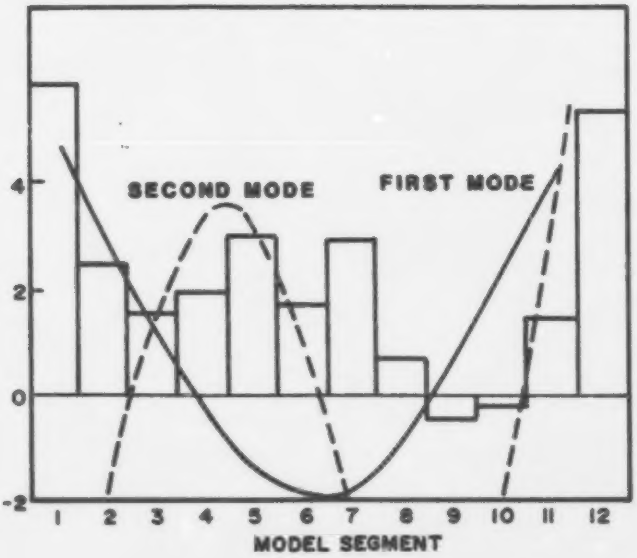

FIGURE 6.4

SEGMENTAL DISTRIBUTION OF MEAN ADDED MASS

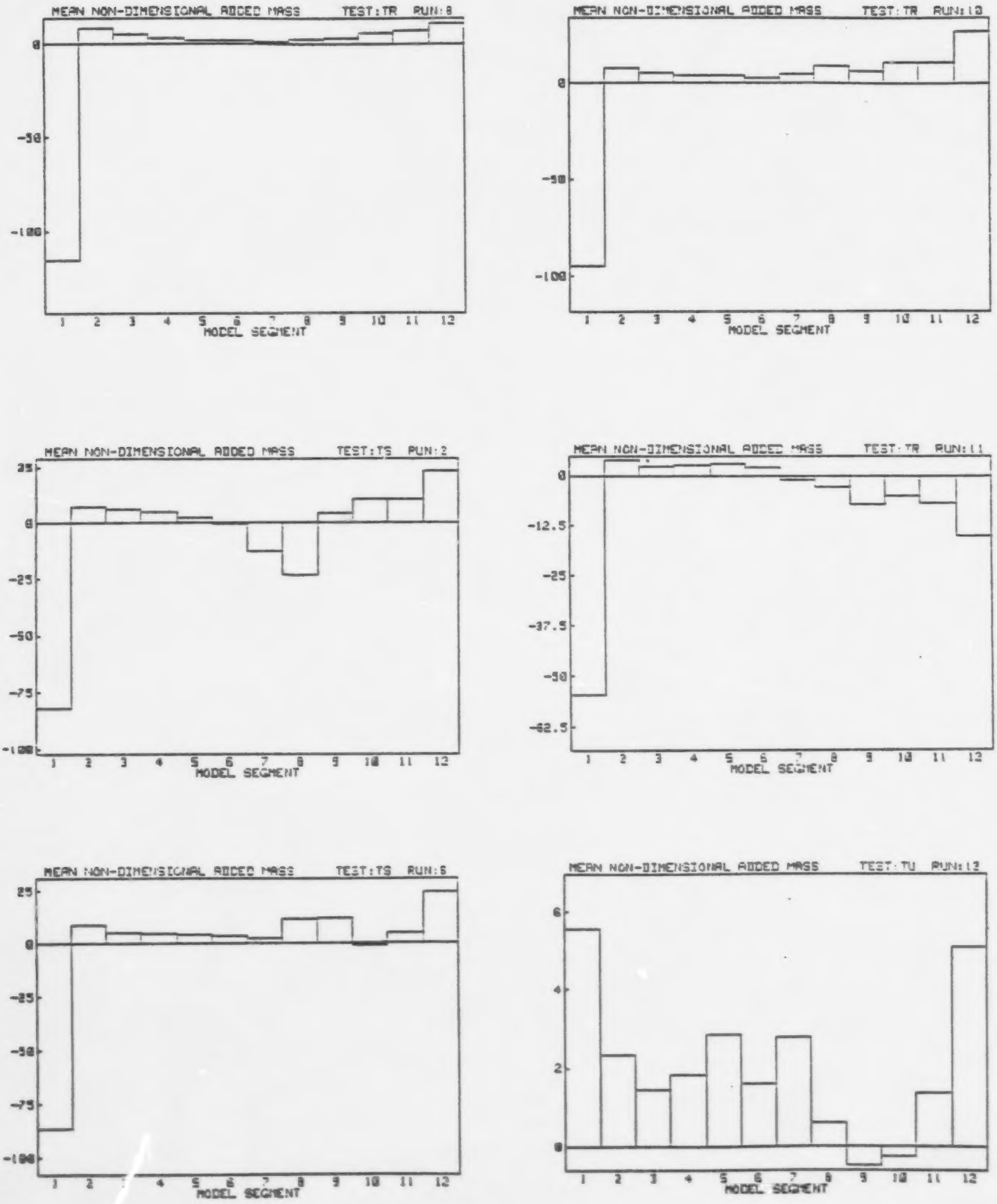

FIGURE 6.4 (continued)

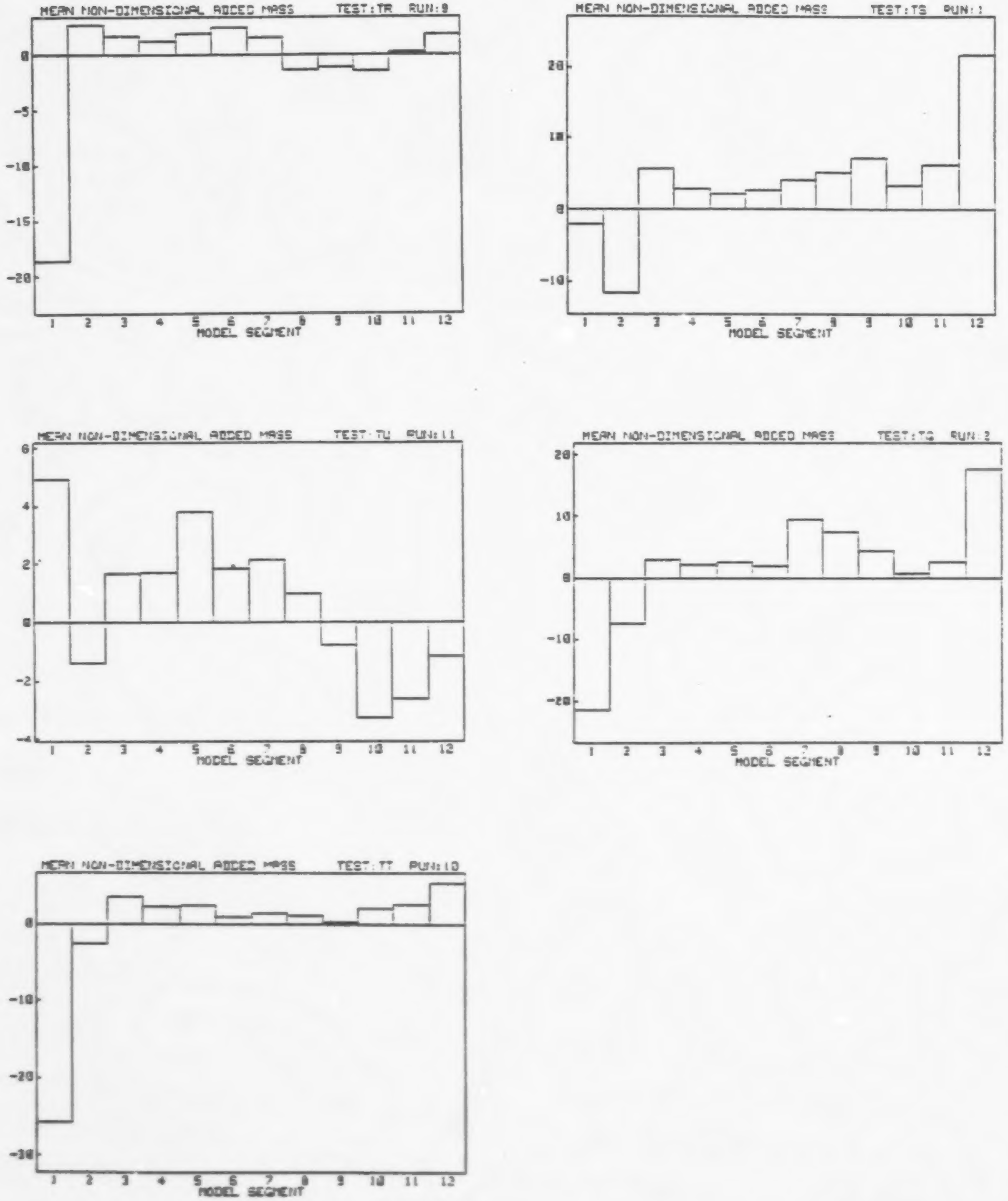

It was pointed out earlier that due to low levels of acceleration the computation of added mass of the aft segments is severely curtailed for tests involving low impact velocities. More than one half of the data points have been excluded as a consequence of acceleration data less than the threshold value. The different tests also exhibit singularity peaks associated with acceleration zero crossings, as observed for Test TU-11 in the preceding sections.

Mean segment added mass as well as the entire motion and force data sets have been tabulated for each test case in Appendix A. Table 6.1 and 6.2 compute the mean values of the segment hydrodynamic inertial force and added mass respectively for the selected tests. The cumulative mean values over the entire model are also given. It was found that ship speed affected the results, but the large standard deviations obscured meaningful quantitative assessment of trends. However, a qualitative description of distribution of means of the hydrodynamic inertial force along the model has provided a number of insights. In particular the slope of the force curves along the parallel midbody appear to increase as a function of ship speed. They occupy a range of about 100 Newtons which spreads out with negative values forward of Segment 7 and positive values aft. The higher speeds tend towards the extremes. At the bow segment the hydrodynamic inertia force has a positive peak which increases with ship speed. The effect is spread onto the second segment at higher speeds. The aft values are positive and typically reduced from the local maxima at segments 10 or 11. On the other hand the added mass cumulative mean over all segments does not show any trend with ship speeds.

There was an apparent variation in the hydrodynamic force trend between the model configurations with and without the forefoot knife. The test case with the forefoot knife showed larger hydrodynamic inertial forces over the aft segments. This may have been an artifact of the uncorrected motions data in this test. On the other hand, it may have been a consequence of the greater whipping response at the stern that is observed with the forefoot knife present. The preliminary results have shown the need for further tests and analysis to assess the influence of bow geometry.

The mean segment added mass obtained in the selected tests exhibit large standard deviations as a result of singularity peaks and sign changes at acceleration zero crossings. This error is compounded in low velocity tests by the large number of data points excluded by accelerations less than the threshold value. This problem is greater for segments near amidships. Hence it was not found meaningful to use the mean added mass over the entire interaction period as an indicator of hydrodynamic effects in transient ship-ice interaction.

TABLE 6.1

SEGMENTAL DISTRIBUTION OF TOTAL HYDRODYNAMIC FORCE

TEST	TS-6	TS-2	TR-8	TR-10	TR-11	TU-12	TR-9	TU-11	TT-10	TS-1	TG-2*
VEL. (m/s)	.24	.37	.37	.58	.67	.73	.86	.98	1.03	1.14	1.12
SEGMENT	MEAN (N)	MEAN (N)	MEAN (N)	MEAN (N)	MEAN (N)	MEAN (N)	MEAN (N)	MEAN (N)	MEAN (N)	MEAN (N)	MEAN (N)
1	67.2	160	149.8	192.5	239.9	322.4	367.5	343.8	290.7	292.1	212
2	-24.5	-57.4	-42.5	-62	-83.6	-99.8	-123.2	-20.8	13.4	137.1	88.4
3	-20	-58.4	-35.2	-48.5	-84.2	-80.4	-91.2	-119.8	-112.4	-116	-96
4	-8.6	-48.5	-23	-29.8	-85.5	-61.4	-64.3	-85.3	-72.8	-62.9	-46.6
5	3.5	-41.4	-16.5	-19.1	-98.7	-51.4	-56.2	-73.8	-58.4	-37.5	-18
6	14.2	-33.5	-9.8	-5.1	-107.8	-36.8	-44.4	-59.3	-40.8	-12.3	23.2
7	26.1	-22.9	-.6	12.5	-109.2	-13.6	-26.1	-35.7	-12.6	25.4	73.2
8	36.8	-10.2	10.4	31.8	-107.1	11.3	-3.3	-5.4	18.7	67.9	124.5
9	46	-.8	21.5	45.9	-105.3	30.5	17.4	18.8	45.2	102.2	157.1
10	62.3	6.2	34.2	64.8	-123.3	45.5	33	37	72	139.9	187.1
11	58.9	12.5	31.5	62.5	-96.6	42.2	30.5	34.8	68.9	136.1	169.6
12	28.7	5.9	-.9	35	-69.8	21	13.9	3.6	35	104.6	182

Note: *Original MV ARCTIC Bow Geometry

TABLE 6.2

SEGMENTAL DISTRIBUTION OF NON-DIMENSIONAL ADDED MASS

TEST	TS-6	TS-2	TR-8	TR-10	TR-11	TU-12	TR-9	TU-11	TT-10	TS-1	TG-2*
VEL. (m/s)	.24	.37	.37	.58	.67	.73	.86	.98	1.03	1.14	1.12
SEGMENT	MEAN	MEAN	MEAN	MEAN	MEAN	MEAN	MEAN	MEAN	MEAN	MEAN	MEAN
1	-86.5	-81.9	-114.9	-94.7	-54.7	5.6	-18.7	4.9	-25.8	-2.1	-21.4
2	9.0	7.6	9.0	7.8	3.8	2.3	2.7	-1.4	-2.7	-11.7	-7.4
3	5.0	6.2	5.8	5.4	2.2	1.4	1.7	1.7	3.6	5.7	2.9
4	4.9	5.2	3.8	4.2	2.6	1.8	1.3	1.7	2.2	2.9	2.2
5	4.0	2.3	2.5	3.9	3.0	2.8	2.0	3.8	2.3	2.1	2.5
6	3.3	-.4	1.9	2.6	1.9	1.6	2.4	1.8	0.9	2.7	2.0
7	2.3	-12.7	1.3	4.4	-1.0	2.8	1.6	2.1	1.5	4.1	9.5
8	11.7	-23.7	3.1	8.8	-2.9	0.6	-1.3	1.0	1.1	5.1	7.5
9	12.1	4.5	3.3	6.4	-7.1	-.5	-1.1	-.8	0.3	7.0	4.3
10	-1.1	10.9	6.1	10.9	-5.0	-.2	-1.4	-3.3	2.0	3.4	0.7
11	4.8	10.9	7.4	10.8	-6.8	1.3	0.3	-2.6	2.6	6.2	2.5
12	24.7	23.0	11.3	27.2	-15.0	5.1	1.8	-1.2	5.3	21.7	17.5

Note: Non-Dimensional added mass with respect to segment mass displacement.
* Original MV ARCTIC Bow Geometry.

A general trend in the distribution of the effective added mass along the model may be based on six of the tests. Neglecting the lower speed tests reduced the amount of scatter due to the acceleration threshold. The non-dimensional added mass was found to average -4.0 at the bow and at the second segment. It may be concluded that this was associated with confinement effects. Over the remaining 9 segments the ratio averaged 2.3. A division of the segment added mass time histories into selected time intervals corresponding to different phases of the interaction would be a useful next step in this analysis. This would provide discrete added mass values for the initial contact, ride-up, and slide-off phases.

A valid frequency domain assessment of the added mass results has not been attempted at this time, largely because added mass and damping have not been separated. In addition, the smoothing of the pitch data and the corresponding segment-by-segment calculation of heave and buoyancy values will have distorted the frequency content of the added mass time histories. Nonetheless it would be advantageous to have frequency or mode shape dependent added mass and damping data for the transient impact case to compare with experimental data obtained in the dry mode and wet mode oscillation tests. This could be achieved by Fourier analysis of the hydrodynamic force and each segments' corresponding acceleration time histories.

6.4 Observations

In the course of implementing the added mass extraction procedures it was observed that a number of factors significantly affected the results:

- The accuracy of the bow motions was dependent on the resolution of the six coupled motion channels measured by the MST system.

  It was seen that the uncoupling process introduced small errors in the pitch, heave and roll respectively. The measurement errors at the bow segment were thought to be less than five percent. As such they would not constitute a significant source of error in the calculation of the first segment buoyancy; nor in the correction of the acceleration measurements to account for roll and pitch. However, the initial errors in the bow pitch and heave were amplified at segments further aft, since the segment-by-segment extrapolation of heave depended on the bow motions and an assumed model stiffness. Although the buoyancy force time histories at the stern segments appeared reasonable, there was concern that the frequency content had been distorted by the extrapolation process and by the required smoothing of the pitch data. An independent set of motion measurements at each segment would be one way to avoid this step-by-step accumulation of error.

- Shear difference time histories were calculated from the measured bending moment distributions via the shear distributions derived at each time step. The magnitude of the shear difference at each of the parallel midbody segment was not sensitive enough to account for ice effects at the bow. Modifications included bending moment corrections for the influence of the longitudinal ice force and for the portion of the bow mass forward of the ice force. The location and distribution of the ice load were approximated from the measured model motions. It was assumed that the force was equally divided with respect to the centroid between the base region and apex region of the instantaneous impact notch. Shear values for the first, second and twelfth segment were observed to change as a consequence of these corrections. Generally the trends in added mass were unchanged, although the magnitudes were substantially altered.

- A noticeable repercussion of the inexact location and distribution of ice loading is that the distinction between segment 1 and segment 2 results was blurred. In addition the ice force was shown to be the dominant influence on the bow segment added mass. This was shown by the reflection of the ice loading time histories in the corresponding hydrodynamic inertial force time histories. These latter forces are very large, suggesting that there are large added mass or damping effects associated with the presence as well as interaction with the ice in the notch region. It has not been possible from the data, to identify the mechanisms involved in this process, although it is thought that ice removal, friction, notch confinement and proximity effects have significant influence on the calculated added mass.

- A limited amount of wave profile data was available on video and high speed camera. This was used to visually examine the bow wave associated with the surge deceleration. The wave profile constituted a small departure from the segment buoyancies calculated on the basis of model motions, and has been considered a second order effect in this study.

- The vertical and horizontal ice force components exhibit a gradual increase in magnitude over the 0.25 second interval prior to ship-ice contact. At higher impact velocities the magnitudes of these forces approached 100 Newtons, or about 10 percent of the typical peak ice force. This force may have been caused by the influence of the water surface depression in advance of the bow wave acting on the force balance. However results from separate tests in which the model was stopped prior to contact with the ice did not reproduce this effect. Nonetheless this error may be considered small in view of the overwhelming importance of the ice force on the bow's hydrodynamic inertial force.

- It also remains a possibility that some computed shear data may have resulted in significant errors in the observed hydrodynamic inertial forces on the bow. This concern could not be addressed, since there was no direct shear measurements included in the existing data sets. A physical model with a shear instrumentation system, or redundancy between shear and bending moment sensors, would be helpful in resolving this question and assessing the extent of error in the methodology.

- Added mass and fluid damping effects have been lumped together in this study. Structural damping is incorporated within the shear difference loading and therefore has not been assessed. An iterative procedure to isolate the two hydrodynamic components has been proposed, but has not been attempted in the current study. This would involve a determination of an optimum pair of added mass and fluid damping coefficients for each segment from a matrix of possible combinations. The root mean square of the difference between the hydrodynamic inertial force and the sum of the ship speed and acceleration dependent components will be minimized over the time interval selected.

7. CONCLUSIONS

7.1 Overview

A time domain analysis of data obtained from ramming tests with a segmented MV ARCTIC model has been carried out. This involved an assessment of a number of data sets which resulted in the selection of 12 tests for subsequent study. An added mass extraction procedure was developed which involved a dynamic balancing of all vertical forces acting on each segment of the model. The procedure was implemented on an HP 9816 computer system and the test cases analyzed. The method developed is unique in that a time domain approach to the problem has not been attempted in the past and hence no comparable reference has been found to correlate or validate the results (see Volume I). The sensitivities of the procedures to a number of factors have been assessed and refinements suggested in several areas. The principal findings and weaknesses of this study are summarized below.

7.2 Inference from Results

1. It has been possible to obtain time histories of the total hydrodynamic force from the existing model test data. From this, hydrodynamic added mass was determined assuming that hydrodynamic damping effects are negligible.

2. The results have shown that the added mass may be expected to assume values much larger than the mass displacement over the interaction period. Generally the largest added mass effects are observed at the bow. This is believed to be associated with the proximity and confinement influence of the ice, since the magnitude of the hydrodynamic inertial force at the bow segment parallels the ice force time history. The magnitudes of added mass are typically reduced at segments further aft along the model.

3. The trends in the results are relatively well defined for the hydrodynamic inertial force. However the trends in the added mass are obscured by the small magnitudes of segment accelerations and acceleration zero crossings which result in large computed added mass both positive and negative.

4. The results indicate clearly that the consideration of added mass in the extraction of loads from response data is complex, and that traditional approaches in which added mass is considered as being time independent are not adequate. The phenomenon has been shown to be a local one, with large and negative values occurring. Thus the project has as planned provided a greater understanding of the phenomenon, and indicated where caution must be used in the interpretation of the impact process. It has also shown where further investigation is required.

7.3 Observed Weaknesses and Possible Improvements

1. Several limitations in the present experimental data were observed. If experimental programs were designed specifically to obtain appropriate data for extracting added mass distributions, then several improvements in experiment design would be recommended as follows:

   ° the direct measurement of shear at the segment interfaces to provide this information directly, rather than by deduction from bending moment.

   ° a more accurate motions measurement system, preferably allowing an independent measurement set for each segment.

   ° direct measurement of the centre of action of the ice forces. This would entail resolving forces and moments accurately in all six degrees of freedom.

   ° improved wave profile data from relative motion sensors mounted both on the model segments and on the ice block. The latter measurements would allow assessment of ice load measurement errors due to changes in ice block buoyancy.

2. The difficulty encountered in determining the influence of ship speed on the added mass could be alleviated by increasing the number of test cases considered to an adequately larger number. In addition the total period for the overall interaction could be divided into a number of intervals corresponding to the different phases in the hull-ice-interaction process.

3. Frequency domain values of added mass have not been calculated in this study, because separate time histories of added mass and damping could not be derived. An alternative approach involving normal modes and Fourier transforms may be used for this purpose. This would provide a means of linking the present time history analysis to parallel experimental data obtained from dry mode and wet mode tests.

4. A further separation of the two components of the total hydrodynamic force has been proposed using an iterative search procedure. This would result in a pair of time histories representing the hydrodynamic coefficients (added mass, damping) for each test.

The hydrodynamic inertial force $F_{HI}(t)$, is determined at each time step for each segment. In addition both the apparent heave velocities and the segment accelerations are known. The added mass coefficient and damping coefficient can therefore be found by solving the following equation:

$$F_{HI}(t)_i = m_{ia}(t)Z_i(t) + c_i(t)Z_i(t)$$

Since there are two unknowns and only one equation, it is not possible to solve the above equation directly. However if at successive time steps the expressions are independent, then an adequately accurate solution becomes possible provided the time steps are sufficiently small. It has not been possible to implement this method in the present task, but would be a logical next step in the future.

REFERENCES:

[1] Continuation of Parametric Model Study of M.V. ARCTIC Hydroelastic Response During Multi-Year Ice Impacts, Volume I - Methodology and Results, ACL Report FR 1942C, TP#7976E, August 1986.

[2] Daley, C.G., Phillips, L.P., Parametric Model Study of MV ARCTIC Hydroelastic Response During Multi-year Ice Impacts, Transport Canada Report TP6536E, 1985, submitted by Arctec Canada Limited.

[3] Riska, K., Daley, C.G. Physical Modelling on Ship/Ice Interaction. Report 1 of the Joint Research Project Arrangement III. Submitted to Transport Canada, 1986.

[4] Canarctic/NS&E, Test Ice for Dedicated Tests, MV ARCTIC 1984, Vol. 1 [illegible] 2, Transport Canada TP6270E, by Norland Science and Engineering Limited, 1984.

[5] Melville/VTT, MV ARCTIC Dynamic Exciter Tests, Transport Canada TP5891E, by Melville Shipping Limited and Technical Research Centre of Finland, 1982.

[6] G&M/VTT, MV ARCTIC Dedicated Field Tests, Test Results and Analysis, Transport Canada TP6207E by German and Milne Inc. and Technical Research Centre of Finland, 1985.

[7] Canmar, KIGORIAK and ROBERT LEMEUR 1983 Ice Impact Tests, Refinement of Model Ship/Ice Interaction Energies. Transport Canada TP6813E by Canmar Marine Drilling Limited, 1985.

[8] Popov, J.N., Kheisin, D.Ie., Ice Navigation Qualities of Ships. CRREL Translation 417, 1973.

[9] Vaughan H., Flexural Response of Icebreaking Ships to Impact Loads, RINA, 1986.

[10] Hakala, M.K., Application of the Finite Element Method to Fluid Structure Interaction in Ship Vibrations, VTT Report, 1985.

[11] Investigation of the Added Mass Phenomenon with a Flexible Model of the M.V. ARCTIC: A Review of Existing Methods, Available Data and Summary of Experimental Results, prepared for TDC by Arctec Canada Limited, March 1987.

[12] Investigation of the Added Mass Phenomenon with a Flexible Model of the M.V. ARCTIC: Model Experiments in Open Water and In Ice, prepared for TDC, by Arctec Canada Limited, March 1987.

APPENDIX A

TEST DATA AND RESULTS

MV ARCTIC MODEL TESTS
ADDED MASS CALCULATION

TEST: TR
RUN NUMBER: 8

NOMINAL IMPACT VELOCITY:	.38	m/s
NOMINAL SHIP SPEED:	4.7	kt
TIME TO MAXIMUM SURGE:	1.056	s
TIME FROM IMPACT TO BACKOFF:	2.141	s

TIME INCREMENT:	.004	s
ACCELEROMETER THRESHOLD:	.05	m/s^2

MODEL MASS:	596	kg
WATER DEPTH:	1.85	m
MODEL DRAFT:	0.275	m
ICE FREEBOARD:	0.025	m

SEGMENT ADDED MASS NORMALIZED BY DISPLACED MASS

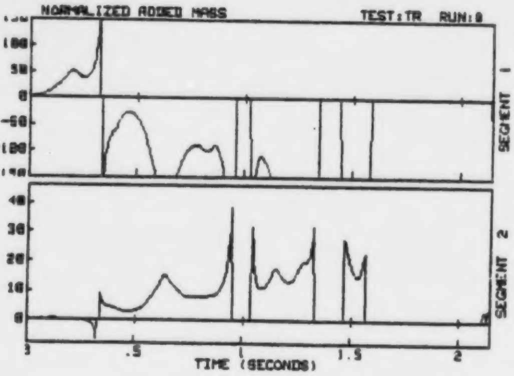

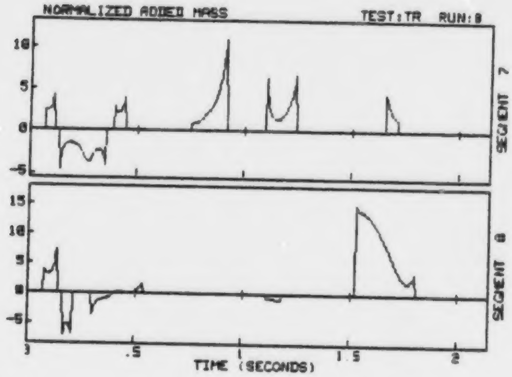

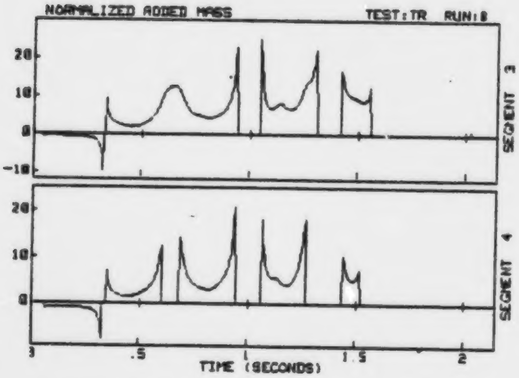

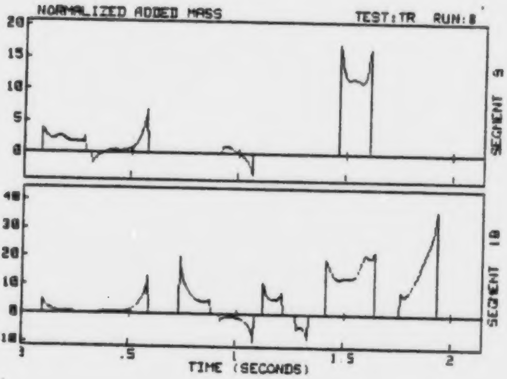

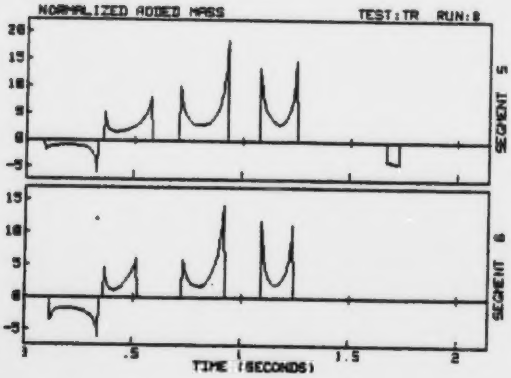

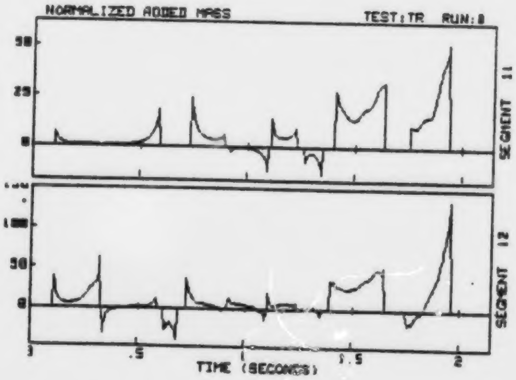

SEGMENT HYDRODYNAMIC FORCE

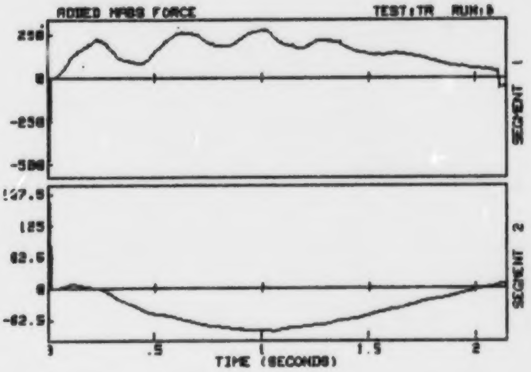

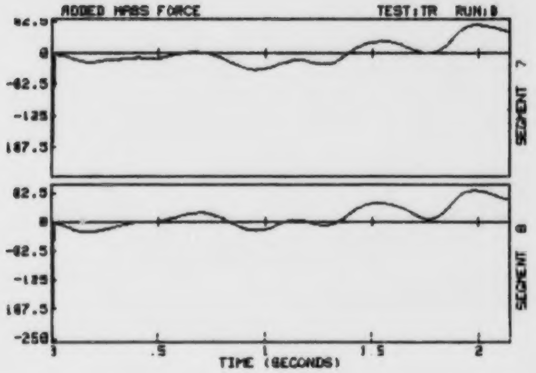

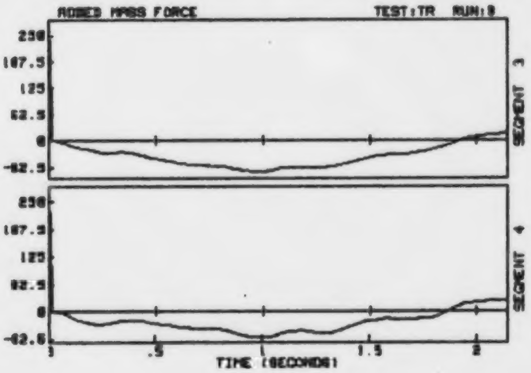

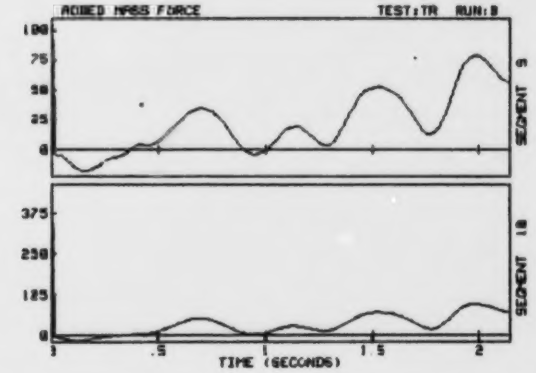

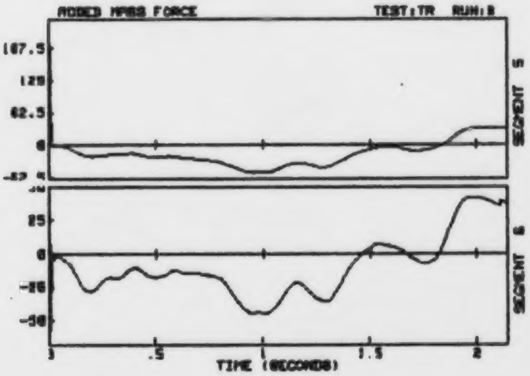

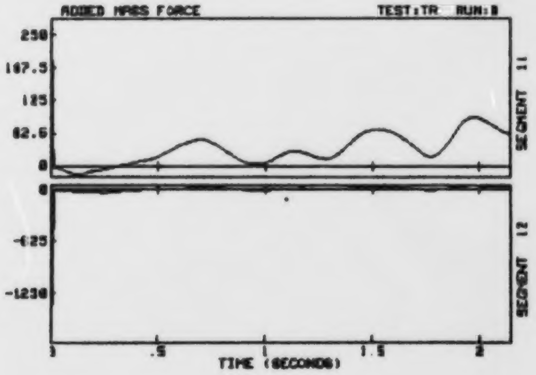

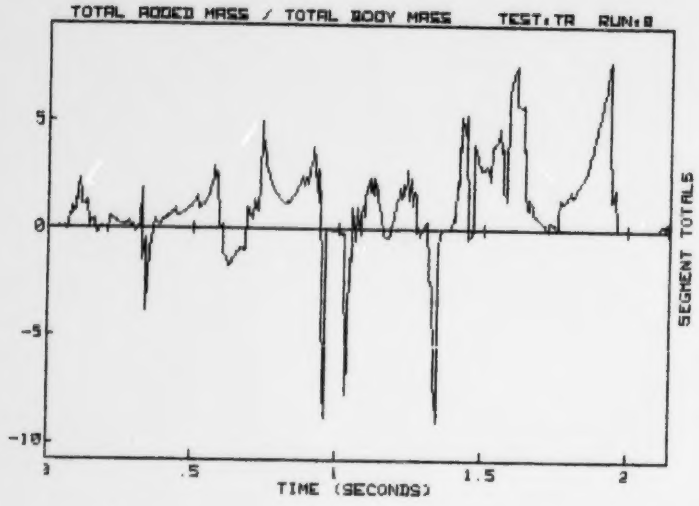

NON-DIMENSIONAL SEGMENTAL ADDED MASS STATISTICS

SEGMENT	MIN	MAX	MEAN	S.D.	NPTS
1	-541.6	246.4	-114.9	114.4	345
2	-6.6	38.5	9	7.5	328
3	-9.8	24.9	5.8	5.3	319
4	-7.8	21.1	3.8	4.4	264
5	-5.9	18.7	2.5	4	228
6	-6	14.2	1.9	3.6	179
7	-4.6	11	1.3	3.1	168
8	-7.1	15.1	3.1	5.6	167
9	-3.4	17.2	3.3	4.8	187
10	-9.7	37	6.1	8.3	330
11	-14	51.8	7.4	11.1	350
12	-40.7	135.9	11.3	22.4	390
MEAN MODEL ADDED MASS =			1.99		3255

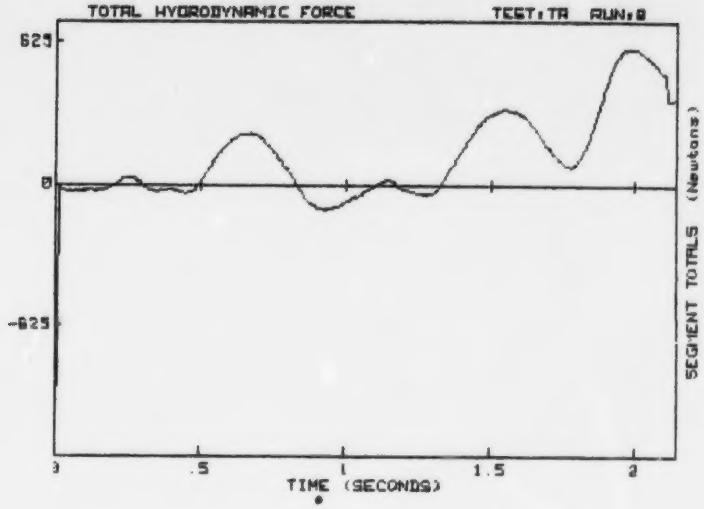

HYDRODYNAMIC FORCE SUMMARY STATISTICS

SEGMENT	MIN	MAX	MEAN	S.D.	NPTS
1	-476	278.6	149.8	83.9	532
2	-86.3	172	-42.5	34.6	532
3	-72.8	239.4	-35.2	29.5	532
4	-58.3	238.4	-23	28.9	532
5	-53.3	202.5	-16.5	26.3	532
6	-56.8	41.9	-9.8	22.6	532
7	-203.6	55.9	-.6	26.2	532
8	-214.5	69.1	10.4	27.5	532
9	-18.4	91.4	21.5	25.3	532
10	-16.3	387.9	34.2	36.8	532
11	-16.9	234.8	31.5	30.4	532
12	-1550.7	50.7	-.9	98.7	532
MEAN HYDRODYNAMIC FORCE =			9.93		6384

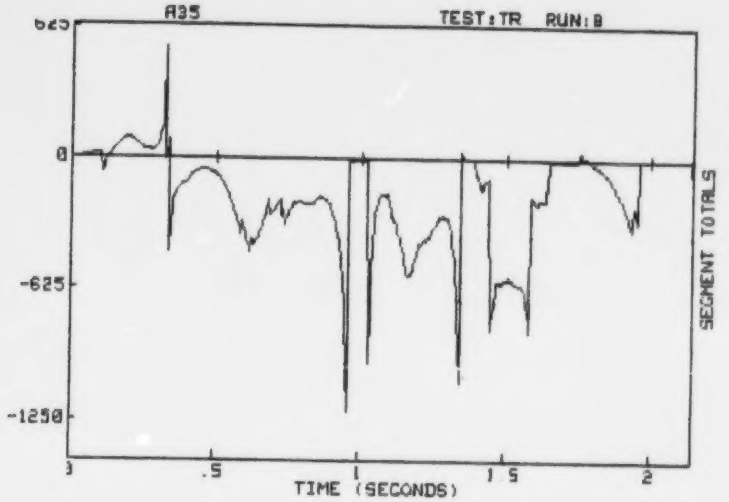

HEAVE/PITCH COUPLED ADDED MASS SUMMARY STATISTICS

SEGMENT	MIN	MAX	MEAN	S.D.	NPTS
1	-1188.7	540.7	-252.3	251.1	345
2	-12.1	71	16.6	13.9	328
3	-14	35.7	8.3	7.6	319
4	-8	21.6	3.9	4.5	264
5	-3.6	11.5	1.5	2.5	228
6	-1.2	2.9	.4	.7	179
7	-2.3	.9	-.3	.6	168
8	-9.3	4.4	-1.9	3.4	167
9	-17.6	3.5	-3.4	4.9	187
10	-53	13.8	-8.7	11.9	330
11	-95	25.7	-13.5	20.3	350
12	-303.9	91	-25.2	50.1	390
MEAN A35 MODEL ADDED MASS =			-3.43		3255

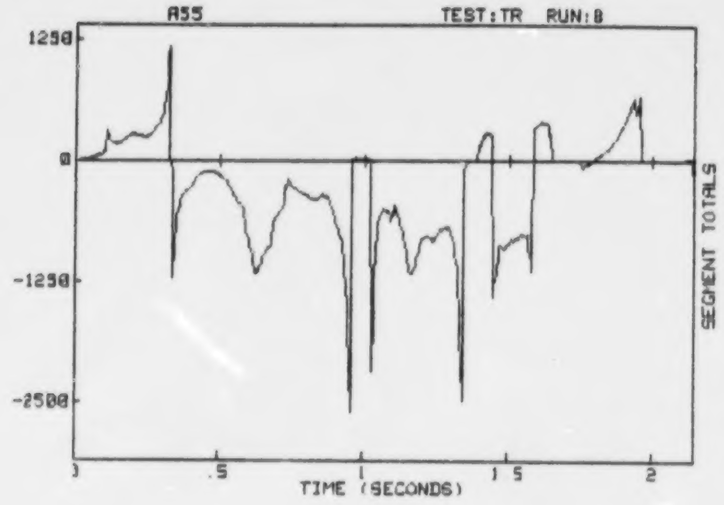

PITCH ADDED MASS MOMENT OF INERTIA SUMMARY STATISTICS

SEGMENT	MIN	MAX	MEAN	S.D.	NPTS
1	-2609.3	1186.9	-553.8	251.1	345
2	-22.4	131	30.6	13.9	328
3	-20.1	51.2	11.9	7.6	319
4	-8.2	22.2	3.9	4.5	264
5	-2.2	7.1	.9	2.5	228
6	-.3	.6	.1	.7	179
7	-.2	.5	.1	.6	168
8	-2.7	5.7	1.2	3.4	167
9	-3.6	18	3.5	4.9	187
10	-19.8	75.8	12.5	11.9	330
11	-47.1	174.1	24.8	20.3	350
12	-203.5	679.5	56.4	50.1	390

MEAN A55 MODEL ADDED MASS = -.64 3255

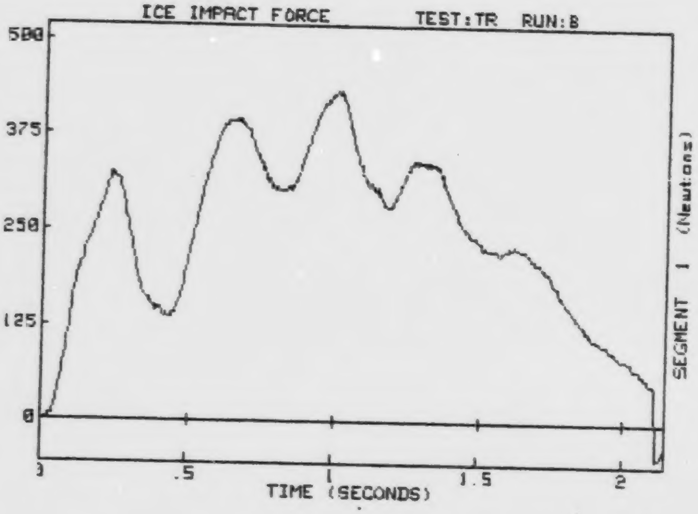
ICE IMPACT FORCE
TEST:TR RUN:8
500
375
250
125
0
0
.5
1
1.5
2
TIME (SECONDS)
SEGMENT 1 (Newtons)

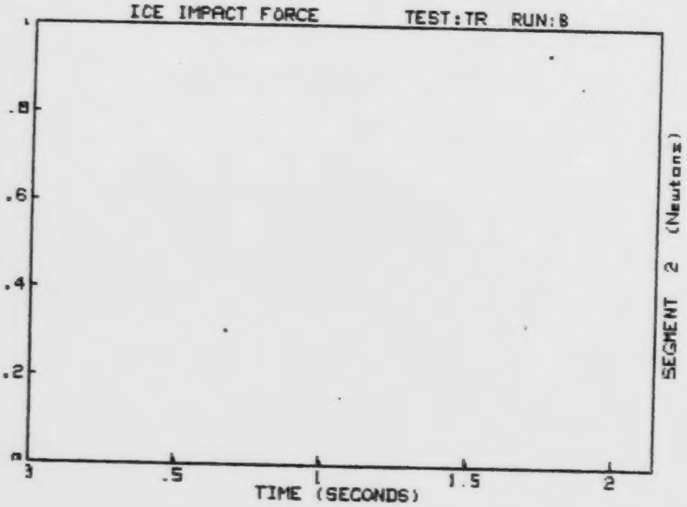
ICE IMPACT FORCE
TEST:TR RUN:8
1
.8
.6
.4
.2
0
0
.5
1
1.5
2
TIME (SECONDS)
SEGMENT 2 (Newtons)

IMPACT VELOCITY= .37 m/s
SHIP SPEED= 4.53 kt

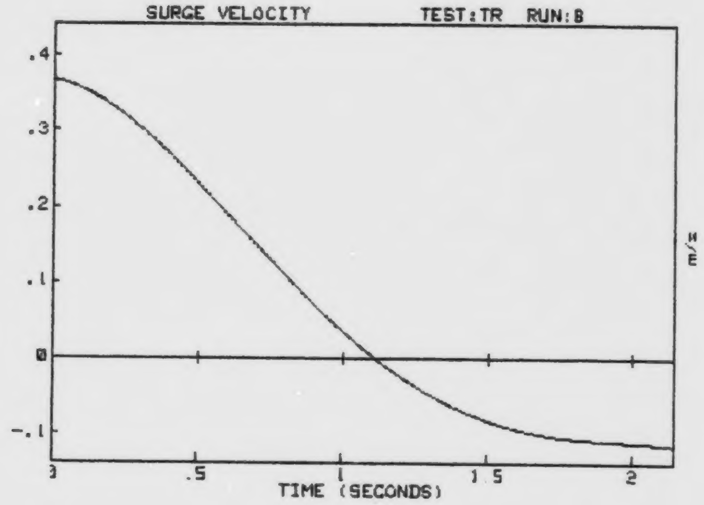

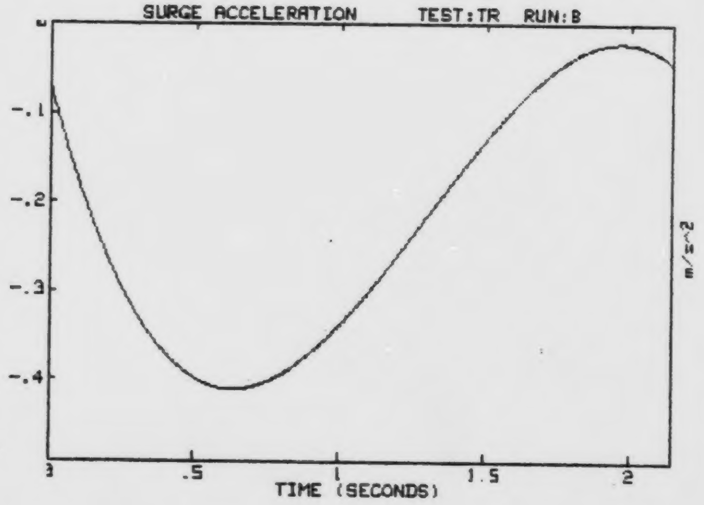

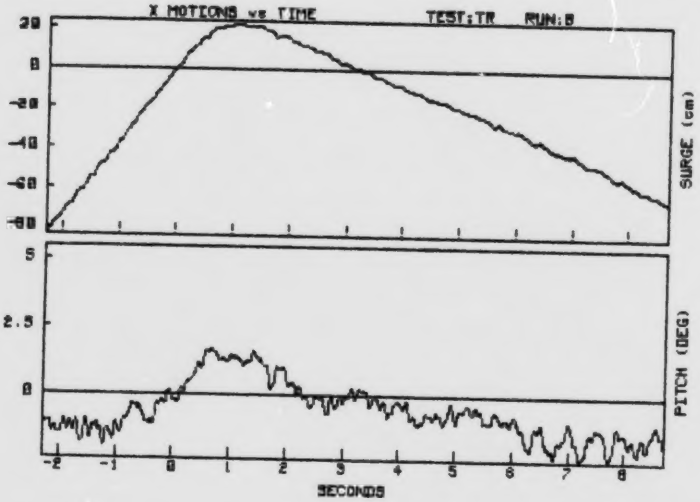
X MOTIONS vs TIME
TEST:TR RUN:8
20
0
-20
-40
-60
-80
SURGE (cm)
5
2.5
0
PITCH (DEG)
-2
-1
0
1
2
3
4
5
6
7
8
SECONDS

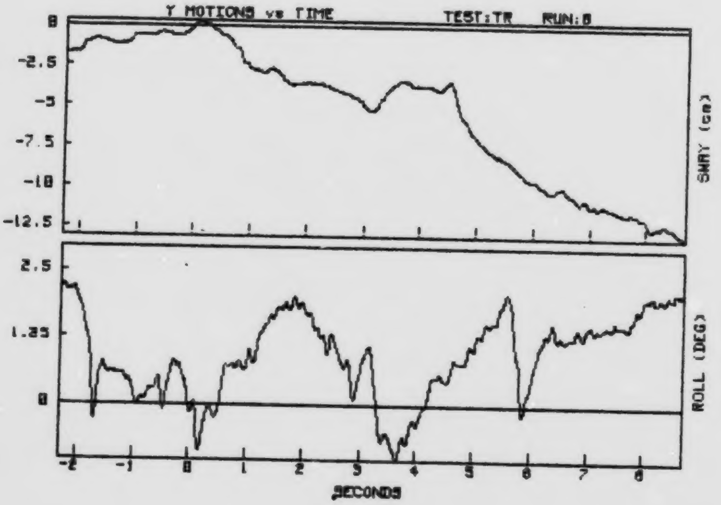
Y MOTIONS vs TIME
TEST:TR RUN:8
0
-2.5
-5
-7.5
-10
-12.5
SWAY (cm)
2.5
1.25
0
ROLL (DEG)
-2
-1
0
1
2
3
4
5
6
7
8
SECONDS

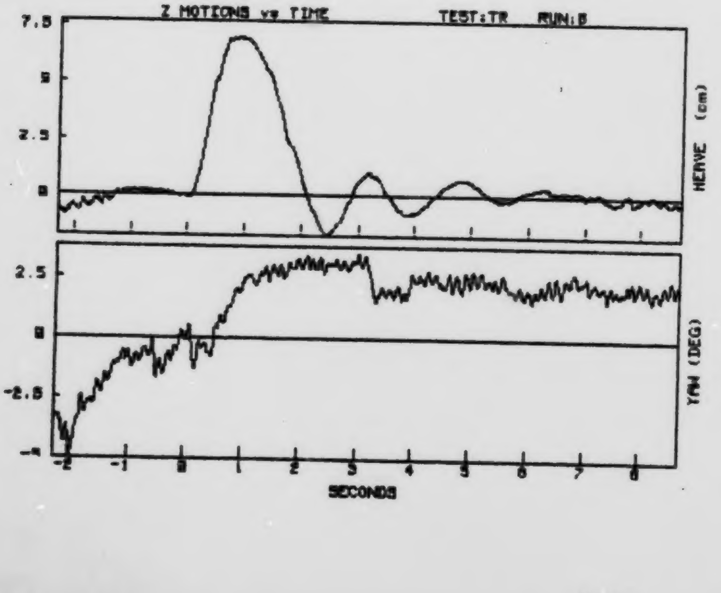
Z MOTIONS vs TIME
TEST:TR RUN:8
7.5
5
2.5
0
HEAVE (cm)
2.5
0
-2.5
-5
YAW (DEG)
-2
-1
0
1
2
3
4
5
6
7
8
SECONDS

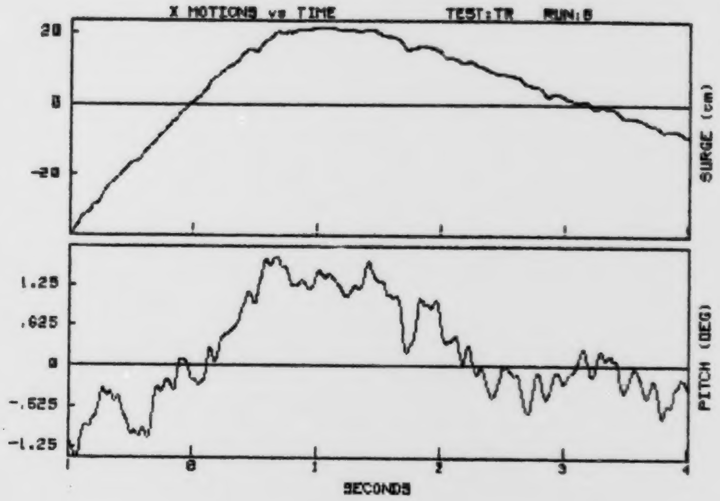
X MOTIONS vs TIME
TEST:TR RUN:8
20
0
-20
SURGE (cm)
1.25
.625
0
-.625
-1.25
PITCH (DEG)
0
1
2
3
4
SECONDS

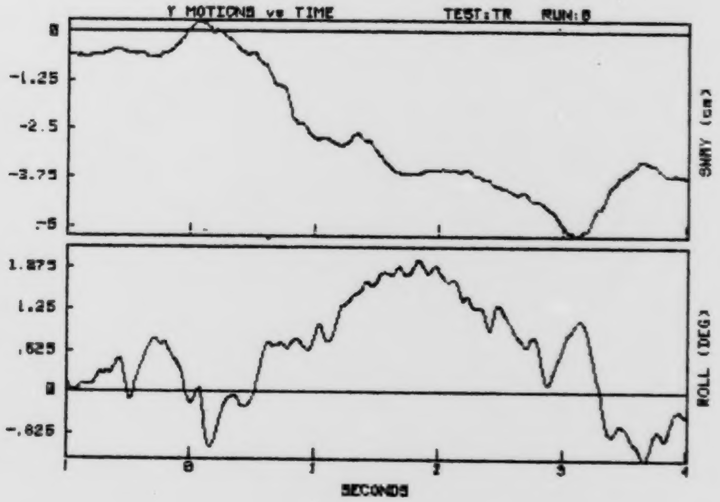
Y MOTIONS vs TIME
TEST:TR RUN:8
0
-1.25
-2.5
-3.75
-5
SWAY (cm)
1.875
1.25
.625
0
-.625
ROLL (DEG)
0
1
2
3
4
SECONDS

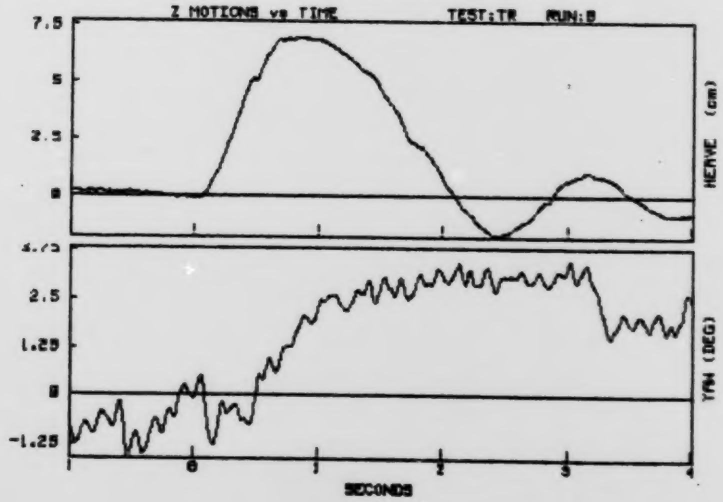
Z MOTIONS vs TIME
TEST:TR RUN:8
7.5
5
2.5
0
HEAVE (cm)
3.75
2.5
1.25
0
-1.25
YAW (DEG)
0
1
2
3
4
SECONDS

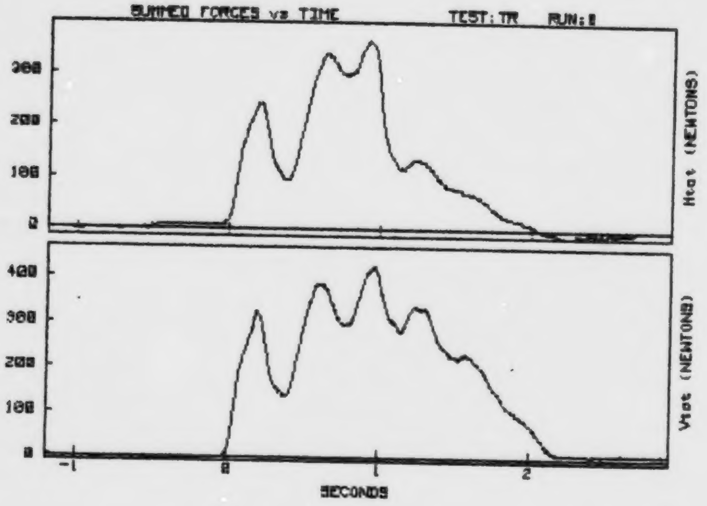
SUMMED FORCES vs TIME
TEST: TR
RUN: 8
300
200
100
0
Htot (NEWTONS)
400
300
200
100
0
Vtot (NEWTONS)
-1
0
1
2
SECONDS

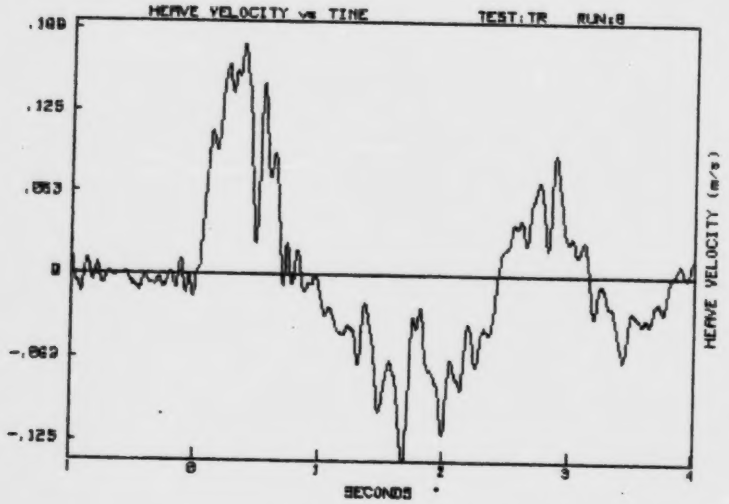
HEAVE VELOCITY vs TIME
TEST: TR
RUN: 8
.188
.125
.063
0
-.063
-.125
HEAVE VELOCITY (m/s)
1
0
1
2
3
4
SECONDS

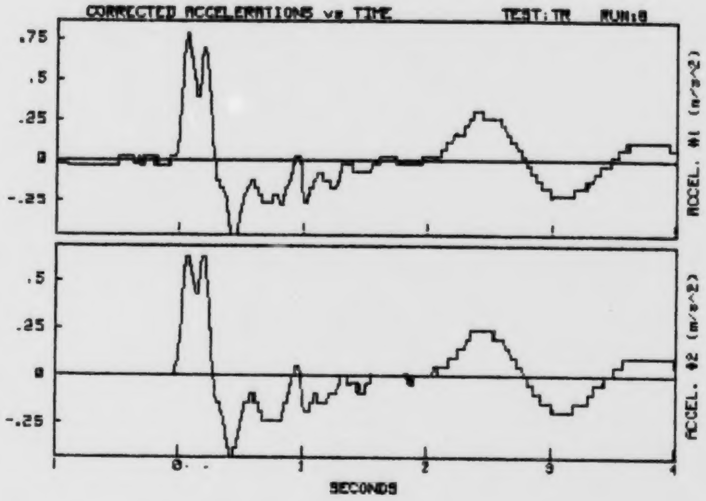
CORRECTED ACCELERATIONS vs TIME
TEST:TR
RUN:8
.75
.5
.25
0
-.25
ACCEL. #1 (m/s^2)
.5
.25
0
-.25
ACCEL. #2 (m/s^2)
-1
0
1
2
3
4
SECONDS

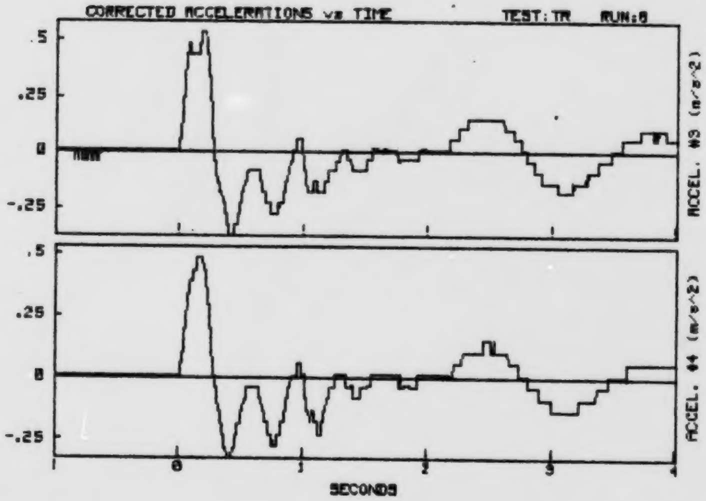
CORRECTED ACCELERATIONS vs TIME
TEST:TR
RUN:8
.5
.25
0
-.25
ACCEL. #3 (m/s^2)
.5
.25
0
-.25
ACCEL. #4 (m/s^2)
-1
0
1
2
3
4
SECONDS

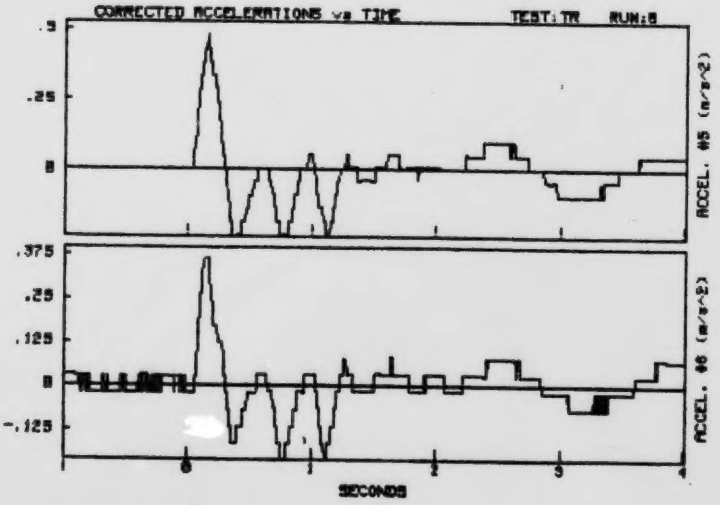
CORRECTED ACCELERATIONS vs TIME
TEST:TR
RUN:8
.5
.25
0
ACCEL. #5 (m/s^2)
.375
.25
.125
0
-.125
ACCEL. #6 (m/s^2)
-1
0
1
2
3
4
SECONDS

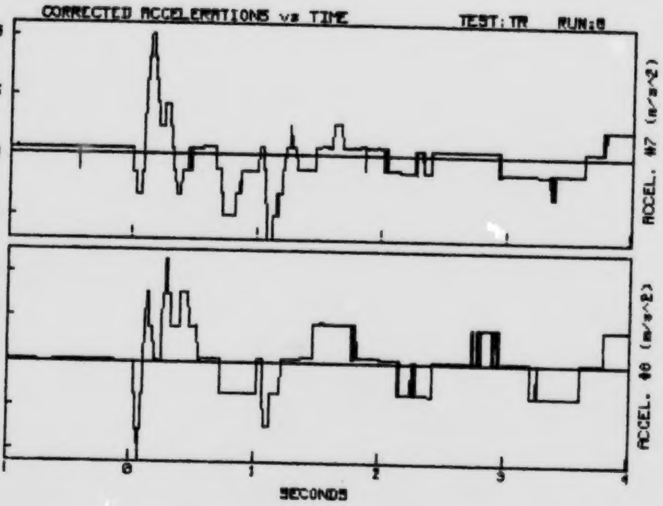
CORRECTED ACCELERATIONS vs TIME
TEST: TR
RUN: 8
.25
.125
0
-.125
ACCEL. #7 (m/s^2)
.125
.063
0
-.063
-.125
ACCEL. #8 (m/s^2)
1
0
1
2
3
4
SECONDS

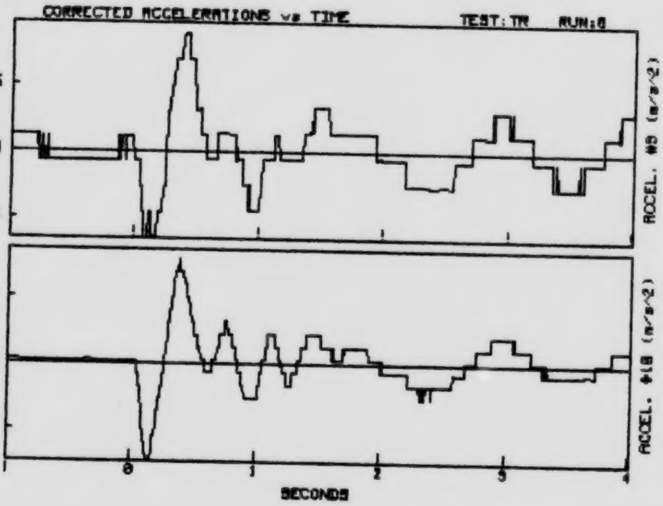
CORRECTED ACCELERATIONS vs TIME
TEST: TR
RUN: 8
.125
0
-.125
ACCEL. #9 (m/s^2)
.25
0
-.25
ACCEL. #10 (m/s^2)
1
0
1
2
3
4
SECONDS

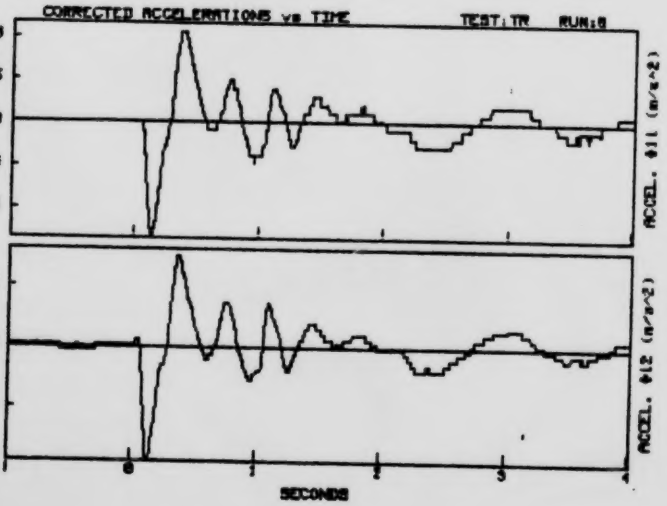
CORRECTED ACCELERATIONS vs TIME
TEST: TR
RUN: 8
.5
.25
0
-.25
-.5
ACCEL. #11 (m/s^2)
.5
0
-.5
ACCEL. #12 (m/s^2)
1
0
1
2
3
4
SECONDS

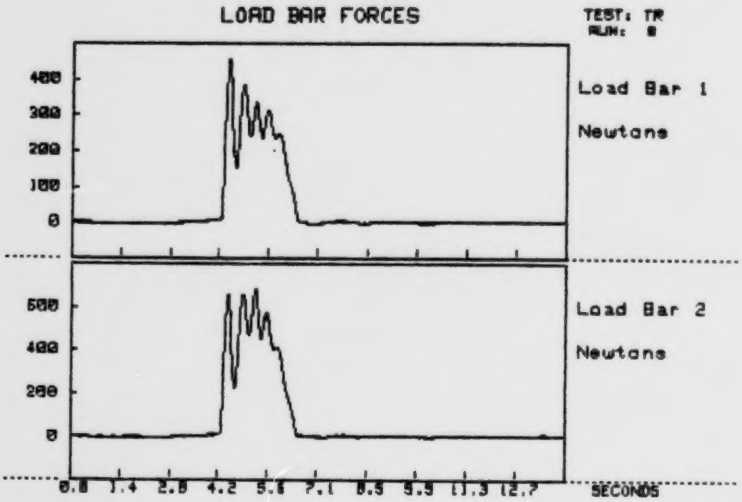
LOAD BAR FORCES
TEST: TR
RUN: 8
400
300
200
100
0
Load Bar 1
Neutons
600
400
200
0
Load Bar 2
Neutons
0.0
1.4
2.8
4.2
5.6
7.1
8.5
9.9
11.3
12.7
SECONDS

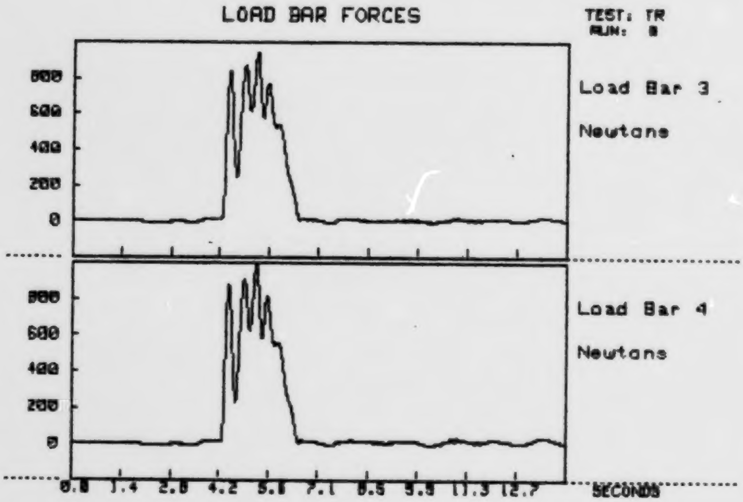
LOAD BAR FORCES
TEST: TR
RUN: 8
800
600
400
200
0
Load Bar 3
Neutons
800
600
400
200
0
Load Bar 4
Neutons
0.0
1.4
2.8
4.2
5.6
7.1
8.5
9.9
11.3
12.7
SECONDS

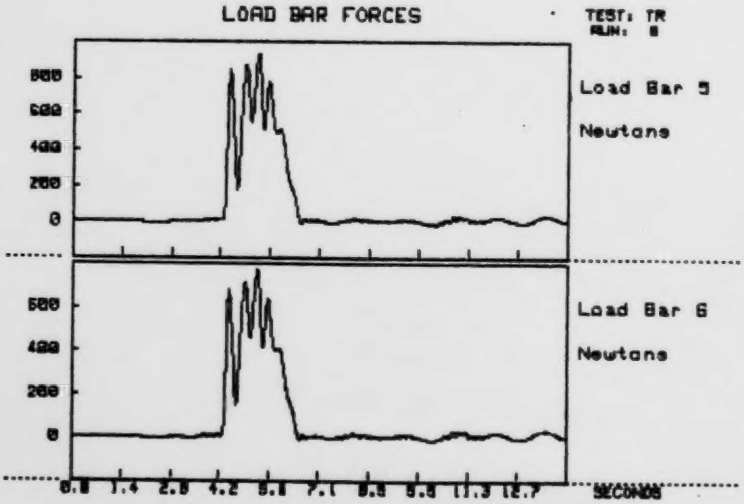
LOAD BAR FORCES
TEST: TR
RUN: 8
800
600
400
200
0
Load Bar 5
Neutons
600
400
200
0
Load Bar 6
Neutons
0.0
1.4
2.8
4.2
5.6
7.1
8.5
9.9
11.3
12.7
SECONDS

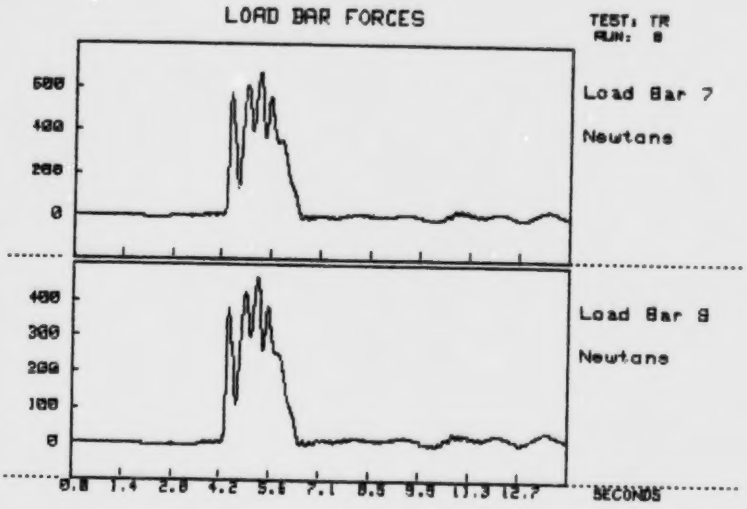
LOAD BAR FORCES
TEST: TR
RUN: 8
600
400
200
0
Load Bar 7
Newtons
400
300
200
100
0
Load Bar 8
Newtons
0.0
1.4
2.8
4.2
5.6
7.1
8.5
9.9
11.3
12.7
SECONDS

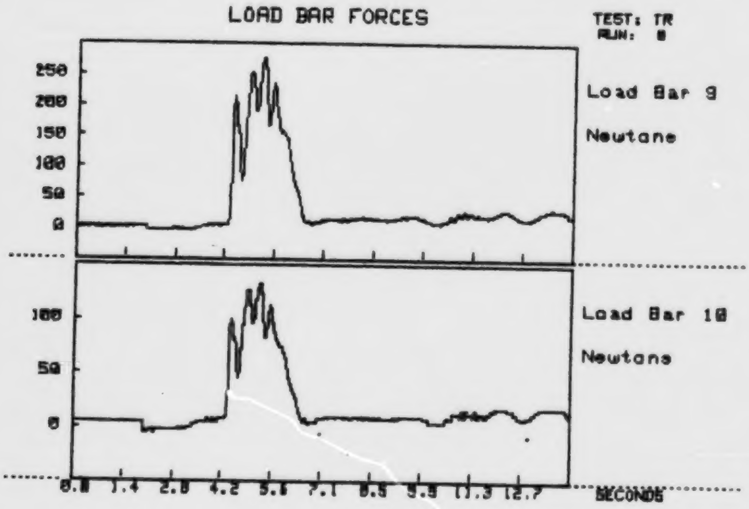
LOAD BAR FORCES
TEST: TR
RUN: 8
250
200
150
100
50
0
Load Bar 9
Newtons
100
50
0
Load Bar 10
Newtons
0.0
1.4
2.8
4.2
5.6
7.1
8.5
9.9
11.3
12.7
SECONDS

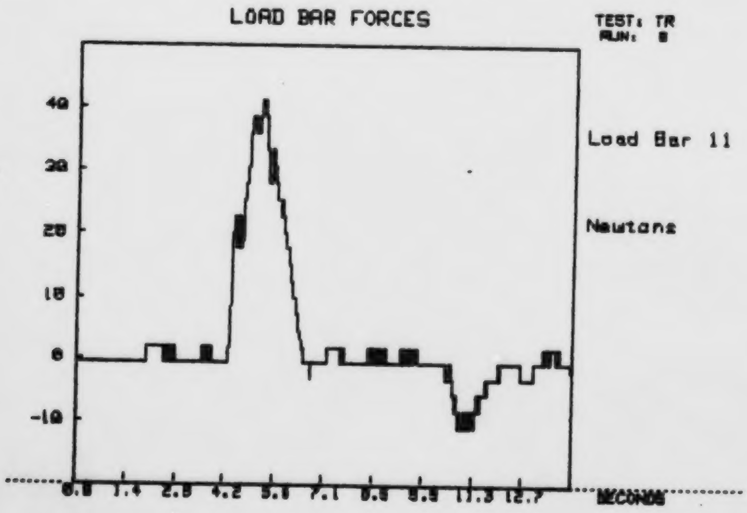
LOAD BAR FORCES
TEST: TR
RUN: 8
40
30
20
10
0
-10
Load Bar 11
Newtons
0.0
1.4
2.8
4.2
5.6
7.1
8.5
9.9
11.3
12.7
SECONDS

```
                 MV  ARCTIC MODEL TESTS
                 ADDED MASS CALCULATION



                    TEST:          TR
                    RUN NUMBER:    9


          NOMINAL IMPACT VELOCITY:              .84      m/s
          NOMINAL SHIP SPEED:                   10.3     kt
          TIME TO MAXIMUM SURGE:                .79      s
          TIME FROM IMPACT TO BACKOFF:          1.633    s


          TIME INCREMENT:                        .004    s
          ACCELEROMETER THRESHOLD:               .05     m/s^2


          MODEL MASS:                             596    kg
          WATER DEPTH:                            1.85   m
          MODEL DRAFT:                            0.275  m
          ICE FREEBOARD:                          0.025  m
```

SEGMENT ADDED MASS NORMALIZED BY DISPLACED MASS

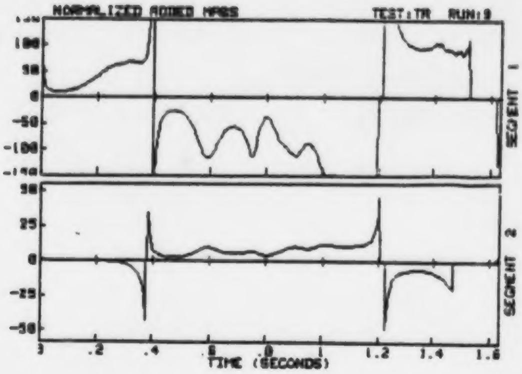

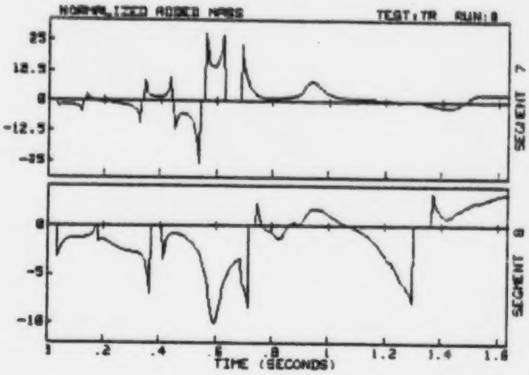

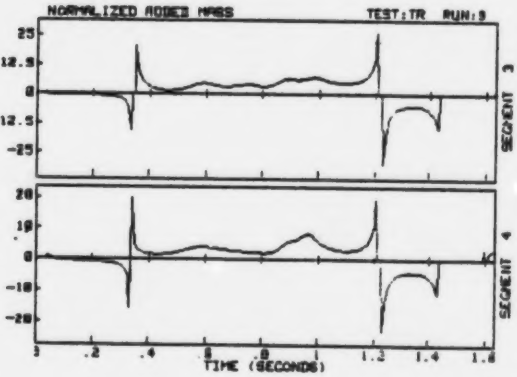

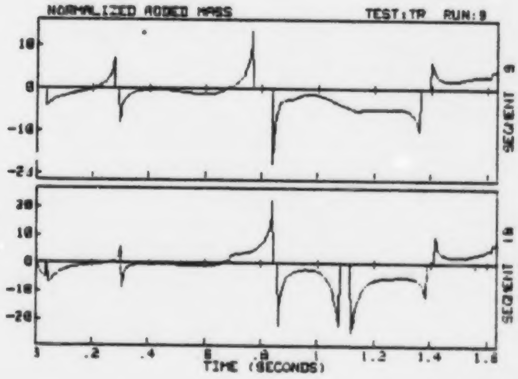

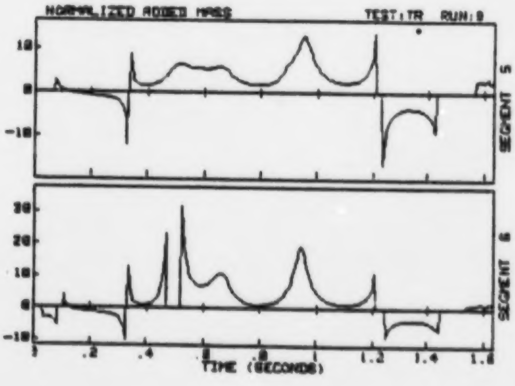

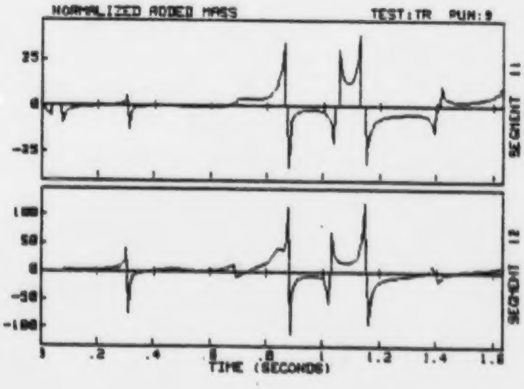

SEGMENT HYDRODYNAMIC FORCE

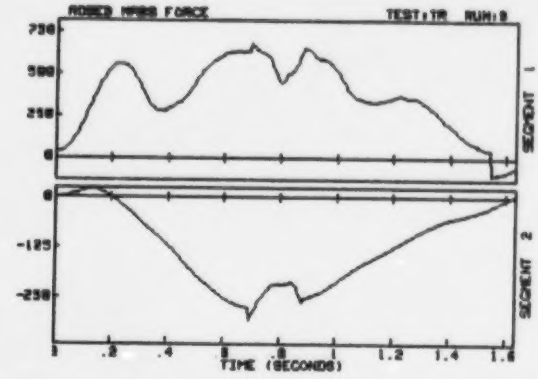

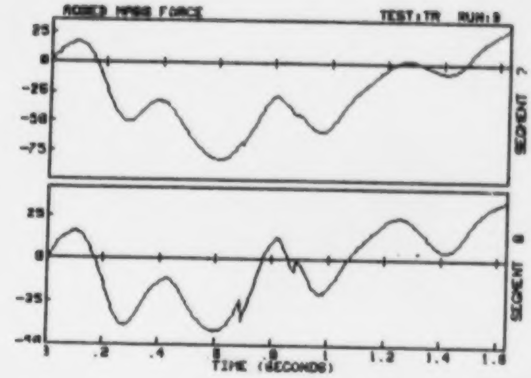

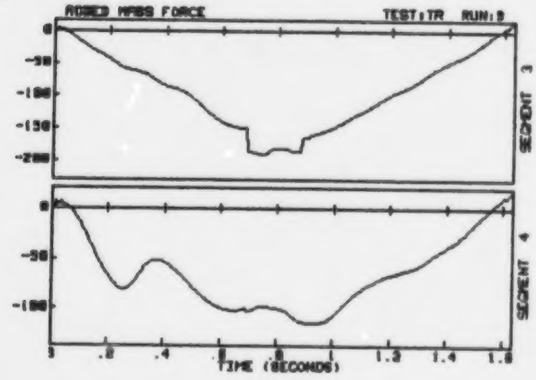

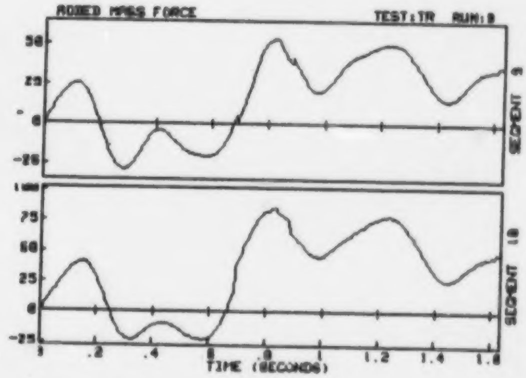

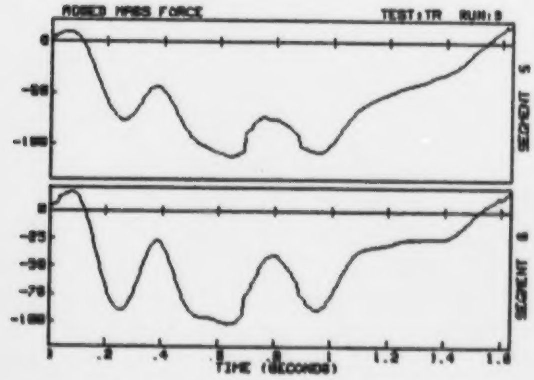

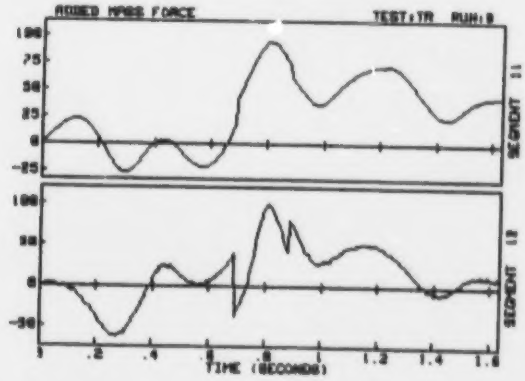

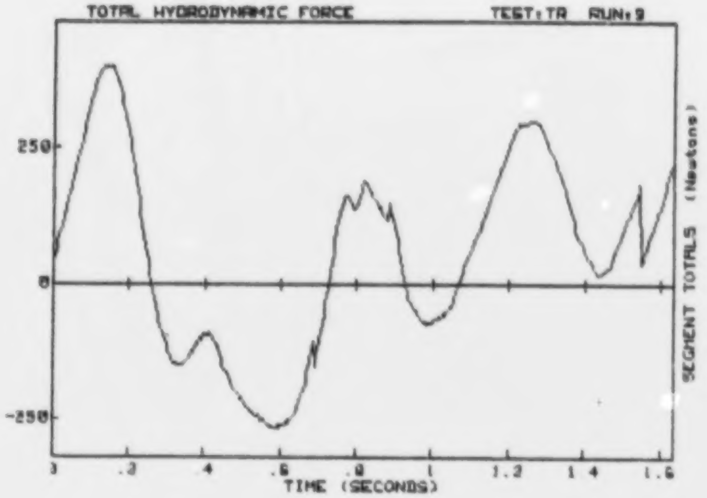

HYDRODYNAMIC FORCE SUMMARY STATISTICS

SEGMENT	MIN	MAX	MEAN	S.D.	NPTS
1	-108.1	681.9	367.5	202.9	406
2	-307.9	22.4	-123.2	96.7	406
3	-191	14.3	-91.2	58.6	406
4	-115.2	17.4	-64.3	36.5	406
5	-112.1	18.4	-56.2	37.5	406
6	-102.1	17.8	-44.4	34.9	406
7	-82	29.5	-26.1	29.9	406
8	-42.1	34.9	-3.3	21.4	406
9	-28.6	54.1	17.4	24.2	406
10	-23	85.6	33	33.9	406
11	-26.3	95.3	30.5	33.3	406
12	-62.3	100.8	13.9	33.9	406
MEAN HYDRODYNAMIC FORCE =			4.47		4872

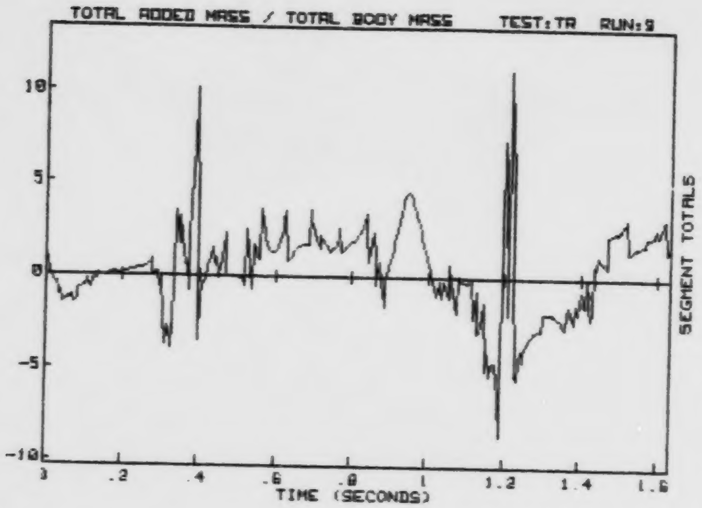

NON-DIMENSIONAL SEGMENTAL ADDED MASS STATISTICS

SEGMENT	MIN	MAX	MEAN	S.D.	NPTS
1	-715.4	803.5	-18.7	135.4	375
2	-48.8	46.1	2.7	9.7	362
3	-30.1	26.3	1.7	5.8	342
4	-23	19.7	1.3	4.6	348
5	-16.6	13.7	2	4.5	345
6	-9.8	31.4	2.4	5.8	346
7	-26.3	28	1.6	5.8	348
8	-10.1	3.6	-1.3	2.9	359
9	-17.9	13.5	-1.1	3.3	366
10	-24.6	22.5	-1.4	5.4	382
11	-33.6	38.5	.3	7.4	379
12	-110.5	121.7	1.8	19.6	375
MEAN MODEL ADDED MASS =			.44		4327

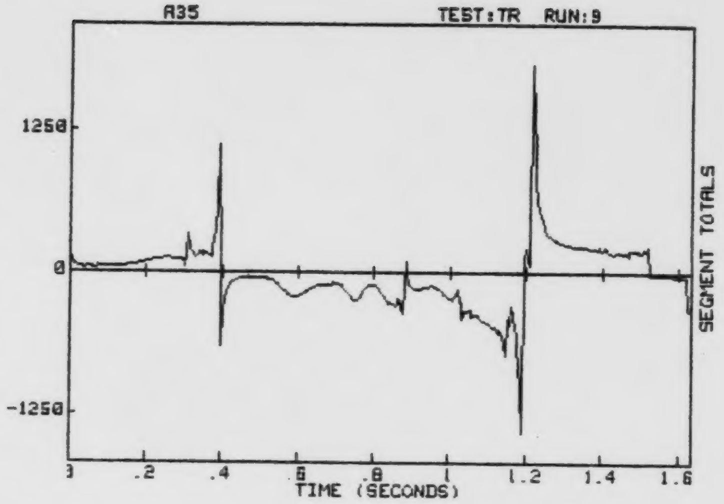

HEAVE/PITCH COUPLED ADDED MASS SUMMARY STATISTICS

SEGMENT	MIN	MAX	MEAN	S.D.	NPTS
1	-1570.3	1763.6	-41	297.1	375
2	-89.9	84.9	5	17.8	362
3	-43.1	37.7	2.4	8.3	342
4	-23.6	20.1	1.3	4.7	348
5	-10.2	8.4	1.2	2.7	345
6	-2	6.4	.5	1.2	346
7	-5.7	5.4	-.3	1.2	348
8	-2.2	6.2	.8	1.8	359
9	-13.8	18.3	1.2	3.3	366
10	-32.1	35.2	2	7.8	382
11	-70.6	61.7	-.5	13.5	379
12	-272.1	247.1	-4.1	43.7	375
MEAN A35 MODEL ADDED MASS =			.48		4327

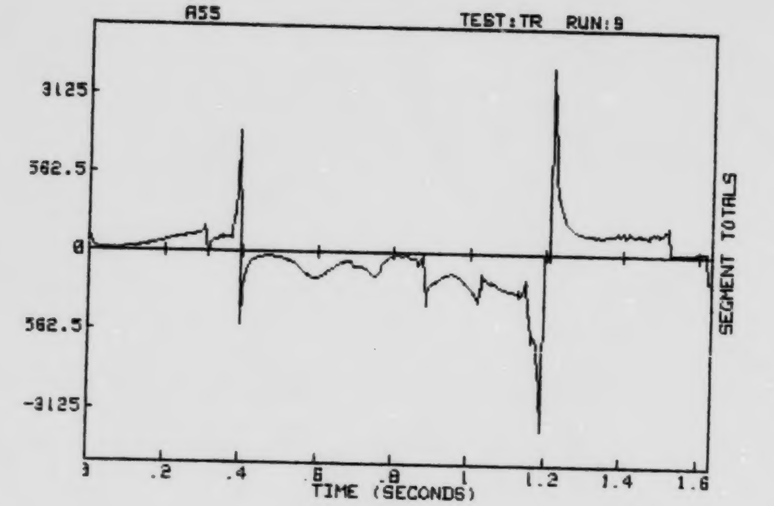

PITCH ADDED MASS MOMENT OF INERTIA SUMMARY STATISTICS

SEGMENT	MIN	MAX	MEAN	S.D.	NPTS
1	-3446.8	3871.1	-89.9	297.1	375
2	-165.8	156.6	9.2	17.8	362
3	-61.8	54.1	3.5	8.3	342
4	-24.2	20.6	1.3	4.7	348
5	-6.3	5.2	.7	2.7	345
6	-.4	1.3	.1	1.2	346
7	-1.1	1.2	.1	1.2	348
8	-3.8	1.4	-.5	1.8	359
9	-18.7	14.1	-1.2	3.3	366
10	-50.3	46	-2.9	7.8	382
11	-113	129.4	1	13.5	379
12	-552.6	608.5	9.2	43.7	375
MEAN A55 MODEL ADDED MASS =			-.33		4327

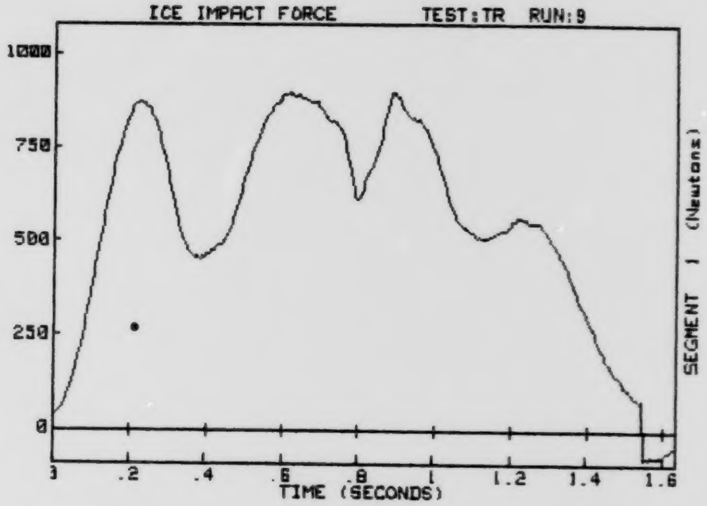
ICE IMPACT FORCE TEST:TR RUN:9
1000
750
500
250
0
0
.2
.4
.6
.8
1
1.2
1.4
1.6
TIME (SECONDS)
SEGMENT 1 (Newtons)

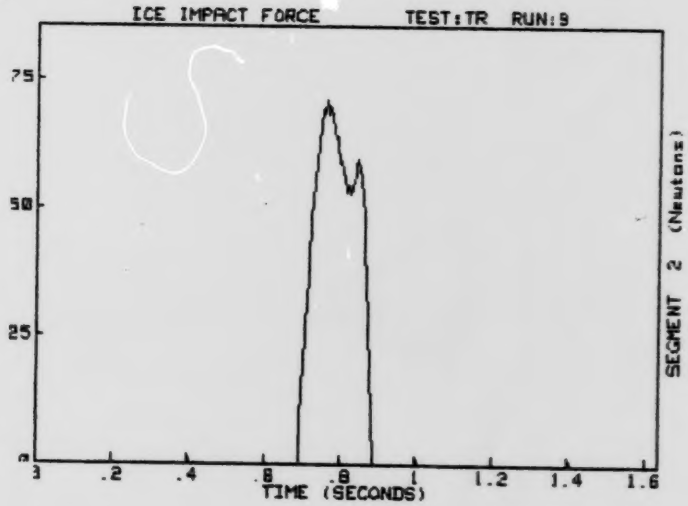
ICE IMPACT FORCE TEST:TR RUN:9
75
50
25
0
0
.2
.4
.6
.8
1
1.2
1.4
1.6
TIME (SECONDS)
SEGMENT 2 (Newtons)

IMPACT VELOCITY= .86 m/s
SHIP SPEED= 10.63 kt

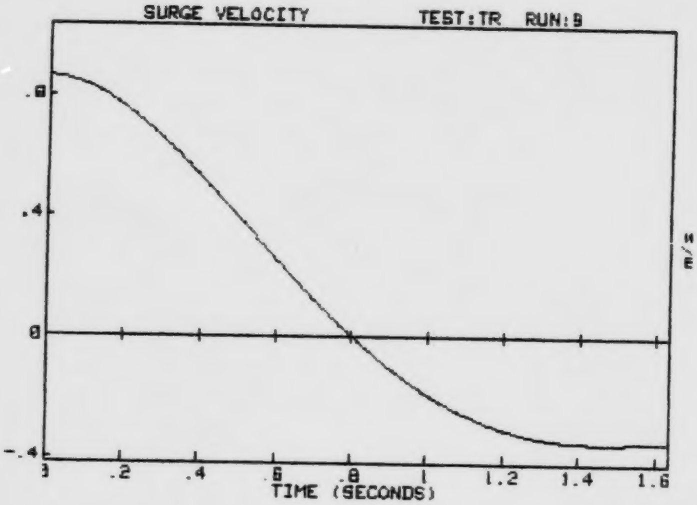

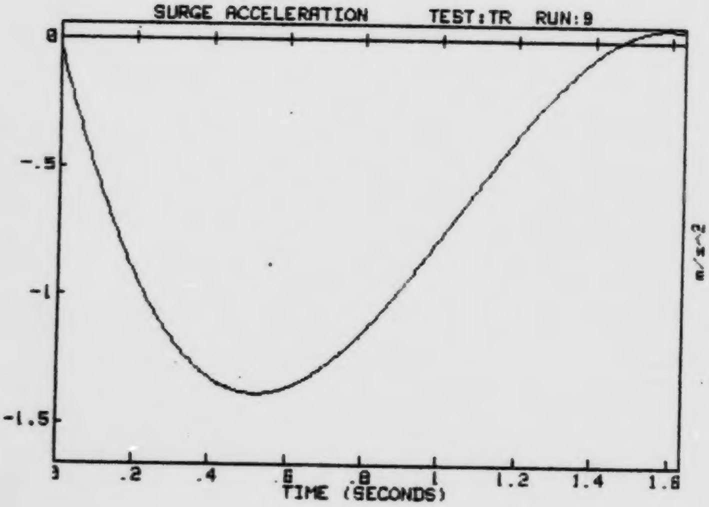

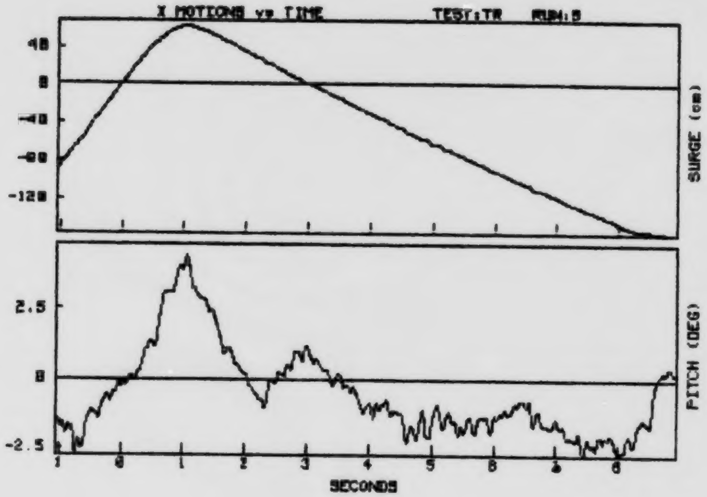
X MOTIONS vs TIME
TEST:TR
RUN:5
40
0
-40
-80
-120
SURGE (cm)
2.5
0
-2.5
PITCH (DEG)
0
1
2
3
4
5
6
8
SECONDS

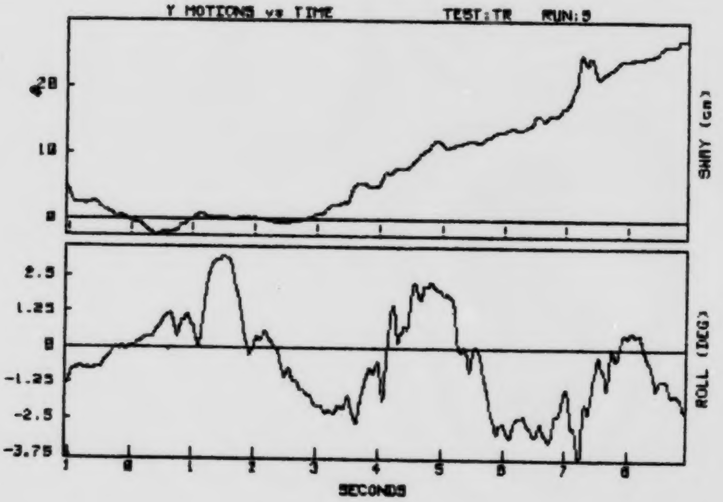
Y MOTIONS vs TIME
TEST:TR
RUN:5
20
10
0
SWAY (cm)
2.5
1.25
0
-1.25
-2.5
-3.75
ROLL (DEG)
0
1
2
3
4
5
6
7
8
SECONDS

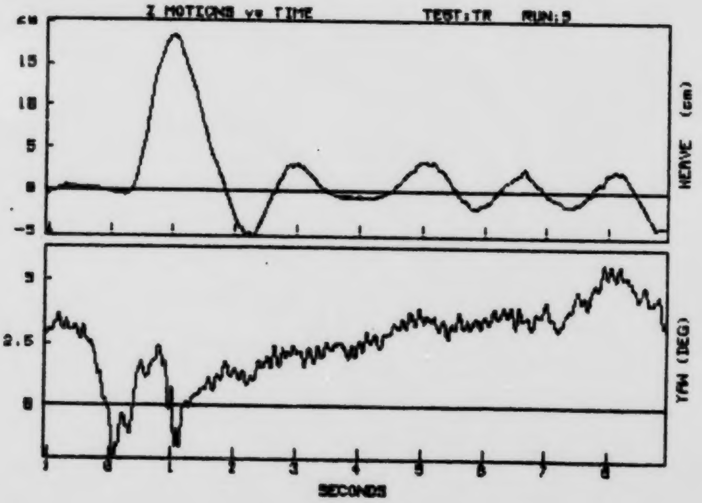
Z MOTIONS vs TIME
TEST:TR
RUN:5
15
10
5
0
-5
HEAVE (cm)
5
2.5
0
YAW (DEG)
0
1
2
3
4
5
6
7
8
SECONDS

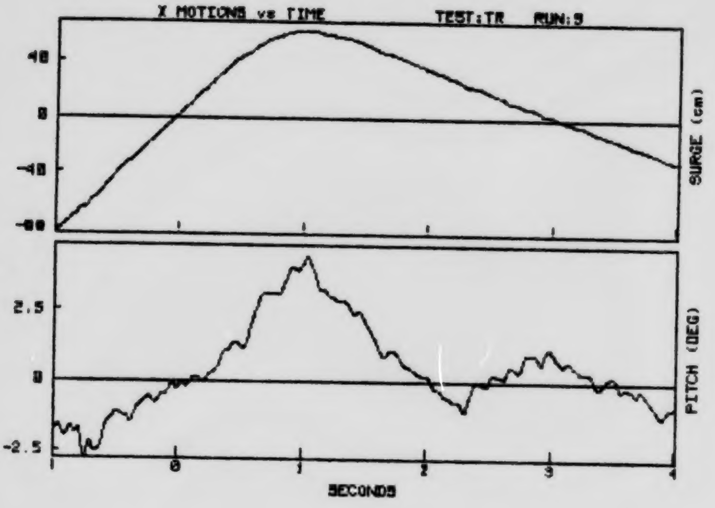
X MOTIONS vs TIME
TEST:TR RUN:5
40
0
-40
-80
SURGE (cm)
2.5
0
-2.5
PITCH (DEG)
0
1
2
3
4
SECONDS

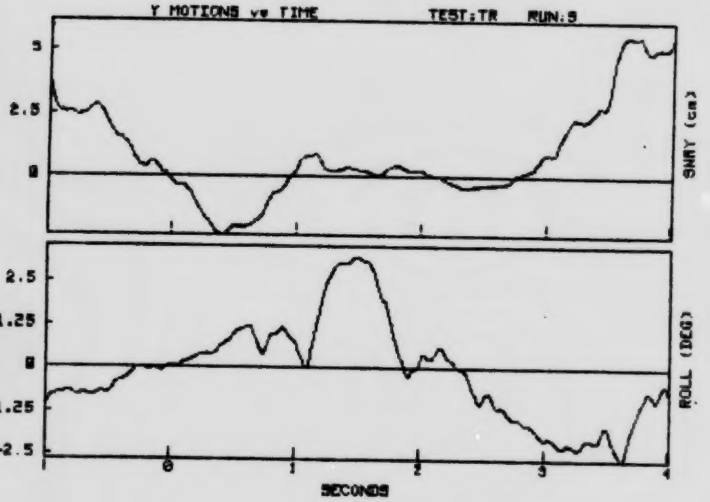
Y MOTIONS vs TIME
TEST:TR RUN:5
5
2.5
0
SWAY (cm)
2.5
1.25
0
-1.25
-2.5
ROLL (DEG)
0
1
2
3
4
SECONDS

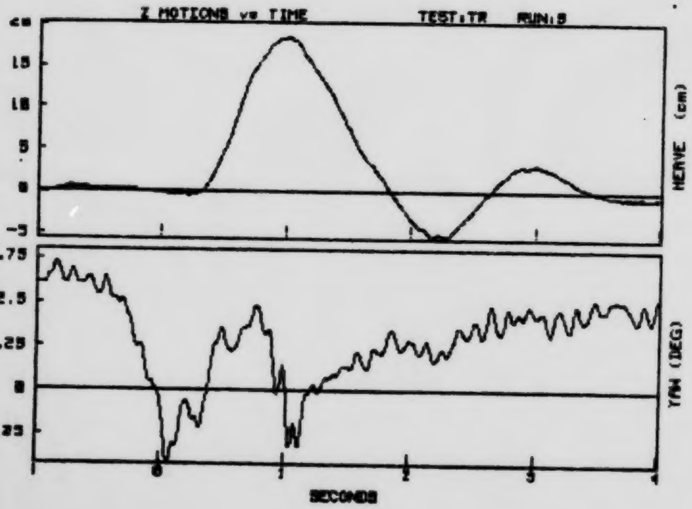
Z MOTIONS vs TIME
TEST:TR RUN:5
20
15
10
5
0
-5
HEAVE (cm)
3.75
2.5
1.25
0
-1.25
YAW (DEG)
0
1
2
3
4
SECONDS

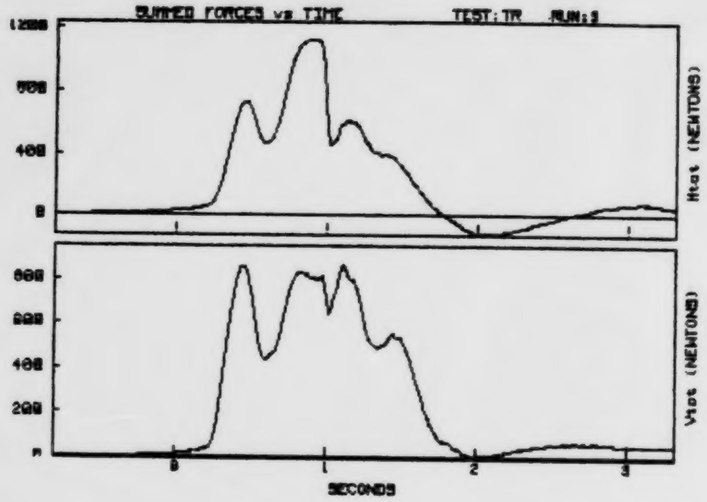
SUMMED FORCES vs TIME
TEST:TR RUN:9
1200
800
400
0
Htot (NEWTONS)
800
600
400
200
0
Vtot (NEWTONS)
0
1
2
3
SECONDS

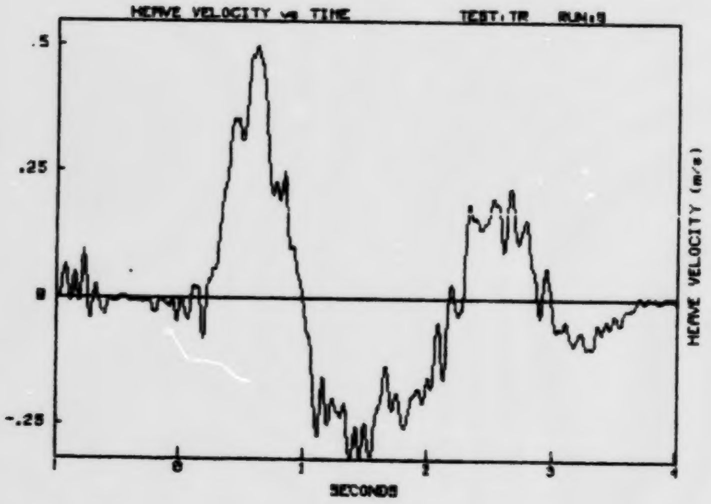
HEAVE VELOCITY vs TIME
TEST:TR RUN:9
.5
.25
0
-.25
HEAVE VELOCITY (m/s)
0
1
2
3
4
SECONDS

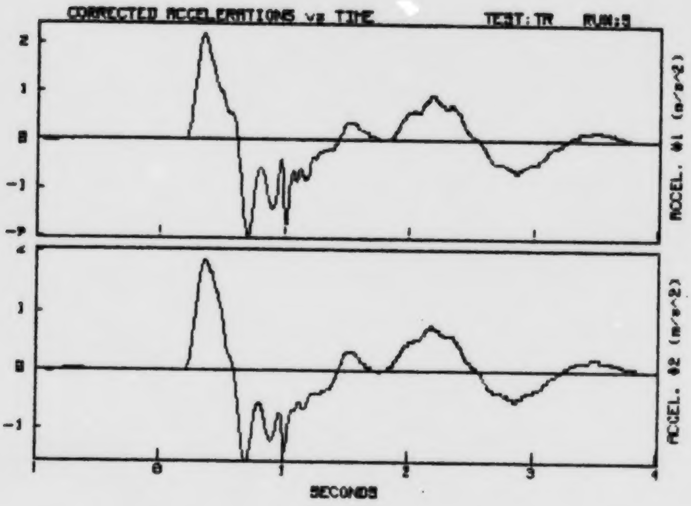
CORRECTED ACCELERATIONS vs TIME
TEST:TR RUN:5
ACCEL. #1 (m/s^2)
ACCEL. #2 (m/s^2)
2
1
0
-1
-2
1
0
-1
0
1
2
3
4
SECONDS

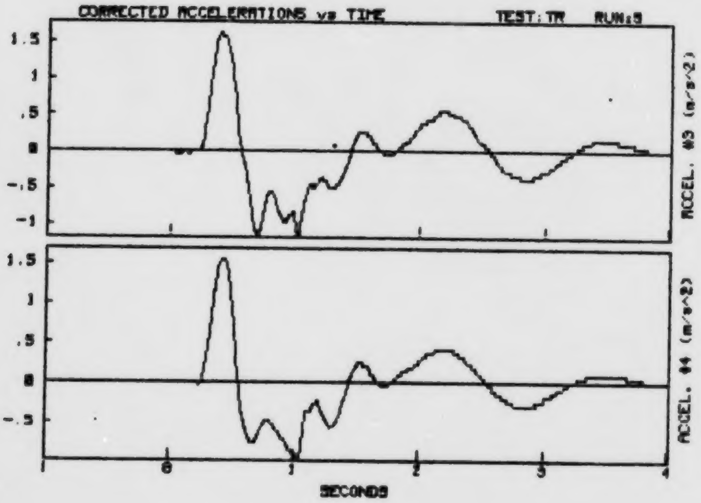
CORRECTED ACCELERATIONS vs TIME
TEST:TR RUN:5
ACCEL. #3 (m/s^2)
ACCEL. #4 (m/s^2)
1.5
1
.5
0
-.5
-1
1.5
1
.5
0
-.5
0
1
2
3
4
SECONDS

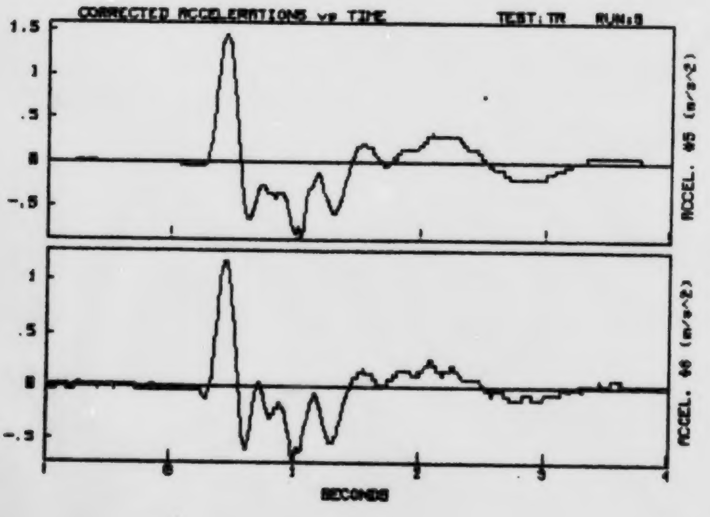
CORRECTED ACCELERATIONS vs TIME
TEST:TR RUN:5
ACCEL. #5 (m/s^2)
ACCEL. #6 (m/s^2)
1.5
1
.5
0
-.5
1
.5
0
-.5
0
1
2
3
4
SECONDS

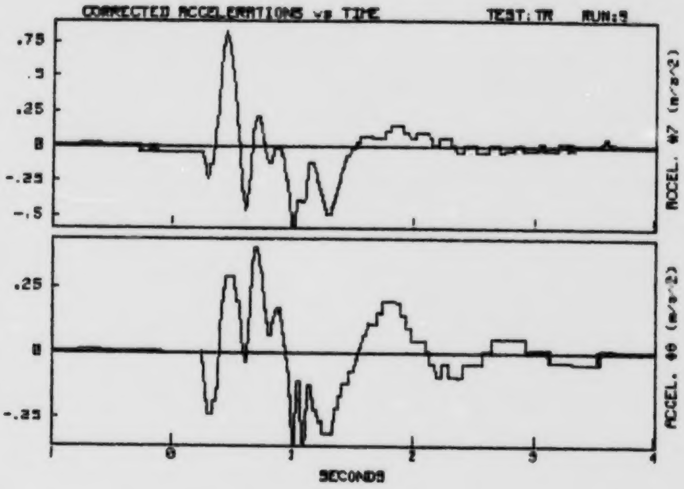
CORRECTED ACCELERATIONS vs TIME
TEST: TR
RUN: 9
.75
.5
.25
0
-.25
-.5
ACCEL. #7 (m/s^2)
.25
0
-.25
ACCEL. #8 (m/s^2)
0
1
2
3
4
SECONDS

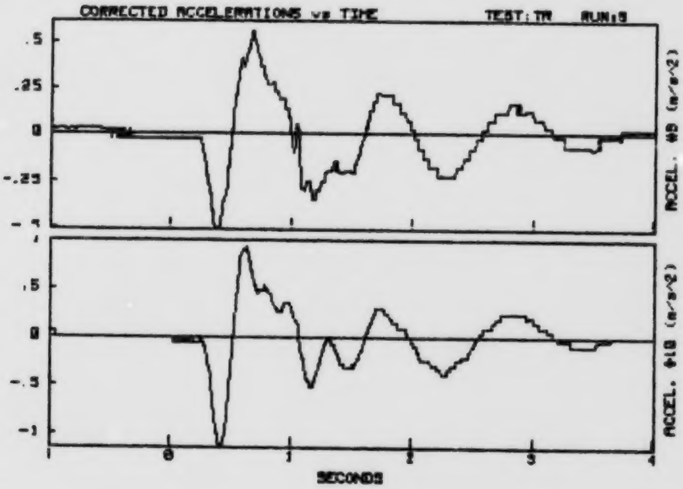
CORRECTED ACCELERATIONS vs TIME
TEST: TR
RUN: 9
.5
.25
0
-.25
-.5
ACCEL. #9 (m/s^2)
1
.5
0
-.5
-1
ACCEL. #10 (m/s^2)
0
1
2
3
4
SECONDS

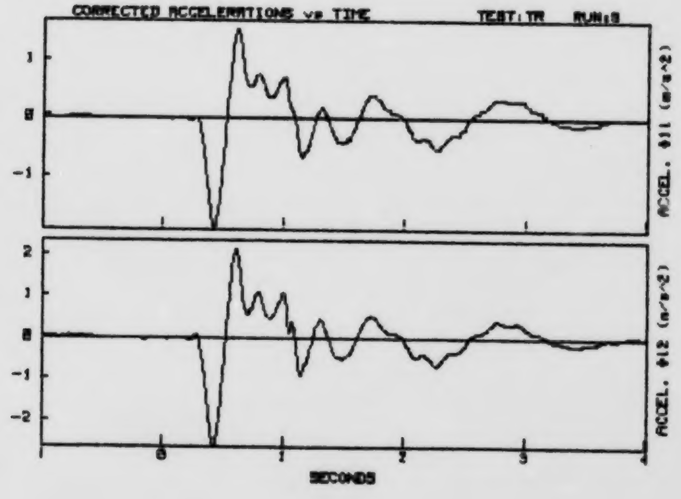
CORRECTED ACCELERATIONS vs TIME
TEST: TR
RUN: 9
1
0
-1
ACCEL. #11 (m/s^2)
2
1
0
-1
-2
ACCEL. #12 (m/s^2)
0
1
2
3
4
SECONDS

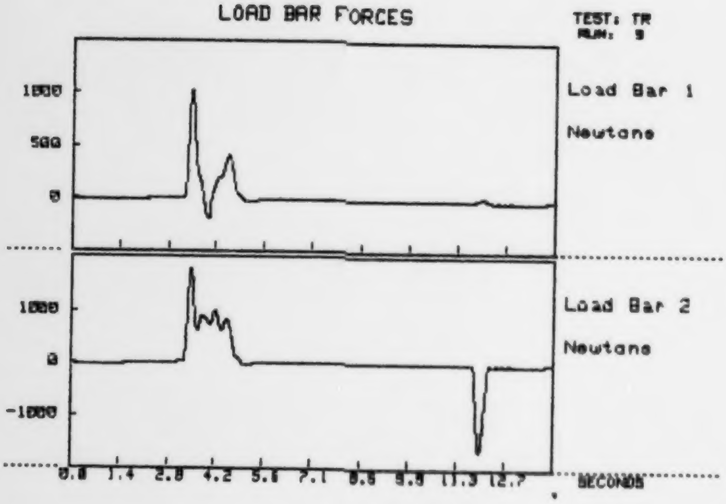
LOAD BAR FORCES
TEST: TR
RUN: 9
1000
500
0
Load Bar 1
Newtons
1000
0
-1000
Load Bar 2
Newtons
0.0 1.4 2.8 4.2 5.6 7.1 8.5 9.9 11.3 12.7
SECONDS

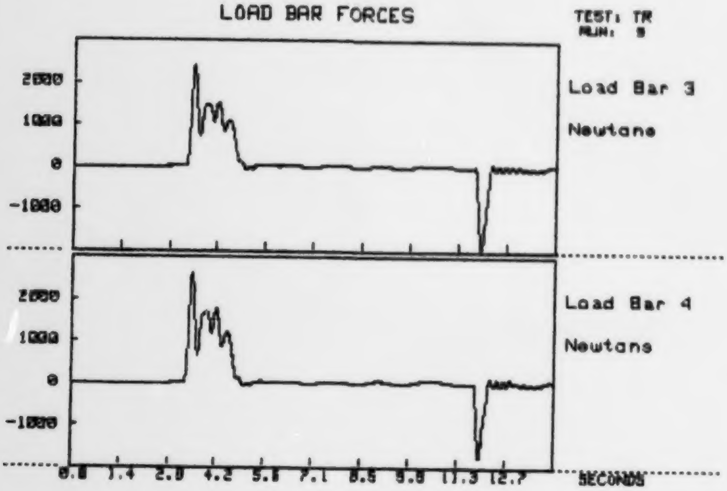
LOAD BAR FORCES
TEST: TR
RUN: 9
2000
1000
0
-1000
Load Bar 3
Newtons
2000
1000
0
-1000
Load Bar 4
Newtons
0.0 1.4 2.8 4.2 5.6 7.1 8.5 9.9 11.3 12.7
SECONDS

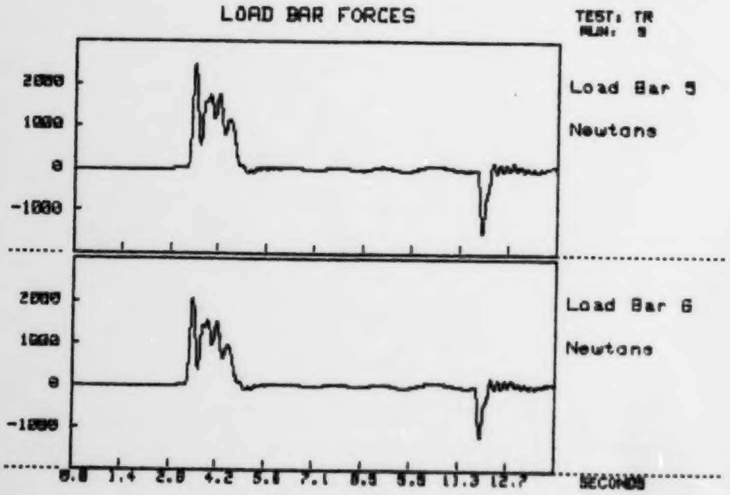
LOAD BAR FORCES
TEST: TR
RUN: 9
2000
1000
0
-1000
Load Bar 5
Newtons
2000
1000
0
-1000
Load Bar 6
Newtons
0.0 1.4 2.8 4.2 5.6 7.1 8.5 9.9 11.3 12.7
SECONDS

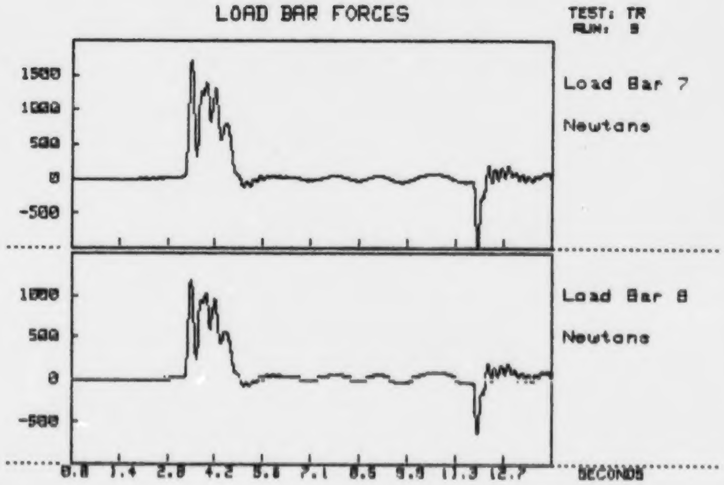
LOAD BAR FORCES
TEST: TR
RUN: 9
1500
1000
500
0
-500
Load Bar 7
Newtons
1000
500
0
-500
Load Bar 8
Newtons
0.0
1.4
2.8
4.2
5.6
7.1
8.5
9.9
11.3
12.7
SECONDS

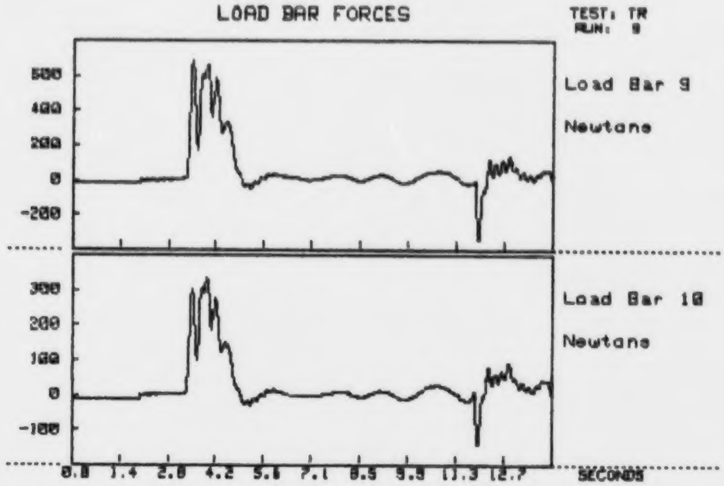
LOAD BAR FORCES
TEST: TR
RUN: 9
600
400
200
0
-200
Load Bar 9
Newtons
300
200
100
0
-100
Load Bar 10
Newtons
0.0
1.4
2.8
4.2
5.6
7.1
8.5
9.9
11.3
12.7
SECONDS

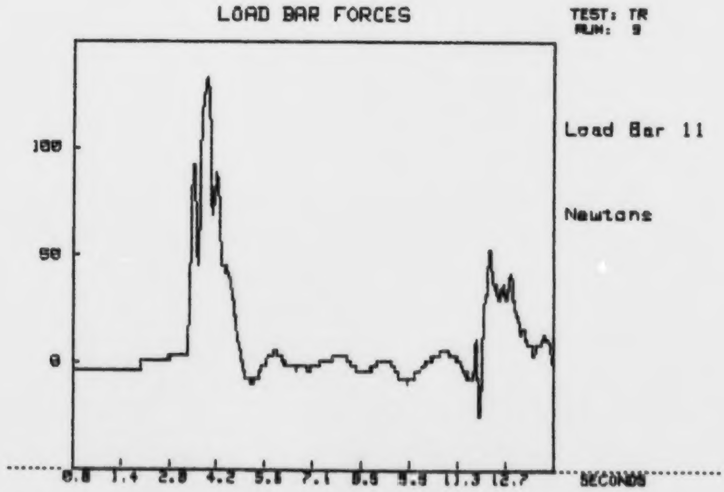
LOAD BAR FORCES
TEST: TR
RUN: 9
100
50
0
Load Bar 11
Newtons
0.0
1.4
2.8
4.2
5.6
7.1
8.5
9.9
11.3
12.7
SECONDS

MV ARCTIC MODEL TESTS
ADDED MASS CALCULATION

TEST:	TR
RUN NUMBER:	10

NOMINAL IMPACT VELOCITY:	.54	m/s
NOMINAL SHIP SPEED:	6.6	kt
TIME TO MAXIMUM SURGE:	1.145	s
TIME FROM IMPACT TO BACKOFF:	2.085	s

TIME INCREMENT:	.004	s
ACCELEROMETER THRESHOLD:	.05	m/s^2

MODEL MASS:	596	kg
WATER DEPTH:	1.85	m
MODEL DRAFT:	0.275	m
ICE FREEBOARD:	0.025	m

SEGMENT ADDED MASS NORMALIZED BY DISPLACED MASS

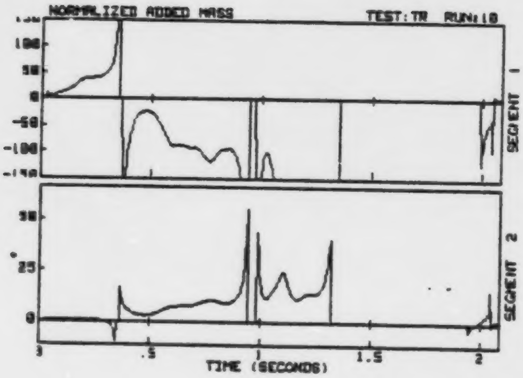

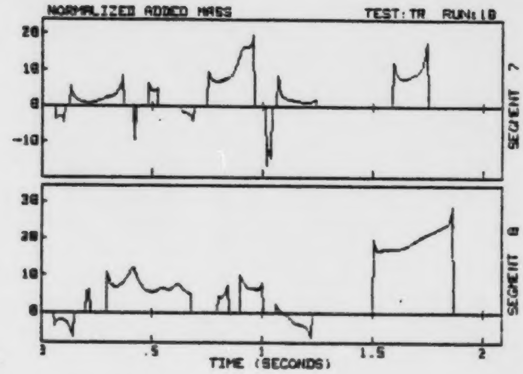

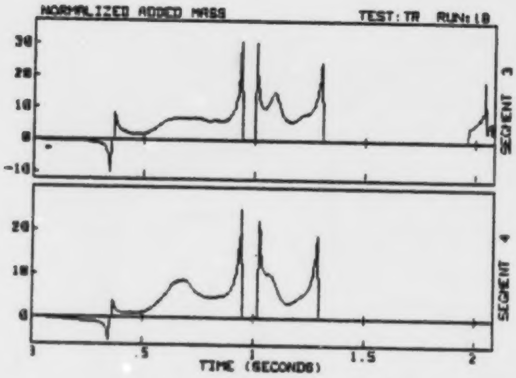

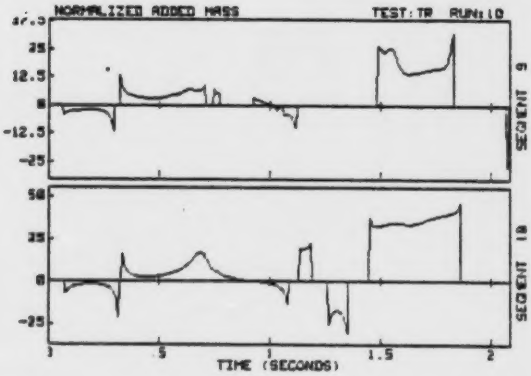

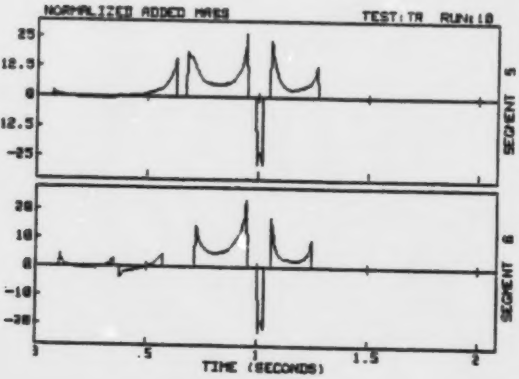

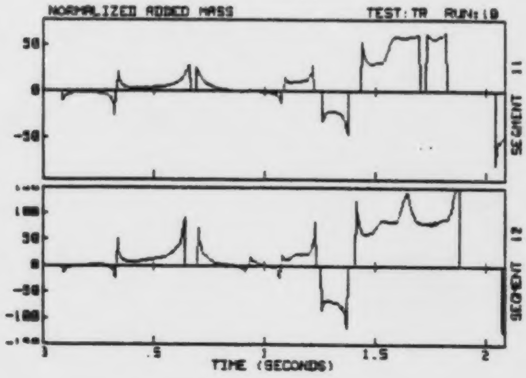

SECTION HYDRODYNAMIC FORCE

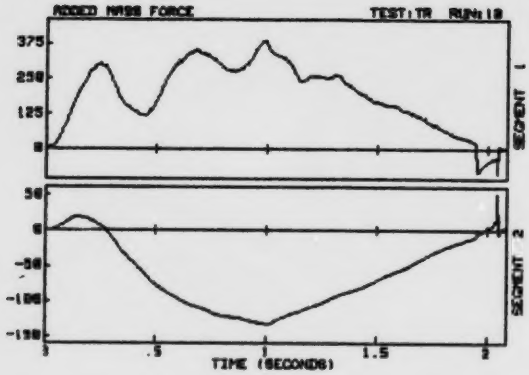

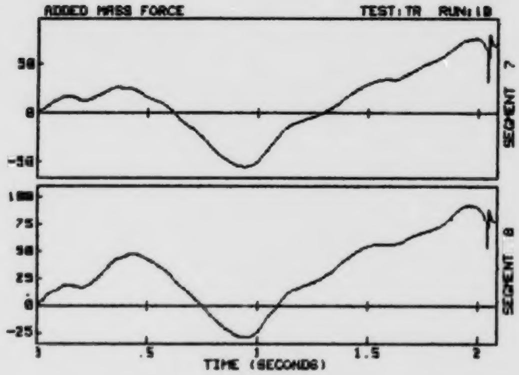

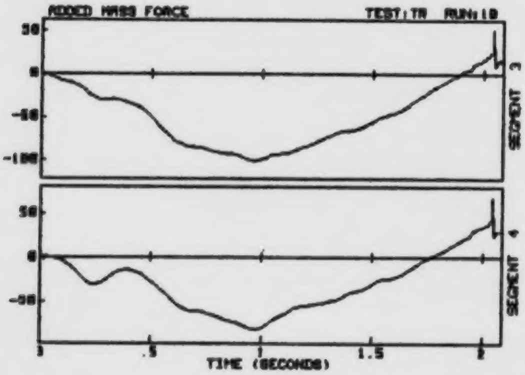

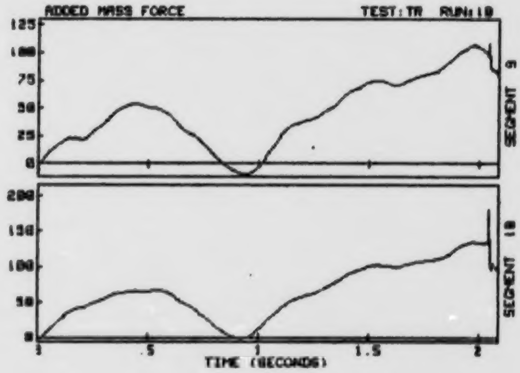

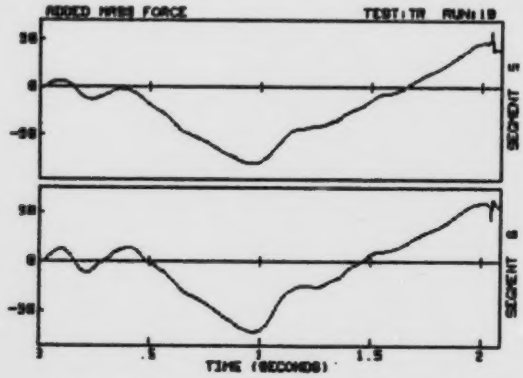

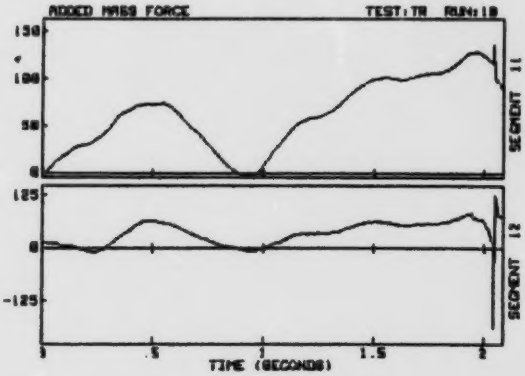

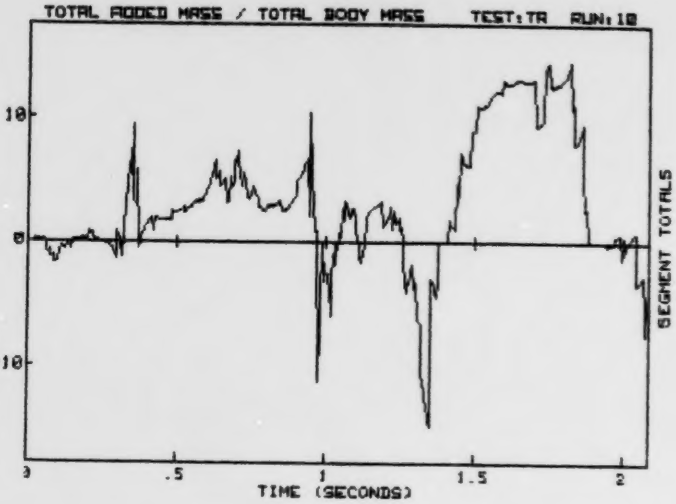

NON-DIMENSIONAL SEGMENTAL ADDED MASS STATISTICS

SEGMENT	MIN	MAX	MEAN	S.D.	NPTS
1	-727.2	355.6	-94.7	128.7	343
2	-9.8	55.3	7.8	8.4	343
3	-10.1	31.1	5.4	5.5	326
4	-5.1	24.9	4.2	4.6	286
5	-28.6	26.6	3.9	7.2	263
6	-23.1	23.4	2.6	6.1	221
7	-16.6	20	4.4	6.2	237
8	-6.9	28.7	8.8	8.3	290
9	-27.2	31.9	6.4	9.7	291
10	-31.2	46.5	10.9	17.8	374
11	-78.8	64.5	10.8	26.4	388
12	-126.2	187.6	27.2	51.6	409
MEAN MODEL ADDED MASS =			4.23		3771

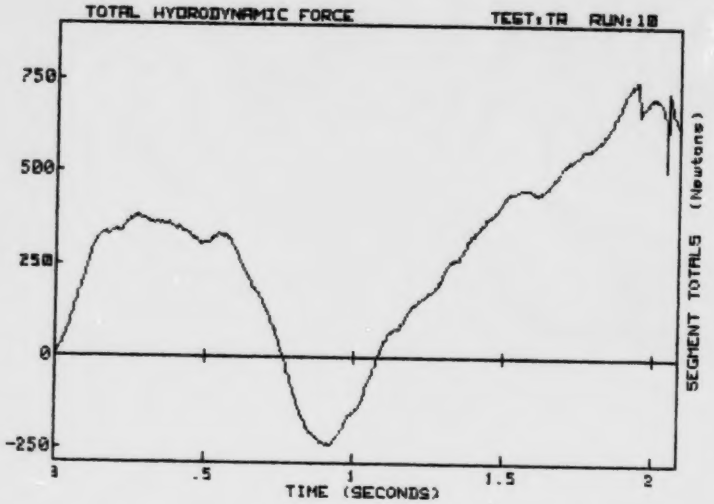

HYDRODYNAMIC FORCE SUMMARY STATISTICS

SEGMENT	MIN	MAX	MEAN	S.D.	NPTS
1	-87.1	383.6	192.5	114.6	518
2	-133.5	52.4	-62	49.3	518
3	-100.7	52.7	-48.5	35.9	518
4	-81.7	67.5	-29.8	31.8	518
5	-80.5	58.8	-19.1	34.4	518
6	-71.1	62.7	-5.1	34.3	518
7	-54.5	80.1	12.5	34.4	518
8	-29.8	92.2	31.8	32.4	518
9	-9.1	108.4	45.9	31.4	518
10	-5	180.2	64.8	38.3	518
11	-3.5	136.2	62.5	37.9	518
12	-189.8	124.5	35	28.6	518
MEAN HYDRODYNAMIC FORCE =			23.37		6216

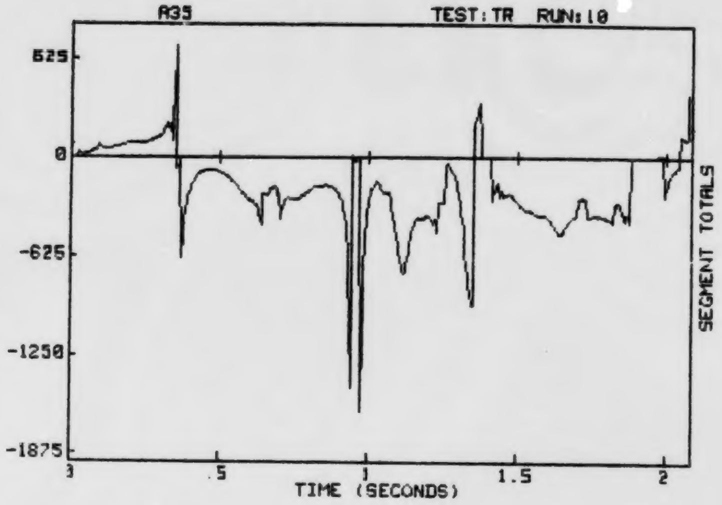

HEAVE/PITCH COUPLED ADDED MASS SUMMARY STATISTICS

SEGMENT	MIN	MAX	MEAN	S.D.	NPTS
1	-1596.2	780.5	-207.8	282.5	343
2	-18.2	102	14.4	15.5	343
3	-14.5	44.6	7.8	7.9	326
4	-5.2	25.5	4.3	4.7	286
5	-17.6	16.3	2.4	4.4	263
6	-4.7	4.8	.5	1.2	221
7	-4.1	3.4	-.9	1.3	237
8	-17.6	4.2	-5.4	5.1	290
9	-32.7	27.9	-6.5	9.9	291
10	-66.5	44.7	-15.7	25.4	374
11	-118.2	144.5	-19.9	48.3	388
12	-419.4	282.1	-60.8	115.5	409
MEAN A35 MODEL ADDED MASS =			-4.89		3771

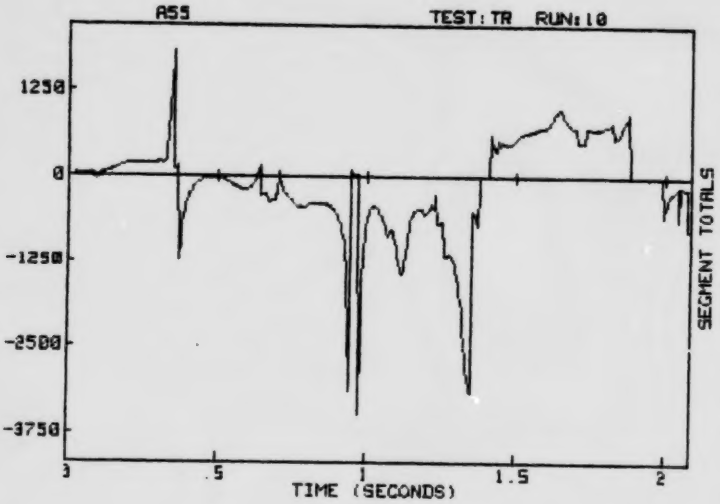

PITCH ADDED MASS MOMENT OF INERTIA SUMMARY STATISTICS

SEGMENT	MIN	MAX	MEAN	S.D.	NPTS
1	-3503.7	1713.2	-456.1	282.5	343
2	-33.5	188.1	26.6	15.5	343
3	-20.8	63.9	11.2	7.9	326
4	-5.4	26.1	4.4	4.7	286
5	-10.8	10	1.5	4.4	263
6	-1	1	.1	1.2	221
7	-.7	.8	.2	1.3	237
8	-2.6	10.8	3.3	5.1	290
9	-28.5	33.5	6.7	9.9	291
10	-64	95.1	22.4	25.4	374
11	-264.9	216.6	36.4	48.3	388
12	-630.8	937.7	135.9	115.5	409
MEAN ASS MODEL ADDED MASS =			3.42		3771

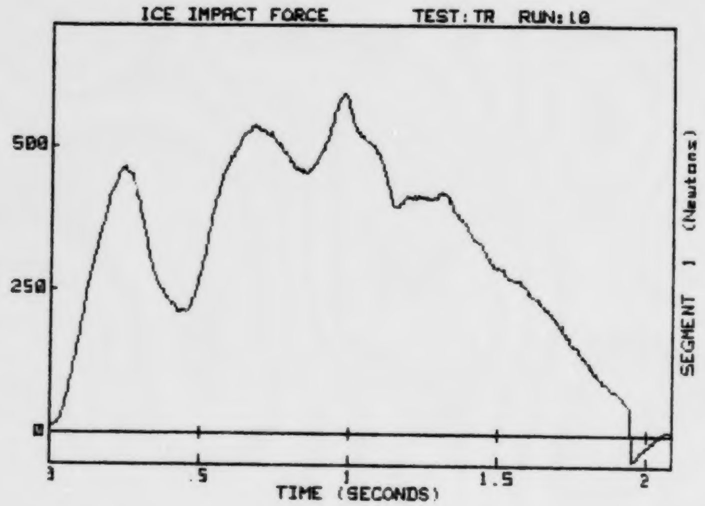
ICE IMPACT FORCE
TEST: TR RUN: 10
500
250
0
0
.5
1
1.5
2
TIME (SECONDS)
SEGMENT 1 (Newtons)

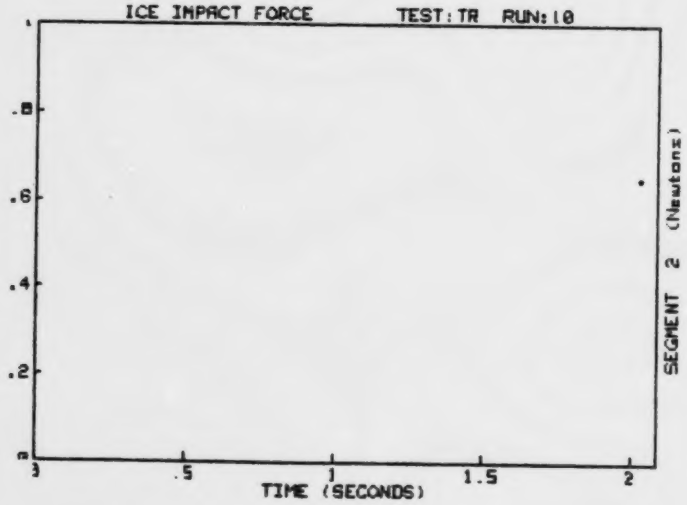
ICE IMPACT FORCE
TEST: TR RUN: 10
1
.8
.6
.4
.2
0
0
.5
1
1.5
2
TIME (SECONDS)
SEGMENT 2 (Newtons)

IMPACT VELOCITY= .58 m/s
SHIP SPEED= 7.13 kt

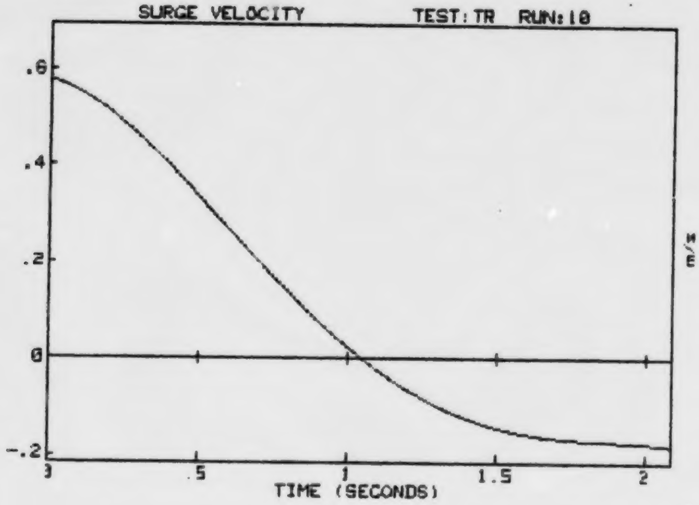

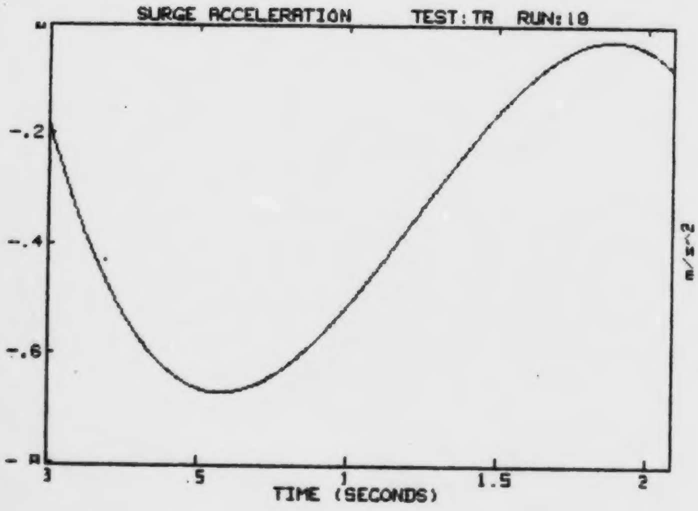

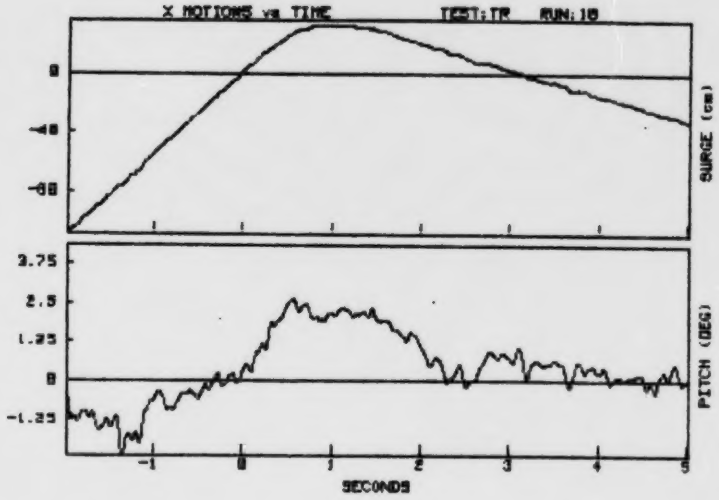
X MOTIONS vs TIME
TEST: TR
RUN: 10
0
-40
-80
SURGE (cm)
3.75
2.5
1.25
0
-1.25
PITCH (DEG)
-1
0
1
2
3
4
5
SECONDS

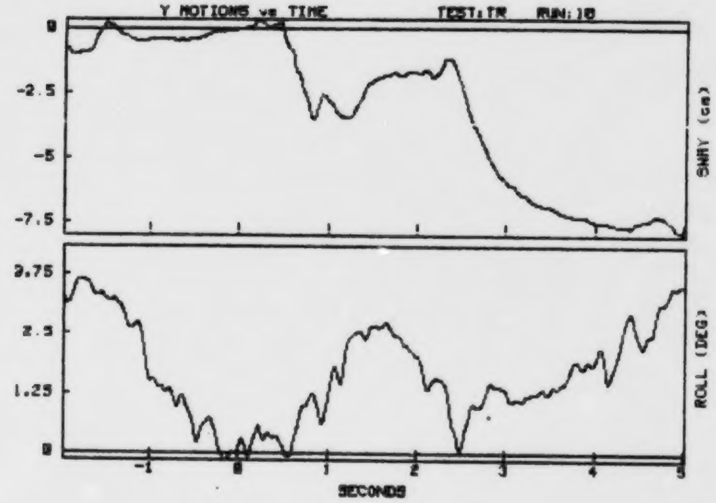
Y MOTIONS vs TIME
TEST: TR
RUN: 10
0
-2.5
-5
-7.5
SWAY (cm)
3.75
2.5
1.25
0
ROLL (DEG)
-1
0
1
2
3
4
5
SECONDS

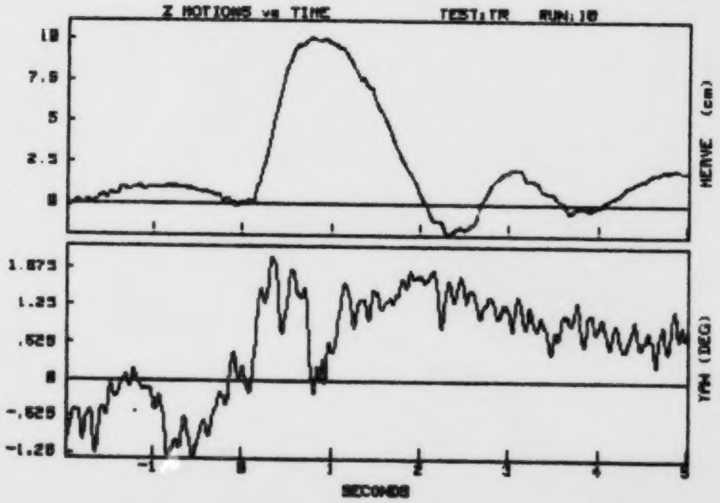
Z MOTIONS vs TIME
TEST: TR
RUN: 10
10
7.5
5
2.5
0
HEAVE (cm)
1.875
1.25
.625
0
-.625
-1.25
YAW (DEG)
-1
0
1
2
3
4
5
SECONDS

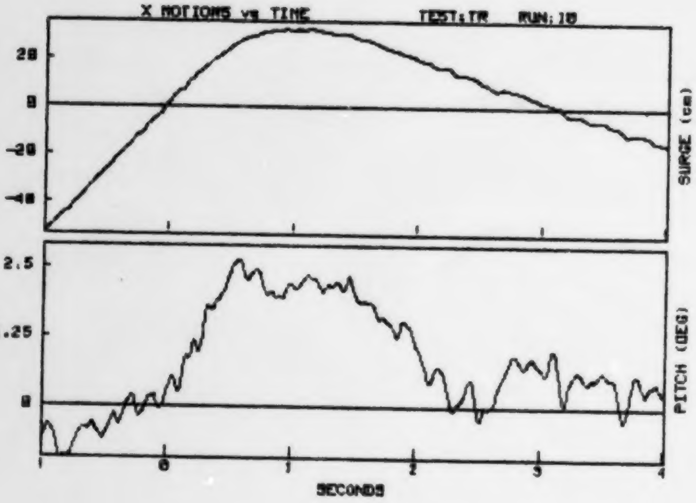
X MOTIONS vs TIME
TEST:TR RUN:10
20
0
-20
-40
SURGE (cm)
2.5
1.25
0
PITCH (DEG)
0
1
2
3
4
SECONDS

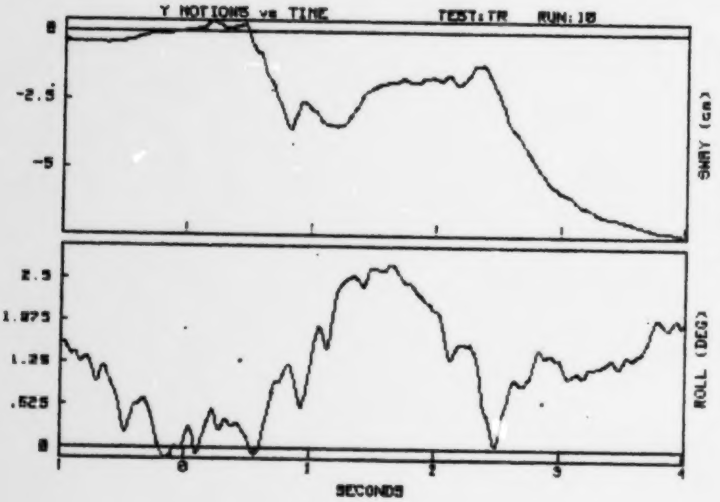
Y MOTIONS vs TIME
TEST:TR RUN:10
0
-2.5
-5
SWAY (cm)
2.5
1.875
1.25
.625
0
ROLL (DEG)
0
1
2
3
4
SECONDS

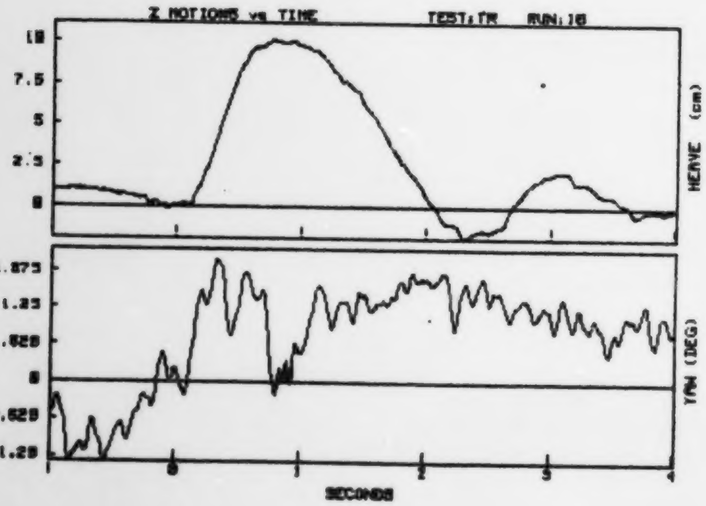
Z MOTIONS vs TIME
TEST:TR RUN:10
10
7.5
5
2.5
0
HEAVE (cm)
1.875
1.25
.625
0
-.625
-1.25
YAW (DEG)
0
1
2
3
4
SECONDS

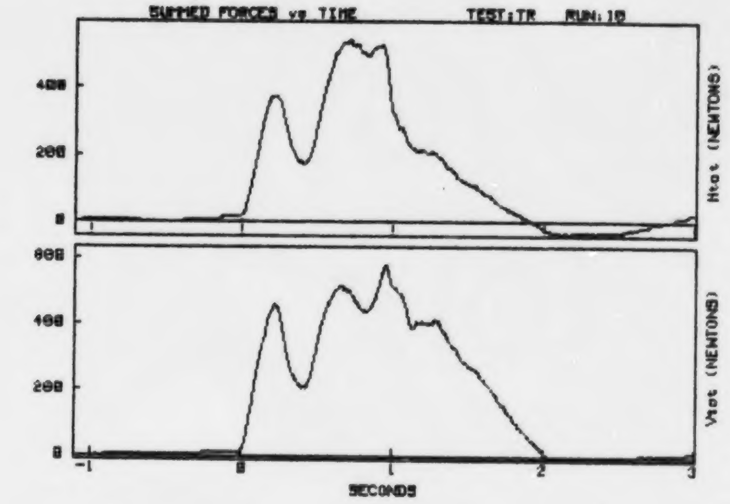
SUMMED FORCES vs TIME
TEST:TR
RUN:10
400
200
0
Htot (NEWTONS)
600
400
200
0
Vtot (NEWTONS)
-1
0
1
2
3
SECONDS

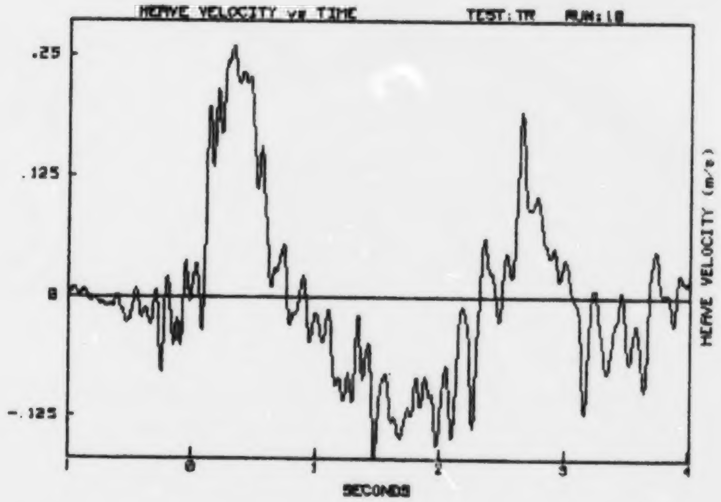
HEAVE VELOCITY vs TIME
TEST:TR
RUN:10
.25
.125
0
-.125
HEAVE VELOCITY (m/s)
0
1
2
3
4
SECONDS

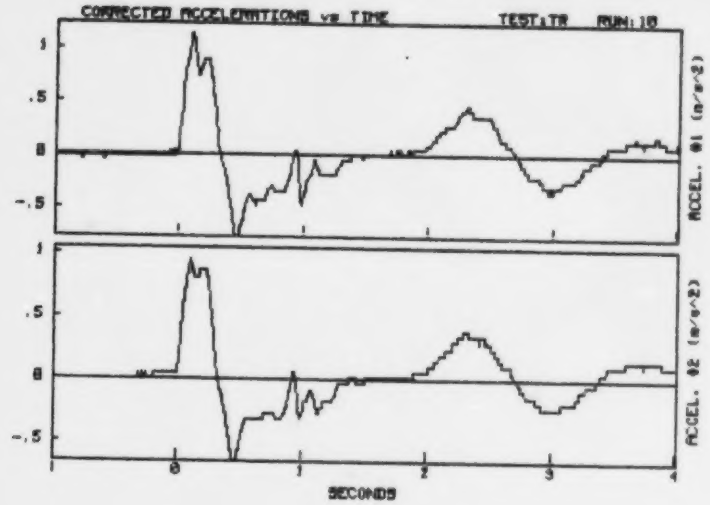
CORRECTED ACCELERATIONS vs TIME
TEST:TR
RUN:10
1
.5
0
-.5
ACCEL. #1 (m/s^2)
1
.5
0
-.5
ACCEL. #2 (m/s^2)
0
1
2
3
4
SECONDS

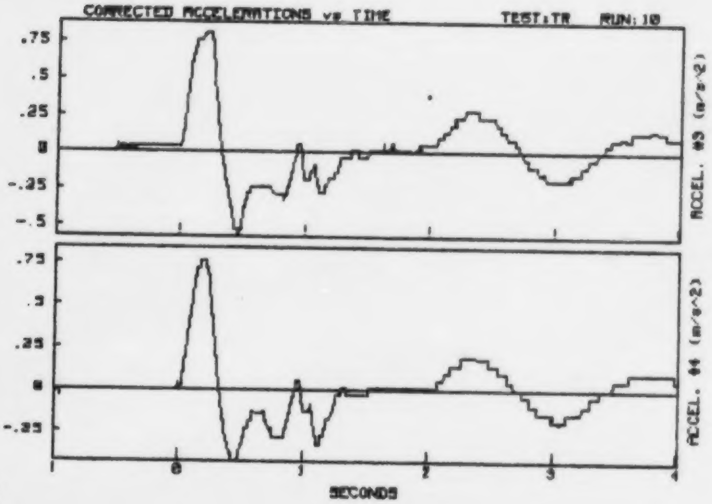
CORRECTED ACCELERATIONS vs TIME
TEST:TR
RUN:10
.75
.5
.25
0
-.25
-.5
ACCEL. #3 (m/s^2)
.75
.5
.25
0
-.25
ACCEL. #4 (m/s^2)
0
1
2
3
4
SECONDS

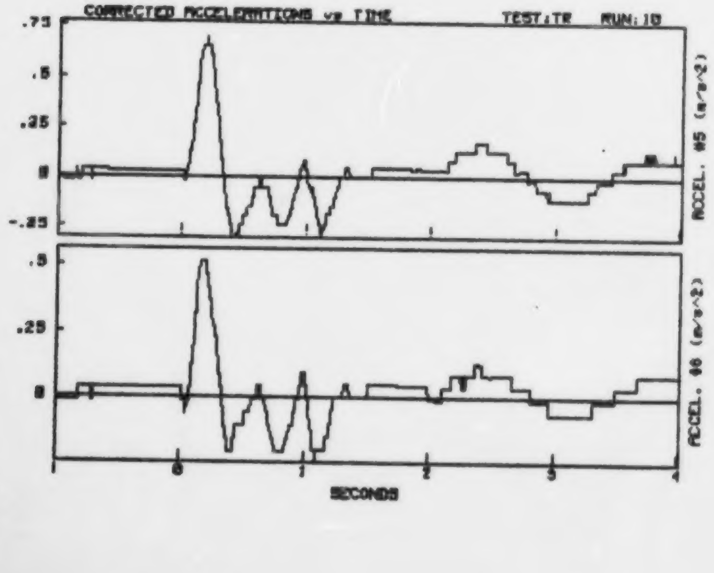
CORRECTED ACCELERATIONS vs TIME
TEST:TR
RUN:10
.75
.5
.25
0
-.25
ACCEL. #5 (m/s^2)
.5
.25
0
ACCEL. #6 (m/s^2)
0
1
2
3
4
SECONDS

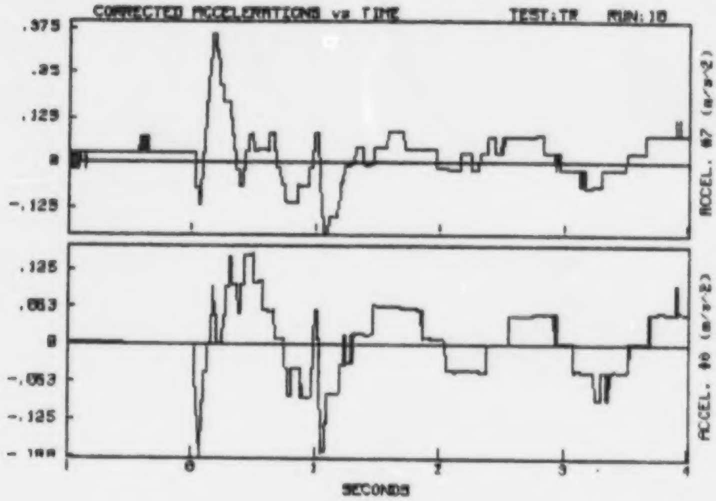
CORRECTED ACCELERATIONS vs TIME
TEST:TR RUN:10
.375
.25
.125
0
-.125
ACCEL. #7 (m/s^2)
.125
.063
0
-.063
-.125
-.188
ACCEL. #8 (m/s^2)
0
1
2
3
4
SECONDS

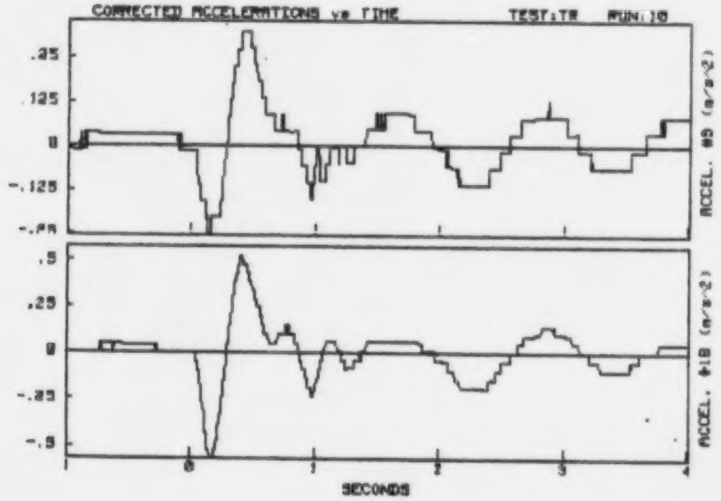
CORRECTED ACCELERATIONS vs TIME
TEST:TR RUN:10
.25
.125
0
-.125
-.25
ACCEL. #9 (m/s^2)
.5
.25
0
-.25
-.5
ACCEL. #10 (m/s^2)
0
1
2
3
4
SECONDS

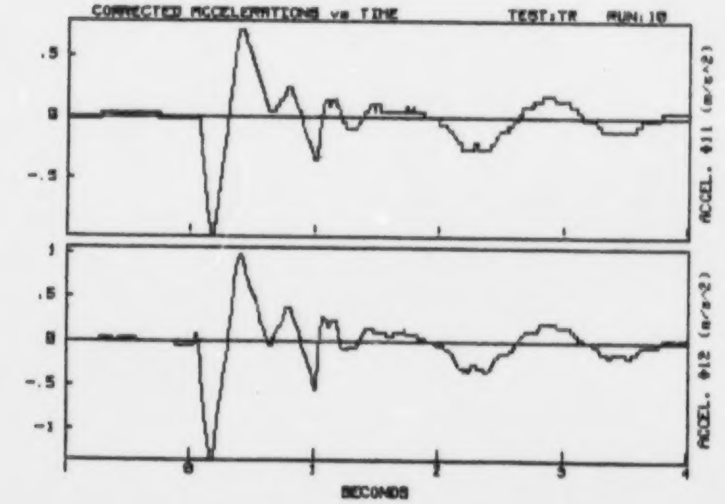
CORRECTED ACCELERATIONS vs TIME
TEST:TR RUN:10
.5
0
-.5
ACCEL. #11 (m/s^2)
1
.5
0
-.5
-1
ACCEL. #12 (m/s^2)
0
1
2
3
4
SECONDS

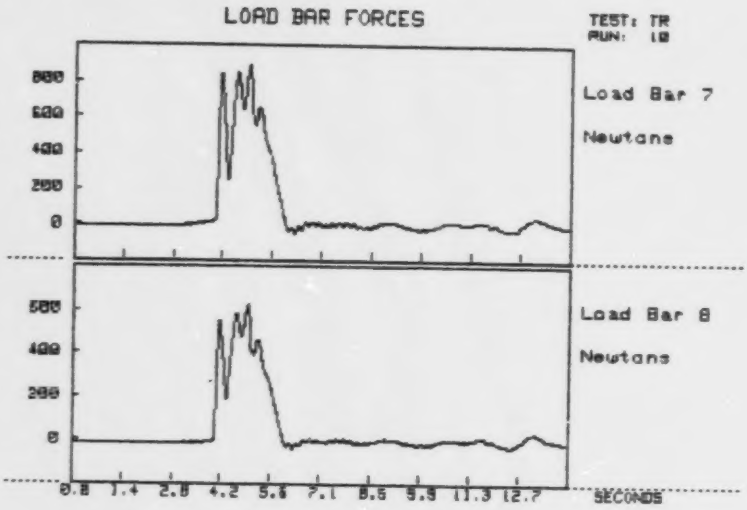
LOAD BAR FORCES
TEST: TR
RUN: 10
800
600
400
200
0
Load Bar 7
Newtons
500
400
200
0
Load Bar 8
Newtons
0.0
1.4
2.8
4.2
5.6
7.1
8.5
9.9
11.3
12.7
SECONDS

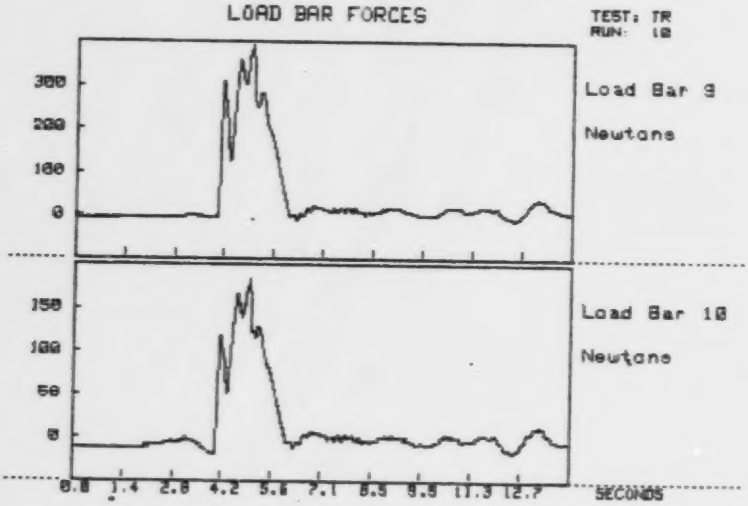
LOAD BAR FORCES
TEST: TR
RUN: 10
300
200
100
0
Load Bar 9
Newtons
150
100
50
0
Load Bar 10
Newtons
0.0
1.4
2.8
4.2
5.6
7.1
8.5
9.9
11.3
12.7
SECONDS

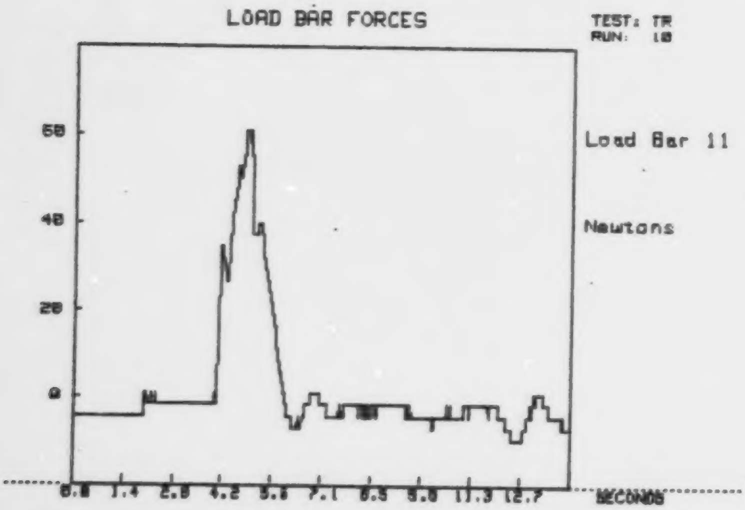
LOAD BAR FORCES
TEST: TR
RUN: 10
60
40
20
0
Load Bar 11
Newtons
0.0
1.4
2.8
4.2
5.6
7.1
8.5
9.9
11.3
12.7
SECONDS

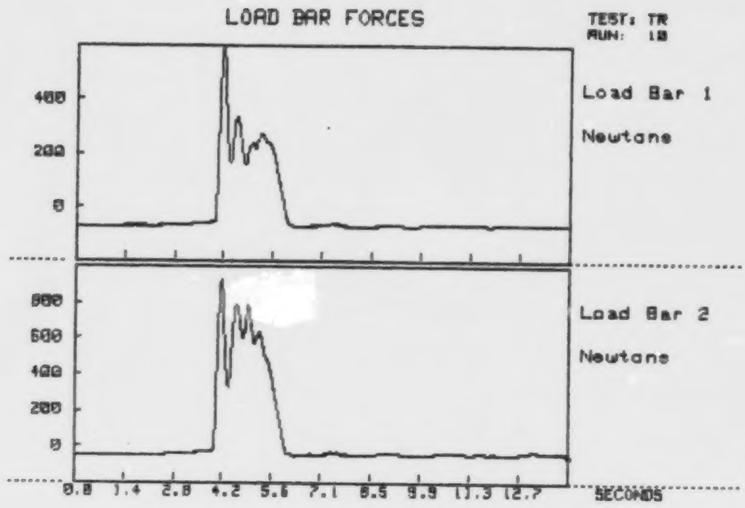
LOAD BAR FORCES
TEST: TR
RUN: 10
Load Bar 1
Newtons
400
200
0
Load Bar 2
Newtons
800
600
400
200
0
0.0
1.4
2.8
4.2
5.6
7.1
8.5
9.9
11.3
12.7
SECONDS

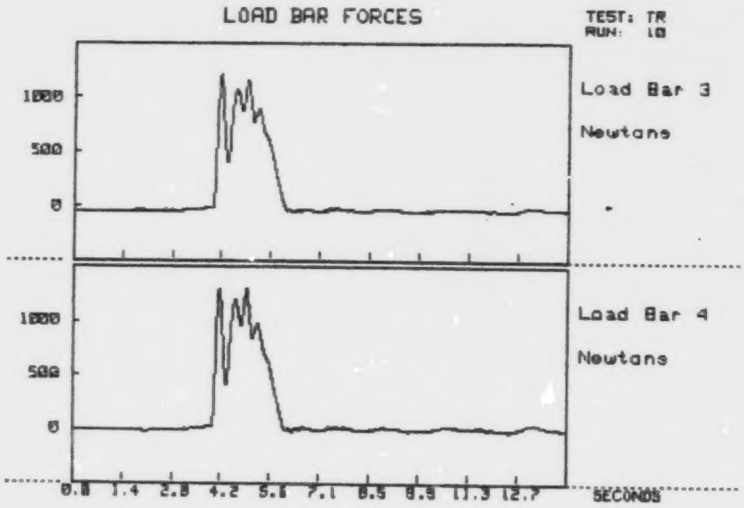
LOAD BAR FORCES
TEST: TR
RUN: 10
Load Bar 3
Newtons
1000
500
0
Load Bar 4
Newtons
1000
500
0
0.0
1.4
2.8
4.2
5.6
7.1
8.5
9.9
11.3
12.7
SECONDS

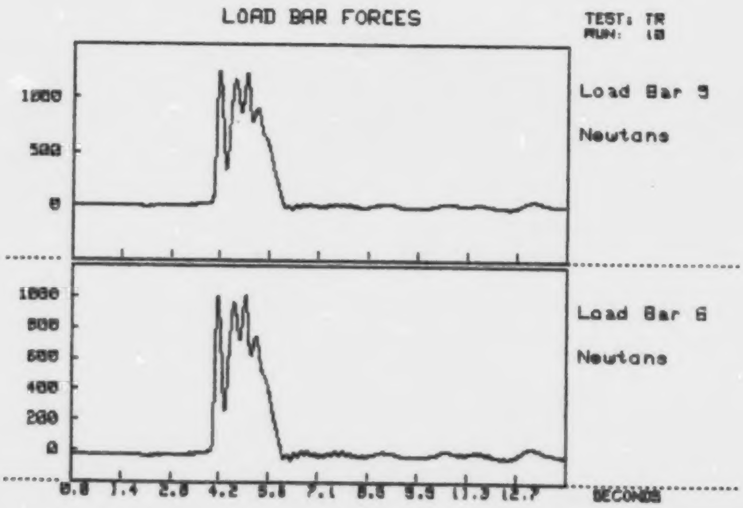
LOAD BAR FORCES
TEST: TR
RUN: 10
Load Bar 5
Newtons
1000
500
0
Load Bar 6
Newtons
1000
800
600
400
200
0
0.0
1.4
2.8
4.2
5.6
7.1
8.5
9.9
11.3
12.7
SECONDS

```
                MV  ARCTIC MODEL TESTS
                ADDED MASS CALCULATION



                   TEST:            TR
                   RUN NUMBER:      11


         NOMINAL IMPACT VELOCITY:            .63      m/s
         NOMINAL SHIP SPEED:                 7.7      kt
         TIME TO MAXIMUM SURGE:              1.194    s
         TIME FROM IMPACT TO BACKOFF:        1.762    s


         TIME INCREMENT:                     .004     s
         ACCELEROMETER THRESHOLD:            .05      m/s^2


         MODEL MASS:                          596     kg
         WATER DEPTH:                         1.85    m
         MODEL DRAFT:                         0.275   m
         ICE FREEBOARD:                       0.025   m
```

SEGMENT ADDED MASS NORMALIZED BY DISPLACED MASS

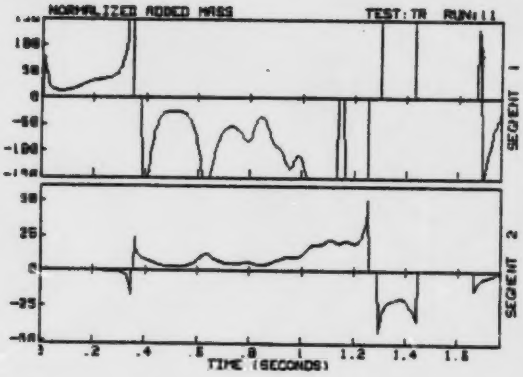

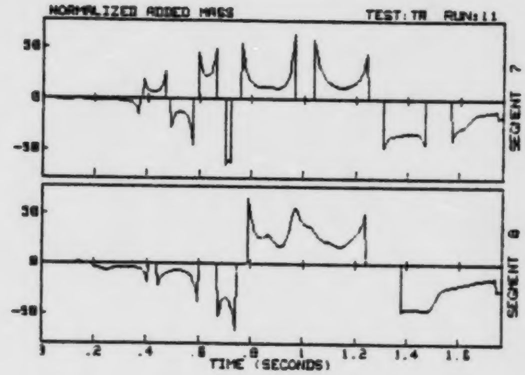

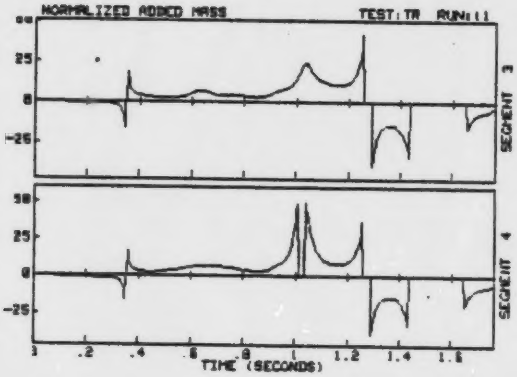

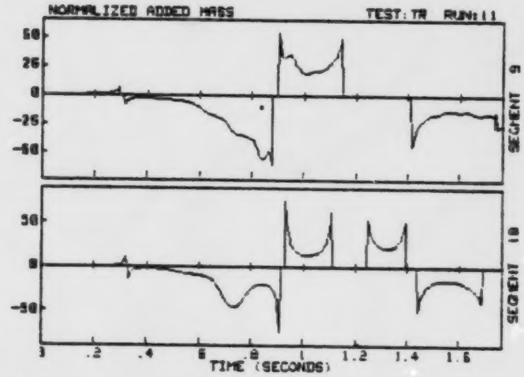

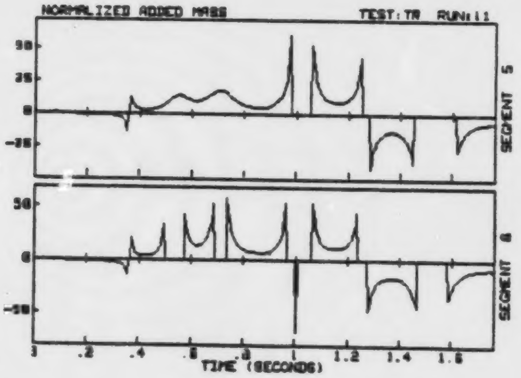

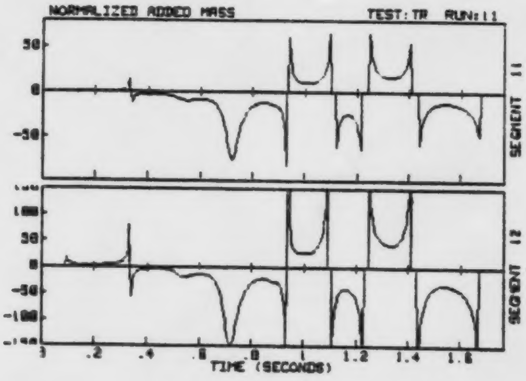

SEGMENT HYDRODYNAMIC FORCE

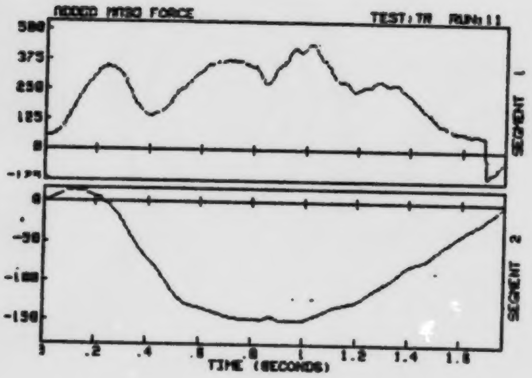

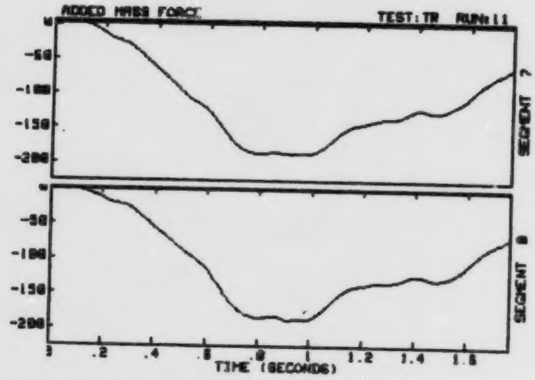

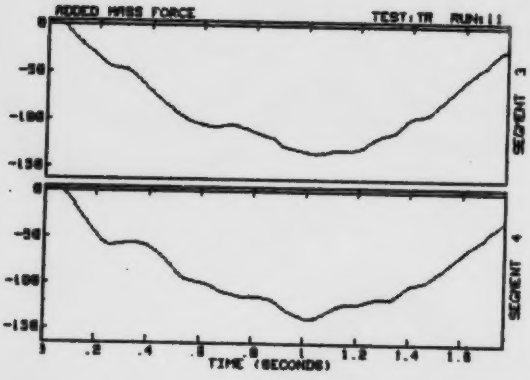

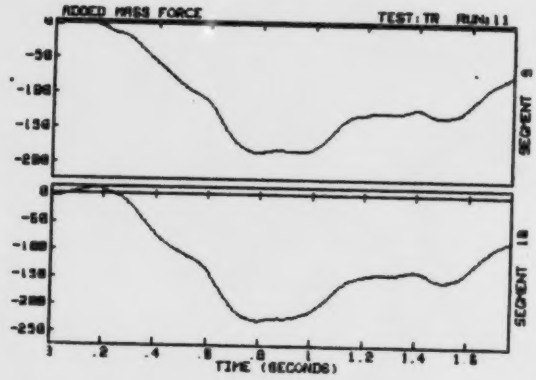

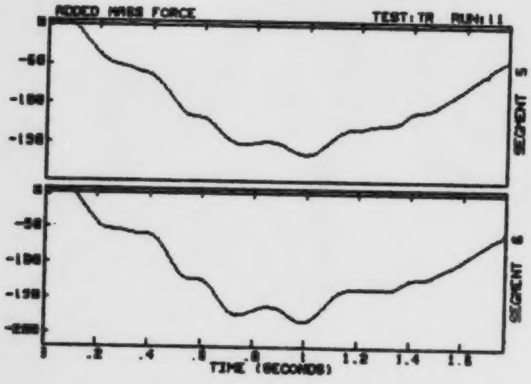

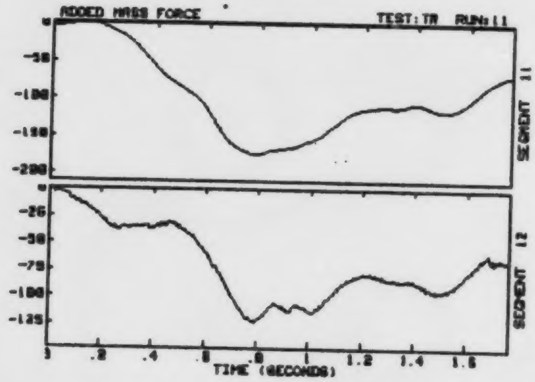

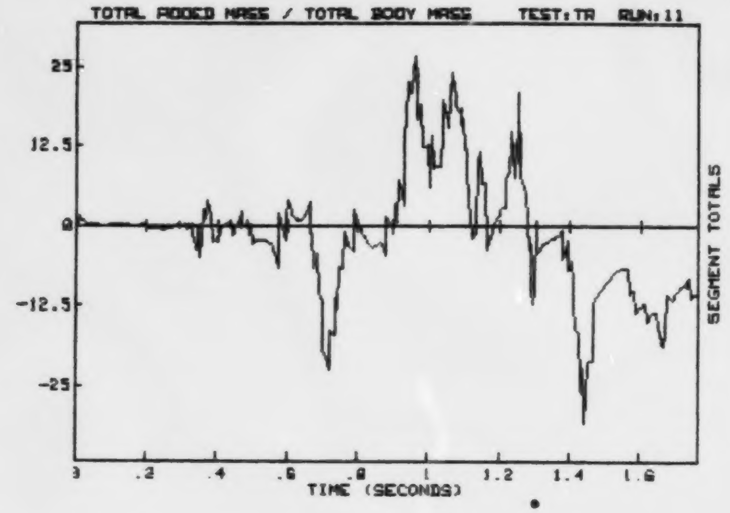

NON-DIMENSIONAL SEGMENTAL ADDED MASS STATISTICS

SEGMENT	MIN	MAX	MEAN	S.D.	NPTS
1	-682.1	589.1	-54.7	203.6	348
2	-43.4	50.8	3.8	12.8	370
3	-39.7	42.1	2.2	10.5	365
4	-38.8	50.4	2.6	12	357
5	-41.4	59.8	3	13.6	348
6	-67.7	57.6	1.9	18.9	316
7	-64.3	64.1	-1	23.2	330
8	-66.8	64.8	-2.9	26.9	342
9	-61.4	54.3	-7.1	21.3	344
10	-75.3	75.1	-5	22.3	350
11	-81	66.3	-6.8	22.4	369
12	-245.7	189.7	-15	56.8	374
MEAN MODEL ADDED MASS =			-1.6		4213

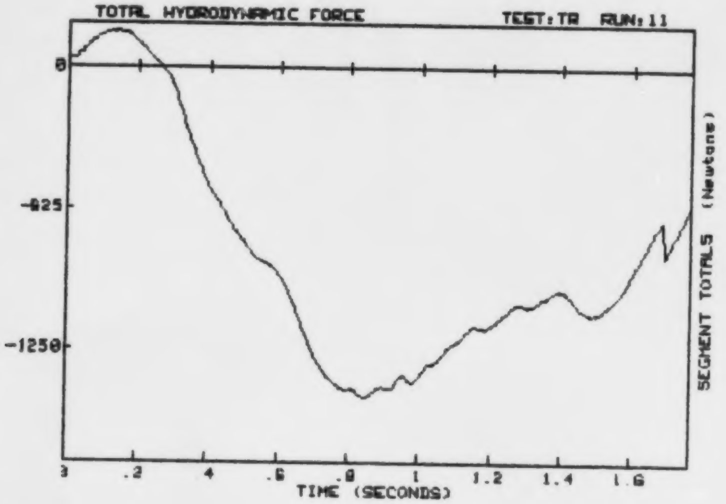

HYDRODYNAMIC FORCE SUMMARY STATISTICS

SEGMENT	MIN	MAX	MEAN	S.D.	NPTS
1	-107.7	447.1	239.9	124.6	438
2	-150.1	15	-83.6	56.8	438
3	-134.7	3.6	-84.2	39.9	438
4	-138.3	4.4	-85.5	38	438
5	-164.4	4.2	-98.7	48.1	438
6	-183.5	5.2	-107.8	52.9	438
7	-187.9	3.9	-109.2	60.2	438
8	-188.8	1.8	-107.1	60	438
9	-184.7	2.6	-105.3	59	438
10	-229.2	12.3	-123.3	74	438
11	-174.4	1.8	-96.6	53.8	438
12	-123.6	.5	-69.8	33.7	438

MEAN HYDRODYNAMIC FORCE = -69.26 5256

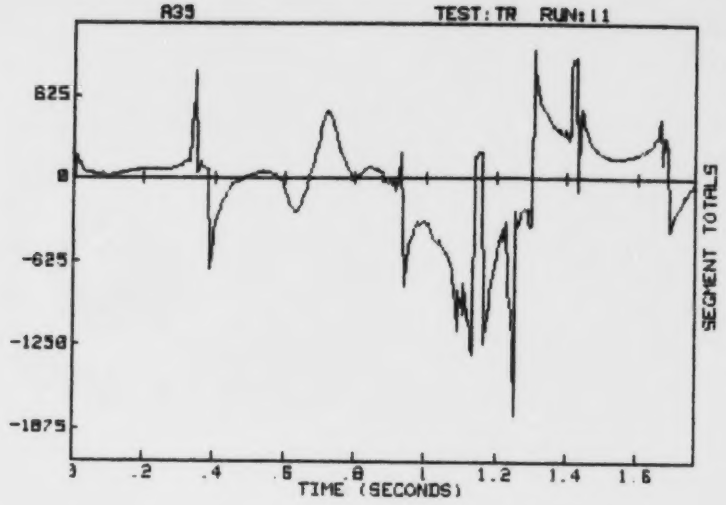

HEAVE/PITCH COUPLED ADDED MASS SUMMARY STATISTICS

SEGMENT	MIN	MAX	MEAN	S.D.	NPTS
1	-1497.2	1293	-120	446.9	348
2	-79.9	93.7	7	23.6	370
3	-56.9	60.4	3.2	15.1	365
4	-39.7	51.6	2.7	12.3	357
5	-25.4	36.8	1.8	8.4	348
6	-13.9	11.8	.4	3.9	316
7	-13.1	13.2	.2	4.8	330
8	-39.9	41.1	1.8	16.5	342
9	-55.6	62.9	7.3	21.8	344
10	-107.4	107.7	7.1	31.9	350
11	-121.5	148.4	12.5	41.1	369
12	-424.1	549.4	33.5	127.1	374
MEAN A35 MODEL ADDED MASS =			2.04		4213

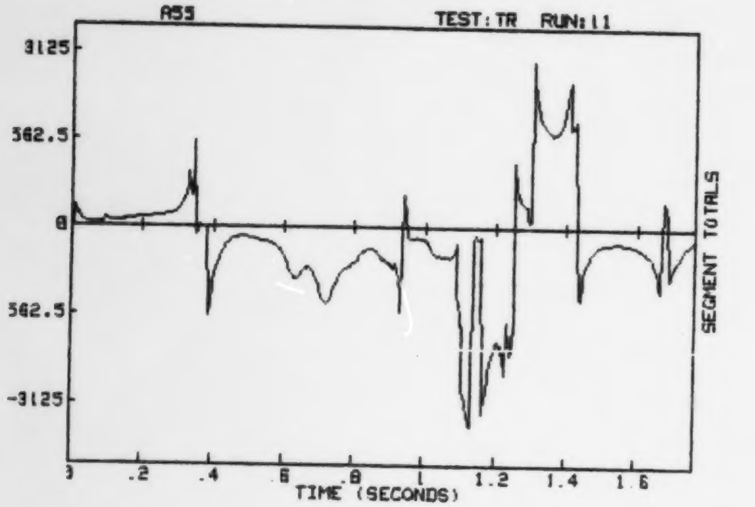

PITCH ADDED MASS MOMENT OF INERTIA SUMMARY STATISTICS

SEGMENT	MIN	MAX	MEAN	S.D.	NPTS
1	-3286.4	2838.2	-263.3	446.9	348
2	-147.4	172.8	12.9	23.6	370
3	-81.6	86.7	4.6	15.1	365
4	-40.7	52.8	2.7	12.3	357
5	-15.6	22.6	1.1	8.4	348
6	-2.8	2.4	.1	3.9	316
7	-2.7	2.7	0	4.8	330
8	-25.3	24.5	-1.1	16.5	342
9	-64.4	56.9	-7.4	21.8	344
10	-154.1	153.8	-10.2	31.9	350
11	-272.1	222.8	-22.9	41.1	369
12	-1228.5	948.4	-75	127.1	374
MEAN A55 MODEL ADDED MASS =			-5.86		4213

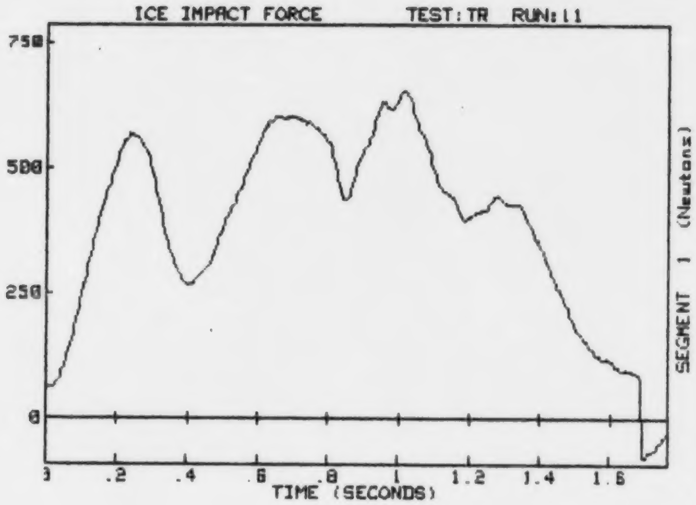
ICE IMPACT FORCE TEST:TR RUN:11
750
500
250
0
0
.2
.4
.6
.8
1
1.2
1.4
1.6
TIME (SECONDS)
SEGMENT 1 (Newtons)

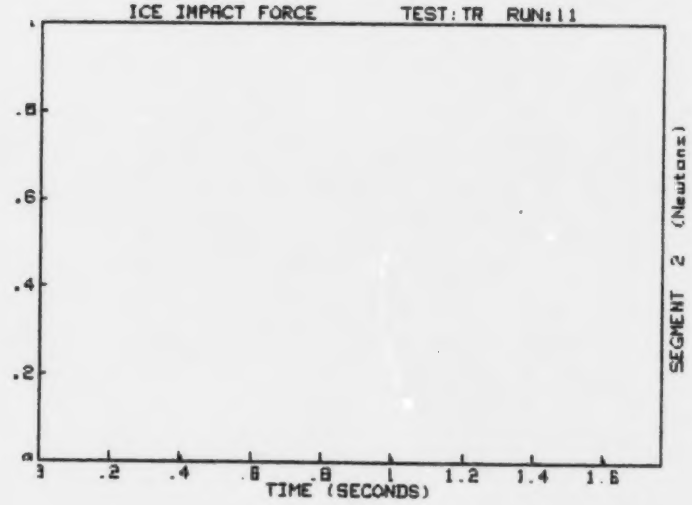
ICE IMPACT FORCE TEST:TR RUN:11
1
.8
.6
.4
.2
0
0
.2
.4
.6
.8
1
1.2
1.4
1.6
TIME (SECONDS)
SEGMENT 2 (Newtons)

IMPACT VELOCITY= .67 m/s
SHIP SPEED= 8.18 kt

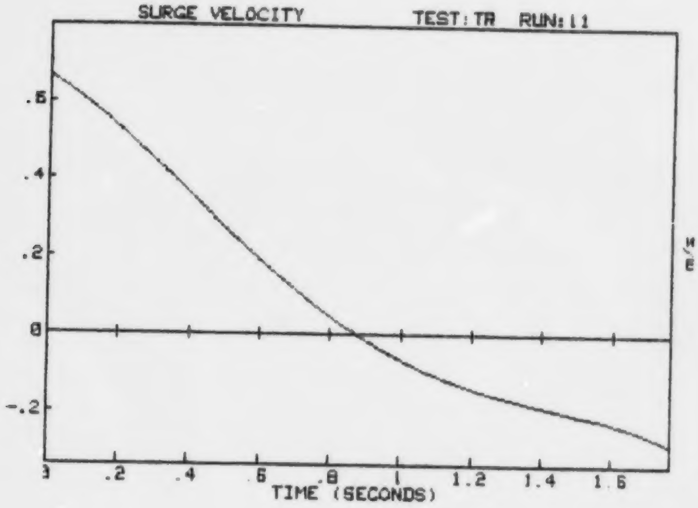

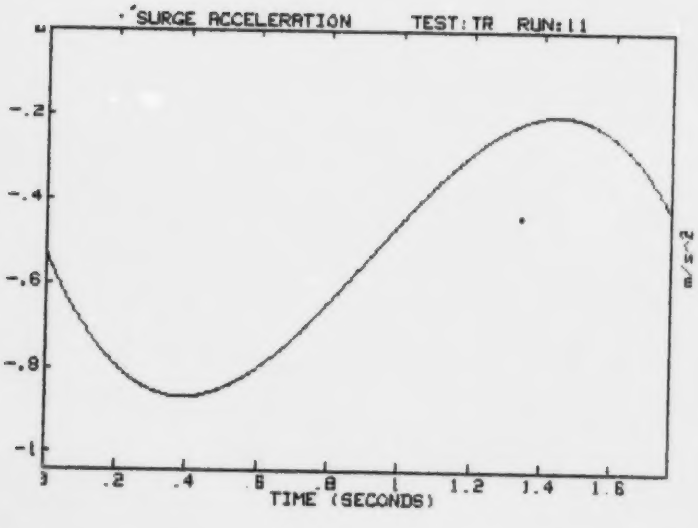

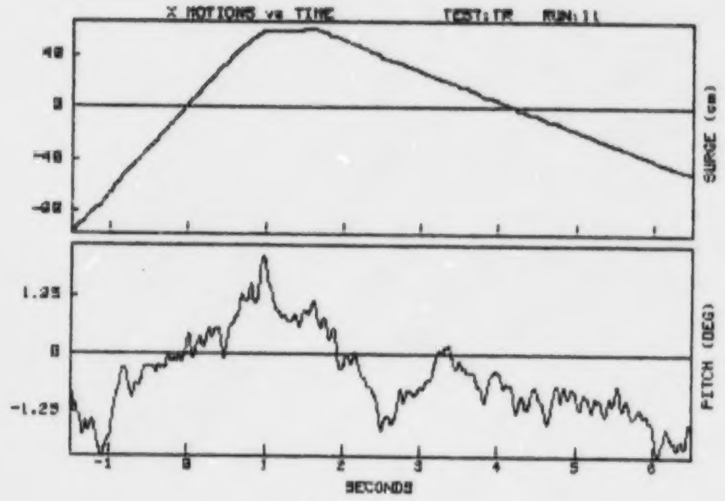
X MOTIONS vs TIME
TEST:TR RUN:11
40
0
-40
-80
SURGE (cm)
1.25
0
-1.25
PITCH (DEG)
-1
0
1
2
3
4
5
6
SECONDS

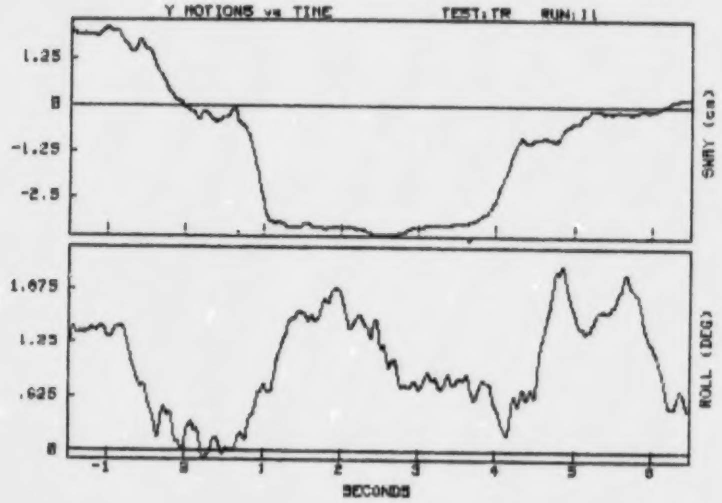
Y MOTIONS vs TIME
TEST:TR RUN:11
1.25
0
-1.25
-2.5
SWAY (cm)
1.875
1.25
.625
0
ROLL (DEG)
-1
0
1
2
3
4
5
6
SECONDS

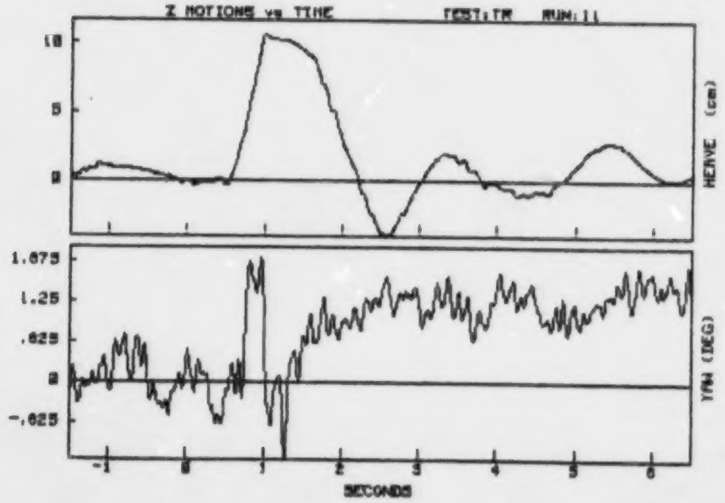
Z MOTIONS vs TIME
TEST:TR RUN:11
10
5
0
HEAVE (cm)
1.875
1.25
.625
0
-.625
YAW (DEG)
-1
0
1
2
3
4
5
6
SECONDS

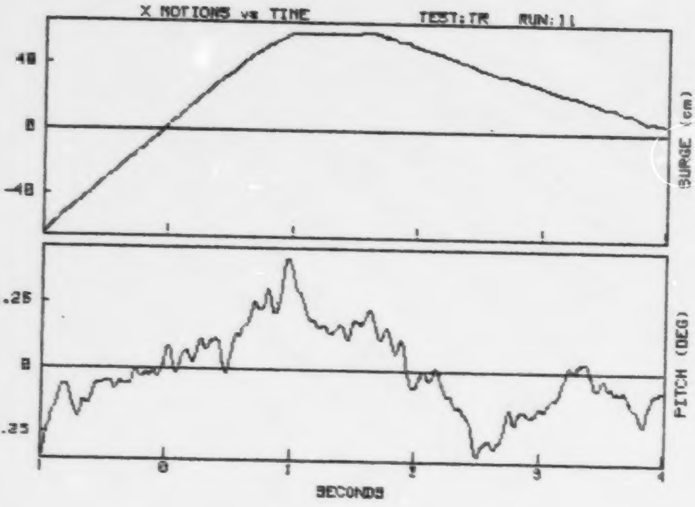
X MOTIONS vs TIME
TEST:TR RUN:11
40
0
-40
SURGE (cm)
1.25
0
-1.25
PITCH (DEG)
0
1
2
3
4
SECONDS

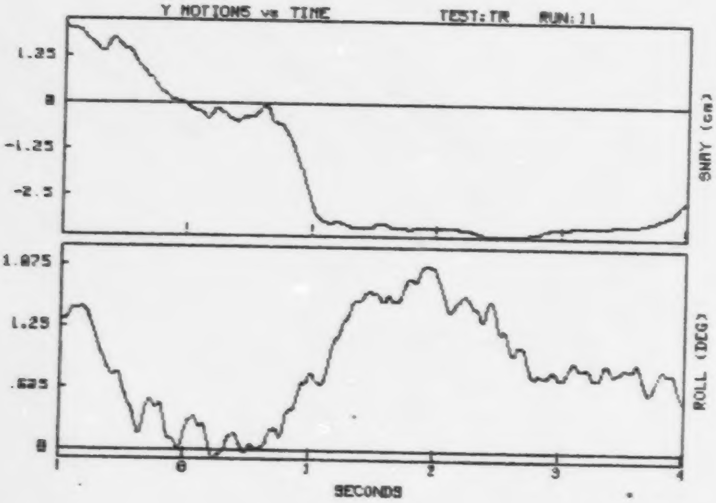
Y MOTIONS vs TIME
TEST:TR RUN:11
1.25
0
-1.25
-2.5
SWAY (cm)
1.875
1.25
.625
0
ROLL (DEG)
0
1
2
3
4
SECONDS

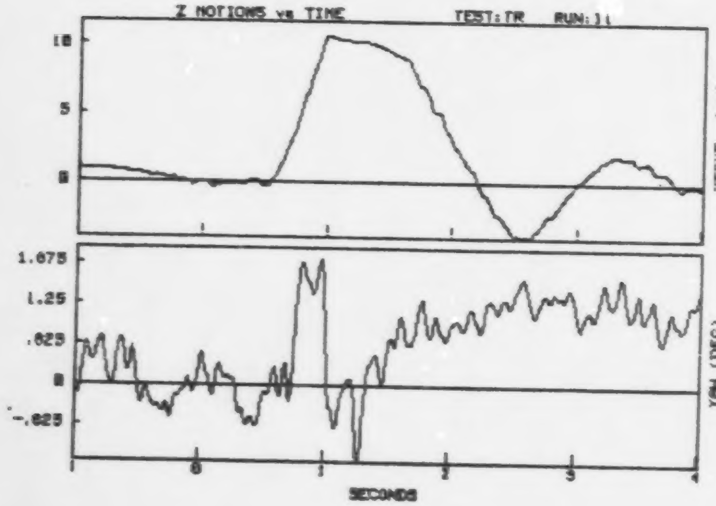
Z MOTIONS vs TIME
TEST:TR RUN:11
10
5
0
HEAVE (cm)
1.875
1.25
.625
0
-.625
YAW (DEG)
0
1
2
3
4
SECONDS

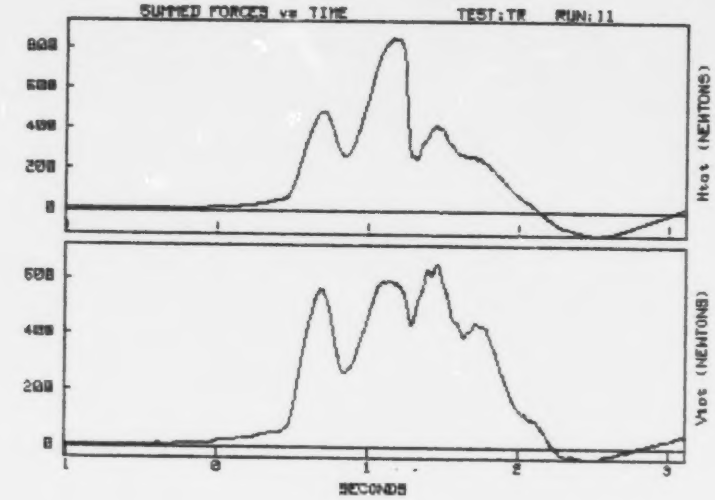
SUMMED FORCES vs TIME
TEST: TR RUN: 11
800
600
400
200
0
Htot (NEWTONS)
600
400
200
0
Vtot (NEWTONS)
1
0
1
2
3
SECONDS

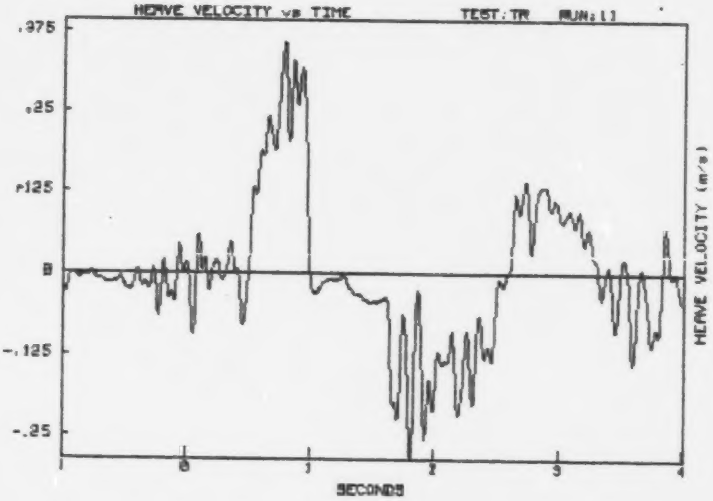
HEAVE VELOCITY vs TIME
TEST: TR RUN: 11
.375
.25
.125
0
-.125
-.25
HEAVE VELOCITY (m/s)
1
0
1
2
3
4
SECONDS

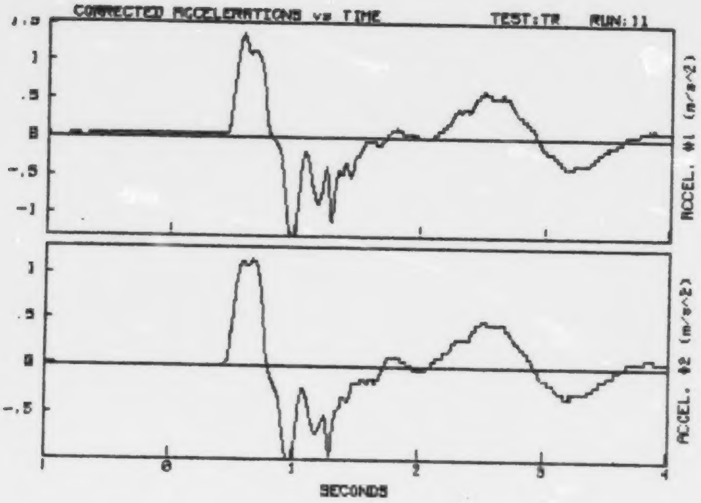
CORRECTED ACCELERATIONS vs TIME
TEST:TR RUN:11
1.5
1
.5
0
-.5
-1
ACCEL. #1 (m/s^2)
1
.5
0
-.5
ACCEL. #2 (m/s^2)
0
1
2
3
4
SECONDS

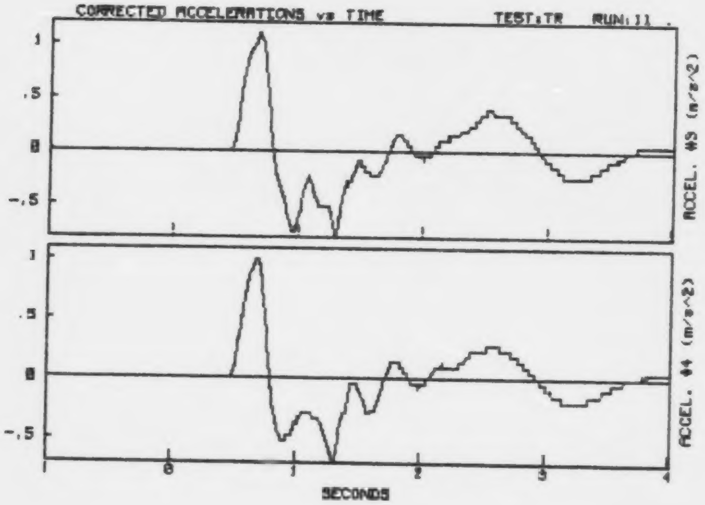
CORRECTED ACCELERATIONS vs TIME
TEST:TR RUN:11
1
.5
0
-.5
ACCEL. #3 (m/s^2)
1
.5
0
-.5
ACCEL. #4 (m/s^2)
0
1
2
3
4
SECONDS

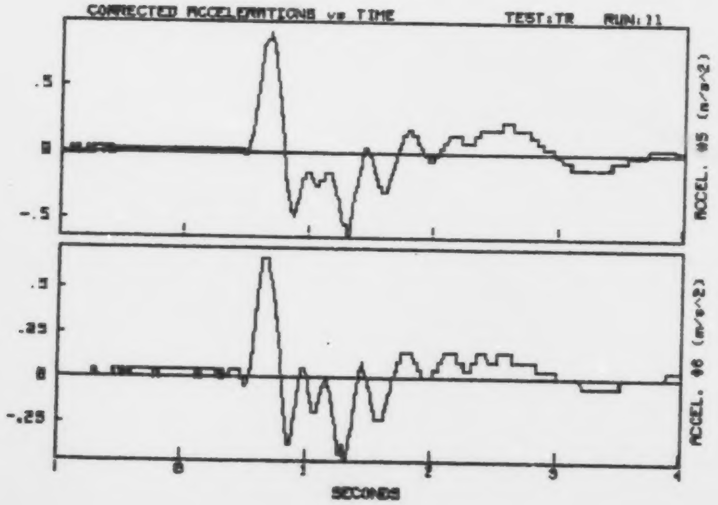
CORRECTED ACCELERATIONS vs TIME
TEST:TR RUN:11
.5
0
-.5
ACCEL. #5 (m/s^2)
.5
.25
0
-.25
ACCEL. #6 (m/s^2)
0
1
2
3
4
SECONDS

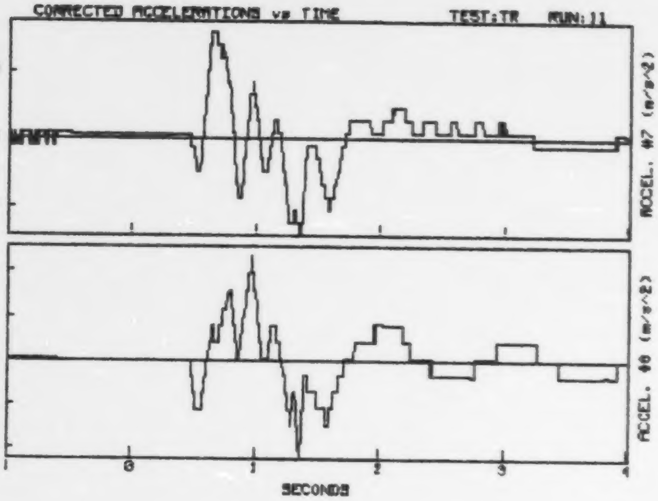
CORRECTED ACCELERATIONS vs TIME
TEST:TR RUN:11
.25
0
-.25
ACCEL. #7 (m/s^2)
.25
.125
0
-.125
-.25
ACCEL. #8 (m/s^2)
0
1
2
3
4
SECONDS

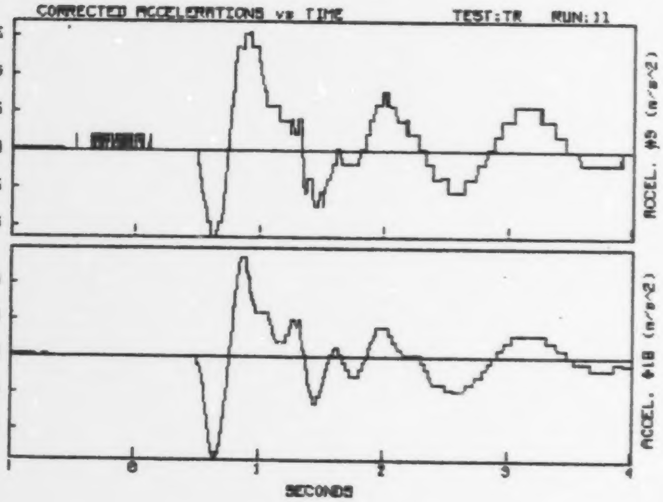
CORRECTED ACCELERATIONS vs TIME
TEST:TR RUN:11
.375
.25
.125
0
-.125
-.25
ACCEL. #9 (m/s^2)
.5
.25
0
-.25
-.5
ACCEL. #10 (m/s^2)
0
1
2
3
4
SECONDS

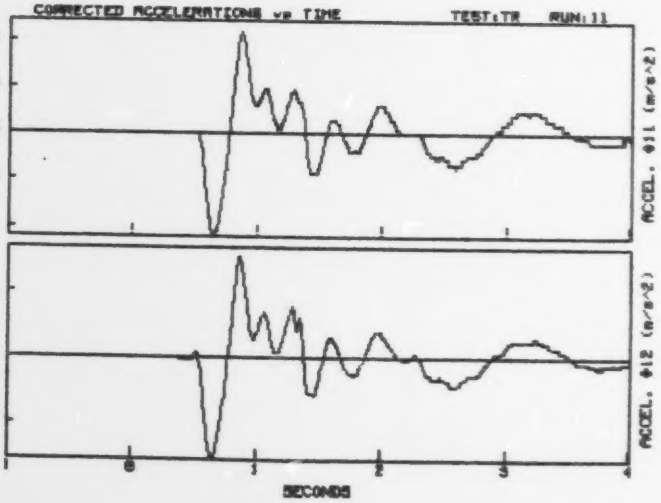
CORRECTED ACCELERATIONS vs TIME
TEST:TR RUN:11
1
.5
0
-.5
-1
ACCEL. #11 (m/s^2)
1
0
-1
ACCEL. #12 (m/s^2)
0
1
2
3
4
SECONDS

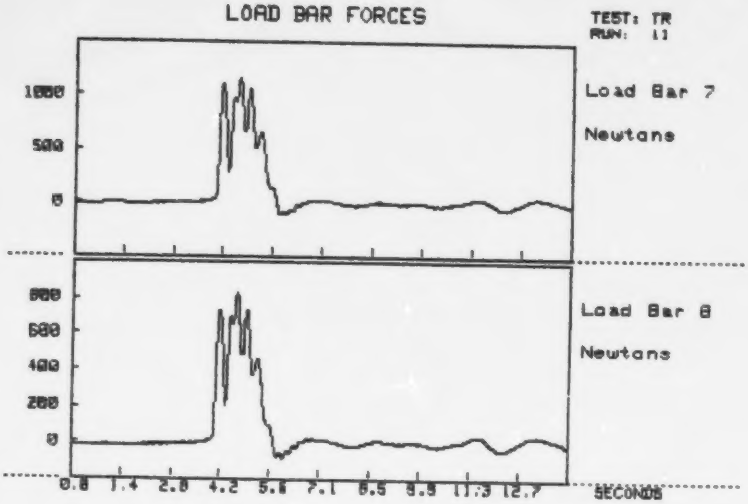
LOAD BAR FORCES
TEST: TR
RUN: 11
1000
500
0
Load Bar 7
Newtons
800
600
400
200
0
Load Bar 8
Newtons
0.0
1.4
2.8
4.2
5.6
7.1
8.5
9.9
11.3
12.7
SECONDS

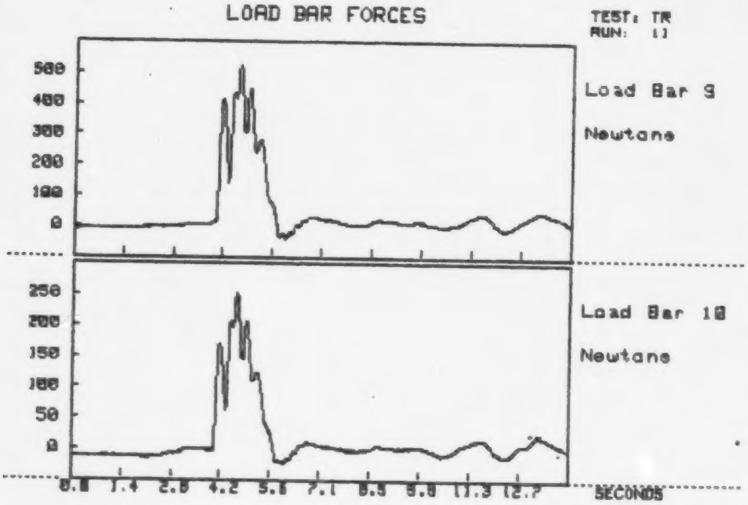
LOAD BAR FORCES
TEST: TR
RUN: 11
500
400
300
200
100
0
Load Bar 9
Newtons
250
200
150
100
50
0
Load Bar 10
Newtons
0.0
1.4
2.8
4.2
5.6
7.1
8.5
9.9
11.3
12.7
SECONDS

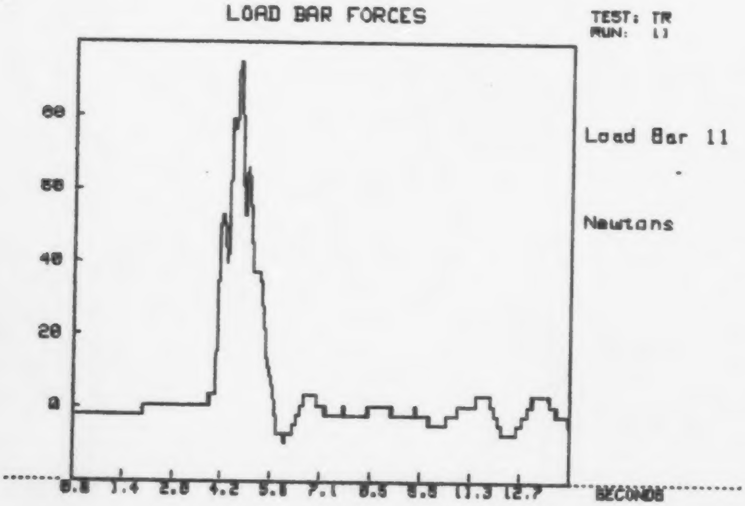
LOAD BAR FORCES
TEST: TR
RUN: 11
80
60
40
20
0
Load Bar 11
Newtons
0.0
1.4
2.8
4.2
5.6
7.1
8.5
9.9
11.3
12.7
SECONDS

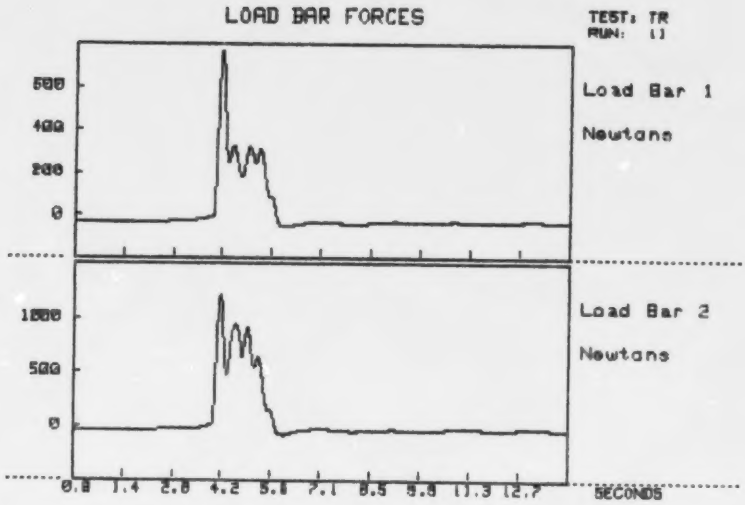
LOAD BAR FORCES
TEST: TR
RUN: 11
600
400
200
0
Load Bar 1
Neutons
1000
500
0
Load Bar 2
Neutons
0.0
1.4
2.8
4.2
5.6
7.1
8.5
9.9
11.3
12.7
SECONDS

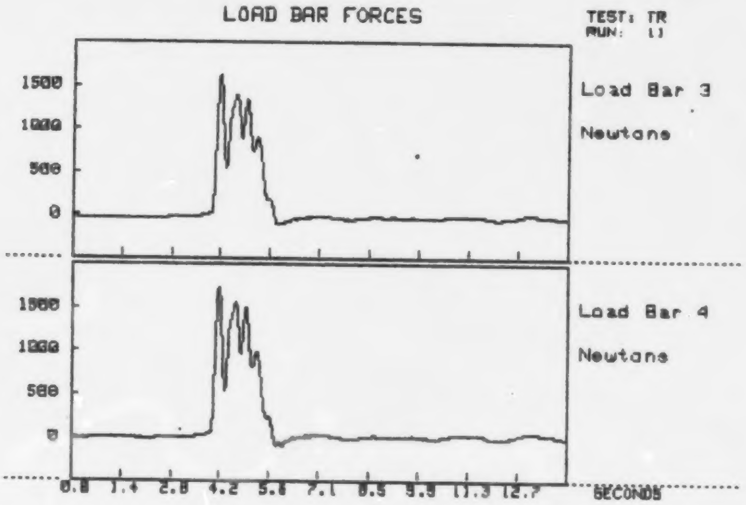
LOAD BAR FORCES
TEST: TR
RUN: 11
1500
1000
500
0
Load Bar 3
Neutons
1500
1000
500
0
Load Bar 4
Neutons
0.0
1.4
2.8
4.2
5.6
7.1
8.5
9.9
11.3
12.7
SECONDS

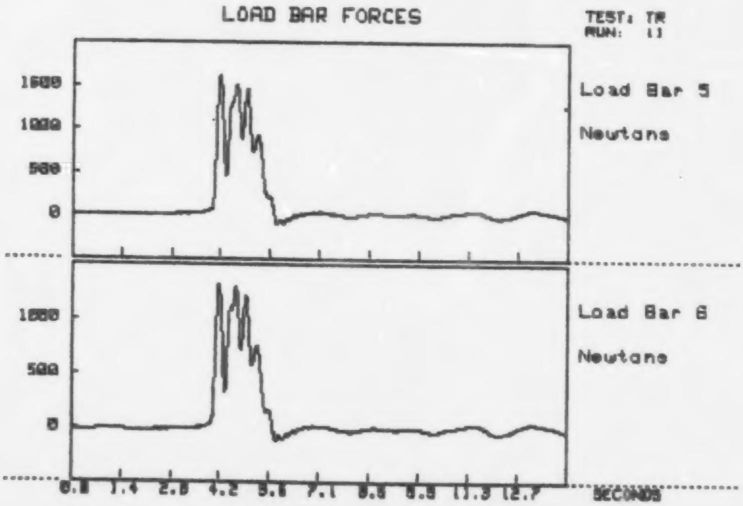
LOAD BAR FORCES
TEST: TR
RUN: 11
1500
1000
500
0
Load Bar 5
Neutons
1000
500
0
Load Bar 6
Neutons
0.0
1.4
2.8
4.2
5.6
7.1
8.5
9.9
11.3
12.7
SECONDS

```
MV  ARCTIC MODEL TESTS
ADDED MASS CALCULATION



TEST:          TS
RUN NUMBER:    1



NOMINAL IMPACT VELOCITY:            1.26      m/s
NOMINAL SHIP SPEED:                 15.5      kt
TIME TO MAXIMUM SURGE:              1.056     s
TIME FROM IMPACT TO BACKOFF:        1.919     s



TIME INCREMENT:                      .004     s
ACCELEROMETER THRESHOLD:             .05      m/s^2



MODEL MASS:                          596      kg
WATER DEPTH:                         1.85     m
MODEL DRAFT:                         0.275    m
ICE FREEBOARD:                       0.025    m
```

SEGMENT ADDED MASS NORMALIZED BY DISPLACED MASS

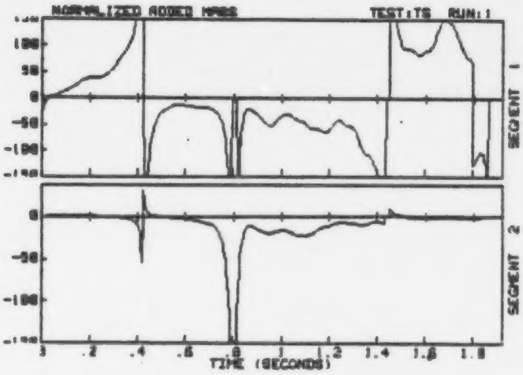

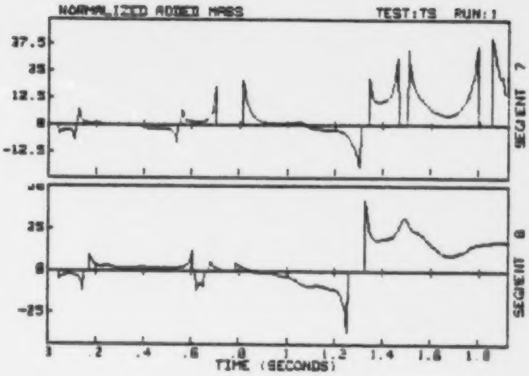

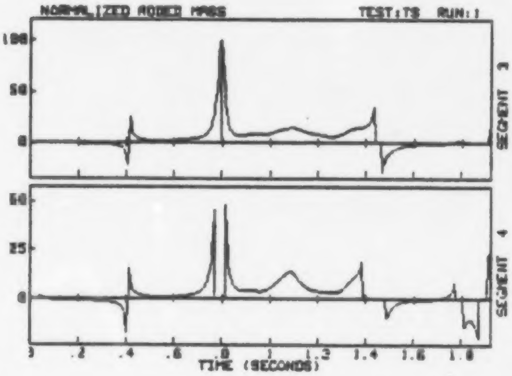

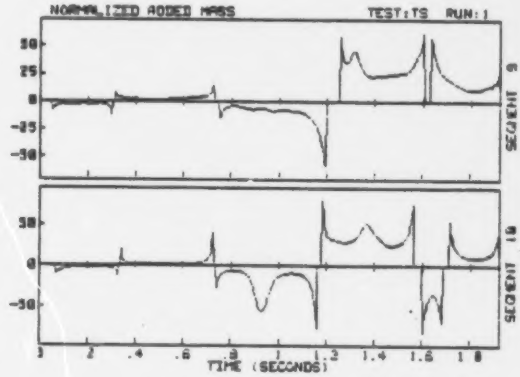

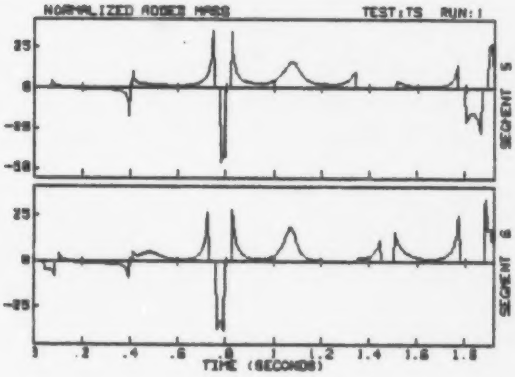

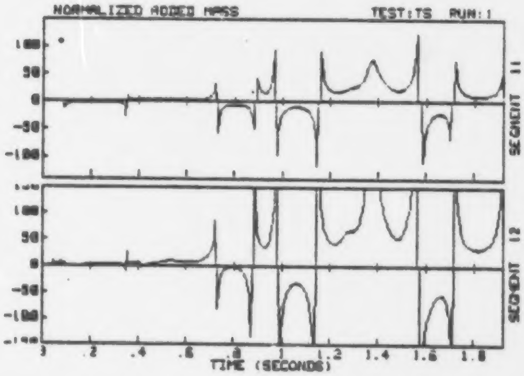

SEGMENT HYDRODYNAMIC FORCE

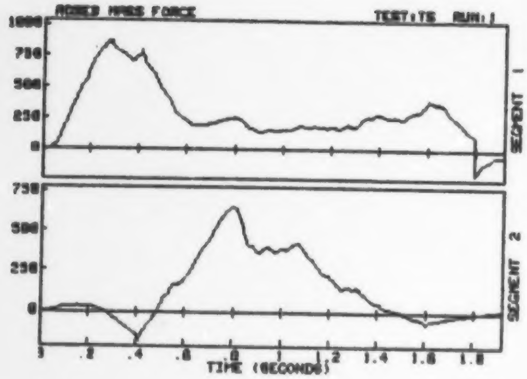

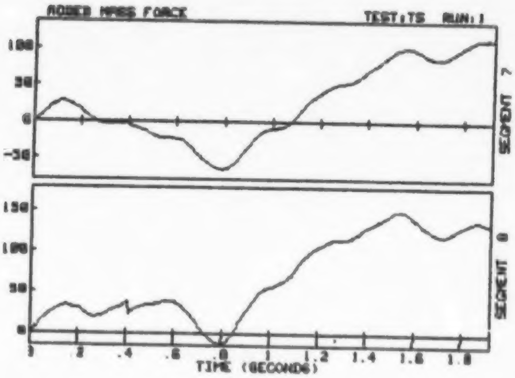

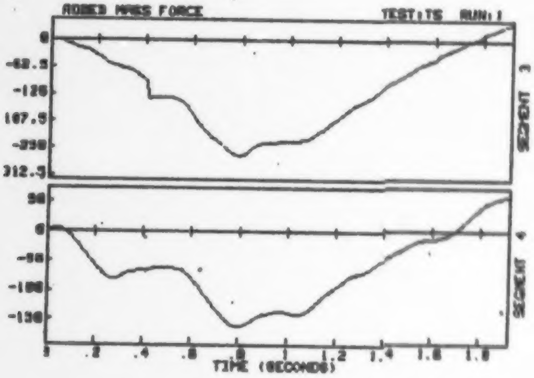

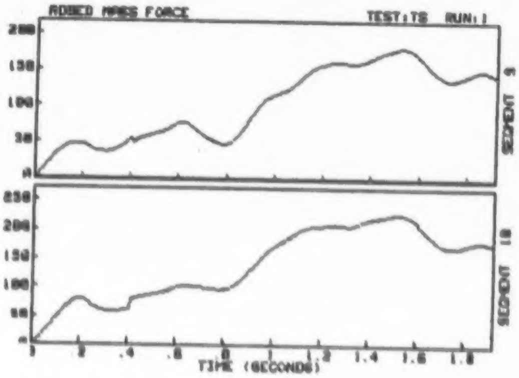

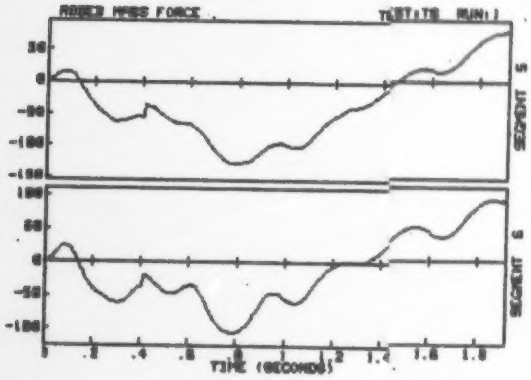

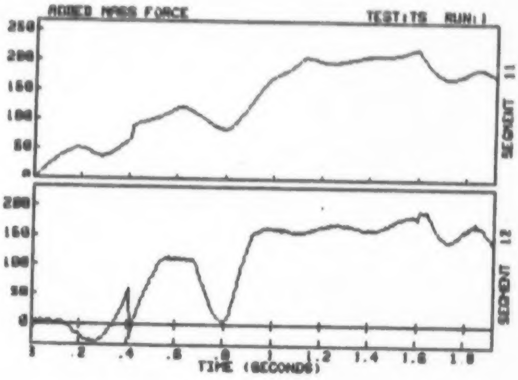

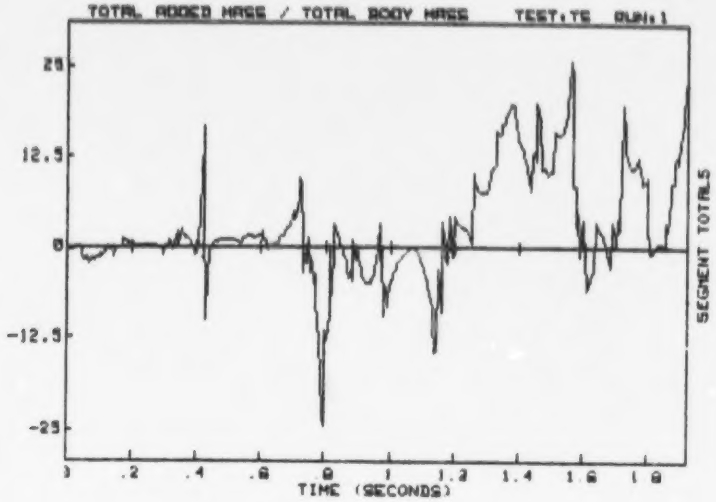

NON-DIMENSIONAL SEGMENTAL ADDED MASS STATISTICS

SEGMENT	MIN	MAX	MEAN	S.D.	NPTS
1	-846.6	787.5	-2.1	115.5	450
2	-257.6	32.6	-11.7	29	443
3	-29.2	100.1	5.7	12.8	431
4	-19.7	48.1	2.9	7.2	413
5	-46.6	35.2	2.1	8.7	386
6	-38.1	34.5	2.7	7.9	393
7	-20.1	40.7	4.1	9	398
8	-36.9	42.1	5.1	11.4	418
9	-58.3	61.6	7	17.5	434
10	-81.6	79.7	3.4	25	434
11	-116.1	124.1	6.2	27.5	435
12	-409.5	373.8	21.7	84.9	449
MEAN MODEL ADDED MASS =			2.67		5084

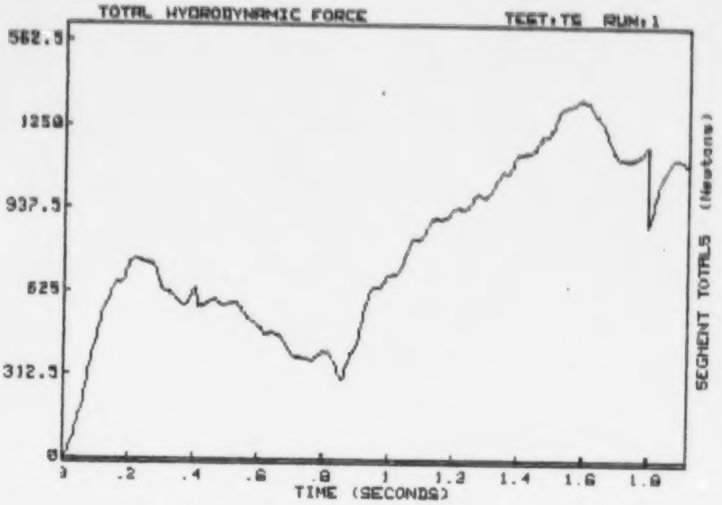

HYDRODYNAMIC FORCE SUMMARY STATISTICS

SEGMENT	MIN	MAX	MEAN	S.D.	NPTS
1	-196.8	865.9	292.1	227	477
2	-181.9	649.7	137.1	200.5	477
3	-268.5	40.8	-116	92.5	477
4	-160.9	62.4	-62.9	58.7	477
5	-128	79.4	-37.5	55.3	477
6	-105.2	92.6	-12.3	52	477
7	-65.5	115.2	25.4	53.2	477
8	-13	149.5	67.9	51.5	477
9	-1.3	180.6	102.2	52.8	477
10	.3	227.2	139.9	63	477
11	0	220.9	136.1	64.6	477
12	-30.1	194.5	104.6	72.9	477
MEAN HYDRODYNAMIC FORCE =			64.72		5724

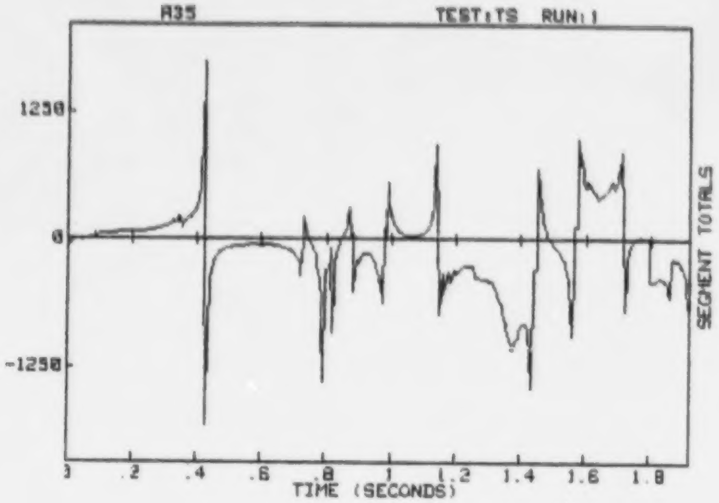

HEAVE/PITCH COUPLED ADDED MASS SUMMARY STATISTICS

SEGMENT	MIN	MAX	MEAN	S.D.	NPTS
1	-1858.4	1728.5	-4.7	253.5	450
2	-475	60.2	-21.6	53.5	443
3	-41.9	143.5	8.2	18.3	431
4	-20.2	49.3	3	7.4	413
5	-28.7	21.6	1.3	5.4	386
6	-7.8	7.1	.6	1.6	393
7	-8.3	4.1	-.8	1.8	398
8	-25.9	22.7	-3.2	7	418
9	-63.1	59.7	-7.2	18	434
10	-114	116.8	-4.8	35.7	434
11	-227.6	212.7	-11.3	50.4	435
12	-835.8	915.7	-48.4	189.7	449

MEAN A35 MODEL ADDED MASS = -3.05 5084

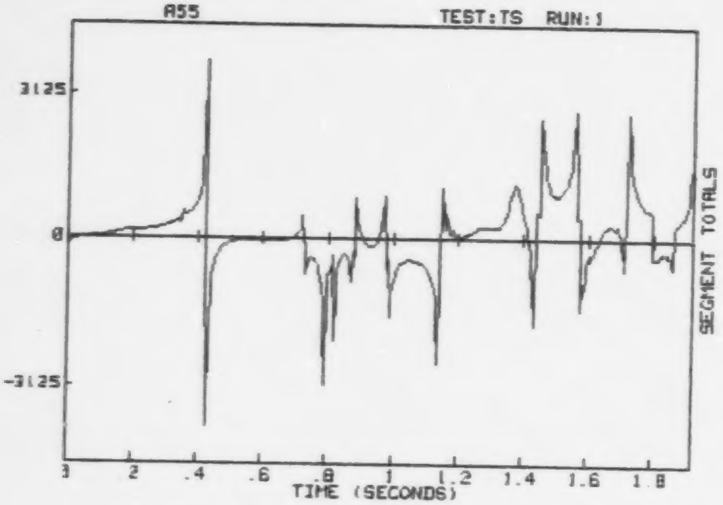

PITCH ADDED MASS MOMENT OF INERTIA SUMMARY STATISTICS

SEGMENT	MIN	MAX	MEAN	S.D.	NPTS
1	-4079.1	3794.2	-10.2	253.5	450
2	-876	110.9	-39.8	53.5	443
3	-60.1	205.8	11.7	18.3	431
4	-20.6	50.5	3	7.4	413
5	-17.6	13.3	.8	5.4	386
6	-1.6	1.4	.1	1.6	393
7	-.8	1.7	.2	1.8	398
8	-13.9	15.9	1.9	7	418
9	-61.1	64.6	7.4	18	434
10	-167.2	163.1	6.9	35.7	434
11	-389.9	417.1	20.7	50.4	435
12	-2047.5	1868.8	108.3	189.7	449
MEAN A55 MODEL ADDED MASS =			2.36		5084

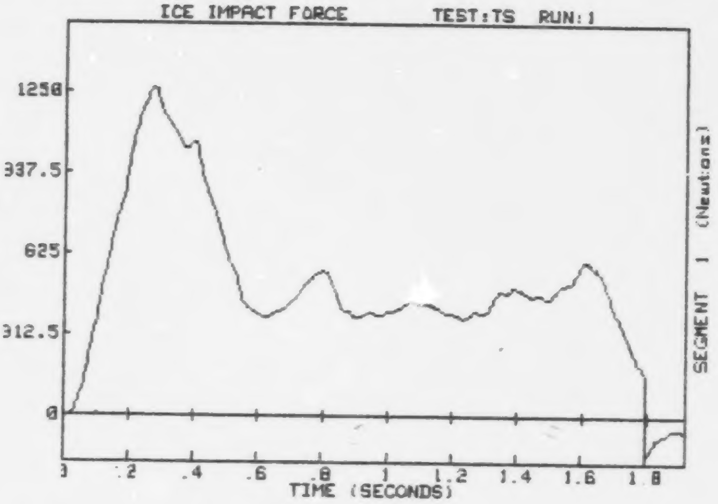
ICE IMPACT FORCE
TEST:TS RUN:1
1250
937.5
625
312.5
0
0
.2
.4
.6
.8
1
1.2
1.4
1.6
1.8
TIME (SECONDS)
SEGMENT 1 (Newtons)

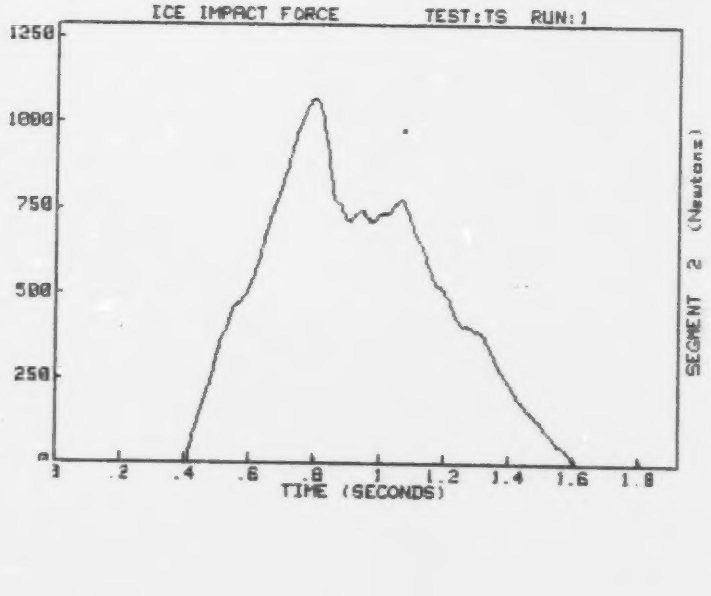
ICE IMPACT FORCE
TEST:TS RUN:1
1250
1000
750
500
250
0
0
.2
.4
.6
.8
1
1.2
1.4
1.6
1.8
TIME (SECONDS)
SEGMENT 2 (Newtons)

IMPACT VELOCITY= 1.14 m/s
SHIP SPEED= 14.06 kt

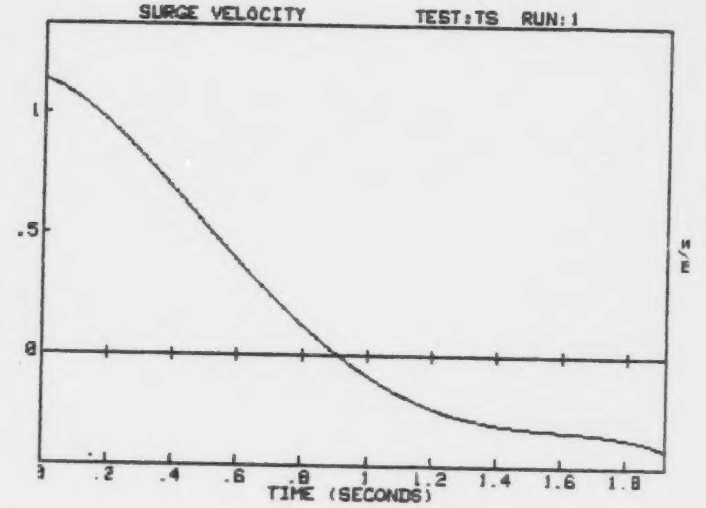

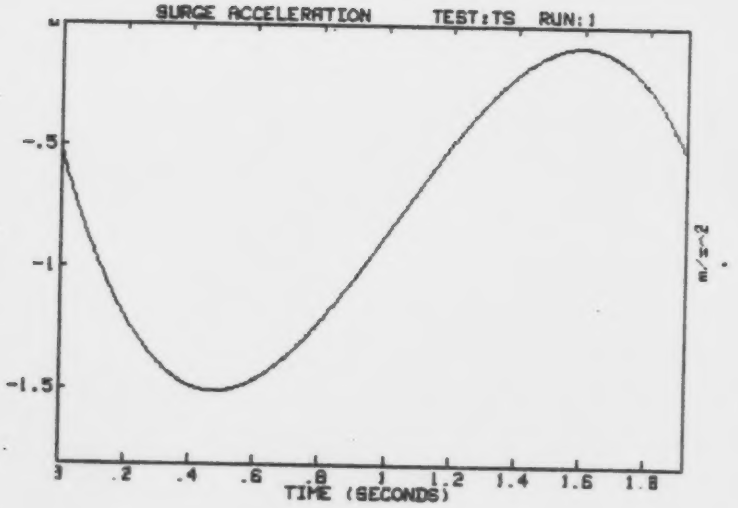

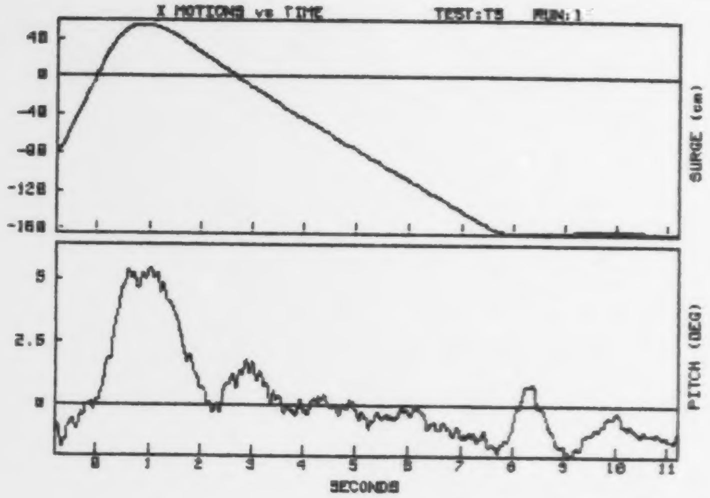

X MOTIONS vs TIME
TEST:T3 RUN:1
40
0
-40
-80
-120
-160
SURGE (cm)
5
2.5
0
PITCH (DEG)
0
1
2
3
4
5
6
7
8
9
10
11
SECONDS

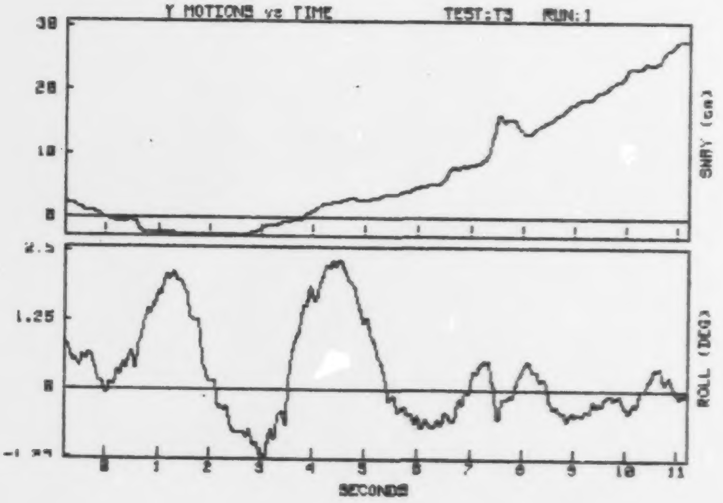

Y MOTIONS vs TIME
TEST:T3 RUN:1
30
20
10
0
SWAY (cm)
2.5
1.25
0
-1.25
ROLL (DEG)
0
1
2
3
4
5
6
7
8
9
10
11
SECONDS

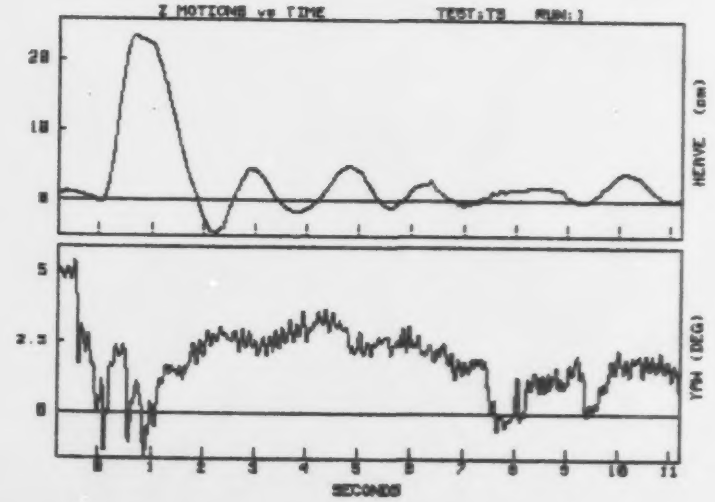

Z MOTIONS vs TIME
TEST:T3 RUN:1
20
10
0
HEAVE (cm)
5
2.5
0
YAW (DEG)
0
1
2
3
4
5
6
7
8
9
10
11
SECONDS

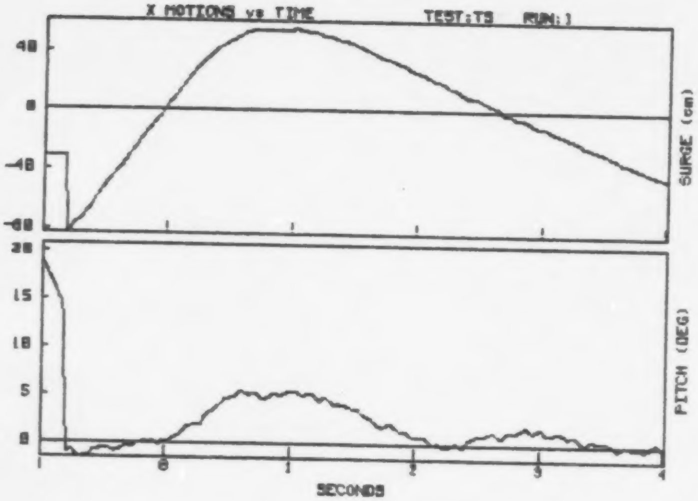
X MOTIONS vs TIME
TEST:TS RUN:1
40
0
-40
-80
SURGE (cm)
20
15
10
5
0
PITCH (DEG)
0
1
2
3
4
SECONDS

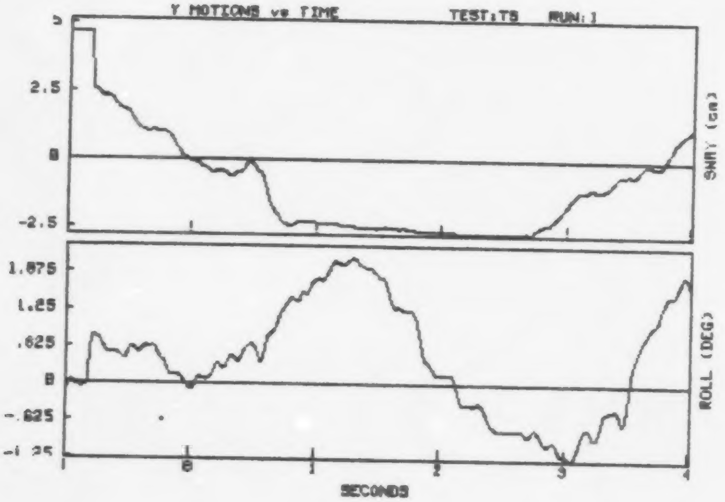
Y MOTIONS vs TIME
TEST:TS RUN:1
5
2.5
0
-2.5
SWAY (cm)
1.875
1.25
.625
0
-.625
-1.25
ROLL (DEG)
0
1
2
3
4
SECONDS

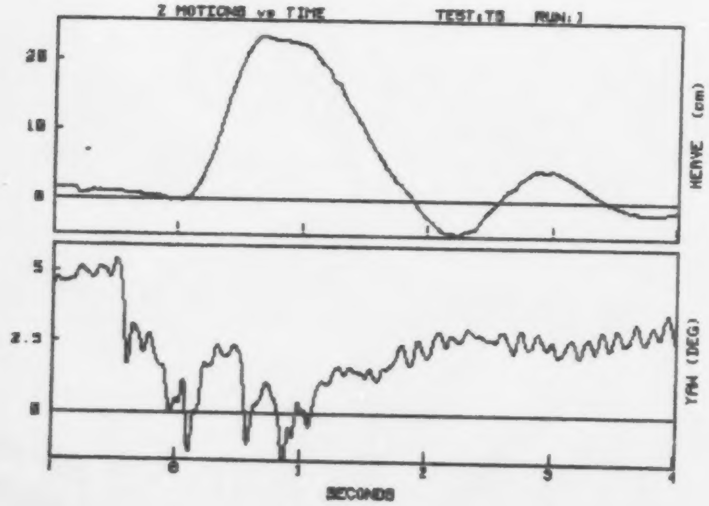
Z MOTIONS vs TIME
TEST:TS RUN:1
20
10
0
HEAVE (cm)
5
2.5
0
YAW (DEG)
0
1
2
3
4
SECONDS

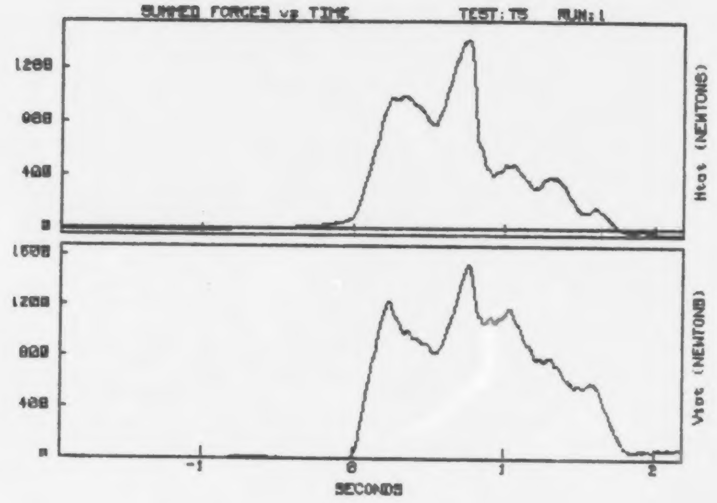
SUMMED FORCES vs TIME
TEST: T5
RUN: 1
1200
800
400
0
Htot (NEWTONS)
1600
1200
800
400
0
Vtot (NEWTONS)
-1
0
1
2
SECONDS

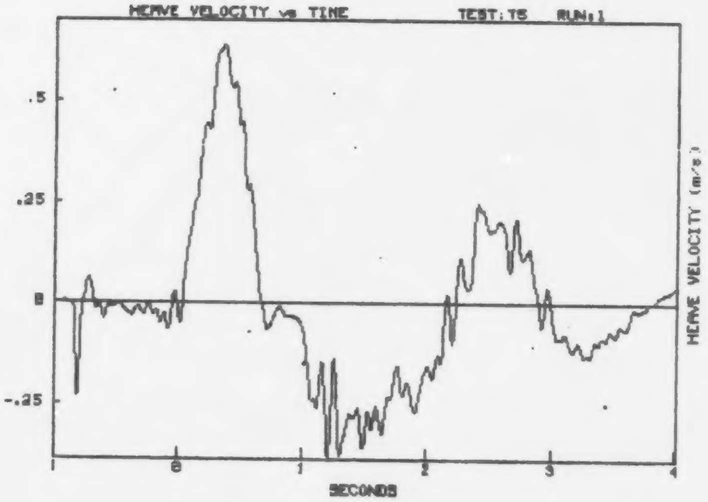
HEAVE VELOCITY vs TIME
TEST: T5
RUN: 1
.5
.25
0
-.25
HEAVE VELOCITY (m/s)
1
0
1
2
3
4
SECONDS

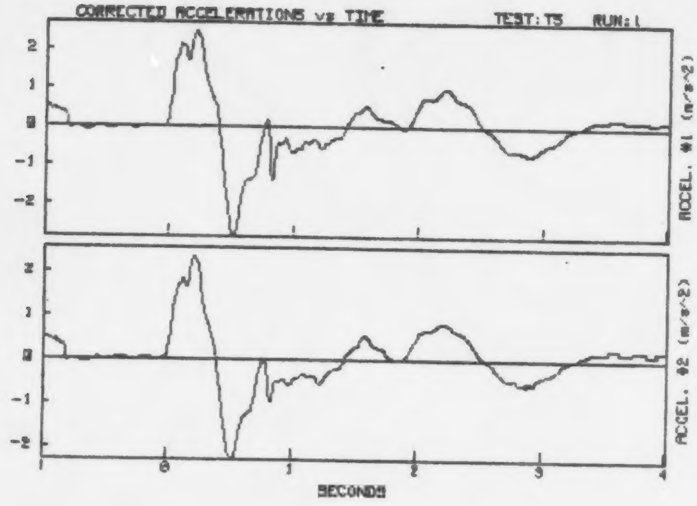
CORRECTED ACCELERATIONS vs TIME
TEST: T5 RUN: 1
ACCEL. #1 (m/s^2)
2
1
0
-1
-2
ACCEL. #2 (m/s^2)
2
1
0
-1
-2
0
1
2
3
4
SECONDS

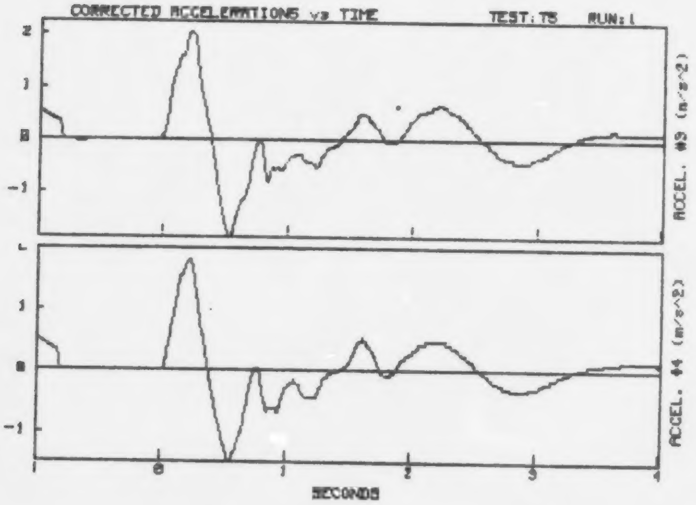
CORRECTED ACCELERATIONS vs TIME
TEST: T5 RUN: 1
ACCEL. #3 (m/s^2)
2
1
0
-1
ACCEL. #4 (m/s^2)
1
0
-1
0
1
2
3
4
SECONDS

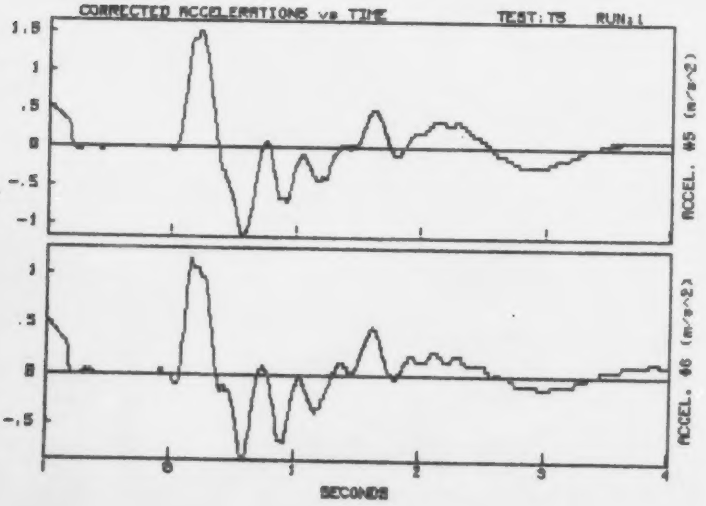
CORRECTED ACCELERATIONS vs TIME
TEST: T5 RUN: 1
ACCEL. #5 (m/s^2)
1.5
1
.5
0
-.5
-1
ACCEL. #6 (m/s^2)
1
.5
0
-.5
0
1
2
3
4
SECONDS

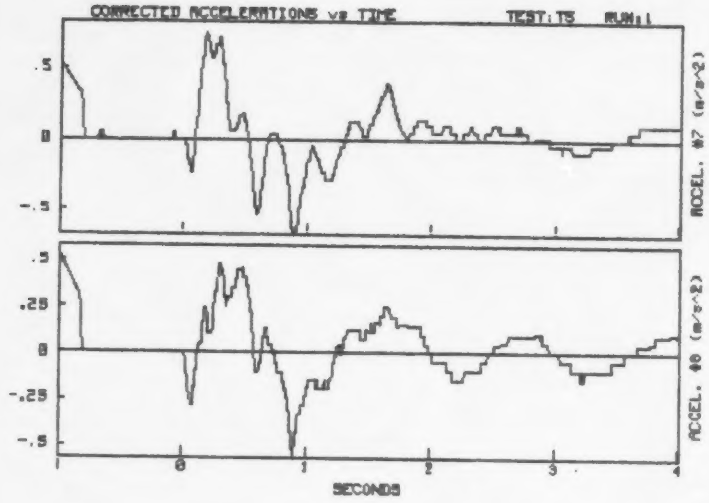
CORRECTED ACCELERATIONS vs TIME
TEST: T5 RUN: 1
.5
0
-.5
ACCEL. #7 (m/s^2)
.5
.25
0
-.25
-.5
ACCEL. #8 (m/s^2)
0
1
2
3
4
SECONDS

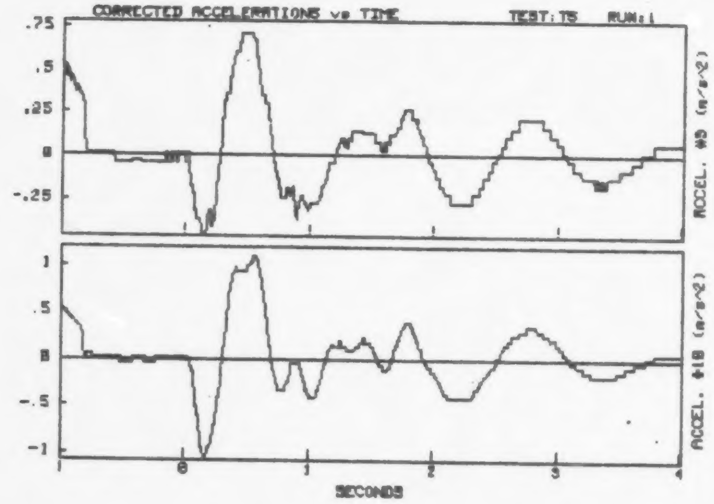
CORRECTED ACCELERATIONS vs TIME
TEST: T5 RUN: 1
.75
.5
.25
0
-.25
ACCEL. #9 (m/s^2)
1
.5
0
-.5
-1
ACCEL. #10 (m/s^2)
0
1
2
3
4
SECONDS

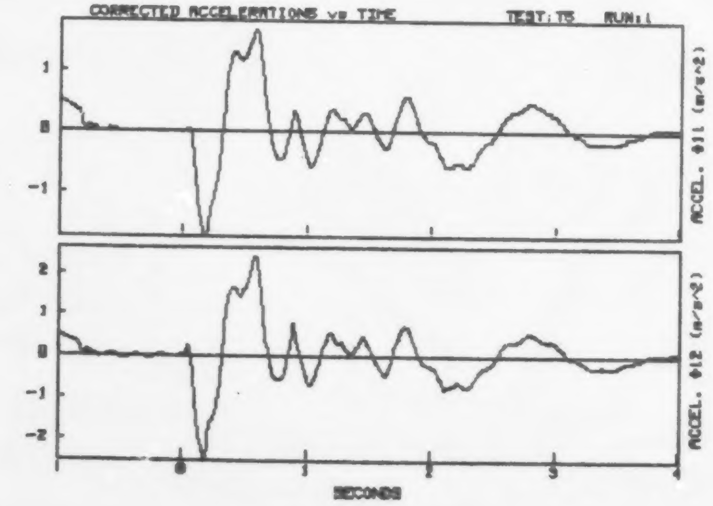
CORRECTED ACCELERATIONS vs TIME
TEST: T5 RUN: 1
1
0
-1
ACCEL. #11 (m/s^2)
2
1
0
-1
-2
ACCEL. #12 (m/s^2)
0
1
2
3
4
SECONDS

```
                    MV  ARCTIC MODEL TESTS
                    ADDED MASS CALCULATION



                       TEST:          TS
                       RUN NUMBER:    2



              NOMINAL IMPACT VELOCITY:          .38       m/s
              NOMINAL SHIP SPEED:               4.7       kt
              TIME TO MAXIMUM SURGE:            1.097     s
              TIME FROM IMPACT TO BACKOFF:      2.153     s



              TIME INCREMENT:                    .004     s
              ACCELEROMETER THRESHOLD:           .05      m/s^2



              MODEL MASS:                        596      kg
              WATER DEPTH:                       1.85     m
              MODEL DRAFT:                       0.275    m
              ICE FREEBOARD:                     0.025    m
```

SEGMENT ADDED MASS NORMALIZED BY DISPLACED MASS

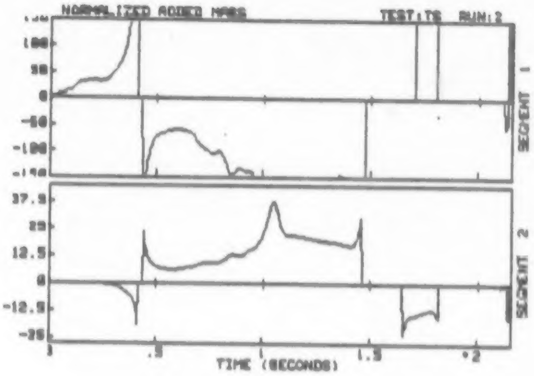

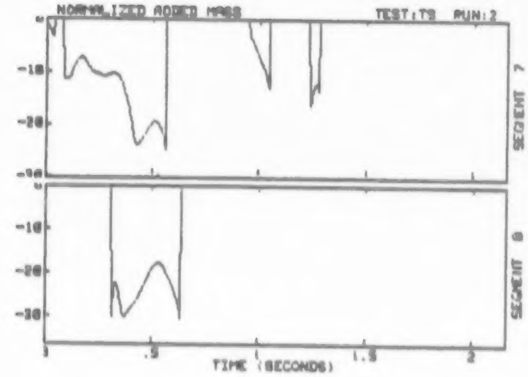

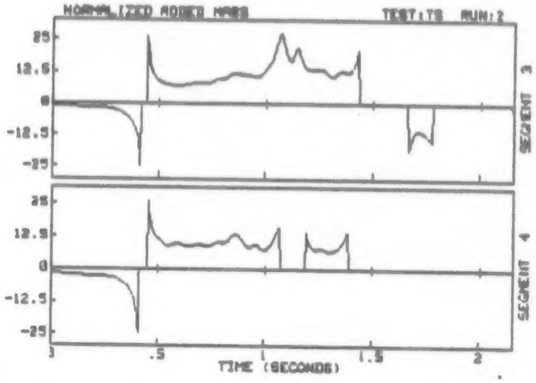

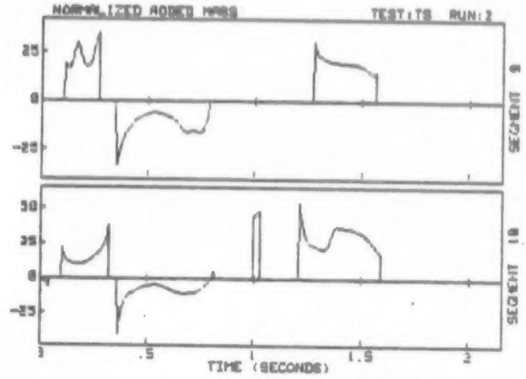

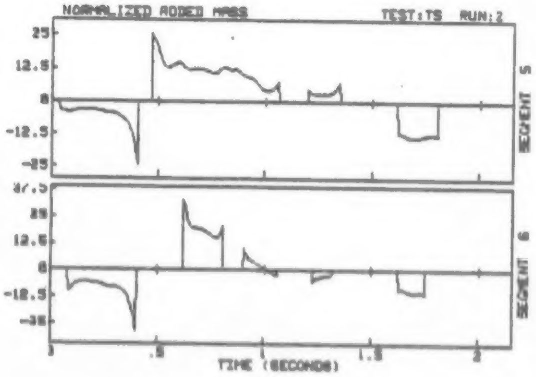

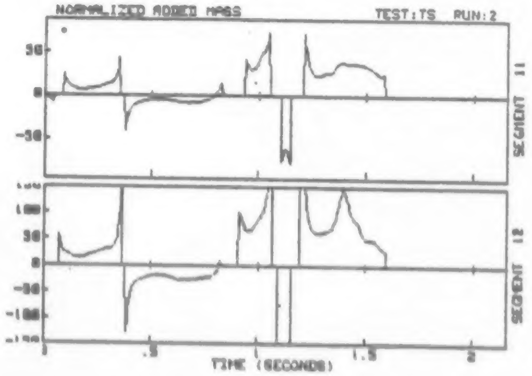

SEGMENT HYDRODYNAMIC FORCE

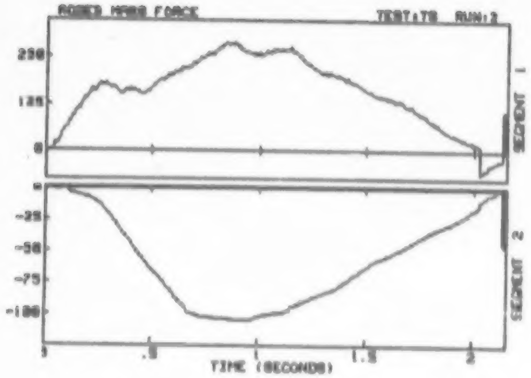

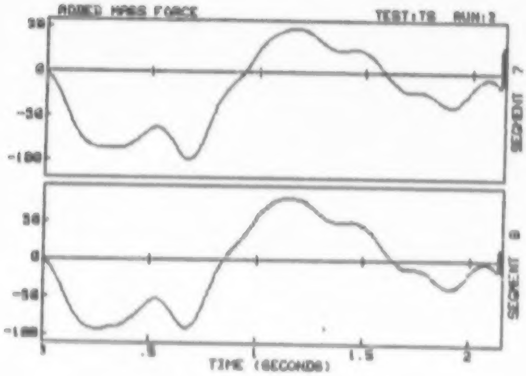

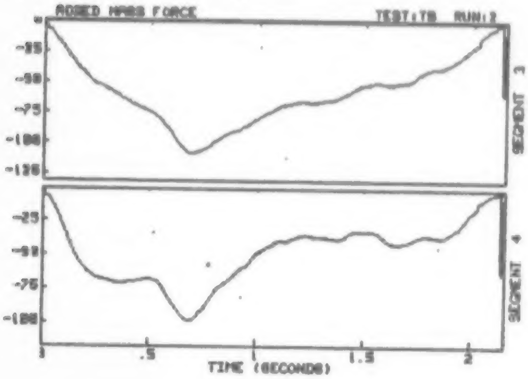

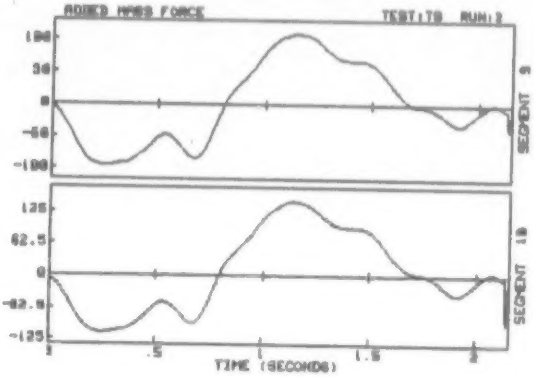

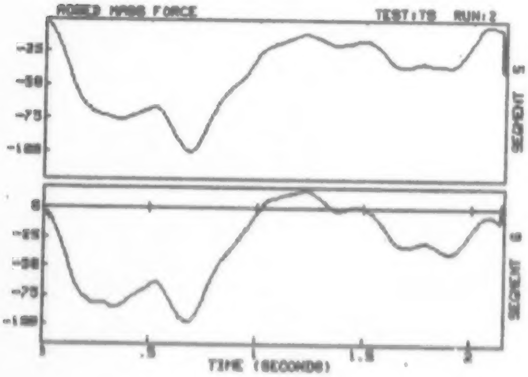

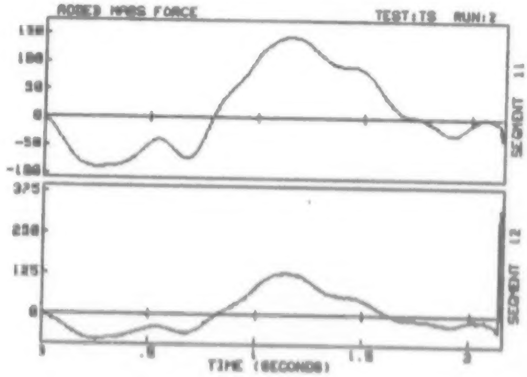

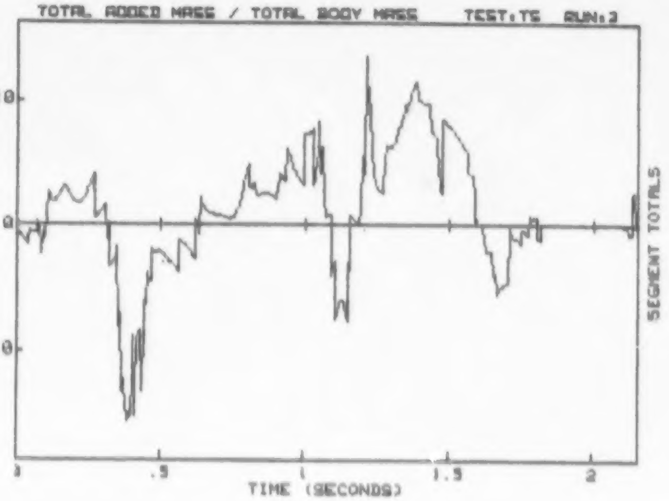

NON-DIMENSIONAL SEGMENTAL ADDED MASS STATISTICS

SEGMENT	MIN	MAX	MEAN	S.D.	NPTS
1	-405.2	331	-81.9	144.2	393
2	-23.1	37.6	7.6	12.3	411
3	-24.9	27.3	6.2	9.8	380
4	-24.6	26.2	5.2	7.3	302
5	-24.4	25.8	2.3	10.1	323
6	-28.9	32.6	-.4	11.7	218
7	-25.1	0	-12.7	6.1	163
8	-30.5	0	-23.7	3.9	81
9	-33.5	34.9	4.5	17.3	219
10	-40	54.3	10.9	19	279
11	-80	73.7	10.9	25.1	321
12	-333	317.4	23	81.8	335
MEAN MODEL ADDED MASS =			-.48		3425

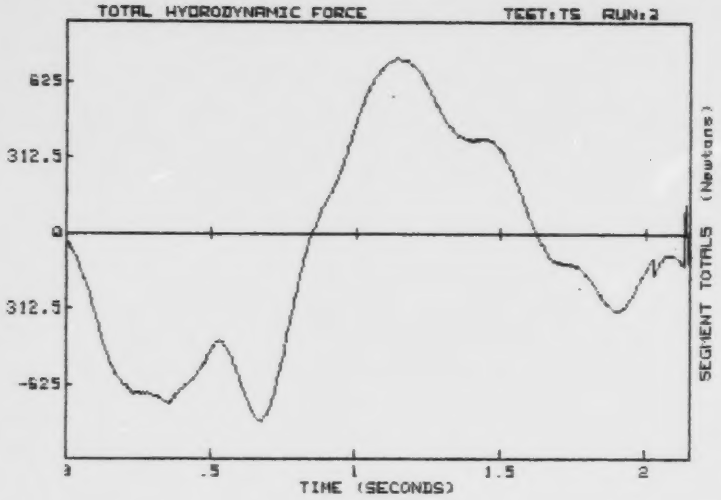

HYDRODYNAMIC FORCE SUMMARY STATISTICS

SEGMENT	MIN	MAX	MEAN	S.D.	NPTS
1	-60.9	291.5	160	89.9	535
2	-103.9	1.1	-57.4	35.7	535
3	-108.8	.5	-58.4	26.8	535
4	-98.9	-1.2	-48.5	23.2	535
5	-100.1	-1.4	-41.4	26.6	535
6	-98.1	15.4	-33.5	34.1	535
7	-98.8	47.9	-22.9	44.4	535
8	-92.9	83.3	-10.2	55.1	535
9	-96	108.6	-.8	63.5	535
10	-112.5	144.6	6.2	79.6	535
11	-89	144.8	12.5	72.8	535
12	-76.1	329.5	5.9	62.9	535
MEAN HYDRODYNAMIC FORCE =			-7.37		6420

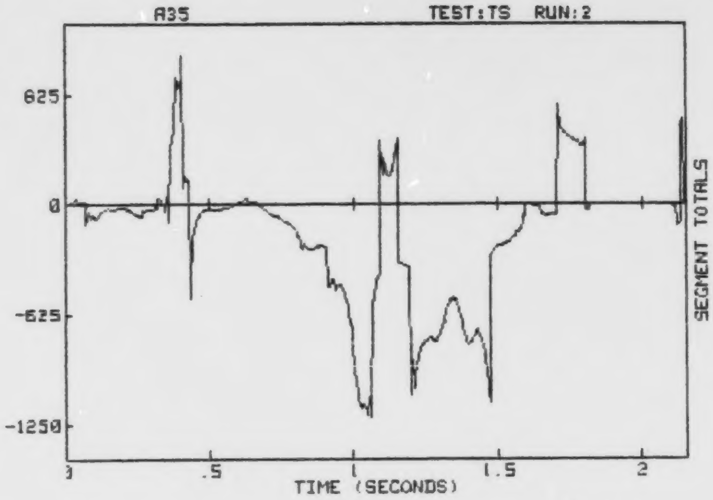

HEAVE/PITCH COUPLED ADDED MASS SUMMARY STATISTICS

SEGMENT	MIN	MAX	MEAN	S.D.	NPTS
1	-889.4	726.5	-179.8	316.5	393
2	-42.7	69.3	14	22.7	411
3	-35.7	39.1	8.9	14.1	380
4	-25.2	26.9	5.4	7.5	302
5	-15	15.9	1.4	6.2	323
6	-5.9	6.7	-.1	2.4	218
7	0	5.1	2.6	1.2	163
8	0	18.7	14.6	2.4	81
9	-35.8	34.3	-4.6	17.7	219
10	-77.7	57.3	-15.7	27.2	279
11	-135.2	146.6	-20	46.1	321
12	-709.7	744.7	-51.5	182.8	335

MEAN A35 MODEL ADDED MASS = -2.1 3425

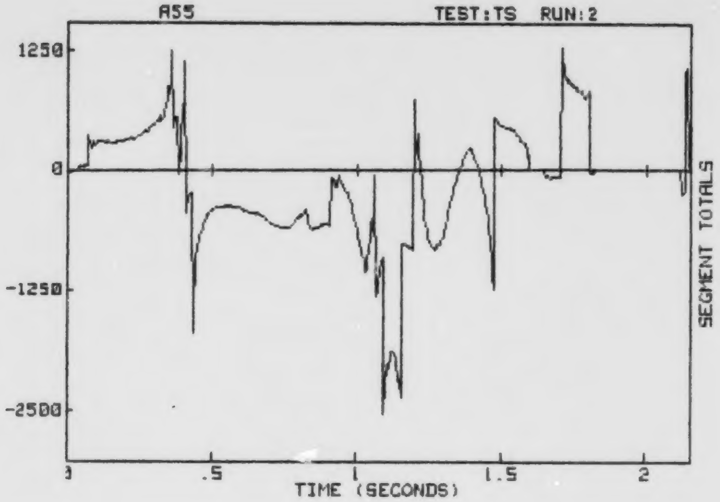

PITCH ADDED MASS MOMENT OF INERTIA SUMMARY STATISTICS

SEGMENT	MIN	MAX	MEAN	S.D.	NPTS
1	-1952.2	1594.7	-394.7	316.5	393
2	-78.7	127.9	25.8	22.7	411
3	-51.2	56.1	12.8	14.1	380
4	-25.8	27.5	5.5	7.5	302
5	-9.2	8.8	.9	6.2	323
6	-1.2	1.4	0	2.4	218
7	-1.1	0	-.5	1.2	163
8	-11.5	0	-9	2.4	81
9	-35.1	36.6	4.7	17.7	219
10	-82	111.2	22.4	27.2	279
11	-268.7	247.8	36.7	46.1	321
12	-1665.1	1586.8	115.2	182.8	335

MEAN A55 MODEL ADDED MASS = 2.82 3425

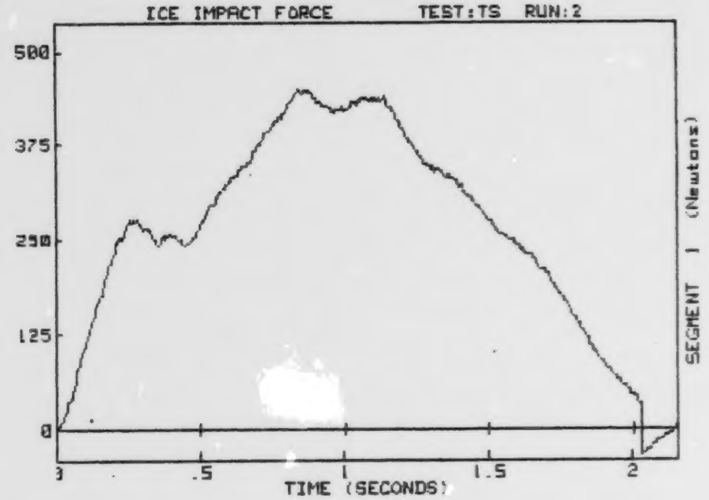
ICE IMPACT FORCE
TEST:TS RUN:2
500
375
250
125
0
0
.5
1
1.5
2
TIME (SECONDS)
SEGMENT 1 (Newtons)

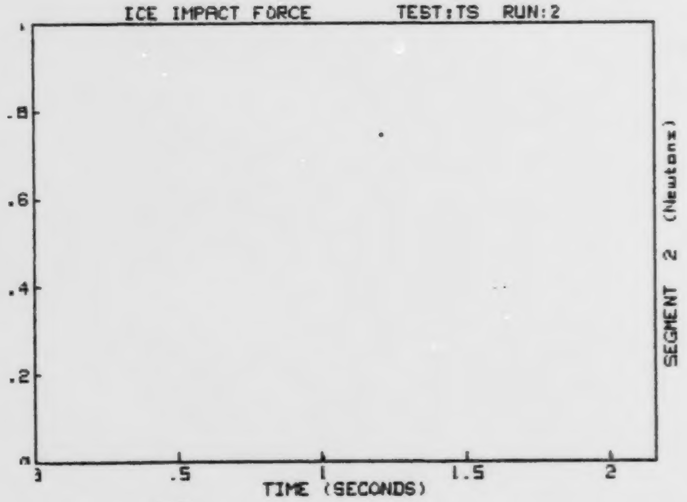
ICE IMPACT FORCE
TEST:TS RUN:2
1
.8
.6
.4
.2
0
0
.5
1
1.5
2
TIME (SECONDS)
SEGMENT 2 (Newtons)

IMPACT VELOCITY= .37 m/s
SHIP SPEED= 4.5 kt

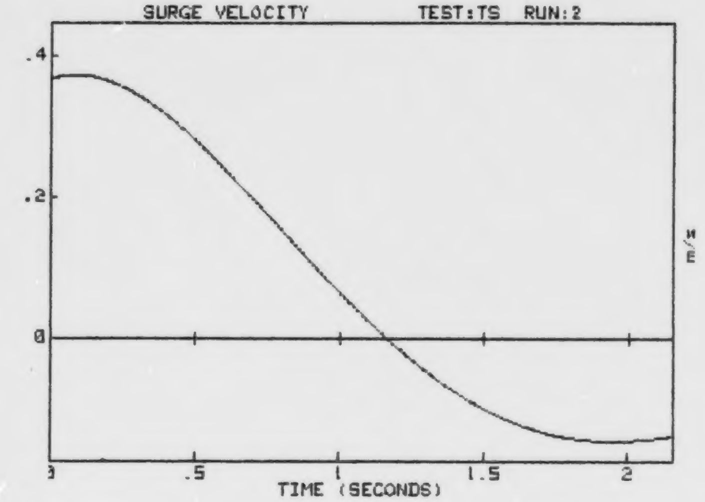

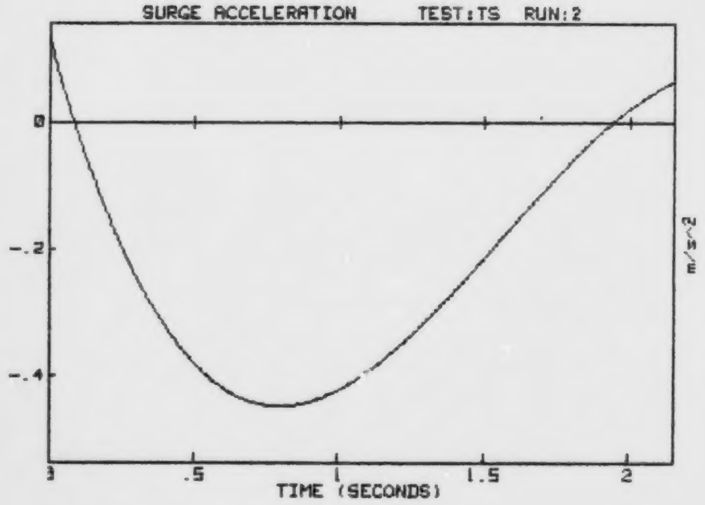

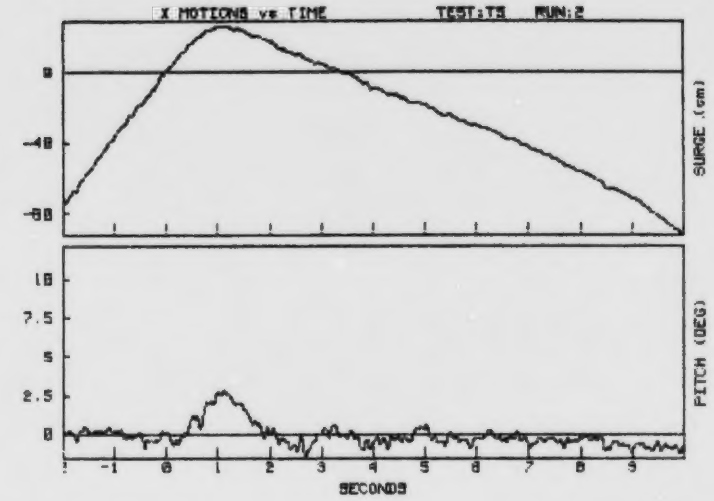
X MOTIONS vs TIME
TEST:TS RUN:2
0
-40
-80
SURGE (cm)
10
7.5
5
2.5
0
PITCH (DEG)
-1
0
1
2
3
4
5
6
7
8
9
SECONDS

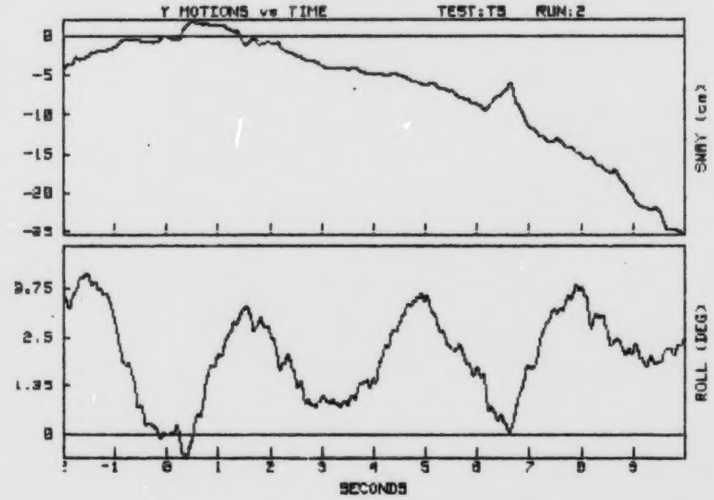
Y MOTIONS vs TIME
TEST:TS RUN:2
0
-5
-10
-15
-20
-25
SWAY (cm)
3.75
2.5
1.25
0
ROLL (DEG)
-1
0
1
2
3
4
5
6
7
8
9
SECONDS

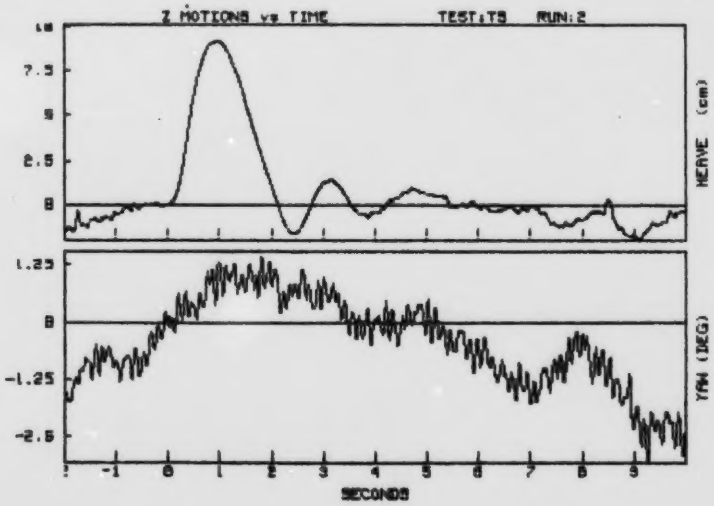
Z MOTIONS vs TIME
TEST:TS RUN:2
10
7.5
5
2.5
0
HEAVE (cm)
1.25
0
-1.25
-2.5
YAW (DEG)
-1
0
1
2
3
4
5
6
7
8
9
SECONDS

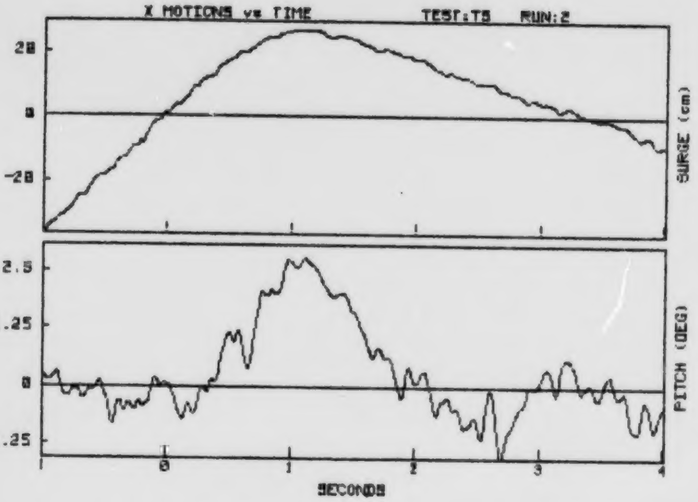
X MOTIONS vs TIME
TEST:T5 RUN:2
20
0
-20
SURGE (cm)
2.5
1.25
0
-1.25
PITCH (DEG)
0
1
2
3
4
SECONDS

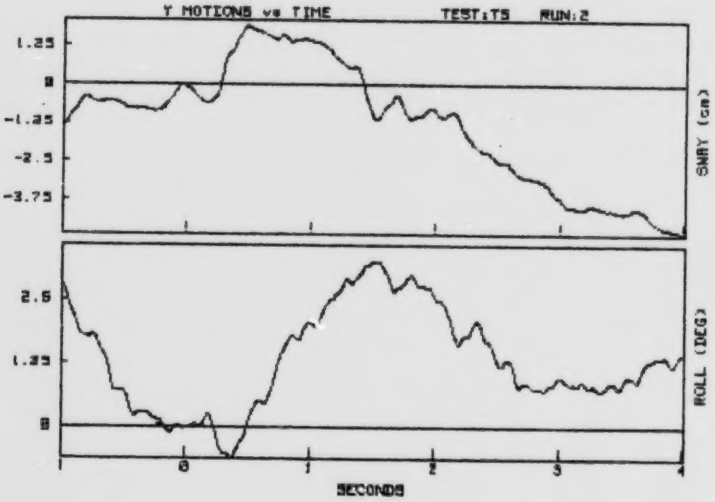
Y MOTIONS vs TIME
TEST:T5 RUN:2
1.25
0
-1.25
-2.5
-3.75
SWAY (cm)
2.5
1.25
0
ROLL (DEG)
0
1
2
3
4
SECONDS

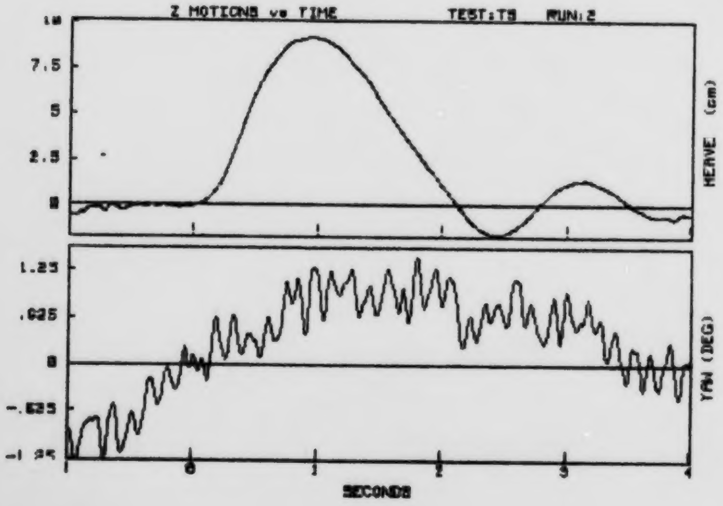
Z MOTIONS vs TIME
TEST:T5 RUN:2
10
7.5
5
2.5
0
HEAVE (cm)
1.25
.625
0
-.625
-1.25
YAW (DEG)
0
1
2
3
4
SECONDS

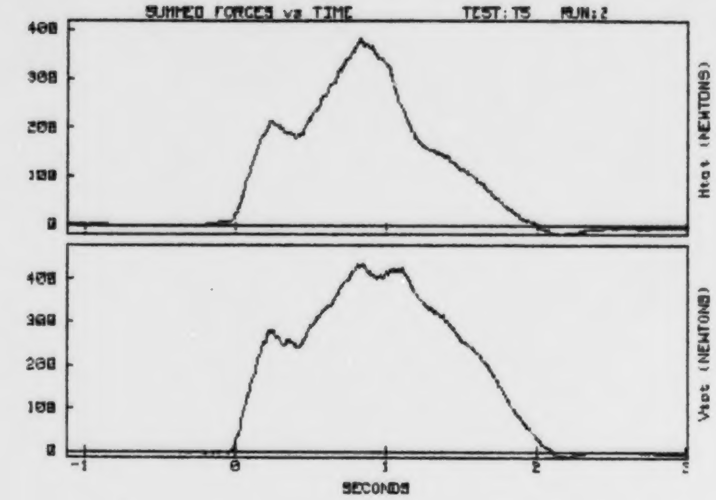
SUMMED FORCES vs TIME TEST: T5 RUN: 2
400
300
200
100
0
Htot (NEWTONS)
400
300
200
100
0
Vtot (NEWTONS)
-1
0
1
2
3
SECONDS

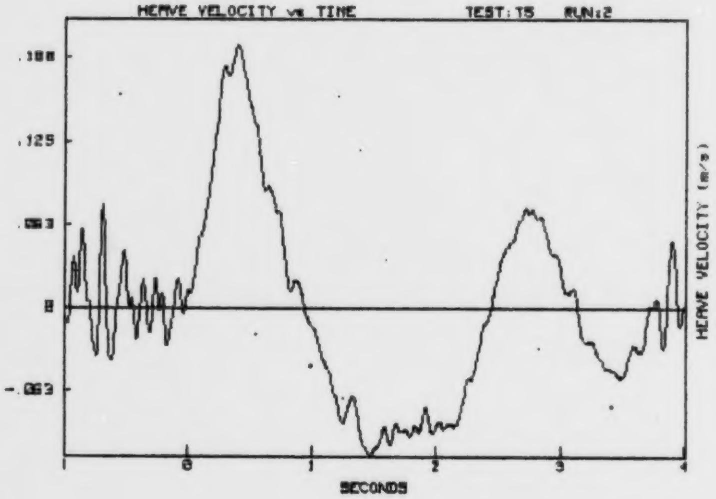
HEAVE VELOCITY vs TIME TEST: T5 RUN: 2
.188
.125
.063
0
-.063
HEAVE VELOCITY (m/s)
-1
0
1
2
3
4
SECONDS

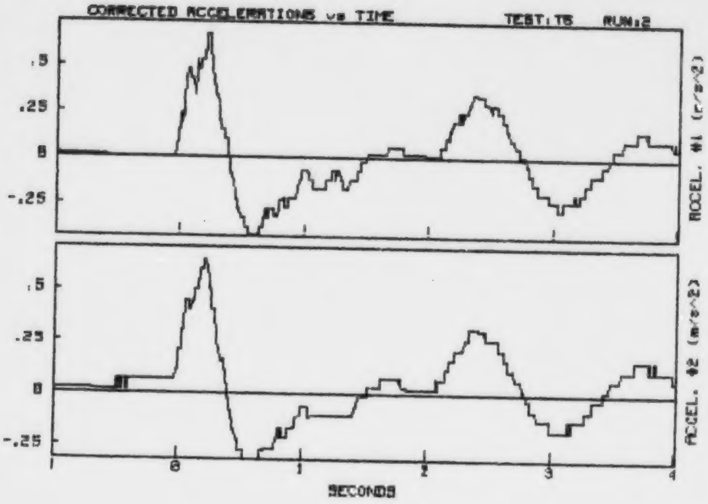
CORRECTED ACCELERATIONS vs TIME
TEST:T5 RUN:2
.5
.25
0
-.25
ACCEL. #1 (m/s^2)
.5
.25
0
-.25
ACCEL. #2 (m/s^2)
0
1
2
3
4
SECONDS

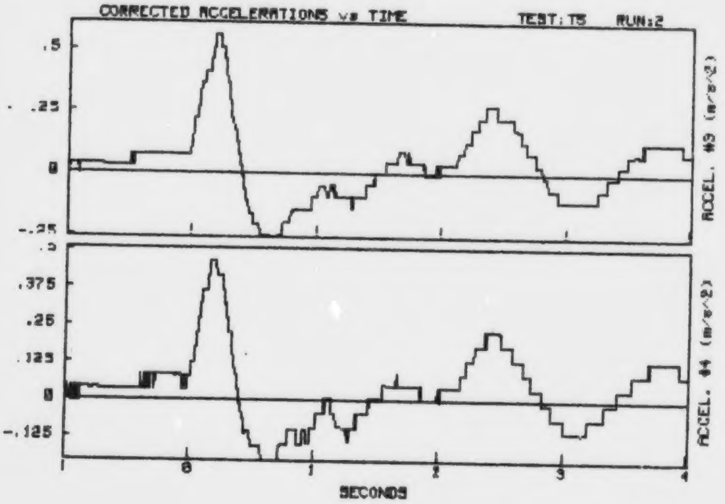
CORRECTED ACCELERATIONS vs TIME
TEST:T5 RUN:2
.5
.25
0
-.25
ACCEL. #3 (m/s^2)
.5
.375
.25
.125
0
-.125
ACCEL. #4 (m/s^2)
0
1
2
3
4
SECONDS

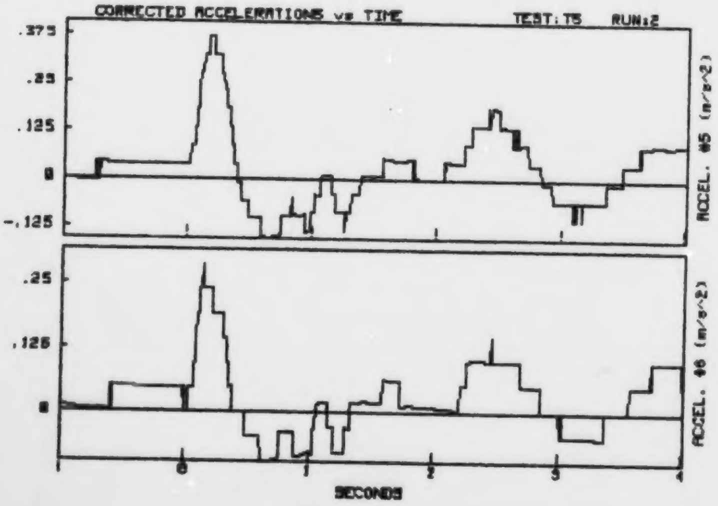
CORRECTED ACCELERATIONS vs TIME
TEST:T5 RUN:2
.375
.25
.125
0
-.125
ACCEL. #5 (m/s^2)
.25
.125
0
ACCEL. #6 (m/s^2)
0
1
2
3
4
SECONDS

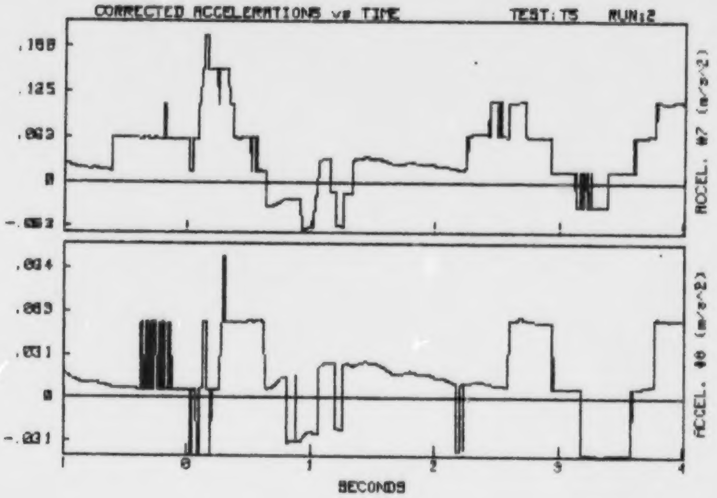
CORRECTED ACCELERATIONS vs TIME
TEST:T5 RUN:2
.188
.125
.063
0
-.063
ACCEL. #7 (m/s^2)
.094
.063
.031
0
-.031
ACCEL. #8 (m/s^2)
0
1
2
3
4
SECONDS

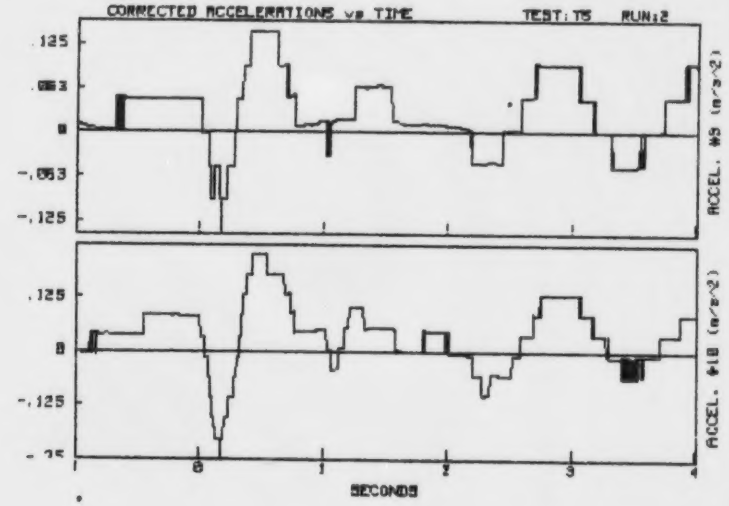
CORRECTED ACCELERATIONS vs TIME
TEST:T5 RUN:2
.125
.063
0
-.063
-.125
ACCEL. #9 (m/s^2)
.125
0
-.125
-.25
ACCEL. #10 (m/s^2)
0
1
2
3
4
SECONDS

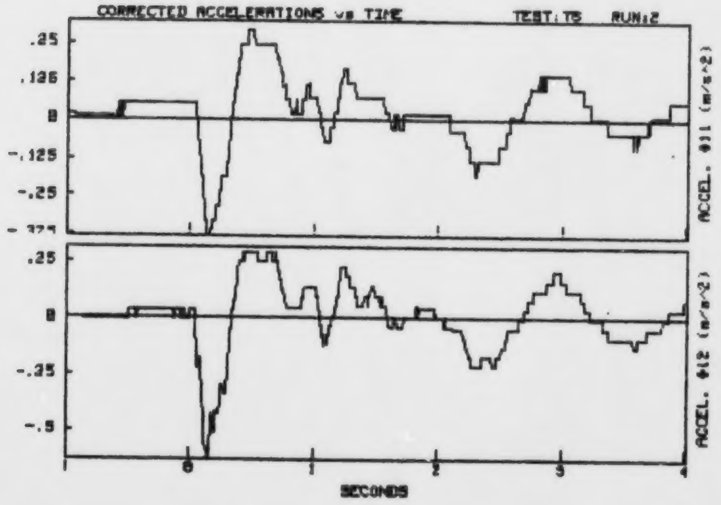
CORRECTED ACCELERATIONS vs TIME
TEST:T5 RUN:2
.25
.125
0
-.125
-.25
-.375
ACCEL. #11 (m/s^2)
.25
0
-.25
-.5
ACCEL. #12 (m/s^2)
0
1
2
3
4
SECONDS

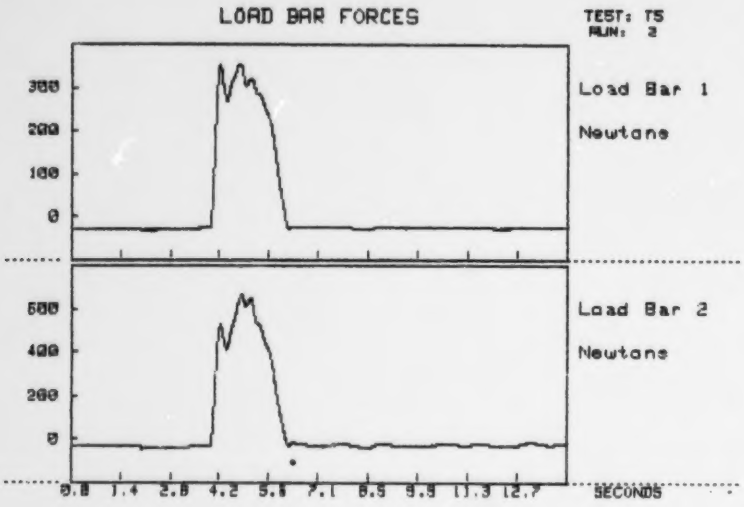
LOAD BAR FORCES
TEST: T5
RUN: 2
300
200
100
0
Load Bar 1
Newtons
600
400
200
0
Load Bar 2
Newtons
0.0
1.4
2.8
4.2
5.6
7.1
8.5
9.9
11.3
12.7
SECONDS

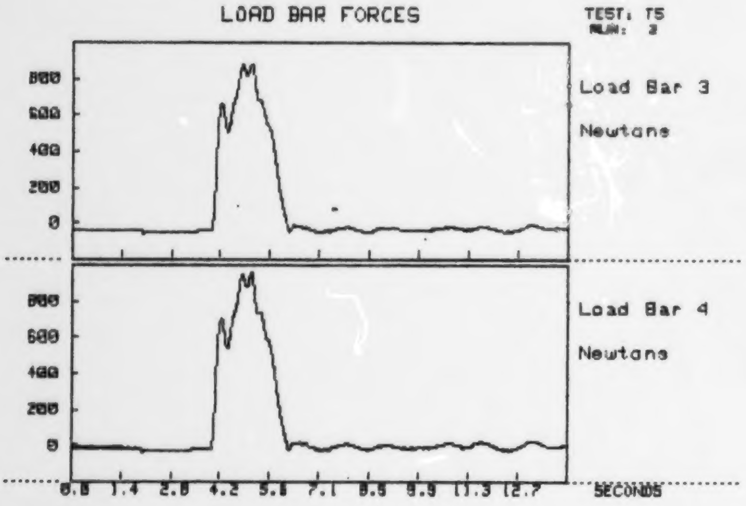
LOAD BAR FORCES
TEST: T5
RUN: 2
800
600
400
200
0
Load Bar 3
Newtons
800
600
400
200
0
Load Bar 4
Newtons
0.0
1.4
2.8
4.2
5.6
7.1
8.5
9.9
11.3
12.7
SECONDS

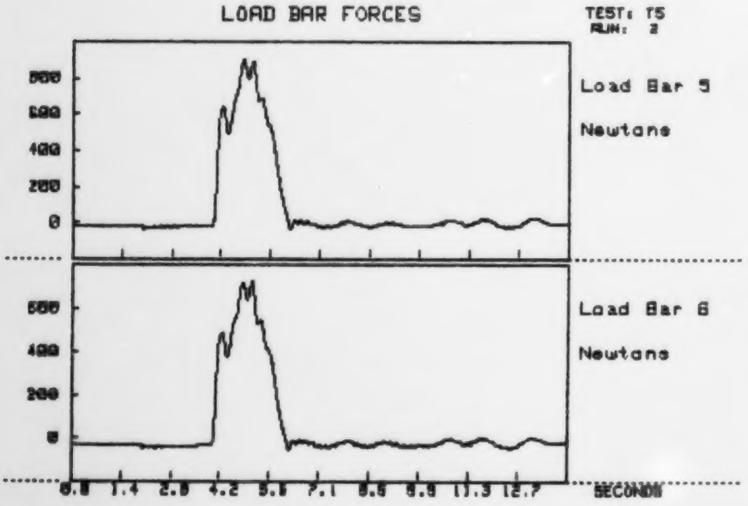
LOAD BAR FORCES
TEST: T5
RUN: 2
800
600
400
200
0
Load Bar 5
Newtons
600
400
200
0
Load Bar 6
Newtons
0.0
1.4
2.8
4.2
5.6
7.1
8.5
9.9
11.3
12.7
SECONDS

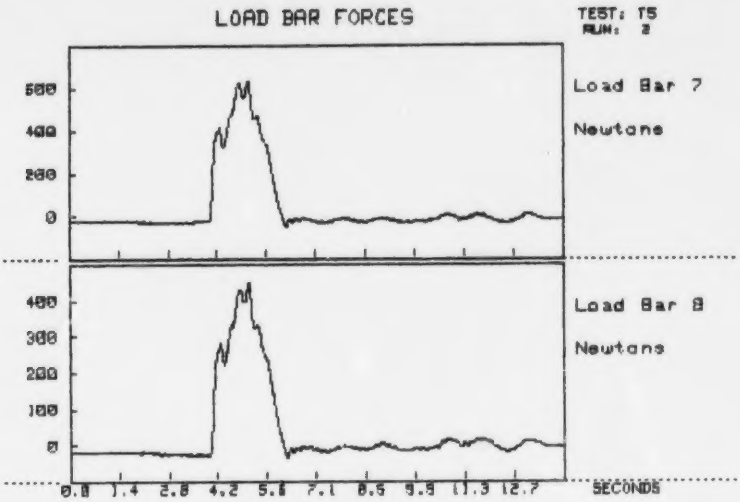
LOAD BAR FORCES
TEST: T5
RUN: 2
Load Bar 7
Newtons
600
400
200
0
Load Bar 8
Newtons
400
300
200
100
0
0.0 1.4 2.8 4.2 5.6 7.1 8.5 9.9 11.3 12.7
SECONDS

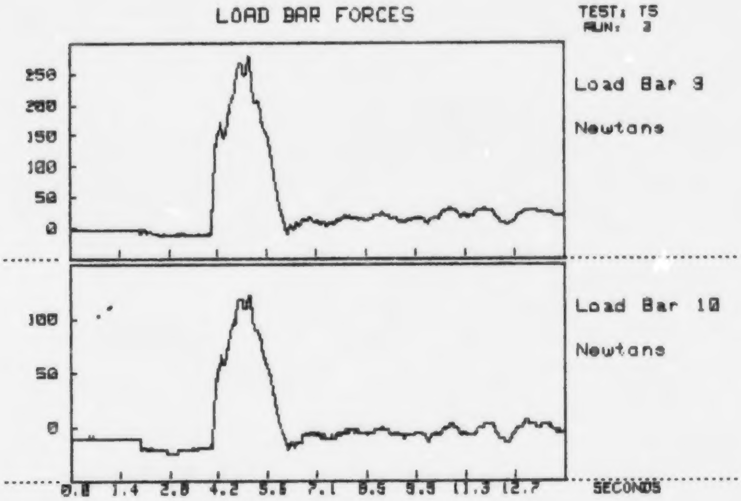
LOAD BAR FORCES
TEST: T5
RUN: 2
Load Bar 9
Newtons
250
200
150
100
50
0
Load Bar 10
Newtons
100
50
0
0.0 1.4 2.8 4.2 5.6 7.1 8.5 9.9 11.3 12.7
SECONDS

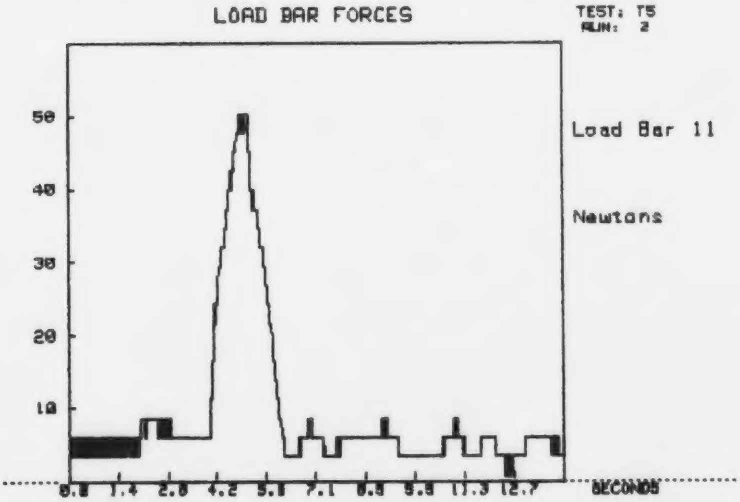
LOAD BAR FORCES
TEST: T5
RUN: 2
Load Bar 11
Newtons
50
40
30
20
10
0.0 1.4 2.8 4.2 5.6 7.1 8.5 9.9 11.3 12.7
SECONDS

ADDED MASS CALCULATION

```
                    TEST:          TS
                    RUN NUMBER:    6



NOMINAL IMPACT VELOCITY:         .24        m/s
NOMINAL SHIP SPEED:              3          kt
TIME TO MAXIMUM SURGE:           1.234      s
TIME FROM IMPACT TO BACKOFF:     2.343      s



TIME INCREMENT:                   .004      s
ACCELEROMETER THRESHOLD:          .05       m/s^2



MODEL MASS:                        596    kg
WATER DEPTH:                       1.85   m
MODEL DRAFT:                       0.275  m
ICE FREEBOARD:                     0.025  m
```

SEGMENT ADDED MASS NORMALIZED BY DISPLACED MASS

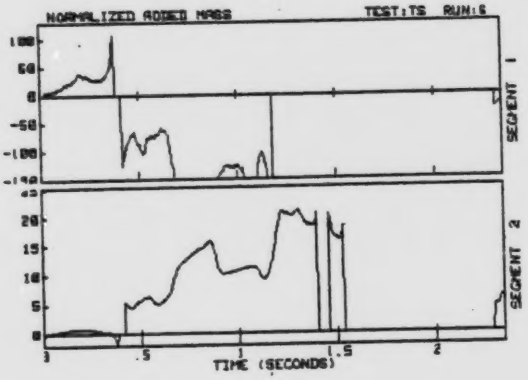

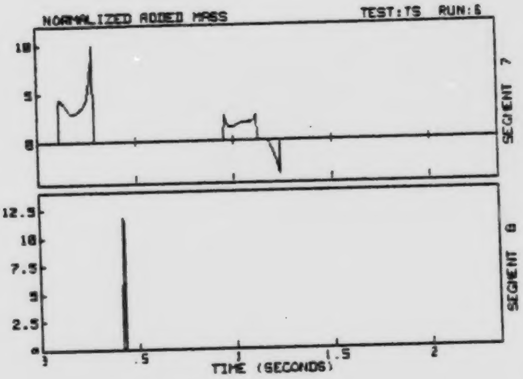

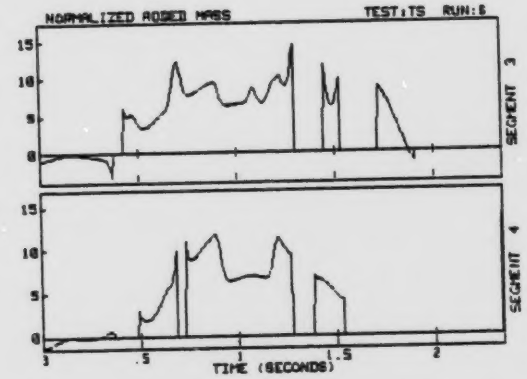

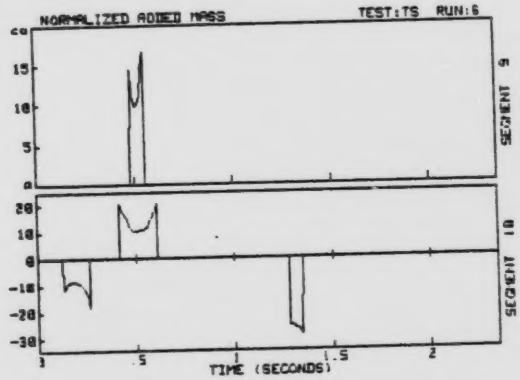

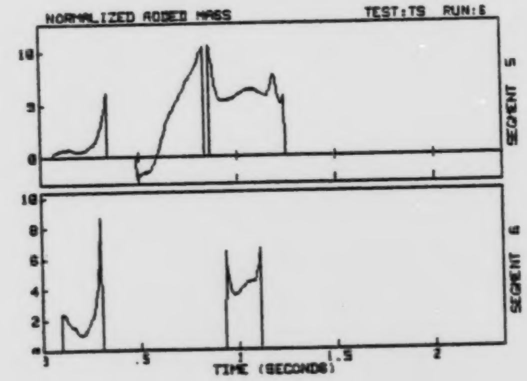

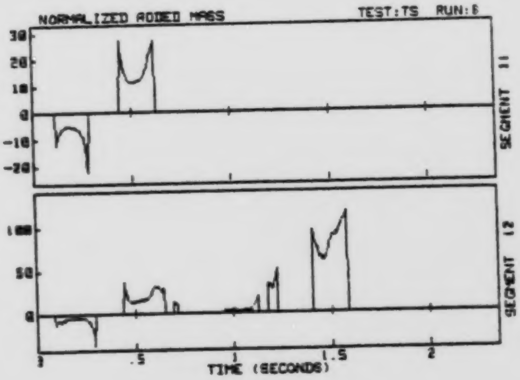

SEGMENT HYDRODYNAMIC FORCE

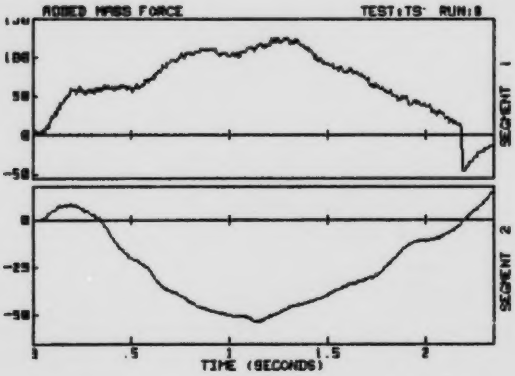

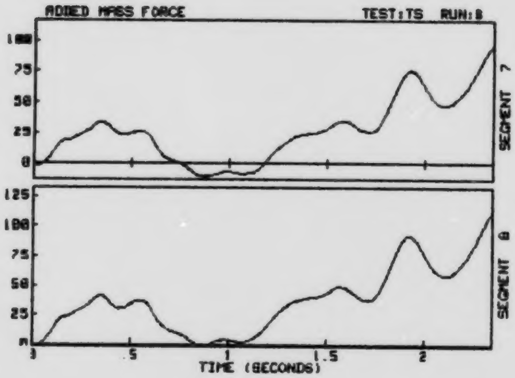

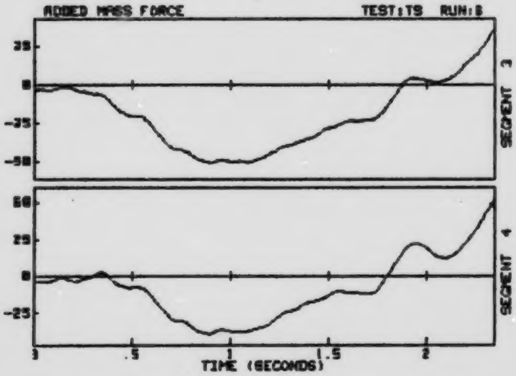

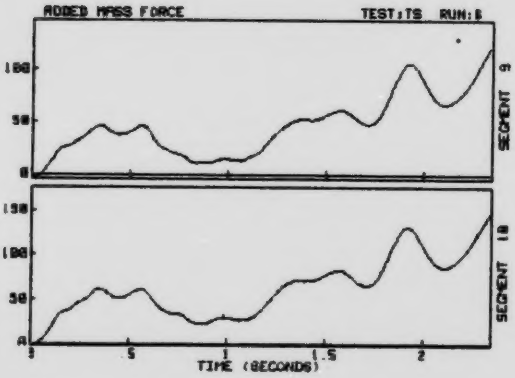

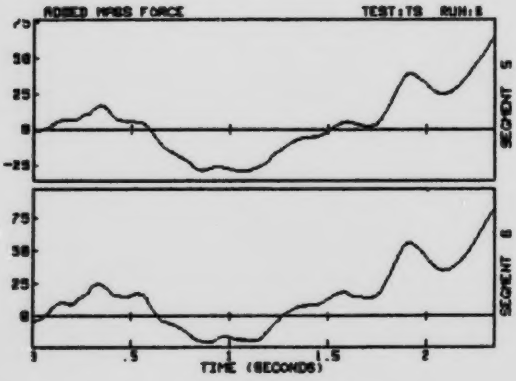

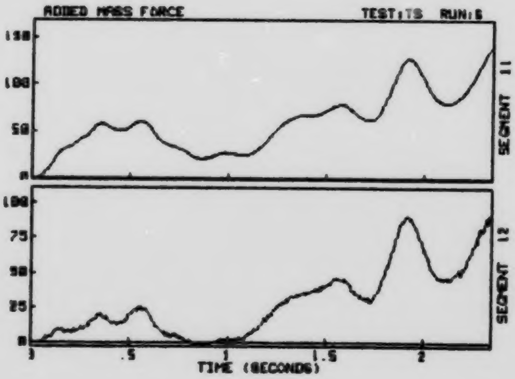

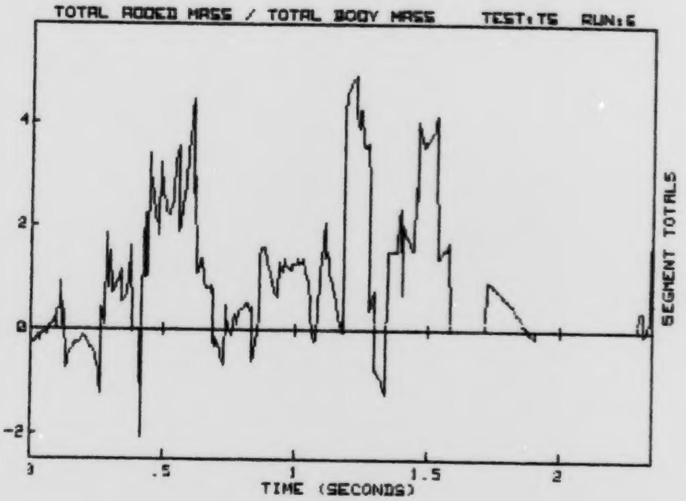

NON-DIMENSIONAL SEGMENTAL ADDED MASS STATISTICS

SEGMENT	MIN	MAX	MEAN	S.D.	NPTS
1	-257	106.8	-86.5	90.1	288
2	-1.9	21.1	9	6.8	368
3	-3.3	14.5	5	4	375
4	-1.3	14.1	4.9	4.1	317
5	-2.1	10.6	4	3.2	248
6	0	8.6	3.3	1.7	95
7	-3.5	9.9	2.3	2.3	100
8	0	11.8	11.7	.1	2
9	0	16.7	12.1	2.2	18
10	-28.8	20.7	-1.1	15.8	97
11	-22.2	27.5	4.8	13	86
12	-35.1	117.7	24.7	34.7	207
MEAN MODEL ADDED MASS =			3.74		2201

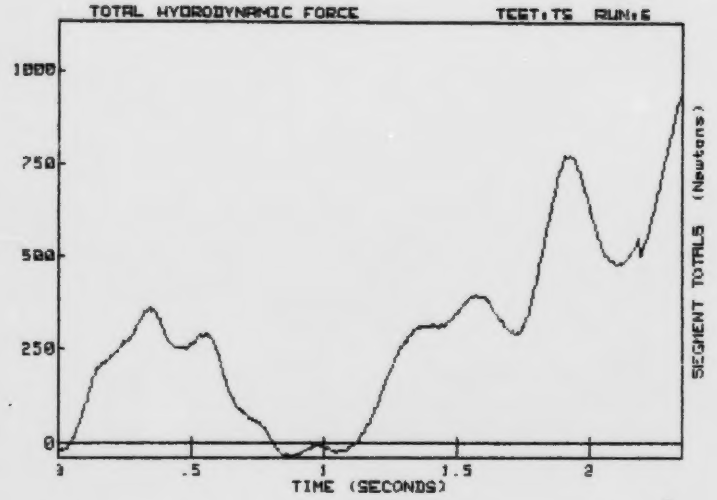

HYDRODYNAMIC FORCE SUMMARY STATISTICS

SEGMENT	MIN	MAX	MEAN	S.D.	NPTS
1	-45.8	125.1	67.2	41	582
2	-54.4	15	-24.5	21	582
3	-51.1	35.7	-20	21.7	582
4	-39.3	50.2	-8.6	20.9	582
5	-29.5	64.4	3.5	22.2	582
6	-19.6	81.2	14.2	23.5	582
7	-10.2	97	26.1	25.6	582
8	-1.2	111.1	36.8	27.4	582
9	-3.3	122.6	46	28.6	582
10	-2	147.2	62.3	33.2	582
11	-.5	140.6	58.9	31.7	582
12	-2.8	92.7	28.7	25.6	582
MEAN HYDRODYNAMIC FORCE =			24.21		6984

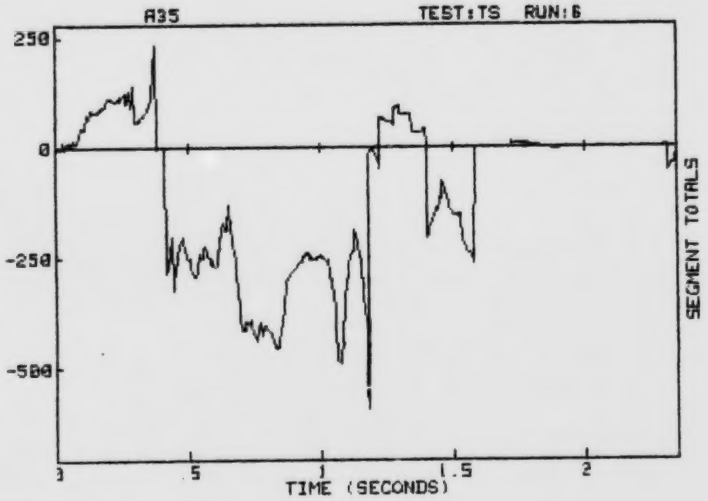

HEAVE/PITCH COUPLED ADDED MASS SUMMARY STATISTICS

SEGMENT	MIN	MAX	MEAN	S.D.	NPTS
1	-564.1	234.3	-189.9	197.8	288
2	-3.4	38.9	16.6	12.5	368
3	-4.7	20.8	7.2	5.7	375
4	-1.3	14.4	5	4.2	317
5	-1.3	6.5	2.4	2	248
6	0	1.8	.7	.3	95
7	-2	.7	-.5	.5	100
8	-7.2	0	-7.2	.1	2
9	-17.1	0	-12.4	2.2	18
10	-29.6	41.1	1.5	22.6	97
11	-50.3	40.7	-8.8	23.8	86
12	-263.3	78.5	-55.3	77.5	207

MEAN A35 MODEL ADDED MASS = -2.99 2201

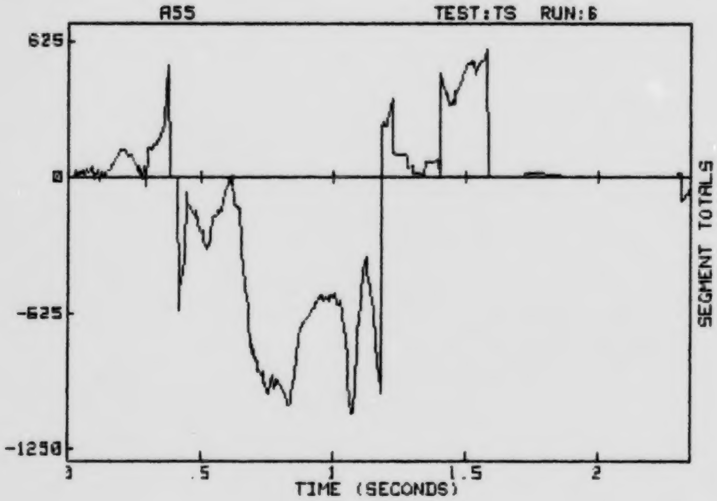

PITCH ADDED MASS MOMENT OF INERTIA SUMMARY STATISTICS

SEGMENT	MIN	MAX	MEAN	S.D.	NPTS
1	-1238.3	514.4	-416.8	197.8	288
2	-6.3	71.8	30.6	12.5	368
3	-6.7	29.8	10.4	5.7	375
4	-1.3	14.8	5.1	4.2	317
5	-.8	4	1.5	2	248
6	0	.4	.1	.3	95
7	-.1	.4	.1	.5	100
8	0	4.4	4.4	.1	2
9	0	17.5	12.7	2.2	18
10	-58.9	42.4	-2.2	22.6	97
11	-74.5	92.3	16.2	23.8	86
12	-175.5	588.6	123.6	77.5	207
MEAN A55 MODEL ADDED MASS =			1.56		2201

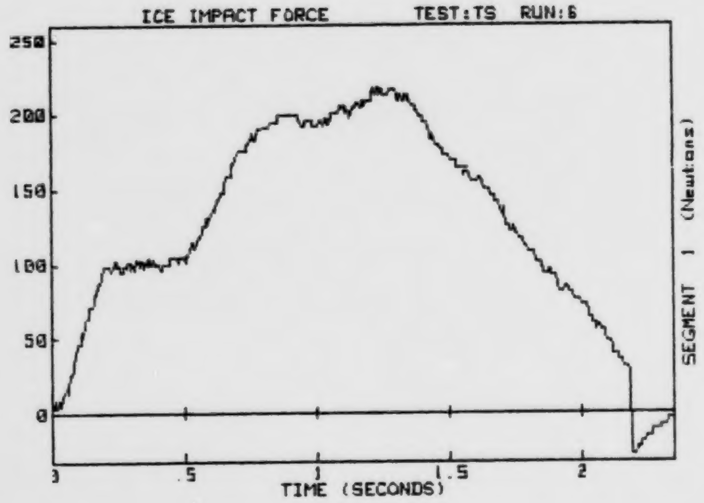
ICE IMPACT FORCE
TEST:TS RUN:6
250
200
150
100
50
0
0
.5
1
1.5
2
TIME (SECONDS)
SEGMENT 1 (Newtons)

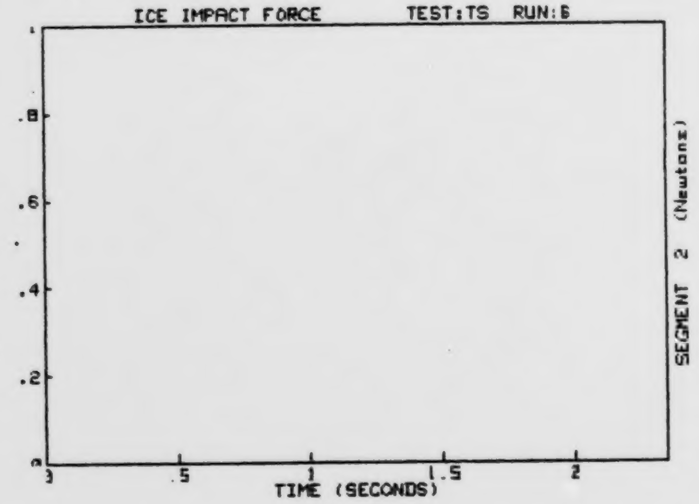
ICE IMPACT FORCE
TEST:TS RUN:6
1
.8
.6
.4
.2
0
0
.5
1
1.5
2
TIME (SECONDS)
SEGMENT 2 (Newtons)

IMPACT VELOCITY= .24 m/s
SHIP SPEED= 2.98 kt

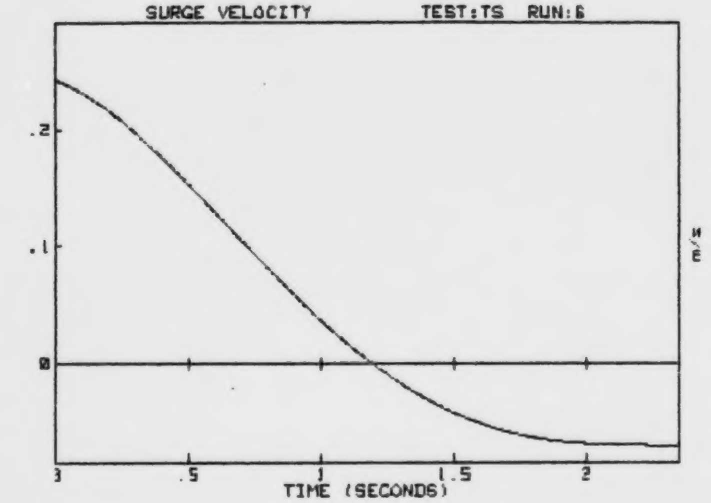

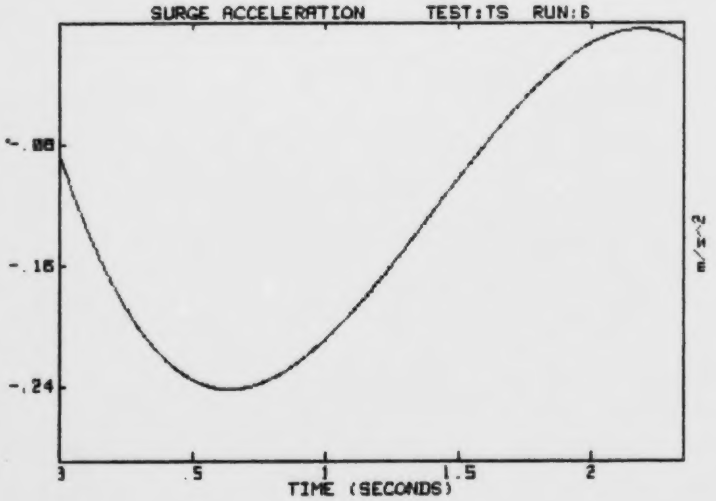

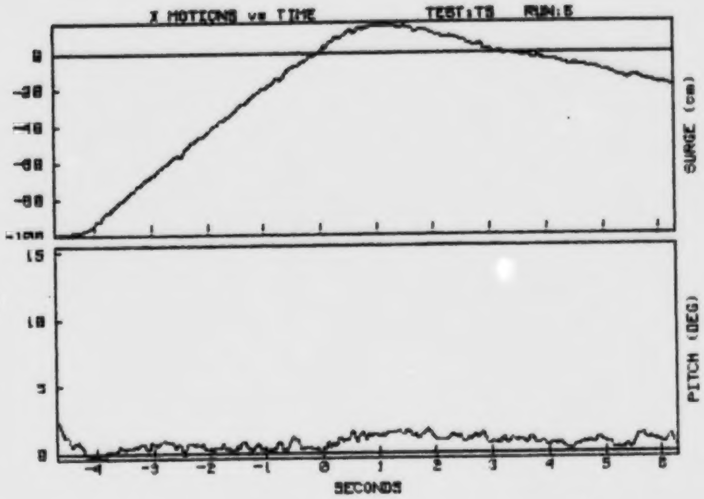
X MOTIONS vs TIME
TEST:TS RUN:5
SURGE (cm)
0
-20
-40
-60
-80
-100
PITCH (DEG)
15
10
5
0
-4
-3
-2
-1
0
1
2
3
4
5
6
SECONDS

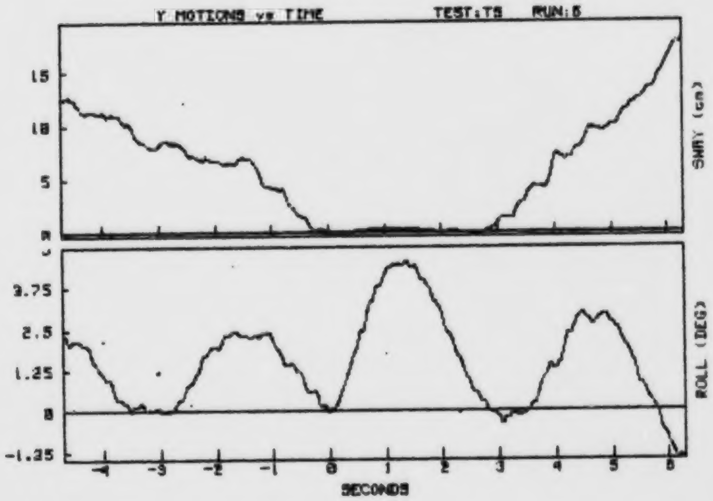
Y MOTIONS vs TIME
TEST:TS RUN:5
SWAY (cm)
15
10
5
0
ROLL (DEG)
3.75
2.5
1.25
0
-1.25
-4
-3
-2
-1
0
1
2
3
4
5
6
SECONDS

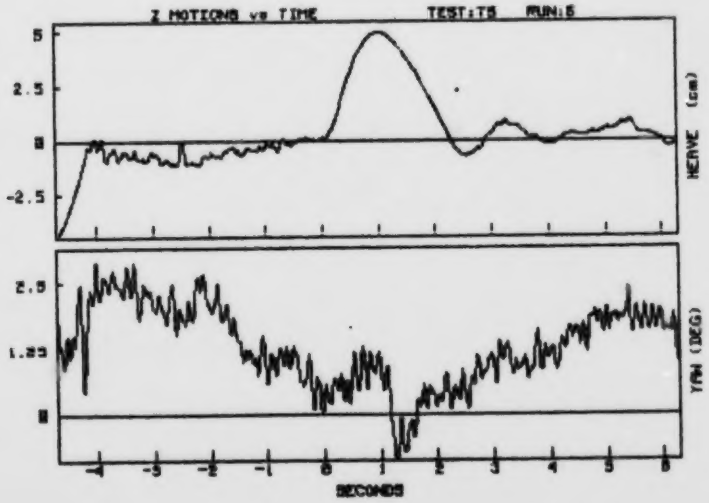
Z MOTIONS vs TIME
TEST:TS RUN:5
HEAVE (cm)
5
2.5
0
-2.5
YAW (DEG)
2.5
1.25
0
-4
-3
-2
-1
0
1
2
3
4
5
6
SECONDS

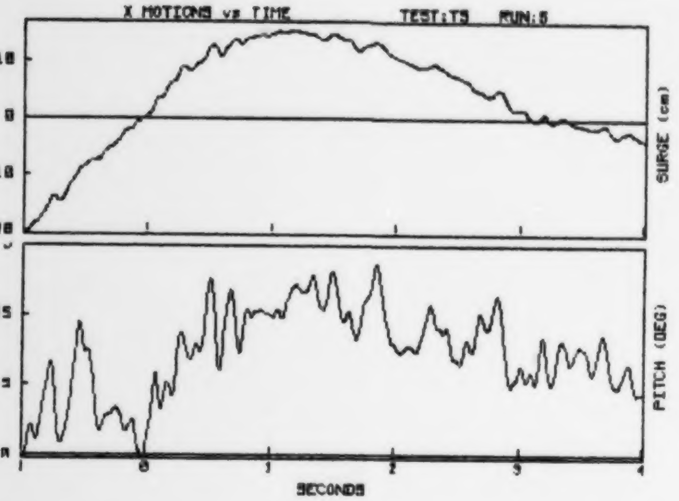
X MOTIONS vs TIME
TEST:T5
RUN:6
10
0
-10
-20
SURGE (cm)
1.25
.625
0
PITCH (DEG)
0
1
2
3
4
SECONDS

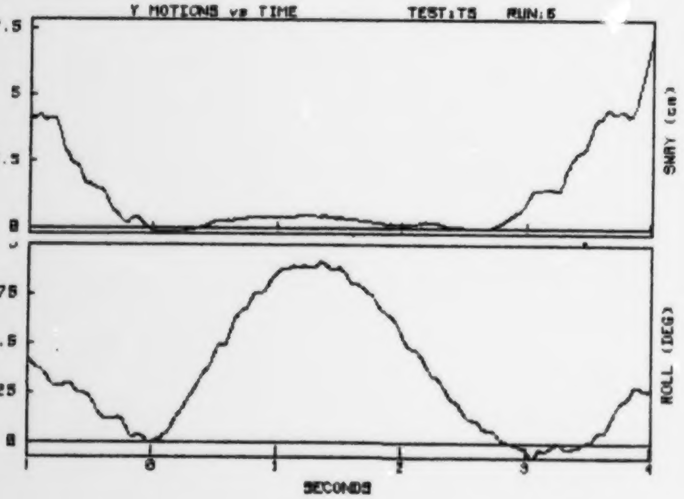
Y MOTIONS vs TIME
TEST:T5
RUN:6
7.5
5
2.5
0
SWAY (cm)
3.75
2.5
1.25
0
ROLL (DEG)
0
1
2
3
4
SECONDS

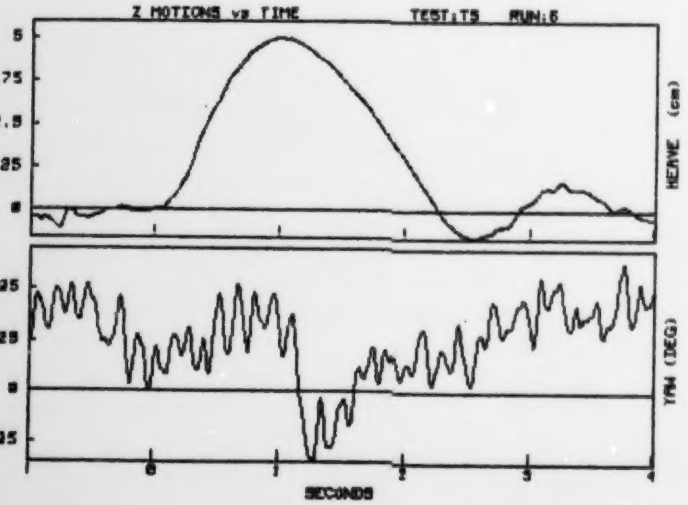
Z MOTIONS vs TIME
TEST:T5
RUN:6
5
3.75
2.5
1.25
0
HEAVE (cm)
1.25
.625
0
-.625
YAW (DEG)
0
1
2
3
4
SECONDS

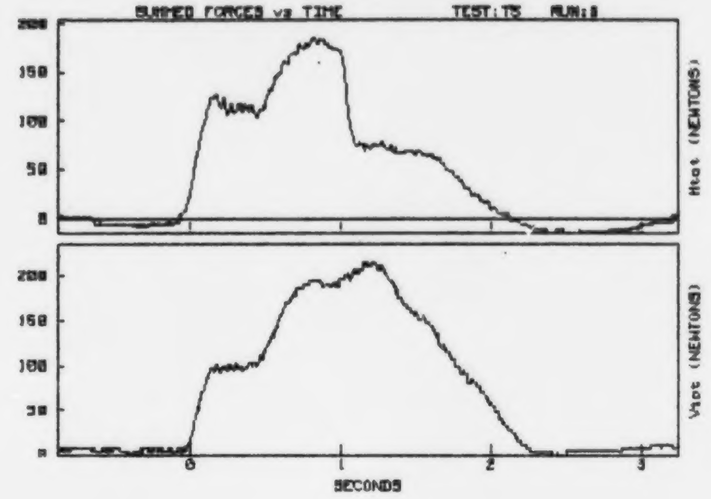
SUMMED FORCES vs TIME
TEST: T5 RUN: 8
200
150
100
50
0
Htot (NEWTONS)
200
150
100
50
0
Vtot (NEWTONS)
0
1
2
3
SECONDS

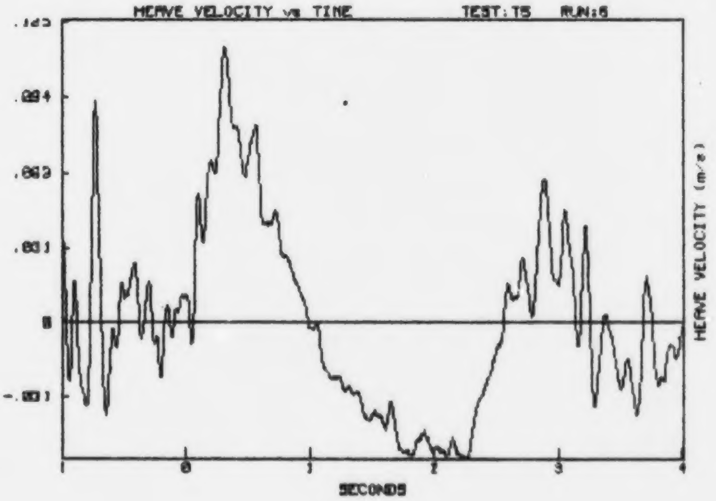
HEAVE VELOCITY vs TIME
TEST: T5 RUN: 6
.125
.094
.063
.031
0
-.031
HEAVE VELOCITY (m/s)
1
0
1
2
3
4
SECONDS

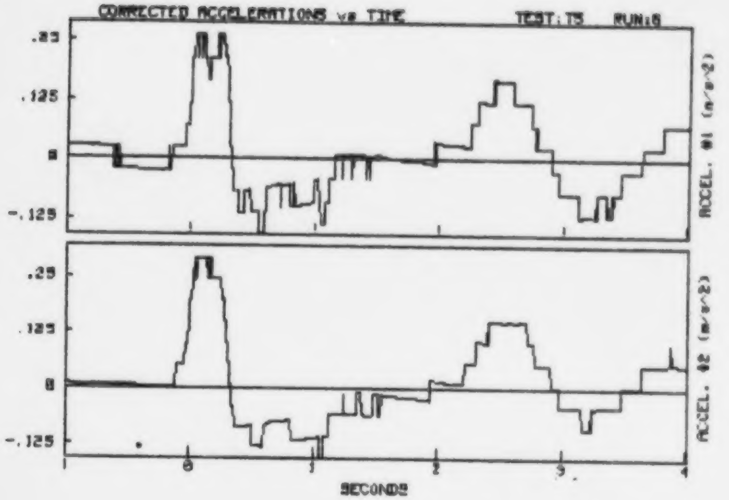
CORRECTED ACCELERATIONS vs TIME
TEST: T5 RUN: 6
.25
.125
0
-.125
ACCEL. #1 (m/s^2)
.25
.125
0
-.125
ACCEL. #2 (m/s^2)
0
1
2
3
4
SECONDS

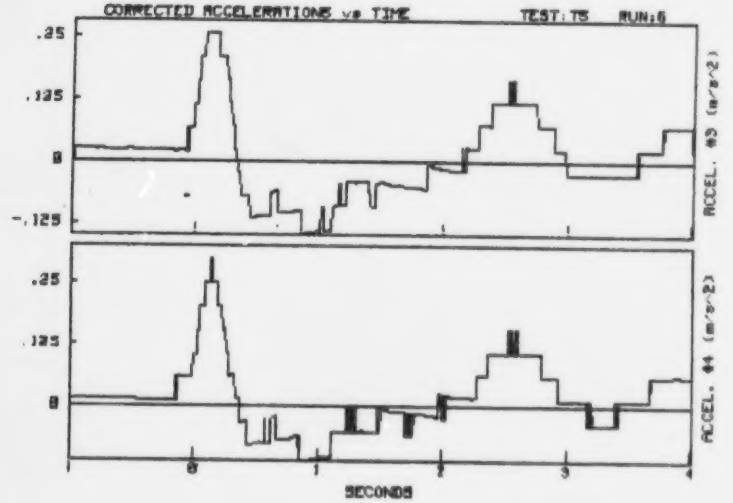
CORRECTED ACCELERATIONS vs TIME
TEST: T5 RUN: 6
.25
.125
0
-.125
ACCEL. #3 (m/s^2)
.25
.125
0
ACCEL. #4 (m/s^2)
0
1
2
3
4
SECONDS

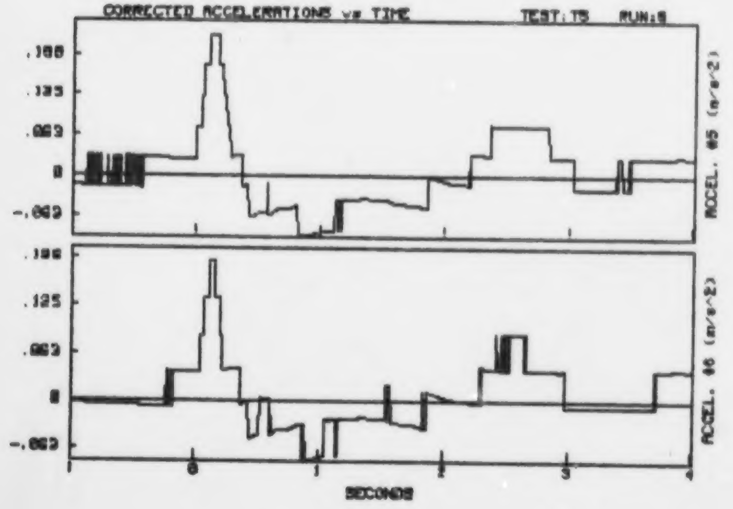
CORRECTED ACCELERATIONS vs TIME
TEST: T5 RUN: 6
.188
.125
.063
0
-.063
ACCEL. #5 (m/s^2)
.188
.125
.063
0
-.063
ACCEL. #6 (m/s^2)
0
1
2
3
4
SECONDS

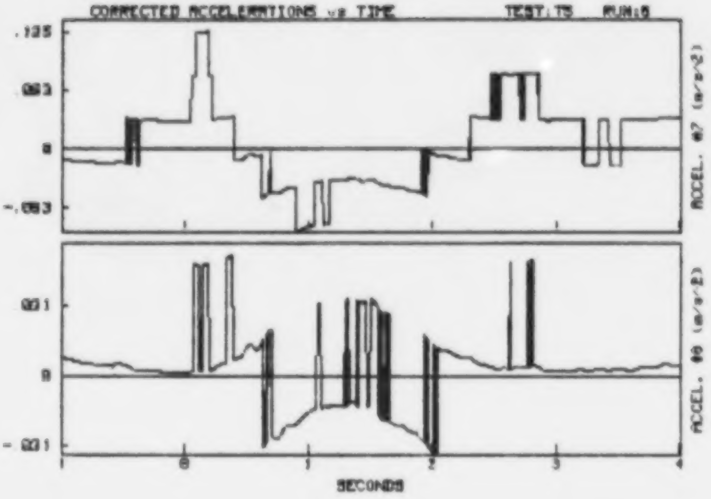
CORRECTED ACCELERATIONS vs TIME
TEST:T5 RUN:5
.125
.063
0
-.063
ACCEL. #7 (m/s^2)
.031
0
-.031
ACCEL. #8 (m/s^2)
0
1
2
3
4
SECONDS

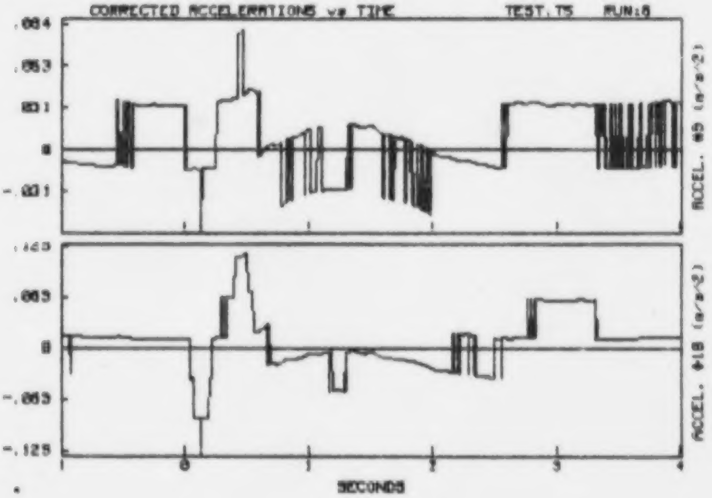
CORRECTED ACCELERATIONS vs TIME
TEST:T5 RUN:5
.094
.063
.031
0
-.031
ACCEL. #9 (m/s^2)
.125
.063
0
-.063
-.125
ACCEL. #10 (m/s^2)
0
1
2
3
4
SECONDS

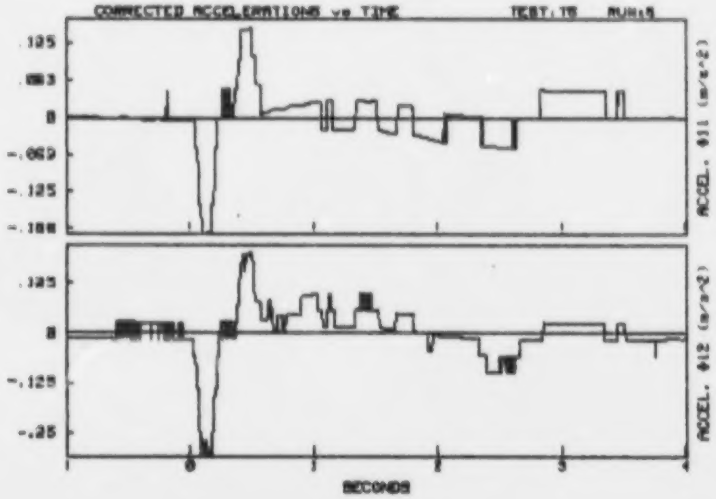
CORRECTED ACCELERATIONS vs TIME
TEST:T5 RUN:5
.125
.063
0
-.063
-.125
-.188
ACCEL. #11 (m/s^2)
.125
0
-.125
-.25
ACCEL. #12 (m/s^2)
0
1
2
3
4
SECONDS

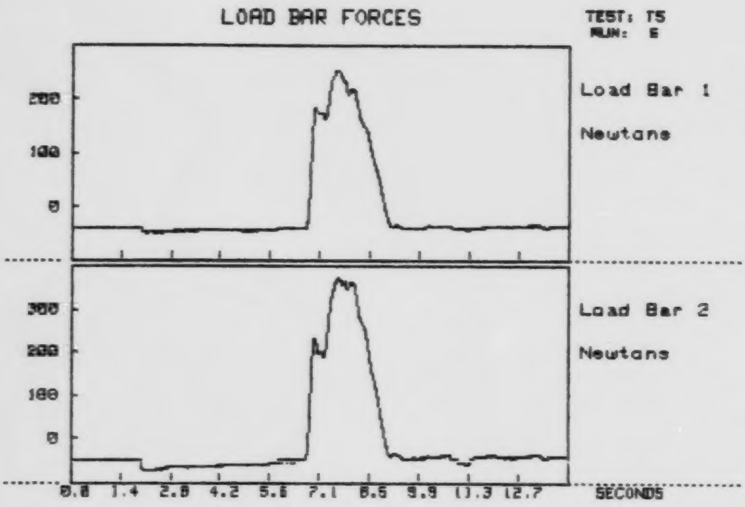
LOAD BAR FORCES
TEST: T5
RUN: 6
200
100
0
Load Bar 1
Newtons
300
200
100
0
Load Bar 2
Newtons
0.0
1.4
2.8
4.2
5.6
7.1
8.5
9.9
11.3
12.7
SECONDS

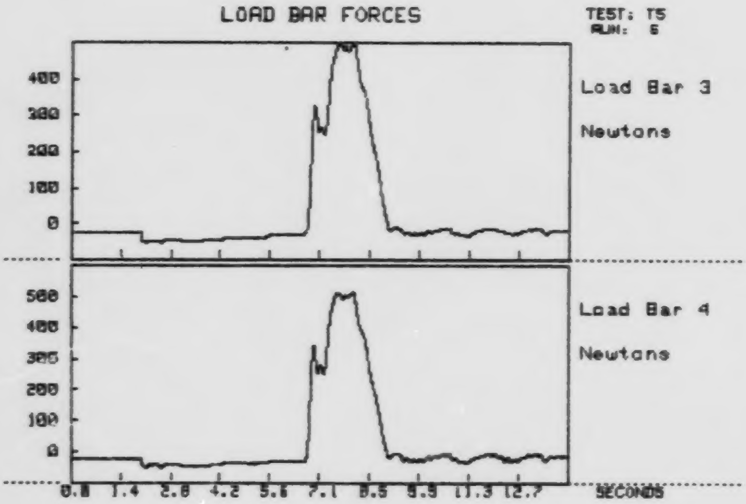
LOAD BAR FORCES
TEST: T5
RUN: 6
400
300
200
100
0
Load Bar 3
Newtons
500
400
300
200
100
0
Load Bar 4
Newtons
0.0
1.4
2.8
4.2
5.6
7.1
8.5
9.9
11.3
12.7
SECONDS

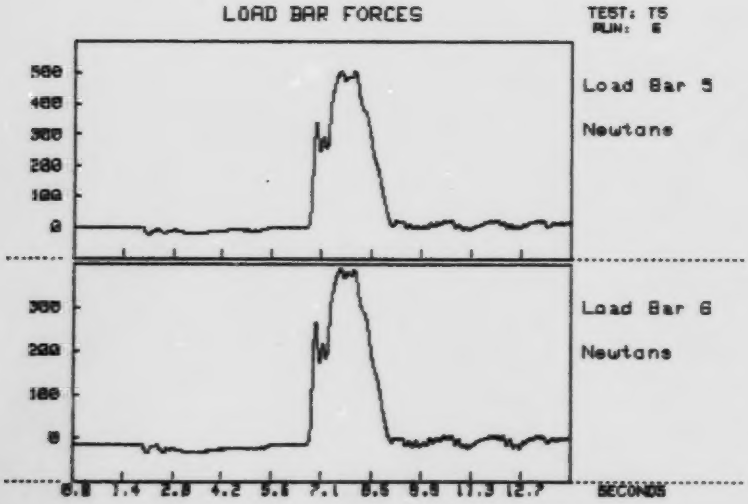
LOAD BAR FORCES
TEST: T5
RUN: 6
500
400
300
200
100
0
Load Bar 5
Newtons
300
200
100
0
Load Bar 6
Newtons
0.0
1.4
2.8
4.2
5.6
7.1
8.5
9.9
11.3
12.7
SECONDS

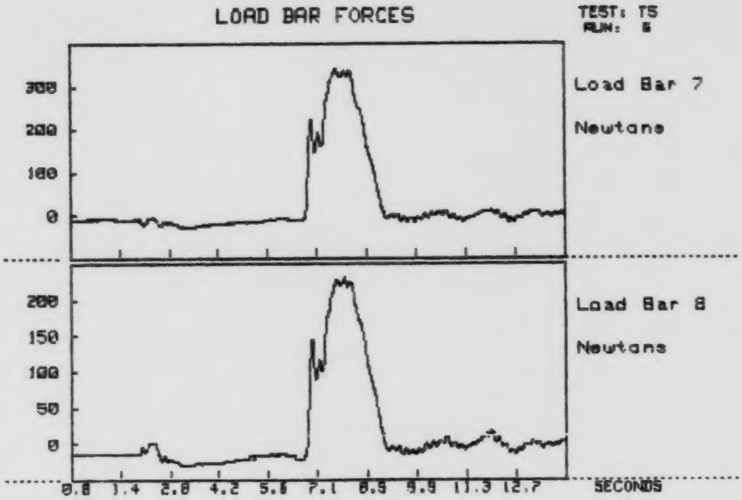
LOAD BAR FORCES
TEST: T5
RUN: 6
300
200
100
0
Load Bar 7
Newtons
200
150
100
50
0
Load Bar 8
Newtons
0.0
1.4
2.8
4.2
5.6
7.1
8.5
9.9
11.3
12.7
SECONDS

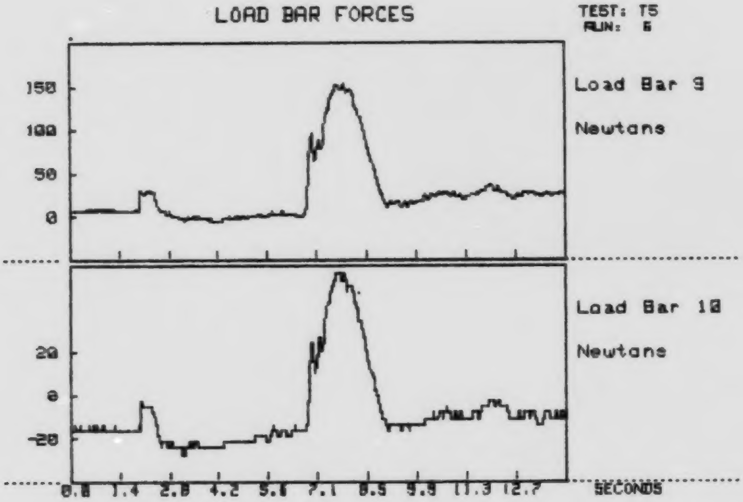
LOAD BAR FORCES
TEST: T5
RUN: 6
150
100
50
0
Load Bar 9
Newtons
20
0
-20
Load Bar 10
Newtons
0.0
1.4
2.8
4.2
5.6
7.1
8.5
9.9
11.3
12.7
SECONDS

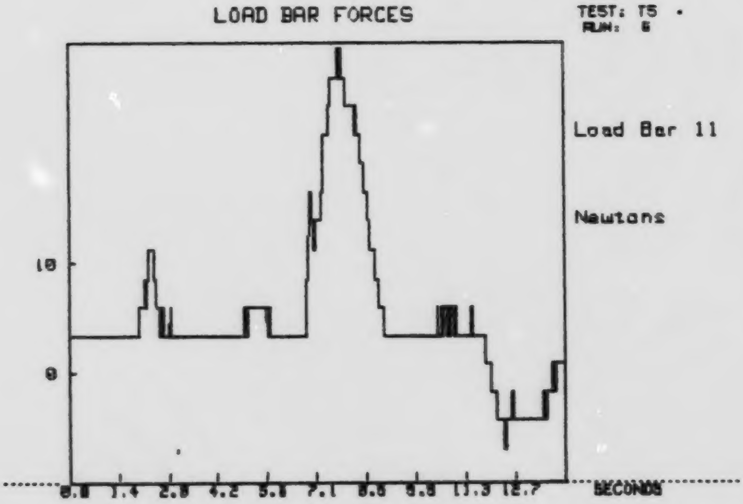
LOAD BAR FORCES
TEST: T5
RUN: 6
10
0
Load Bar 11
Newtons
0.0
1.4
2.8
4.2
5.6
7.1
8.5
9.9
11.3
12.7
SECONDS

```
                 MV  ARCTIC MODEL TESTS
                 ADDED MASS CALCULATION



                    TEST:          TT
                    RUN NUMBER:    10



         NOMINAL IMPACT VELOCITY:          1.05      m/s
         NOMINAL SHIP SPEED:               12.9      kt
         TIME TO MAXIMUM SURGE:            .802      s
         TIME FROM IMPACT TO BACKOFF:      1.806     s



         TIME INCREMENT:                    .004     s
         ACCELEROMETER THRESHOLD:           .05      m/s^2



         MODEL MASS:                         596     kg
         WATER DEPTH:                        1.85    m
         MODEL DRAFT:                        0.275   m
         ICE FREEBOARD:                      0.025   m
```

SEGMENT ADDED MASS NORMALIZED BY DISPLACED MASS

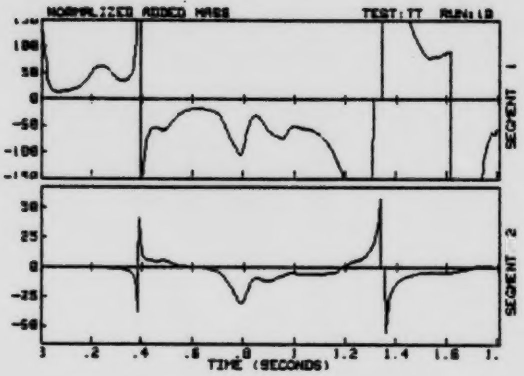

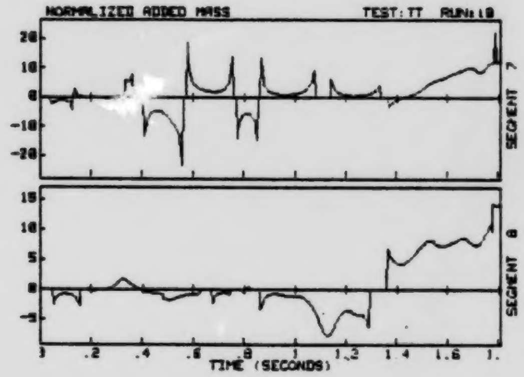

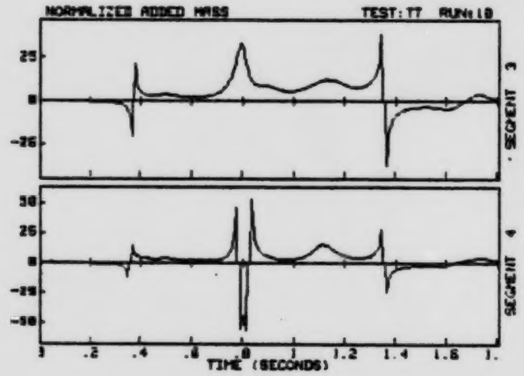

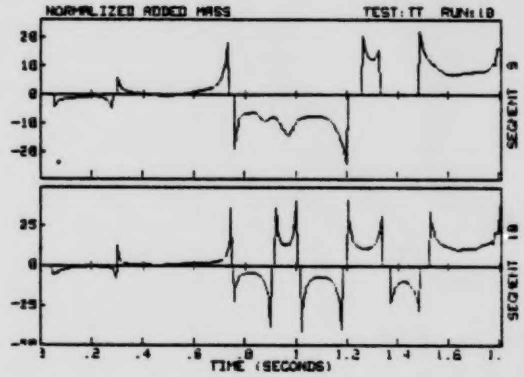

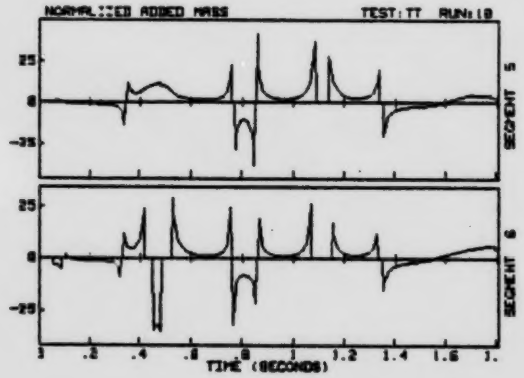

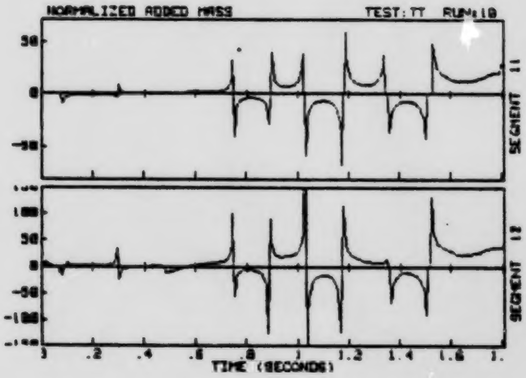

SEGMENT HYDRODYNAMIC FORCE

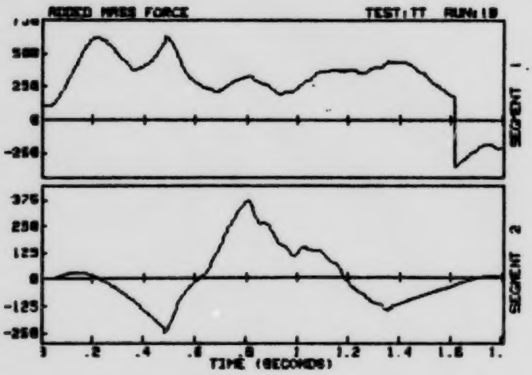

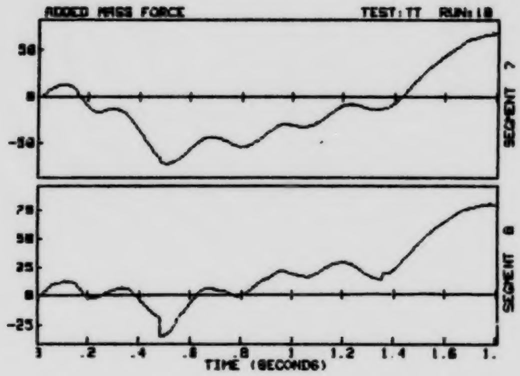

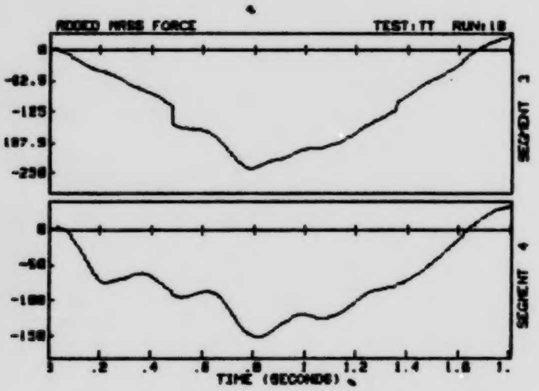

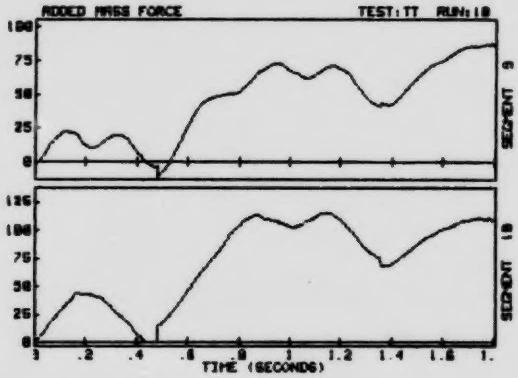

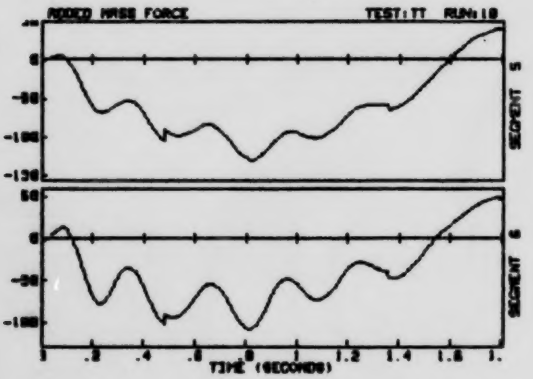

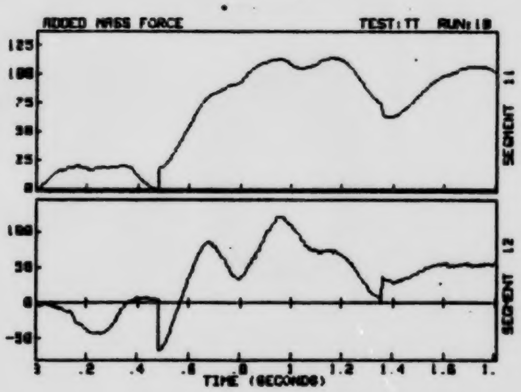

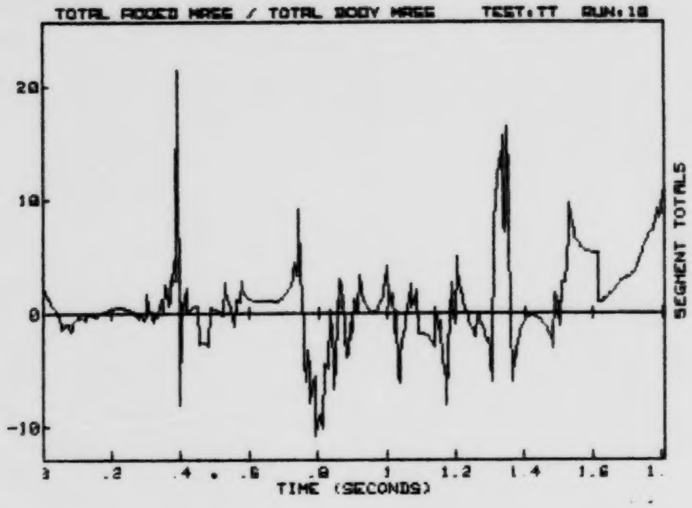

NON-DIMENSIONAL SEGMENTAL ADDED MASS STATISTICS

SEGMENT	MIN	MAX	MEAN	S.D.	NPTS
1	-847.8	992.2	-25.8	167.6	440
2	-54.5	56.9	-2.7	9.6	443
3	-37.8	38.5	3.6	7.9	434
4	-57	53	2.2	9.1	424
5	-38.4	41.4	2.3	7.4	408
6	-34.8	28.9	.9	7.9	379
7	-23.3	22	1.5	5.7	386
8	-7.8	14.2	1.1	4.7	378
9	-24.4	22	.3	8.3	370
10	-41.8	41.4	2	12.3	403
11	-67.4	59.3	2.6	13.3	411
12	-183.1	182.5	5.3	29.2	426
MEAN MODEL ADDED MASS =			.88		4902

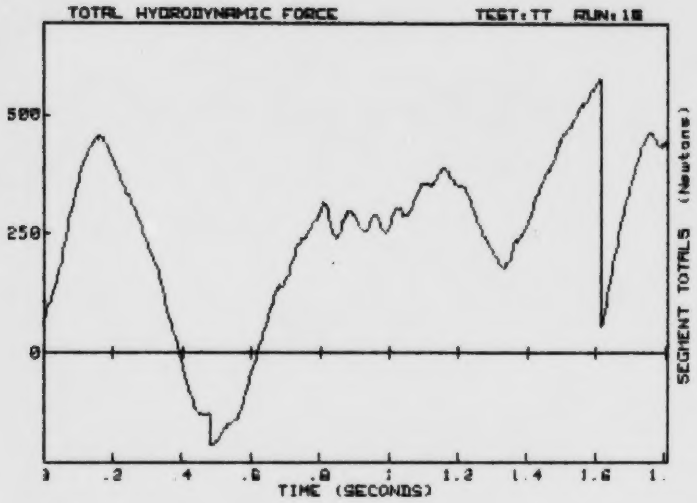

HYDRODYNAMIC FORCE SUMMARY STATISTICS

SEGMENT	MIN	MAX	MEAN	S.D.	NPTS
1	-359.8	627.7	290.7	218	449
2	-248.2	371.4	13.4	131.1	449
3	-240.7	27.6	-112.4	80.3	449
4	-152.3	33.5	-72.8	48.8	449
5	-129.7	41.7	-58.4	45.5	449
6	-107.9	49.9	-40.8	40.6	449
7	-72.1	68.8	-12.6	36.5	449
8	-34.8	80.6	18.7	26.9	449
9	-10.4	87.8	45.2	27.4	449
10	-3.1	115.5	72	37.3	449
11	-1.8	114.2	68.9	39.2	449
12	-67.3	120.7	35	43	449
MEAN HYDRODYNAMIC FORCE =			20.56		5388

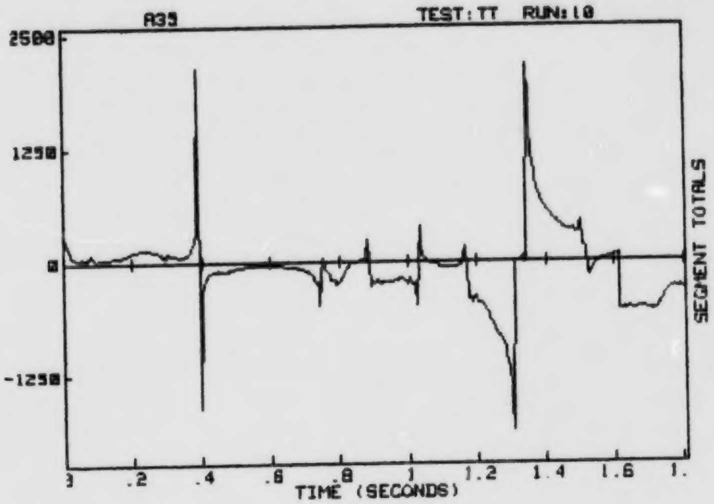

HEAVE/PITCH COUPLED ADDED MASS SUMMARY STATISTICS

SEGMENT	MIN	MAX	MEAN	S.D.	NPTS
1	-1860.9	2177.9	-56.7	367.9	440
2	-100.6	104.9	-5	17.7	443
3	-54.1	55.3	5.1	11.4	434
4	-58.3	54.3	2.3	9.3	424
5	-23.6	25.5	1.4	4.6	408
6	-7.1	5.9	.2	1.6	379
7	-4.5	4.8	-.3	1.2	386
8	-8.7	4.8	-.7	2.9	378
9	-22.5	24.9	-.3	8.5	370
10	-59.2	59.8	-2.8	17.7	403
11	-108.6	123.6	-4.7	24.4	411
12	-408.1	409.4	-11.9	65.3	426
MEAN A35 MODEL ADDED MASS =			-1.1		4902

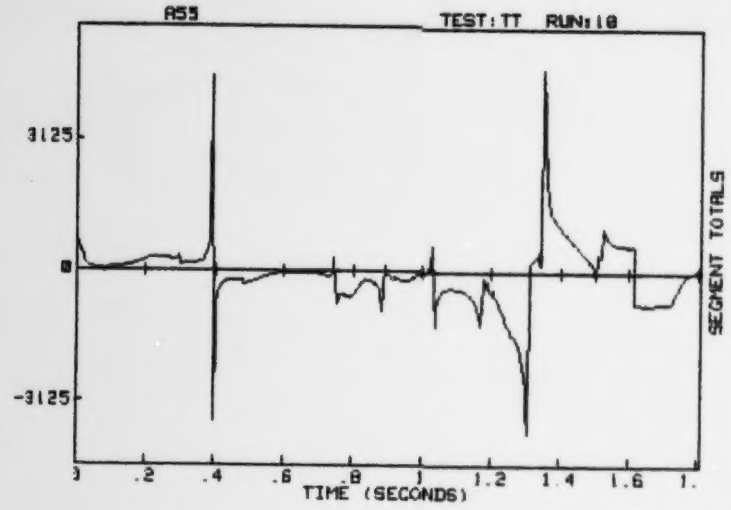

PITCH ADDED MASS MOMENT OF INERTIA SUMMARY STATISTICS

SEGMENT	MIN	MAX	MEAN	S.D.	NPTS
1	-4084.6	4780.4	-124.5	367.9	440
2	-185.5	193.4	-9.2	17.7	443
3	-77.6	79.2	7.3	11.4	434
4	-59.8	55.6	2.3	9.3	424
5	-14.5	15.7	.9	4.6	408
6	-1.5	1.2	0	1.6	379
7	-1	.9	.1	1.2	386
8	-3	5.4	.4	2.9	378
9	-25.5	23.1	.3	8.5	370
10	-85.6	84.7	4.1	17.7	403
11	-226.5	199.1	8.6	24.4	411
12	-915.4	912.6	26.5	65.3	426
MEAN A55 MODEL ADDED MASS =			-.25		4902

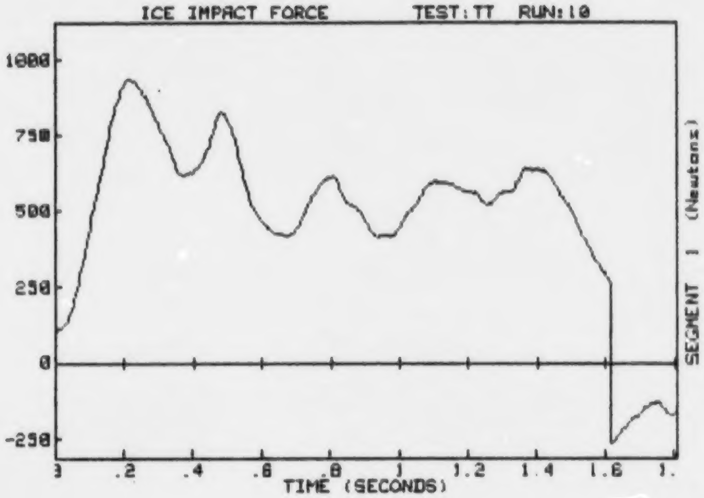
ICE IMPACT FORCE
TEST: TT RUN: 10
1000
750
500
250
0
-250
0
.2
.4
.6
.8
1
1.2
1.4
1.6
1.
TIME (SECONDS)
SEGMENT 1 (Newtons)

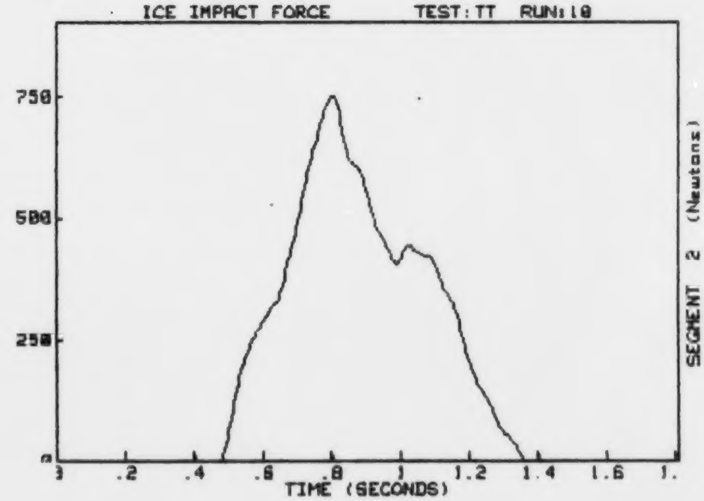
ICE IMPACT FORCE
TEST: TT RUN: 10
750
500
250
0
0
.2
.4
.6
.8
1
1.2
1.4
1.6
1.
TIME (SECONDS)
SEGMENT 2 (Newtons)

IMPACT VELOCITY= 1.03 m/s
SHIP SPEED= 12.72 kt

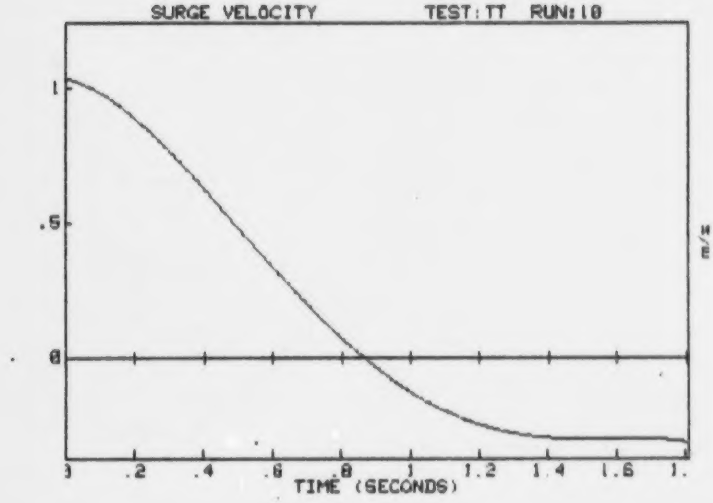

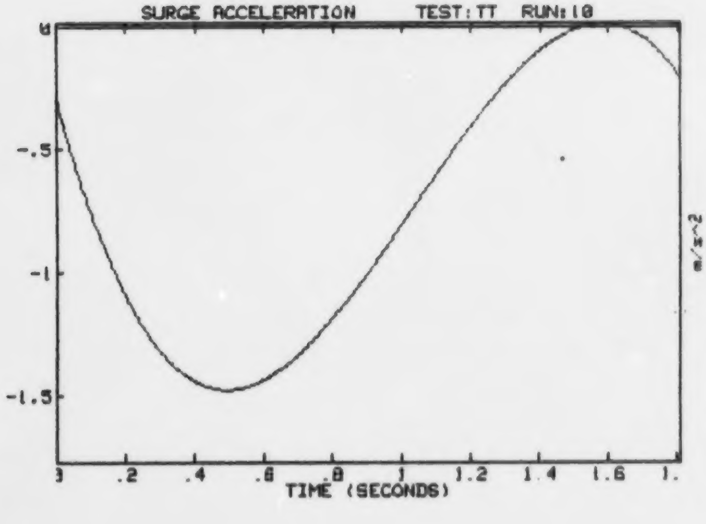

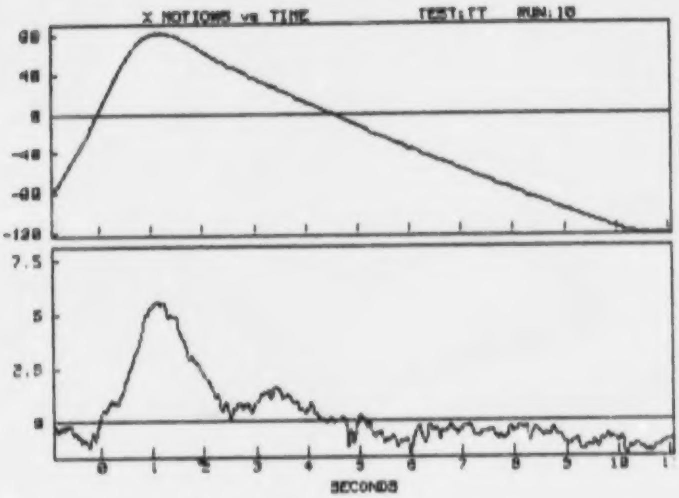
X MOTIONS vs TIME
TEST:TT RUN:10
80
40
0
-40
-80
-120
SURGE (cm)
7.5
5
2.5
0
PITCH (DEG)
0
1
2
3
4
5
6
7
8
9
10
1
SECONDS

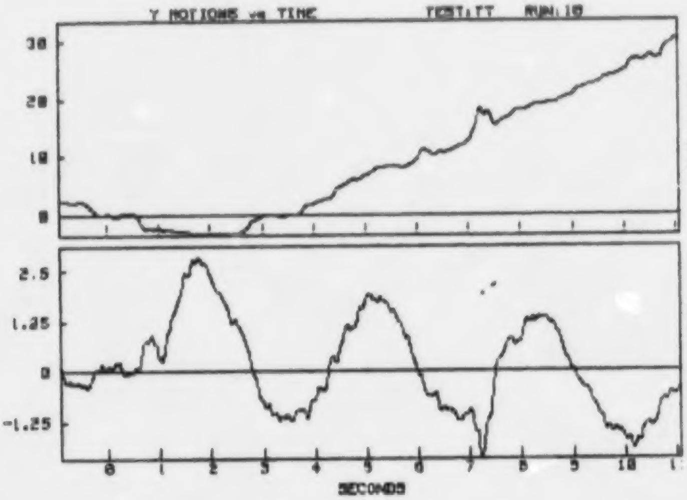
Y MOTIONS vs TIME
TEST:TT RUN:10
30
20
10
0
SWAY (cm)
2.5
1.25
0
-1.25
ROLL (DEG)
0
1
2
3
4
5
6
7
8
9
10
1
SECONDS

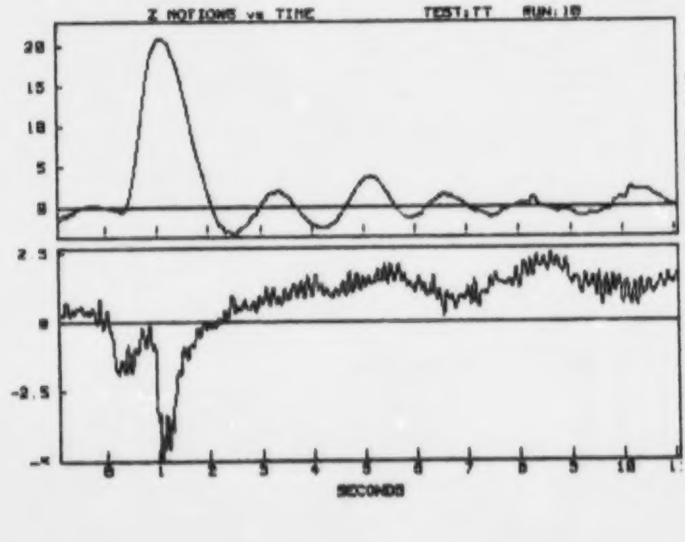
Z MOTIONS vs TIME
TEST:TT RUN:10
20
15
10
5
0
HEAVE (cm)
2.5
0
-2.5
-5
YAW (DEG)
0
1
2
3
4
5
6
7
8
9
10
1
SECONDS

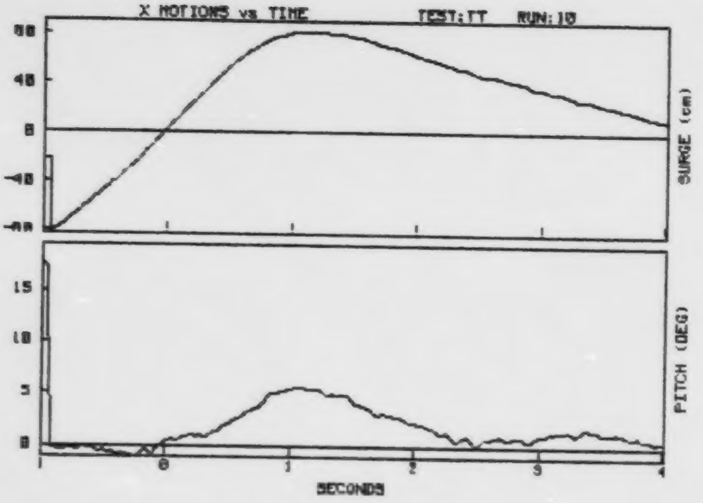
X MOTIONS vs TIME
TEST:TT RUN:10
80
40
0
-40
-80
SURGE (cm)
15
10
5
0
PITCH (DEG)
-1
0
1
2
3
4
SECONDS

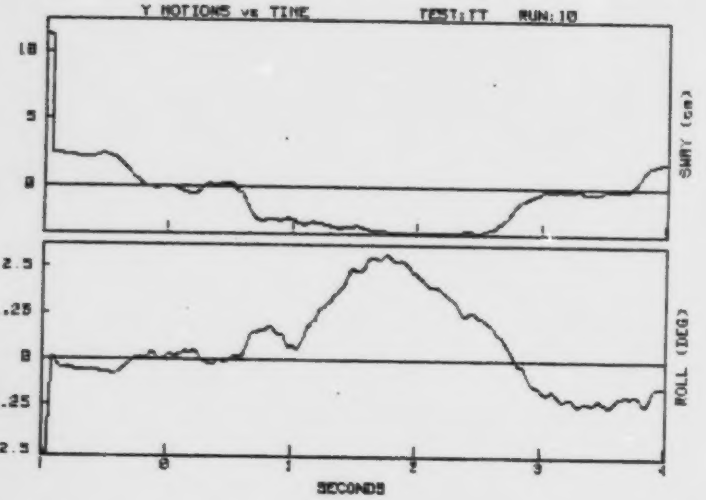
Y MOTIONS vs TIME
TEST:TT RUN:10
10
5
0
SWAY (cm)
2.5
1.25
0
-1.25
-2.5
ROLL (DEG)
-1
0
1
2
3
4
SECONDS

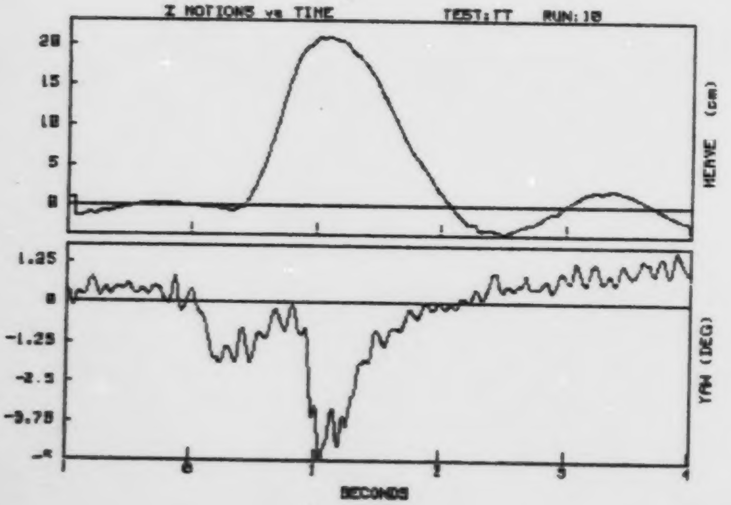
Z MOTIONS vs TIME
TEST:TT RUN:10
20
15
10
5
0
HEAVE (cm)
1.25
0
-1.25
-2.5
-3.75
-5
YAW (DEG)
-1
0
1
2
3
4
SECONDS

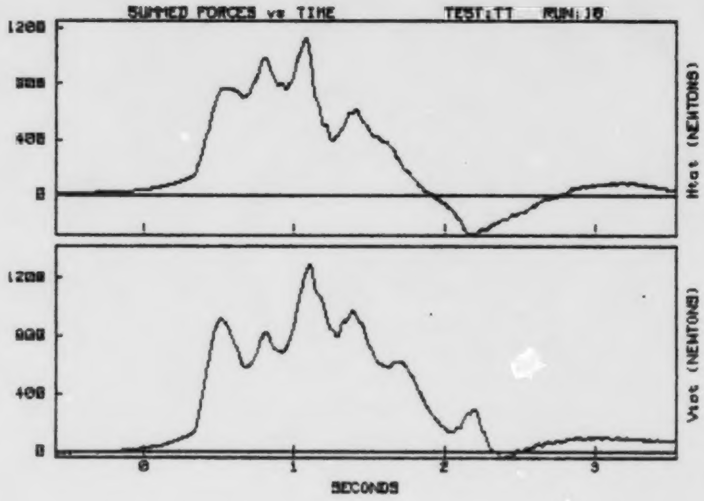
SUMMED FORCES vs TIME
TEST:TT RUN:10
1200
800
400
0
Htot (NEWTONS)
1200
800
400
0
Vtot (NEWTONS)
0
1
2
3
SECONDS

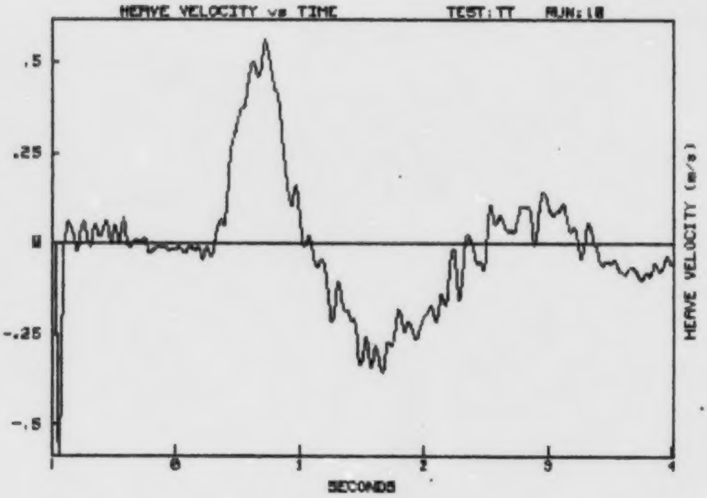
HEAVE VELOCITY vs TIME
TEST:TT RUN:10
.5
.25
0
-.25
-.5
HEAVE VELOCITY (m/s)
0
1
2
3
4
SECONDS

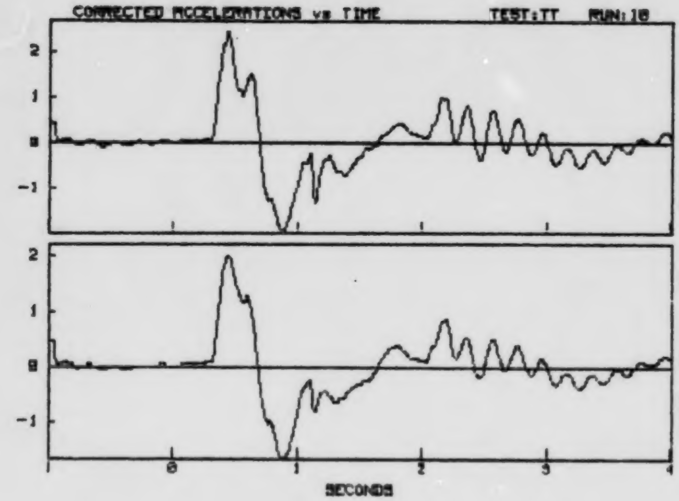
CORRECTED ACCELERATIONS vs TIME
TEST:TT RUN:10
ACCEL. #1 (m/s^2)
ACCEL. #2 (m/s^2)
2
1
0
-1
SECONDS
0
1
2
3
4

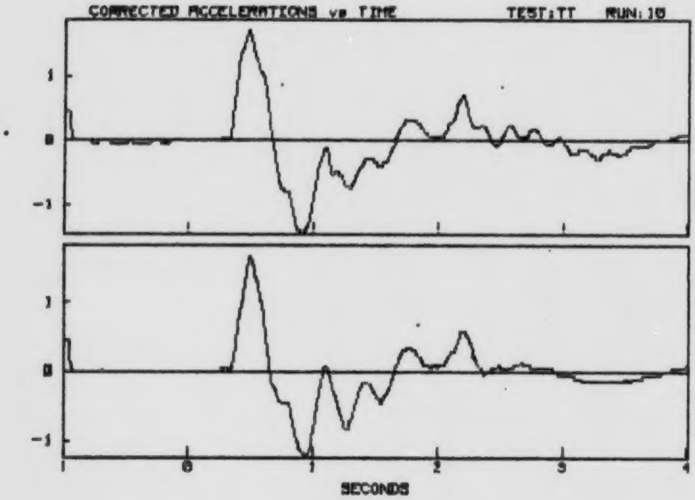
CORRECTED ACCELERATIONS vs TIME
TEST:TT RUN:10
ACCEL. #3 (m/s^2)
ACCEL. #4 (m/s^2)
1
0
-1
SECONDS
0
1
2
3
4

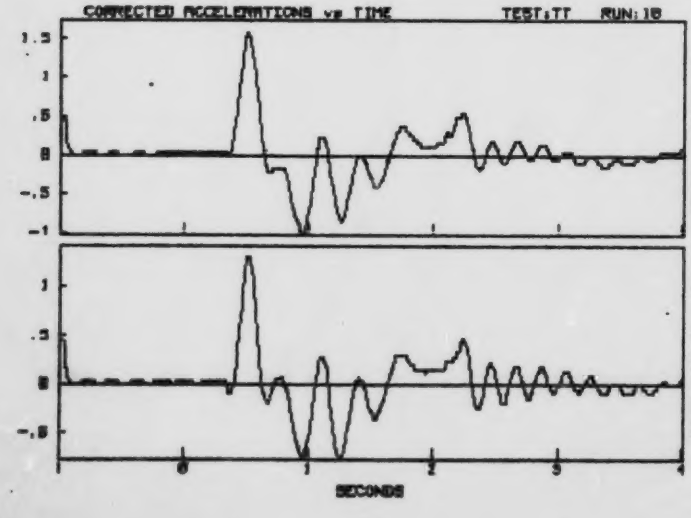
CORRECTED ACCELERATIONS vs TIME
TEST:TT RUN:10
ACCEL. #5 (m/s^2)
ACCEL. #6 (m/s^2)
1.5
1
.5
0
-.5
-1
SECONDS
0
1
2
3
4

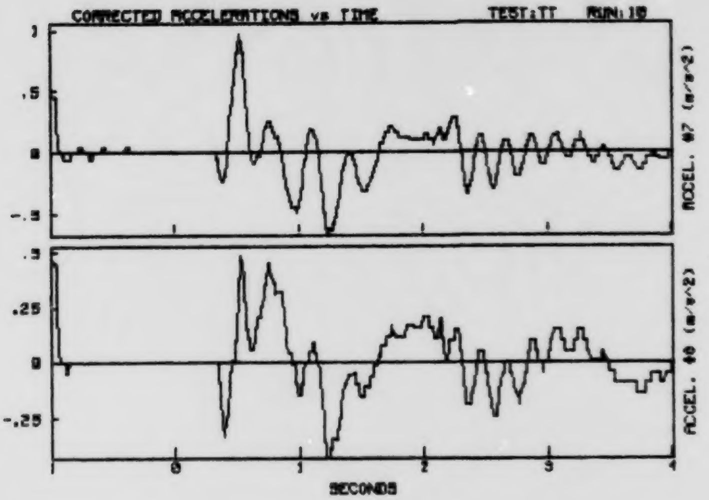
CORRECTED ACCELERATIONS vs TIME
TEST: TT
RUN: 18
1
.5
0
-.5
ACCEL. #7 (m/s^2)
.5
.25
0
-.25
ACCEL. #8 (m/s^2)
0
1
2
3
4
SECONDS

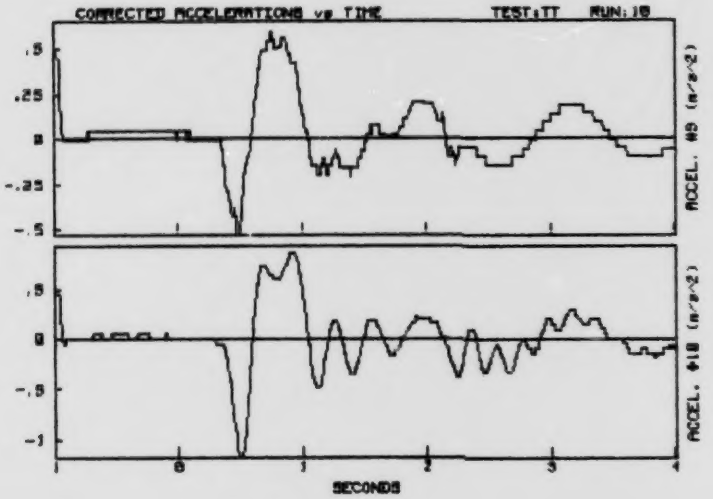
CORRECTED ACCELERATIONS vs TIME
TEST: TT
RUN: 18
.5
.25
0
-.25
-.5
ACCEL. #9 (m/s^2)
.5
0
-.5
-1
ACCEL. #10 (m/s^2)
0
1
2
3
4
SECONDS

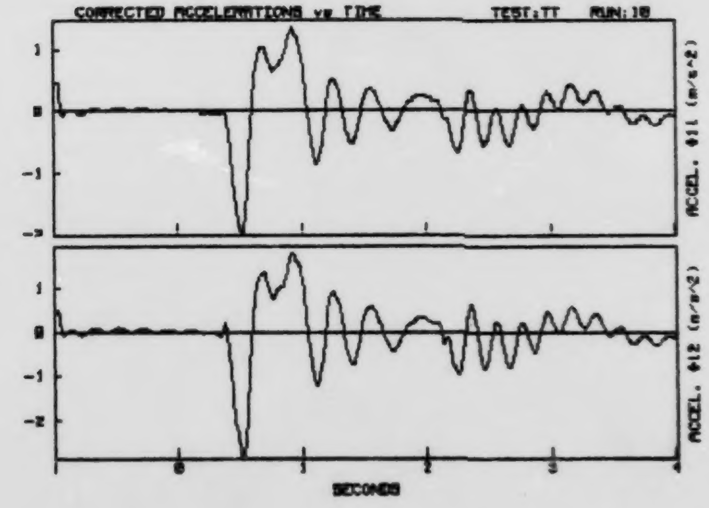
CORRECTED ACCELERATIONS vs TIME
TEST: TT
RUN: 18
1
0
-1
-2
ACCEL. #11 (m/s^2)
1
0
-1
-2
ACCEL. #12 (m/s^2)
0
1
2
3
4
SECONDS

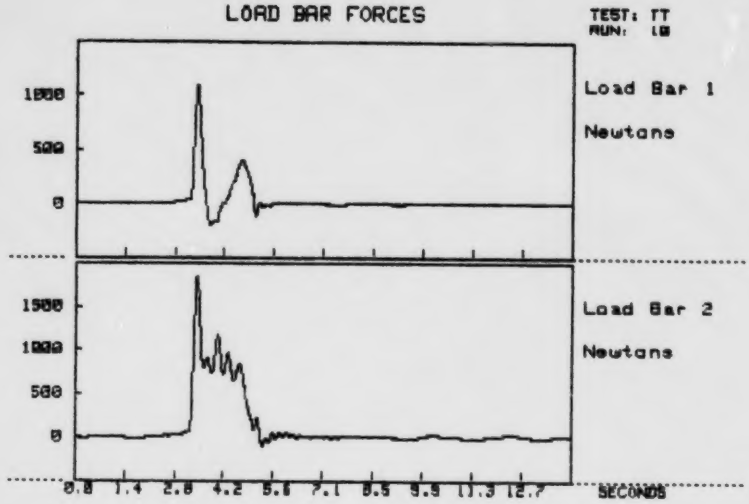
LOAD BAR FORCES
TEST: TT
RUN: 10
1000
500
0
Load Bar 1
Neutons
1500
1000
500
0
Load Bar 2
Neutons
0.0
1.4
2.8
4.2
5.6
7.1
8.5
9.9
11.3
12.7
SECONDS

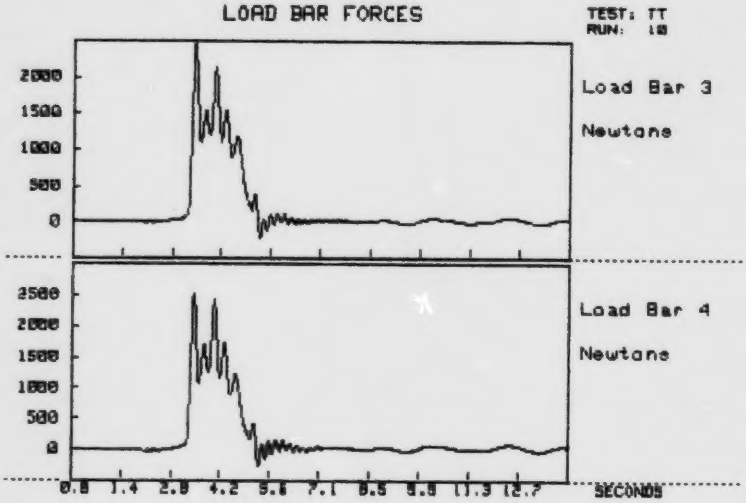
LOAD BAR FORCES
TEST: TT
RUN: 10
2000
1500
1000
500
0
Load Bar 3
Neutons
2500
2000
1500
1000
500
0
Load Bar 4
Neutons
0.0
1.4
2.8
4.2
5.6
7.1
8.5
9.9
11.3
12.7
SECONDS

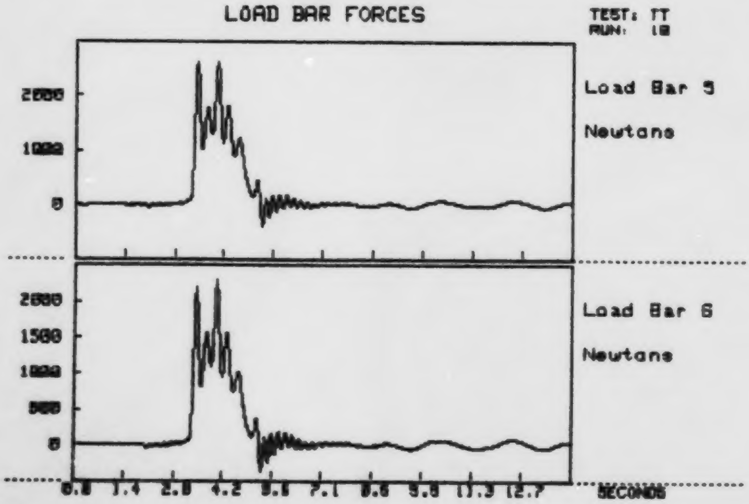
LOAD BAR FORCES
TEST: TT
RUN: 10
2000
1000
0
Load Bar 5
Neutons
2000
1500
1000
500
0
Load Bar 6
Neutons
0.0
1.4
2.8
4.2
5.6
7.1
8.5
9.9
11.3
12.7
SECONDS

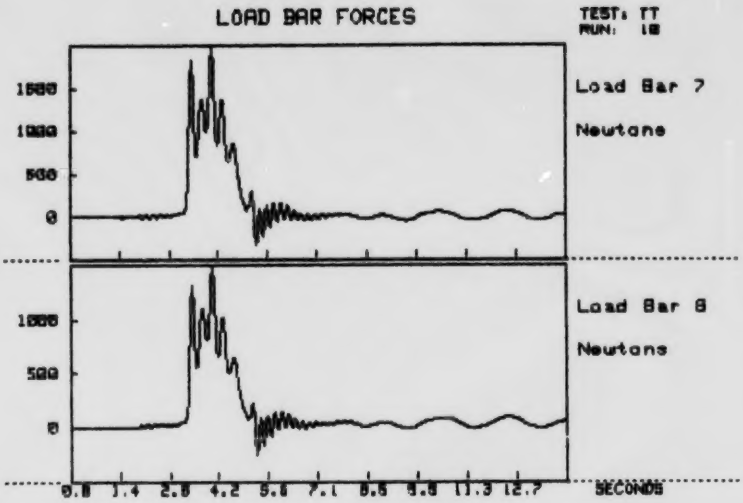
LOAD BAR FORCES
TEST: TT
RUN: 10
1500
1000
500
0
Load Bar 7
Newtons
1000
500
0
Load Bar 8
Newtons
0.0
1.4
2.8
4.2
5.6
7.1
8.5
9.9
11.3
12.7
SECONDS

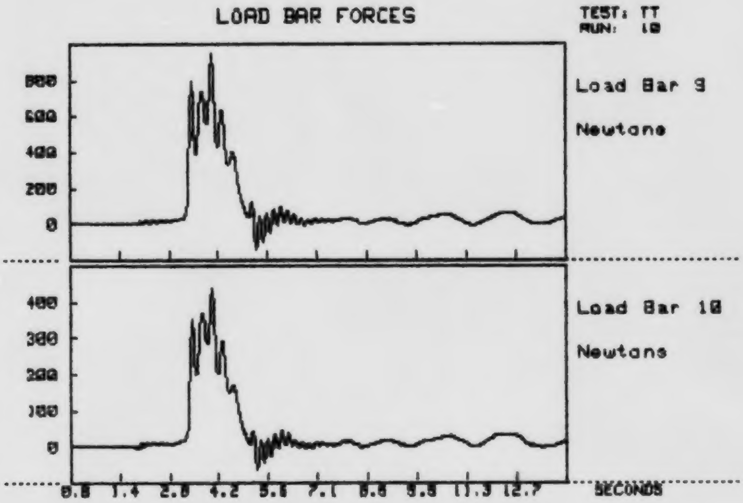
LOAD BAR FORCES
TEST: TT
RUN: 10
800
600
400
200
0
Load Bar 9
Newtons
400
300
200
100
0
Load Bar 10
Newtons
0.0
1.4
2.8
4.2
5.6
7.1
8.5
9.9
11.3
12.7
SECONDS

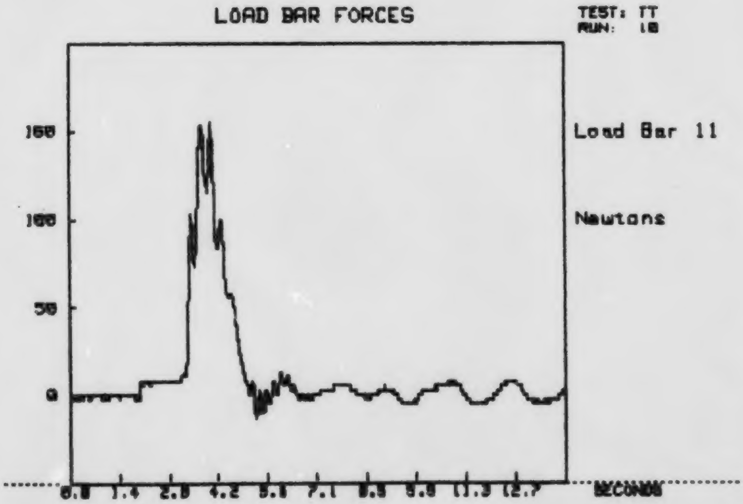
LOAD BAR FORCES
TEST: TT
RUN: 10
150
100
50
0
Load Bar 11
Newtons
0.0
1.4
2.8
4.2
5.6
7.1
8.5
9.9
11.3
12.7
SECONDS

MV ARCTIC MODEL TESTS
ADDED MASS CALCULATION

TEST:	TU
RUN NUMBER:	11

NOMINAL IMPACT VELOCITY:	.98	m/s
NOMINAL SHIP SPEED:	12	kt
TIME TO MAXIMUM SURGE:	.814	s
TIME FROM IMPACT TO BACKOFF:	1.676	s

TIME INCREMENT:	.004	s
ACCELEROMETER THRESHOLD:	.05	m/s^2

MODEL MASS:	596	kg
WATER DEPTH:	1.85	m
MODEL DRAFT:	0.275	m
ICE FREEBOARD:	0.025	m

SEGMENT ADDED MASS NORMALIZED BY DISPLACED MASS

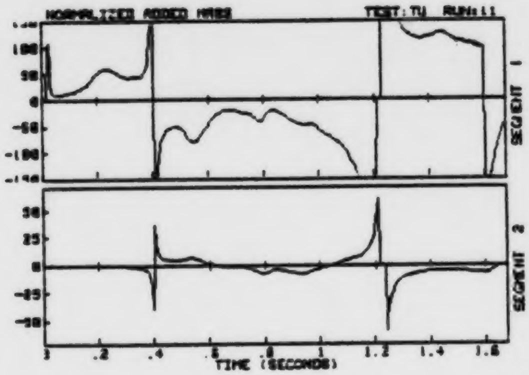

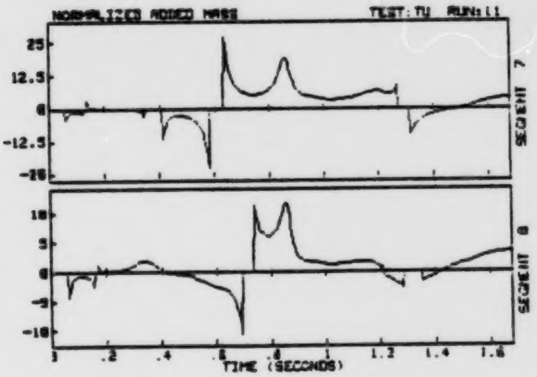

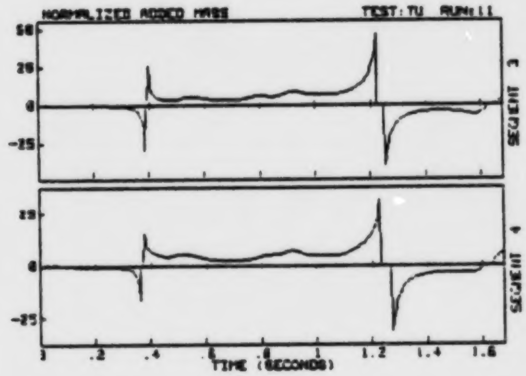

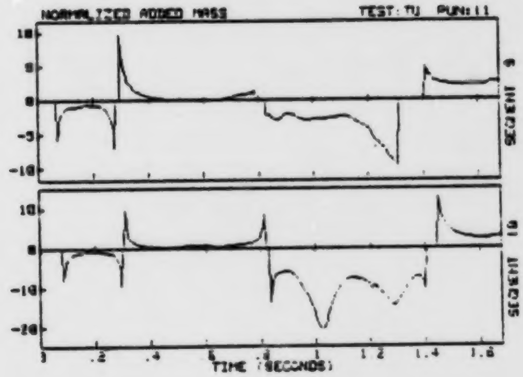

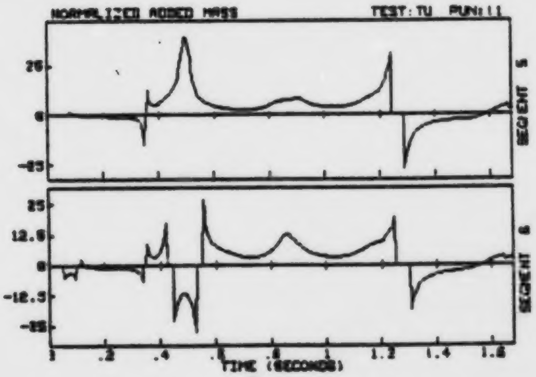

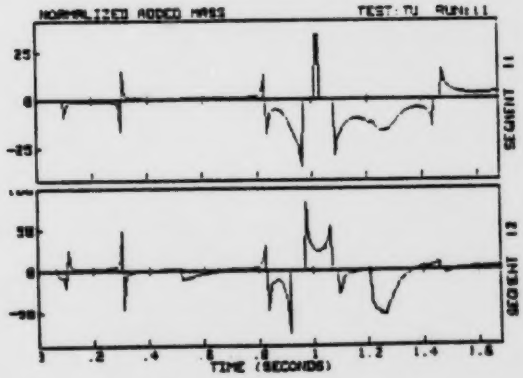

SEGMENT HYDRODYNAMIC FORCE

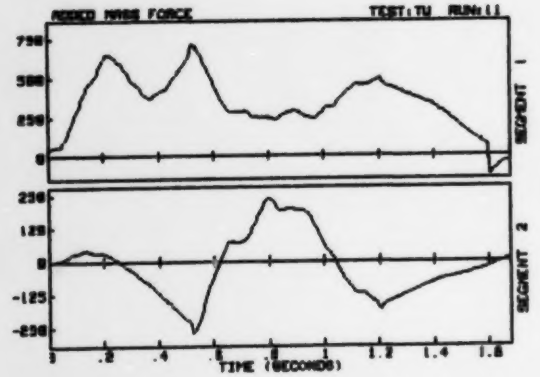

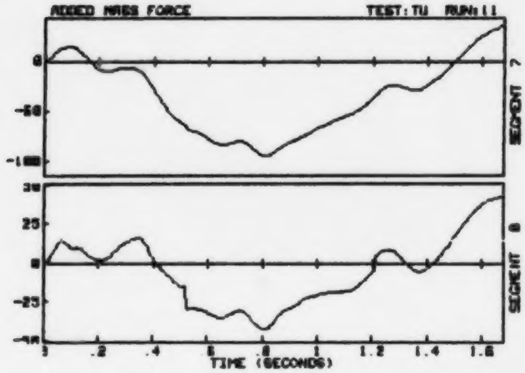

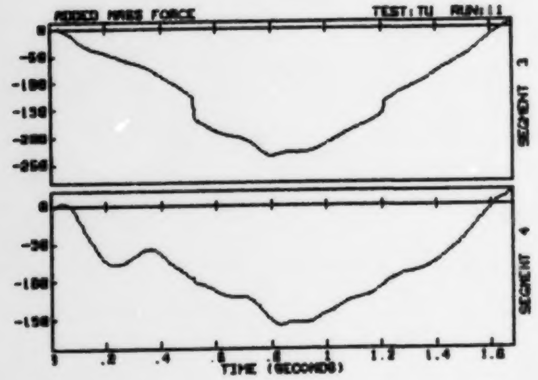

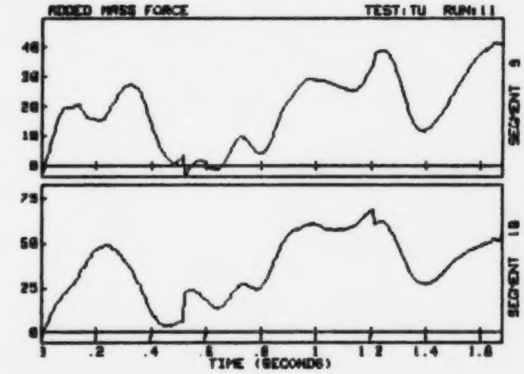

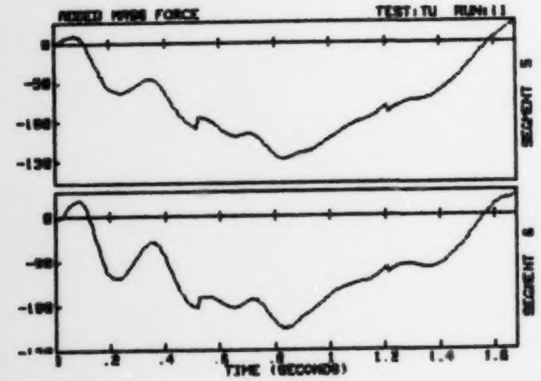

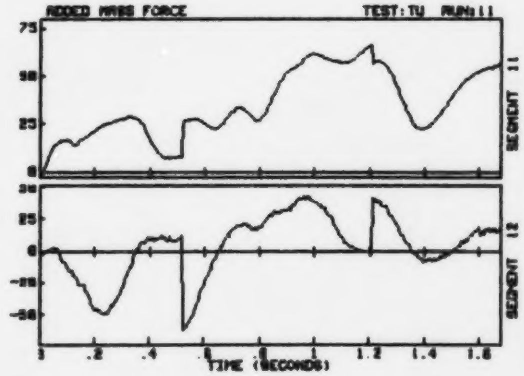

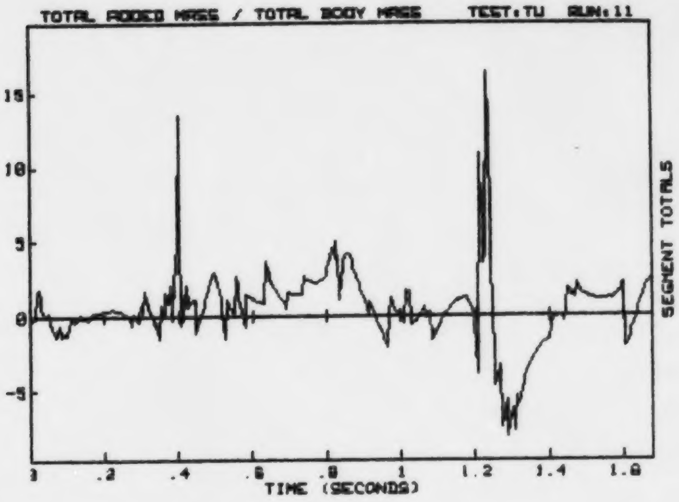

NON-DIMENSIONAL SEGMENTAL ADDED MASS STATISTICS

SEGMENT	MIN	MAX	MEAN	S.D.	NPTS
1	-854.2	921.7	4.9	135.8	404
2	-59.4	59.6	-1.4	9.5	395
3	-40.8	45.9	1.7	8.1	401
4	-31.5	31.2	1.7	6.3	387
5	-26.7	39.3	3.8	8.2	382
6	-27.6	26.7	1.8	7.1	370
7	-23	27.5	2.1	5.9	358
8	-10.6	11.8	1	3.1	368
9	-9.7	9.6	-.8	2.8	361
10	-20.6	12.6	-3.3	6.3	378
11	-34.6	34.7	-2.6	8.4	357
12	-76.5	83.4	-1.2	17.2	371
MEAN MODEL ADDED MASS =			.56		4532

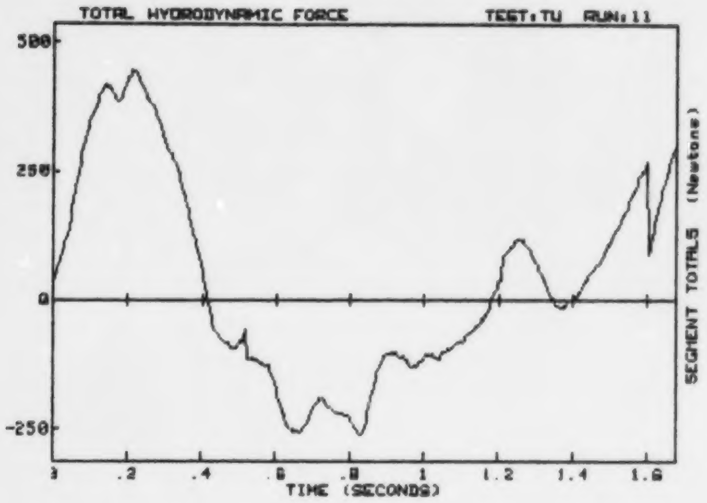

HYDRODYNAMIC FORCE SUMMARY STATISTICS

SEGMENT	MIN	MAX	MEAN	S.D.	NPTS
1	-115.6	718.2	343.8	171.8	415
2	-267.5	234.2	-20.8	113.8	415
3	-235.4	10.4	-119.8	77.3	415
4	-157.7	16.7	-85.3	47.5	415
5	-147.6	21.6	-73.8	46.8	415
6	-125.1	24.1	-59.3	40.2	415
7	-95.4	35.6	-35.7	37	415
8	-42.7	42.7	-5.4	21.5	415
9	-2.9	41.5	18.8	12	415
10	-4.9	69	37	17.9	415
11	-2.4	66.4	34.8	17.3	415
12	-61.5	43	3.6	24.1	415
MEAN HYDRODYNAMIC FORCE =			0		4980

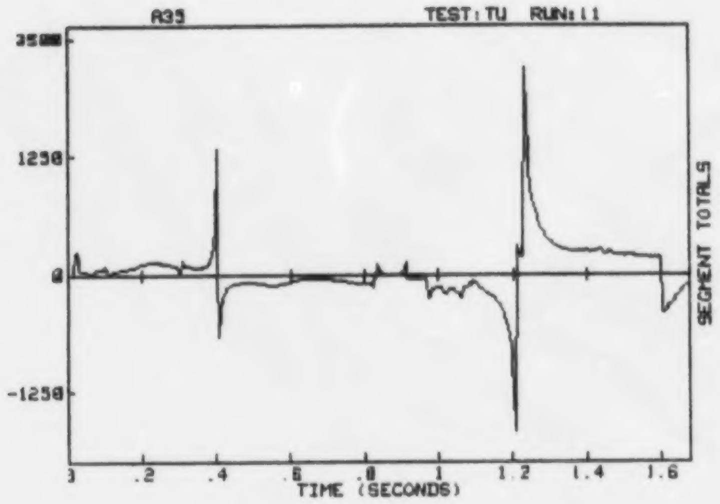

HEAVE/PITCH COUPLED ADDED MASS SUMMARY STATISTICS

SEGMENT	MIN	MAX	MEAN	S.D.	NPTS
1	-1874.9	2023	10.8	298	404
2	-109.6	109.8	-2.6	17.4	395
3	-58.5	65.8	2.4	11.6	401
4	-32.3	31.9	1.8	6.5	387
5	-16.4	24.2	2.4	5	382
6	-5.6	5.5	.4	1.5	370
7	-5.6	4.7	-.4	1.2	358
8	-7.3	6.5	-.6	1.9	368
9	-9.9	10	.8	2.9	361
10	-18	29.4	4.7	9	378
11	-63.6	63.4	4.8	15.3	357
12	-186.6	171	2.6	38.4	371
MEAN A35 MODEL ADDED MASS =			1.25		4532

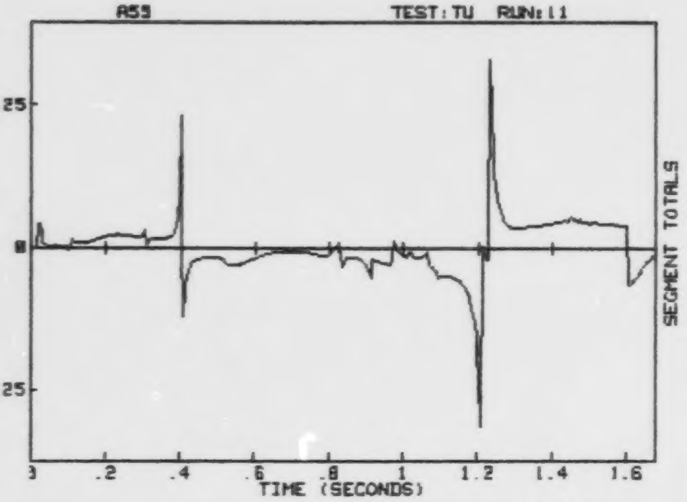

PITCH ADDED MASS MOMENT OF INERTIA SUMMARY STATISTICS

SEGMENT	MIN	MAX	MEAN	S.D.	NPTS
1	-4115.5	4440.5	23.8	298	404
2	-202.1	202.5	-4.7	17.4	395
3	-83.9	94.4	3.4	11.6	401
4	-33.1	32.7	1.8	6.5	387
5	-10.1	14.9	1.4	5	382
6	-1.2	1.1	.1	1.5	370
7	-1	1.2	.1	1.2	358
8	-4	4.5	.4	1.9	368
9	-10.2	10.1	-.8	2.9	361
10	-42.1	25.8	-6.7	9	378
11	-116.2	116.6	-8.8	15.3	357
12	-382.5	417.2	-5.9	38.4	371

MEAN A55 MODEL ADDED MASS = -.54 4532

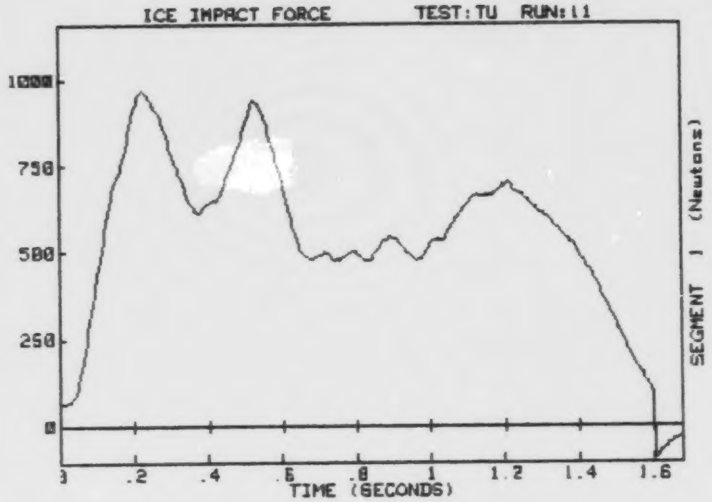
ICE IMPACT FORCE
TEST: TU RUN: 11
1000
750
500
250
0
0
.2
.4
.6
.8
1
1.2
1.4
1.6
TIME (SECONDS)
SEGMENT 1 (Newtons)

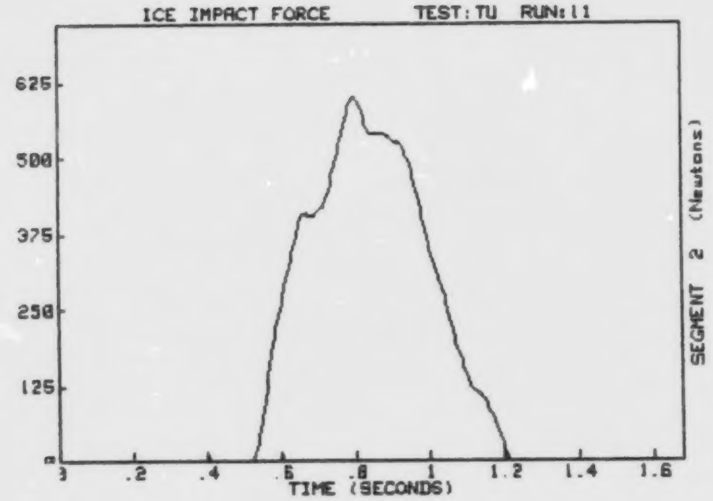
ICE IMPACT FORCE
TEST: TU RUN: 11
625
500
375
250
125
0
0
.2
.4
.6
.8
1
1.2
1.4
1.6
TIME (SECONDS)
SEGMENT 2 (Newtons)

IMPACT VELOCITY= .98 m/s
SHIP SPEED= 12.06 kt

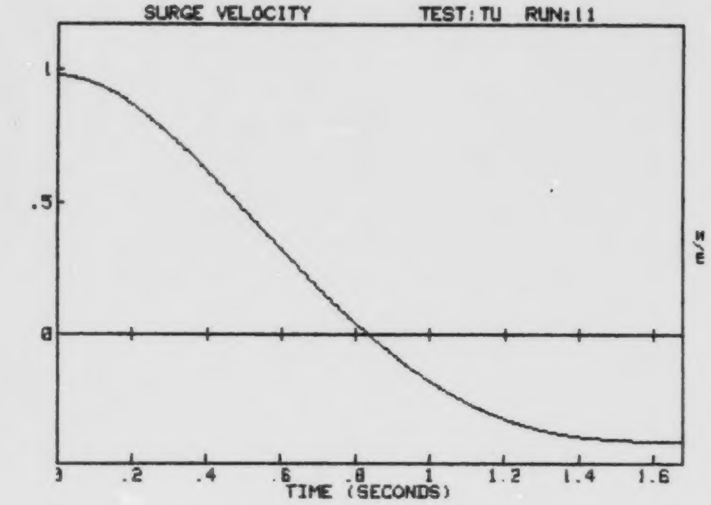

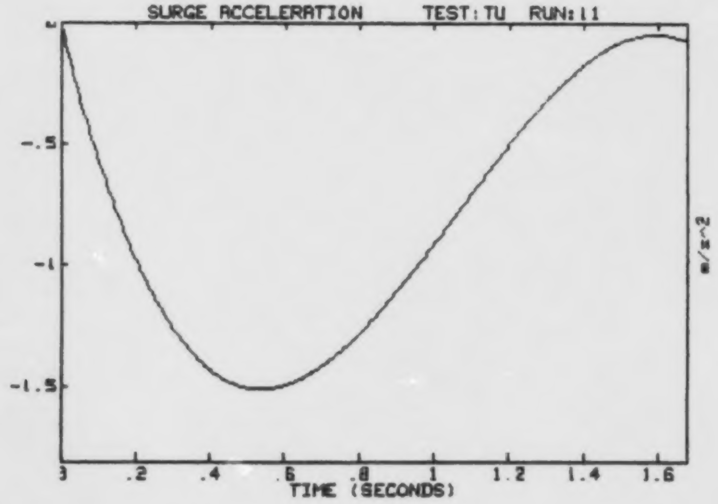

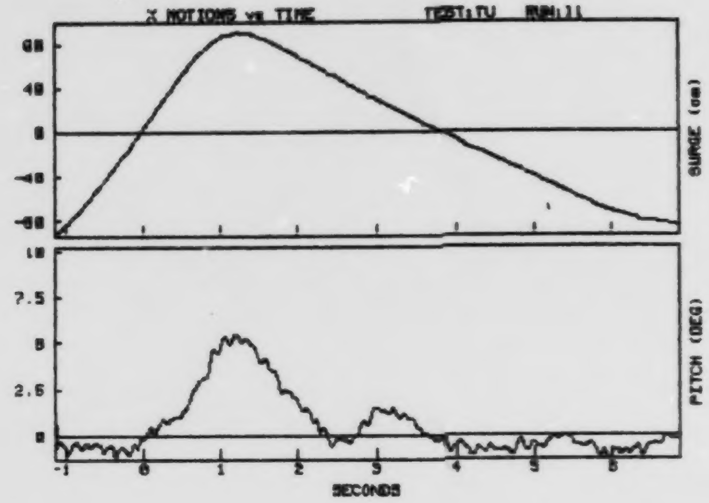
X MOTIONS vs TIME
TEST:TU RUN:11
80
40
0
-40
-80
SURGE (cm)
10
7.5
5
2.5
0
PITCH (DEG)
-1
0
1
2
3
4
5
6
SECONDS

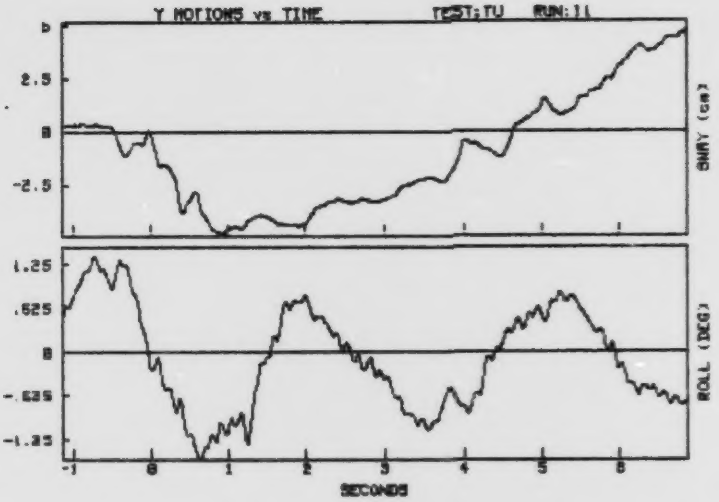
Y MOTIONS vs TIME
TEST:TU RUN:11
5
2.5
0
-2.5
SWAY (cm)
1.25
.625
0
-.625
-1.25
ROLL (DEG)
-1
0
1
2
3
4
5
6
SECONDS

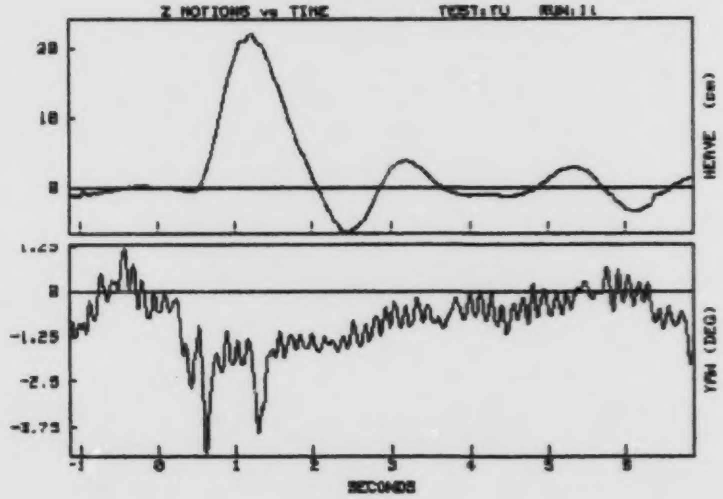
Z MOTIONS vs TIME
TEST:TU RUN:11
20
10
0
HEAVE (cm)
1.25
0
-1.25
-2.5
-3.75
YAW (DEG)
-1
0
1
2
3
4
5
6
SECONDS

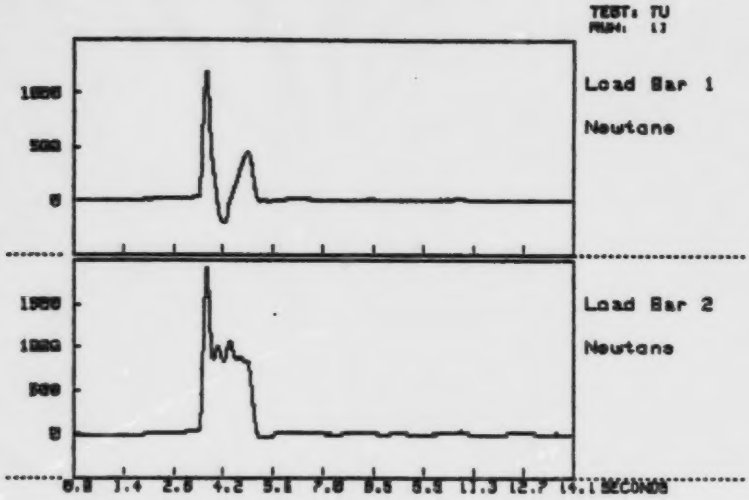
TEST: TU
RUN: 11
Load Bar 1
Newtons
1000
500
0
Load Bar 2
Newtons
1500
1000
500
0
0.0 1.4 2.8 4.2 5.6 7.0 8.5 9.9 11.3 12.7 14.1 SECONDS

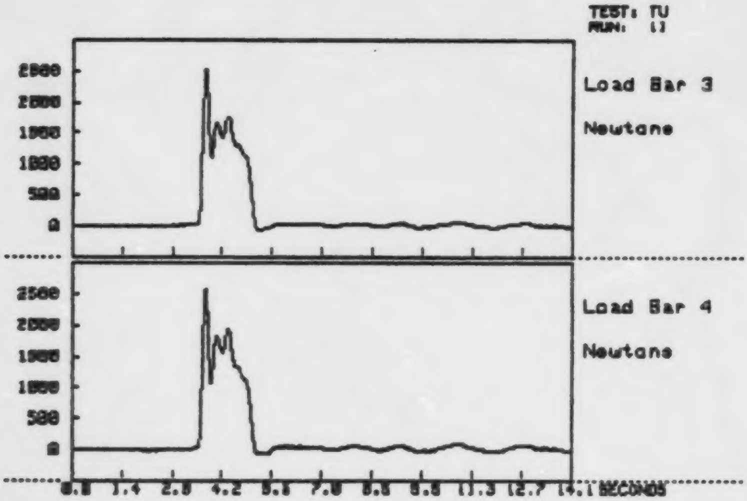
TEST: TU
RUN: 11
Load Bar 3
Newtons
2500
2000
1500
1000
500
0
Load Bar 4
Newtons
2500
2000
1500
1000
500
0
0.0 1.4 2.8 4.2 5.6 7.0 8.5 9.9 11.3 12.7 14.1 SECONDS

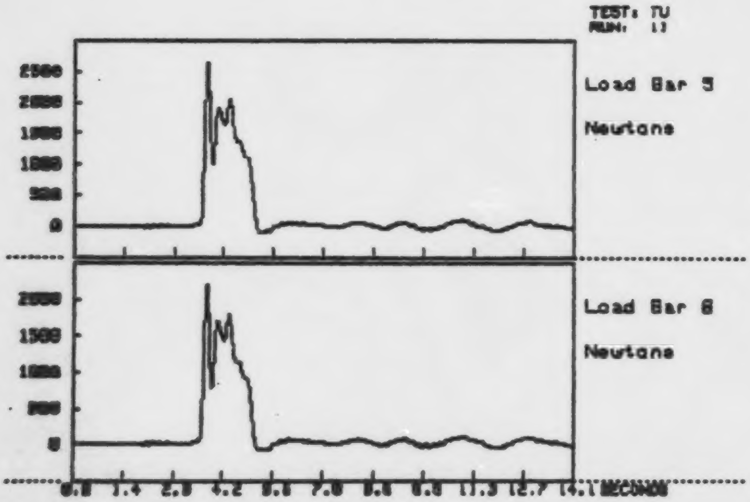
TEST: TU
RUN: 11
Load Bar 5
Newtons
2500
2000
1500
1000
500
0
Load Bar 6
Newtons
2000
1500
1000
500
0
0.0 1.4 2.8 4.2 5.6 7.0 8.5 9.9 11.3 12.7 14.1 SECONDS

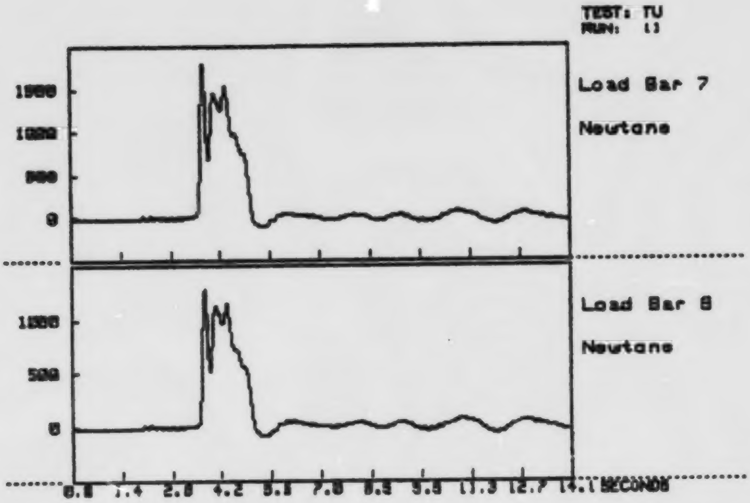
TEST: TU
RUN: 11
Load Bar 7
Newtons
1500
1000
500
0
Load Bar 8
Newtons
1000
500
0
0.0
1.4
2.8
4.2
5.6
7.0
8.5
9.9
11.3
12.7
14.1 SECONDS

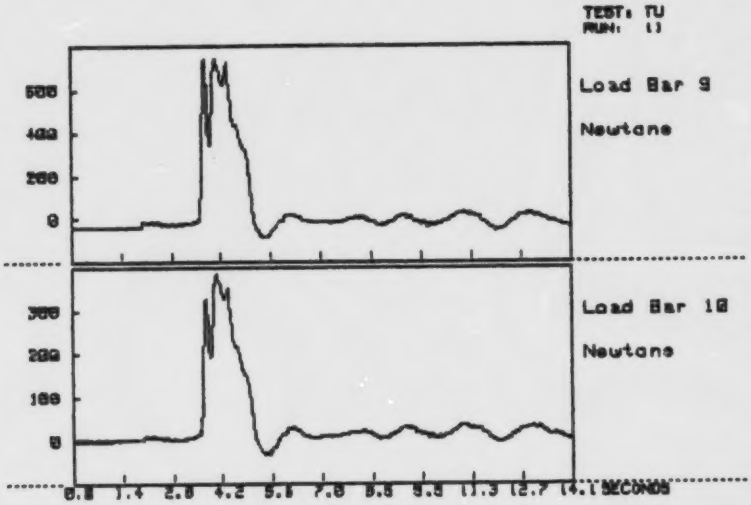
TEST: TU
RUN: 11
Load Bar 9
Newtons
600
400
200
0
Load Bar 10
Newtons
300
200
100
0
0.0
1.4
2.8
4.2
5.6
7.0
8.5
9.9
11.3
12.7
14.1 SECONDS

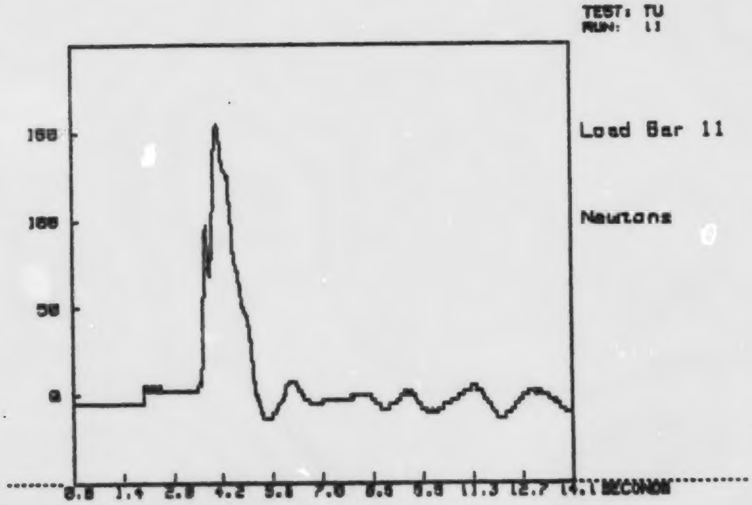
TEST: TU
RUN: 11
Load Bar 11
Newtons
150
100
50
0
0.0
1.4
2.8
4.2
5.6
7.0
8.5
9.9
11.3
12.7
14.1 SECONDS

MV ARCTIC MODEL TESTS
ADDED MASS CALCULATION

TEST: TU
RUN NUMBER: 12

NOMINAL IMPACT VELOCITY:	.68	m/s
NOMINAL SHIP SPEED:	8.4	kt
TIME TO MAXIMUM SURGE:	.883	s
TIME FROM IMPACT TO BACKOFF:	1.726	s

TIME INCREMENT:	.004	s
ACCELEROMETER THRESHOLD:	.05	m/s^2

MODEL MASS:	596	kg
WATER DEPTH:	1.85	m
MODEL DRAFT:	0.275	m
ICE FREEBOARD:	0.025	m

SEGMENT ADDED MASS NORMALIZED BY DISPLACED MASS

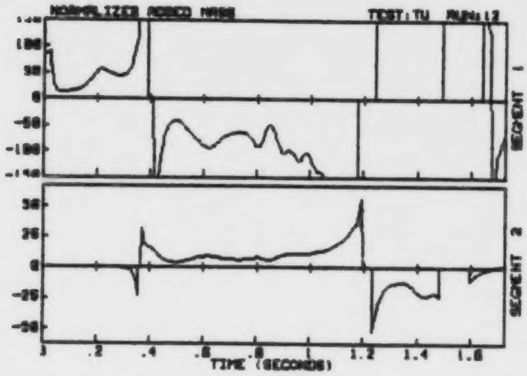

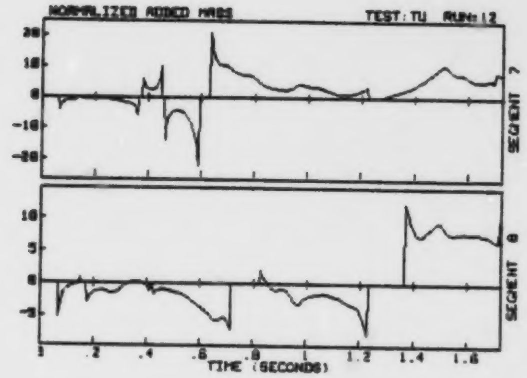

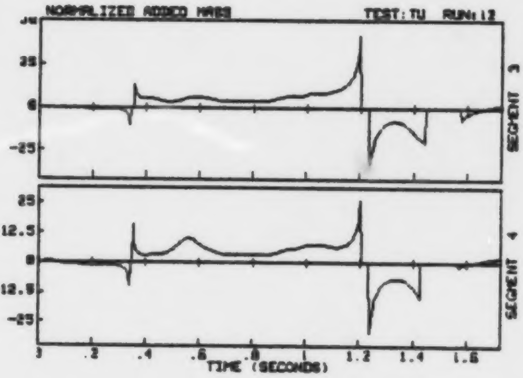

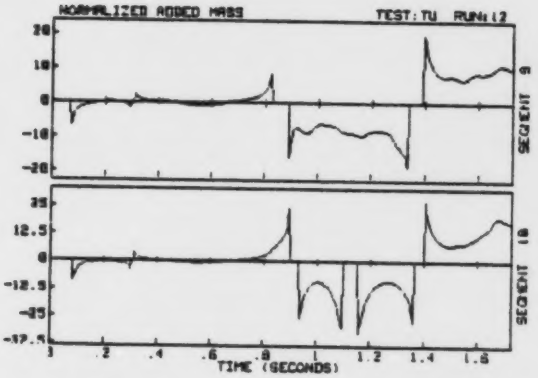

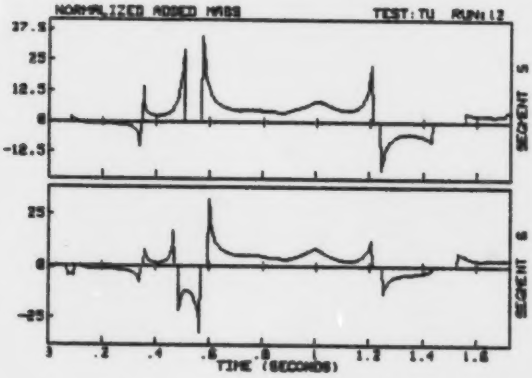

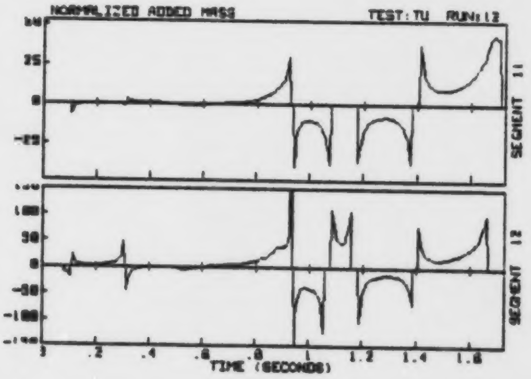

SEGMENT HYDRODYNAMIC FORCE

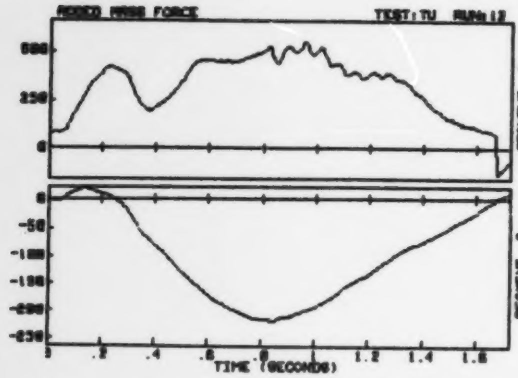

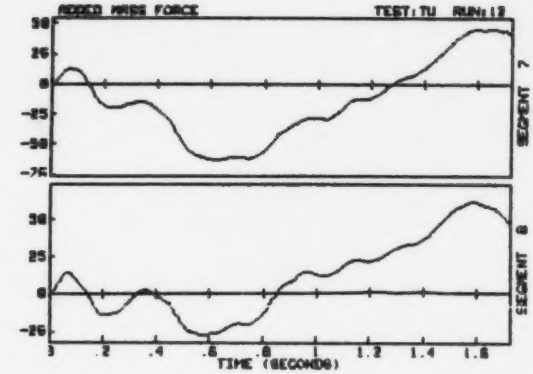

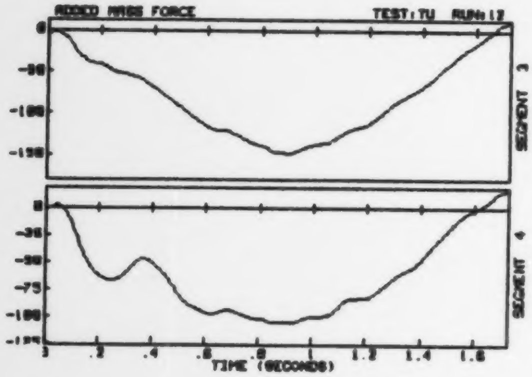

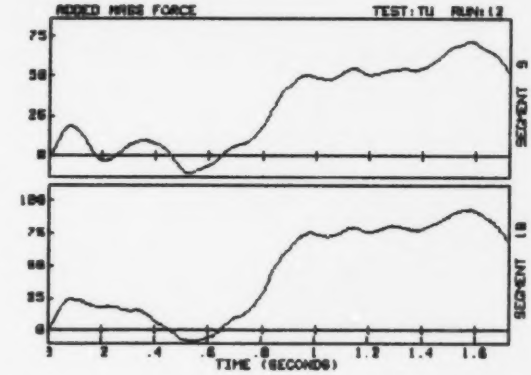

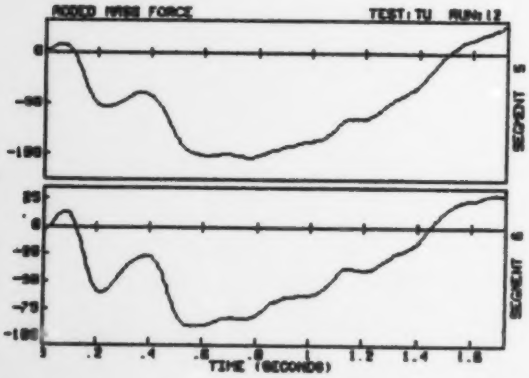

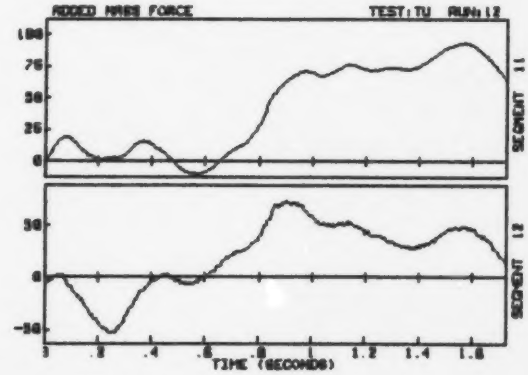

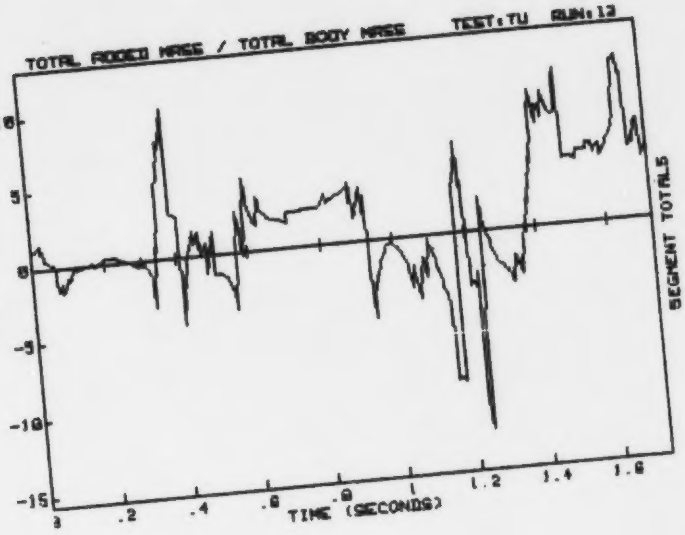

```
                  NON-DIMENSIONAL SEGMENTAL ADDED MASS STATISTICS

SEGMENT     MIN          MAX          MEAN         S.D.         NPTS
   1      -845.8        845.7         5.6         221.1         368
   2       -51.8         56.1         2.3          13.1         388
   3       -34.7         41.9         1.4           8.3         386
   4       -29.3         26.5         1.8           6.2         384
   5       -19.3         34.5         2.8           6.3         351
   6       -31.8         32.3         1.6           6.6         367
   7       -21.9         20.6         2.8           5.1         377
   8        -8.1         12.3          .6           4.7         342
   9       -18.7         19.9         -.5           6.8         377
  10       -32.1         27.7         -.2          10.5         372
  11       -40           43.6          1.3         13.6         359
  12      -153.4        150.3         5.1          33.8         369

 MEAN MODEL ADDED MASS =              1.3                      4440
```

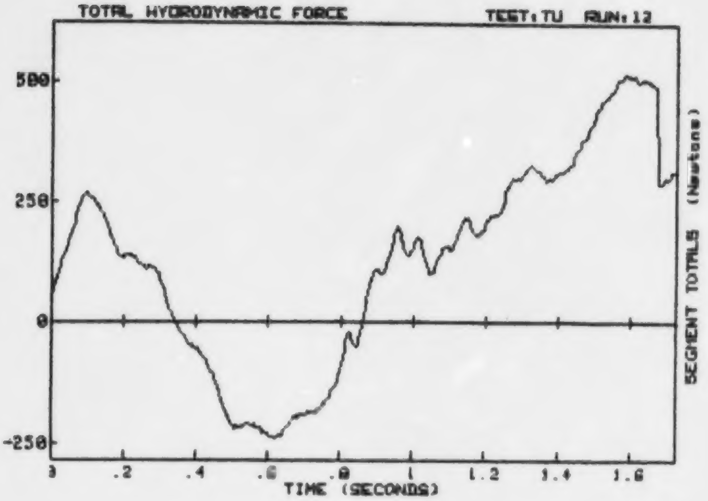

HYDRODYNAMIC FORCE SUMMARY STATISTICS

SEGMENT	MIN	MAX	MEAN	S.D.	NPTS
1	-128.8	548.8	322.4	153.2	429
2	-220.4	20.5	-99.8	79.9	429
3	-149.2	10.6	-80.4	47.4	429
4	-105.3	16	-61.4	36.7	429
5	-103.8	26.5	-51.4	40.3	429
6	-90.6	30	-36.8	36.8	429
7	-63.4	45.8	-13.6	32.8	429
8	-27.3	62.1	11.3	26.2	429
9	-11.3	72	30.5	26.9	429
10	-8.6	93.6	45.5	35.1	429
11	-10.1	93.2	42.2	35.3	429
12	-53.3	74	21	32.4	429
MEAN HYDRODYNAMIC FORCE =			0		5148

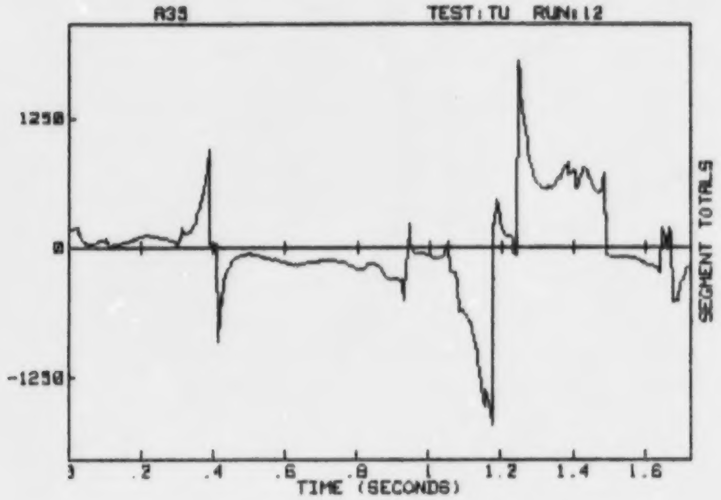

HEAVE/PITCH COUPLED ADDED MASS SUMMARY STATISTICS

SEGMENT	MIN	MAX	MEAN	S.D.	NPTS
1	-1856.6	1856.3	12.2	485.4	368
2	-95.6	103.4	4.3	24.2	388
3	-49.8	60	2.1	11.8	386
4	-30	27.2	1.9	6.4	384
5	-11.9	21.2	1.7	3.8	351
6	-6.5	6.6	.3	1.4	367
7	-4.2	4.5	-.6	1.1	377
8	-7.6	5	-.4	2.9	342
9	-20.3	19.2	.5	6.9	377
10	-39.6	46	.4	15	372
11	-79.9	73.3	-2.5	24.9	359
12	-336	343	-11.3	75.6	369
MEAN A35 MODEL ADDED MASS =			.72		4440

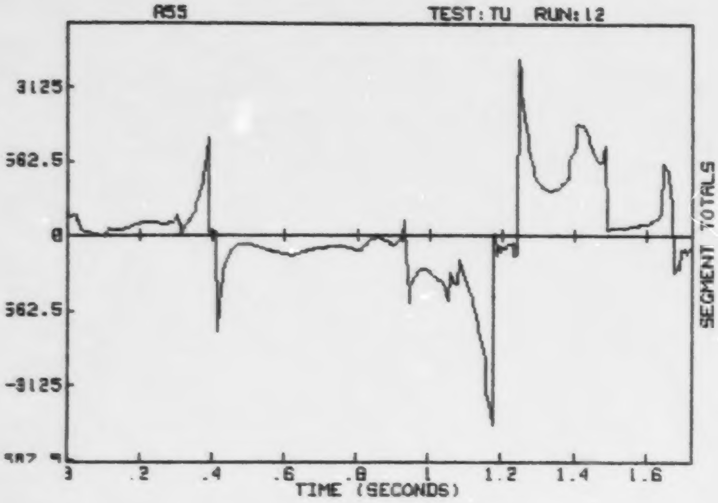

PITCH ADDED MASS MOMENT OF INERTIA SUMMARY STATISTICS

SEGMENT	MIN	MAX	MEAN	S.D.	NPTS
1	-4075.2	4074.6	26.8	485.4	368
2	-176.2	190.6	8	24.2	388
3	-71.4	86.1	3	11.8	386
4	-30.8	27.8	1.9	6.4	384
5	-7.3	13	1.1	3.8	351
6	-1.3	1.4	.1	1.4	367
7	-.9	.9	.1	1.1	377
8	-3.1	4.7	.2	2.9	342
9	-19.6	20.8	-.5	6.9	377
10	-65.8	56.7	-.5	15	372
11	-134.3	146.5	4.5	24.9	359
12	-767	751.2	25.3	75.6	369

MEAN A55 MODEL ADDED MASS = 1.98 4440

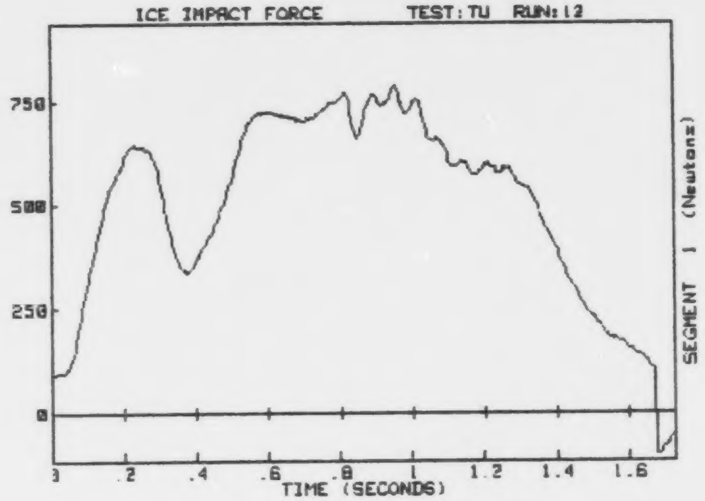
ICE IMPACT FORCE
TEST: TU RUN: 12
750
500
250
0
0
.2
.4
.6
.8
1
1.2
1.4
1.6
TIME (SECONDS)
SEGMENT 1 (Newtons)

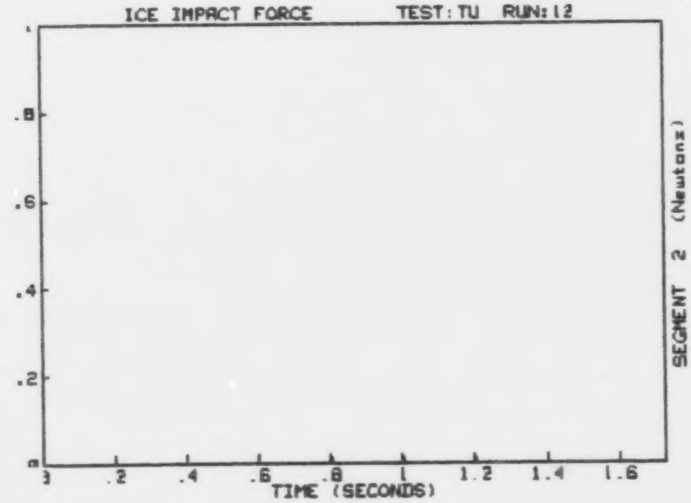
ICE IMPACT FORCE
TEST: TU RUN: 12
.8
.6
.4
.2
0
0
.2
.4
.6
.8
1
1.2
1.4
1.6
TIME (SECONDS)
SEGMENT 2 (Newtons)

IMPACT VELOCITY= .73 m/s
SHIP SPEED= 8.99 kt

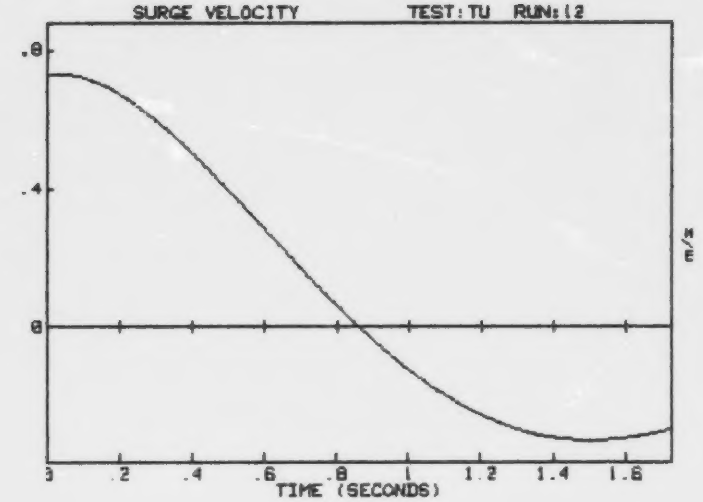

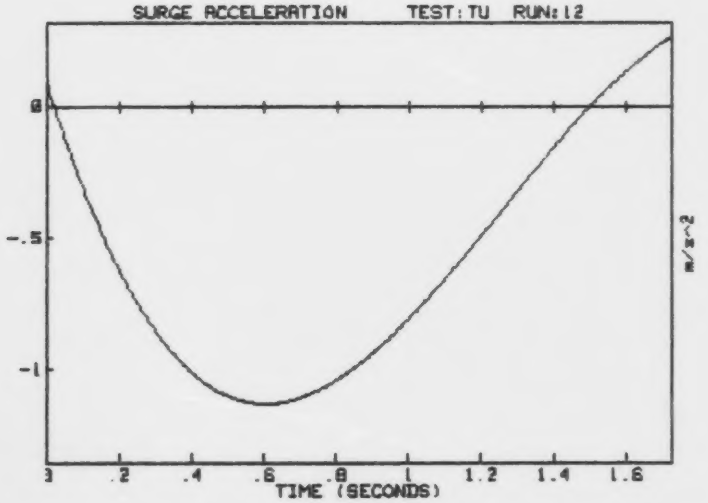

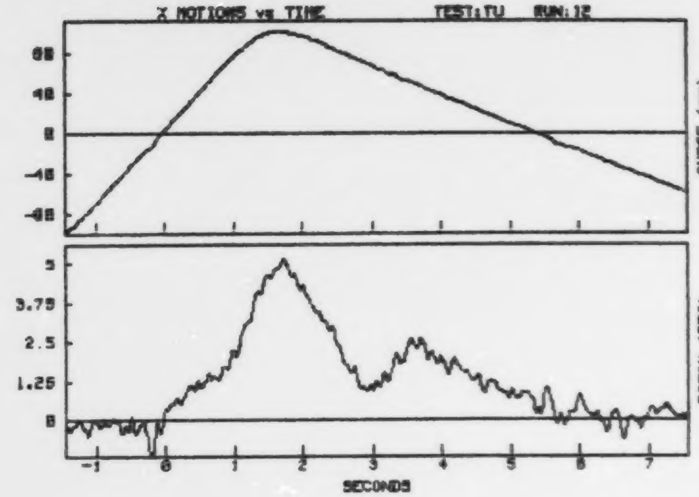
X MOTIONS vs TIME
TEST:TU RUN:12
80
40
0
-40
-80
SURGE (cm)
5
3.75
2.5
1.25
0
PITCH (DEG)
-1
0
1
2
3
4
5
6
7
SECONDS

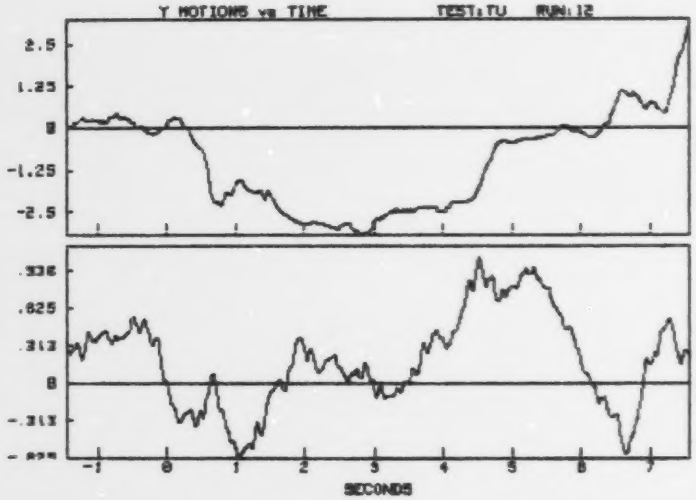
Y MOTIONS vs TIME
TEST:TU RUN:12
2.5
1.25
0
-1.25
-2.5
SWAY (cm)
.938
.625
.313
0
-.313
-.625
ROLL (DEG)
-1
0
1
2
3
4
5
6
7
SECONDS

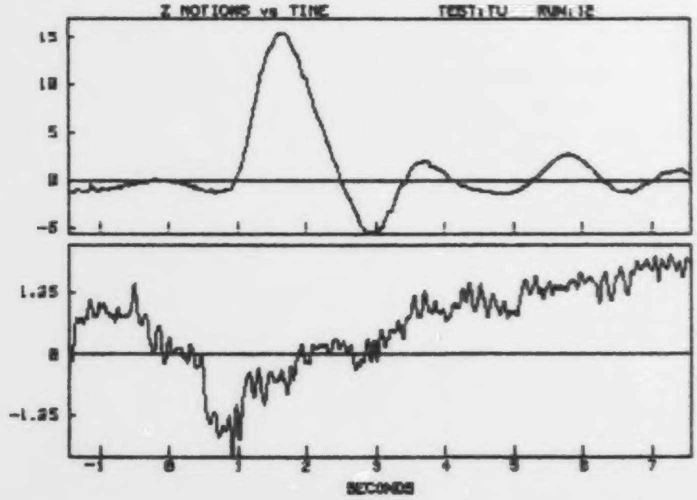
Z MOTIONS vs TIME
TEST:TU RUN:12
15
10
5
0
-5
HEAVE (cm)
1.25
0
-1.25
YAW (DEG)
-1
0
1
2
3
4
5
6
7
SECONDS

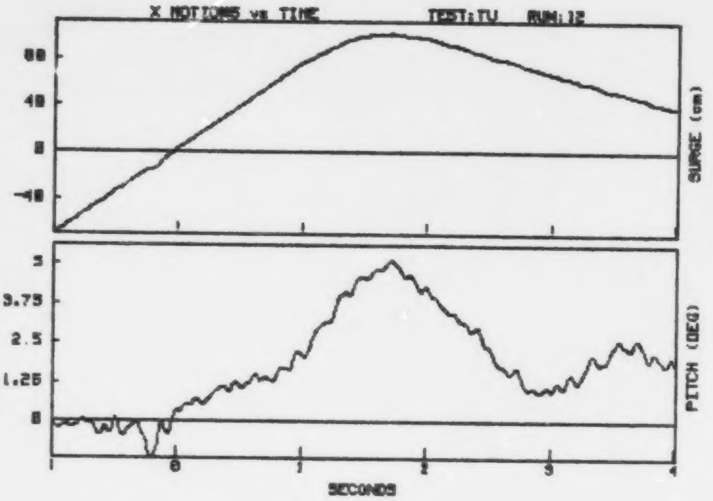
X MOTIONS vs TIME
TEST:TU RUN:12
80
40
0
-40
SURGE (cm)
5
3.75
2.5
1.25
0
PITCH (DEG)
0
1
2
3
4
SECONDS

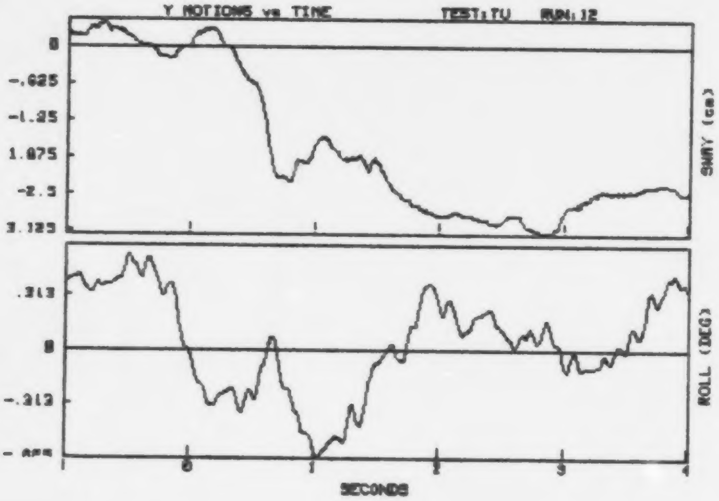
Y MOTIONS vs TIME
TEST:TU RUN:12
0
-.625
-1.25
1.875
-2.5
3.125
SWAY (cm)
.313
0
-.313
-.625
ROLL (DEG)
0
1
2
3
4
SECONDS

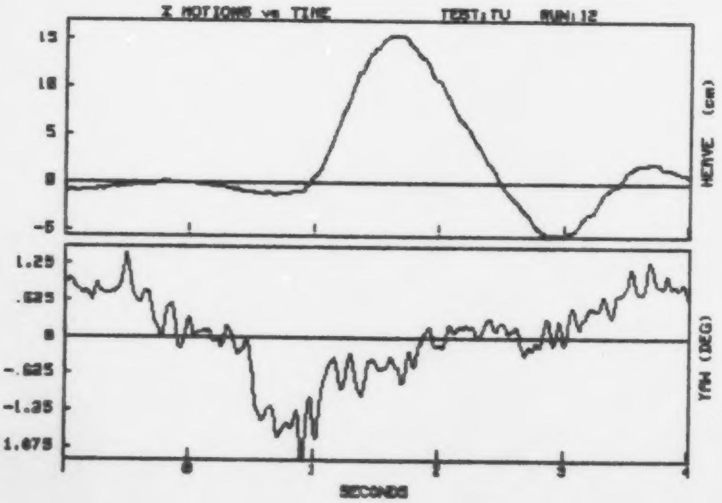
Z MOTIONS vs TIME
TEST:TU RUN:12
15
10
5
0
-5
HEAVE (cm)
1.25
.625
0
-.625
-1.25
1.875
YAW (DEG)
0
1
2
3
4
SECONDS

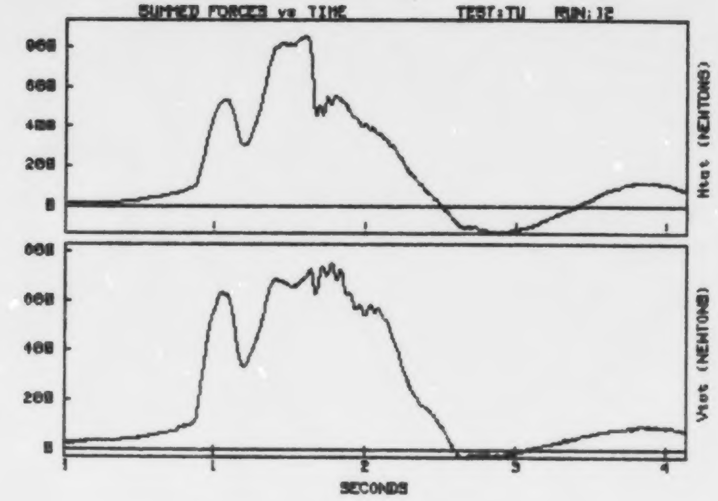
SUMMED FORCES vs TIME
TEST:TU RUN:12
800
600
400
200
0
Htot (NEWTONS)
800
600
400
200
0
Vtot (NEWTONS)
1
2
3
4
SECONDS

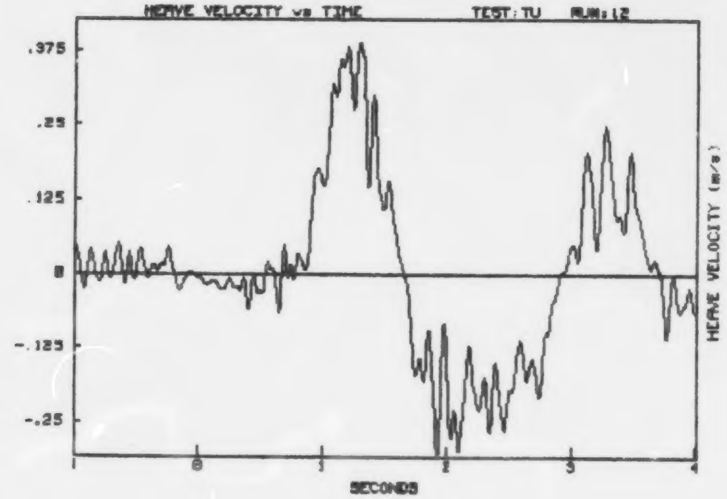
HEAVE VELOCITY vs TIME
TEST:TU RUN:12
.375
.25
.125
0
-.125
-.25
0
1
2
3
4
SECONDS
HEAVE VELOCITY (m/s)

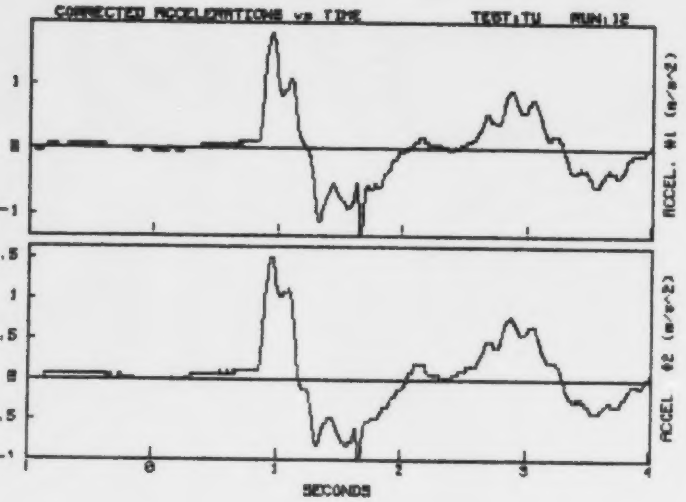
CORRECTED ACCELERATIONS vs TIME
TEST:TU
RUN:12
1
0
-1
1.5
1
.5
0
-.5
-1
ACCEL. #1 (m/s^2)
ACCEL. #2 (m/s^2)
0
1
2
3
4
SECONDS

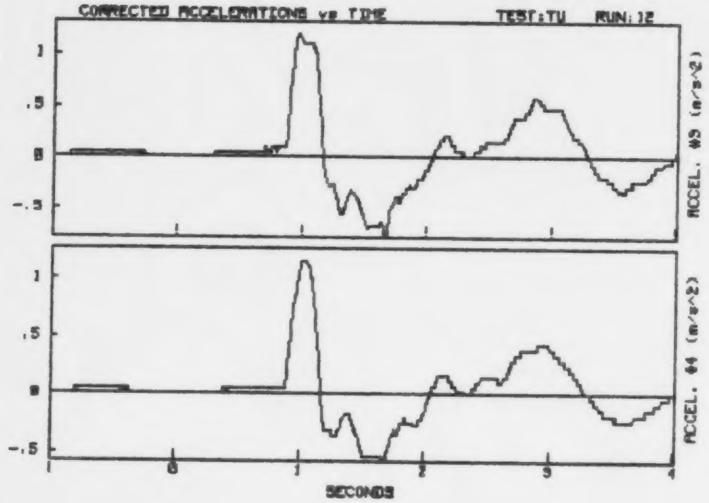
CORRECTED ACCELERATIONS vs TIME
TEST:TU
RUN:12
1
.5
0
-.5
1
.5
0
-.5
ACCEL. #3 (m/s^2)
ACCEL. #4 (m/s^2)
0
1
2
3
4
SECONDS

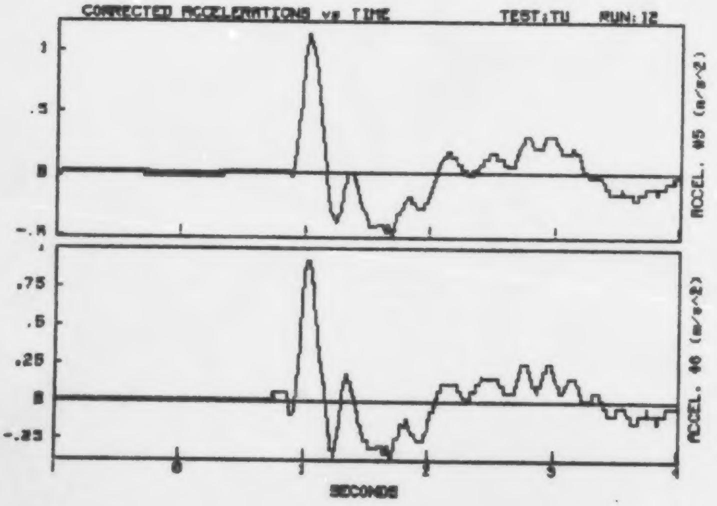
CORRECTED ACCELERATIONS vs TIME
TEST:TU
RUN:12
1
.5
0
-.5
.75
.5
.25
0
-.25
ACCEL. #5 (m/s^2)
ACCEL. #6 (m/s^2)
0
1
2
3
4
SECONDS

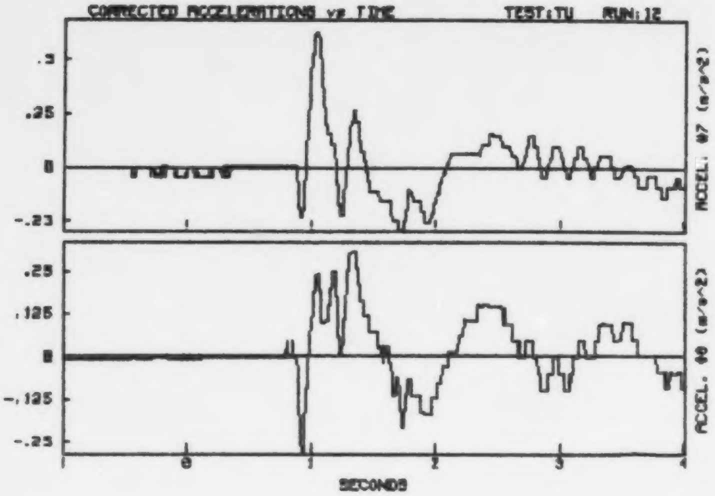
CORRECTED ACCELERATIONS vs TIME
TEST:TU
RUN:12
.3
.25
0
-.23
ACCEL. #7 (m/s^2)
.25
.125
0
-.125
-.25
ACCEL. #8 (m/s^2)
0
1
2
3
4
SECONDS

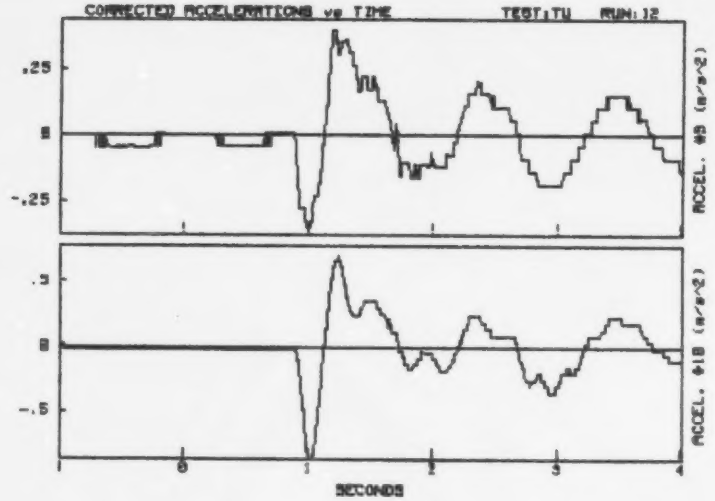
CORRECTED ACCELERATIONS vs TIME
TEST:TU
RUN:12
.25
0
-.25
ACCEL. #9 (m/s^2)
.5
0
-.5
ACCEL. #10 (m/s^2)
0
1
2
3
4
SECONDS

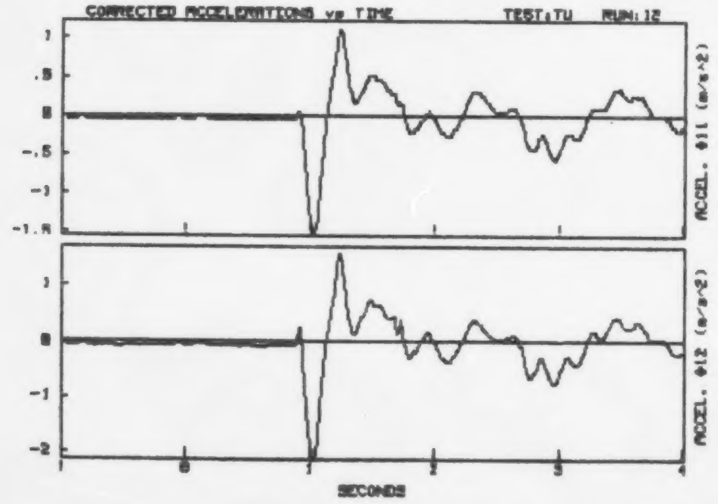
CORRECTED ACCELERATIONS vs TIME
TEST:TU
RUN:12
1
.5
0
-.5
-1
-1.5
ACCEL. #11 (m/s^2)
1
0
-1
-2
ACCEL. #12 (m/s^2)
0
1
2
3
4
SECONDS

```
                    MV  ARCTIC MODEL TESTS
                    ADDED MASS CALCULATION



                       TEST:          TG
                       RUN NUMBER:    2



        NOMINAL IMPACT VELOCITY:          1.04       m/s
        NOMINAL SHIP SPEED:               12.8       kt
        TIME TO MAXIMUM SURGE:            .964       s
        TIME FROM IMPACT TO BACKOFF:      2.355      s



        TIME INCREMENT:                    .004      s
        ACCELEROMETER THRESHOLD:           .05       m/s^2



        MODEL MASS:                         596      kg
        WATER DEPTH:                        1.85     m
        MODEL DRAFT:                        0.275    m
        ICE FREEBOARD:                      0.025    m
```

SEGMENT ADDED MASS NORMALIZED BY DISPLACED MASS

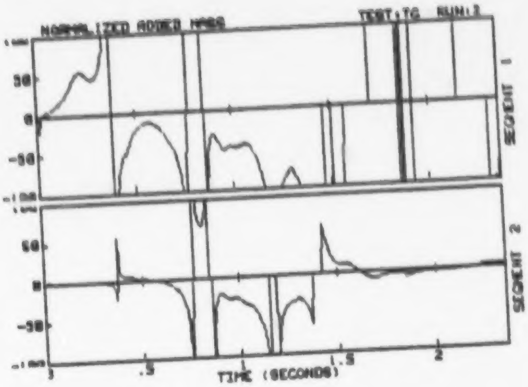

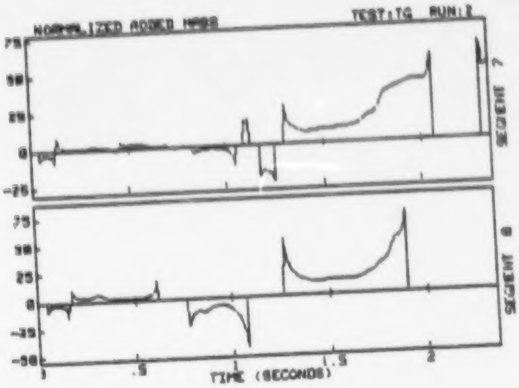

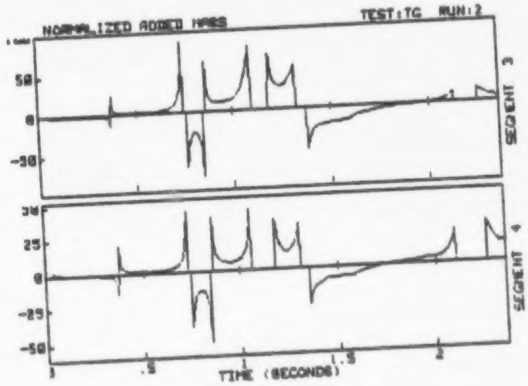

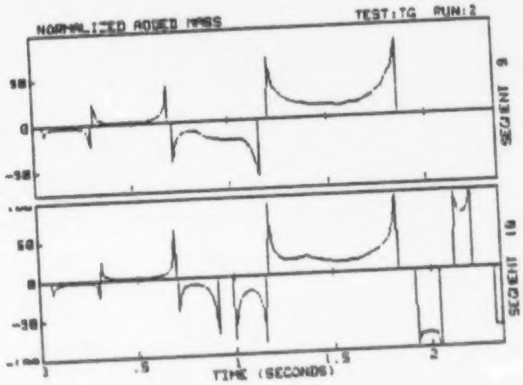

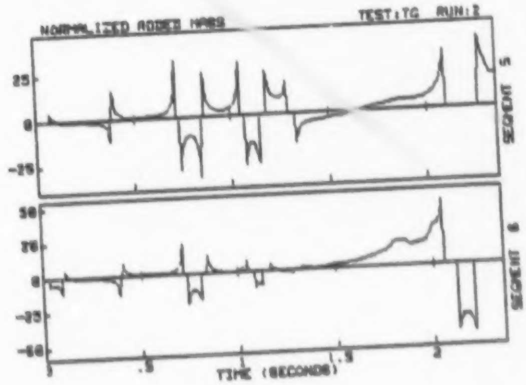

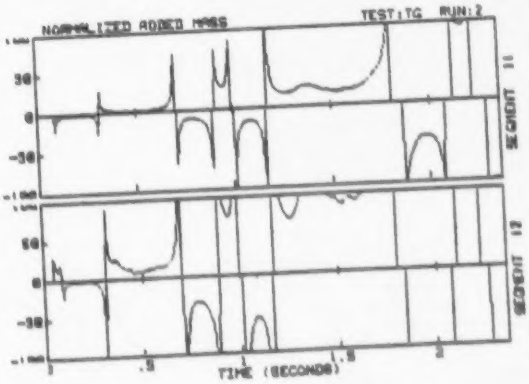

SEGMENT HYDRODYNAMIC FORCE

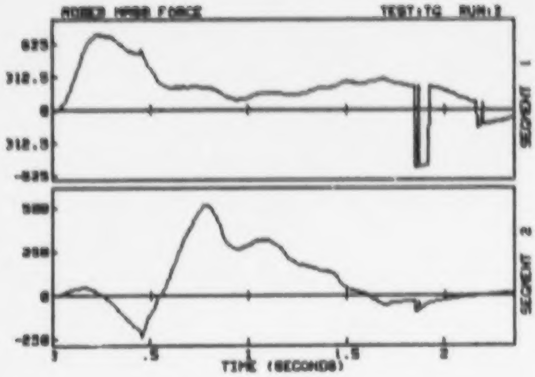

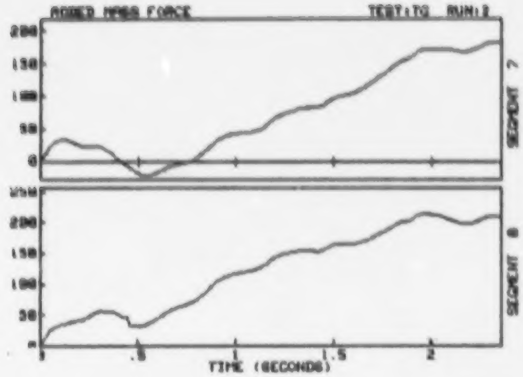

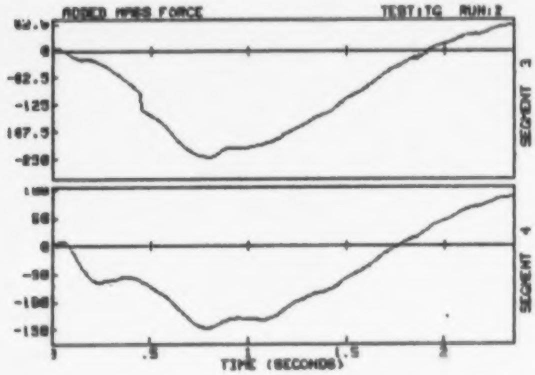

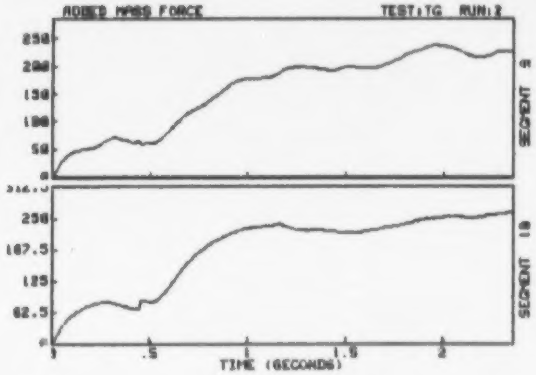

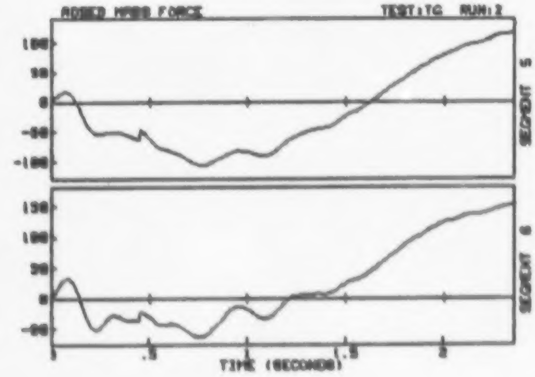

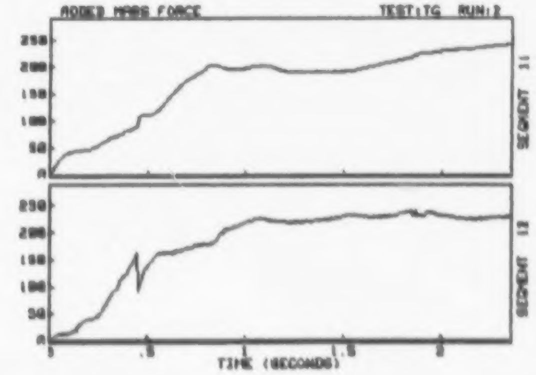

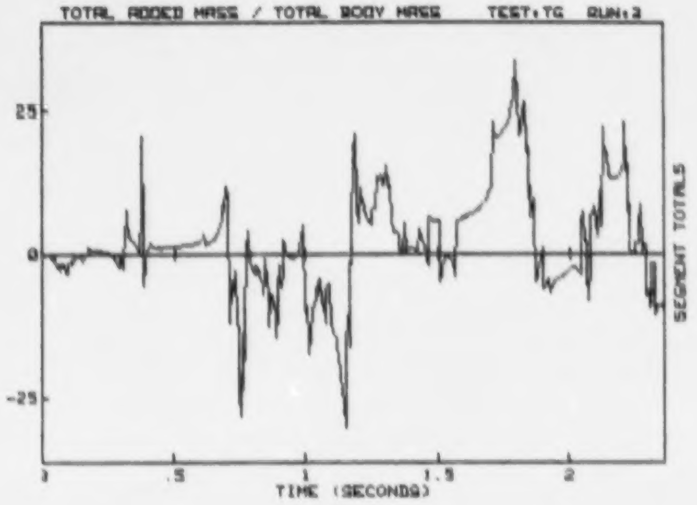

NON-DIMENSIONAL SEGMENTAL ADDED MASS STATISTICS

SEGMENT	MIN	MAX	MEAN	S.D.	NPTS
1	-631.8	740	-21.4	166.5	493
2	-184.5	169.5	-7.4	31.8	534
3	-79.9	88.9	2.9	19.5	502
4	-51	44.1	2.2	10.9	486
5	-33.4	40	2.5	9.9	489
6	-48.6	46.2	2	12.6	474
7	-25.5	64.8	9.5	16.5	450
8	-45.7	73.8	7.5	17.2	369
9	-62.3	82.4	4.3	20.4	426
10	-102	101.3	.7	36.3	467
11	-137.2	138.9	2.5	44.2	504
12	-651.4	628	17.5	173.8	531
MEAN MODEL ADDED MASS =			2.33		5725

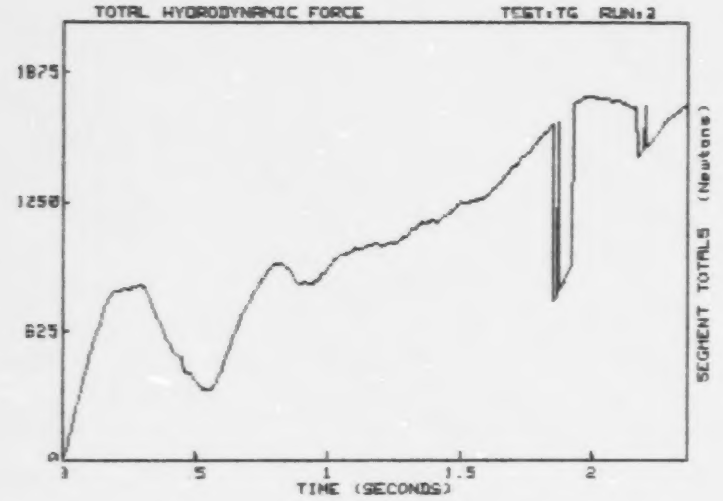

HYDRODYNAMIC FORCE SUMMARY STATISTICS

SEGMENT	MIN	MAX	MEAN	S.D.	NPTS
1	-549.8	722.8	212	231.9	585
2	-239.8	515.7	88.4	166.8	585
3	-246	59.1	-96	97.1	585
4	-147.2	88.2	-46.6	70	585
5	-107.4	116.4	-18	68.3	585
6	-63.2	151.9	23.2	66.5	585
7	-22.7	181	73.2	66	585
8	-.6	214.2	124.5	65.5	585
9	-1.1	237.9	157.1	67.9	585
10	-1.3	262.6	187.1	73.4	585
11	-1.8	241.5	169.6	64.1	585
12	-4.1	241.3	182	69.1	585
MEAN HYDRODYNAMIC FORCE =			0		7020

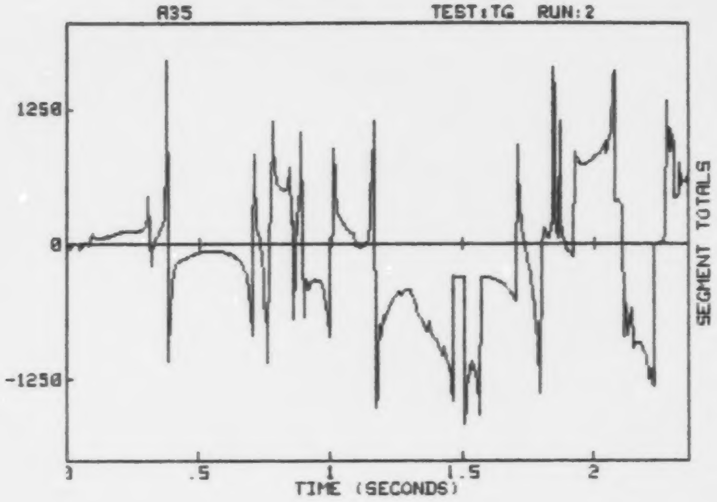

HEAVE/PITCH COUPLED ADDED MASS SUMMARY STATISTICS

SEGMENT	MIN	MAX	MEAN	S.D.	NPTS
1	-1386.9	1624.3	-47.1	365.5	493
2	-340.1	312.6	-13.7	58.6	534
3	-114.6	127.5	4.2	28	502
4	-52.2	45.2	2.2	11.1	486
5	-20.5	24.6	1.5	6.1	489
6	-10	9.5	.4	2.6	474
7	-13.3	5.2	-1.9	3.4	450
8	-45.4	28.1	-4.6	10.6	369
9	-84.4	63.8	-4.4	20.9	426
10	-145	145.9	-1	52	467
11	-254.7	251.5	-4.6	81.1	504
12	-1404.3	1456.5	-39.2	388.6	531

MEAN A35 MODEL ADDED MASS = -2.68 5725

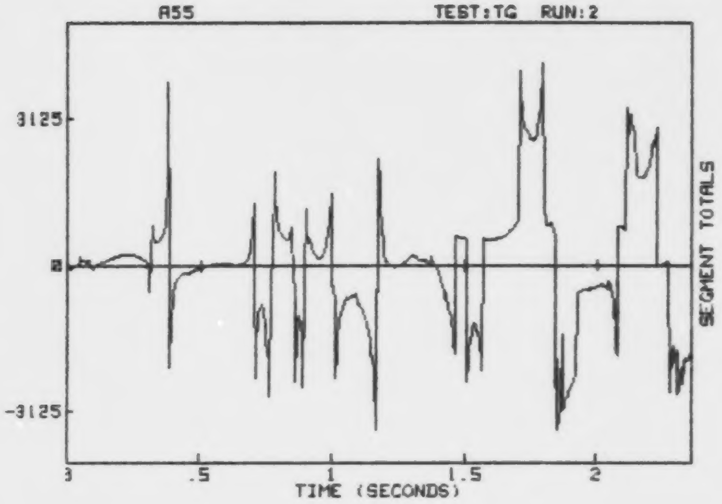

PITCH ADDED MASS MOMENT OF INERTIA SUMMARY STATISTICS

SEGMENT	MIN	MAX	MEAN	S.D.	NPTS
1	-3044.2	3565.3	-103.3	365.5	493
2	-627.2	576.3	-25.3	58.6	534
3	-164.3	182.8	6	28	502
4	-53.5	46.3	2.3	11.1	486
5	-12.6	15.1	.9	6.1	489
6	-2	1.9	.1	2.6	474
7	-1.1	2.7	.4	3.4	450
8	-17.3	27.9	2.8	10.6	369
9	-65.4	86.4	4.5	20.9	426
10	-208.9	207.5	1.4	52	467
11	-461	466.8	8.5	81.1	504
12	-3256.8	3140	87.6	388.6	531
MEAN A55 MODEL ADDED MASS =			-.05		5725

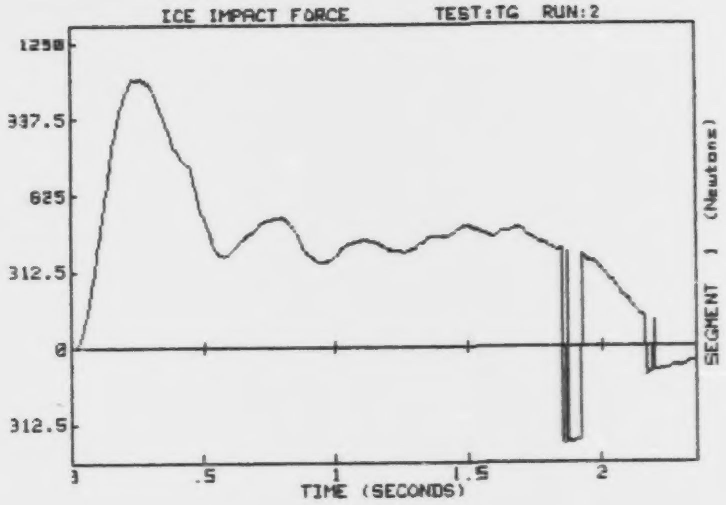
ICE IMPACT FORCE
TEST:TG RUN:2
1250
937.5
625
312.5
0
312.5
0
.5
1
1.5
2
TIME (SECONDS)
SEGMENT 1 (Newtons)

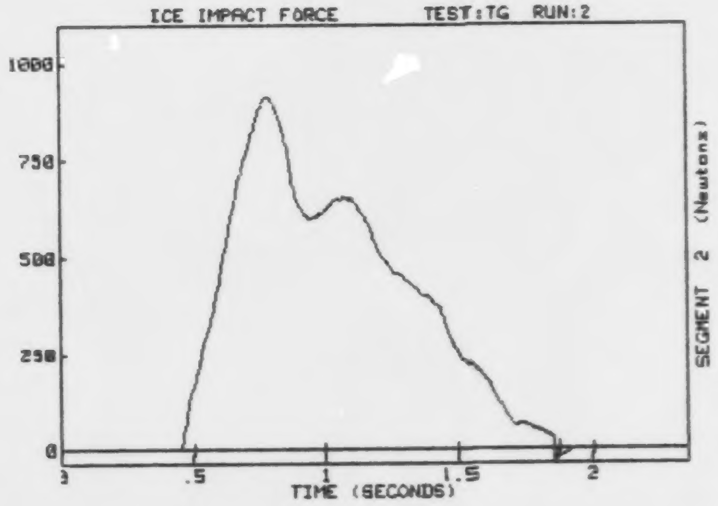
ICE IMPACT FORCE
TEST:TG RUN:2
1000
750
500
250
0
0
.5
1
1.5
2
TIME (SECONDS)
SEGMENT 2 (Newtons)

IMPACT VELOCITY= 1.12 m/s
SHIP SPEED= 13.82 kt

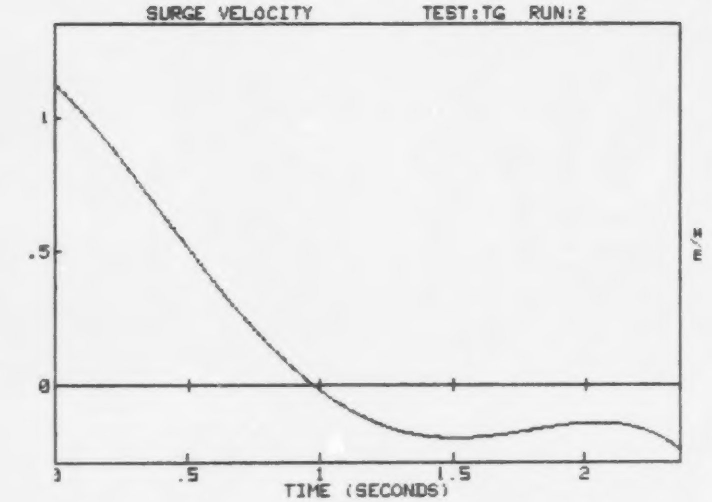

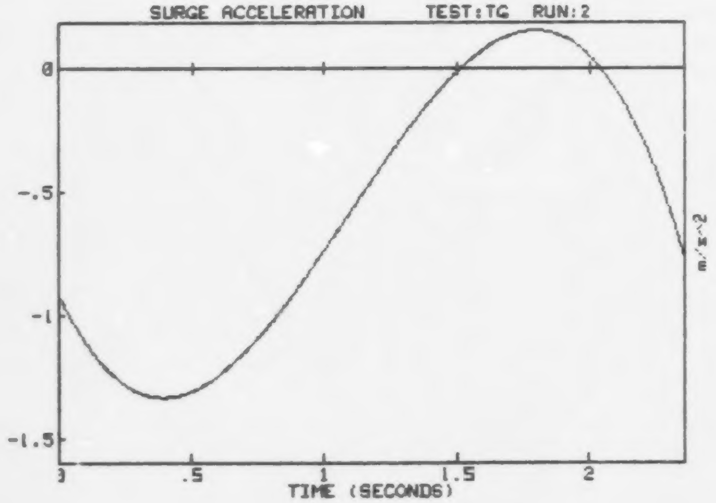

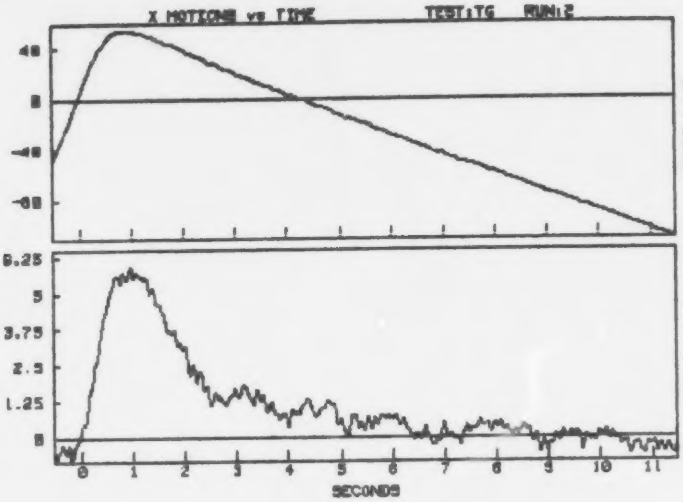
X MOTIONS vs TIME TEST:TG RUN:2

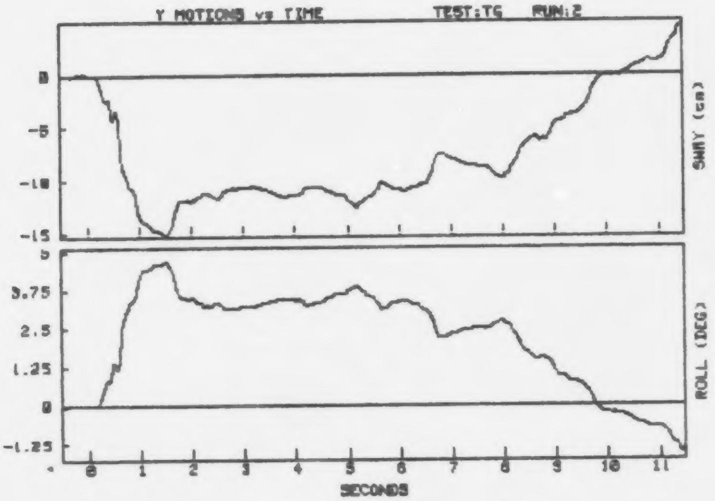
Y MOTIONS vs TIME TEST:TG RUN:2

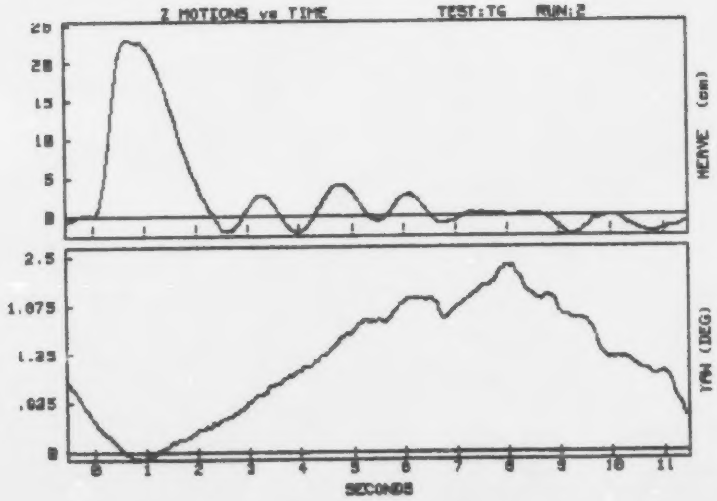
Z MOTIONS vs TIME TEST:TG RUN:2

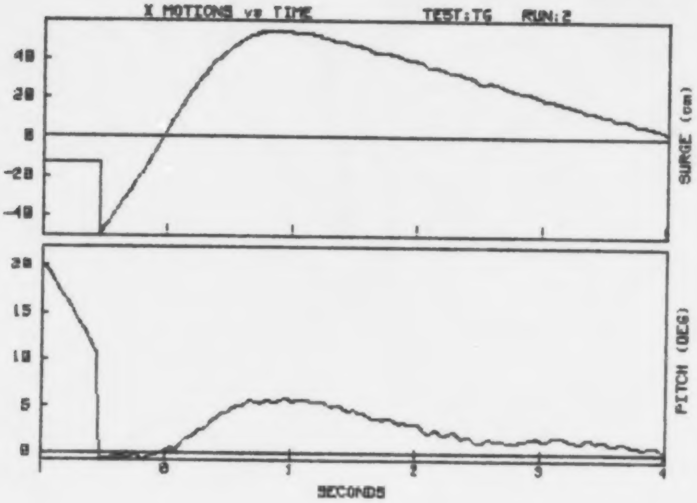
X MOTIONS vs TIME
TEST:TG RUN:2
40
20
0
-20
-40
SURGE (cm)
20
15
10
5
0
PITCH (DEG)
0
1
2
3
4
SECONDS

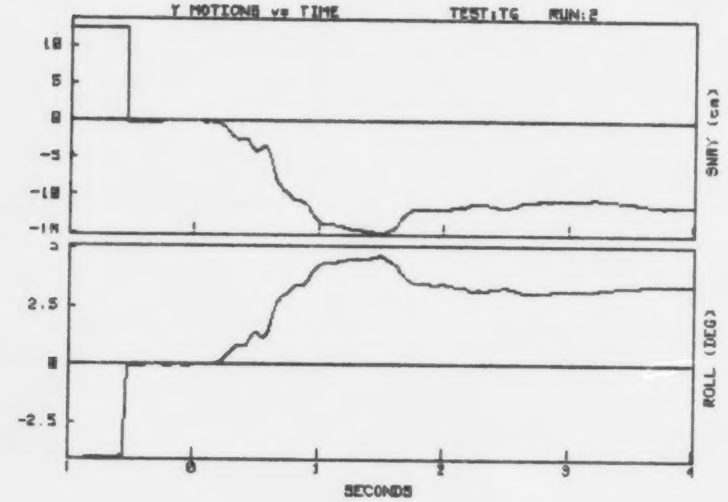
Y MOTIONS vs TIME
TEST:TG RUN:2
10
5
0
-5
-10
-15
SWAY (cm)
5
2.5
0
-2.5
ROLL (DEG)
0
1
2
3
4
SECONDS

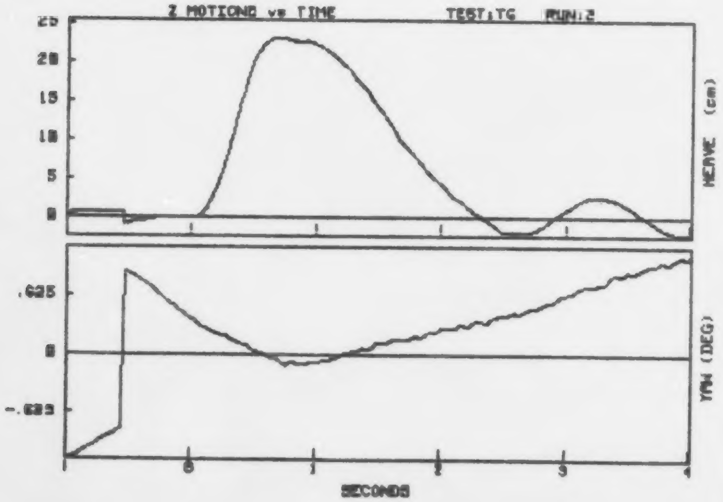
Z MOTIONS vs TIME
TEST:TG RUN:2
25
20
15
10
5
0
HEAVE (cm)
.025
0
-.025
YAW (DEG)
0
1
2
3
4
SECONDS

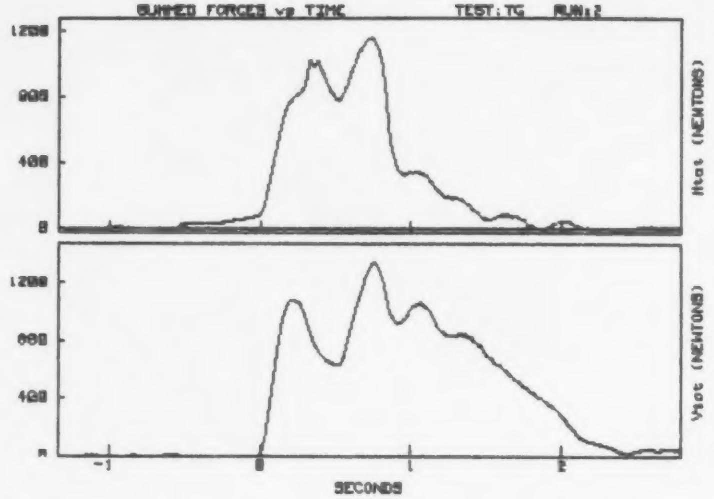
SUMMED FORCES vs TIME
TEST:TG
RUN:2
1200
800
400
0
Htot (NEWTONS)
1200
800
400
0
Ytot (NEWTONS)
-1
0
1
2
SECONDS

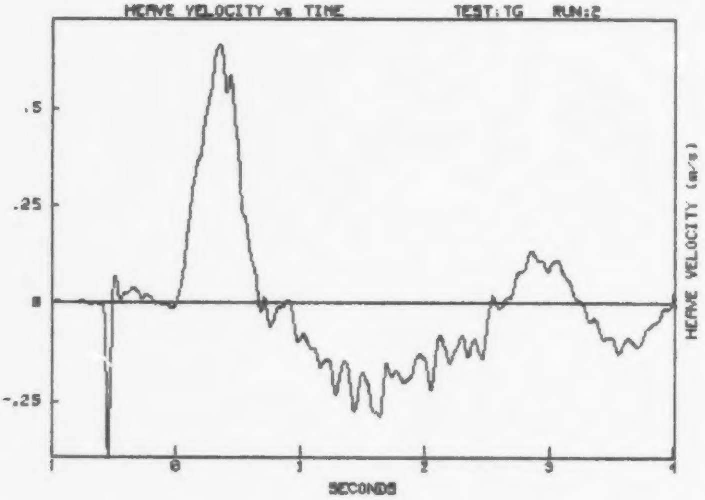
HEAVE VELOCITY vs TIME
TEST:TG
RUN:2
.5
.25
0
-.25
HEAVE VELOCITY (m/s)
0
1
2
3
4
SECONDS

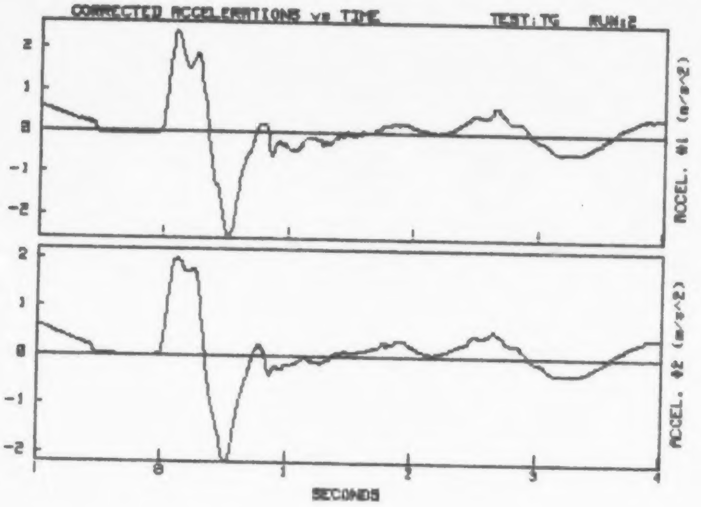
CORRECTED ACCELERATIONS vs TIME
TEST:TG RUN:2
2
1
0
-1
-2
ACCEL. #1 (m/s^2)
2
1
0
-1
-2
ACCEL. #2 (m/s^2)
0
1
2
3
4
SECONDS

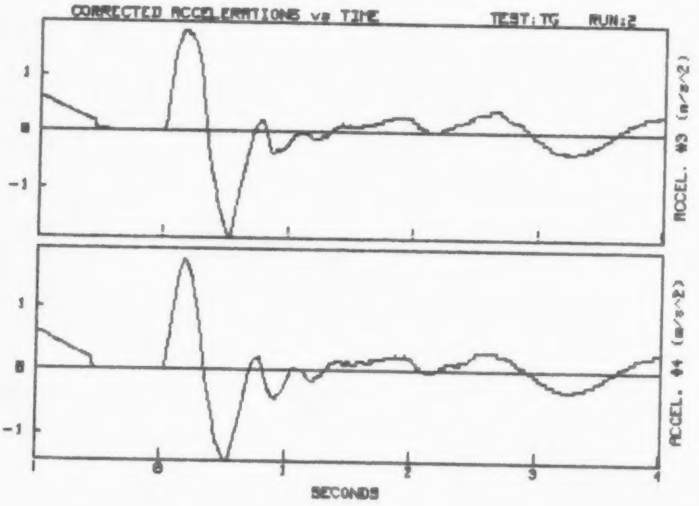
CORRECTED ACCELERATIONS vs TIME
TEST:TG RUN:2
1
0
-1
ACCEL. #3 (m/s^2)
1
0
-1
ACCEL. #4 (m/s^2)
0
1
2
3
4
SECONDS

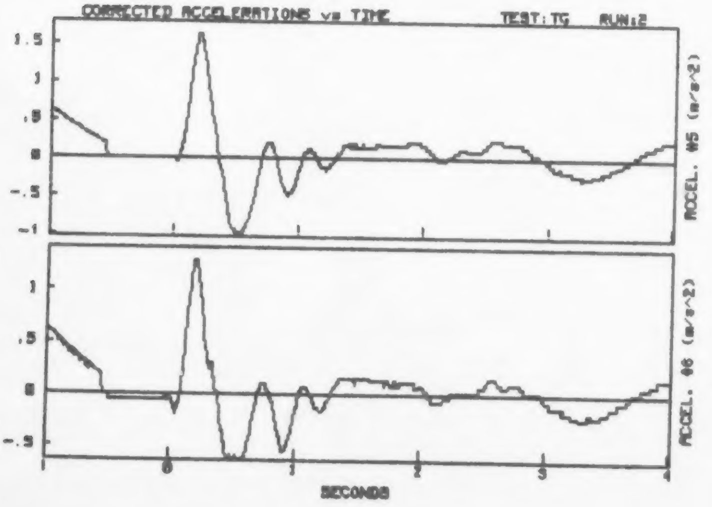
CORRECTED ACCELERATIONS vs TIME
TEST:TG RUN:2
1.5
1
.5
0
-.5
-1
ACCEL. #5 (m/s^2)
1
.5
0
-.5
ACCEL. #6 (m/s^2)
0
1
2
3
4
SECONDS

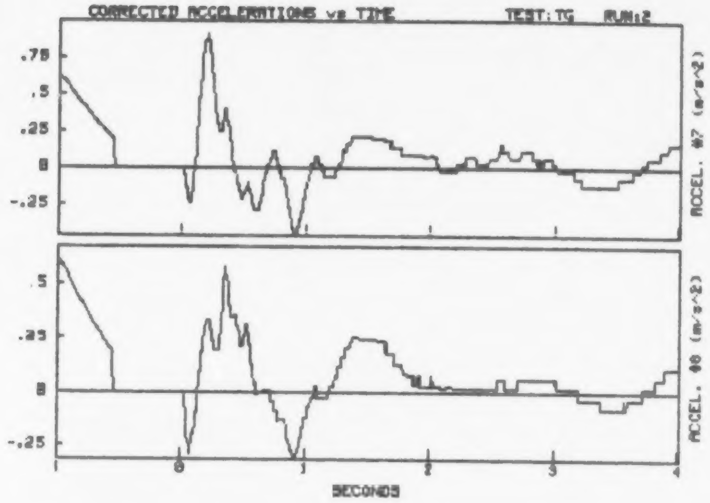

CORRECTED ACCELERATIONS vs TIME
TEST:TG RUN:2
.75
.5
.25
0
-.25
ACCEL. #7 (m/s^2)
.5
.25
0
-.25
ACCEL. #8 (m/s^2)
0
1
2
3
4
SECONDS

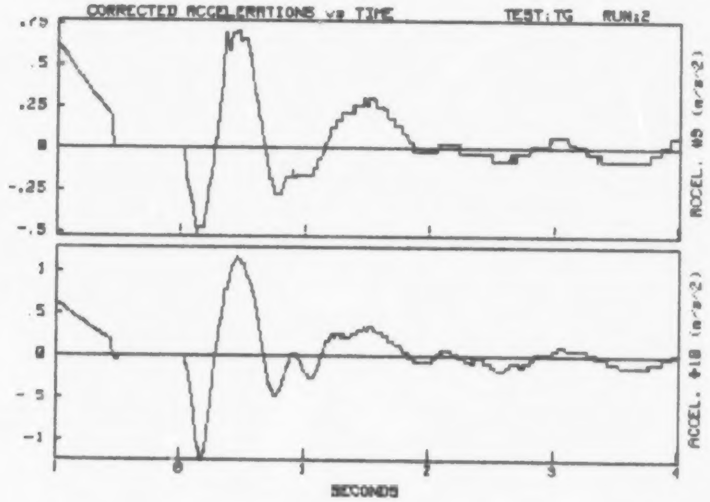

CORRECTED ACCELERATIONS vs TIME
TEST:TG RUN:2
.75
.5
.25
0
-.25
-.5
ACCEL. #9 (m/s^2)
1
.5
0
-.5
-1
ACCEL. #10 (m/s^2)
0
1
2
3
4
SECONDS

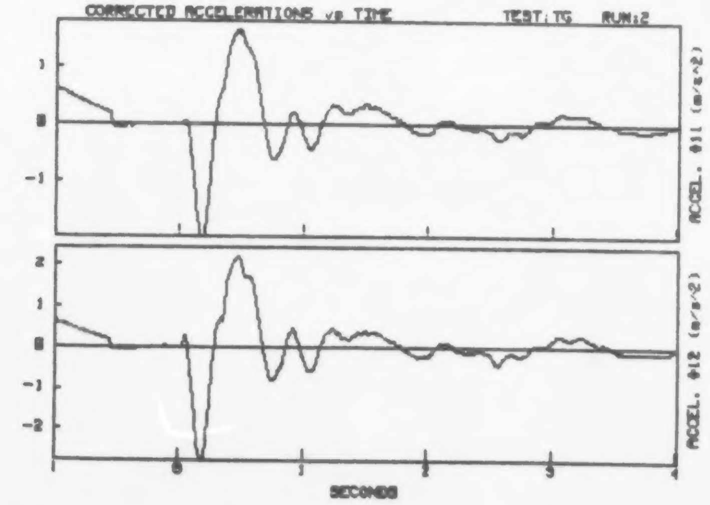

CORRECTED ACCELERATIONS vs TIME
TEST:TG RUN:2
1
0
-1
ACCEL. #11 (m/s^2)
2
1
0
-1
-2
ACCEL. #12 (m/s^2)
0
1
2
3
4
SECONDS

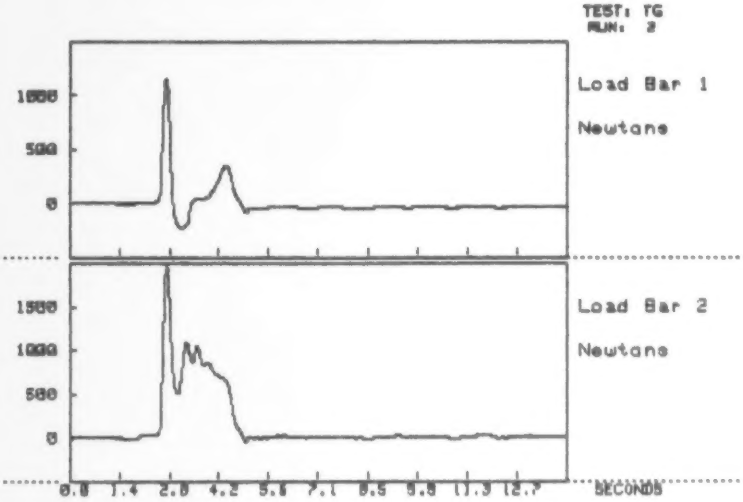
TEST: TG
RUN: 2
Load Bar 1
Neutons
1000
500
0
Load Bar 2
Neutons
1500
1000
500
0
0.0
1.4
2.8
4.2
5.6
7.1
8.5
9.9
11.3
12.7
SECONDS

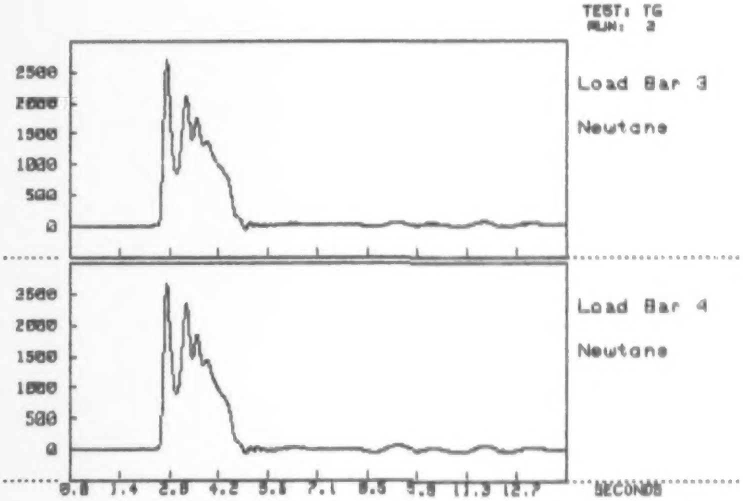
TEST: TG
RUN: 2
Load Bar 3
Neutons
2500
2000
1500
1000
500
0
Load Bar 4
Neutons
2500
2000
1500
1000
500
0
0.0
1.4
2.8
4.2
5.6
7.1
8.5
9.9
11.3
12.7
SECONDS

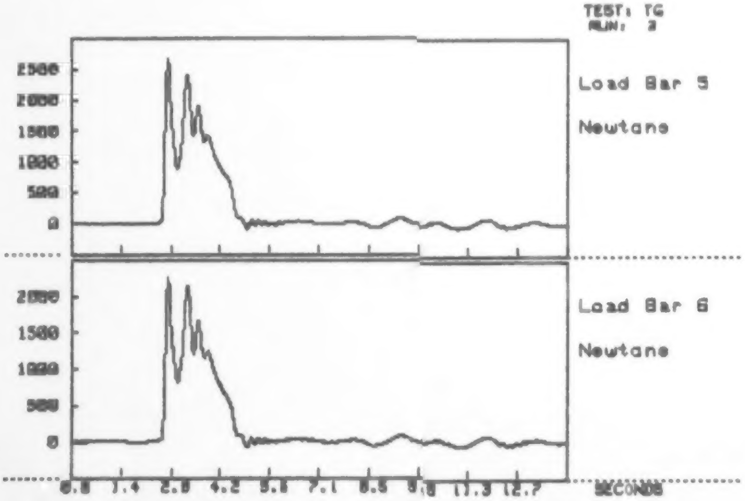
TEST: TG
RUN: 2
Load Bar 5
Neutons
2500
2000
1500
1000
500
0
Load Bar 6
Neutons
2000
1500
1000
500
0
0.0
1.4
2.8
4.2
5.6
7.1
8.5
9.9
11.3
12.7
SECONDS

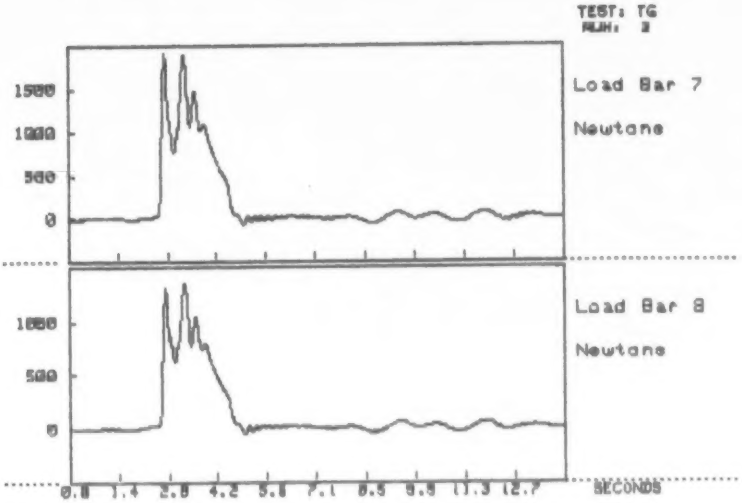
TEST: TG
RUN: 2
1500
1000
500
0
Load Bar 7
Newtons
1000
500
0
Load Bar 8
Newtons
0.0 1.4 2.8 4.2 5.6 7.1 8.5 9.9 11.3 12.7
SECONDS

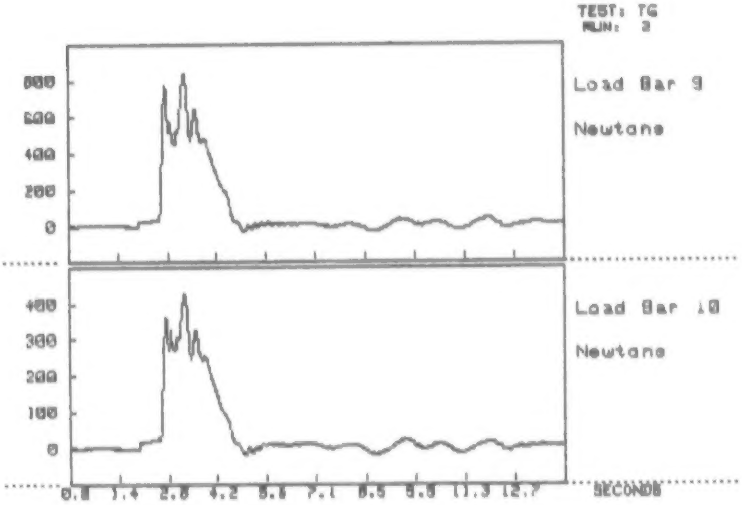
TEST: TG
RUN: 2
800
600
400
200
0
Load Bar 9
Newtons
400
300
200
100
0
Load Bar 10
Newtons
0.0 1.4 2.8 4.2 5.6 7.1 8.5 9.9 11.3 12.7
SECONDS

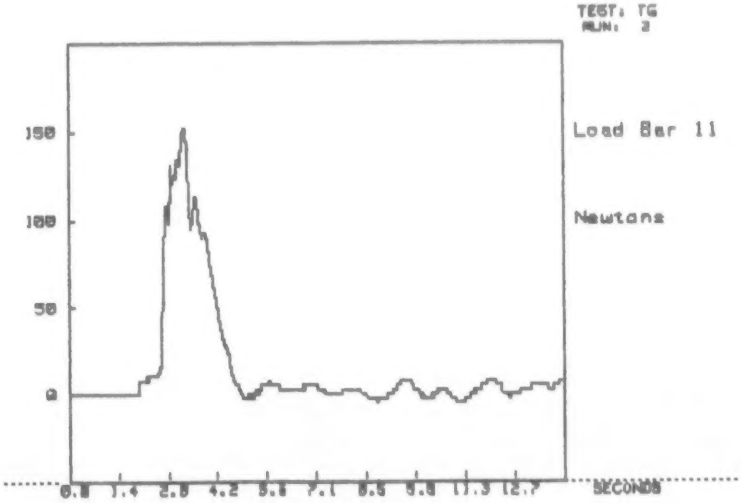
TEST: TG
RUN: 2
150
100
50
0
Load Bar 11
Newtons
0.0 1.4 2.8 4.2 5.6 7.1 8.5 9.9 11.3 12.7
SECONDS

Volume

3

ARCTEC CANADA LIMITED

[redacted]

ARCTEC CANADA LIMITED 1957C

TP 8797E

INVESTIGATION OF THE ADDED MASS PHENOMENON WITH A FLEXIBLE MODEL OF THE M.V. ARCTIC: VOLUME 3 - MODEL EXPERIMENTS IN OPEN WATER AND IN ICE

PREPARED FOR: TRANSPORTATION DEVELOPMENT CENTRE

by

D.J. Howard
B.C. Menon

MARCH 1987

PREPARED BY:

ARCTEC CANADA LIMITED
311 Legget Drive,
Kanata, Ontario.
K2K 1Z8

PROJECT TEAM:

Balji Menon, Project Manager
Claude Daley, In-house Consultant
David Howard, (Project Engineer - Task 3)
Loyd Phillips, (Project Engineer - Task 2)
Carlos Ferregut (Structural Analyst)
Michael Steele, (Systems Analyst)
Al Tudhope, (Technician)
Andre Lemieux, (Technician)

DISCLAIMER: The contents of this report reflect the views of the authors and not necessarily the official view or opinions of the Transportation Development Centre of Transport Canada.

Un sommaire en français de ce rapport est inclus avant la table des matières.

Approved by: ______________________________

Transport Canada Transports Canada

Development Développement

REPORT DOCUMENTATION FORM

1. Transport Canada Report No.
TP 8797E

2. TDC Project No.
6637/6639

3. Recipient's Catalogue No.

4. Title and Subtitle
INVESTIGATION OF THE ADDED MASS PHENOMENON WITH A FLEXIBLE MODEL OF THE M.V. ARCTIC: VOLUME 3 - MODEL EXPERIMENTS IN OPEN WATER AND IN ICE

5. Report Date
March 1987

6. Performing Organization Report No.
1957C

7. Author(s)
D.J. Howard and B.C. Menon

8. Transport Canada File No.
D1460-231

9. Performing Organization Name and Address
Arctec Canada Limited
311 Legget Drive
Kanata, Ontario
K2K 1Z8

10. DSS File No.
11SD.T8200-5-5595

11. DSS or Transport Canada Contract No.
11SD.T8200-5-5595/01-SD

12. Sponsoring Agency Name and Address
Transportation Development Centre (TDC)
200 Dorchester Blvd. West
Suite 601, West Tower
Montreal, Quebec H2Z 1X4

13. Type of Report and Period Covered
Final

14. Sponsoring Agency Code

15. Supplementary Notes See also:
Volume 1: Review of Existing Methods, Available Data and Summary of Experimental Results. Volume 2: Time Domain Analysis of Hull Response During Ramming.

16. TDC Project Officer
C. Nowicki, I.M. Bayly

17. Abstract

The comprehensive model experimental program reported in this volume aims at obtaining a semi-empirical data base of hydrodynamic added mass and damping applicable to longitudinal vertical plane response of the MV ARCTIC hull form. A 40:1, segmented, flexible model of the bulk carrier was subjected to hammer (impulse) and shaker (oscillation) tests in both air (dry) and in water (wet). The dry tests were aimed at identifying the dynamic mode shapes and frequencies of the hull form as well as to quantify the internal (structural) hull damping. The wet tests were carried out in the stationary mode as well as at forward speed. Additional wet tests were performed to assess shallow water effects as well as the influence of level unbroken ice cover. Processing of the test data was carried out using modal analysis methods. The results showed that the hydrodynamic added mass and damping are dependent on the frequency. Their distributions along the length of the hull are dependent on the mode shape. It was seen that the physical model used was capable of reproducing realistically the first two flexural modes of the full-scale ship. Results showed that added mass expressed as J-factors increased with frequency in shallow water as well as in the presence of ice cover. Damping was found to be almost independent of forward speed.

18. Key Words
Hydrodynamic Added Mass, Damping, MV ARCTIC, Segmented Model, Flexural Modes, Level Ice, Impulse Tests, Oscillation Tests.

19. Distribution Statement
A limited number of copies are available from the Transportation Development Centre.

20. Security Classification (of this report)
Unclassified

21. Security Classification (of this page)
Unclassified

22. No. of Pages
228

23. Price

TDC/CDT 79-005
Rev 86

Canada

Transports Canada Transport Canada
Développement Development

FORMULE DOCUMENTAIRE DU RAPPORT

1. N° du rapport Transports Canada
TP 8797E

2. N° de l'étude — CDT
6637/6639

3. N° de catalogue du destinataire

4. Titre et sous-titre
INVESTIGATION OF THE ADDED MASS PHENOMENON WITH A FLEXIBLE MODEL OF THE M.V. ARCTIC: VOLUME 3 - MODEL EXPERIMENTS IN OPEN WATER AND IN ICE

5. Date du rapport
mars 1987

6. N° du rapport de l'organisme exécutant
1957C

7. Auteur(s)
D.J. Howard et B.C. Menon

8. N° de dossier Transports Canada
D1460-231

9. Nom et adresse de l'organisme exécutant
Arctec Canada Limited
311 Legget Drive
Kanata (Ontario)
K2K 1Z8

10. N° de dossier — ASC
11SD.T8200-5-5595

11. N° de contrat — ASC ou Transports Canada
11SD.T8200-5-5595/01-SD

12. Nom et adresse de l'organisme parrain
Centre de développement des transports (CDT)
200 ouest, boul. Dorchester
Suite 601, tour ouest
Montréal (Québec) H2Z 1X4

13. Genre de rapport et période visée
Final

14. Code de l'organisme parrain

15. Remarques additionnelles
Voir également:
Volume 1: Review of Existing Methods, Available Data and Summary of Experimental Results. Volume 2: Time Domain Analysis of Hull Response During Ramming.

16. Agent de projet — CDT
C. Nowicki, I.M. Bayly

17. Résumé

Le programme global d'expérimentation du modèle exposé dans le présent volume vise à recueillir une base de données semi-empiriques sur la masse hydrodynamique ajoutée et sur l'amortissement, applicables au comportement longitudinal sur le plan vertical de la configuration de la coque du N.M. ARCTIC. Un modèle flexible segmenté du cargo, à l'échelle de 1/40, a été soumis à des essais d'impulsion et d'oscillation à la fois dans l'air (à sec) et dans l'eau (mouillés). Les essais à sec tendaient à identifier les formes de modes dynamiques et les fréquences de la configuration de la coque, et à quantifier l'amortissement interne (structure) de la coque. Les essais mouillés ont été réalisés en mode stationnaire et en vitesse avant. D'autres essais mouillés ont été entrepris pour évaluer les effets en eau peu profonde et l'influence d'une couverture de glace plane non fragmentée. Le traitement des données d'essai a été réalisé par méthodes d'analyse modale. Les résultats démontrent que la masse hydrodynamique ajoutée et l'amortissement dépendent de la fréquence. Leur répartition le long de la coque dépend de la forme du mode. Il a été démontré que le modèle physique utilisé pouvait reproduire de façon réaliste les deux premiers modes de flexion du navire réel. Les résultats indiquent que la masse ajoutée exprimée en facteurs J augmente avec la fréquence en eau peu profonde et en présence d'une couverture de glace. On a noté que l'amortissement est pratiquement indépendant de la vitesse avant.

18. Mots-clés
Masse hydrodynamique ajoutée, amortissement, N.M. ARCTIC, modèle segmenté, modes de flexion, glace plane, essais d'impulsion, essais d'oscillation.

19. Diffusion
Le Centre de développement des transports dispose d'un nombre limité d'exemplaires.

20. Classification de sécurité (de ce rapport)
non classifié

21. Classification de sécurité (de cette page)
non classifiée

22. Nombre de pages
228

23. Prix
—

CDT/TDC 79-005
Rev 86

Canada

SUMMARY

The purpose of the work reported in this and associated volumes was to investigate the hydrodynamic added mass phenomenon as it occurs during ship-ice interaction, to enable effective analysis and future calculation of global impact loads from experimental data.

This volume describes the model experiments undertaken to quantify the hydrodynamic added mass and damping associated with longitudinal hull response in calm, ice-free water and in level unbroken ice. These experiments are distinct from those referred to in Volume II, in that the present series falls into the category of steady-state, constant frequency, constant amplitude oscillation tests, wherein the model is excited at one point on the forward segment of the hull and the responses of all the segments are measured. The experiments included oscillation tests in the wet and dry modes with the following objectives:

- Determine the magnitude and distribution of the hydrodynamic added mass and damping in the various testing modes.
- Determine the effects of excitation frequency and forward speed on the above parameters.
- Assess the influence of water depth on added mass and damping.
- Quantify the modifications to the hydrodynamic coefficients due to the presence of level unbroken ice cover.

A 40:1 dynamically scaled model of the MV ARCTIC designed to replicate the vertical bending modes of the ship was used in the experimental program. The model is composed of 12 individual segments linked along the neutral axis. The stiffness distribution along the model length is obtained by connecting the adjacent segments with simply supported spring bars. Prior to the tests, response frequencies in the first four modes were measured and compared with scaled target frequencies of the ship. It was seen that the first flexural modal frequency compared to within 6% of the target value, while the second flexural modal frequency was within 10%. At higher modes, the discrepancies were larger, indicating that the flexible scale model does not behave like a free-free beam at the higher modes. The instrumentation system consisted of 12 vertically referenced accelerometers on the model, one at each segment. The input forcing function was measured using a strain gauged dynamometer.

The dry tests were conducted using a specially built metal frame, on which the model was supported. The model was hung from the frame through calibrated metal springs which represented the waterplane "stiffness" of each model segment. Both hammer and shaker tests were conducted with this set up. The wet tests were conducted in the towing tank with the model restrained in roll, surge, sway and yaw. Again, hammer and shaker tests were conducted both in the stationary mode as well as at forward speed. An electrodynamic shaker capable of achieving a frequency range of 0 - 100 Hz and an amplitude range of 0.1 to 5 mm was used in the dry and wet tests. The wet tests were conducted in water with depth to draft ratio of 5.2. In order to assess the influence of water depth on hull response, the hammer tests were repeated in shallower water (depth to draft ratio 1.5). A limited series of ice tests was performed with the model stationary in level unbroken ice cover with uniform thickness (1.1 m full scale). For additional tests to investigate the hydrodynamic added mass and damping in the rigid body modes, the model was further stiffened and the wet shaker tests were repeated. A final series of tests was carried out to determine the dependence of the oscillation amplitudes on the test results.

The test procedures and data processing method followed for the hammer tests were essentially the same for all hammer tests, including the frame tests, the dry hammer tests and the wet hammer tests. Similarly, the methods followed for the shaker tests were the same for all shaker tests, including the dry shaker tests, the stationary and towed wet shaker tests, and the shaker tests in ice.

All acceleration and force time series were subjected to Fast Fourier Transforms (FFT) with 1024 data points for the hammer tests and 2048 data points for shaker tests. The hull response transfer functions for each segment were then determined from the acceleration and force spectra. The dynamic properties of the system were calculated using a standard modal analysis software. This exercise generated, for each flexural mode (up to the fifth), the segmental distribution of the frequency, percentage damping, peak response, phase angle, generalized stiffness and the generalized mass. They are, therefore, termed the modal frequency, modal damping and so on. The modal mass determined in the dry tests was removed from the modal mass extracted from the wet tests to give the modal added mass. The modal added mass was then expressed as a ratio of the dry modal mass as well as the displaced mass of a half cylinder of length equal to that of the segment and radius equal to half of the mean segment beam. The latter is commonly referred to as the J-factor, which is dependent on the mode.

Examination of the transfer functions from the zero-speed dry, wet and ice cover tests depicted substantial differences in modal frequencies resulting from the hydrodynamic added mass effects. Forward speed effects were found to be significant at second and higher flexural modes of response. Two effects are apparent - modal frequencies increase with forward speed; for the first and second mode of response, the damping is higher at higher speeds, but for the higher modes, the damping is lower than that for the zero-speed case.

From the dry hammer tests, it is seen that the structural (internal) hull damping increases with the mode number up to the third mode and at the fourth mode drops below that at the third mode. Variation of hull damping along the length of the hull is significant in the first mode. But, at higher modes, damping is essentially uniform through the length of the hull. These damping factors are applicable to damped oscillation cases.

From the dry shaker tests, on the other hand, it is clearly observed that internal hull damping is a function of the frequency of oscillation. Further, significant variation of damping along the hull is observed only in the first mode. Once again, the magnitude of damping increases with the mode number up to the third mode, beyond which it drops slightly.

From zero-speed hammer tests in deep water, it is seen that the hydrodynamic added mass, expressed as J-factors, varies along the length of the hull attaining large values near the nodes. In general, positive values are obtained for J-factors. However, in the third mode negative values are registered locally at segments where accelerations are very low (i.e. near the nodal points). Damping factor is nearly constant at 10% for the forward and aft segment of the hull, while for the intermediate segments the damping drops to roughly 4%. It is also seen that the damping is mode dependent, roughly 50% lower for the second mode.

From zero-speed hammer tests in shallow water, it is seen that the hydrodynamic added mass is roughly 40% higher at the bow and the forward segments, while at the stern segments it is 55 to 65% higher than those determined from the deep water tests. At or near the second nodal point, the increase is much higher, of the order of 100%. Damping, on the other hand, is roughly 50% higher at the forward end of the hull and about 20% higher at the aft end.

In general, considerably lower added mass values (J-factors) were obtained from the zero-speed shaker tests. As shaker tests are inherently more accurate than the hammer tests, it is concluded that these numbers are appropriate for all application purposes. It is also observed that damping is considerably higher in the zero-speed shaker tests and tends to increase in magnitude with the mode number.

From the shaker tests with forward speed, it is seen that hydrodynamic added mass dropped as much as 30% at a moderate speed of 3 knots. Towards higher speeds (6 knots), this trend is reversed and the added mass shows fairly large fluctuations with associated local negative J-factors. Damping, on the other hand, remains essentially unchanged from the zero-speed tests, indicating that it is almost independent of forward speed.

SOMMAIRE

L'objet des travaux exposés dans le présent document et dans les volumes connexes consiste à étudier le phénomène de la masse hydrodynamique ajoutée, tel qu'il survient lors de l'interaction navire-glaces, afin de permettre une analyse sérieuse et des calculs ultérieurs des charges d'impact globales à partir de données expérimentales.

Le présent volume décrit l'expérimentation réalisée sur modèle afin de quantifier la masse hydrodynamique ajoutée et l'amortissement touchant le comportement longitudinal de la coque en eau calme et libre de glaces, et en glace plane non fragmentée. Ces expériences sont différentes de celles indiquées dans le volume II, car elles font partie de la catégorie des essais en régime permanent, de fréquence constante et d'oscillation à amplitude constante, avec excitation du modèle à un point du segment avant de la coque et mesure du comportement de tous les segments. Les expériences ont comporté des essais d'oscillation à sec et mouillés visant les objectifs suivants:

- Établir la grandeur et la répartition de la masse hydrodynamique ajoutée et de l'amortissement dans les divers modes d'essai.
- Établir les effets de la fréquence d'excitation et de la vitesse avant sur les paramètres susmentionnés.
- Évaluer l'influence de la profondeur de l'eau sur la masse ajoutée et sur l'amortissement.
- Quantifier les modifications aux coefficients hydrodynamiques découlant de la présence d'une couverture de glace plane non fragmentée.

Pour le programme expérimental, on a utilisé un modèle dynamique à l'échelle de 1/40 du N.M. ARCTIC, destiné à reproduire les modes de flexion verticale du navire. Le modèle comporte 12 segments distincts reliés le long de l'axe neutre. La répartition de la rigidité le long du modèle s'obtient en reliant les segments adjacents par des barres à ressort simplement soutenues. Avant les essais, les fréquences de comportement des premiers quatre modes ont été mesurées et comparées aux fréquences cibles à l'échelle. Il a été démontré que la première fréquence modale de flexion se comparait à quelque 6 p. 100 de la valeur cible, tandis que la deuxième fréquence modale de flexion se situait à 10 p. 100 près. À des modes plus élevés, les écarts étaient plus considérables, indiquant ainsi que le modèle flexible à l'échelle ne se comporte pas comme un poutre libre-libre aux modes plus élevés. L'ensemble des instruments se composait de 12 accéléromètres à référence verticale sur le modèle, soit un à chaque segment. La fonction de force d'entrée était mesurée par un dynamomètre à extensomètre.

Les essais à sec ont été réalisés à l'aide d'un bâti métallique spécial destiné à supporter le modèle. Ce dernier était suspendu au bâti à l'aide de ressorts métalliques calibrés représentant la "rigidité" du plan de flottaison de chaque segment du modèle. Les essais d'impulsion et d'oscillation ont été menés de cette façon. Les essais mouillés ont été réalisés dans le bassin des carènes avec le modèle contrôlé en roulis, houle, balancement et embardée. Les essais d'impulsion et d'oscillation ont été menés en mode stationnaire et en vitesse avant. Un vibreur électrodynamique d'une plage de fréquences de 0 à 100 Hz et d'amplitude de 0,1 à 5 mm a servi aux essais à sec et mouillés. Les essais mouillés ont été réalisés dans l'eau avec rapport profondeur-tirant d'eau de 5,2. Afin d'évaluer l'influence de la profondeur de l'eau sur le comportement de la coque, les essais d'impulsion ont été repris en eau moins profonde (rapport profondeur-tirant d'eau de 1,5). Une courte série d'essais dans les glaces a été faite avec le modèle stationnaire dans une couverture de glace plane non fragmentée d'épaisseur uniforme (1,1 mm grandeur réelle). Pour réaliser des essais supplémentaires destinés à étudier la masse hydrodynamique ajoutée et l'amortissement en mode corps rigide, le modèle a été encore rigidifié et les essais d'oscillation mouillés ont été répétés. Une dernière série d'essais a permis d'établir la dépendance des amplitudes d'oscillation sur les résultats des essais.

Les méthodes d'essai et de traitement des données utilisées dans le cas des essais d'impulsion ont été essentiellement les mêmes pour tous les essais de ce genre, y compris les essais sur bâti, les essais d'impulsion à sec et mouillés. De la même façon, les méthodes utilisées pour les essais d'oscillation ont été identiques pour tous les essais du genre, y compris les essais d'oscillation à sec, les essais mouillés sur modèle stationnaire et remorqué, et les essais d'oscillation dans les glaces.

Toutes les séries temporelles d'accélération et de force ont été soumises à la transformation accélérée de Fourier avec 1024 points de mesure pour les essais d'impulsion et 2048 points pour les essais d'oscillation. Les fonctions de transfert de comportement de la coque pour chaque segment ont été ensuite déterminées à partir du spectre d'accélération et de force. Les propriétés dynamiques du système ont été calculées à l'aide d'un logiciel ordinaire d'analyse modale. Cet exercice a engendré, pour chaque mode de flexion (jusqu'au cinquième) la répartition segmentaire de la fréquence, l'amortissement en pourcentage, la réponse de pointe, le déphasage, la rigidité généralisée et la masse généralisée. Ils sont donc qualifiés de fréquence modale, amortissement modal et ainsi de suite. La masse modale calculée lors des essais à sec a été soustraite de la masse modale tirée des essais mouillés pour obtenir la masse modale ajoutée. Cette masse modale ajoutée a ensuite été exprimée comme un rapport de la masse modale sèche ainsi que la masse déplacée d'un demi-cylindre de longueur égale à celle du segment et de rayon étale à la moitié de la poutre moyenne du segment. Il s'agit de ce qui est habituellement appelé le facteur J, qui dépend du mode.

L'étude des fonctions de transfert des essais à sec vitesse zéro, puis mouillés et avec couverture de glace, a révélé de nettes différences dans les fréquences modales résultant des effets de la masse hydrodynamique ajoutée. On a noté que les effets en vitesse avant sont importants au deuxième et aux modes de flexion plus élevés. Deux effets sont apparents: les fréquences modales augmentent avec la vitesse avant; pour le premier et le deuxième mode de comportement, l'amortissement est plus marqué aux hautes vitesses mais, pour les modes supérieurs, l'amortissement est moindre que celui noté dans le cas de la vitesse zéro.

À partir des essais d'impulsion à sec, on note que l'amortissement interne (structural) de la coque augmente avec le numéro du mode jusqu'au troisième, puis diminue au quatrième mode au-dessous de celui du troisième mode. La différence d'amortissement de la coque sur sa longueur est importante dans le premier mode. Cependant, dans les modes plus élevés, l'amortissement est essentiellement uniforme sur toute la longueur de la coque. Ces facteurs d'amortissement s'appliquent aux cas d'oscillation amortie.

D'autre part, à la lumière des essais d'oscillation à sec, il est évident que l'amortissement interne de la coque est fonction de la fréquence d'oscillation. En outre, la différence marquée de l'amortissement le long de la coque n'est observée que dans le premier mode. Encore une fois, l'ampleur de l'amortissement augmente avec le numéro du mode jusqu'au troisième mode, au-delà duquel elle diminue quelque peu.

À la suite des essais d'impulsion à vitesse zéro en eau profonde, on remarque que la masse hydrodynamique ajoutée, exprimée en facteurs J, varie sur la longueur de la coque et atteint des valeurs importantes près des points nodaux. En général, des valeurs positives sont obtenues pour les facteurs J. Cependant, dans le troisième mode, on enregistre des valeurs négatives localement aux segments où les accélérations sont très faibles (par exemple à proximité des points nodaux). Le facteur d'amortissement est pratiquement constant à 10 p. 100 pour le segment avant et arrière de la coque, alors que, dans le cas des segments intermédiaires, l'amortissement diminue à quelque 4 p. 100. On note en outre que l'amortissement dépend du mode, soit environ 50 p. 100 moins élevé dans le cas du deuxième mode.

À partir des essais d'impulsion à vitesse zéro en eau peu profonde, on remarque que la masse hydrodynamique ajoutée est de plus ou moins 40 p. 100 supérieure à la proue et dans les segments avant, tandis que dans les segments de poupe, elle est de 55 à 65 p. 100 plus élevée que celle mesurée à partir des essais en eau profonde. Sur le deuxième point nodal ou à proximité, l'augmentation est nettement plus élevée, soit d'environ 100 p. 100. D'autre part, l'amortissement est d'environ 50 p. 100 plus élevé à l'extrémité avant de la coque et d'environ 20 p. 100 plus élevé à l'extrémité arrière.

En général, les essais d'oscillation à vitesse zéro ont engendré des valeurs de masse ajoutée (facteurs J) considérablement moins élevées. Étant donné que les essais d'oscillation sont, de façon inhérente, plus précis que les essais d'impulsion, on en déduit que ces valeurs conviennent à toutes les applications. On a noté en outre que l'amortissement est considérablement plus élevé lors des essais d'oscillation à vitesse zéro et tend à augmenter avec le numéro du mode.

À la suite des essais d'oscillation en vitesse avant, on note que la masse hydrodynamique ajoutée diminue jusqu'à 30 p. 100 à vitesse modérée de 3 noeuds. Lorsque la vitesse augmente (6 noeuds), cette tendance s'inverse et la masse ajoutée indique des fluctuations assez considérables associées à des facteurs J locaux négatifs. D'autre part, l'amortissement demeure essentiellement inchangé à vitesse zéro, ce qui indique qu'il est pratiquement indépendant de la vitesse avant.

ACKNOWLEDGEMENTS

The authors would like to acknowledge the support of Mr. Sydney Mathews of Coldstream Maritime Incorporated, who as technical liaison officer to TDC provided guidance and encouragement through close participation in all phases of this project. In addition, we would also like to thank Mr. Chris Nowicki for his assistance in the contractual and administrative aspects of this work.

TABLE OF CONTENTS

1. INTRODUCTION....................1
   1.1 Background....................1
   1.2 Test Objectives....................2

2. MODEL DESCRIPTION....................3
   2.1 Characteristics of Segmented Flexible Model....................3
   2.2 Modal Properties of MV ARCTIC Model Using F.E.Methods..8

3. TEST PROGRAM....................13
   3.1 Overview....................13
   3.2 Vibration Test Equipment....................13
   3.3 Dry Mode Tests....................13
   3.4 Wet Mode Tests....................17
   3.5 Ice Cover Tests....................20
   3.6 Miscellaneous Tests....................22
   3.7 Instrumentation System....................24

4. TEST PROCEDURES AND DATA PROCESSING....................28
   4.1 Test Preparations....................28
   4.2 Hammer Tests....................30
   4.3 Shaker Tests....................31
   4.4 Modal Analysis....................32

5. EXPERIMENTAL RESULTS....................36
   5.1 Hammer Tests....................36
   5.2 Shaker Tests....................38
   5.3 Miscellaneous Test Results....................43

6. MODAL ANALYSIS....................49
   6.1 Dry Tests....................49
   6.2 Stationary Wet Tests....................55
   6.3 Towed Wet Tests....................60
   6.4 Tests in Uniform Ice Cover....................75

7. CONCLUSIONS....................79

8. RECOMMENDATIONS....................81

9. REFERENCES....................82

APPENDIX A - SPECIFICATIONS OF MB-50 ELECTRODYNAMIC SHAKER

APPENDIX B - RESPONSE TRANSFER FUNCTIONS AND MODE SHAPES

LIST OF FIGURES

2.1 Plate of the Segmented Flexible Model........................4
2.2 Assembly of Nodes and Elements..............................9
2.3 First Flexural Mode..10
2.4 Second Flexural Mode.......................................11

3.1 Operational Characteristics of Hydraulic and Electrodynamic Vibration Machine..........................14
3.2 Set-up for Dry Tests.......................................16
3.3 Heave Staff for Wet Shaker Tests...........................19
3.4 Pre-cut Ice Cover for Stationary Tests in Ice..............21
3.5 Position of Model Relative to Ice Sheet....................23
3.6 Instrumentation Data Acquisition System....................25
3.7 MV ARCTIC Model Instrumentation............................26
3.8 Instrumentation Used During Frame Hammer Tests.............27

4.1 Overview of Oscillation Test Procedure & Data Processing...29
4.2 Single Degree-of-Freedom Transfer Function Definition Sketch..33

5.1 Hammer Test Results..37
5.2 Stationary Shaker Test Results.............................39
5.3 Towed Shaker Test Results..................................40
5.4 Variation of the Normalized Response Transfer Function With Forcing Amplitude at 5.4 Hz..........................47
5.5 Variation of the Normalized Response Transfer Function With Forcing Amplitude at 10.3 Hz.........................48

6.1 Definition Sketch for Single Degree-of-Freedom System......51
6.2 Dry Shaker...53
6.3 Dry Hammer...54
6.4 Variation of the "J" Factor Along Model....................59
6.5 Stationary Wet Hammer Tests (Deep Water)...................61
6.6 Stationary Wet Hammer Tests (Shallow Water)................62
6.7 Stationary Wet Shaker Tests (Deep Water)...................63
6.8(a) Stationary Shaker Tests Excited at the CG..............65
6.8(b) Stationary Rigid Body Tests............................68
6.8(c) Rigid Body Tests at 6 Knots............................69
6.9 Variation of the "J" Factor with Velocity..................73
6.10 Wet Shaker Tests at 1 Knot................................74
6.11 Variation of "J" Factor Due to the Presence of Ice........77
6.12 Stationary Tests in Ice...................................78

LIST OF TABLES

2.1 MV ARCTIC Principal Particulars.....5
2.2 Model Ballast Distribution.....6
2.3 MV ARCTIC Modal Properties.....7
2.4 Predicted and Measured Dry Natural Frequencies.....12

3.1 Experimental Test Program.....15
3.2 Segment Details.....18

5.1 Water Properties.....41
5.2 Elastic Modulus of the Test Ice Sheet.....42
5.3 Ice Thickness Profile.....43
5.4 Forcing Amplitude Variation Tests at 5.4 Hz.....44
5.5 Forcing Amplitude Variation Tests at 10.3 Hz.....45

6.1 Modal Results from the Dry Hammer Tests.....50
6.2 Modal Results from the Dry Shaker Tests.....52
6.3 Modal Results from the Stationary Hammer Tests in Deep Water.....56
6.4 Modal Results from the Stationary Hammer Tests in Shallow Water.....57
6.5 Modal Results from the Stationary Shaker Tests in Deep Water.....58
6.6 Modal Results from the Stationary Shaker Tests Excited from the CG.....64
6.7 Modal Results from the Stationary Rigid Body Tests.....66
6.8 Modal Results from the Rigid Body Tests at 6 knots.....67
6.9 Modal Results from the Shaker Tests at 1 knot.....70
6.10 Modal Results from the Shaker Tests at 3 knots.....71
6.11 Modal Results from the Shaker Tests at 6 knots.....72
6.12 Modal Results from the Shaker Tests in Level Ice.....76

NOMENCLATURE

B = Beam
$\bar{B}$ = Model's average waterline beam
C = Damping coefficient
C_b = Block coefficient
C_{bf} = Block coefficient, forward
C_p = Prismatic coefficient
C_w = Water-plane area coefficient
D = Displacement
$F(t)$ = Forcing function
K = Stiffness
L_{bp} = Length, between perpendiculars
L_{oa} = Length, overall
M = Mass
M_a = Total hydrodynamic added mass
T = Draft
x = Motion variable

α, β, γ = Hull line angles
ω_d = Damped natural frequency (rad/sec)
ω_n = Undamped natural frequency (rad/sec)
ζ = Damping factor
ρ = Density of water

1. INTRODUCTION

1.1 Background

In the study of ship motions and hull loads, the usual convention, which dates back to Lewis (1929), is to express the coupling between hydrodynamic forces and structural response in terms of added mass and damping effects. These effects are usually quantified by the so called coefficients which are expressed as functions of hull geometry, fluid density, frequency of oscillation and modal response shape. A considerable amount of research has been carried out in the development of methods to derive these coefficients for ship hull forms in open water. These methods take into account the influence of the free surface as well as the three-dimensional effects at the bow and stern ends of the hull. In the presence of continuous ice cover and in transient response situations, such as that encountered during ramming operations, the influence of the free surface and the flow around the ends of the hull will differ significantly from the open water case. It is therefore, essential to investigate experimentally the effects of ice cover on the hydrodynamic reactions on the hull in its various modes of responses. It is our understanding that no serious effort has been made in the past to quantify hydrodynamic added mass and damping applicable to icebreaking ships, and there are no experimental data in the literature which are specific to these hull forms.

It is well known that ship hull hydrodynamic coefficients cannot be measured directly from experiments. What can be measured are the loads on and the responses of the model. From these measurements, the hydrodynamic coefficients can then be derived using a suitable ship response theory. The coefficients so determined are, strictly speaking, those associated with that particular theory and therefore, inherit all the limitations and approximations of the theory. However, once measurements are obtained from experiments, suitability of various theories may be investigated, and a simple theory, if appropriate may be used. The accuracy of the hydrodynamic coefficients depends not only on the measurement accuracies of the loads and responses of the model, but also on the accuracy of the hull response formulation.

The contents of this volume deals with a special series of tests carried out with the 40:1 flexible scale model of the MV ARCTIC in open water and in level unbroken ice. All the tests were carried out with the specific aim of extracting hydrodynamic added mass and damping in the vibratory mode. This work is independent of (but complimentary to) a concurrent task involving analysis of existing scale model test data reported in Volume 2. Volume 1 provides a background to the subject of hydrodynamic added mass and damping by reviewing the state-of-the art theoretical methods and available experimental data.

1.2 Objectives

The ultimate goal of the present experimental program is to conduct scale model tests in the 'wet' as well as 'dry' modes so that the following objectives can be achieved:

i) Isolation of the hydrodynamic forces acting on the hull and determination of the magnitude and distribution of the hydrodynamic added mass and damping from the measured hull responses to specified excitation.

ii) Determine the effects of excitation frequency and forward speed on the hydrodynamic coefficients.

iii) Assess the influence of water depth on the hydrodynamic coefficients.

iv) Quantify the modifications to the coefficients of hydrodynamic reaction due to the presence of level, uniform, unbroken ice cover.

v) Correlate measured hydrodynamic coefficients with those derived by calculations from existing semi-empirical or theoretical methods.

In addition to the above project objectives, a number of specific tasks can be identified that were carefully drawn up to systematically lead into those listed above. These were:

i) To instrument the flexible MV ARCTIC model for measurement of accelerations at the centre of each of the segments. The bending strains between segments are to be sensed by the built-in strain-gauged strength elements.

ii) To design and fabricate a test rig for stationary 'dry' oscillation tests with the flexible model.

iii) To design and fabricate a test rig for towed tests in water.

iv) To determine the specification as well as fabricate/-procure a forcing mechanism that will be capable of oscillating the model over the required range of excitation frequencies and amplitudes.

v) To develop or procure modal analysis software that will allow extraction of hydrodynamic added mass and damping to be readily carried out.

vi) To carry out oscillation tests in air, in deep and shallow water as well as in the presence of level unbroken ice cover, acquires and processes the bulk of the data so that the most pertinent parameters can be summarized in graphical as well as tabular form.

2. MODEL DESCRIPTION

2.1 Characteristics of Segmented Flexible Model

A dynamically scaled model of the MV ARCTIC was used in the experimental program. This model was designed to replicate the first two vertical bending modes of the ship as a means of investigating hull girder stresses during ship-ice ramming interactions. The results of these studies have been reported in [1] and [2]. This model retains the original MV ARCTIC bow, and is at a scale of 1/40 (Figure 2.1). Table 2.1 lists the model particulars. It is composed of 12 individual segments linked along the neutral axis by self-aligning bearings. This gives the model its flexibility in the longitudinal midship plane. The joints between the segments are sealed with a flexible neoprene membrane of negligible stiffness to obtain a water-tight joint.

Each segment was individually ballasted to simulate the weight distribution of the prototype vessel during the 1984 dedicated trials reported in [3]. Table 2.2 lists the scaled target weight distribution during these trials, the bare shell weight distribution, and the test weight distribution which was achieved during these tests. The exact weight distribution during the 1984 trials could not be modelled since the bare shell weight of three segments is larger than required. To correct this problem, the excess weight is redistributed to adjacent segments keeping the first moment about the centre of gravity constant. However, this is not considered to produce serious distortion in the mode shapes, since it did not exhibit noticeable distortions in earlier testing.

The stiffness distribution along the model is obtained by connecting adjacent segments with simply-supported spring bars at a known distance above the neutral axis bearing. The stiffness of each joint is adjusted by varying the clamp of the spring bar. This provides a convenient method for altering the natural vertical bending frequencies of the model. However, the vertical bending frequencies of the model were not adjusted during these tests. The target vertical vibratory frequencies given in [3] were scaled to produce the target frequencies for the model. Table 2.3 lists the target frequencies and the actual vibratory frequencies measured. The pitch response frequency measured in the hammer tests is to within 1.2% of the target. The first vertical bending frequency in these tests is approximately 6.0% below target, and the second vertical bending frequency is approximately 10.6% above target. These were considered acceptable. However, it should be mentioned that discrepancies between the shaker and hammer tests were observed in the prediction of the vibratory frequencies. This discrepancy will be discussed later, but since hammer tests were originally used to adjust the model properties in previous test programs, only the hammer test results are used here.

FIGURE 2.1

PLATE OF THE SEGMENTED FLEXIBLE MODEL

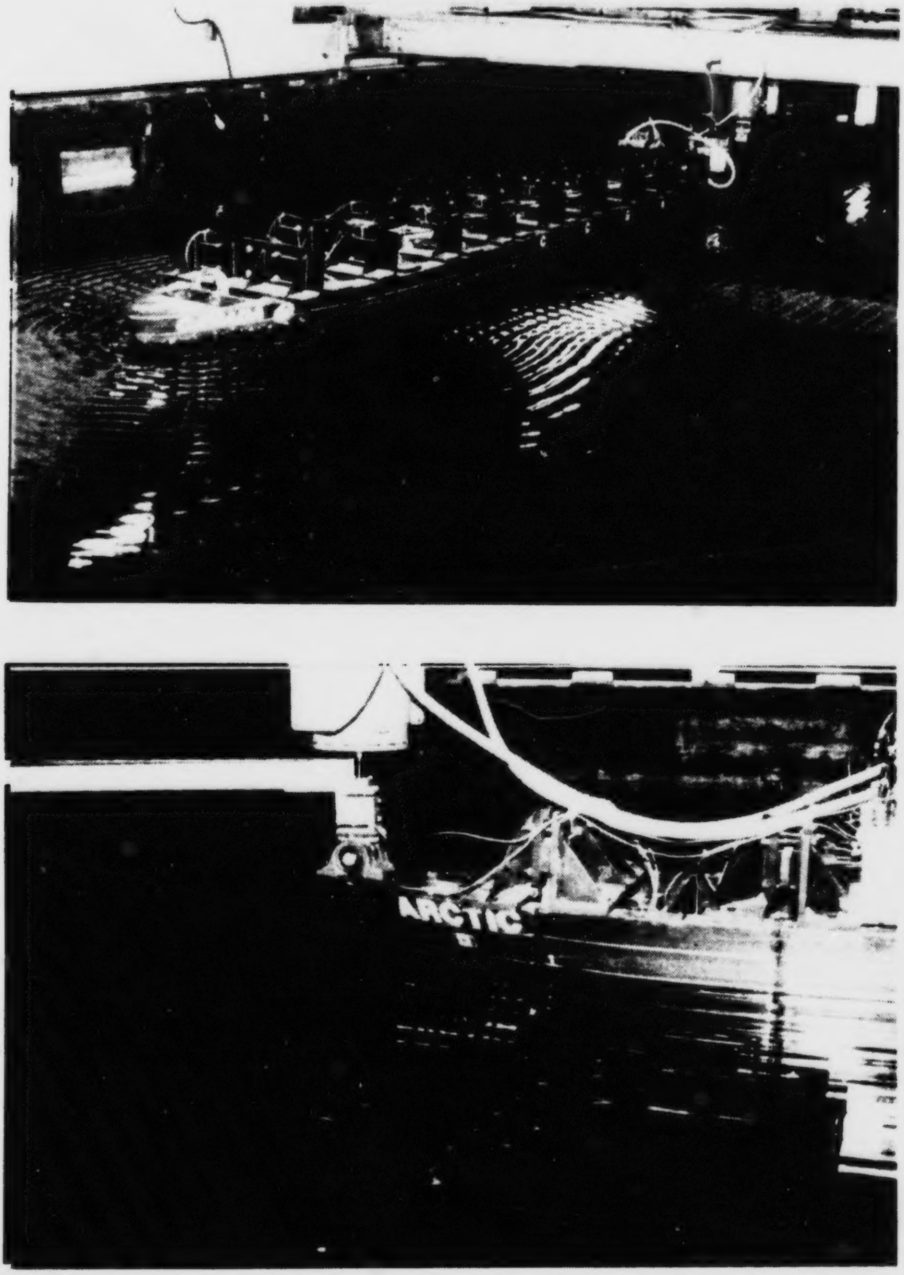

TABLE 2.1

MV ARCTIC PRINCIPAL PARTICULARS

SHIP HULL DATA SHEET

SHIP NAME: MV ARCTIC (Original Bow) **SCALE:** 1:40

DIMENSIONAL PARAMETERS	F.S.	M.S.	DIMENSIONLESS PARAMETERS	
L_{oa} =	209.5	5.24 (m)	Cb = .76	β_5 = 0 deg.
L_{bp} =	196.6	4.91 (m)	Cbf = .80	
B =	22.9	0.57 (m)	Cp = .76	f = 0.1
T =	10.97	0.27 (m)	C_w = .88	
D =	38,104	0.595 (tonne)	γ = 30 deg	

STATION	0	1/2	1	2	3	4	5
α	32.8	30.8	27.2	15.2	6.3	0	0
β	55.4	44.1	35.0	19.6	6.3	0	0

TABLE 2.2

MODEL BALLAST DISTRIBUTION

SEGMENT	TARGET TEST MASS* (kg)	ACTUAL SHELL MASS (kg)	REQUIRED BALLAST (kg)	ACTUAL LEAD BALLAST (kg)	ACTUAL TEST MASS (kg)
BOW 1	27.0	22.62	4.38	0.00	22.62
2	16.8	31.71	(-14.91)	0.00	31.71
3	57.1	41.19	15.91	5.38	46.57
4	77.6	37.04	40.56	40.56	77.60
5	73.1	37.03	36.07	36.07	73.10
6	88.9	36.21	52.69	52.69	88.90
7	44.2	36.79	7.41	3.27	40.00
8	33.4	36.79	(-3.39)	0.00	36.79
9	56.8	36.79	20.01	20.76	57.55
10	64.7	36.21	28.49	28.49	64.70
11	37.2	32.70	4.50	3.43	36.13
12	18.7	19.77	(-1.07)	0.00	19.77
TOTAL	595.5	404.83	190.67	190.66	595.44

* Based on full-scale weight distribution during 1984 trials.

TABLE 2.3

MV ARCTIC MODAL PROPERTIES

VIBRATORY MODES	CALCULATED FREQUENCIES		MEASURED FREQUENCY**
	FULL SCALE* (Hz)	MODEL SCALE (Hz)	(Hz)
Quasi rigid - heave/pitch	0.11	.70	-
Quasi rigid - pure pitch	0.13	.82	0.83
1st Vertical Bending	0.93	5.88	5.53
2nd Vertical Bending	1.98	12.5	13.82
3rd Vertical Bending	3.12	19.7	24.50
4th Vertical Bending	3.98	25.2	33.38
5th Vertical Bending	4.86	30.7	-
6th Vertical Bending	5.26	33.3	-
7th Vertical Bending	5.80	36.7	-

* Vibratory frequencies estimated using a finite element model in [2].

**Measured frequencies from the wet hammer tests in deep water [2].

2.2 Modal Properties of MV ARCTIC Model Using Finite-Element Methods

As discussed in Section 2.1, it is necessary to determine the dry mode shapes and frequencies of the scaled structural model in the absolute, free-free state. This can only be achieved in a numerical model.

A simple structural model of the MV ARCTIC based on the finite element approach was built to predict the hull response modes in the longitudinal midship plane. A lumped spring-mass idealization was used to model the hull girder response and the associated masses of the ship segments. The approximation inherent in modelling the ship as a series of beam elements is that plane sections remain plane and the bending stress distribution varies linearly through the depth of the section. It is believed that for present applications such assumptions will be sufficient to accurately predict the first few modes of hull response. The essential structural properties required to prepare the stiffness model for bending in the longitudinal midship plane are the second moment of area of the sections about the neutral axis and the Young's modulus. These values were first estimated from the full scale properties and then refined through a trial and error procedure that improved the comparison between the predicted and measured modal frequencies. The nodes of the hull girder finite element model were chosen to coincide with the location of the accelerometers. In total 12 nodes were used along the hull. The stiffness of the hull was characterized by 'beam' finite elements having three degrees of freedom at each node. Two translations parallel and perpendicular to the keel and a rotation about the normal to these axes.

Experimental determination of the dry mode shapes and frequencies were carried out using a specially built test rig as described in Section 3.1. In order to confirm that the numerical prediction is capable of reproducing the mode shapes and frequencies in the dry test mode, the supporting frame and springs were also incorporated in the finite element model. Beam elements were used for the frame and struts with equivalent stiffness for the springs. The complete assembly of nodes and elements is shown in Figure 2.2.

Computed Dry Natural Frequencies and Mode Shapes

The natural frequencies and mode shapes predicted using the finite element model were compared with those measured in the experiments in Figures 2.3 and 2.4. The finite element model predicts the first two natural frequencies very closely. The errors in the prediction are shown in Table 2.4. In both Figures 2.3 and 2.4 the data points marked 'multi degree of freedom' show close agreement with the predictions. The third flexural frequency measured from the physical model is substantially different from that predicted by the beam element numerical model, indicating that the segmented physical model does not behave as a non-uniform beam at this frequency. In general, there is very good agreement between the measured and the predicted mode shapes. However, Figure 2.4 suggests that further calibration of the model is required before using it for analyzing higher mode shapes and frequencies.

FIGURE 2.2 ASSEMBLY OF NODES AND ELEMENTS

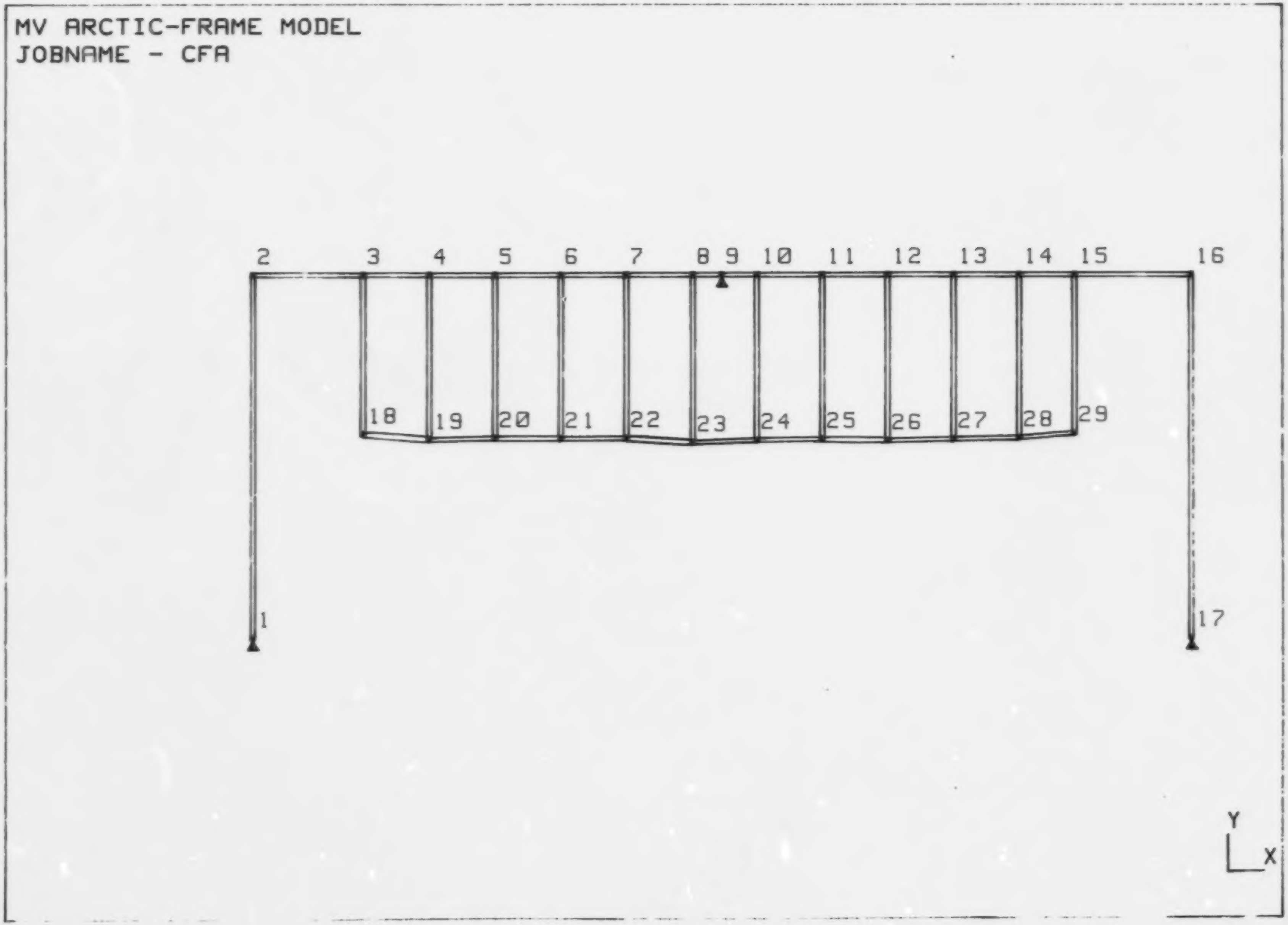

FIGURE 2.3 FIRST FLEXURAL MODE

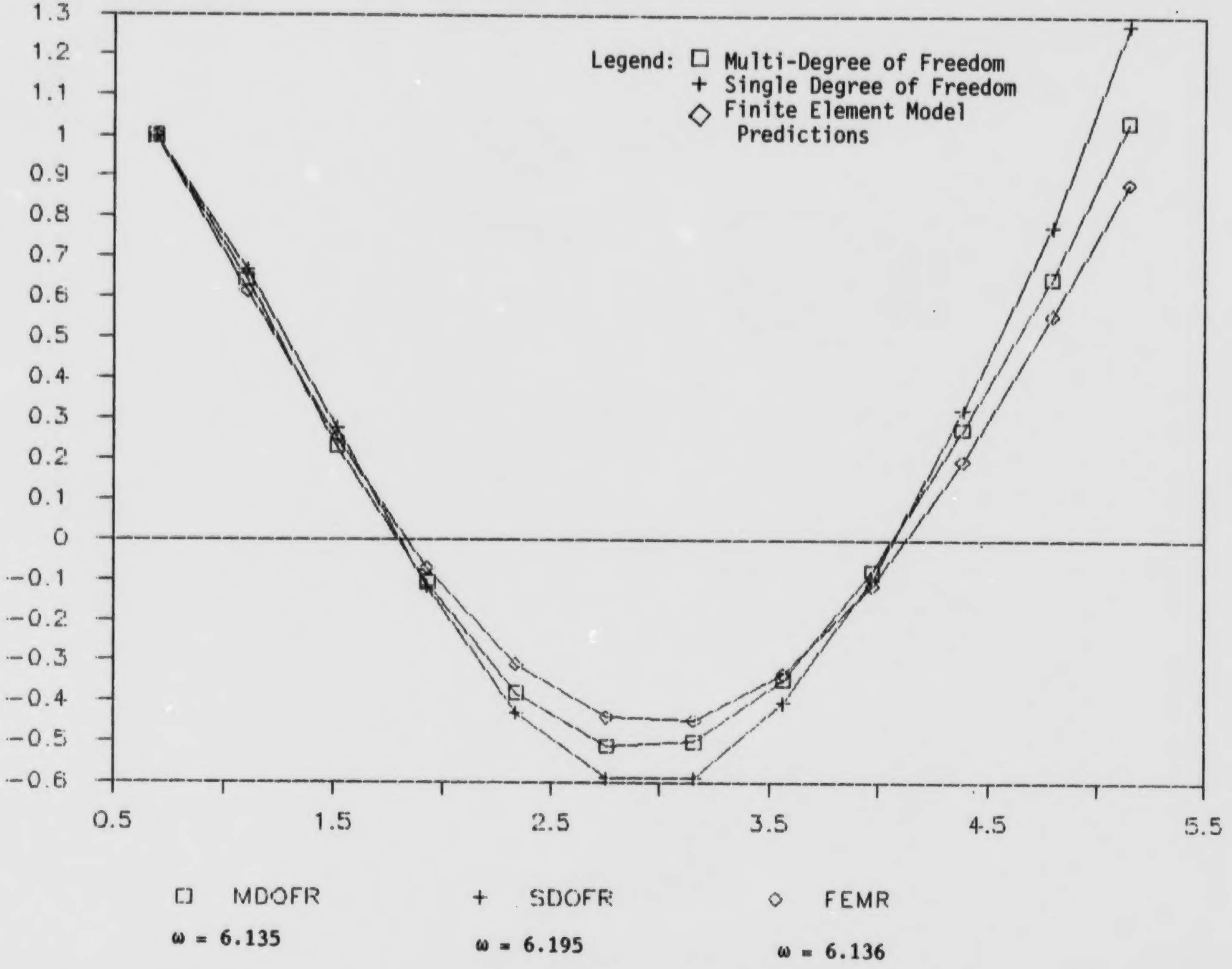

FIGURE 2.4 SECOND FLEXURAL MODE

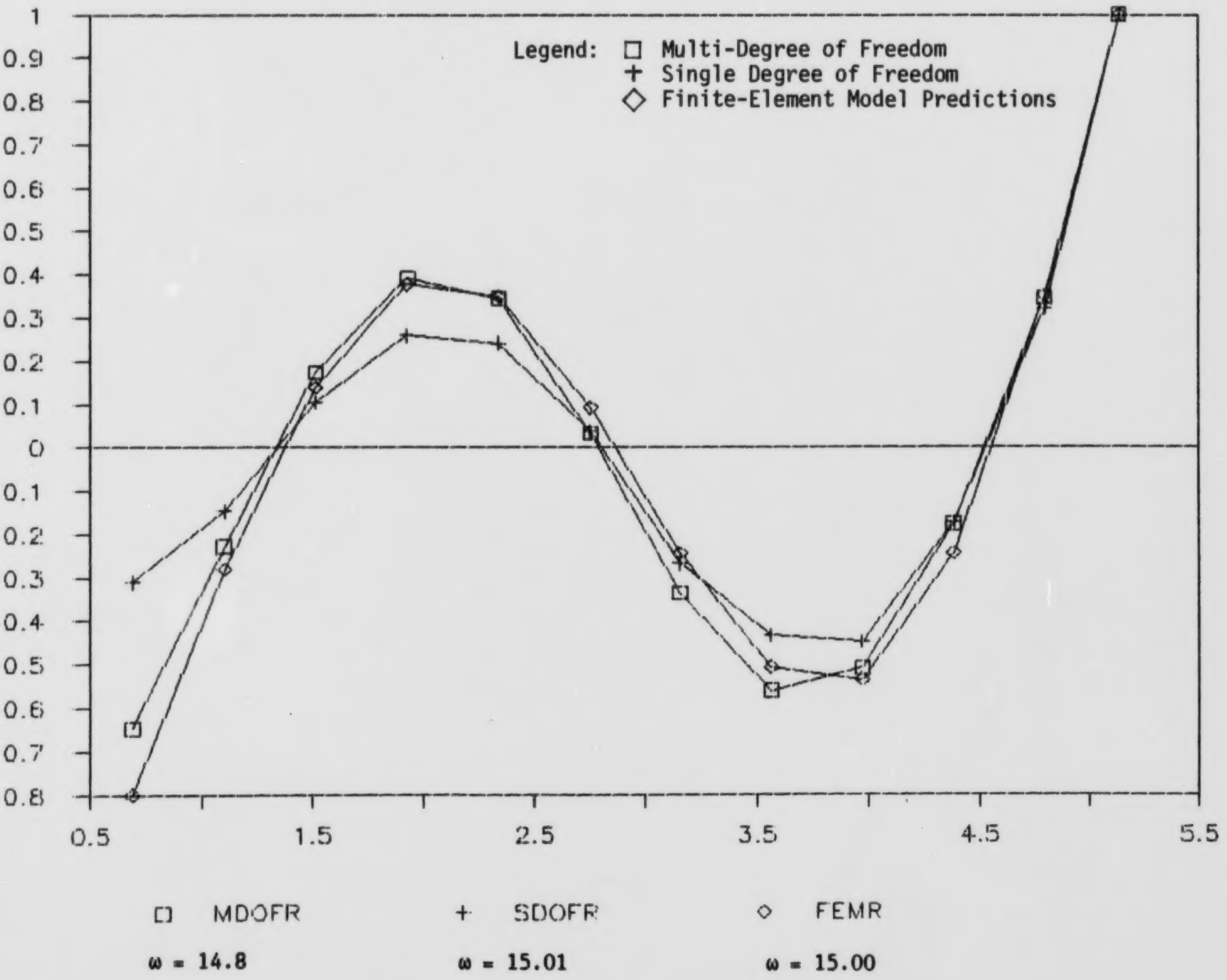

TABLE 2.4

PREDICTED AND MEASURED DRY NATURAL FREQUENCIES

MODE No.	Type	NATURAL FREQUENCY, Hz Measured	Predicted	Error %
1	Flexural	6.135	6.136	0.01
2	Flexural	14.80	15.00	1.35
3	Flexural	21.50	26.85	12.48

3. TEST PROGRAM

3.1 Overview

The overall experimental program can be divided into two major categories: Dry tests with the model supported by 'buoyancy' springs; Wet tests with model in open water as well as in ice. Additional tests were also attempted in the wet rigid body modes to isolate hydrodynamic added mass and damping characteristic of those cases. Table 3.1 summarizes the entire model test program, listing the primary objective of each series, file names assigned for data logging and other identifying test parameters.

3.2 Vibration Test Equipment

Common to all types of present-day vibration testing is the use of an electrically controlled vibration machine which produces the mechanical motion to which the test specimen is subjected. The most widely used vibration machine is the electrodynamic shaker, which is basically a large "loud-speaker" system. Another frequently used shaker is based on electrohydraulic principles. While the electrohydraulic shaker is capable of operating at very low frequencies (theoretically down to DC), it allows very large strokes (up to 30 cm), and has a very high force capability (over 50 tons of oscillatory force). The electrodynamic shaker has a number of advantages specific to this project:

- Precise control of stroke at low frequencies
- Over 200 Newton (45 lb.) from a shaker weighing just over over 20 kg (50 lb).
- 1-5000 Hz continuously variable frequency range
- Voltage feedback amplifier provides random and transient excitation capability

For the present tests, it is adequate to achieve a frequency range of 0-100 Hz and deflection amplitude range of 0.1 to 5 mm. A chart showing the typical regions of operation of the two types of vibration machines is shown in Figure 3.1. An MB Modal 50 electrodynamic shaker was chosen for the present application. A complete list of specifications of the shaker is attached to Appendix A, along with a brief description of the principle of operation.

3.3 Dry Mode Tests

The apparatus used for the dry tests is shown in Figure 3.2. The support framework was built from steel I beams and C channels. The minimum static stiffness of this structure was calculated to be 1300 times that of the corresponding spring. Therefore, statically this structure was adequate. However, the natural frequency of this structure was within the range of the desired model response frequency. To increase the natural frequency of this structure to

Figure 3.1

OPERATIONAL CHARACTERISTICS OF HYDRAULIC AND ELECTRODYNAMIC VIBRATION MACHINE

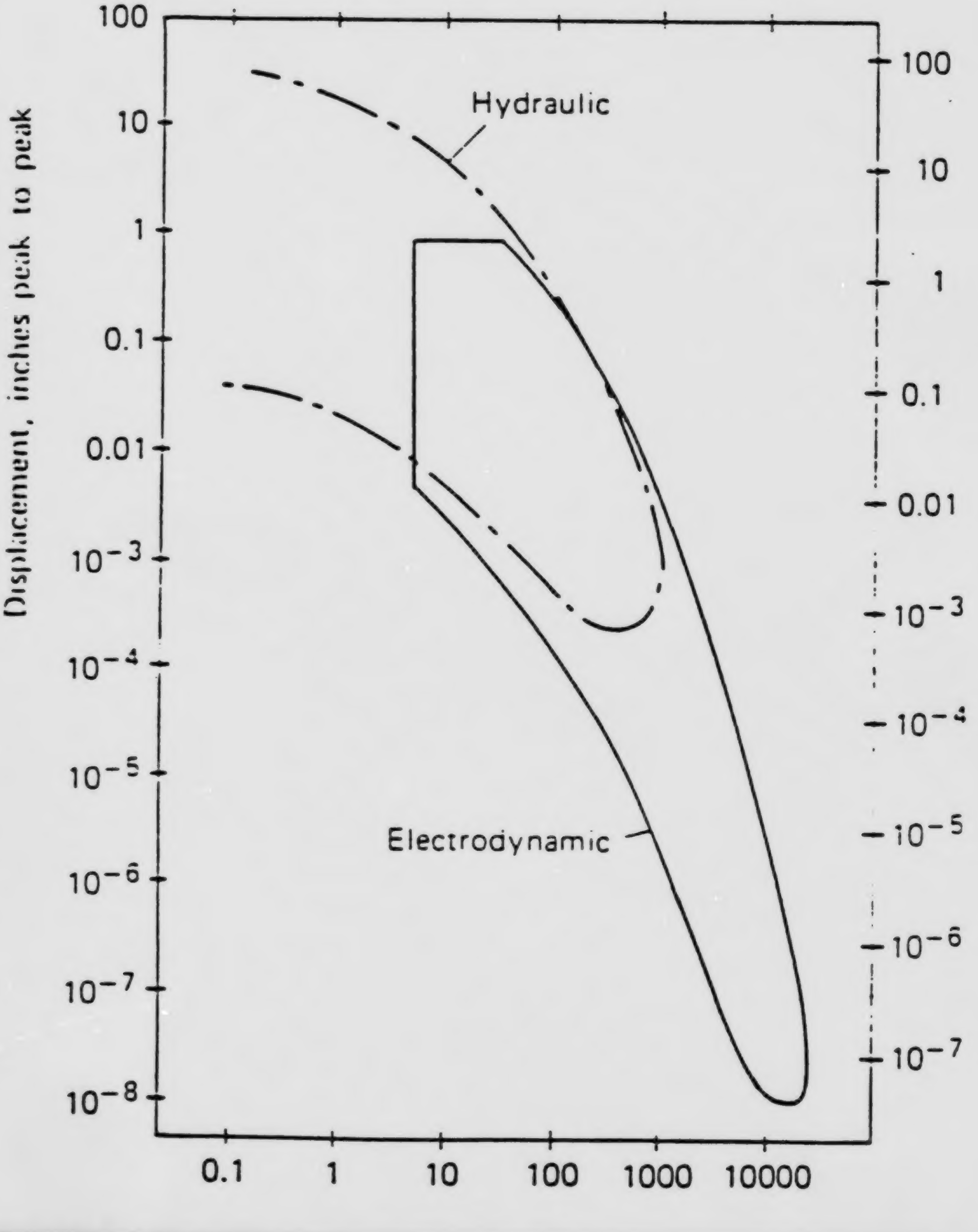

TABLE 3.1
EXPERIMENTAL TEST PROGRAM

TEST NAME	WATER DEPTH (m)	FULL SCALE VELOCITY (knots)	EXCITER LOCATION	OBJECTIVE	BEGINNING FILENAME	LAST FILENAME	NUMBER OF TESTS *1	FREQUENCY RANGE (Hz)
Frame Tests	N.A.	N.A.	as noted	Hammer tests on dry support frame to determine its modal properties	FRM01	FRM13	13	0 - 50
Dry Hammer	N.A.	N.A.	Bow	Hammer tests on the model supported by springs, to determine its dry modal properties	DRYH01	DRYH39	38*[2]	0 - 50
Dry Shaker	N.A.	N.A.	Bow	Shaker tests on the model supported by springs, to determine its steady state dry modal properties	DRY01	DRY144	143*[3]	0.8 - 100
Wet Hammer	1.424	0	Bow	Hammer tests on the model to determine its hydrodynamic added mass	WETH01	WETH40	40	0 - 50
	0.411	0	Bow	Hammer tests on the model to determine the effect water depth has on added mass	WETH51	WET90	40	0 - 50
Wet Shaker	1.424	0	Bow	Shaker tests on the model to determine its steady state hydrodynamic added mass	WET001	WET120	120	0.8 - 50
	1.424	1	Bow	same as above	WET201	WET252	52	1.1 - 35*[4]
	1.424	3	Bow	same as above	WET301	WET339	39	1.1 - 35*[5]
	1.424	6	Bow	same as above	WET401	WET452	52	1.1 - 35*[4]
	1.22	0	LCG	Shaker tests on the model to determine its steady state modal properties in heave	WET501	WET513	13	0.8 - 5
Level Ice	1.424	0	Bow	Shaker tests on the model while surrounded by ice, to determine the effect a level ice sheet has on the hydrodynamic added mass	ICE001	ICE105	105	0.8 - 35
Rigid Model	1.424	0	Bow	Shaker tests on the model modified with stiffeners to determine if the flexibility of the model influences the added mass	RIG001	RIG009	9	0.8 - 1.6
	1.424	6	Bow	same as above	RIG101	RIG109	9	0.8 - 1.6
Amplitude Variation	1.424	0	Bow	Shaker tests on the model in water to determine the effect forcing amplitude has on the model's motion	AMP001	AMP011	11	5.4
	1.424	0	Bow	same as above	AMP012	AMP022	11	10.3

*1 This is the number of separate tests, however some tests may have more than one file.

*2 One test had a poor data channel, and was dropped from the analysis.

*3 One test was never digitized, and was later repeated.

*4 Only the first two flexural modes were analyzed in detail due to time limitations.

*5 Only the first flexural mode was analyzed in detail due to time limitations.

Figure 3.2 SET-UP FOR DRY TESTS

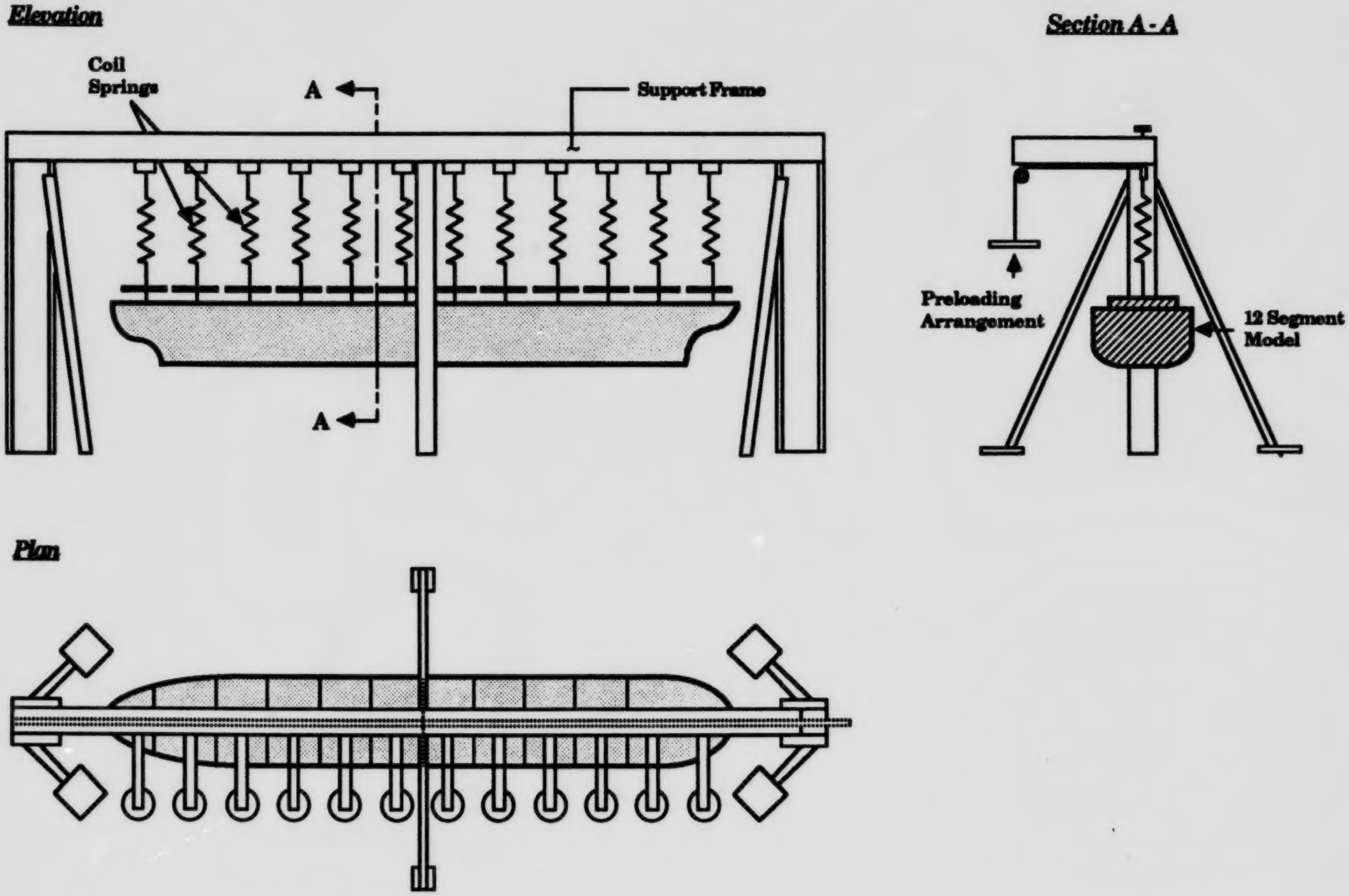

above 30Hz, would require an enormous frame. Therefore, the approach taken was to measure and record the frame response, and adjust the data accordingly, if necessary. The model was supported by twelve wire cables. Each cable was attached to the model through springs mounted approximately at the waterplane centerline for that segment. The values of the spring constants for each segment are given in Table 3.2.

The wire above the springs was fed through a cable clamp, and over a pulley to a loading pan. The cable clamps and pulleys were rigidly mounted above the model.

Before the test, the mass for each segment was determined, and the segments ballasted accordingly. Once the model was completely ballasted, the loading pans were loaded to the same weight. The model was then lifted off the ground, connected to the shaker, and trimmed with the model level. The cable clamps were then tightened, and the test was ready to begin.

The shaker was mounted on the bow segment in such a way as not to interfere with the spring support system. The top of the shaker was mounted in such a manner as to apply only a vertical excitation.

3.4 Wet Mode Tests

The wet tests were performed in Arctec Canada's Kanata ice basin. The model was restrained in roll, surge and sway with a low mass and low inertia heavestaff as shown in Figure 3.3. To provide sufficient surge restraint with as little mass as possible, a horizontal "A frame" was constructed using aluminum. At one end a bearing arrangement was fixed to the carriage. At the apex of the "A frame", the shaker had its base fixed to the carriage, and its actuator fixed to the heavestaff. Between the end of the heavestaff and the model a vertical dynamometer recorded the excitation to the model.

The wet hammer tests performed on the model were done with the model approximately in the centre of the basin. Due to the test configuration, no velocity effect could be examined. The first series of tests were in 1.424 meters of water, or a depth to draft ratio of approximately 5.2. The second series of hammer tests were performed in 0.411 meters of water. This depth represents a depth to draft ratio of 1.5. It should be noted that due to physical limitations of reaching the model at this shallow depth, two obstacles were placed in the water in the vicinity of the bow. Their profile, in the direction of wave propagation was kept to a minimum. They were both placed approximately 0.75 meters from the starboard bow, and had a horizontal profile each of approximately 0.10 meters. Their effect is not known, however, it is thought that their influence should be negligible.

TABLE 3.2

SEGMENT DETAILS

SEGMENT NO.	SPRING CONSTANT (kg/m)	SEGMENT MASS (kg)	SEGMENT CENTROID (m)
BOW: 1	94.48	22.62	4.648
2	207.63	31.71	4.291
3	233.73	46.57	3.891
4	234.07	77.60	3.481
5	234.07	73.10	3.072
6	234.07	88.90	2.662
7	234.07	40.00	2.253
8	234.07	36.79	1.843
9	233.74	57.55	1.434
10	224.99	64.70	1.027
11	186.19	36.13	.625
STERN:12	111.63	19.77	.222
TOTAL		595.44	

Figure 3.3 HEAVE STAFF for WET SHAKER TESTS

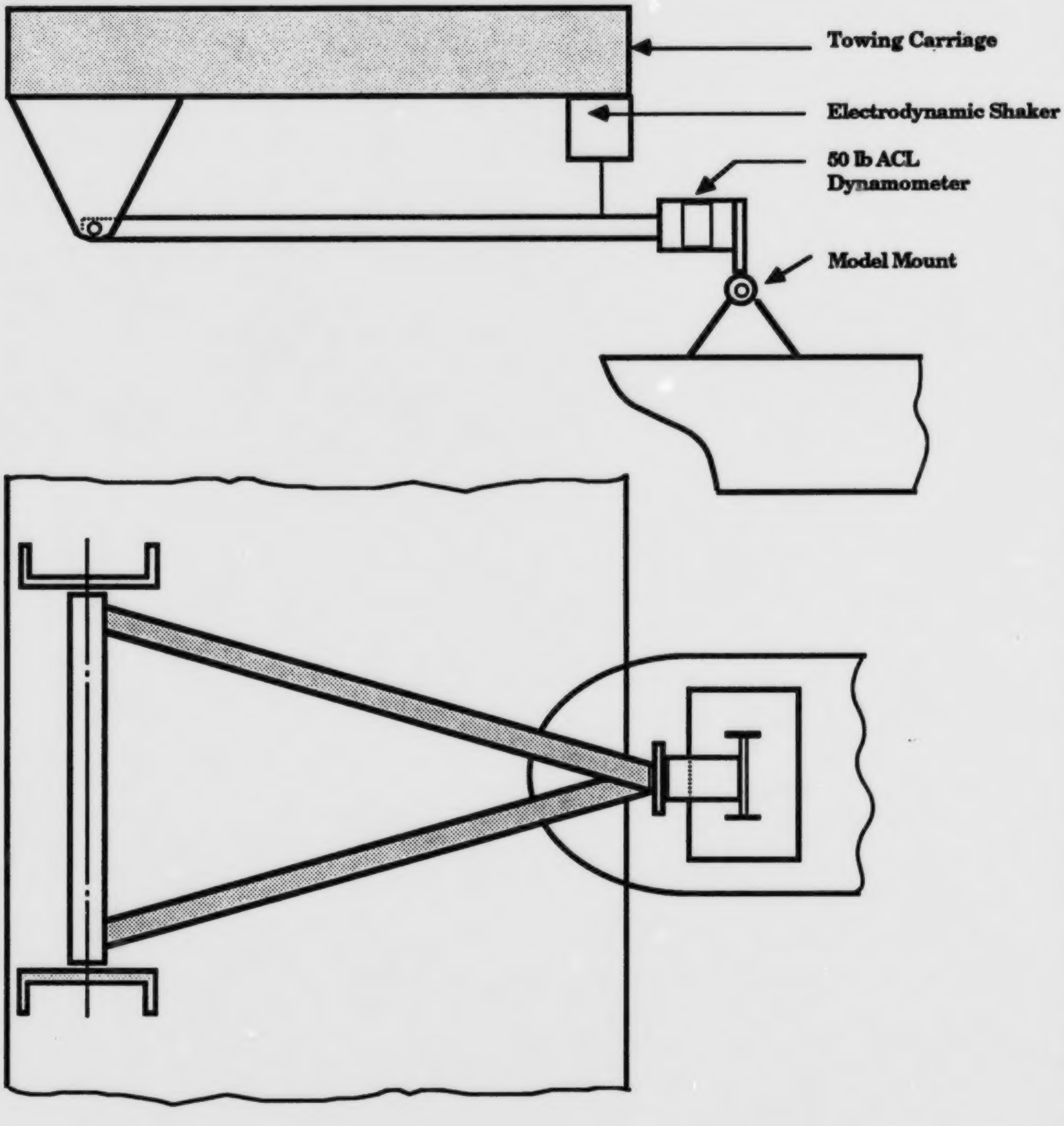

The stationary wet shaker tests were performed in the centre of the basin. There was approximately 2.16 meters to each of the side walls and approximately 12.5 meters to each end wall. No wave absorbing device was thought to be necessary during these tests due to the short wave lengths generated. However, rather long wavelengths were generated for frequencies between 0.8 and 1.5 hz. These waves were generated lengthwise along the basin with a wavelength of approximately twice the ship length. As such, tests performed within this frequency range had to be performed immediately following the shaker's excitation, to eliminate any reflected wave effect. Usually, for tests within this frequency range, a number of tests were performed and the best one used in the data analysis.

The towed shaker tests were also performed as close to the centre of the basin as possible. At 1.0 knots, the model would travel approximately 0.83 meters while the test was being performed. However, at 6.0 knots, the model would travel about 5 meters during the actual test. Including acceleration length, deceleration distance, and letting the model come to steady state, two thirds of the basin was used. For some tests at 6.0 knots some wave reflection problems were observed before the test began when the model was nearer to the end wall. However, once the towing carriage was started and the model moved away from the wall, these problems subsided to the point that they were not observed during the steady state portion in the middle of the basin when the data was collected.

The final wet tests were performed using the same test rig described above, however the shaker location was moved to the CG. For these tests, the shaker position was directly over the joint between segments six and seven, but was only connected to segment seven. Because the shaker location was above a joint, the shaker mount on the model had to move upwards by 0.20 meters to provide clearance under the towing carriage. As a result, the water level in the basin had to be lowered by the same amount. This reduced the depth to draft ratio from 5.2 to 4.4. From work completed by [4], this reduction will have negligible effect on the results.

3.5 Ice Cover Tests

The ice cover tests were performed using the same apparatus described for the wet tests. However for the ice test, a scale model ice sheet with a full scale thickness equivalent to 1.1 meters and an elastic modulus of approximately 660 MPa was prepared. The ice sheet was pre-cut as shown in Figure 3.4 for approximately 10 meters. The remaining 14 meters of ice was used to monitor the ice properties during the day. The channel width was selected to be 10% larger than the model's beam, plus twice the ice thickness. This produced a channel width of 0.68 meters. The individual floes were cut to a ratio of 4:1.

Figure 3.4 PRE-CUT ICE COVER FOR STATIONARY TESTS IN ICE

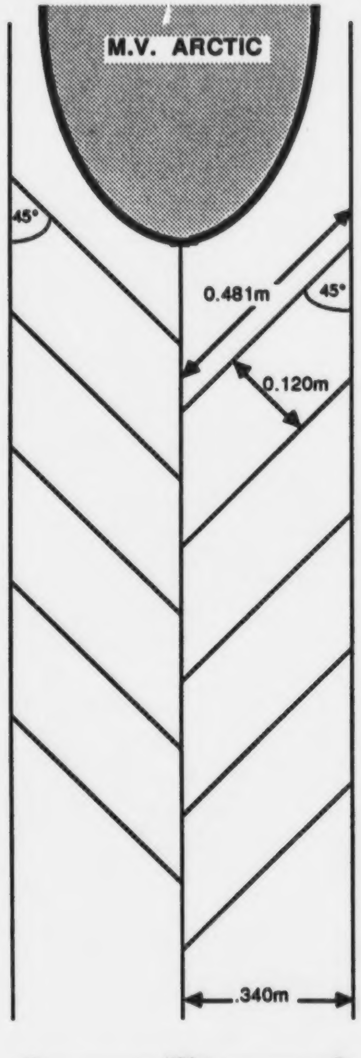

Once the ice sheet was cut, the model was slowly towed into position trying to displace only the ice floes that would normally be displaced during level icebreaking. The model was towed until the bow touched the last set of pre-cut floes, and the test was ready to begin. Figure 3.5 shows the position of the model in the ice sheet for these tests.

Since the time taken to perform the shaker tests was approximately 6 hours, during this time the ice would naturally decay. Every effort was made to keep the ice sheet as constant as possible, however, it is a property of doped refrigerated ice that once the temperature rises to the point where the ice stops growing, the ice begins to rot. In typical ice tests, the ice sheet is permitted to decay to the desired strength and then tested. However, since the duration of the shaker tests was rather long, this approach was not possible. Instead, the important ice properties were measured periodically during the shaker tests to record the condition of the ice. Since the elastic flexure of the ice was considered to be an important factor in influencing the hydrodynamic added mass, the elastic modulus was measured periodically. During the shaker tests the ice sheet never fails. Therefore the flexural strength was not considered to be important, and possibly detrimental to the shaker tests, and not measured. The ice thickness was also considered to be important. However, the ice thickness was reasonably stable with time, and therefore only measured once.

3.6 Miscellaneous Tests

As well as the above tests, two other small series of tests were performed. For the first series, the model was stiffened by bolting each segment together. With the model almost rigid, shaker tests in the frequency range of the rigid body modes of heave and pitch were performed. These tests were performed with the model stationary and at a speed of 6 knots.

Although the model was considerably stiffer than before, flexural modes could still be observed. To stiffen this model to the point of being considered rigid would require a continuous keel. These modifications were beyond the scope of this project.

The second series of tests were to investigate the effect of changing forcing amplitude. This was necessary since during the tests, the forcing amplitude was varied to give the maximum signal output without damaging the model or the instrumentation. The reason for this approach was that for a linear elastic system, motion varies linearly with force. Therefore, it does not matter what force is chosen if the system is linear. These tests were performed to check this hypothesis.

The amplitude tests were performed in water with the model stationary using the same method described for the wet tests. Two frequencies were selected: approximately the first flexural mode and approximately half way between the first and second flexural modes. For each frequency, 10 forcing amplitudes were used.

Figure 3.5 **POSITION OF MODEL RELATIVE TO ICE SHEET**

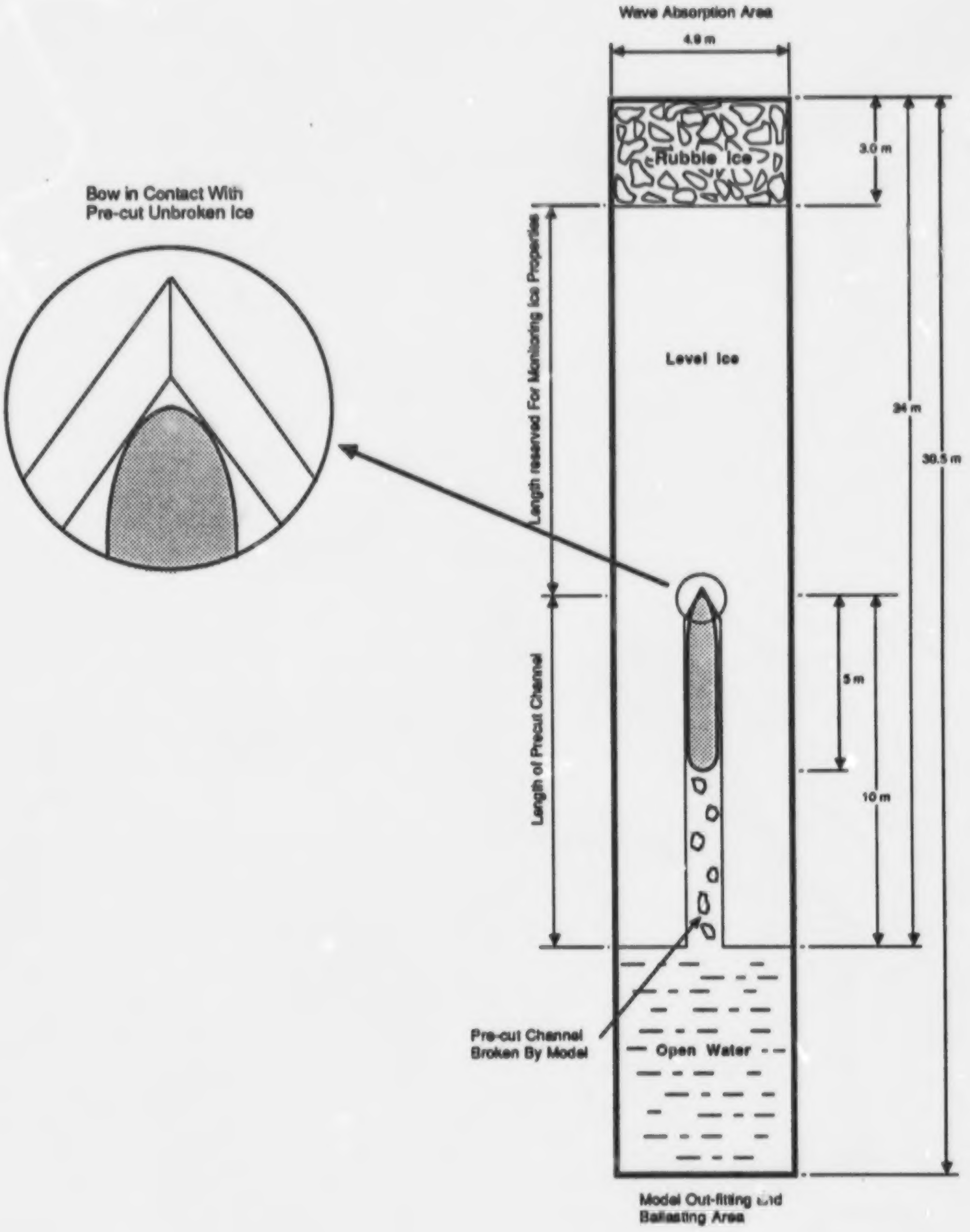

3.7 Instrumentation System

A schematic of the instrumentation system is shown in Figure 3.6. Twelve accelerometers were located on the model one at each segment. Between each segment a strain gauged bar measured the hull bending moments. These were conditioned with Vishay model 2100 series strain gauge amplifiers.

The forcing function was measured with a 25 kg (55 lb) strain gauge dynamometer for the shaker tests, and a 1000 kg (2200 lb) strain gauge dynamometer for the hammer tests. Both of these were conditioned with Vishay model 2100 series strain gauge amplifiers.

Figure 3.7 shows the precise location of each transducer for all ship model tests.

The carriage speed and position for the towed wet tests were measured with the standard potentiometer pick-up on the ice carriage drive system.

All 26 analog channels plus one voice channel were recorded on a Honeywell 5600E 28 channel Analog Tape recorder. The accelerometer data, forcing function data, and carriage speed data were recorded digitally with a 16 channel A/D 200 scanning card mounted in a HP9816S Computer. The digital data was then stored on an HP9144A tape drive.

For the tests performed on the dry support frame, nine accelerometers and one force dynamometer were used. These accelerometers and force dynamometers are the same ones used for the ship tests. Figure 3.8 shows the location of each transducer for the frame tests.

Figure 3.6 INSTRUMENTATION DATA ACQUISITION SYSTEM

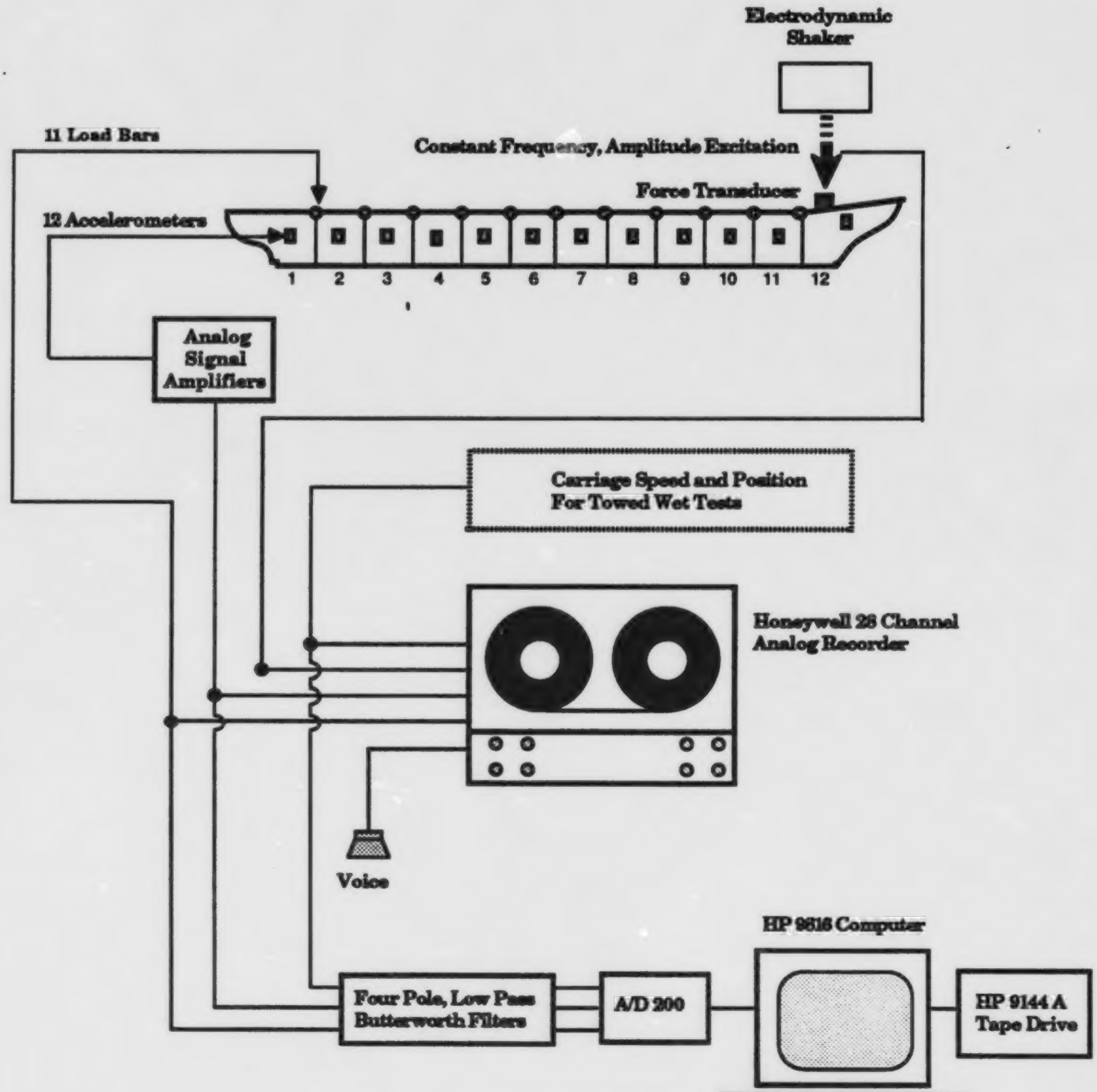
Electrodynamic Shaker
11 Load Bars
Constant Frequency, Amplitude Excitation
Force Transducer
12 Accelerometers
1
2
3
4
5
6
7
8
9
10
11
12
Analog Signal Amplifiers
Carriage Speed and Position For Towed Wet Tests
Honeywell 28 Channel Analog Recorder
Voice
HP 9816 Computer
Four Pole, Low Pass Butterworth Filters
A/D 200
HP 9144 A Tape Drive

Figure 3.7 MV ARCTIC MODEL INSTRUMENTATION

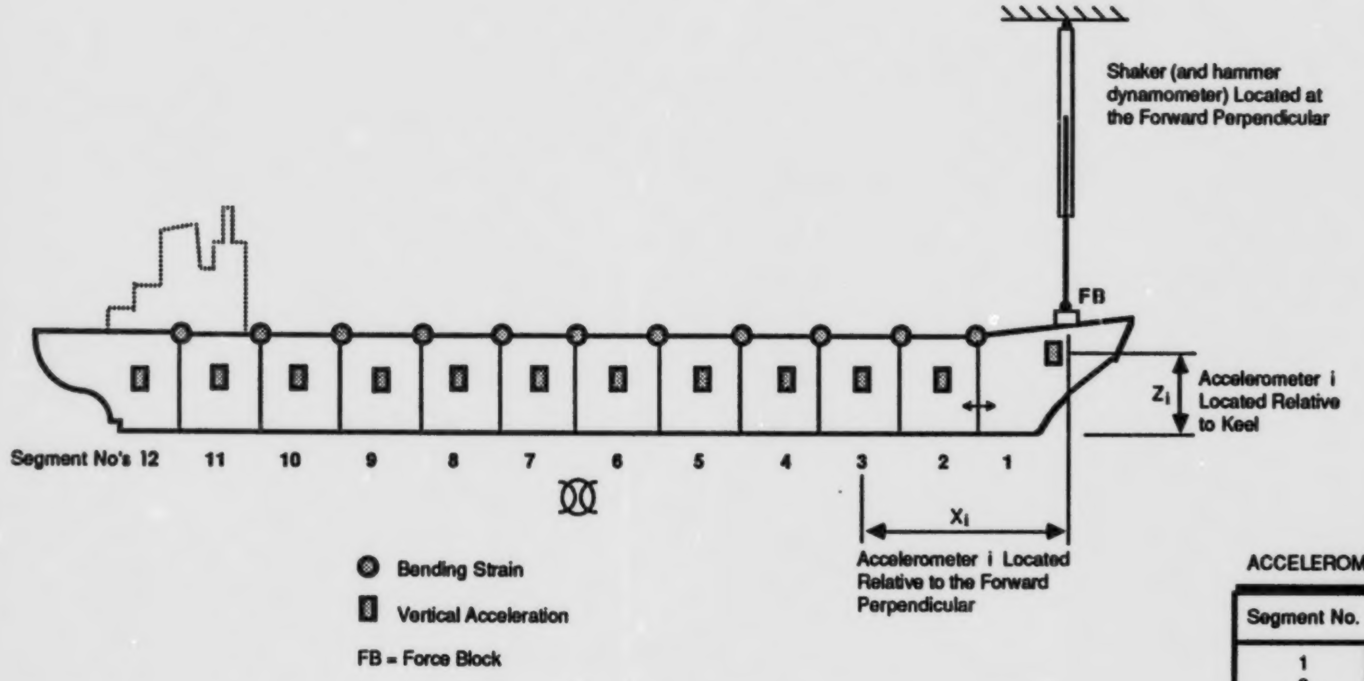
Shaker (and hammer dynamometer) Located at the Forward Perpendicular
FB
Z_i
Accelerometer i Located Relative to Keel
Segment No's 12
11
10
9
8
7
6
5
4
3
2
1
X_i
Accelerometer i Located Relative to the Forward Perpendicular
Bending Strain
Vertical Acceleration
FB = Force Block

ACCELEROMETER LOCATIONS

Segment No.	X_i (m)	Z_i (m)
1	.224	.333
2	.657	.298
3	1.050	.307
4	1.463	.303
5	1.873	.307
6	2.288	.310
7	2.689	.295
8	3.099	.301
9	3.507	.291
10	3.919	.301
11	4.329	.309
12	4.675	.339

Figure 3.8 **INSTRUMENTATION USED DURING FRAME HAMMER TESTS**

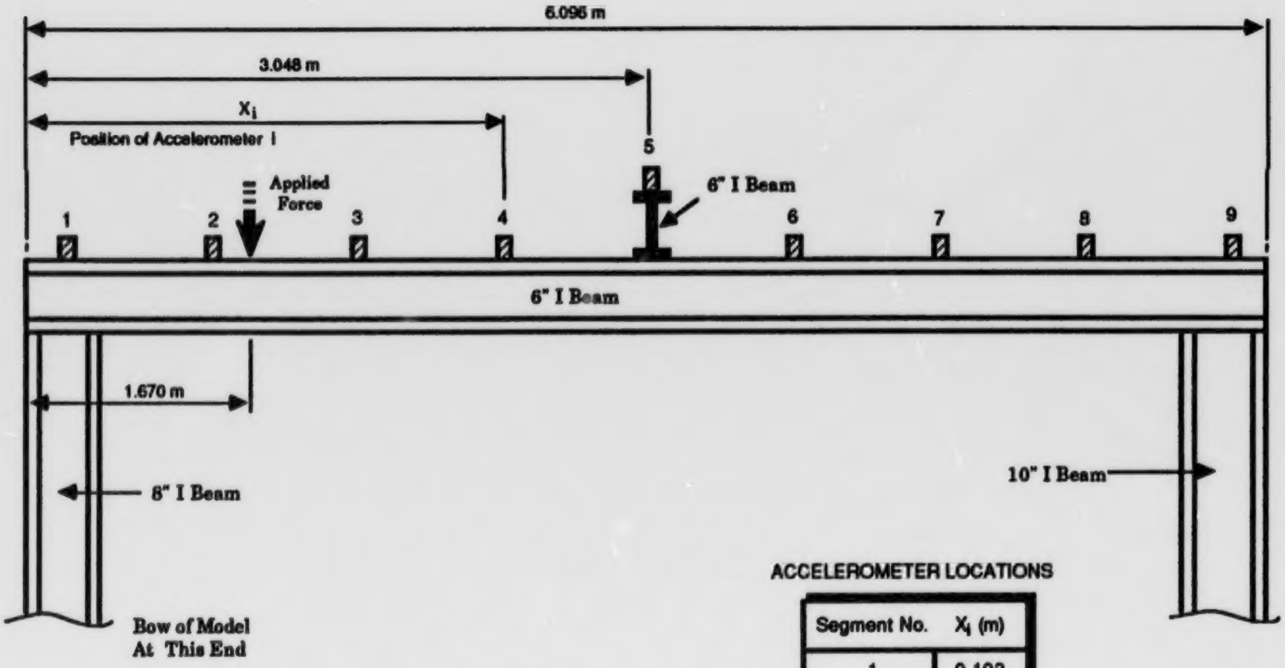

ACCELEROMETER LOCATIONS

Segment No.	X_i (m)
1	0.102
2	0.838
3	1.575
4	2.311
5	3.048
6	3.778
7	4.509
8	5.239
9	5.969

4. TEST PROCEDURES AND DATA PROCESSING

The test procedures and data processing method followed for the hammer tests were essentially the same for all hammer tests, including the frame tests, the dry hammer tests and the wet hammer tests. Similarly, the methods followed for the shaker tests were the same for all shaker tests, including the dry shaker tests, the stationary and towed wet shaker tests, and the ice shaker tests. Therefore, a discussion of each individual test will not be necessary, and only a general discussion on the two types of tests will be provided. Also included will be a description of the pre test preparations and post test analysis. Figure 4.1 shows a schematic flow chart of the entire test procedure and data processing method.

4.1 Test Preparations

The first step was the calibration of all transducers and equipment used. This included a calibration of the analog tape recorder, analog amplifiers and digital A/D unit. Once the individual components were calibrated and gained, the accelerometers and force dynamometers were calibrated through the complete system. Each transducer was assigned a specific data channel, analog filter, analog amplifier and computer channel. Although all components are interchangeable, this reduces the possible sources for error and improves the quality and accuracy of the results.

The accelerometers were expected to see approximately a 1 g acceleration. Therefore they were all calibrated statically on a tilt table from -1 to +1g. The force dynamometers were calibrated using a precision set of dead weights up to a maximum of 180N and 240N for the shaker and hammer dynamometers respectively. The dynamic range of interest for the tests was the first three flexural modes and the rigid body mode. This required a frequency range of up to 30 Hz. Therefore, the filter cut off frequency was set to 50 Hz, and the scanning frequency was set to be 200 Hz per channel (four times the filter frequency). For those shaker tests where frequencies above 50 Hz were required, a filter frequency of 150 Hz and a scanning frequency of 600 Hz per channel was selected.

A property of the filters used is that a phase shift occurs, and the phase shift depends on the ratio of the signal frequency to the filter cut off frequency. To remove errors associated with this phenomenon, all filters were set to the same cut off frequency. Therefore, the phase shift observed on all channels at each frequency will be the same.

Figure 4.1

OVERVIEW OF OSCILLATION TEST PROCEDURE AND DATA PROCESSSING

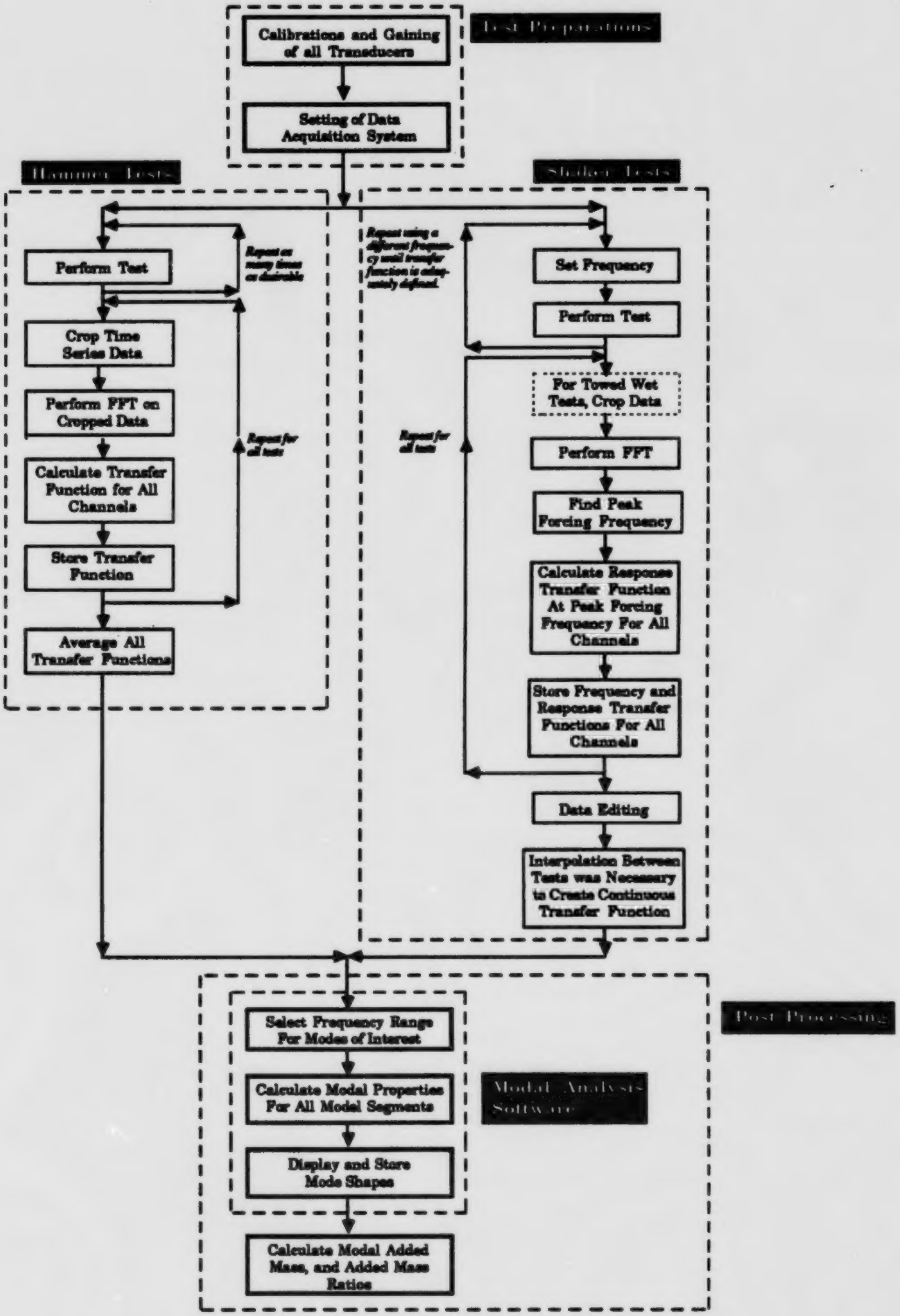
Test Preparations
Calibrations and Gaining of all Transducers
Setting of Data Acquisition System
Hammer Tests
Shaker Tests
Perform Test
Repeat as many times as desirable
Crop Time Series Data
Perform FFT on Cropped Data
Repeat for all tests
Calculate Transfer Function for All Channels
Store Transfer Function
Average All Transfer Functions
Repeat using a different frequency until transfer function is adequately defined.
Set Frequency
Perform Test
For Towed Wet Tests, Crop Data
Repeat for all tests
Perform FFT
Find Peak Forcing Frequency
Calculate Response Transfer Function At Peak Forcing Frequency For All Channels
Store Frequency and Response Transfer Functions For All Channels
Data Editing
Interpolation Between Tests was Necessary to Create Continuous Transfer Function
Post Processing
Select Frequency Range For Modes of Interest
Calculate Modal Properties For All Model Segments
Modal Analysis Software
Display and Store Mode Shapes
Calculate Modal Added Mass, and Added Mass Ratios

4.2 Hammer Tests

Once the system was calibrated, the hammer tests were ready to be performed. Since the average transfer function is to be derived by combining the results from a number of tests, the testing and data processing were performed separately. A large number of trials are required because the error in the frequency response amplitude decreases from unity as the square root of the number of repetitions. Therefore, the larger the number of tests, the better the results.

The hammer test was performed by impacting the force dynamometer with a rubber hammer. The rubber hammer was sufficiently rigid to excite frequencies well above 50 Hz, yet pliable enough not to damage the instrumentation. An attempt was made to only apply a vertical excitation with little influence from the arm holding the hammer.

Before the impact, the computer data acquisition system was started. Approximately 2 seconds of data was collected as a zero reference before the impact. Then an additional 8 to 13 seconds of data was collected following impact. Once data collection was finished and stored, a quick glance summary was displayed on the computer to show the maximum and minimum of all channels. If any channels approached or exceeded the A/D limit, voltage limit, or transducer limit, then corrective actions were taken. The summary was also used to check if all transducers were functioning, and if there was a doubt, the suspected channel was plotted and checked. When the data quality was verified, the test cycle was repeated.

When all hammer tests were complete, for each type of test, then the computer processing cycle began. The computer would first select the window to perform the FFT (Fast Fourier Transform). The FFT requires that the number of data points be to a power of 2. For the hammer tests, the window was selected to be 1024 data points. This represents a frequency resolution of approximately 0.20 Hz.

The window was automatically selected by finding the maximum force. The computer would then step backwards from the maximum force until the force was less than 1% of the maximum. This was defined as the beginning. The end was defined to be 1024 data points later. The FFT was calculated for all channels using the window defined from the force channel. The transfer function was then calculated and stored by dividing each acceleration spectrum by the force spectrum. This same process was repeated for all tests.

Once all transfer functions were calculated for any particular type of test, then the real and imaginary components for all tests at each frequency were numerically averaged. This produced a single transfer function for each type of test. This average transfer function is then used to calculate the modal properties which will be described later.

4.3 Shaker Tests

The shaker tests were performed using virtually the same equipment used in the hammer tests with the exception of the force dynamometer. For the shaker tests, the force dynamometer used for the hammer tests was replaced with a more sensitive dynamometer rigidly mounted to the model in surge, sway, heave, roll and yaw with freedom to pitch.

The first step for the shaker tests was to select the excitation frequency. The shaker tests were typically done in two phases. The first phase would be to excite the model at frequency intervals of 1 Hz throughout the desired frequency range. Then the first set of data would be processed and the natural frequencies approximately defined. The second phase would be at a frequency interval of 0.1 Hz for a range of approximately ±1 Hz around each natural frequency of interest.

Once the frequency was selected the shaker would be started. When the model reached steady state oscillation, the computer data acquisition system was started. For all stationary tests, the computer was set to collect 2048 data points per channel. At a scanning frequency of 200 Hz, this represents a frequency resolution of approximately 0.1 Hz. This number was selected because the FFT requires that the number of data points be a power of 2, and by using this number, no cropping of the data was required. However, for the towed tests, approximately 25 to 30 seconds of data was collected. Following the towed test, 2048 data points were manually selected by viewing the velocity and force signal and selecting the steady state data.

The data collection process continued until the transfer function was well enough defined at the frequencies of interest to calculate the modal properties.

When the data collection was finished, the data processing would begin. The FFT was performed on all data channels for the selected time series data. The frequency at which the maximum force amplitude occurred was found. The real and imaginary accelerations at this frequency were divided by the real and imaginary force. These values were the real and imaginary transfer function component at this particular frequency. The transfer function components for all twelve accelerometers were stored along with the frequency for each test. Upon completion of all data processing, the transfer function components were all accumulated into one file to produce the response transfer function.

Since this test method enabled different tests occurring at the same frequency, a data editing procedure was required. In most situations where two or more tests occurred at the same frequency, the real and imaginary components were numerically averaged. For some frequencies where problems were noted during testing, the tests were intentionally repeated. If there was a small difference between these tests, they were averaged. However, if there was a significant difference between them, by analyzing the time series signal and by comparing their frequency resolution, the one with the poorest data was deleted. This was necessary for the tests in water around 1 Hz. During testing it was noted that large longitudinal waves were created. Following about 10 seconds, these waves were reflected back on the model. Because there was not sufficient time for the model to reach steady state before the wave returned, a number of tests were repeated and the best one used in the analysis.

Once all data editing was finished, the transfer function was made continuous by linearly interpolating between frequencies. Since the modal analysis software required a continuous transfer function, and the frequency steps from these tests varied from about 0.1 Hz near a natural frequency, to 1 Hz away from a natural frequency, and even higher beyond the range of interest for the frequency, interpolation was required. The frequency step chosen to perform the modal analysis on was approximately 0.2 Hz; the same step used for the hammer tests.

With the transfer function continuous and in the same form as the hammer test results, the modal properties are ready to be calculated.

4.4 Modal Analysis

Given either the transfer function produced by the hammer or shaker tests, the dynamic properties can be calculated using a modal analysis approach. The modal analysis approach permits the calculation of the mass, damping factor and stiffness at each modal frequency. The software used to calculate the modal properties was the "Entek Easy" package.

Given a single degree of freedom response transfer function obtained by dividing an acceleration spectrum by the forcing spectrum as shown in Figure 4.2, the modal properties can be calculated as follows. The first property to be deduced is the damped natural frequency. The damped natural frequency is the frequency at which the amplitude is a maximum. If there is low damping, the damped natural frequency is virtually the same as the undamped natural frequency.

The sharpness of the transfer function peak is an indication of the damping. A sharp peak has little damping where as a broad peak has high damping. By measuring the width of the peak, the damping can be calculated.

Figure 4.2

SINGLE DEGREE-OF-FREEDOM TRANSFER FUNCTION DEFINITION SKETCH

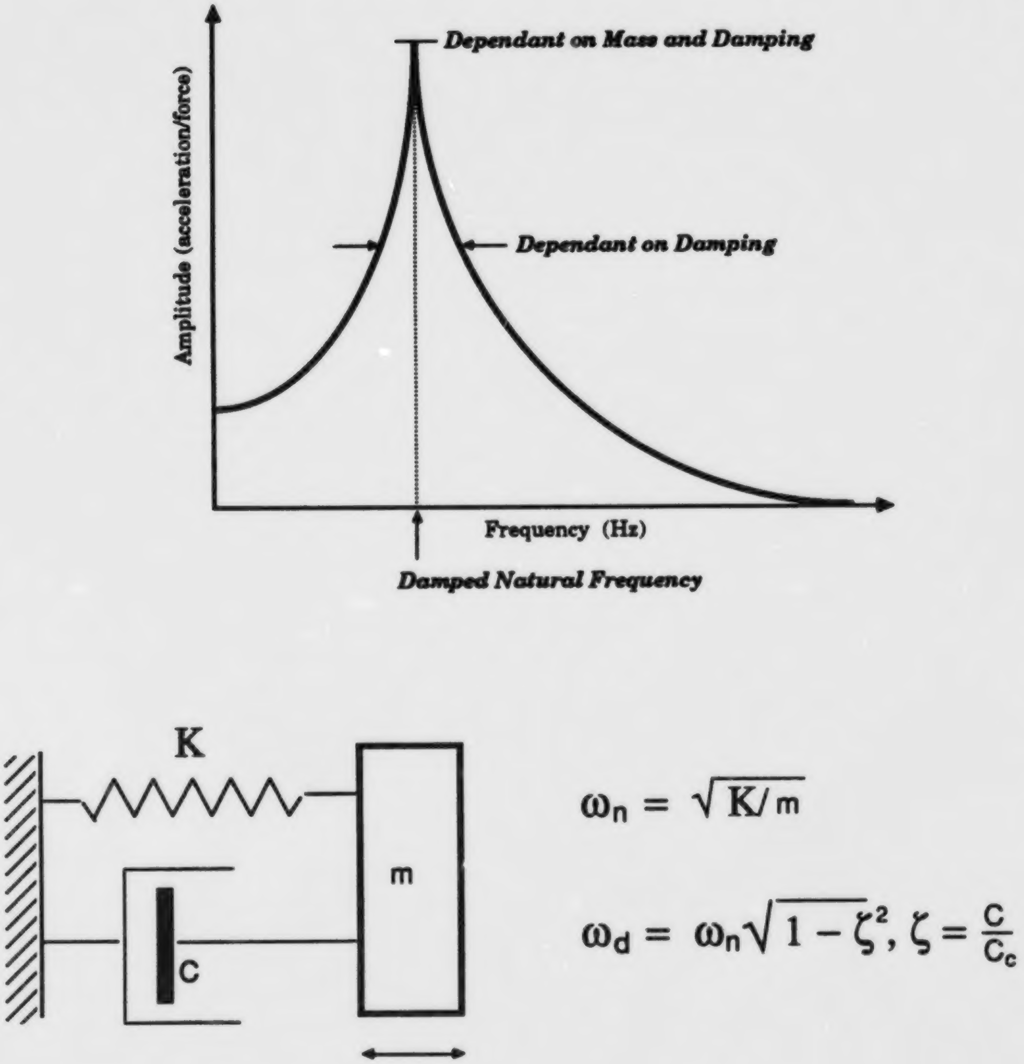

$$\omega_n = \sqrt{K/m}$$

$$\omega_d = \omega_n\sqrt{1-\zeta^2}, \zeta = \frac{C}{C_c}$$

The height of the transfer function peak is an indication of the mass of the system. If the mass is large the ratio of the acceleration to force at the natural frequency will be small. Therefore, by knowing the damping and the transfer function peak, the mass can be calculated.

The stiffness and undamped natural frequency can be calculated as follows:

$$\omega_n = \omega_d \,/\, \sqrt{1 - \zeta^2} \qquad (4.1)$$

and $$\omega_n = \sqrt{K/M} \qquad (4.2)$$

where ω_d = damped natural frequency (rad/sec)

ω_n = undamped natural frequency (rad/sec)

ζ = damping factor

K = stiffness

M = mass

Although the above method can be used to calculate the modal properties, the Entek Easy software package uses a more sophisticated method. The method chosen to calculate the modal properties with Entek Easy was the Single Degree of Freedom Rational Fraction Polynomial Curve Fitting method (note: Entek Easy has a number of calculation methods).

The Rational Fraction Polynomial Curve Fitting method fits a polynomial to the transfer function data using the least-squares method. The polynomial curve, which has the irregularities of typical test data smoothed out, is used to accurately calculate the modal properties in a manner similar to what was described earlier.

Although the Entek Easy package permits the calculation of multi-degree of freedom systems, in this analysis a number of single degree of freedom calculations were made instead. For systems with well defined and well spaced modes, and a damping of below 20 to 30%, a single degree of freedom calculation will suffice and be faster. Different calculation methods for the dry hammer tests were tried, and there was not a significant difference between single and multi-degree of freedom calculations.

To perform the Single Degree of Freedom Rational Fraction Polynomial curve fit calculation, the frequencies of interest must first be identified. By viewing any of the twelve transfer functions and selecting the frequency range for each mode of interest, the calculations could be performed.

Following the modal analysis calculations performed by the Entek Easy package, the modal mass from the dry tests was removed from the modal mass from the tests in water and in ice to give the modal added mass. The modal added mass was divided by the modal mass from the dry tests to give the added mass ratio. The modal added mass was also divided by the mass displaced by a half cylinder of length equal to the waterline length and radius equal to half of the mean model breadth. The details of these calculations are in section 5.

5. EXPERIMENTAL RESULTS

The measured transfer functions presented in this section were obtained using the methods described in Section 4. However, due to the number of tests performed, it is not possible to present all the raw data. In fact, only the processed transfer functions will be given in this report, and the majority will only be given in the appendices. The following sections will show only typical examples of the transfer function results. However, the processed modal properties, which are of primary interest in this report, will all be given in this section.

Tests performed to validate the experimental procedures and equipment used will also be found in the appendices. These include tests on the dry test support frame, and the shaker tests where the forcing amplitude was varied.

5.1 Hammer Tests

The transfer functions for the hammer tests are given in Appendix B, with a typical example shown in Figure 5.1. These figures show the dry hammer test results and those from the shallow and deep-water hammer tests. The water temperature measured during the wet tests are listed in Table 5.1. Also included is the approximate water density for these temperatures.

The first five vibratory modes can be seen in these figures. The first mode, the rigid body coupled heave and pitch mode, occurs approximately at 1 Hz. The first, second, third and fourth flexural modes occur at approximately 5, 15, 25 and 35 Hz respectively.

The rigid body mode and the first two flexural modes are well defined and well behaved. The third flexural mode for the dry hammer tests is not as well defined as the other modes. This indicates that another vibratory mode, which is closely spaced (in frequency) to the third flexural mode, is influencing the model's behaviour. Presence of this mode could indicate an apparent weakness in the model's dynamic properties, or an influence from the support structure.

The fourth flexural mode, although heavily damped, is also not as well defined and well behaved as the first few modes. Again this is more noticeable from the dry tests.

FIGURE 5.1
HAMMER TEST RESULTS

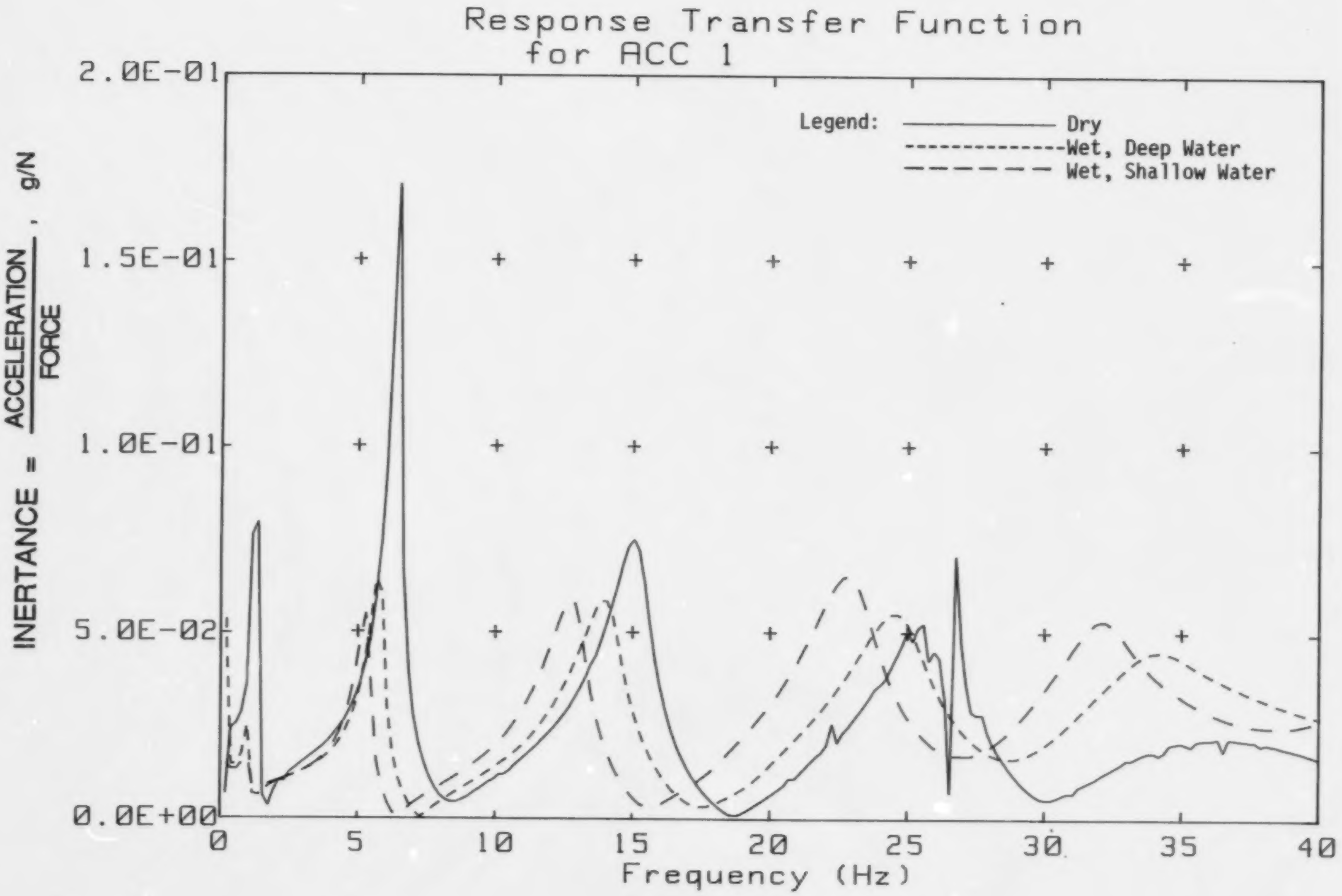

The decrease in modal frequency observed between the dry hammer tests and the deep and shallow water hammer tests is primarily the result of increase in the effective mass of the model. This increase in effective mass can be directly attributed to hydrodynamic inertia of the surrounding water. The decrease in modal amplitude observed is primarily caused by the increase in damping. Therefore, one can conclude that for the rigid body mode and at least the first two flexural modes, the hydrodynamic added mass and damping increase with a reduction of water depth. The higher modes are less consistent.

5.2 Shaker Tests

The transfer functions from the dry shaker tests, and those from the shaker tests in open-water as well as the shaker tests in ice-covered water are given in Figure 5.2. Note that all these tests correspond to stationary (zero-speed) conditions. The transfer functions for the towed shaker tests in water are given in Figure 5.3. The water property data for these tests are given in Table 5.1 and the ice property data in Tables 5.2 and 5.3.

The position of the accelerometers are the same as those in the dry shaker tests. They have been arranged so that accelerometer 1 is in the bow and each subsequent accelerometer progresses towards the stern.

The first vibratory mode shown in Figure 5.2 is the rigid body coupled mode of heave and pitch. The remaining modes are the flexural modes. The rigid body mode and the first two flexural modes are well defined and reasonably well behaved. The third flexural mode from the dry shaker tests exhibits some irregularities as observed earlier in the dry hammer tests. To fully explain these irregularities, more data is required at a finer frequency resolution. The third flexural mode from the shaker tests in open-water and in ice-covered water appear reasonably smooth.

The fourth flexural mode for the dry shaker tests is not completely defined in Figure 5.2 since the data is only shown up to 40 Hz. However, the dry shaker tests were performed well beyond this limit. The fourth flexural mode for the shaker tests in open-water is completely defined, but is slightly irregular. The shaker tests in ice covered water only went to 35 Hz, and therefore did not completely define the fourth flexural mode.

Figure 5.3 shows the effect of forward speed in water on the shaker test results. Although the stationary shaker tests were completely defined throughout this frequency range, the 1 and 6 knot tests were only accurately defined for the first and second flexural modes, and approximately defined for the rigid body mode and the third flexural mode. The 3 knot tests were only accurately defined for the first flexural mode, and approximately defined for the rigid body mode and the second and third flexural modes.

FIGURE 5.2

STATIONARY SHAKER TEST RESULTS

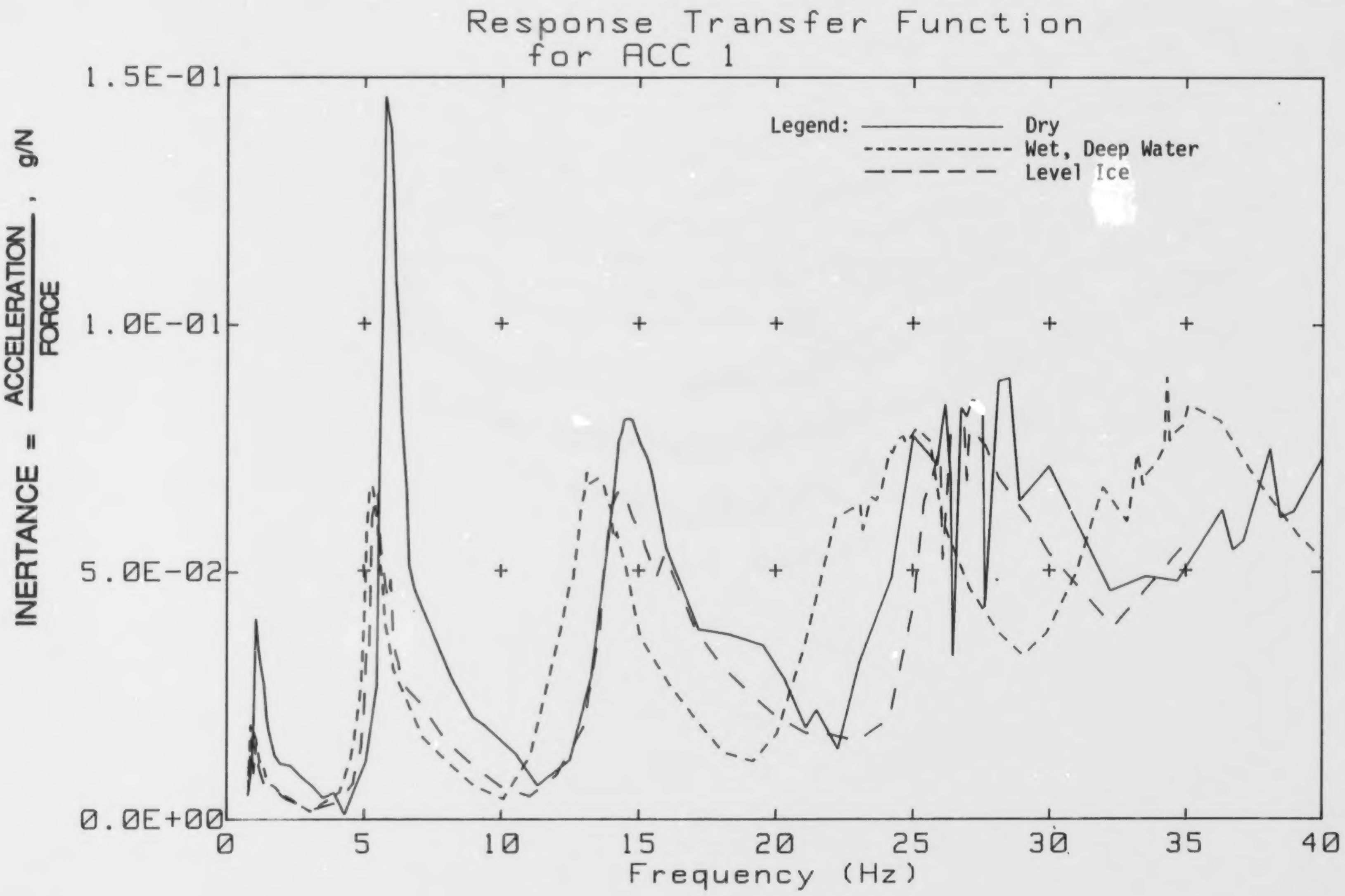

FIGURE 5.3

TOWED SHAKER TEST RESULTS

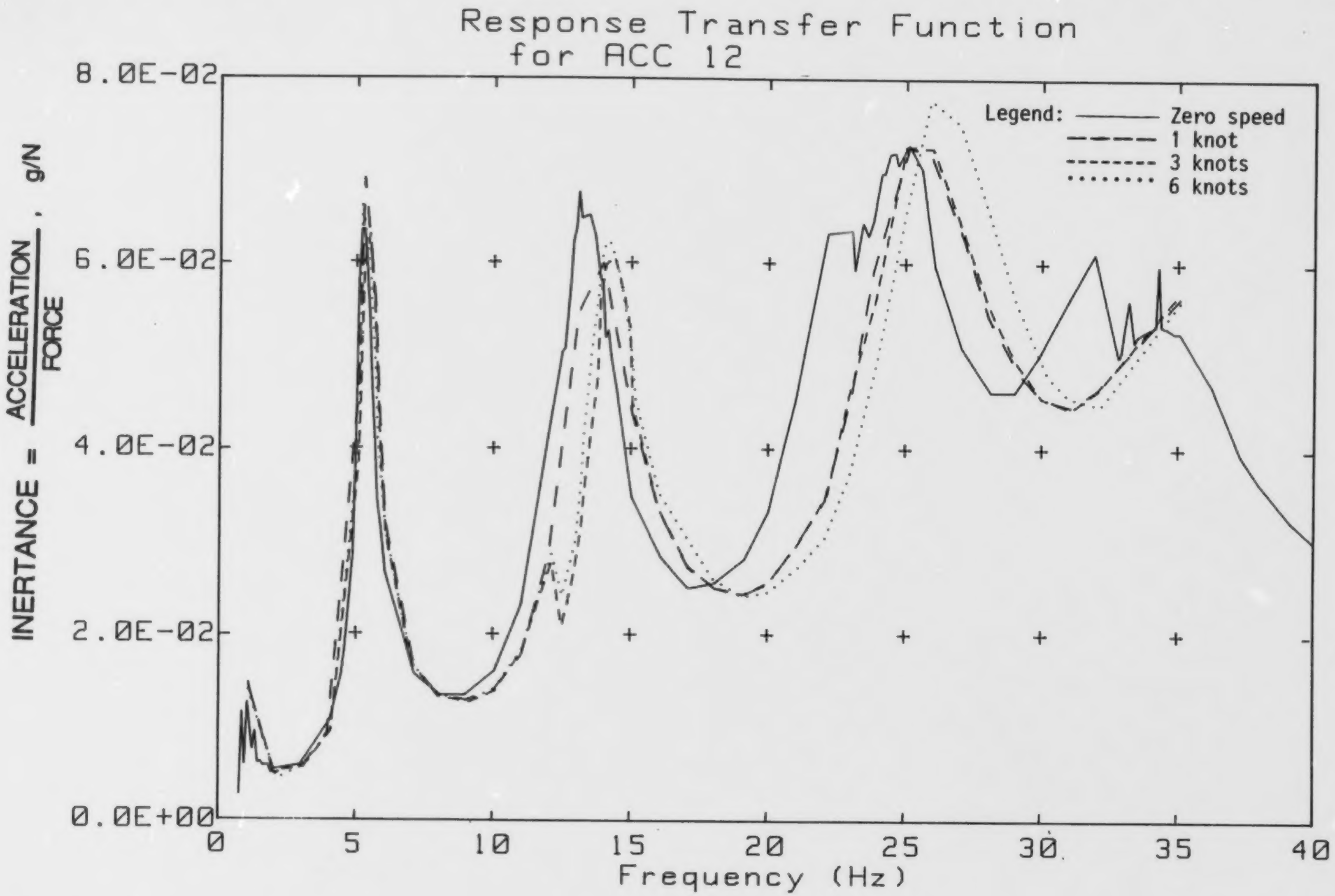

TABLE 5.1

WATER PROPERTIES

TEST NAME	WATER TEMPERATURE (°C)	APPROXIMATE WATER DENSITY (kg/m^3) *1
Hammer Tests (deep water)	1	999.42
Hammer Tests (shallow water)	3	999.45
Shaker Tests (0 knots)	4	999.46
Shaker Tests (1 knot)	3 / 0.5 *2	999.45 / 999.39 *2
Shaker Tests (3 knots)	3 / 0.5 *2	999.45 / 999.39 *2
Shaker Tests (6 knots)	1.0 / 0.5 *2	999.42 / 999.39 *2
Ice Tests	0.0	999.35
Rigid Model Tests	1	999.42
Amplitude Variation Tests	1	999.42

*1 These values were estimated knowing the density of pure water at these temperatures, and correcting for a 5.5% Urea solution knowing the relative density difference at 20°C.

*2 These tests were performed at two different times, resulting in two different water temperatures.

TABLE 5.2

ELASTIC MODULUS OF THE TEST ICE SHEET

TIME	CHARACTERISTIC LENGTH (m)	ELASTIC MODULUS (MPa)	LOCATION* (m)	COMMENTS
11:45	.235	21.09	9.0	Before Ice Shaker Tests
15:35	.215	13.62	9.5	During Ice Shaker Tests
17:40	.218	14.68	8.5	After Ice Shaker Tests

* Location refers to position along the basin length. All properties were measured in the transverse centre.

TABLE 5.3

ICE THICKNESS PROFILE

LOCATION FROM (m)	LOCATION TO (m)	AVERAGE THICKNESS (mm)	THICKNESS DEVIATION (mm)	NO. OF OBSERVATIONS	COMMENTS
5	13	26.79	1.00	18	Unbroken level ice sheet in front of model.
14	19	28.72	1.60	12	Ice sheet surrounding model.
19	24	28.29	1.36	10	Broken channel astern of model.
5	24	27.65	1.45	38	Entire ice sheet.

The first flexural mode does not appear to have any appreciable forward speed effects, since all four curves almost coincide. The second flexural mode at 1 knot and 6 knots also nearly coincide but are considerably different from that observed in stationary tests. The 3 knot tests, although not accurately defined, does not appear to follow either the stationary tests or the other forward speed tests.

Although not accurately defined at the third flexural mode, the 1 and 3 knot tests appear to be almost identical, and approximately in the middle of the stationary and 6 knot tests.

5.3 Miscellaneous Test Results

5.3.1 Forcing Amplitude Variation Tests

The purpose of these tests was to determine if the system behaves linearly, permitting the variation of the forcing amplitude, between tests. If the system is linear, the response transfer function will be independent of the force since it is derived by dividing the acceleration spectrum by the force spectrum.

These tests were considered important because of the shaker's specifications. The shaker's output was constant at high frequencies. However as the frequency approached 1 Hz, the forcing amplitude would decrease considerably. Therefore, the force used to shake the model at 30 Hz may not be obtainable at 1 Hz. Conversely, the maximum shaker force at 1 Hz may not produce sufficient model response at 30 Hz to measure the model's motion. As a compromise, the approach used in the test program was to select the largest force without exceeding the capacity of the instrumentation or the model.

This made it necessary to check if the model does behave linearly. Two frequencies and ten amplitude settings were selected. The first amplitude setting selected was the maximum force for that frequency. The amplitude dial was then decreased in equal increments to the minimum setting.

Since the instrumentation resolution would change throughout these tests, it was not wanted to introduce more variables by gaining up the signals as they got smaller. Therefore, an eleventh test was performed by repeating the test at the lowest force at a different gain. For this additional test, all transducers were gained up to give the best signal possible.

Tables 5.4 and 5.5 list the results of the Forcing Amplitude Variation Tests. The model was oscillated in water at the first flexural frequency and half way between the first and second flexural frequencies respectively. Listed is the forcing amplitude and the corresponding response transfer function for each accelerometer.

TABLE 5.4
FORCING AMPLITUDE VARIATION TESTS AT 5.4 Hz

FORCE (N)	RESPONSE TRANSFER FUNCTION X 10^2, 1/kg											
	ACC 1	ACC 2	ACC 3	ACC 4	ACC 5	ACC 6	ACC 7	ACC 8	ACC 9	ACC 10	ACC 11	ACC 12
53.29	7.07	4.46	2.18	.317	1.94	2,85	2.79	1.84	.201	2.04	4.28	6.53
48.17	7.05	4.41	2.17	.317	1.94	2.84	2.78	1.83	.200	2.03	4.26	6.50
44.81	7.11	4.42	2.19	.325	1.96	2.87	2.81	1.85	.200	2.06	4.31	6.57
41.61	7.25	4.47	2.22	.341	2.01	2.94	2.87	1.88	.202	2.11	4.40	6.71
37.87	7.32	4.48	2.23	.351	2.04	2.97	2.90	1.89	.201	2.14	4.46	6.79
33.70	7.45	4.52	2.25	.369	2.09	3.03	2.95	1.92	.200	2.19	4.55	6.93
28.84	7.56	4.54	2.27	.393	2.15	3.10	3.00	1.94	.196	2.25	4.65	7.06
22.82	7.64	4.49	2.24	.440	2.21	3.15	3.04	1.93	.191	2.31	4.75	7.20
15.53	7.22	4.09	2.04	.493	2.17	3.02	2.89	1.76	.178	2.26	4.56	6.89
5.03	4.61	2.44	1.13	.501	1.55	2.03	1.88	1.09	.161	1.59	30.8	4.62
4,85	4.32	2.28	1.04	.491	1.49	1.92	1.77	1.01	.153	1.51	2.91	4.36

TABLE 5.5
FORCING AMPLITUDE VARIATION TESTS AT 10.3 Hz

FORCE (N)	RESPONSE TRANSFER FUNCTION X 10^2, 1 k/g											
	ACC 1	ACC 2	ACC 3	ACC 4	ACC 5	ACC 6	ACC 7	ACC 8	ACC 9	ACC 10	ACC 11	ACC 12
104.28	.388	.58L	.821	.666	.246	.318	.695	.766	.460	.116	.792	1.54
95.89	.388	.582	.821	.664	.244	.319	.694	.763	.458	.117	.791	1.54
85.91	.386	.588	.820	.657	.237	.321	.691	.755	.451	.118	.786	1.53
75.48	.385	.595	.819	.648	.227	.325	.687	.743	.443	.121	.779	1.51
66.45	.386	.603	.817	.639	.219	.327	.684	.732	.435	.123	.774	1.49
58.32	.388	.610	.816	.631	.210	.331	.680	.721	.427	.125	.768	1.48
48.65	.395	.620	.814	.619	.199	.335	.676	.704	.416	.128	.761	1.46
37.42	.408	.634	.811	.605	.184	.340	.670	.681	.403	.131	.753	1.44
24.17	.435	.654	.809	.586	.164	.348	.664	.665	.385	.136	.742	1.41
8.01	.503	.688	.804	.553	.128	.363	.654	.635	.358	.145	.727	1.36
8.37	.513	.693	.803	.549	.123	.365	.654	.632	.354	.146	.725	1.36

A slight variation in the response transfer function is observed in Tables 5.4 and 5.5. To examine the relative magnitudes of these variations, the data are normalized and shown in Figures 5.4 and 5.5. The normalizing is done by dividing the response transfer function for each accelerometer by the corresponding value at the maximum force. This produces a ratio which approaches 1 as the force increases. If the normalized response transfer function is unity for all forcing amplitudes, then the system can be called a linear system.

Figure 5.4 shows that the transfer functions for most accelerometers are low for lower forces, increasing above 1 for moderate forces, and then decreasing slightly to 1 as the force approaches the maximum. There are two accelerometer which do not follow the same trend as the others; these are accelerometers 4 and 9. These two accelerometers happen to be at the two nodes of the first mode, where the acceleration is almost an order of magnitude below the others. Removing accelerometer 4, all accelerometers are linear to within 15% for all but the lowest force at the frequency of 5.4 Hz.

Figure 5.5 shows less of a trend than observed in Figure 5.4. In Figure 5.5, accelerometer 3 behaves almost linearly, varying by only 2% over the entire force range. Output of accelerometer 7 is also satisfactory varying by approximately 6% over the entire force range. However, accelerometers 1 and 5 vary by approximately +30% and -50% respectively.

Comparing the linearity of the accelerometers with the magnitude of the accelerations show that for Figure 5.5, the four best accelerometer signals for system linearity have the second highest, fifth highest, third highest, and highest accelerations respectively. The three worst accelerometers have the second lowest, fourth lowest, and lowest accelerations respectively.

Therefore, a clear trend exists that the larger the acceleration, the more independent the data is from the forcing amplitude. Thus, the slight non linearities observed could be caused by an acceleration which is too small for the instrumentation system to detect, and not necessarily due to non linearities in the system. Regardless, non linearities within a range of 10 to 15% are satisfactory since the approach used was to select the largest force without exceeding the capacity of the instrumentation or the model.

Figure 5.4

VARIATION OF THE NORMALIZED RESPONSE TRANSFER FUNCTION
WITH FORCING AMPLITUDE AT 5.4 Hz

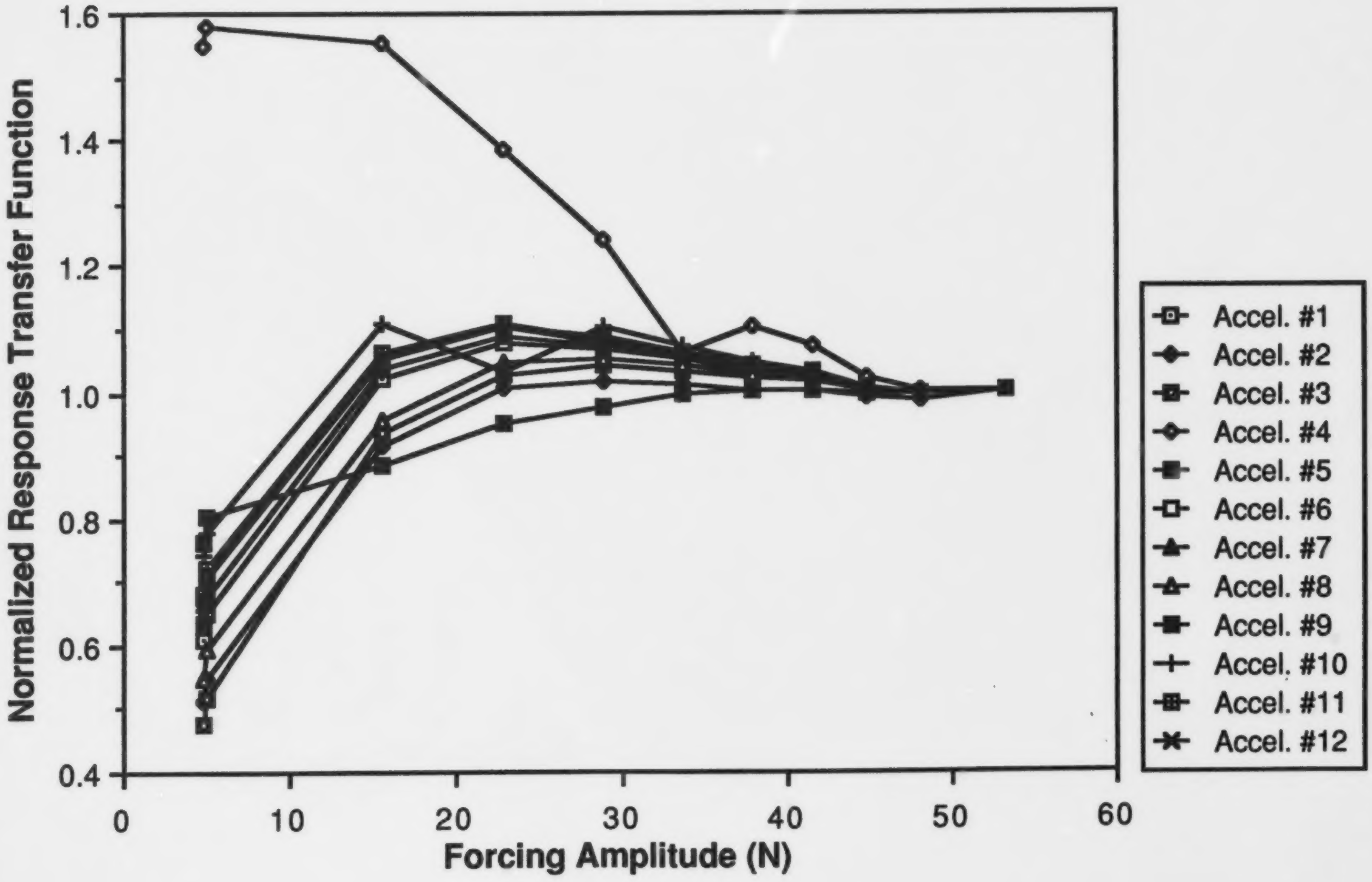

Figure 5.5

VARIATION OF THE NORMALIZED RESPONSE TRANSFER FUNCTION
WITH FORCING AMPLITUDE AT 10.3 Hz

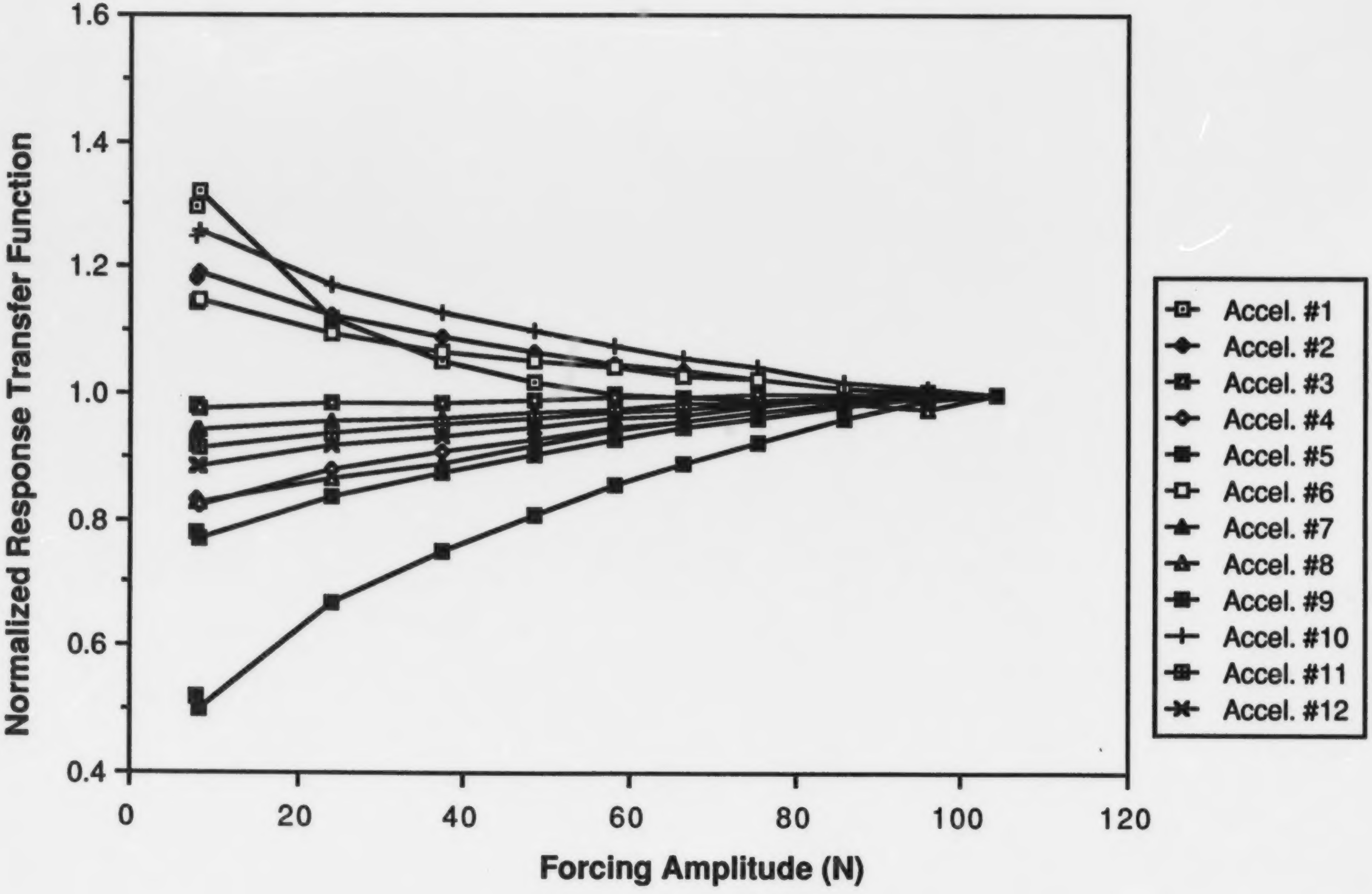

6. MODAL ANALYSIS

The analysis procedure is described in Section 4.4. The data from which the following results are obtained, is given in graphical form in Section 5.

6.1 Dry Tests

Table 6.1 gives the modal properties from the dry hammer tests obtained using the modal analysis software. Since the method used to produce these results was based on a single degree of freedom system, each calculation is independent of the others. As a result, the properties calculated for segment 1 are independent of those calculated for segment 2. Figure 6.1 shows a schematic representation of what each calculation gives. Depending on where the centre of force is, different motions will occur. If the forcing function is applied directly at the centre of gravity of a rigid body, then pure heave motion will occur. In this mode, no matter where the accelerometer is placed, the generalized values of mass, stiffness and damping will the same. However, if the forcing function is not applied at the centre of gravity of a rigid body, then a coupled heave and pitch mode will occur. In this mode, the accelerometer will produce a generalized mass and stiffness for each location. If an accelerometer is placed at a node, or a point where there is little or no motion, then to satisfy the equation of motion the mass and stiffness must be infinite. Therefore, the values of the Generalized Mass, Stiffness and damping given in Table 6.1 represent the properties for the entire hull for a given modes, at specific points.

Since the model is not a rigid body, the analysis is somewhat more complicated. If the model was excited at precisely the centre of gravity, the flexure of the model would result in variations of the modal properties with position. The generalized mass, stiffness and damping will vary.

Table 6.1 lists the modal properties from the dry hammer tests for the first five modes and Table 6.2 gives the same properties from the dry shaker tests. Since each calculation is independent of the others, variations in the natural frequency are observed. Typically, where the variation is small, the quality of the results is high. For example, the standard deviation for the calculated frequency at the first flexural model (or model #2) from the dry hammer tests is .004 Hz. At the fourth flexural mode (or mode #5), the standard deviation for the dry hammer test frequency is .71 Hz. As described earlier, the dynamic model does not respond well above the second flexural mode. This is seen in these results.

By comparing the phase angle and peak for each accelerometer the modal shape can be obtained. Figures 6.2 and 6.3 show the first five mode shapes from the Dry Hammer and Shaker tests respectively.

TABLE 6.1

MODAL RESULTS FROM THE DRY HAMMER TESTS

MODE #	SEGMENT #	FREQ (hz)	DAMPING (%)	PEAK (m)	PHASE (deg)	GENERALIZED STIFFNESS (N/m)	GENERALIZED MASS (kg)
1	1	1.10	2.900	2.383E-01	98	3.441E+03	7.235E+01
1	2	1.09	3.143	1.761E-01	101	4.254E+03	9.036E+01
1	3	1.08	3.024	1.555E-01	103	4.929E+03	1.063E+02
1	4	1.07	2.796	1.432E-01	108	5.668E+03	1.249E+02
1	5	1.05	1.763	1.526E-01	118	8.154E+03	1.858E+02
1	6	1.04	1.114	1.201E-01	146	1.612E+04	3.740E+02
1	7	1.07	3.881	1.553E-02	170	3.753E+04	8.298E+02
1	8	1.11	3.695	3.840E-03	180	1.700E+05	3.524E+03
1	9	1.12	2.483	2.424E-02	-169	4.111E+04	8.305E+02
1	10	1.12	1.563	9.952E-02	-155	1.604E+04	3.214E+02
1	11	1.13	.992	2.452E-01	-146	1.028E+04	2.056E+02
1	12	1.13	.371	9.625E-01	-135	7.023E+03	1.401E+02
2	1	6.19	2.889	1.418E-01	127	1.844E+05	1.220E+02
2	2	6.19	2.970	8.647E-02	121	2.943E+05	1.947E+02
2	3	6.18	2.795	3.278E-02	120	8.237E+05	5.458E+02
2	4	6.19	3.065	1.492E-02	-58	1.653E+06	1.093E+03
2	5	6.19	2.862	5.604E-02	-59	4.712E+05	3.118E+02
2	6	6.19	2.811	7.694E-02	-60	3.492E+05	2.312E+02
2	7	6.19	2.785	7.648E-02	-61	3.545E+05	2.347E+02
2	8	6.19	2.801	5.269E-02	-60	5.118E+05	3.388E+02
2	9	6.18	2.725	1.339E-02	-62	2.068E+06	1.370E+03
2	10	6.19	2.858	4.071E-02	118	6.494E+05	4.297E+02
2	11	6.19	2.831	9.810E-02	117	2.720E+05	1.801E+02
2	12	6.19	2.825	1.591E-01	116	1.680E+05	1.112E+02
3	1	14.94	4.944	3.739E-02	151	2.383E+06	2.705E+02
3	2	14.95	4.927	1.557E-02	140	5.753E+06	6.519E+02
3	3	14.95	4.996	9.871E-03	-32	8.942E+06	1.014E+03
3	4	14.94	4.903	2.683E-02	-38	3.350E+06	3.801E+02
3	5	14.94	4.869	2.479E-02	-39	3.649E+06	4.142E+02
3	6	14.90	4.873	2.973E-03	-36	3.023E+07	3.451E+03
3	7	14.95	4.904	2.445E-02	136	3.678E+06	4.169E+02
3	8	14.95	4.948	4.075E-02	136	2.188E+06	2.480E+02
3	9	14.94	4.920	3.893E-02	132	2.300E+06	2.610E+02
3	10	14.93	4.954	1.443E-02	129	6.153E+06	6.992E+02
3	11	14.95	4.899	2.643E-02	-50	3.406E+06	3.861E+02
3	12	14.94	4.937	7.941E-02	-55	1.124E+06	1.275E+02
4	1	26.14	3.459	2.941E-02	-150	1.327E+07	4.916E+02
4	2	26.03	1.092	9.724E-03	45	1.259E+08	4.707E+03
4	3	25.83	3.154	7.210E-03	12	5.792E+07	2.199E+03
4	4	25.94	3.319	3.879E-03	7	1.032E+08	3.884E+03
4	5	25.87	3.650	6.955E-04	-178	5.204E+08	1.970E+04
4	6	25.88	3.594	8.120E-04	179	4.532E+08	1.713E+04
4	7	25.97	3.381	1.269E-03	-179	3.103E+08	1.165E+04
4	8	26.30	1.880	2.963E-03	22	2.451E+08	8.975E+03
4	9	25.89	3.249	4.797E-03	-12	8.490E+07	3.208E+03
4	10	25.93	3.236	6.823E-03	-16	6.013E+07	2.265E+03
4	11	26.06	3.245	2.294E-03	162	1.800E+08	6.717E+03
4	12	25.95	3.363	3.125E-02	154	1.265E+07	4.757E+02
5	1	35.25	8.100	1.052E-03	172	2.879E+08	5.867E+03
5	2	35.77	10.193	7.115E-05	-6	3.482E+09	6.894E+04
5	3	35.49	8.718	2.987E-03	-16	9.545E+07	1.920E+03
5	4	34.26	1.522	5.704E-03	78	2.668E+08	5.760E+03
5	5	35.70	10.727	3.877E-03	161	6.049E+07	1.202E+03
5	6	35.29	.056	5.404E-02	108	8.096E+08	1.646E+04
5	7	34.75	10.408	1.589E-02	-52	1.441E+07	3.023E+02
5	8	36.73	13.299	3.917E-03	-15	5.111E+07	9.598E+02
5	9	36.24	5.058	3.789E-03	-99	1.353E+08	2.609E+03
5	10	35.01	11.442	1.907E-02	120	1.109E+07	2.292E+02
5	11	36.37	13.030	7.225E-03	133	2.774E+07	5.312E+02
5	12	35.08	9.916	3.428E-02	-68	7.147E+06	1.471E+02

Figure 6.1
DEFINITION SKETCH FOR SINGLE DEGREE-OF-FREEDOM SYSTEM

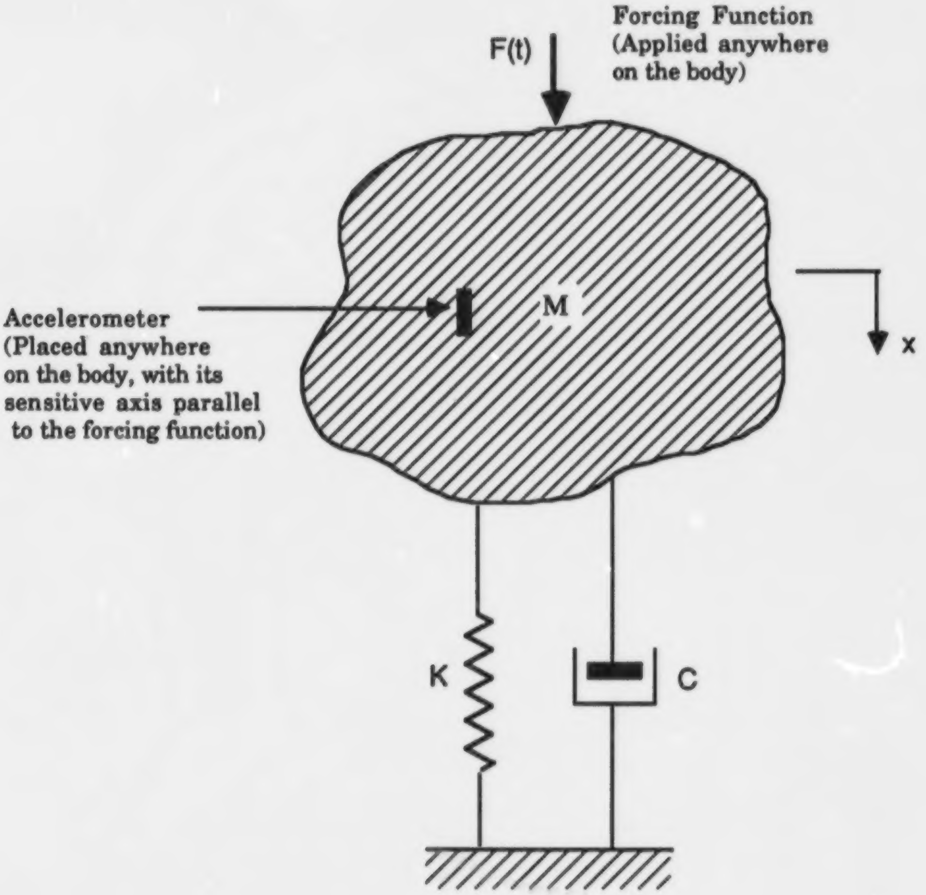

Equation Of Motion Is $M\ddot{x} + C\dot{x} + Kx = F(t)$

TABLE 6.2

MODAL RESULTS FOR THE DRY SHAKER TESTS

MODE #	SEGMENT #	FREQ (hz)	DAMPING (%)	PEAK (m)	PHASE (deg)	GENERALIZED STIFFNESS (N/m)	GENERALIZED MASS (kg)
1	1	1.09	.842	3.764E-01	93	7.342E+03	1.577E+02
1	2	1.09	.720	3.635E-01	94	8.934E+03	1.910E+02
1	3	1.10	.471	5.261E-01	93	9.685E+03	2.019E+02
1	4	1.12	.317	6.227E-01	93	1.255E+04	2.531E+02
1	5	1.14	.176	8.047E-01	93	1.800E+04	3.521E+02
1	6	1.15	.068	1.348E+00	90	2.859E+04	5.458E+02
1	7	1.16	.073	5.820E-01	95	6.305E+04	1.180E+03
1	8	1.18	.062	4.080E-01	-81	1.077E+05	1.970E+03
1	9	1.19	.033	2.732E+00	-89	3.104E+04	5.572E+02
1	10	1.19	.008	1.521E+01	-90	2.199E+04	3.913E+02
1	11	1.20	.019	8.910E+00	-90	1.645E+04	2.895E+02
1	12	1.20	.052	4.214E+00	-89	1.313E+04	2.292E+02
2	1	5.87	3.904	1.410E-01	97	1.235E+05	9.085E+01
2	2	5.87	3.949	8.363E-02	98	2.060E+05	1.514E+02
2	3	5.88	4.026	3.596E-02	98	4.709E+05	3.454E+02
2	4	5.86	3.561	1.095E-02	-87	1.740E+06	1.283E+03
2	5	5.86	3.899	4.749E-02	-88	3.664E+05	2.700E+02
2	6	5.87	3.910	6.493E-02	-96	2.676E+05	1.969E+02
2	7	5.87	3.912	6.546E-02	-88	2.653E+05	1.952E+02
2	8	5.87	3.927	4.735E-02	-87	3.654E+05	2.689E+02
2	9	5.87	4.100	1.295E-02	-83	1.283E+06	9.417E+02
2	10	5.86	3.902	3.287E-02	88	5.293E+05	3.899E+02
2	11	5.87	3.909	8.097E-02	89	2.145E+05	1.580E+02
2	12	5.87	3.910	1.307E-01	88	1.329E+05	9.781E+01
3	1	14.46	5.596	5.716E-02	125	1.290E+06	1.563E+02
3	2	14.42	6.955	2.167E-02	119	2.723E+06	3.318E+02
3	3	14.42	4.841	1.011E-02	-67	8.388E+06	1.021E+03
3	4	14.42	5.750	3.046E-02	-65	2.344E+06	2.854E+02
3	5	14.45	5.915	2.900E-02	-65	2.402E+06	2.915E+02
3	6	14.77	5.219	7.446E-03	-55	1.109E+07	1.287E+03
3	7	14.43	5.724	2.330E-02	106	3.081E+06	3.749E+02
3	8	14.43	5.920	4.368E-02	107	1.590E+06	1.934E+02
3	9	14.42	6.078	4.158E-02	105	1.625E+06	1.978E+02
3	10	14.41	6.219	1.562E-02	104	4.220E+06	5.146E+02
3	11	14.43	6.056	2.643E-02	-79	2.566E+06	3.124E+02
3	12	14.43	6.078	7.672E-02	-82	8.808E+05	1.072E+02
4	1	27.69	5.906	2.842E-02	-159	9.019E+06	2.979E+02
4	2	29.21	.672	2.039E-02	105	1.230E+08	3.651E+03
4	3	26.65	6.973	1.136E-02	-25	1.769E+07	6.312E+02
4	4	27.09	5.440	3.443E-03	-11	7.734E+07	2.670E+03
4	5	27.41	5.497	7.396E-04	172	3.647E+08	1.230E+04
4	6	26.96	1.050	3.002E-02	115	4.550E+07	1.586E+03
4	7	26.57	5.119	1.283E-02	142	2.122E+07	7.614E+02
4	8	28.24	1.009	1.516E-04	0	1.029E+10	3.268E+05
4	9	26.78	5.281	1.923E-02	-49	1.393E+07	4.923E+02
4	10	26.68	5.682	2.423E-02	-60	1.020E+07	3.631E+02
4	11	27.57	4.968	3.859E-03	149	7.825E+07	2.608E+03
4	12	26.81	6.820	7.506E-02	113	2.772E+06	9.768E+01
5	1	38.96	.189	8.620E-04	-180	1.841E+10	3.071E+05
5	2	39.46	1.119	7.478E-03	-17	3.674E+08	5.976E+03
5	3	38.29	1.825	1.340E-02	-31	1.183E+08	2.044E+03
5	4	39.86	.046	4.618E-03	154	1.467E+10	2.339E+05
5	5	38.51	5.618	8.089E-03	142	6.440E+07	1.100E+03
5	6	39.89	.130	4.725E-02	93	5.132E+08	8.171E+03
5	7	38.45	11.118	1.825E-02	-46	1.438E+07	2.464E+02
5	8	38.43	7.966	1.903E-02	-62	1.923E+07	3.298E+02
5	9	38.91	2.430	4.090E-03	-130	3.007E+08	5.030E+03
5	10	38.21	7.022	1.833E-02	109	2.240E+07	3.885E+02
5	11	39.52	4.309	6.452E-03	118	1.109E+08	1.798E+03
5	12	38.51	4.721	3.370E-02	-73	1.840E+07	3.143E+02

FIGURE 6.2
DRY SHAKER

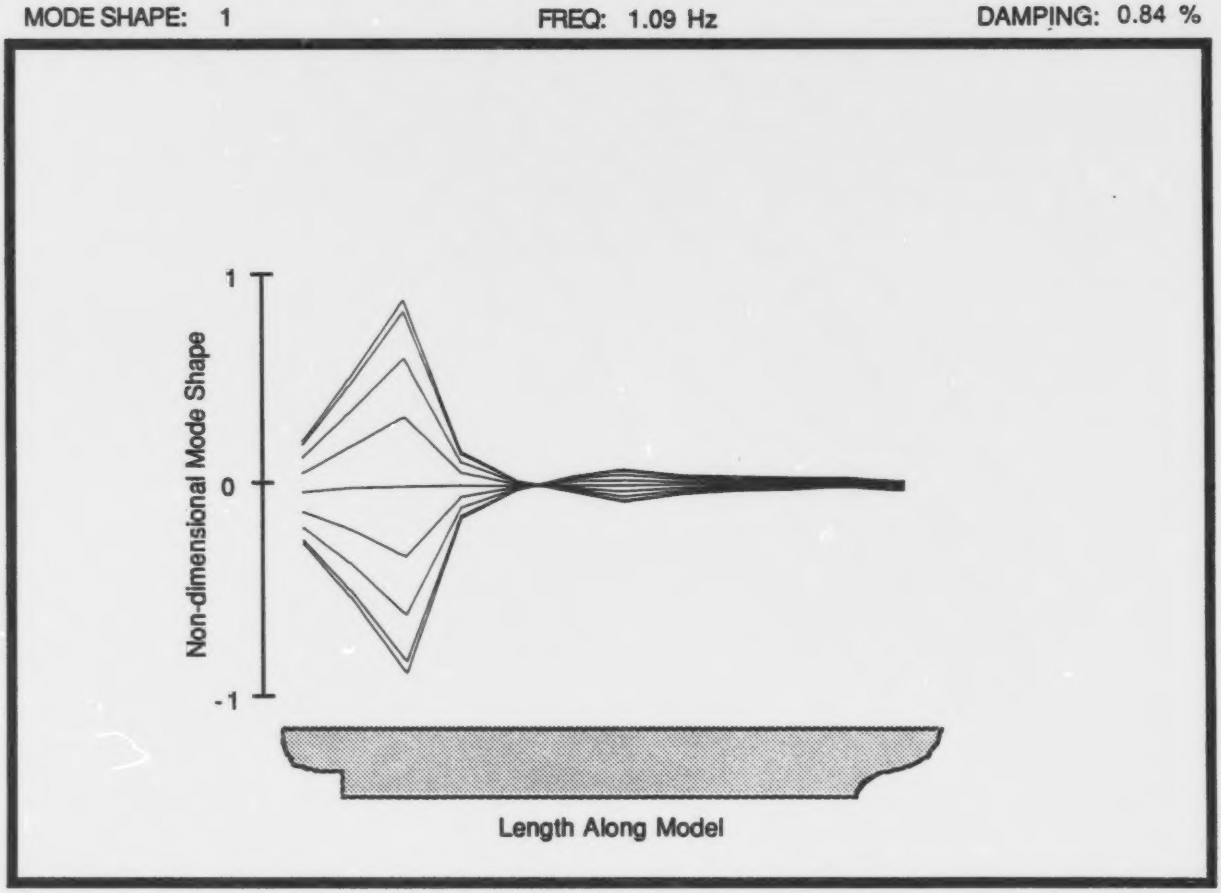

FIGURE 6.3
DRY HAMMER

MODE SHAPE: 1 FREQ: 1.10 Hz DAMPING: 2.90 %

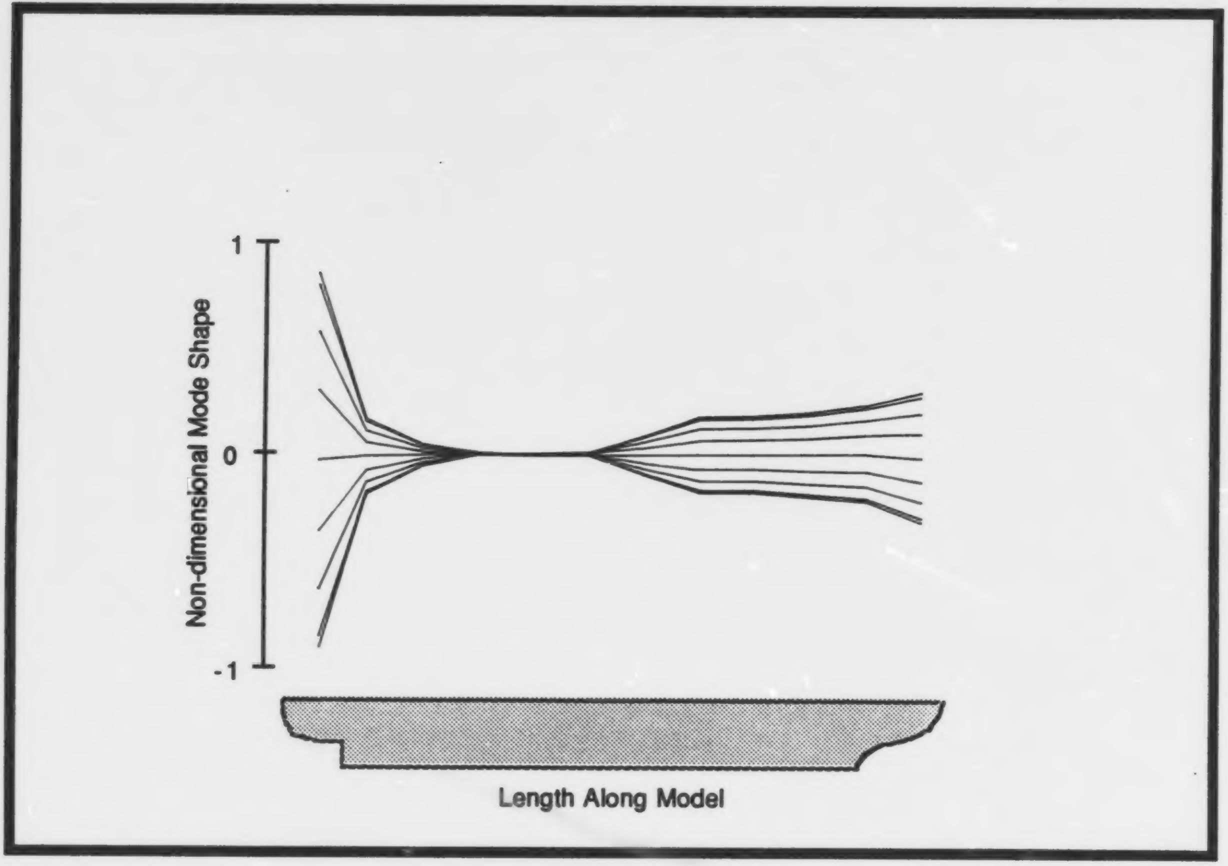

Mode shape 1, (the rigid body mode) for both the hammer and shaker tests is affected by a higher order mode. For the hammer tests, the stern is observed to "whip". Where as for the shaker tests, segment 11 is observed to "whip". The second and third mode shapes (the first and second flexural modes) are quite good, with a small amount of whipping occurring at the stern. The fourth and fifth mode shapes, as described earlier, are not well modelled. As a result, they are not well behaved.

6.2 Stationary Wet Tests

Tables 6.3, 6.4 and 6.5 list the modal properties for the hammer tests in deep water, hammer tests in shallow water, and shaker tests in deep water respectively. The values given on these tables are described in Section 6.1, however three additional columns are added. The generalized added mass is obtained by subtracting the generalized mass in water from the generalized mass in air for each mode shape and position. As described in Section 6.1, the generalized mass represents the mass of the entire body in a given vibratory mode, observed from a given position. Therefore, the generalized added mass is both mode and position dependent.

The mass ratio is obtained by dividing the generalized added mass by the generalized mass obtained from the dry mode tests. The final column, "J" again is a dimensionless ratio. "J" is obtained by dividing the generalized added mass by the mass of a half cylinder with a length equal to the model's waterline length, and a radius of half the model's average waterline beam.

$$J = \frac{M_a}{1/2\ \rho\ \pi\ (\bar{B}/2)^2\ L_{bp}} \qquad (6.1)$$

where M_a = total hydrodynamic added mass

ρ = density of water

$\bar{B}$ = model's average waterline beam

L_{bp} = model's waterline length

Figure 6.4 shows the variation of "J" along the model for the first three modes. Superimposed on each other are the plots for the deep and shallow water hammer tests, and the deep water shaker tests.

TABLE 6.3

MODAL RESULTS FROM THE STATIONARY HAMMER TESTS IN DEEP WATER

MODE #	SEGMENT #	FREQ (hz)	DAMPING (%)	PEAK (m)	PHASE (deg)	GENERALIZED STIFFNESS (N/m)	GENERALIZED MASS (kg)	GENERALIZED ADDED MASS (kg)	MASS RATIO	J
1	1	.82	10.711	1.866E-02	99	6.696E+03	2.501E+02	177.7	2.457	.375
1	2	.82	10.770	1.503E-02	103	8.268E+03	3.088E+02	218.4	2.417	.461
1	3	.81	10.232	1.321E-02	99	9.683E+03	3.698E+02	263.5	2.479	.556
1	4	.81	10.106	1.042E-02	99	1.227E+04	4.750E+02	350.1	2.803	.739
1	5	.81	9.625	7.835E-03	106	1.707E+04	6.630E+02	477.2	2.568	1.008
1	6	.80	6.613	5.118E-03	118	3.769E+04	1.477E+03	1103.0	2.949	2.329
1	7	.81	5.418	2.011E-03	151	1.190E+05	4.589E+03	3759.2	4.530	7.937
1	8	.84	3.869	4.746E-03	-145	7.604E+04	2.723E+03	-801.0	-.227	-1.691
1	9	.85	7.031	7.014E-03	-118	2.921E+04	1.014E+03	183.5	.221	.387
1	10	.86	9.110	1.017E-02	-99	1.585E+04	5.399E+02	218.5	.680	.461
1	11	.85	9.736	1.208E-02	-97	1.226E+04	4.251E+02	219.5	1.068	.463
1	12	.85	9.814	1.534E-02	-95	9.533E+03	3.321E+02	192.0	1.370	.405
2	1	5.55	4.803	5.860E-02	124	2.163E+05	1.776E+02	55.6	.456	.117
2	2	5.55	4.770	3.733E-02	120	3.417E+05	2.808E+02	86.1	.442	.182
2	3	5.55	4.717	1.593E-02	120	8.097E+05	6.656E+02	119.8	.219	.253
2	4	5.55	4.932	4.085E-03	-60	3.019E+06	2.482E+03	1389.0	1.271	2.933
2	5	5.55	4.734	1.980E-02	-61	6.484E+05	5.334E+02	221.6	.711	.468
2	6	5.55	4.622	2.949E-02	-70	4.461E+05	3.668E+02	135.6	.587	.286
2	7	5.55	4.593	2.639E-02	-62	5.016E+05	4.125E+02	177.8	.758	.375
2	8	5.55	4.577	1.639E-02	-63	8.105E+05	6.667E+02	327.9	.968	.692
2	9	5.36	1.223	1.527E-04	-22	3.031E+08	2.677E+05	+2.7E+05	194.401	562.352
2	10	5.55	4.668	2.120E-02	115	6.148E+05	5.054E+02	75.7	.176	.160
2	11	5.55	4.662	4.309E-02	115	3.027E+05	2.489E+02	68.8	.382	.145
2	12	5.55	4.617	6.588E-02	114	1.999E+05	1.644E+02	53.2	.478	.112
3	1	13.82	6.493	3.962E-02	139	1.466E+06	1.944E+02	-76.1	-.281	-.161
3	2	13.84	6.193	1.709E-02	135	3.575E+06	4.725E+02	-179.4	-.275	-.379
3	3	13.81	6.422	5.315E-03	-39	1.103E+07	1.465E+03	451.0	.445	.952
3	4	13.83	6.374	1.932E-02	-45	3.066E+06	4.060E+02	25.9	.068	.055
3	5	13.83	6.267	1.892E-02	-48	3.185E+06	4.217E+02	7.5	.018	.016
3	6	13.75	6.328	5.287E-03	-74	1.115E+07	1.494E+03	-1957.0	-.567	-4.132
3	7	13.86	6.346	1.521E-02	130	3.927E+06	5.180E+02	101.1	.243	.213
3	8	13.85	6.509	2.523E-02	129	2.307E+06	3.045E+02	56.5	.228	.119
3	9	13.83	6.405	2.098E-02	126	2.811E+06	3.720E+02	111.0	.425	.234
3	10	13.75	6.660	3.055E-03	118	1.833E+07	2.457E+03	1757.8	2.514	3.712
3	11	13.85	6.461	2.471E-02	-56	2.372E+06	3.132E+02	-72.9	-.189	-.154
3	12	13.85	6.431	5.833E-02	-59	1.010E+06	1.333E+02	5.8	.045	.012
4	1	24.47	6.237	8.901E-03	167	2.128E+07	9.007E+02	409.1	.832	.864
4	2	24.47	5.508	4.797E-04	170	4.474E+08	1.893E+04	+1.4E+04	3.022	30.032
4	3	24.46	6.282	6.745E-03	-21	2.786E+07	1.180E+03	-1019.0	-.463	-2.152
4	4	24.45	6.189	7.089E-03	-25	2.690E+07	1.140E+03	-2744.0	-.706	-5.794
4	5	24.54	5.914	3.009E-03	150	6.682E+07	2.810E+03	-1.7E+04	-.857	-35.663
4	6	24.50	6.260	2.529E-02	114	7.485E+06	3.158E+02	-1.7E+04	-.982	-35.503
4	7	24.47	6.305	8.893E-03	147	2.107E+07	8.917E+02	-1.1E+04	-.923	-22.716
4	8	24.57	5.862	2.567E-03	-33	7.919E+07	3.323E+03	-5652.0	-.630	-11.934
4	9	24.51	6.318	1.384E-02	-40	1.357E+07	5.719E+02	-2636.1	-.822	-5.566
4	10	24.49	6.482	1.392E-02	-46	1.312E+07	5.541E+02	-1710.9	-.755	-3.613
4	11	24.55	6.277	7.306E-03	139	2.594E+07	1.090E+03	-5627.0	-.838	-11.881
4	12	24.49	6.492	5.086E-02	127	3.587E+06	1.514E+02	-324.3	-.682	-.685
5	1	33.48	7.250	1.610E-03	173	1.896E+08	4.284E+03	-1583.0	-.270	-3.342
5	2	33.53	7.918	2.125E-03	-17	1.319E+08	2.972E+03	-6.6E+04	-.957	-139.291
5	3	33.33	7.350	6.529E-03	-27	4.571E+07	1.042E+03	-878.0	-.457	-1.854
5	4	32.51	6.533	1.009E-03	38	3.164E+08	7.585E+03	1825.0	.317	3.853
5	5	33.42	7.952	8.956E-03	147	3.095E+07	7.020E+02	-500.0	-.416	-1.056
5	6	33.78	6.867	3.917E-03	116	8.373E+07	1.859E+03	-1.5E+04	-.887	-30.830
5	7	33.23	8.238	1.571E-02	-50	1.685E+07	3.864E+02	84.1	.278	.178
5	8	33.27	9.054	1.640E-02	-54	1.472E+07	3.367E+02	-623.1	-.649	-1.316
5	9	33.44	6.867	3.452E-03	137	9.311E+07	2.109E+03	-500.0	-.192	-1.056
5	10	33.25	8.616	2.212E-02	116	1.145E+07	2.623E+02	33.1	.144	.070
5	11	34.04	12.846	4.049E-03	123	4.398E+07	9.613E+02	430.1	.810	.908
5	12	33.25	8.433	5.363E-02	-74	4.825E+06	1.106E+02	-36.5	-.248	-.077

TABLE 6.4

MODAL RESULTS FROM THE STATIONARY HAMMER TESTS IN SHALLOW WATER

MODE #	SEGMENT #	FREQ (hz)	DAMPING (%)	PEAK (m)	PHASE (deg)	GENERALIZED STIFFNESS (N/m)	GENERALIZED MASS (kg)	GENERALIZED ADDED MASS (kg)	MASS RATIO	I
1	1	.80	16.290	9.215E-03	108	8.366E+03	3.331E+02	260.7	3.604	.551
1	2	.79	15.967	7.825E-03	106	9.859E+03	4.002E+02	309.8	3.429	.654
1	3	.77	15.508	7.114E-03	96	1.057E+04	4.532E+02	346.9	3.263	.732
1	4	.78	15.699	5.119E-03	107	1.500E+04	6.221E+02	497.2	3.981	1.050
1	5	.75	13.173	4.495E-03	95	1.862E+04	8.445E+02	658.7	3.545	1.391
1	6	.74	8.497	3.631E-03	92	3.525E+04	1.620E+03	1246.0	3.332	2.631
1	7	.78	4.408	8.147E-04	160	3.354E+05	1.392E+04	+1.3E+04	15.775	27.640
1	8	.83	.392	3.790E-02	-84	9.081E+04	3.368E+03	-156.0	-.044	-.329
1	9	.85	6.702	5.757E-03	-91	3.698E+04	1.296E+03	465.5	.561	.983
1	10	.84	8.577	6.680E-03	-88	2.446E+04	8.727E+02	551.3	1.715	1.164
1	11	.84	12.326	7.435E-03	-86	1.523E+04	5.456E+02	340.0	1.654	.718
1	12	.84	11.469	9.379E-03	-85	1.288E+04	4.648E+02	324.7	2.318	.686
2	1	5.07	4.804	4.992E-02	121	2.118E+05	2.085E+02	86.5	.709	.183
2	2	5.07	4.690	3.238E-02	118	3.337E+05	3.293E+02	134.6	.691	.284
2	3	5.07	4.553	1.526E-02	118	7.291E+05	7.197E+02	173.9	.319	.367
2	4	5.05	4.475	1.865E-03	-71	6.022E+06	5.991E+03	4898.0	4.481	10.342
2	5	5.06	4.554	1.521E-02	-65	7.309E+05	7.218E+02	410.0	1.315	.866
2	6	5.07	4.493	2.279E-02	-73	4.947E+05	4.884E+02	257.2	1.112	.543
2	7	5.07	4.422	2.054E-02	-65	5.578E+05	5.505E+02	315.8	1.346	.667
2	8	5.07	4.378	1.164E-02	-65	9.952E+05	9.809E+02	642.1	1.895	1.356
2	9	5.08	5.143	2.353E-03	115	4.202E+06	4.131E+03	2761.0	2.015	5.830
2	10	5.07	4.600	2.045E-02	113	5.388E+05	5.315E+02	101.8	.237	.215
2	11	5.07	4.564	3.899E-02	112	2.847E+05	2.810E+02	100.9	.560	.213
2	12	5.07	4.528	5.829E-02	112	1.920E+05	1.895E+02	78.3	.704	.165
3	1	12.63	5.874	3.797E-02	141	1.411E+06	2.242E+02	-46.3	-.171	-.098
3	2	12.63	5.797	1.837E-02	135	2.955E+06	4.696E+02	-182.3	-.280	-.385
3	3	12.66	5.916	1.981E-03	-34	2.699E+07	4.267E+03	3253.0	3.208	6.869
3	4	12.63	5.784	1.598E-02	-45	3.406E+06	5.410E+02	160.9	.423	.340
3	5	12.62	5.700	1.708E-02	-48	3.230E+06	5.135E+02	99.3	.240	.210
3	6	12.58	5.528	5.536E-03	-71	1.021E+07	1.634E+03	-1817.0	-.527	-3.837
3	7	12.64	5.802	1.262E-02	131	4.307E+06	6.827E+02	265.8	.638	.561
3	8	12.64	5.848	2.105E-02	130	2.562E+06	4.063E+02	158.3	.638	.334
3	9	12.62	5.795	1.661E-02	127	3.268E+06	5.194E+02	258.4	.990	.546
3	10	12.63	3.615	6.247E-04	-80	1.394E+08	2.214E+04	+2.1E+04	30.665	45.272
3	11	12.63	5.783	2.577E-02	-56	2.113E+06	3.355E+02	-50.6	-.131	-.107
3	12	12.63	5.859	5.590E-02	-58	9.617E+05	1.527E+02	25.2	.198	.053
4	1	22.70	5.919	1.272E-02	165	1.351E+07	6.640E+02	172.4	.351	.364
4	2	22.76	5.942	2.569E-03	164	6.697E+07	3.275E+03	-1432.0	-.304	-3.024
4	3	22.71	5.943	6.778E-03	-22	2.528E+07	1.241E+03	-958.0	-.436	-2.023
4	4	22.70	5.883	7.558E-03	-24	2.288E+07	1.124E+03	-2760.0	-.711	-5.828
4	5	22.76	5.554	2.811E-03	147	6.550E+07	3.203E+03	-1.6E+04	-.837	-34.833
4	6	22.73	5.981	2.483E-02	116	6.868E+06	3.367E+02	-1.7E+04	-.980	-35.459
4	7	22.71	6.048	8.877E-03	148	1.896E+07	9.314E+02	-1.1E+04	-.920	-22.632
4	8	22.73	5.802	3.908E-03	-40	4.498E+07	2.205E+03	-6770.0	-.754	-14.295
4	9	22.73	6.103	1.516E-02	-40	1.103E+07	5.406E+02	-2667.4	-.831	-5.632
4	10	22.73	6.291	1.292E-02	-44	1.255E+07	6.152E+02	-1649.8	-.728	-3.484
4	11	22.76	6.106	1.088E-02	137	1.539E+07	7.529E+02	-5964.1	-.888	-12.593
4	12	22.73	6.286	5.624E-02	129	2.886E+06	1.414E+02	-334.3	-.703	-.706
5	1	31.79	5.224	9.184E-03	-169	4.157E+07	1.042E+03	-4825.0	-.822	-10.188
5	2	32.85	6.480	2.274E-03	46	1.446E+08	3.393E+03	-6.6E+04	-.951	-138.402
5	3	31.78	5.197	9.805E-04	0	3.912E+08	9.812E+03	7892.0	4.110	16.664
5	4	31.54	3.621	4.570E-04	-12	1.187E+09	3.021E+04	+2.4E+04	4.245	51.626
5	5	31.79	5.408	1.666E-03	171	2.214E+08	5.551E+03	4349.0	3.618	9.183
5	6	31.59	4.299	9.912E-03	111	4.622E+07	1.173E+03	-1.5E+04	-.929	-32.278
5	7	31.89	6.176	2.009E-03	-11	1.618E+08	4.029E+03	3726.7	12.328	7.869
5	8	31.73	5.697	6.220E-03	-26	5.609E+07	1.411E+03	451.2	.470	.953
5	9	31.87	5.936	1.522E-03	163	2.219E+08	5.535E+03	2926.0	1.122	6.178
5	10	31.72	5.702	1.133E-02	145	3.074E+07	7.741E+02	544.9	2.377	1.151
5	11	31.12	4.292	1.610E-03	72	2.767E+08	7.235E+03	6703.8	12.620	14.155
5	12	31.68	5.686	3.642E-02	-44	9.567E+06	2.415E+02	94.4	.642	.199

TABLE 6.5

MODAL RESULTS FROM THE STATIONARY SHAKER TESTS IN DEEP WATER

MODE #	SEGMENT #	FREQ (hz)	DAMPING (%)	PEAK (m)	PHASE (deg)	GENERALIZED STIFFNESS (N/m)	GENERALIZED MASS (kg)	GENERALIZED ADDED MASS (kg)	MASS RATIO	J
1	1	1.00	16.342	1.319E-02	106	9.096E+03	2.320E+02	74.3	.471	.157
1	2	1.02	14.653	1.044E-02	108	1.347E+04	3.268E+02	135.8	.711	.287
1	3	.99	15.154	9.810E-03	103	1.309E+04	3.363E+02	134.4	.666	.284
1	4	.98	14.365	7.976E-03	102	1.669E+04	4.364E+02	183.3	.724	.387
1	5	.97	12.552	6.420E-03	99	2.325E+04	6.205E+02	268.4	.762	.567
1	6	.93	9.706	4.890E-03	94	3.610E+04	1.053E+03	507.2	.929	1.071
1	7	.91	4.824	3.991E-03	113	8.576E+04	2.597E+03	1417.0	1.201	2.992
1	8	1.18	8.240	1.149E-03	-68	2.910E+05	5.280E+03	3310.0	1.680	6.989
1	9	1.12	16.102	2.532E-03	-62	6.096E+04	1.226E+03	668.8	1.200	1.412
1	10	1.11	16.446	4.161E-03	-63	3.531E+04	7.307E+02	339.4	.867	.717
1	11	1.08	16.955	5.752E-03	-65	2.353E+04	5.126E+02	223.1	.771	.471
1	12	1.11	15.206	7.866E-03	-67	2.035E+04	4.180E+02	188.8	.824	.399
2	1	5.22	5.425	6.790E-02	98	1.462E+05	1.357E+02	44.9	.494	.095
2	2	5.22	5.248	4.083E-02	97	2.508E+05	2.333E+02	81.9	.541	.173
2	3	5.22	5.544	1.908E-02	97	5.092E+05	4.728E+02	127.4	.369	.269
2	4	5.25	5.173	3.060E-03	-80	3.432E+06	3.159E+03	1876.0	1.462	3.961
2	5	5.23	5.419	1.990E-02	-83	5.012E+05	4.637E+02	193.7	.717	.409
2	6	5.23	5.461	2.856E-02	-92	3.461E+05	3.206E+02	123.7	.628	.261
2	7	5.23	5.469	2.755E-02	-86	3.577E+05	3.318E+02	136.6	.700	.288
2	8	5.22	5.402	1.754E-02	-86	5.681E+05	5.275E+02	258.6	.962	.546
2	9	5.16	3.826	6.617E-04	-76	2.078E+07	1.975E+04	+1.9E+04	19.973	39.713
2	10	5.23	5.474	2.096E-02	93	4.711E+05	4.359E+02	46.0	.118	.097
2	11	5.23	5.466	4.320E-02	92	2.287E+05	2.118E-02	53.8	.341	.114
2	12	5.22	5.478	6.573E-02	91	1.496E+05	1.389E+02	41.1	.420	.087
3	1	13.24	6.995	5.226E-02	124	9.459E+05	1.368E+02	-19.5	-.125	-.041
3	2	13.28	6.665	2.101E-02	123	2.486E+06	3.570E+02	25.2	.076	.053
3	3	13.29	7.392	4.153E-03	-56	1.136E+07	1.629E+03	608.0	.595	1.284
3	4	13.23	7.129	2.203E-02	-63	2.201E+06	3.184E+02	33.0	.116	.070
3	5	13.23	7.001	2.246E-02	-65	2.197E+06	3.179E+02	26.4	.091	.056
3	6	13.20	6.360	6.382E-03	-88	8.474E+06	1.232E+03	-55.0	-.043	-.116
3	7	13.24	7.191	1.575E-02	111	3.056E+06	4.415E+02	66.6	.178	.141
3	8	13.23	7.009	2.847E-02	110	1.731E+06	2.506E+02	57.2	.296	.121
3	9	13.21	6.926	2.381E-02	107	2.090E+06	3.032E+02	105.4	.533	.223
3	10	13.12	6.222	3.957E-03	103	1.380E+07	2.031E+03	1516.4	2.947	3.202
3	11	13.22	7.011	2.647E-02	-76	1.859E+06	2.694E+02	-43.0	-.138	-.091
3	12	13.21	7.004	6.230E-02	-79	7.897E+05	1.146E+02	7.4	.069	.016
4	1	24.88	7.519	7.520E-03	-178	2.162E+07	8.843E+02	586.4	1.968	1.238
4	2	24.80	6.123	3.255E-03	151	6.090E+07	2.509E+03	-1142.0	-.313	-2.411
4	3	24.71	8.304	2.689E-03	-12	5.399E+07	2.239E+03	1607.8	2.547	3.395
4	4	24.88	7.595	3.621E-03	-14	4.444E+07	1.818E+03	-852.0	-.319	-1.799
4	5	24.88	7.133	4.293E-04	-179	3.990E+08	1.633E+04	4030.0	.328	8.509
4	6	24.79	8.236	2.458E-02	121	5.993E+06	2.470E+02	-1339.0	-.844	-2.827
4	7	24.82	7.912	8.524E-03	152	1.803E+07	7.414E+02	-20.0	-.026	-.042
4	8	25.02	4.611	5.211E-04	7	5.143E+08	2.081E+04	-3.1E+05	-.936	-646.094
4	9	24.70	8.730	1.376E-02	-39	1.003E+07	4.161E+02	-76.2	-.155	-.161
4	10	24.73	8.429	1.557E-02	-45	9.200E+06	3.810E+02	17.9	.049	.038
4	11	24.63	9.102	7.033E-03	136	1.870E+07	7.810E+02	-1827.0	-.701	-3.858
4	12	24.72	8.616	5.485E-02	128	2.552E+06	1.058E+02	8.1	.083	.017
5	1	35.23	7.747	4.146E-02	-138	7.627E+06	1.557E+02	-3.1E+05	-.999	-648.109
5	2	35.88	3.074	3.465E-03	58	2.386E+08	4.695E+03	-1281.0	-.214	-2.705
5	3	35.11	8.091	1.194E-02	25	2.519E+07	5.175E+02	-1526.5	-.747	-3.223
5	4	31.45	10.985	7.264E-03	-81	2.447E+07	6.266E+02	-2.3E+05	-.997	-492.554
5	5	35.14	7.808	6.055E-03	-169	5.157E+07	1.058E+03	-42.0	-.038	-.089
5	6	33.30	11.263	1.860E-02	96	1.045E+07	2.387E+02	-7932.3	-.971	-16.749
5	7	35.24	5.574	9.929E-04	-6	4.431E+08	9.035E+03	8788.6	35.668	18.557
5	8	35.21	7.749	1.420E-04	-5	2.224E+09	4.544E+04	+4.5E+04	136.780	95.250
5	9	34.74	3.129	1.661E-03	130	4.585E+08	9.622E+03	4592.0	.913	9.696
5	10	35.18	7.471	5.026E-03	163	6.506E+07	1.331E+03	942.5	2.426	1.990
5	11	34.60	9.674	3.492E-03	143	6.996E+07	1.480E+03	-318.0	-.177	-.671
5	12	35.08	7.657	2.034E-02	-28	1.560E+07	3.210E+02	6.7	.021	.014

Figure 6.4 VARIATION OF THE "J" FACTOR ALONG MODEL

a) Rigid Body Coupled Mode of Heave and Pitch

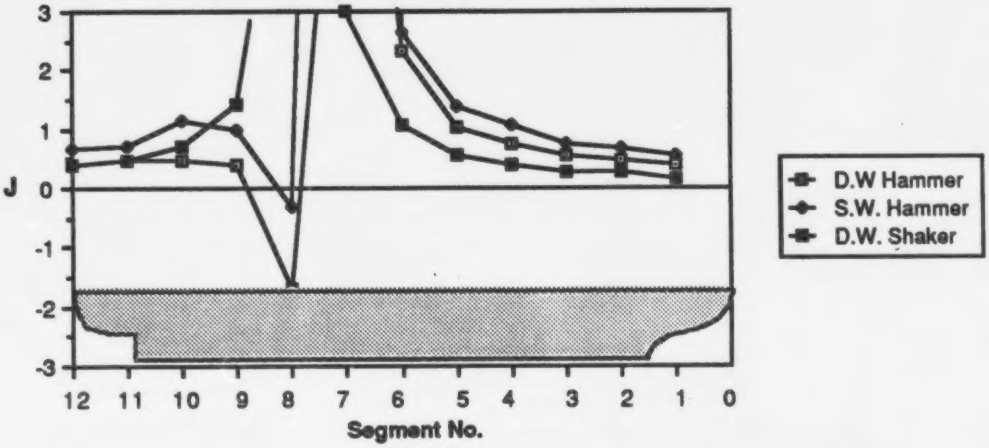

b) First Flexural Mode

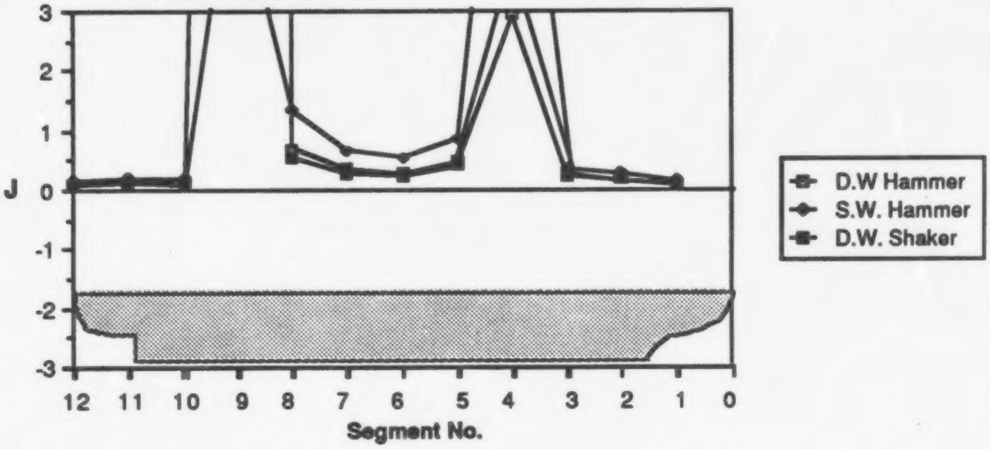

c) Second Flexural Mode

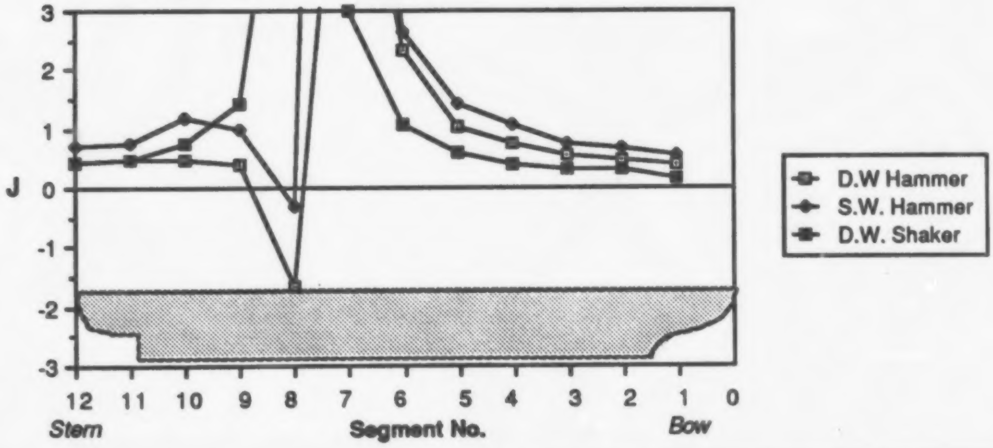

Figures 6.5, 6.6 and 6.7 show the mode shapes for the deep water hammer tests, the shallow water hammer tests, and the deep water shaker tests. The first three mode shapes for the deep water hammer and shaker tests are quite well behaved. The first mode for the shallow water hammer tests has some "whipping" occurring slightly aft of midships. However, the next two modes are well behaved.

Table 6.6 shows the results of the shaker tests with the model excited from the centre of gravity. Figure 6.8a shows the mode shape from these tests. The slight pitching motion seen in figure 6.8a is the reason the generalized mass varies slightly along the model. It is not known whether the pitching motion is due to hydrodynamic effects or by placing the excitation force slightly off the centre of gravity. However, for the calculation of the generalized added mass, mass ratio, and "J", the pitching motion is assumed to be due to hydrodynamic effects. As such, since no dry shaker tests were performed with the model excited from the centre of gravity, the dry modal mass used to calculate the added mass was the model's mass displacement. This assumption would be good as long as the model was excited from its centre of gravity.

Tables 6.7 and 6.8 are the results from the rigid body tests with the model stationary and at a full scale speed of 6 knots respectively. Figures 6.8b and 6.8c show the mode shapes from these tests. Neither figure shows that the model was perfectly rigid, however Figure 6.8c shows some "whipping" at approximately midships. This "whipping" was also observed in the shallow water hammer tests.

6.3 Towed Wet Tests

Tables 6.9, 6.10 and 6.11 list the modal properties for the shaker tests at full scale speeds of 1, 3 and 6 knots respectively. The procedure used to derive these numbers is given in Section 6.1 and 6.2. It must be remembered that only a complete set of data was obtained for the first flexural mode and the 1 and 6 knots speed cases for the second flexural mode. The remainder of the shaker tests could not be performed due to time constraints.

Figure 6.9 shows the variation of "J" as a function of speed and position for the first two flexural modes. The 0, 1 and 3 knot cases are almost identical for the first flexural mode. For these speeds, there is a slight reduction of "J" as speed increases. However, at 6 knots, "J" is considerably different with two large negative peaks at segments 5 and 10.

For the second flexural mode, "J" is less consistent. The value of "J" at 1 knot is slightly higher than for the stationary case. however at 3 knots, the value of "J" is slightly lower than the stationary case. At 6 knots, depending upon the location, "J" is both higher and lower than the stationary case. Two large negative peaks are observed at segments 4 and 7.

Figure 6.10 shows the first mode shape from the towed shaker tests. The rest of the mode shapes are attached to Appendix B.

FIGURE 6.5
STATIONARY WET HAMMER TESTS (Deep Water)

MODE SHAPE: 1 FREQ: .82 Hz DAMPING: 10.71 %

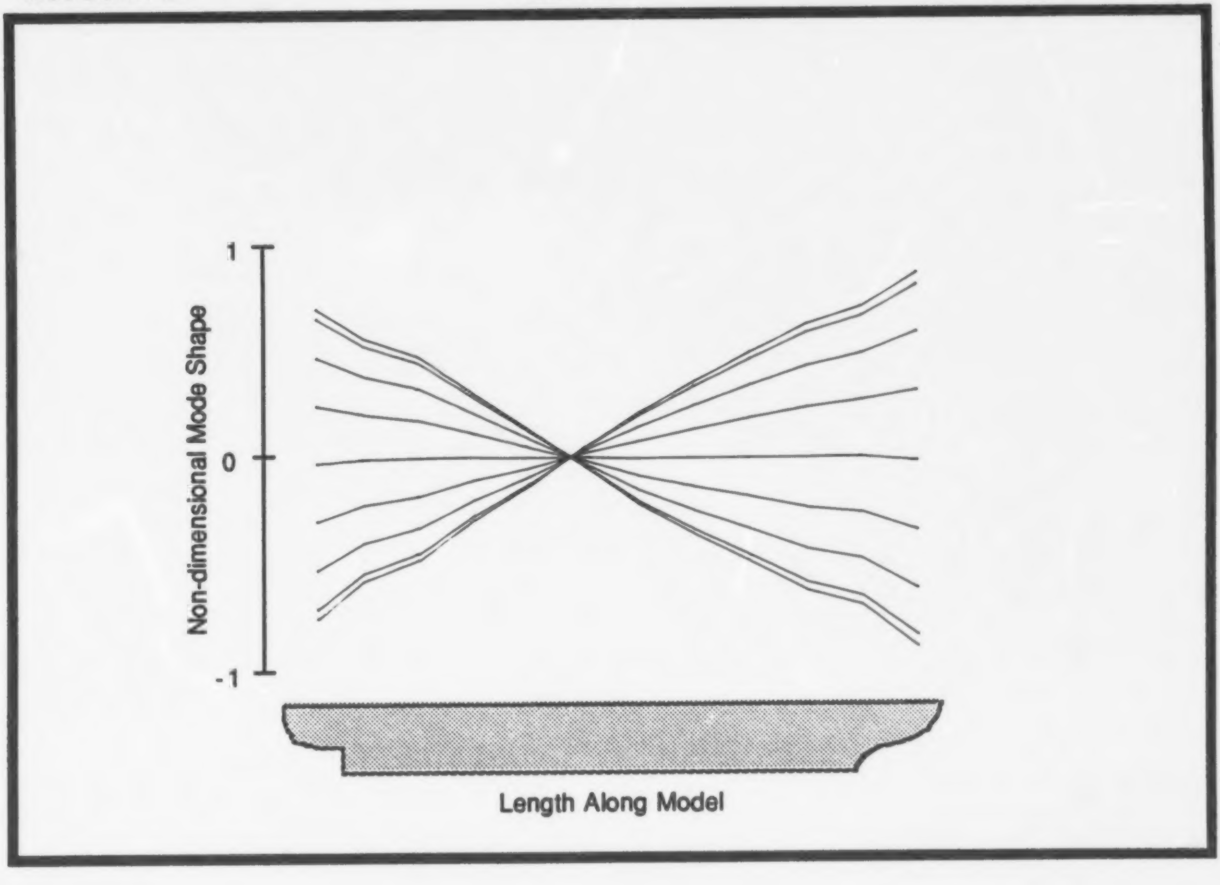

FIGURE 6.6
STATIONARY WET HAMMER TESTS (Shallow Water)

MODE SHAPE: 1 FREQ: .80 Hz DAMPING: 16.29 %

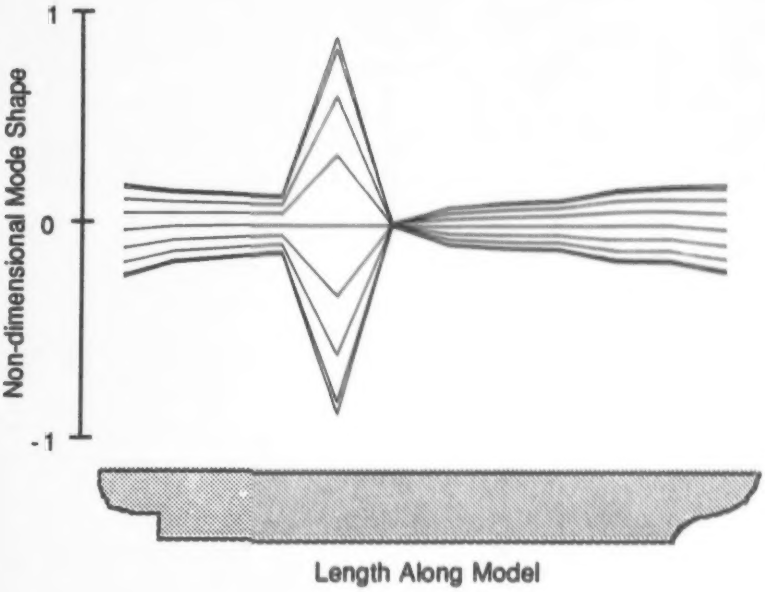

FIGURE 6.7
STATIONARY WET SHAKER TESTS (Deep Water)

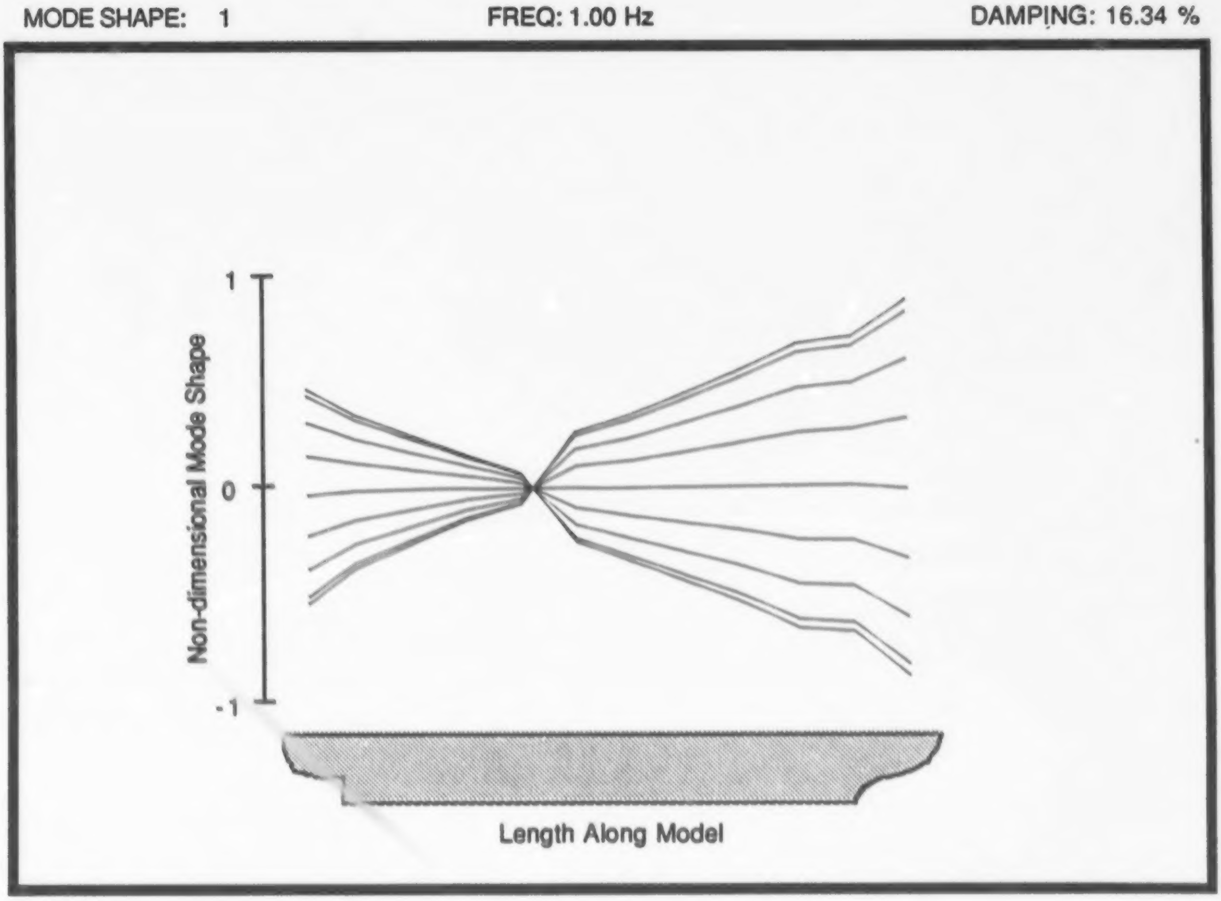

TABLE 6.6

MODAL RESULTS FROM THE STATIONARY SHAKER TESTS EXCITED AT THE CG

MODE NO.	SEGMENT NO.	FREQ. (Hz)	DAMPING (%)	PEAK (m)	PHASE (°)	GENERALIZED STIFFNESS	GENERALIZED MASS	GENERALIZED ADDED MASS	MASS RATIO	J
1	1	1.01	3.747	1.169E-02	120	4.557E+04	1.141E+03	545.5	.916	1.152
1	2	1.01	4.019	1.061E-02	116	4.682E+04	1.172E+03	576.5	.968	1.217
1	3	1.01	4.355	1.069E-02	114	4.292E+04	1.074E+03	478.5	.804	1.010
1	4	1.01	4.613	1.017E-02	111	4.260E+04	1.066E+03	470.5	.790	.993
1	5	1.01	5.091	9.656E-03	107	4.070E+04	1.017E+03	421.5	.708	.890
1	6	1.01	5.445	9.179E-03	104	4.020E+04	1.000E+03	404.5	.679	.854
1	7	1.01	5.901	8.554E-03	102	3.985E+04	9.905E+02	395.0	.663	.834
1	8	1.01	6.627	7.769E-03	101	3.946E+04	9.711E+02	381.6	.641	.806
1	9	1.02	7.176	7.699E-03	99	3.707E+04	3.707E+04	309.5	.520	.654
1	10	1.03	7.543	7.384E-03	99	3.730E+04	8.977E+02	302.2	.507	.638
1	11	1.03	8.168	6.750E-03	98	3.831E+04	9.070E+02	311.5	.523	.658
1	12	1.04	8.414	6.771E-03	99	3.766E+04	8.776E+02	282.1	.474	.596

FIGURE 6.8(a)
STATIONARY SHAKER TESTS EXCITED AT THE CG

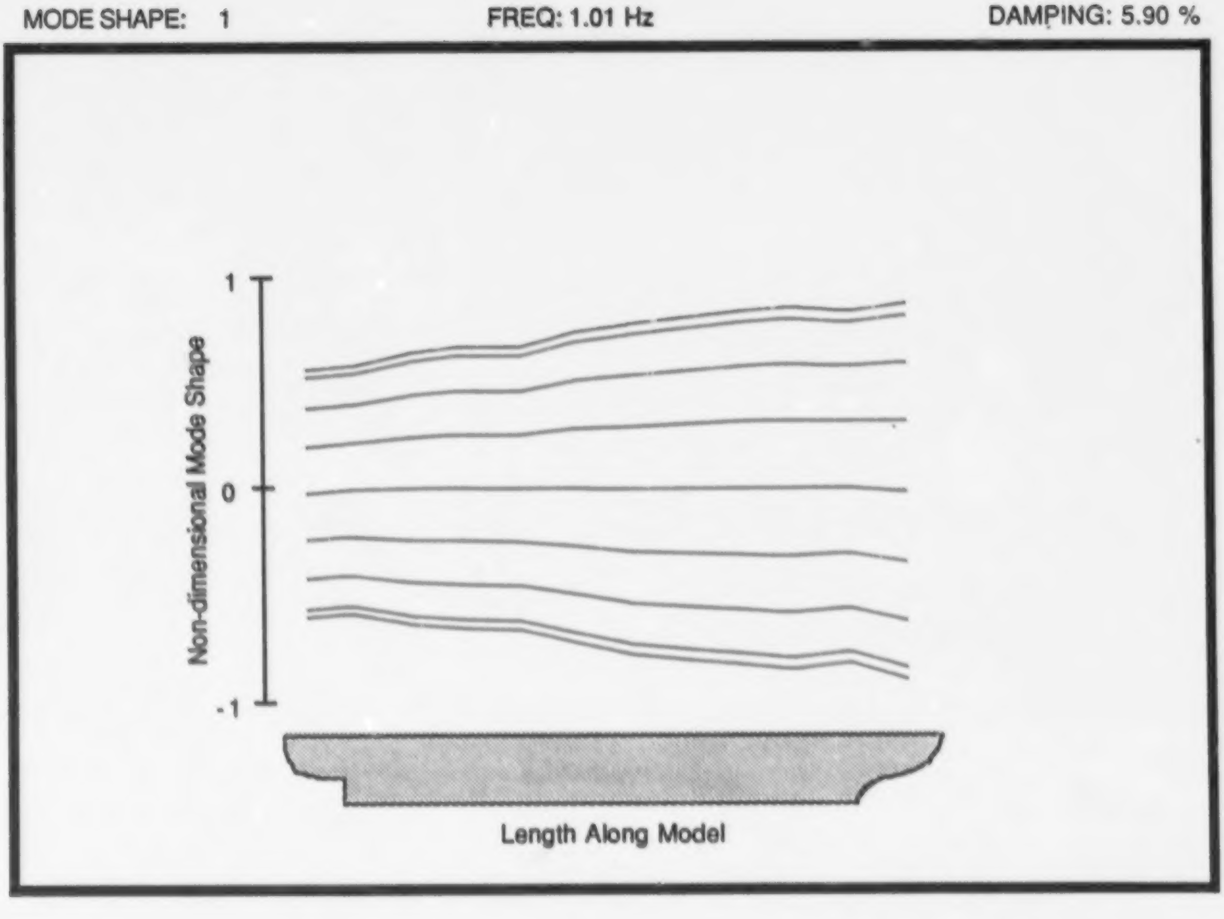

TABLE 6.7

MODAL RESULTS FROM THE STATIONARY RIGID BODY TESTS

MODE #	SEGMENT #	FREQ (hz)	DAMPING (%)	PEAK (m)	PHASE (deg)	GENERALIZED STIFFNESS (N/m)	GENERALIZED MASS (kg)	GENERALIZED ADDED MASS (kg)	MASS RATIO	J
1	1	.94	22.582	1.782E-02	90	4.367E+03	1.243E+02	-33.4	-.212	-.071
1	2	.94	25.338	1.374E-02	89	4.992E+03	1.436E+02	-47.4	-.248	-.100
1	3	.92	21.771	1.276E-02	84	6.058E+03	1.800E+02	-21.9	-.108	-.046
1	4	.91	20.836	1.028E-02	82	7.672E+03	2.335E+02	-19.6	-.077	-.041
1	5	.91	16.948	7.221E-03	83	1.334E+04	4.086E+02	56.5	.160	.119
1	6	.91	11.871	5.232E-03	84	2.603E+04	8.050E+02	259.2	.475	.547
1	7	.95	7.799	3.100E-03	122	7.340E+04	2.068E+03	888.0	.753	1.875
1	8	1.03	5.977	2.091E-03	-146	1.664E+05	4.001E+03	2031.0	1.031	4.288
1	9	1.07	11.205	4.519E-03	-104	4.443E+04	9.875E+02	430.3	.772	.909
1	10	1.08	13.608	5.886E-03	-84	2.891E+04	6.243E+02	233.0	.595	.492
1	11	1.07	16.417	7.343E-03	-77	1.887E+04	4.148E+02	125.3	.433	.265
1	12	1.09	18.054	9.013E-03	-70	1.452E+04	3.073E+02	78.1	.341	.165

TABLE 6.8

MODAL RESULTS FROM THE RIGID BODY TESTS AT 6 KNOTS

MODE #	SEGMENT #	FREQ (hz)	DAMPING (%)	PEAK (m)	PHASE (deg)	GENERALIZED STIFFNESS (N/m)	GENERALIZED MASS (kg)	GENERALIZED ADDED MASS (kg)	MASS RATIO	J
1	1	.95	8.672	2.660E-02	91	7.747E+03	2.168E+02	59.1	.375	.125
1	2	.95	8.622	1.926E-02	90	1.070E+04	3.012E+02	110.2	.577	.233
1	3	.95	8.737	1.803E-02	89	1.121E+04	3.174E+02	115.5	.572	.244
1	4	.94	8.871	1.389E-02	87	1.418E+04	4.059E+02	152.8	.604	.323
1	5	.93	9.044	9.812E-03	83	1.918E+04	5.634E+02	211.3	.600	.446
1	6	.90	8.967	6.179E-03	74	2.907E+04	9.024E+02	356.6	.653	.753
1	7	.88	.380	4.125E-02	79	9.693E+04	3.190E+03	2010.0	1.703	4.244
1	8	1.00	2.340	4.051E-03	-65	2.080E+05	5.276E+03	3306.0	1.678	6.981
1	9	.99	5.574	7.019E-03	-77	4.936E+04	1.278E+03	720.8	1.294	1.522
1	10	.98	6.490	1.074E-02	-81	2.726E+04	7.172E+02	325.9	.833	.688
1	11	.98	6.976	1.465E-02	-82	1.845E+04	4.892E+02	199.7	.690	.422
1	12	.97	7.183	1.7[illegible]7E-02	-85	1.469E+04	3.940E+02	164.8	.719	.348

FIGURE 6.8(b)
STATIONARY RIGID BODY TESTS

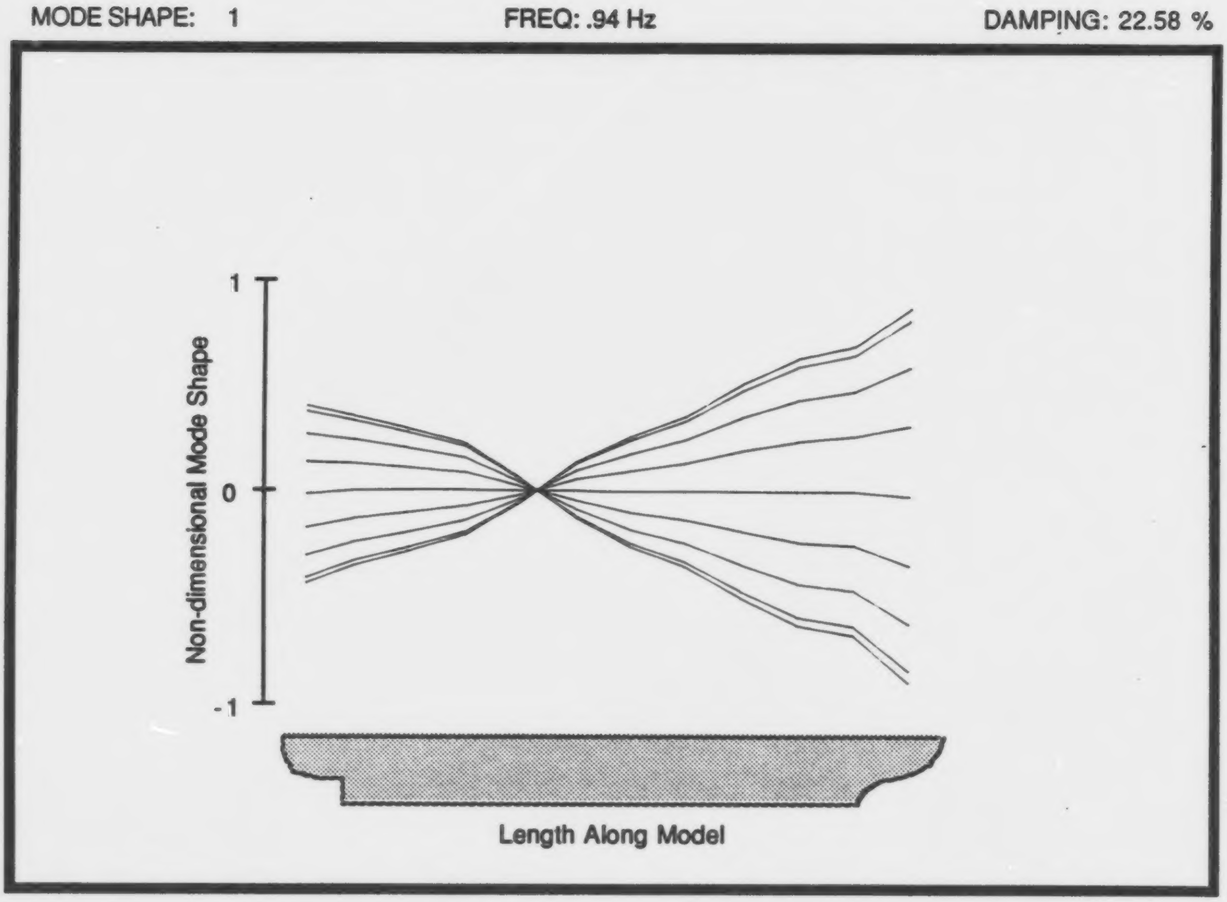

FIGURE 6.8(c)
RIGID BODY TESTS AT 6 KNOTS

MODE SHAPE: 1 FREQ: .95 Hz DAMPING: 8.67 %

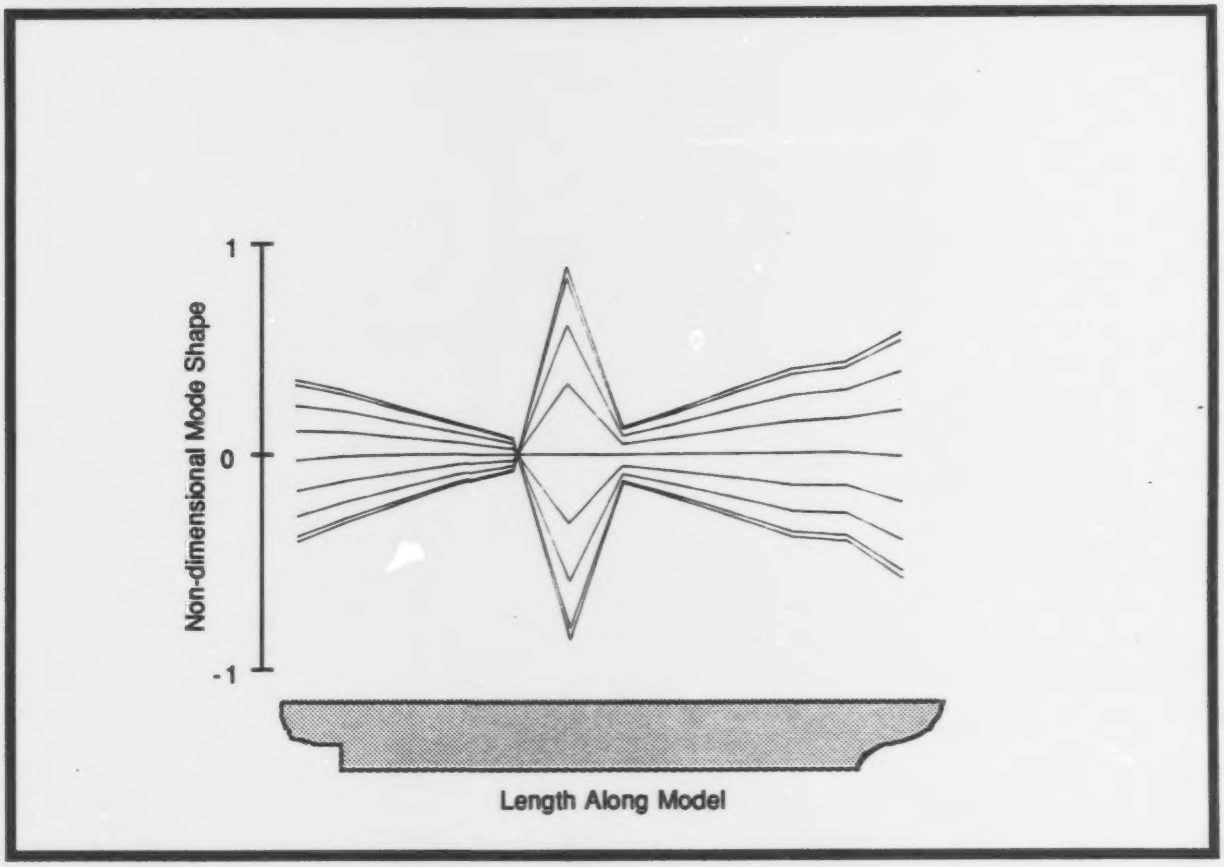

TABLE 6.9

MODAL RESULTS FROM THE SHAKER TESTS AT 1 KNOT

MODE #	SEGMENT #	FREQ (hz)	DAMPING (%)	PEAK (m)	PHASE (deg)	GENERALIZED STIFFNESS (N/m)	GENERALIZED MASS (kg)	GENERALIZED ADDED MASS (kg)	MASS RATIO	J
2	1	5.44	5.779	6.853E-02	107	1.475E+05	1.263E+02	35.5	.390	.075
2	2	5.45	5.368	4.170E-02	109	2.624E+05	2.234E+02	72.0	.476	.152
2	3	5.43	5.821	1.939E-02	104	5.163E+05	4.430E+02	97.6	.283	.206
2	4	5.44	5.535	3.565E-03	-73	2.958E+06	2.534E+03	1251.0	.975	2.641
2	5	5.43	5.677	2.098E-02	-77	4.891E+05	4.197E+02	149.7	.554	.316
2	6	5.44	5.723	2.986E-02	-85	3.413E+05	2.926E+02	95.7	.486	.202
2	7	5.44	5.784	2.758E-02	-78	3.657E+05	3.134E+02	118.2	.606	.250
2	8	5.44	5.924	1.625E-02	-78	6.060E+05	5.193E+02	250.4	.931	.529
2	9	5.49	2.054	1.119E-03	98	2.590E+07	2.176E+04	+2.1E+04	22.107	43.958
2	10	5.44	5.739	2.155E-02	99	4.714E+05	4.042E+02	14.3	.037	.030
2	11	5.44	5.840	4.200E-02	99	2.377E+05	2.038E+02	45.8	.290	.097
2	12	5.43	5.876	6.294E-02	98	1.576E+05	1.352E+02	37.4	.382	.079
3	1	14.31	5.734	5.165E-02	127	1.365E+06	1.688E+02	12.5	.080	.026
3	2	14.24	5.478	2.141E-02	119	3.411E+06	4.262E+02	94.4	.285	.199
3	3	14.43	5.769	4.531E-03	-46	1.573E+07	1.913E+03	892.0	.874	1.883
3	4	14.31	5.477	2.215E-02	-59	3.334E+06	4.122E+02	126.8	.444	.268
3	5	14.29	5.696	2.218E-02	-64	3.190E+06	3.958E+02	104.3	.358	.220
3	6	14.28	4.384	4.932E-03	-100	1.861E+07	2.313E+03	1026.0	.797	2.166
3	7	14.29	5.231	1.812E-02	114	4.251E+06	5.274E+02	152.5	.407	.322
3	8	14.30	5.459	2.913E-02	112	2.537E+06	3.144E+02	121.0	.626	.255
3	9	14.31	5.770	2.166E-02	109	3.234E+06	4.001E+02	202.3	1.023	.427
3	10	14.52	3.752	2.800E-03	96	3.959E+07	4.759E+03	4244.4	8.248	8.962
3	11	14.30	5.599	2.542E-02	-74	2.837E+06	3.513E+02	38.9	.125	.082
3	12	14.30	5.759	5.836E-02	-77	1.201E+06	1.488E+02	41.6	.388	.088

TABLE 6.10

MODAL RESULTS FROM THE SHAKER TESTS AT 3 KNOTS

MODE #	SEGMENT #	FREQ (hz)	DAMPING (%)	PEAK (m)	PHASE (deg)	GENERALIZED STIFFNESS (N/m)	GENERALIZED MASS (kg)	GENERALIZED ADDED MASS (kg)	MASS RATIO	J
2	1	5.37	6.661	6.720E-02	109	1.271E+05	1.116E+02	20.8	.228	.044
2	2	5.38	6.428	3.984E-02	110	2.228E+05	1.952E+02	43.8	.289	.092
2	3	5.37	6.681	1.897E-02	107	4.494E+05	3.946E+02	49.2	.142	.104
2	4	5.40	6.770	3.267E-03	-71	2.600E+06	2.261E+03	978.0	.762	2.065
2	5	5.36	6.605	2.055E-02	-76	4.184E+05	3.684E+02	98.4	.364	.208
2	6	5.37	6.578	2.944E-02	-84	2.938E+05	2.582E+02	61.3	.311	.129
2	7	5.37	6.570	2.740E-02	-76	3.159E+05	2.777E+02	82.5	.423	.174
2	8	5.36	6.447	1.679E-02	-77	5.232E+05	4.619E+02	193.0	.718	.408
2	9	5.66	.049	3.663E-02	61	3.528E+07	2.793E+04	+2.7E+04	28.659	56.985
2	10	5.36	6.598	2.144E-02	100	4.012E+05	3.535E+02	-36.4	-.093	-.077
2	11	5.36	6.591	4.256E-02	100	2.019E+05	1.782E+02	20.2	.128	.043
2	12	5.35	6.577	6.436E-02	99	1.337E+05	1.181E+02	20.3	.207	.043
3	1	13.55	9.332	5.441E-02	116	7.142E+05	9.847E+01	-57.8	-.370	-.122
3	2	13.54	8.984	2.006E-02	113	2.007E+06	2.774E+02	-54.4	-.164	-.115
3	3	13.65	10.117	4.507E-03	-62	8.069E+06	1.096E+03	75.0	.073	.158
3	4	13.55	9.414	2.260E-02	-70	1.703E+06	2.350E+02	-50.4	-.177	-.106
3	5	13.54	9.228	2.248E-02	-73	1.746E+06	2.411E+02	-50.4	-.173	-.106
3	6	13.53	7.913	5.571E-03	-95	8.201E+06	1.134E+03	-153.0	-.119	-.323
3	7	13.55	9.689	1.656E-02	104	2.260E+06	3.117E+02	-63.2	-.169	-.133
3	8	13.54	9.395	2.903E-02	103	1.326E+06	1.833E+02	-10.1	-.052	-.021
3	9	13.53	9.259	2.360E-02	100	1.653E+06	2.288E+02	31.0	.157	.065
3	10	13.52	8.233	3.468E-03	100	1.263E+07	1.751E+03	1236.4	2.403	2.611
3	11	13.53	9.420	2.592E-02	-83	1.480E+06	2.048E+02	-107.6	-.344	-.227
3	12	13.53	9.319	6.086E-02	-86	6.360E+05	8.815E+01	-19.0	-.178	-.040

TABLE 6.11

MODAL RESULTS FROM THE SHAKER TESTS AT 6 KNOTS

MODE #	SEGMENT #	FREQ (hz)	DAMPING (%)	PEAK (m)	PHASE (deg)	GENERALIZED STIFFNESS (N/m)	GENERALIZED MASS (kg)	GENERALIZED ADDED MASS (kg)	MASS RATIO	J
2	1	5.31	5.886	6.547E-02	102	1.442E+05	1.297E+02	-99.5	-.434	-.210
2	2	5.30	5.845	3.933E-02	102	2.416E+05	2.175E+02	126.6	1.394	.267
2	3	5.30	6.129	1.880E-02	99	4.802E+05	4.339E+02	282.5	1.866	.596
2	4	5.32	6.024	3.037E-03	-80	3.052E+06	2.733E+03	2387.6	6.913	5.041
2	5	5.31	5.854	1.935E-02	-81	4.916E+05	4.414E+02	-841.6	-.656	-1.777
2	6	5.31	5.905	2.795E-02	-90	3.369E+05	3.029E+02	32.9	.122	.069
2	7	5.31	5.959	2.672E-02	-83	3.490E+05	3.140E+02	117.1	.595	.247
2	8	5.30	5.914	1.680E-02	-83	5.588E+05	5.034E+02	308.2	1.579	.651
2	9	5.24	4.355	2.421E-04	-49	5.137E+07	4.742E+04	+4.7E+04	175.348	99.559
2	10	5.31	5.931	2.043E-02	95	4.595E+05	4.127E+02	-529.0	-.562	-1.117
2	11	5.31	5.961	4.121E-02	94	2.263E+05	2.035E+02	-186.4	-.478	-.394
2	12	5.31	5.971	6.275E-02	94	1.483E+05	1.334E+02	-24.6	-.156	-.052
3	1	14.11	6.108	5.523E-02	119	1.165E+06	1.482E+02	50.4	.515	.106
3	2	14.07	5.905	2.152E-02	113	3.073E+06	3.935E+02	237.2	1.518	.501
3	3	14.11	5.906	5.360E-03	-65	1.242E+07	1.579E+03	1247.2	3.759	2.633
3	4	14.11	5.984	2.332E-02	-67	2.817E+06	3.583E+02	-662.7	-.649	-1.399
3	5	14.12	6.170	2.271E-02	-69	2.807E+06	3.568E+02	71.4	.250	.151
3	6	14.27	6.626	4.964E-03	-83	1.222E+07	1.520E+03	1228.5	4.214	2.594
3	7	14.08	5.825	1.837E-02	105	3.659E+06	4.673E+02	-819.7	-.637	-1.731
3	8	14.11	5.973	2.982E-02	106	2.206E+06	2.807E+02	-94.2	-.251	-.199
3	9	14.16	6.432	2.209E-02	107	2.787E+06	3.519E+02	158.5	.820	.335
3	10	14.86	6.458	1.387E-03	142	4.870E+07	5.584E+03	5386.2	27.231	11.373
3	11	14.14	6.229	2.535E-02	-78	2.500E+06	3.166E+02	-198.0	-.385	-.418
3	12	14.15	6.350	5.851E-02	-80	1.064E+06	1.346E+02	-177.8	-.569	-.375

Figure 6.9 VARIATION OF THE "J" FACTOR WITH VELOCITY

a) First Flexural Mode

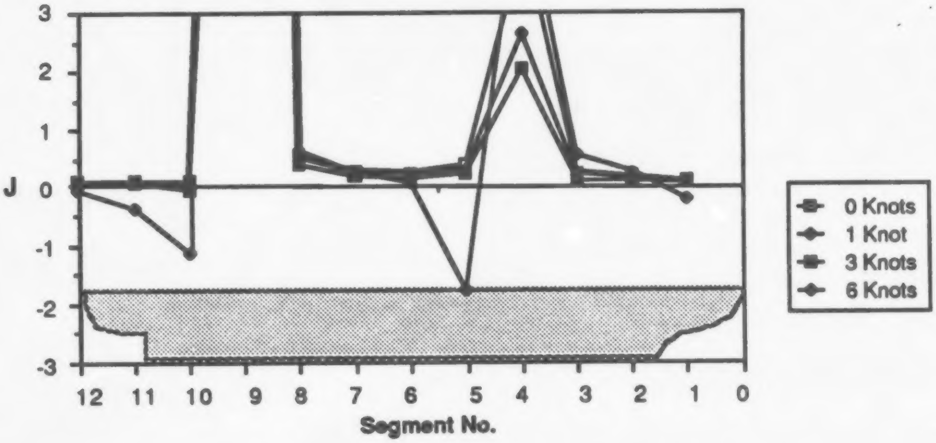

b) Second Flexural Mode

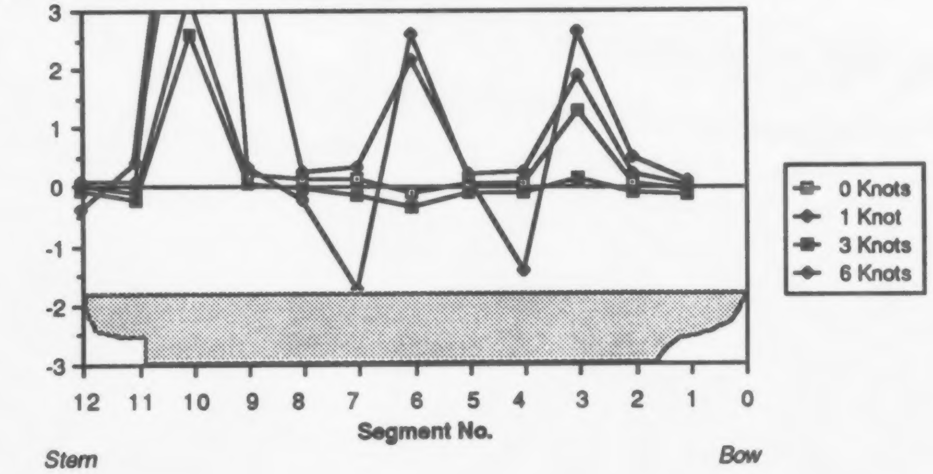

FIGURE 6.10
WET SHAKER TESTS AT 1 KNOT

MODE SHAPE: 2 FREQ: 5.44 Hz DAMPING: 5.78 %

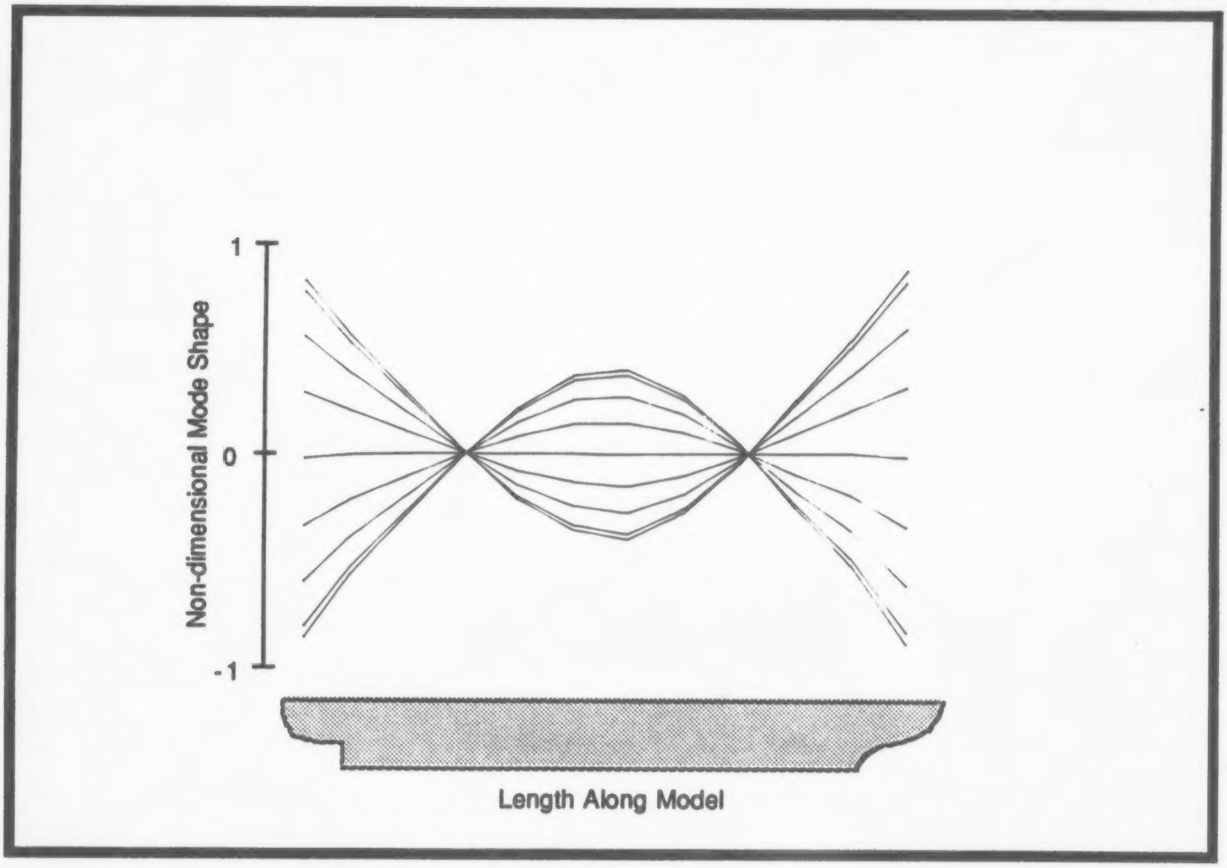

6.4 Tests in Uniform Ice Cover

Table 6.12 lists the modal properties for the shaker tests in ice. The procedure used to derive these numbers is given in section 6.1 and 6.2.

Figure 6.11 shows the effect that ice has on the value of "J". In the rigid body mode, the presence of level ice increases the added mass in the bow by approximately 250%. In the midbody, the increase in added mass due to the ice is larger, however, this is in the vicinity of a node. in the stern, possibly because of an open channel behind the model, the added mass in the presence of ice in only 30 to 40% larger.

For the first flexural mode, the ice does not appear to affect the added mass as much. Typically, the added mass in ice was 10 to 30% above the added mass in open water.

For the second flexural mode, the added mass in ice tends to be lower than the added mass in open water. For the bow half of the model, the added mass in ice was slightly negative. Figure 6.12 shows the mode shapes in ice.

TABLE 6.12

MODAL RESULTS FROM THE SHAKER TESTS IN LEVEL ICE

MODE #	SEGMENT #	FREQ (hz)	DAMPING (%)	PEAK (m)	PHASE (deg)	GENERALIZED STIFFNESS (N/m)	GENERALIZED MASS (kg)	GENERALIZED ADDED MASS (kg)	MASS RATIO	J
1	1	1.02	11.980	9.999E-03	132	1.704E+04	4.174E+02	259.7	1.647	.548
1	2	1.02	12.158	6.503E-03	134	2.589E+04	6.324E+02	441.4	2.311	.932
1	3	1.02	12.523	5.910E-03	136	2.758E+04	6.755E+02	473.6	2.346	1.000
1	4	1.01	13.104	4.019E-03	139	3.824E+04	9.436E+02	690.5	2.728	1.458
1	5	1.01	14.228	2.050E-03	147	6.918E+04	1.714E+03	1361.9	3.868	2.876
1	6	.99	13.980	8.730E-04	155	1.573E+05	4.097E+03	3551.2	6.506	7.498
1	7	.95	6.809	1.313E-04	179	2.002E+06	5.593E+04	+5.5E+04	46.398	115.604
1	8	.99	5.968	3.723E-03	-107	8.775E+04	2.250E+03	280.0	.142	.591
1	9	1.01	6.915	6.507E-03	-81	4.475E+04	1.111E+03	553.8	.994	1.169
1	10	1.02	7.697	8.677E-03	-72	3.050E+04	7.486E+02	357.3	.913	.754
1	11	1.02	8.162	1.055E-02	-69	2.371E+04	5.808E+02	291.3	1.006	.615
1	12	1.02	8.215	1.222E-02	-63	2.050E+04	4.979E+02	268.7	1.172	.567
2	1	5.36	5.391	6.600E-02	92	1.591E+05	1.405E+02	49.6	.547	.105
2	2	5.36	5.119	3.957E-02	93	2.802E+05	2.469E+02	95.5	.631	.202
2	3	5.36	5.607	1.844E-02	92	5.485E+05	4.837E+02	138.3	.400	.292
2	4	5.37	6.212	3.187E-03	-82	2.879E+06	2.526E+03	1243.0	.969	2.625
2	5	5.37	5.481	1.946E-02	-87	5.338E+05	4.688E+02	198.8	.736	.420
2	6	5.36	5.484	2.742E-02	-97	3.778E+05	3.326E+02	135.7	.689	.287
2	7	5.36	5.505	2.634E-02	-91	3.909E+05	3.448E+02	149.6	.766	.316
2	8	5.35	5.256	1.596E-02	-93	6.741E+05	5.960E+02	327.1	1.216	.691
2	9	5.52	6.288	5.199E-04	112	1.841E+07	1.530E+04	+1.4E+04	15.247	30.317
2	10	5.37	5.514	2.023E-02	89	5.111E+05	4.481E+02	58.2	.149	.123
2	11	5.37	5.502	4.003E-02	88	2.584E+05	2.270E+02	69.0	.437	.146
2	12	5.37	5.509	5.962E-02	87	1.731E+05	1.522E+02	54.4	.556	.115
3	1	14.00	7.404	6.500E-02	98	8.035E+05	1.039E+02	-52.4	-.335	-.111
3	2	13.92	8.093	2.417E-02	92	1.957E+06	2.556E+02	-76.2	-.230	-.161
3	3	14.19	8.392	6.196E-03	-71	7.643E+06	9.617E+02	-59.3	-.058	-.125
3	4	14.02	7.513	2.640E-02	-86	1.955E+06	2.521E+02	-33.3	-.117	-.070
3	5	13.98	7.061	2.476E-02	-92	2.206E+06	2.860E+02	-5.5	-.019	-.012
3	6	14.24	3.266	4.317E-03	-108	2.840E+07	3.546E+03	2259.0	1.755	4.770
3	7	14.02	7.738	2.061E-02	88	2.433E+06	3.135E+02	-61.4	-.164	-.130
3	8	14.00	7.234	3.195E-02	86	1.675E+06	2.163E+02	22.9	.118	.048
3	9	14.01	6.930	2.262E-02	83	2.473E+06	3.189E+02	121.1	.612	.256
3	10	14.10	4.924	1.287E-03	72	6.196E+07	7.889E+03	7374.4	14.330	15.571
3	11	14.00	7.178	2.631E-02	-100	2.047E+06	2.648E+02	-47.6	-.152	-.101
3	12	13.99	7.141	5.687E-02	-104	9.511E+05	1.231E+02	15.9	.148	.034
4	1	26.08	6.152	4.966E-02	124	4.395E+06	1.636E+02	-134.3	-.451	-.284
4	2	26.05	7.533	6.964E-03	106	2.554E+07	9.531E+02	-2697.9	-.739	-5.697
4	3	26.03	6.159	1.971E-02	-64	1.102E+07	4.119E+02	-219.3	-.347	-.463
4	4	25.94	6.039	1.917E-02	-77	1.148E+07	4.319E+02	-2238.1	-.838	-4.726
4	5	26.49	6.340	5.105E-03	138	4.279E+07	1.545E+03	-1.1E+04	-.874	-22.709
4	6	25.98	6.180	2.748E-02	64	7.048E+06	2.944E+02	-1291.6	-.814	-2.727
4	7	25.66	6.368	1.583E-02	76	1.289E+07	4.959E+02	-265.5	-.349	-.561
4	8	26.13	6.580	8.717E-03	-69	2.350E+07	8.717E+02	-3.3E+05	-.997	-688.193
4	9	25.70	7.014	2.489E-02	-106	7.470E+06	2.864E+02	-205.9	-.418	-.435
4	10	25.79	8.649	2.227E-02	-111	6.815E+06	2.595E+02	-103.6	-.285	-.219
4	11	25.76	7.153	1.382E-02	75	1.325E+07	5.059E+02	-2102.1	-.806	-4.439
4	12	25.76	8.047	7.033E-02	64	2.315E+06	8.835E+01	-9.3	-.096	-.020

Figure 6.11 VARIATION OF THE "J" FACTOR DUE TO THE PRESENCE OF ICE

a) Rigid Body Coupled Mode of Heave and Pitch

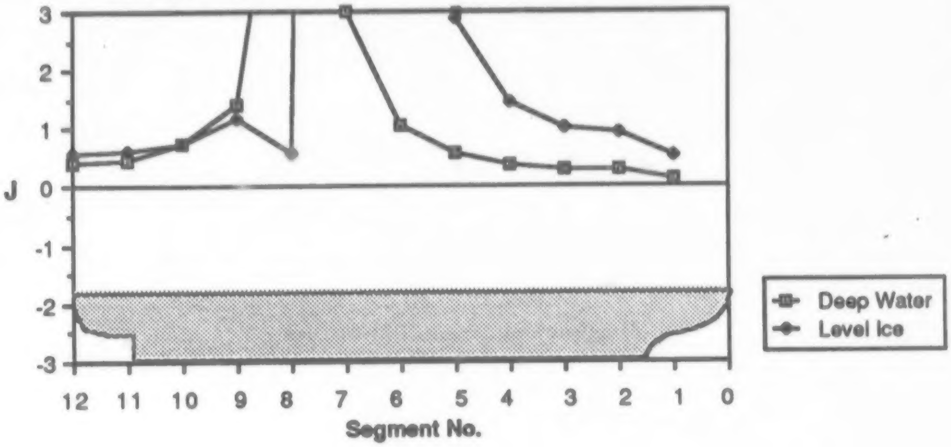

b) First Flexural Mode

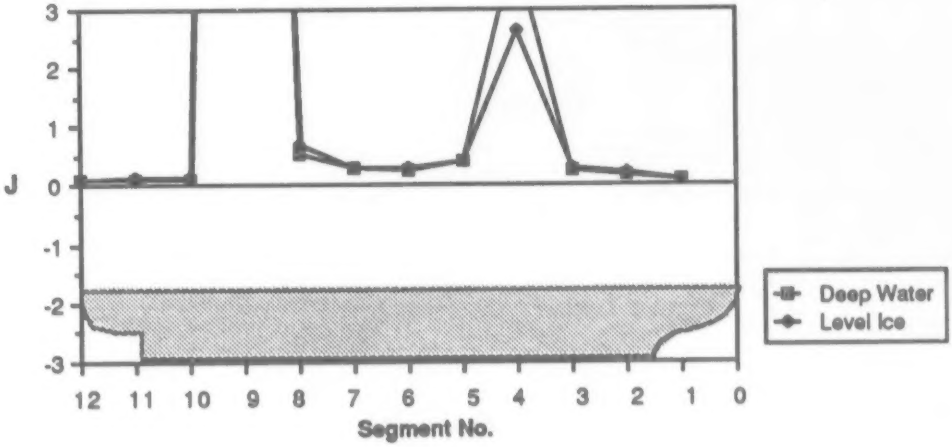

c) Second Flexural Mode

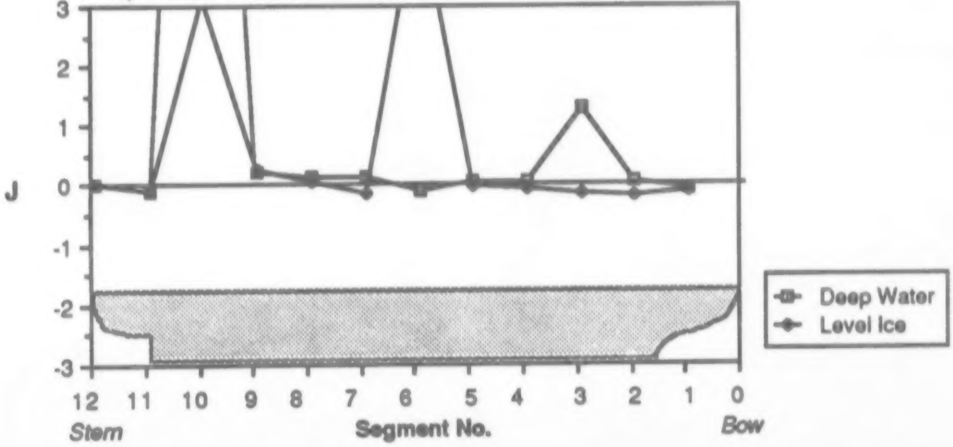

FIGURE 6.12
STATIONARY TESTS IN ICE

MODE SHAPE: 3 FREQ: 14 Hz DAMPING: 7.40 %

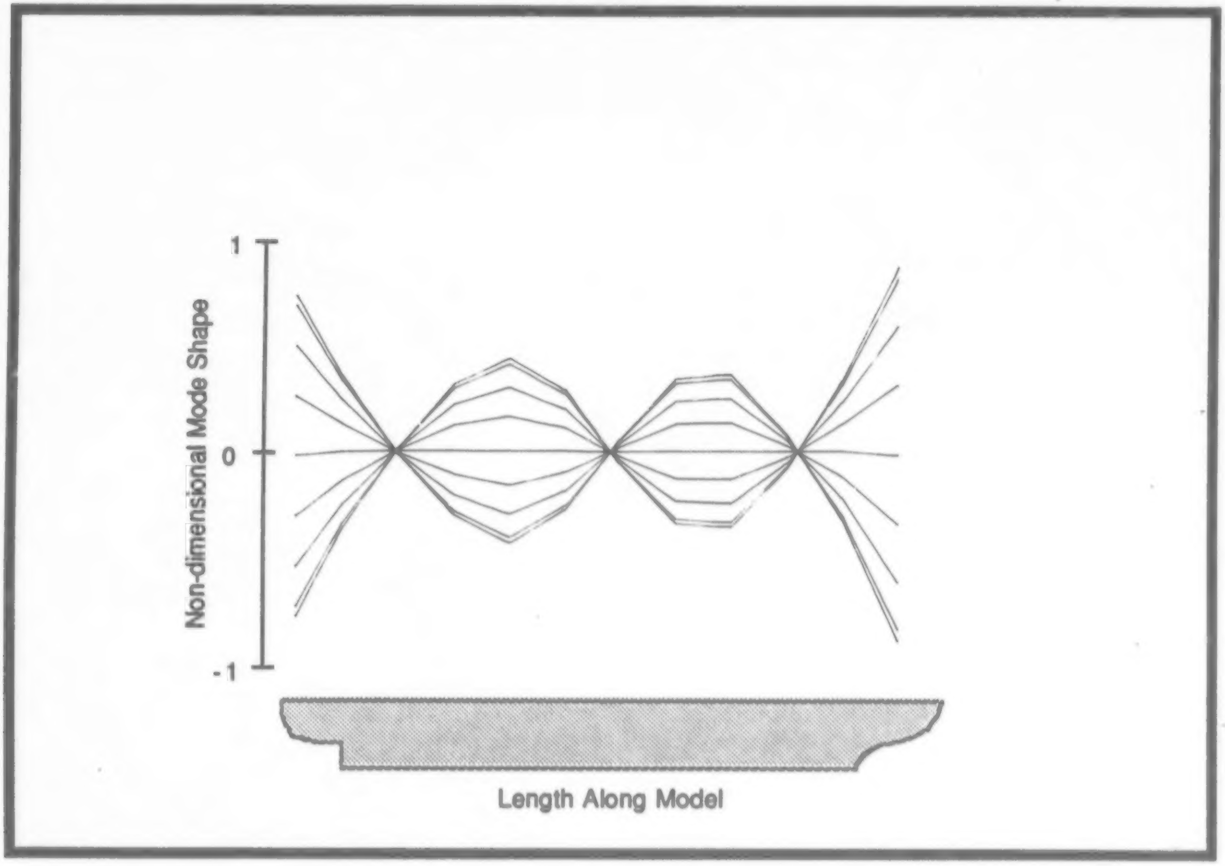

7. CONCLUSIONS

A number of general conclusions can be drawn as a result of the conduct of the model experimental program and the subsequent analysis of the data:

- The test program consisting of dry and wet hammer and shaker tests is a simple but effective means of determining the combined effects of hydrodynamic added mass and damping.
- In the 40:1, segmented, flexible model of the MV ARCTIC used in the present tests, the dynamic flexural modes are easily monitored by the accelerometer system. When compared with full scale, the first and second flexural modes are realistically represented in the physical model.
- Dynamic transfer functions of the model hull exhibit the influence of hydrodynamic added mass and damping qualitatively. They serve as means of comparing the effects of shallow water, forward speed and level ice cover.
- Zero-speed dry, wet and ice cover test data depicted substantial differences in the natural frequencies resulting from the hydrodynamic added mass effects. Similarly relative damping is shown to have moderate influence on the magnitude of response at every mode.
- Forward speed effects are significant at second and higher flexural modes of response. Two effects are apparent - natural frequencies increase with forward speed; for the first and second mode of response, the damping is higher at higher speeds, but for higher modes, the damping is lower than that for the zero-speed case.

The following specific conclusions can be drawn on the hydrodynamic added mass and damping for the MV ARCTIC hull form:

- From the dry hammer tests, it is seen that the structural (internal) hull damping increases with the mode number up to the third mode and at the fourth mode drops below that at the third mode. Variation of hull damping along the length of the hull is significant in the first mode. But at higher modes damping is essentially uniform through the length of the hull. These damping factors are applicable to damped oscillation cases.
- From the dry shaker tests on the other hand, it is clearly observed that internal hull damping is a function of the frequency of oscillation. Further, significant variation of damping along the hull is observed only in the first mode. The magnitude of damping, once again, increases with the mode number up to the third mode, beyond which it drops slightly. However, damping at modes higher than the third, is not considered accurate in the present series of tests.

- From zero-speed hammer tests in deep water, it is seen that the hydrodynamic added mass, expressed as J-factors, varies along the length of the hull attaining large values near the nodes. In general, positive values are obtained for J-factors. However, in the third mode negative values are registered locally at segments where accelerations are very low (i.e. near the nodal points). Added mass values for the fourth and fifth modes are not accurate. Damping factor is nearly constant at 10% for the forward and aft segment of the hull, while for the intermediate segments the damping drops to roughly 4%. It is also seen that the damping is mode dependent, roughly 50% lower for the second mode.

- From zero-speed hammer tests in shallow water, it is seen that the hydrodynamic added mass is roughly 40% higher at the bow and the forward segments, while at the stern segments it is 55 to 65% higher than those determined from the deep water tests. At or near the second nodal point the increase is much higher, of the order of 100%. Damping, on the other hand, is roughly 50% higher at the forward end of the hull and about 20% higher at the aft end.

- In general, considerably lower added mass values (J-factors) were obtained from the zero-speed shaker tests. As shaker tests are inherently more accurate than the hammer tests, it is concluded that these numbers are appropriate for all application purposes. It is also observed that damping is considerably higher in the zero-speed shaker tests and tend to increase in magnitude with the mode number.

- From the shaker tests with forward speed, it is seen that hydrodynamic added mass dropped as much as 30% at a moderate speed of 3 knots. Towards higher speeds (6 knots), this trend is reversed and the added mass shows fairly large fluctuations with associated local negative J-factors. Damping, on the other hand, increases significantly at the moderate speed of 3 knots, but at 6 knots drops down to the level observed at 1 knot.

- From the preliminary shaker tests carried out in level unbroken ice, it is observed that in the rigid body mode, the presence of ice increases the added mass at the bow by approximately 250% and at the stern by roughly 35% compared to those obtained from stationary shaker tests in open water. The increase is substantially lower for the first flexural mode, only by about 30%. Further reduction is observed at the second flexural mode.

8. RECOMMENDATIONS

The model experimental program reported herein has successfully accomplished most of the objectives of the original proposal and those of the statement of work later drawn up based on the proposal. A unique 40:1 scale physical model of the bulk carrier MV ARCTIC was used in the experiments which resulted in a substantial data base of hydrodynamic added mass and damping applicable to hull response calculations in the longitudinal vertical plane. A number of phenomena, such as the influence of hydrodynamic inertia on the natural frequencies of hull response, shallow water effects, forward speed effects and the influence of a level ice cover, were investigated. In order to complement the established results, a number of small tasks involving a limited series of tests have been identified:

- Replication of the hammer tests in air and in water (deep and shallow) to reduce the statistical error in the data processing.

- Conduct of additional shaker tests in the presence of unbroken as well as broken level ice cover of various thicknesses.

- Extension of the tests in ice to situations in which the bow segment is located in a notch or cavity. The thickness of the ice feature in this case will be comparable to the vessel draft.

- Tests to determine the influence of vessel draft on the hydrodynamic parameters.

- The segmented flexible model used in the present study is not adequate for rigid body oscillation tests, as there is no arrangement by which the model can be made totally rigid. A separate series of shaker tests should be carried out with a wooden model to establish accurately the hydrodynamic added mass and damping in the lowest rigid body modes of hull response.

9. REFERENCES

[1] Continuation of Parametric Model Study of MV ARCTIC Hydroelastic Response Durng Multi-Year Ice Impacts, Volume I - Methodology and Results, ACL Report FR 1942C, TP7936E, August 1986.

[2] Daley, C.G., Phillips, L.P., Parametric Model Study of MV ARCTIC Hydroelastic Response During Multi-year Ice Impacts, Transport Canda Report TP6536E, 1985, submitted by Arctec Canada Limited.

[3] Canarctic/NS&E, Test Ice for Dedicated Tests, MV ARCTIC 1984, Vol. 1 and 2, Transport Canada TP6270E, by Norland Science and Engineering Limited, 1984.

[4] Volcy, G.C., "L'amortissement dans le vibrations des Navires", Bulletin Technique du Bureau Veritas, p. 282-291, November 1979.

[5] Investigation of Added Mass With a Flexible Model of the MV ARCTIC, Volume 1 - Review of Existing Methods, Available Data and Summary of Experimental Results, prepared for Transportation Development Centre by Arctec Canada Limited, March 1987.

[6] Investigation of Added Mass With a Flexible Model of the MV ARCTIC, Volume 2 - Time Domain Analysis of Hull Response During Ramming, prepared for Transportation Development Centre by Arctec Canada Limited, March 1987.

APPENDIX A

SPECIFICATIONS OF MB-50 ELECTRODYNAMIC SHAKER

Rev. 86/06/13

MB MODAL 50 Specifications

STANDARD FEATURES

Stroke:	1.0 inch Peak-to-peak (continuous duty) (1.2 inches between stops)
Force Output when cooled by customer's "shop air" supply:	- 50 Pounds(peak)
Force Output when Convection Cooled:	- 25 Pounds(peak)
Stinger Attachments:	Chucks, for stingers (unthreaded) from piano wire up to 3/16" diameter
Shaker Attachments:	- Floor-mount with trunnion base & screw feet - Suspended with multiple turnbuckles
Test Specimen Static Preload:	Capable of tensioning stinger in excess of 50 pounds
Weights:	Shaker with trunnion base: 55 pounds "Bolt on" inertial masses: 30 pounds each - 2 Amplifier : 50 pounds
Suspension Stiffness:	<15 pounds/inch
Bounce Mode of "Large Intertial Configuration" on Armature Suspension:	Approximately 1 Hz
Frequency Range:	1 - 5000 Hz
Armature Weight:	<0.4 pounds
Dimensions:	11-5/8" High (to top of collet chuck with feet retracted) with 7-1/2" x 9-1/4" footprint
Drive Cable Length:	- 30 feet standard (up to 150 ft. optional)
Armature Protection:	- Overtravel switch - Overtravel snubbers
Accessory Kit:	Carrying case for holding chucks, turnbuckles, bolts and nuts for bolt-on masses, and wrenches (which are all supplied with MODAL 50) plus stingers, load cells, etc. (which are supplied by customer)

EXTRA COST OPTIONS

Forced-Air Cooling:	Auxiliary fan with air hose: only necessary if required force exceeds "convection cooled" ratings and if "shop air" supply is not available

APPENDIX B

RESPONSE TRANSFER FUNCTIONS AND MODE SHAPES

- RESPONSE TRANSFER FUNCTION FOR THE HAMMER TESTS
- RESPONSE TRANSFER FUNCTION FOR THE STATIONARY SHAKER TESTS
- RESPONSE TRANSFER FUNCTION FOR THE TOWED SHAKER TESTS
- DRY TEST COMPARISON
- MODE SHAPES FROM THE DRY HAMMER TESTS
- MODE SHAPES FROM THE DRY SHAKER TESTS
- WET TEST COMPARISON
- MODE SHAPES FOR THE DEEP WATER HAMMER TESTS
- MODE SHAPES FOR THE SHALLOW WATER HAMMER TESTS
- MODE SHAPES FOR THE DEEP WATER SHAKER TESTS
- MODE SHAPES FOR THE TOWED SHAKER TESTS
- MODE SHAPES IN ICE
- RESPONSE TRANSFER FUNCTION FOR STRUCTURAL FRAME TESTS

RESPONSE TRANSFER FUNCTION FOR THE HAMMER TESTS

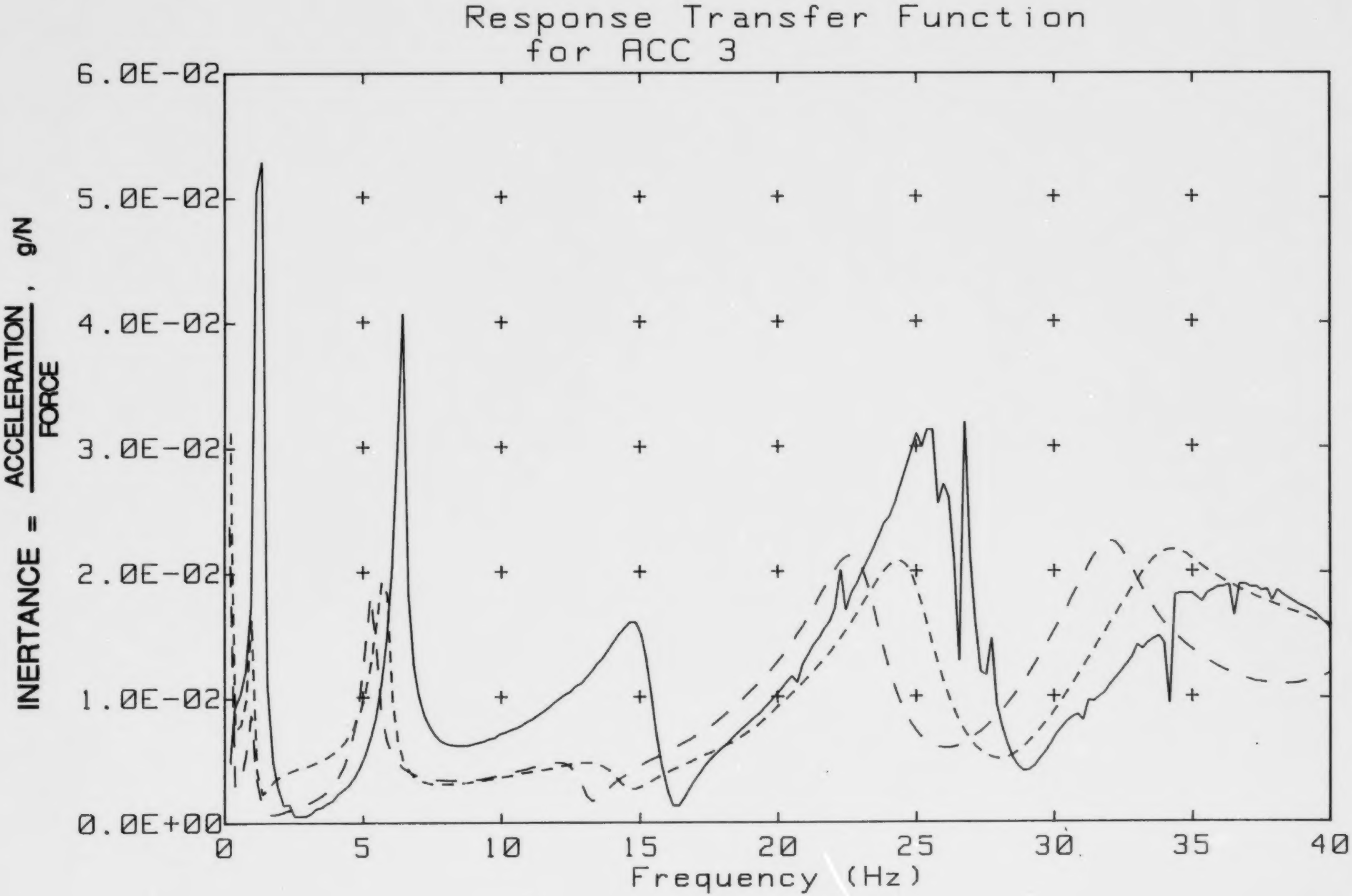
Response Transfer Function
for ACC 3
INERTANCE = ACCELERATION / FORCE , g/N
6.0E-02
5.0E-02
4.0E-02
3.0E-02
2.0E-02
1.0E-02
0.0E+00
0
5
10
15
20
25
30
35
40
Frequency (Hz)

Response Transfer Function
for ACC 4

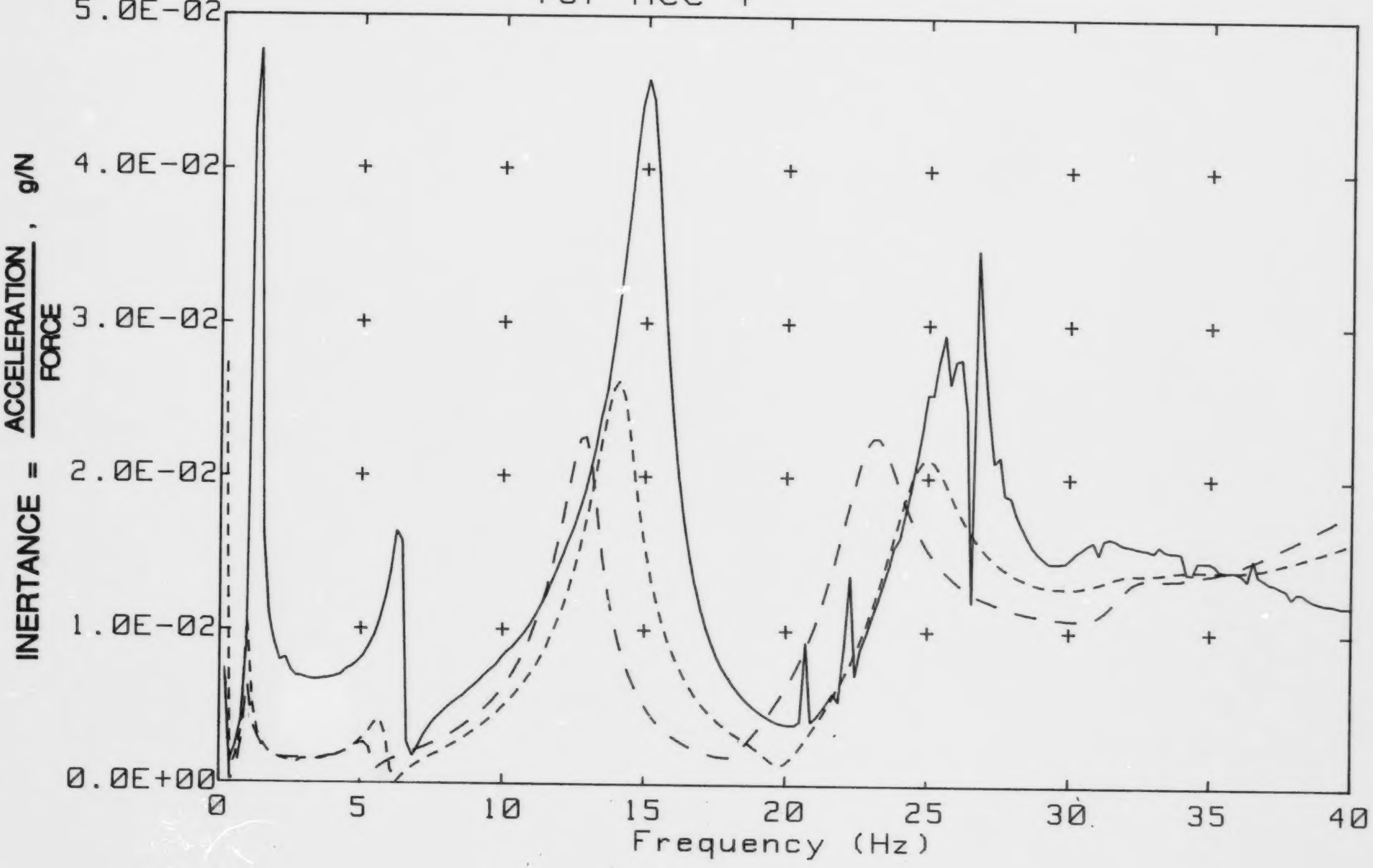

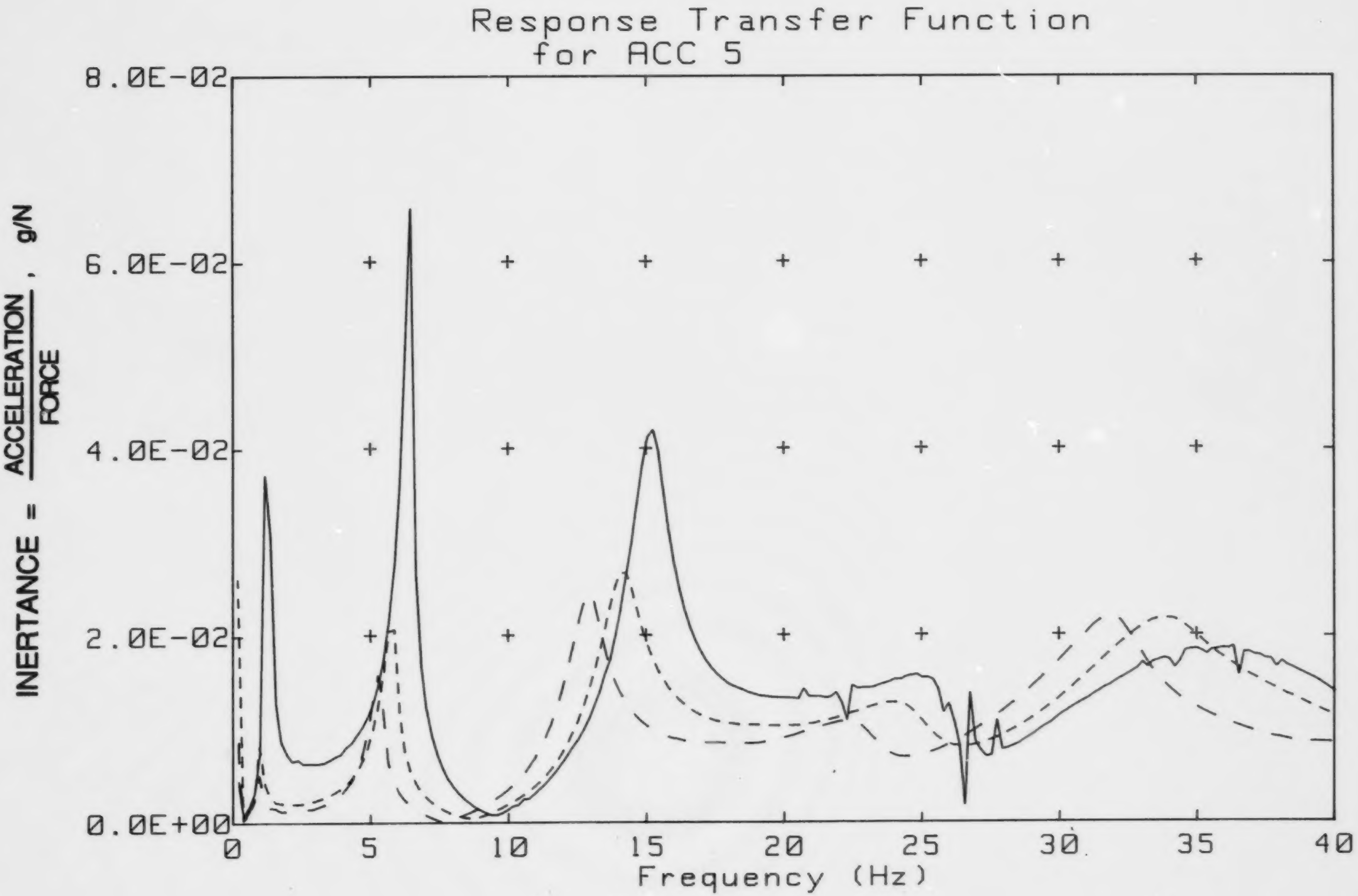
Response Transfer Function
for ACC 5
INERTANCE = ACCELERATION / FORCE , g/N
8.0E-02
6.0E-02
4.0E-02
2.0E-02
0.0E+00
0
5
10
15
20
25
30
35
40
Frequency (Hz)

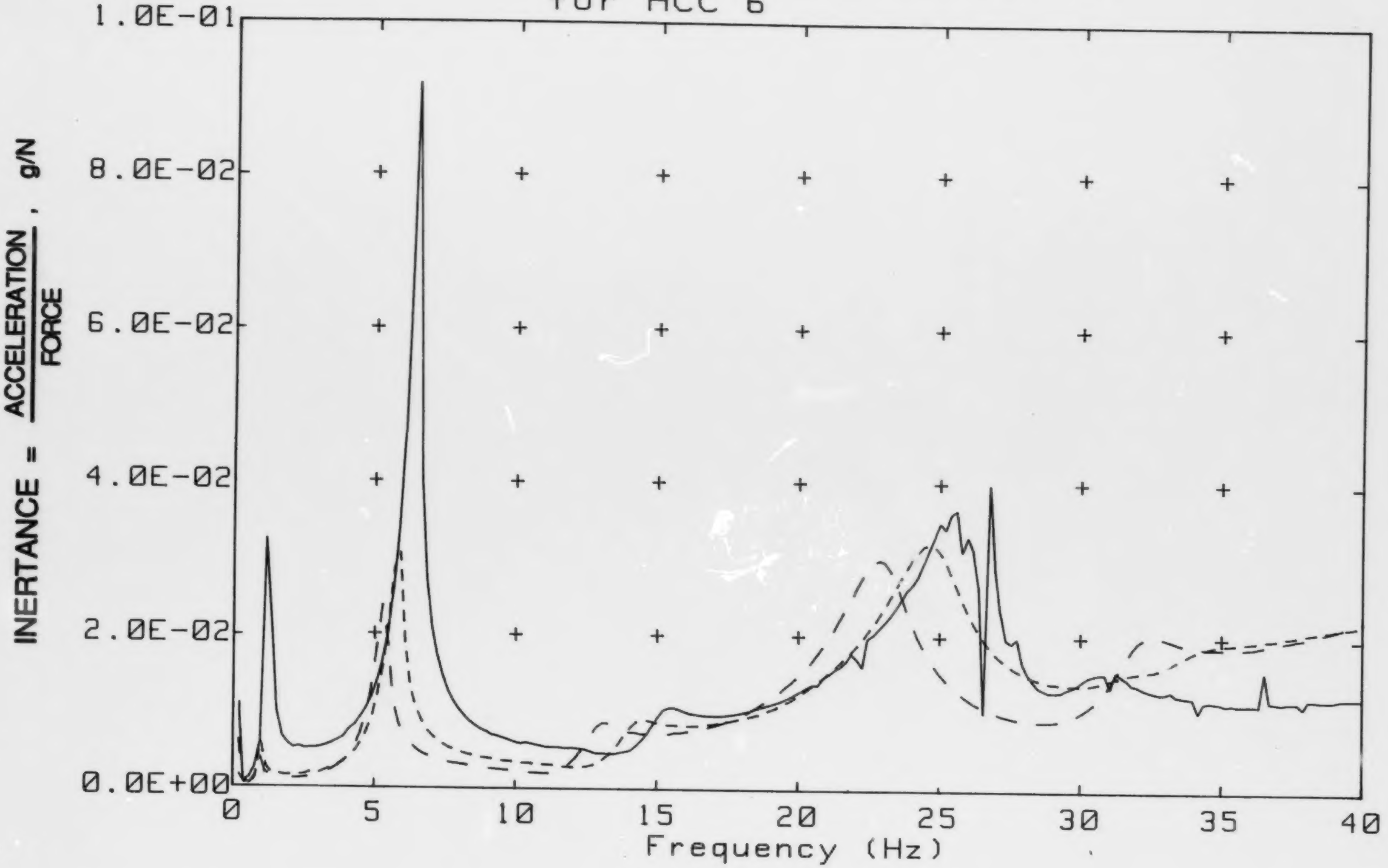

Response Transfer Function
for ACC 6

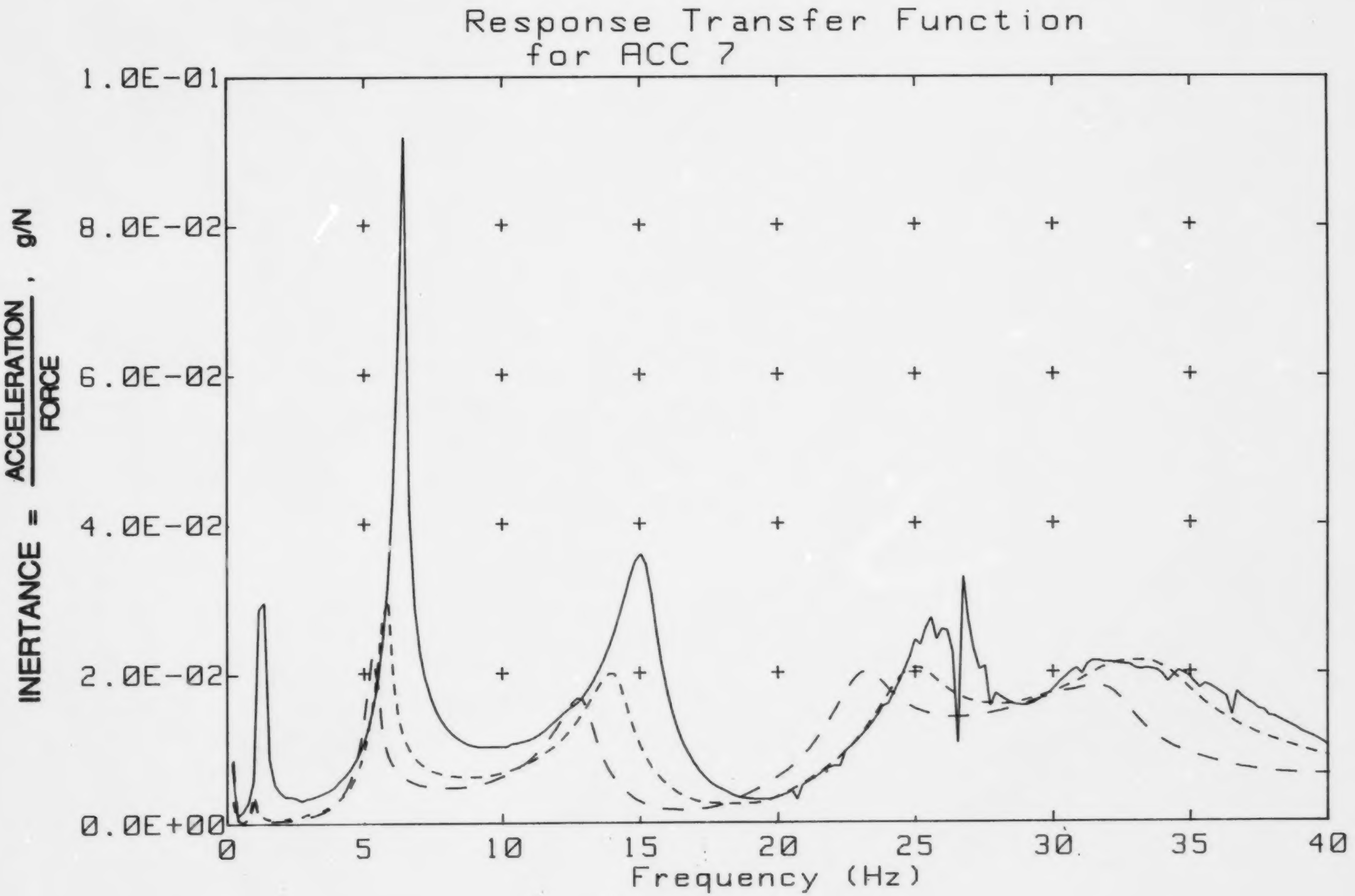
Response Transfer Function
for ACC 7
INERTANCE = ACCELERATION / FORCE , g/N
1.0E-01
8.0E-02
6.0E-02
4.0E-02
2.0E-02
0.0E+00
0
5
10
15
20
25
30
35
40
Frequency (Hz)

Response Transfer Function
for ACC 8

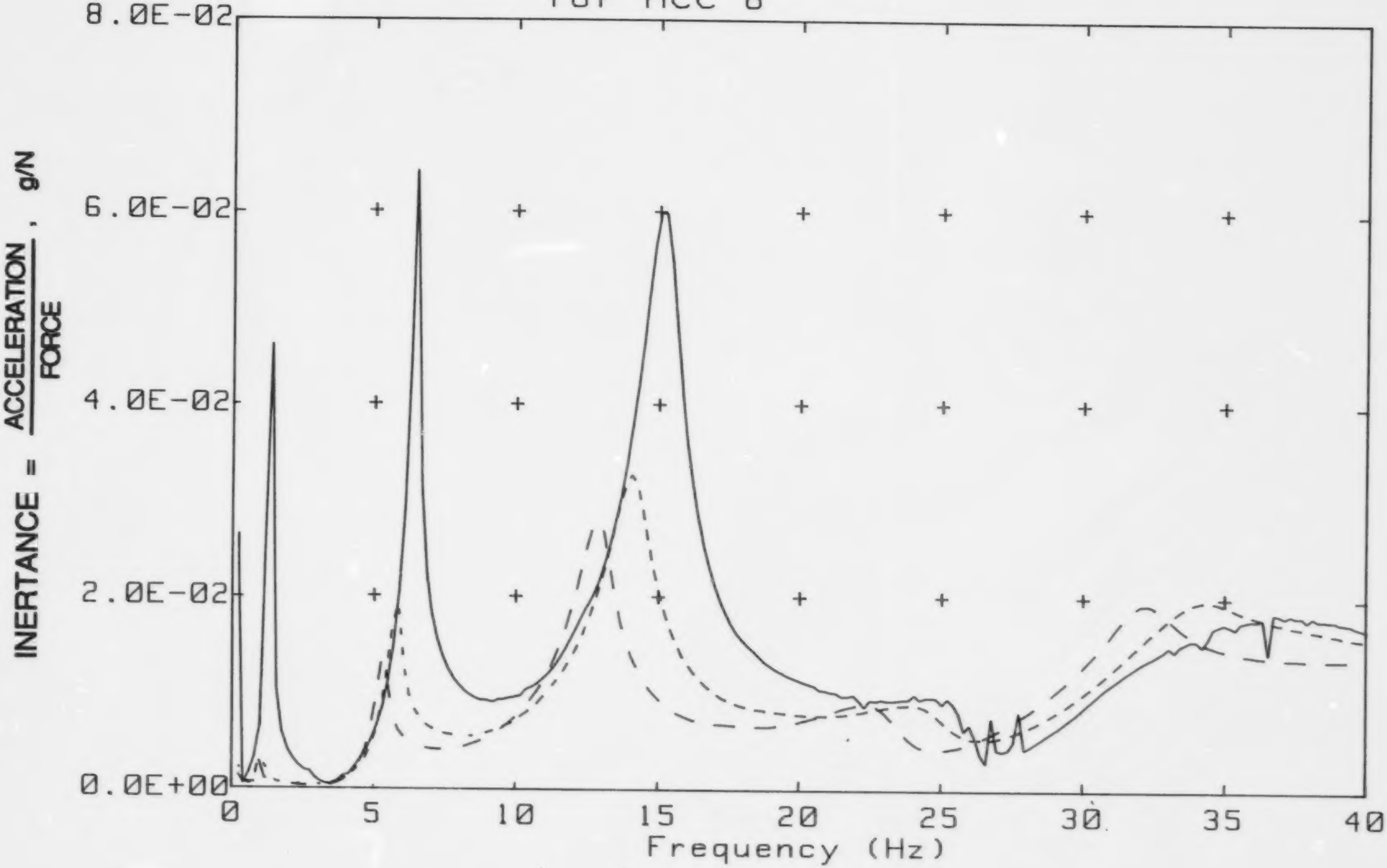

Response Transfer Function
for ACC 2

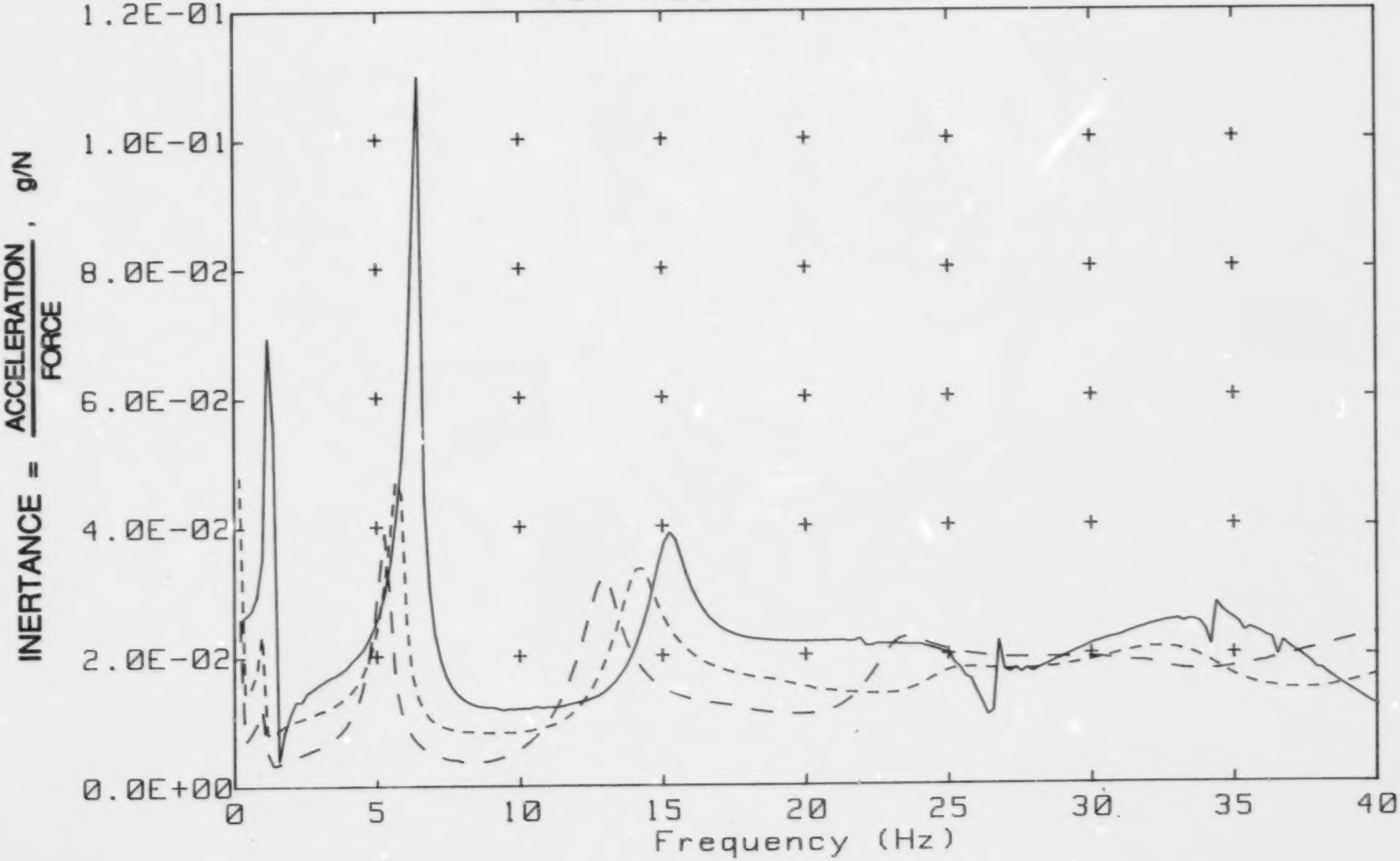

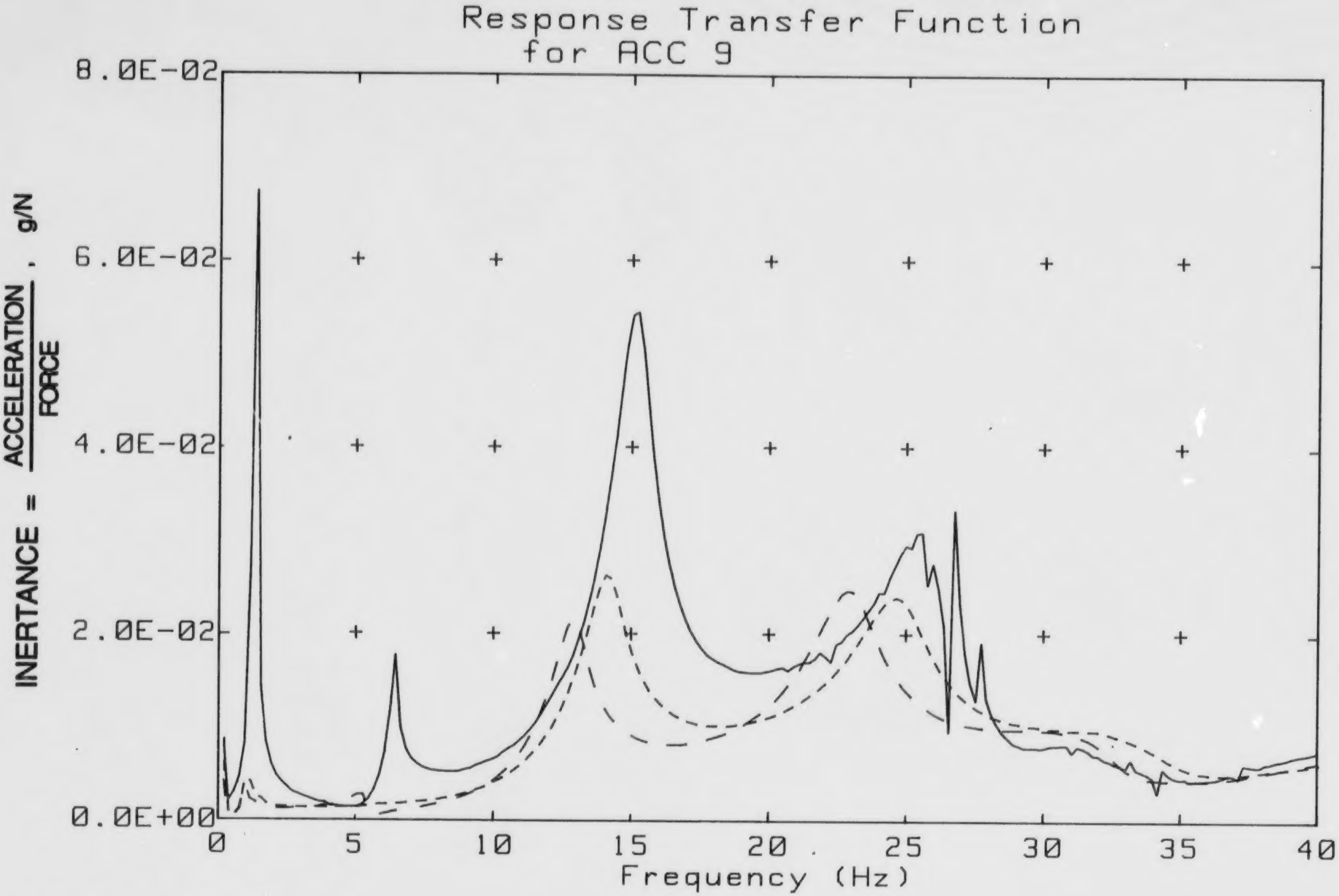
Response Transfer Function
for ACC 9
INERTANCE = ACCELERATION / FORCE , g/N
8.0E-02
6.0E-02
4.0E-02
2.0E-02
0.0E+00
0
5
10
15
20
25
30
35
40
Frequency (Hz)

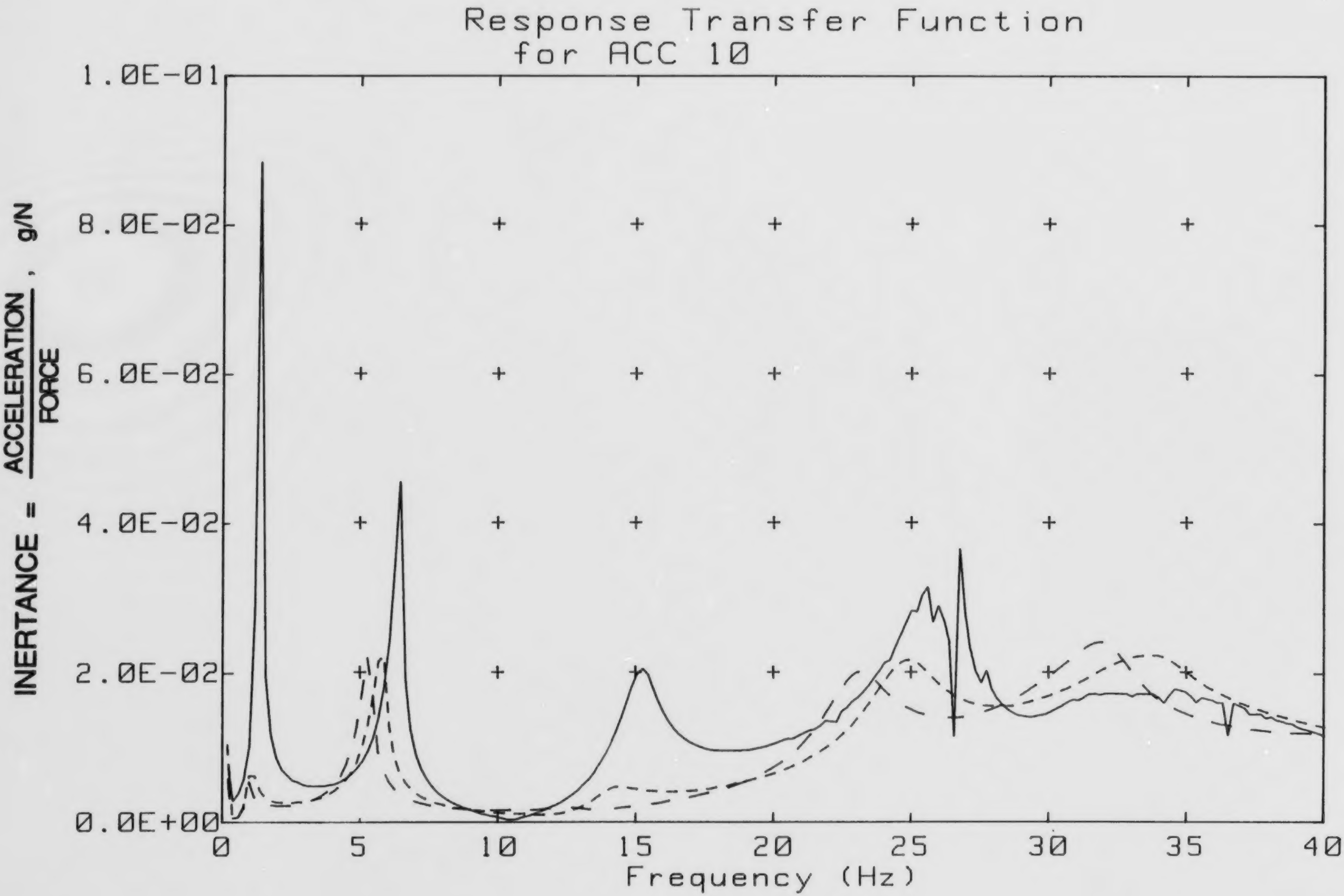
Response Transfer Function
for ACC 10

Response Transfer Function
for ACC 11

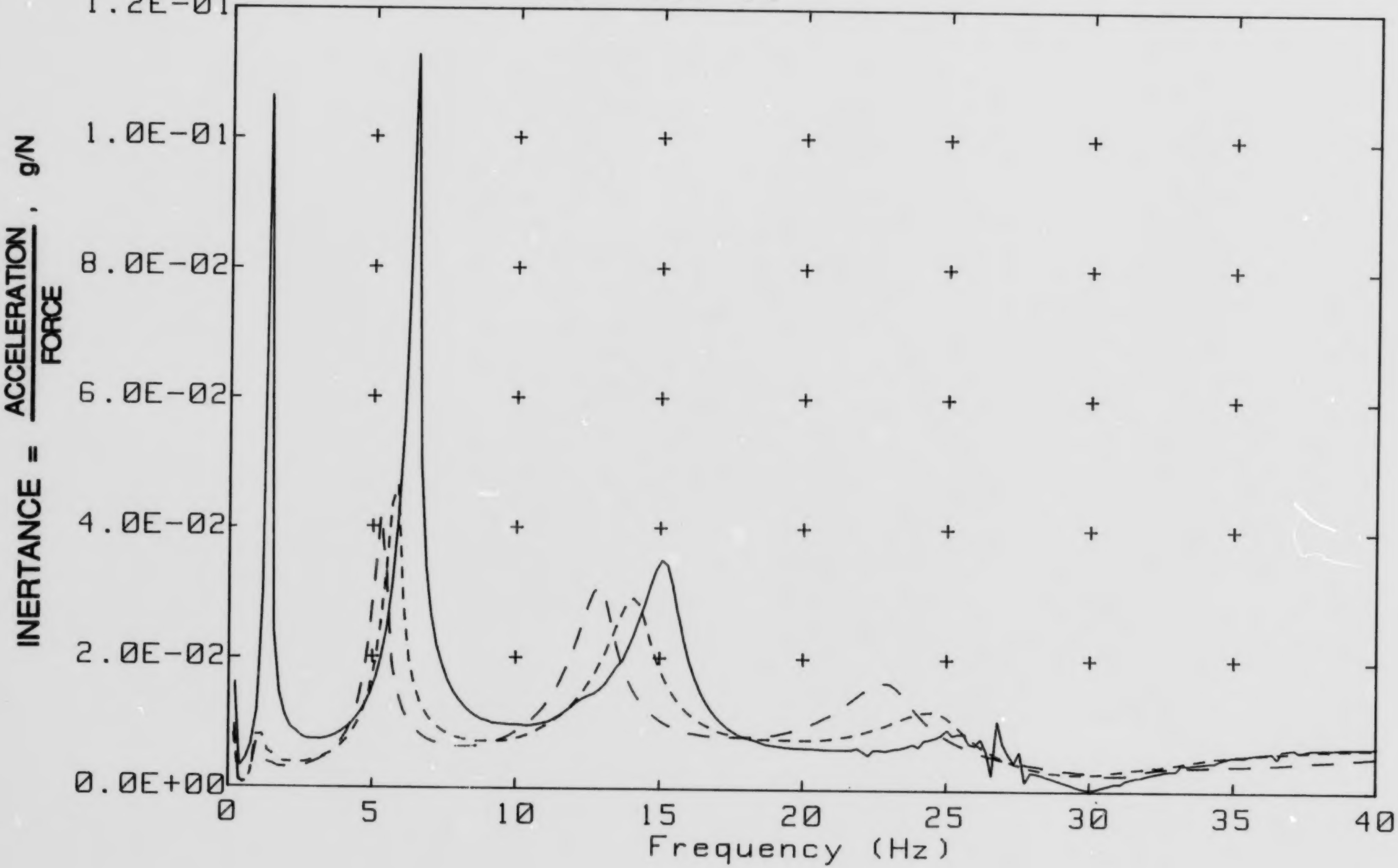

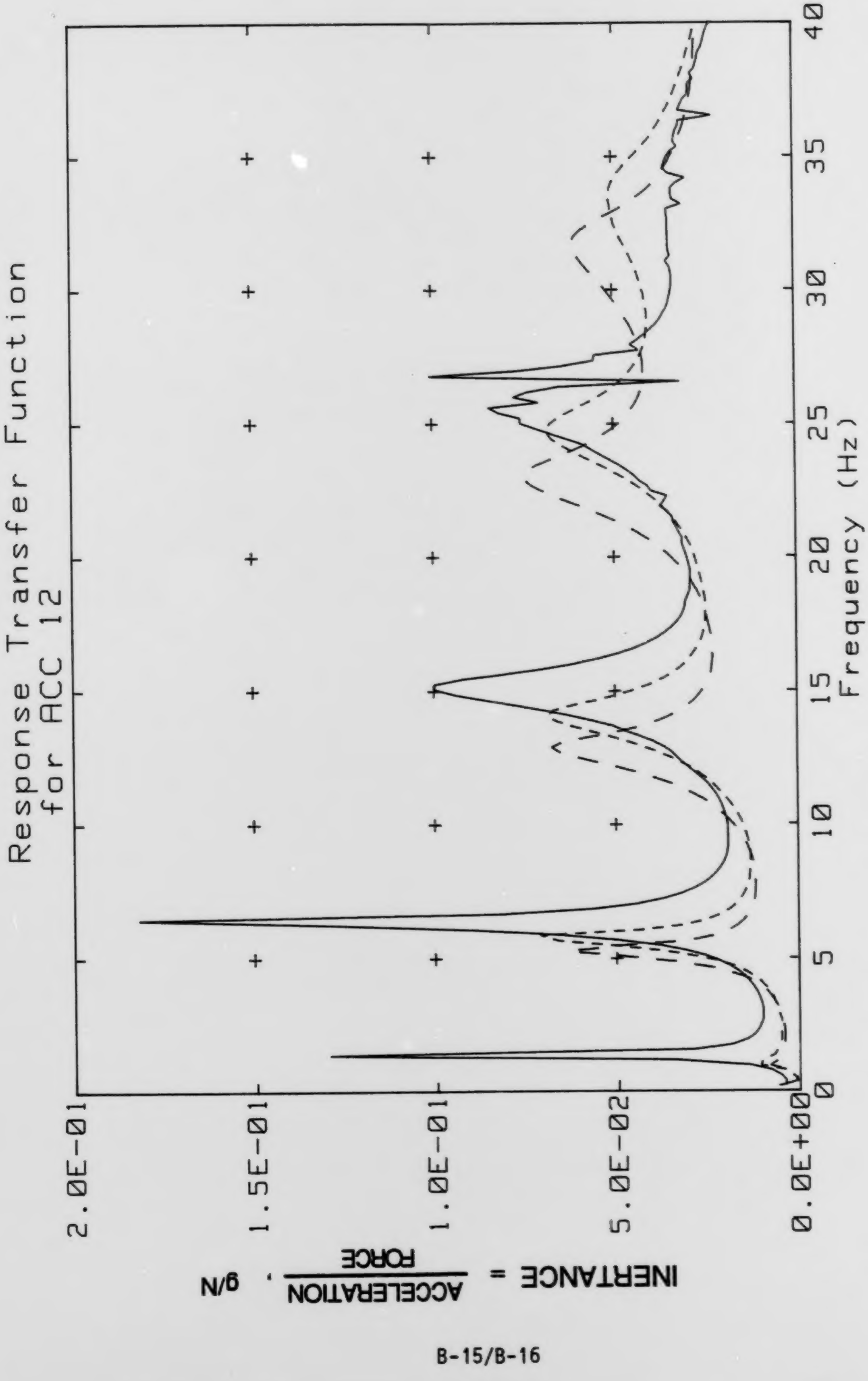

Response Transfer Function for ACC 12

RESPONSE TRANSFER FUNCTION FOR THE STATIONARY SHAKER TESTS

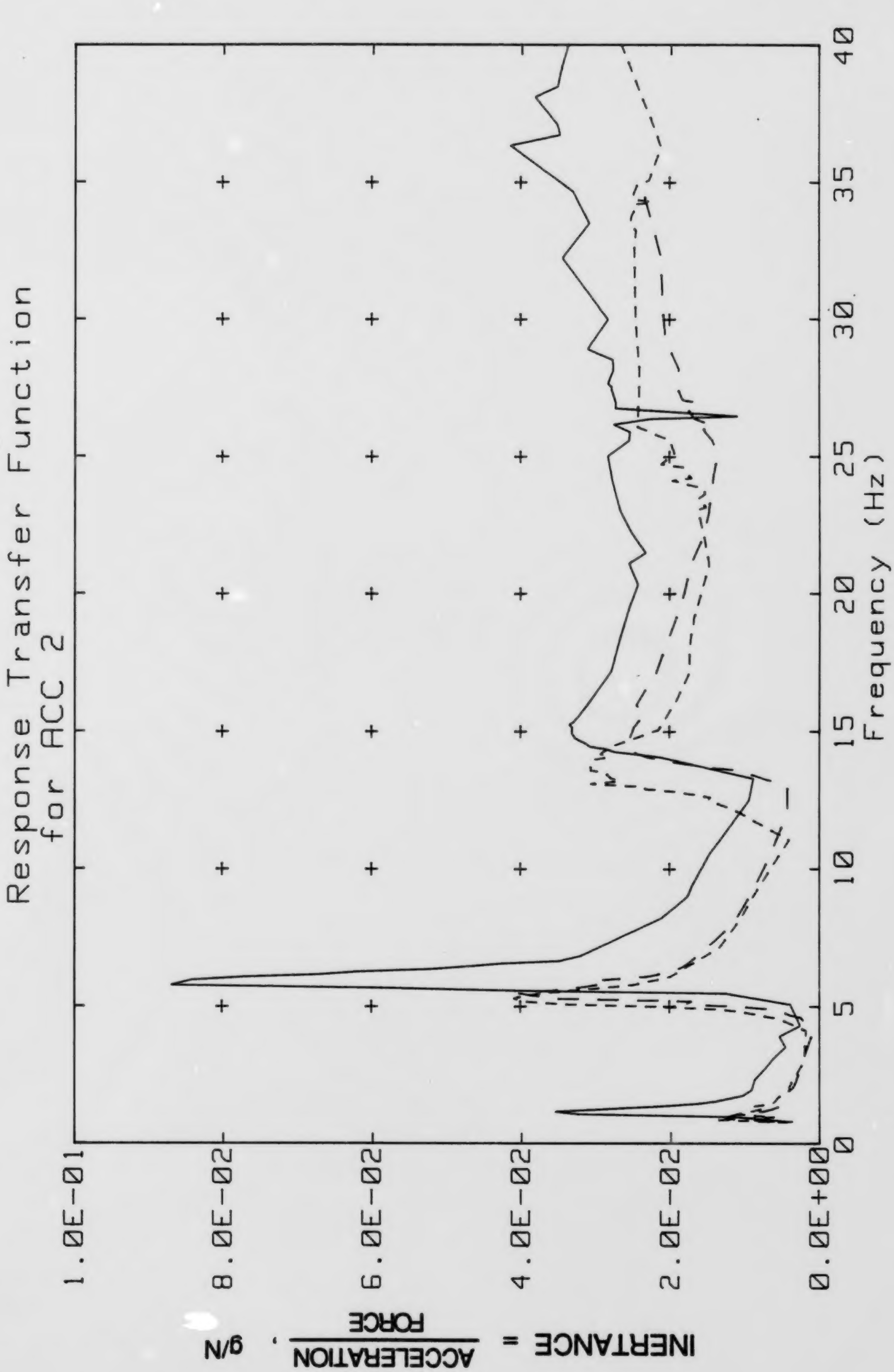

Response Transfer Function for ACC 2

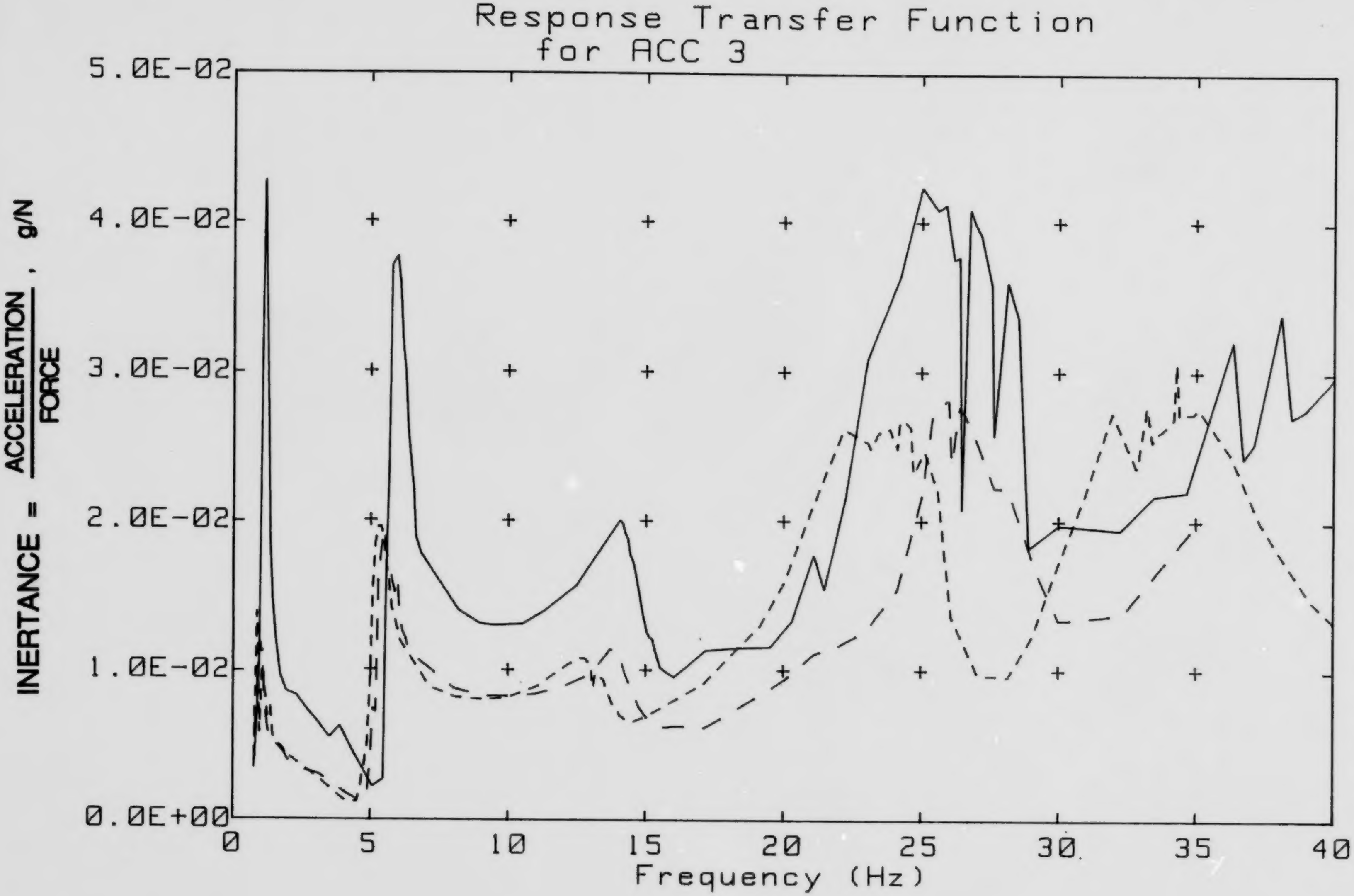
Response Transfer Function
for ACC 3
5.0E-02
4.0E-02
3.0E-02
2.0E-02
1.0E-02
0.0E+00
0
5
10
15
20
25
30
35
40
Frequency (Hz)
INERTANCE = ACCELERATION / FORCE , g/N

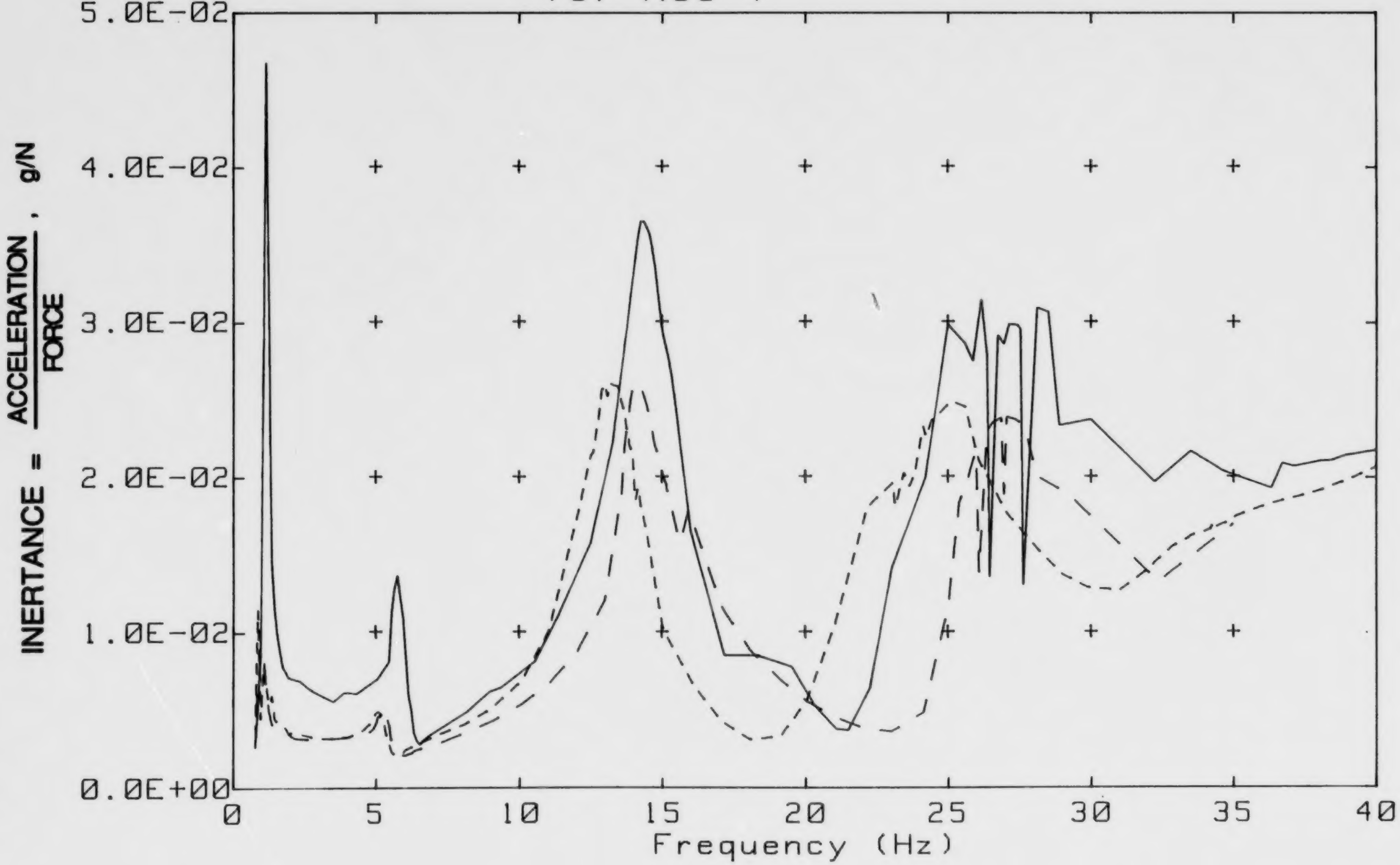

Response Transfer Function
for ACC 4

Response Transfer Function
for ACC 5

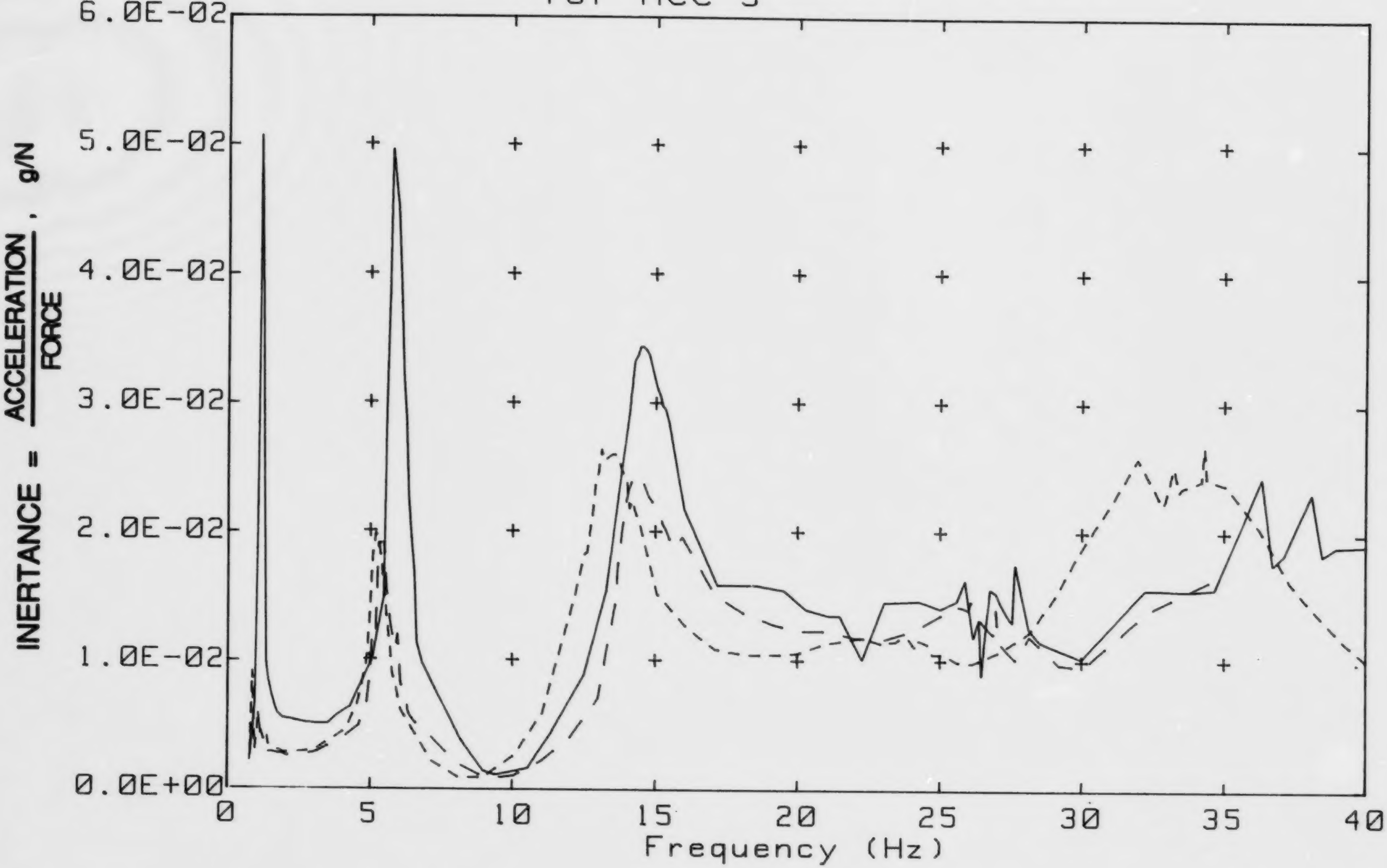

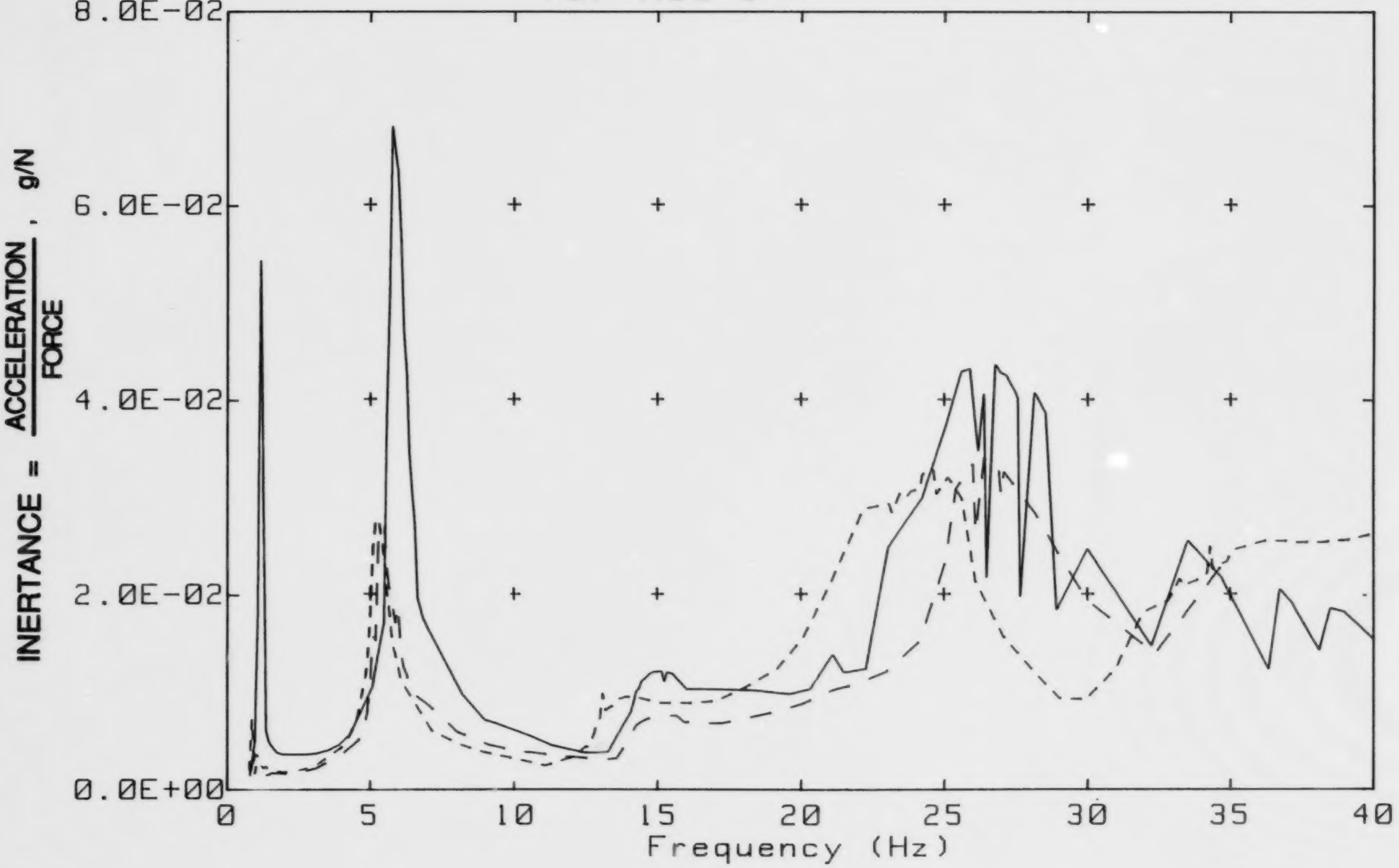

Response Transfer Function
for ACC 6

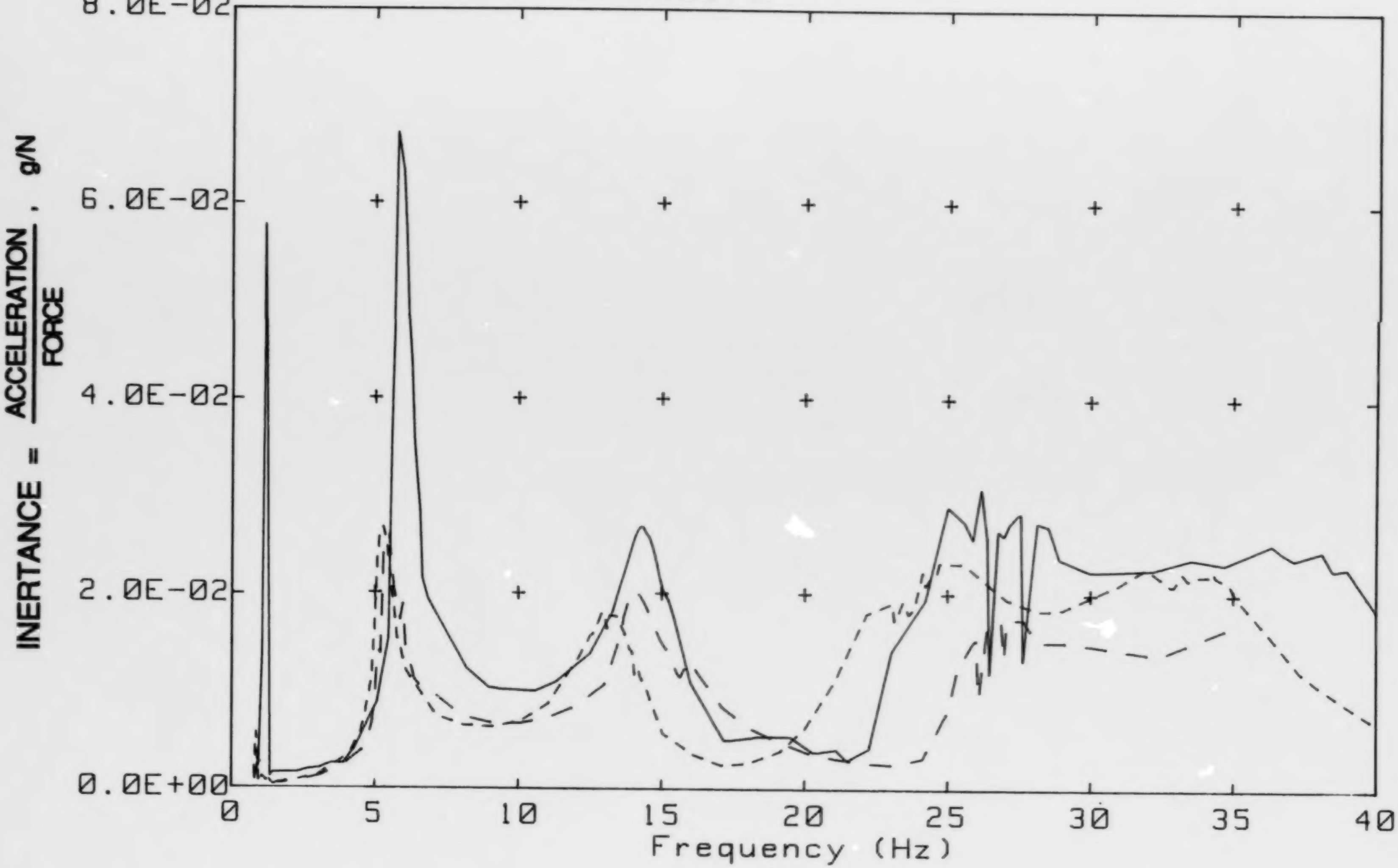
Response Transfer Function
for ACC 7

Response Transfer Function
for ACC 8

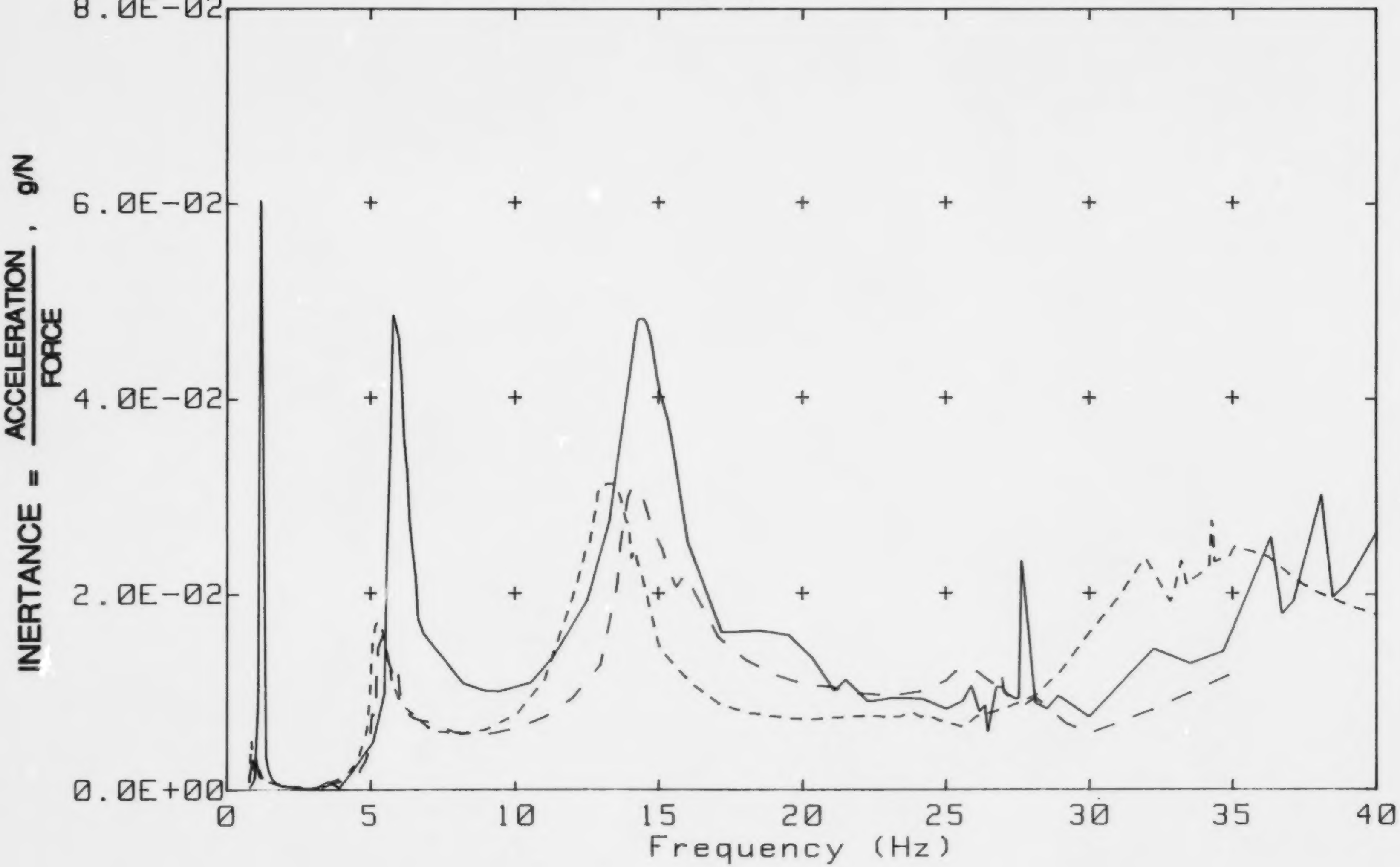

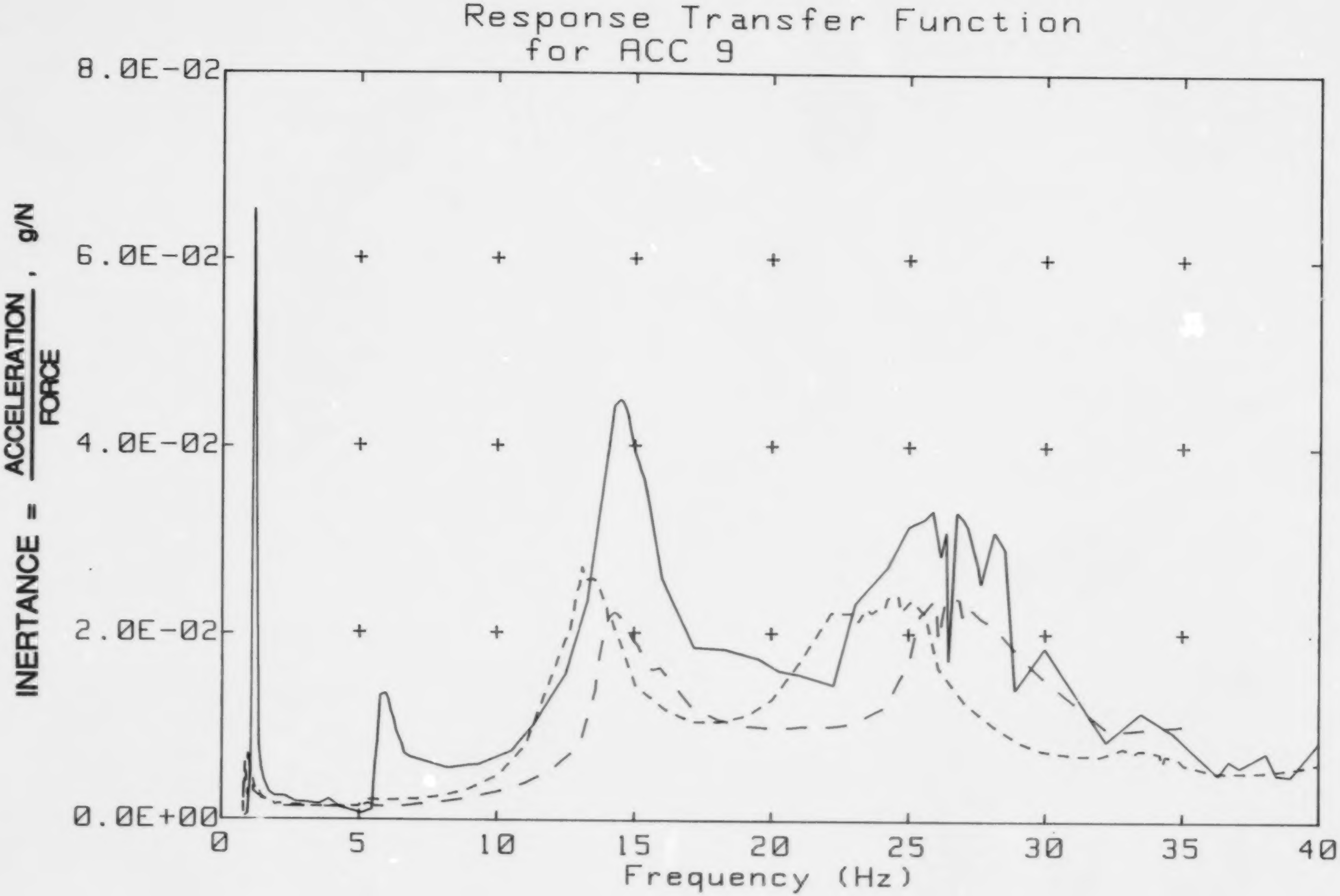
Response Transfer Function
for ACC 9
INERTANCE = ACCELERATION / FORCE , g/N
8.0E-02
6.0E-02
4.0E-02
2.0E-02
0.0E+00
0
5
10
15
20
25
30
35
40
Frequency (Hz)

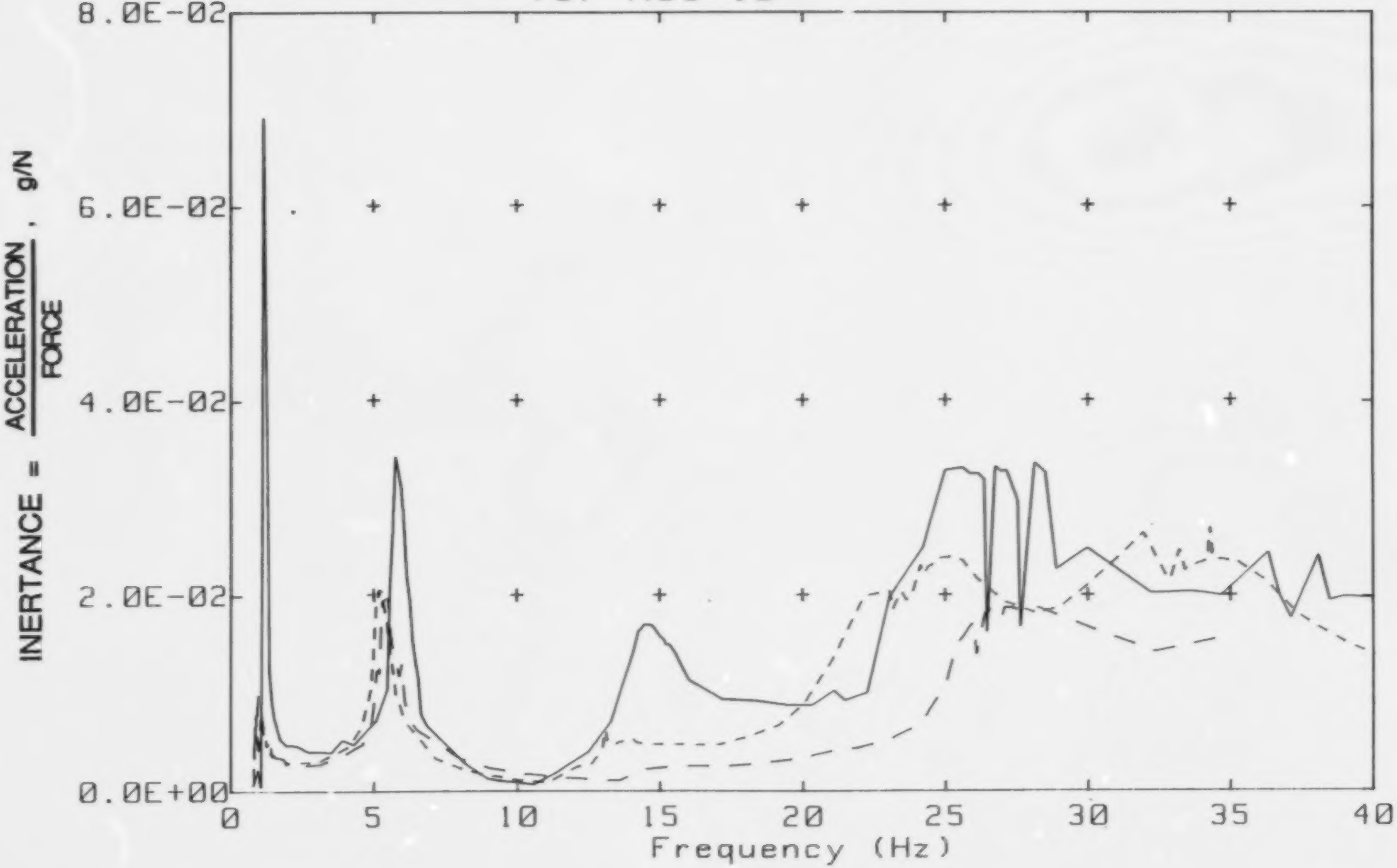

Response Transfer Function
for ACC 10

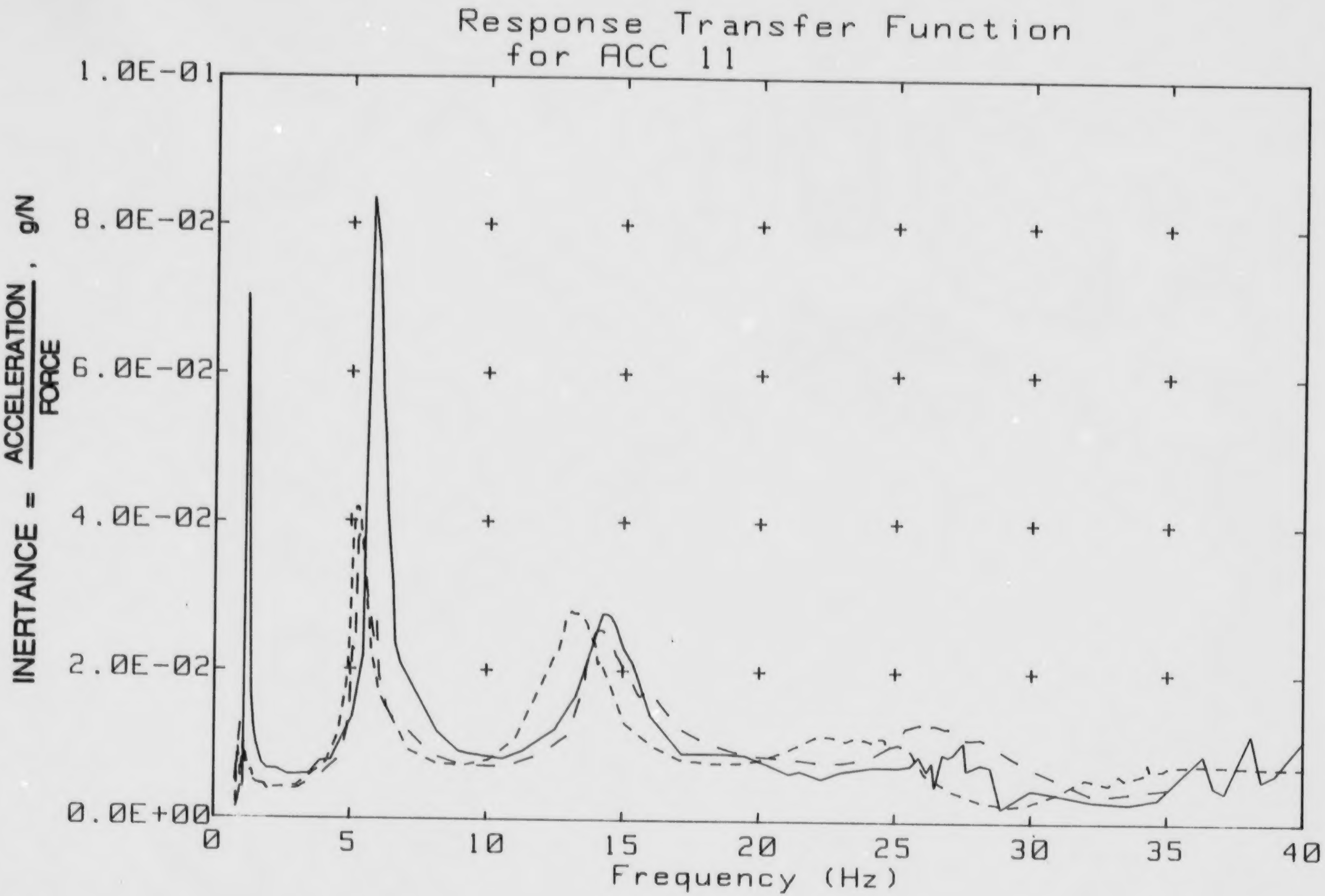
Response Transfer Function
for ACC 11
INERTANCE = ACCELERATION / FORCE , g/N
1.0E-01
8.0E-02
6.0E-02
4.0E-02
2.0E-02
0.0E+00
0
5
10
15
20
25
30
35
40
Frequency (Hz)

Response Transfer Function
for ACC 12

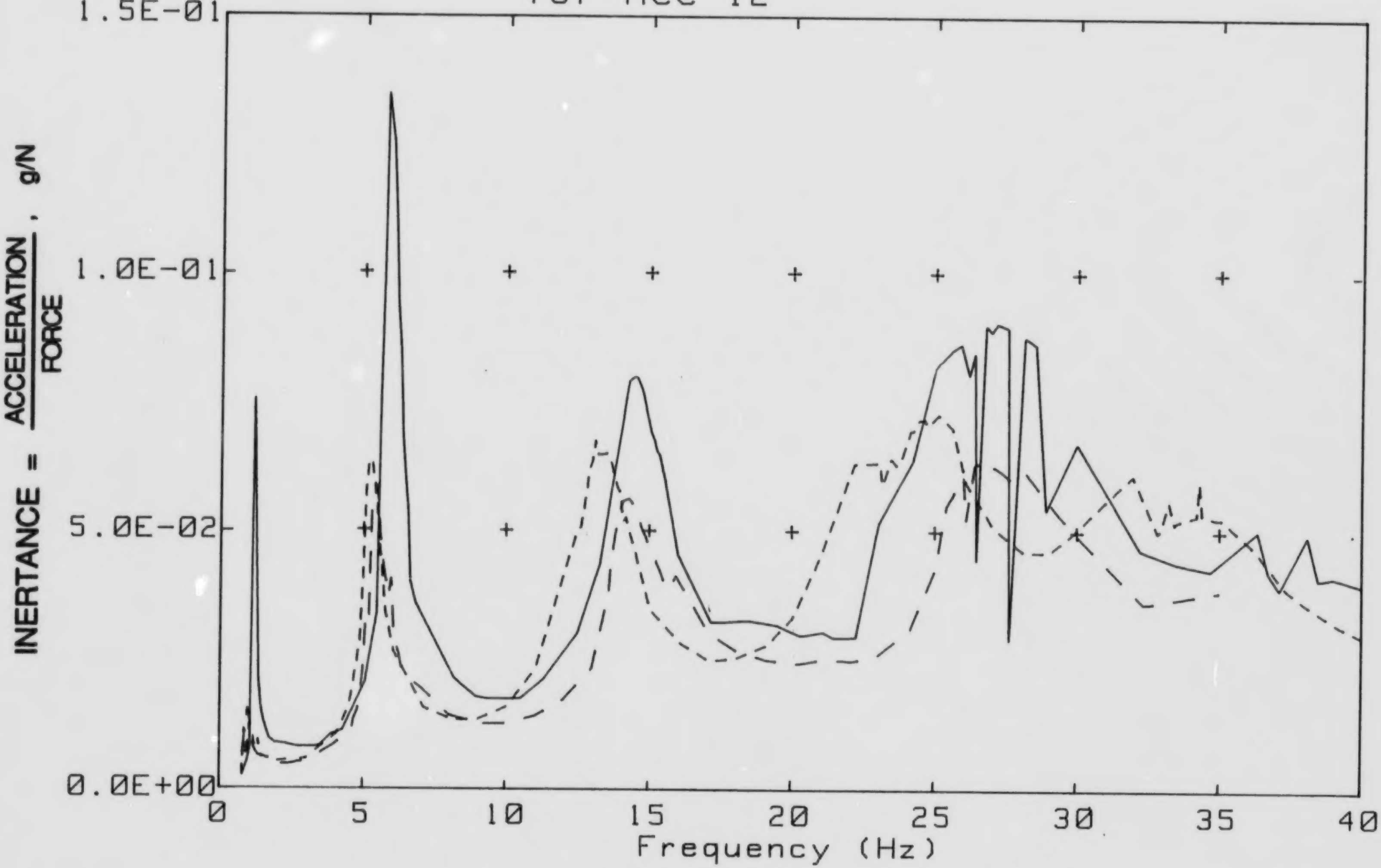

RESPONSE TRANSFER FUNCTION FOR THE TOWED SHAKER TESTS

Response Transfer Function for ACC 1

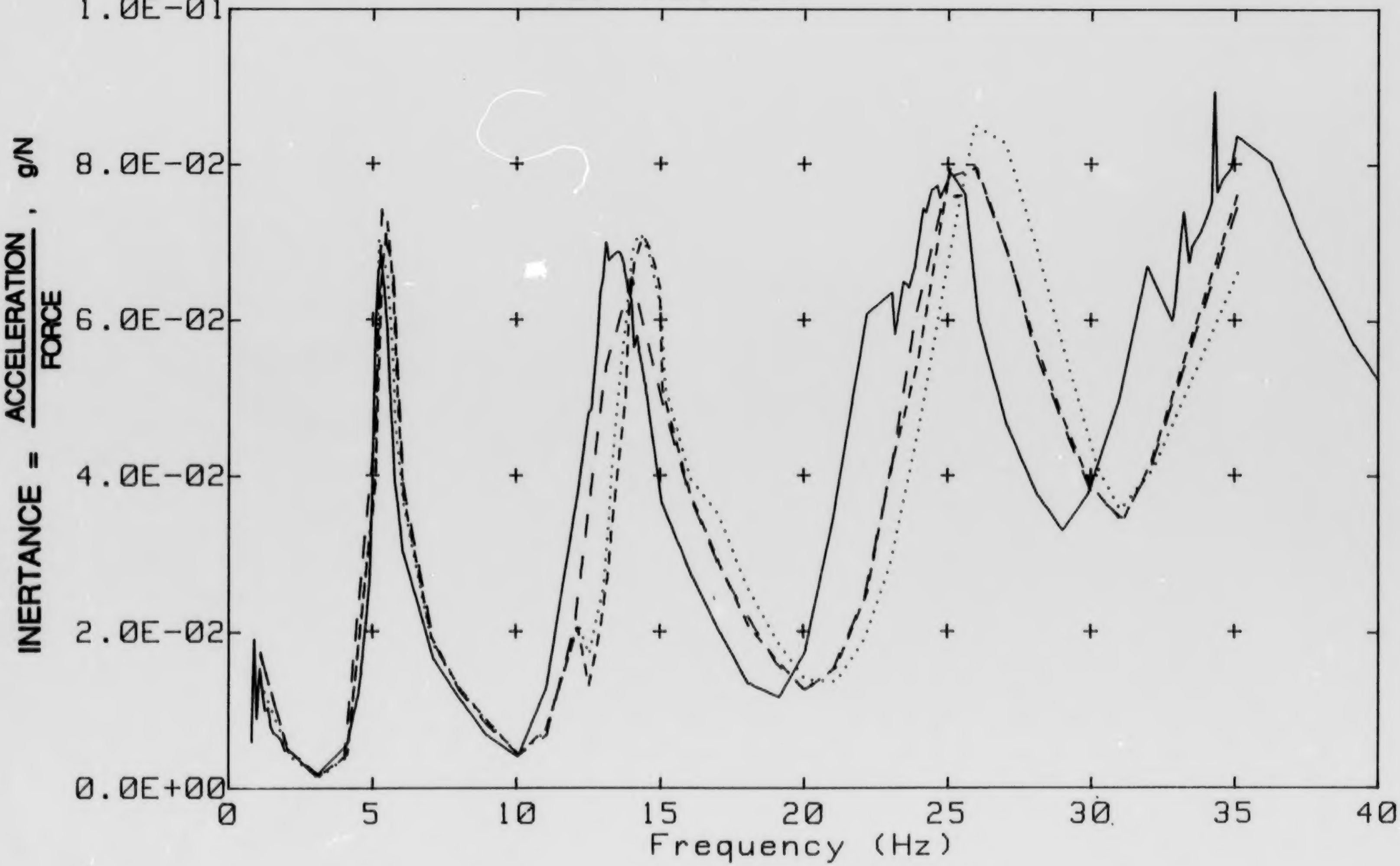

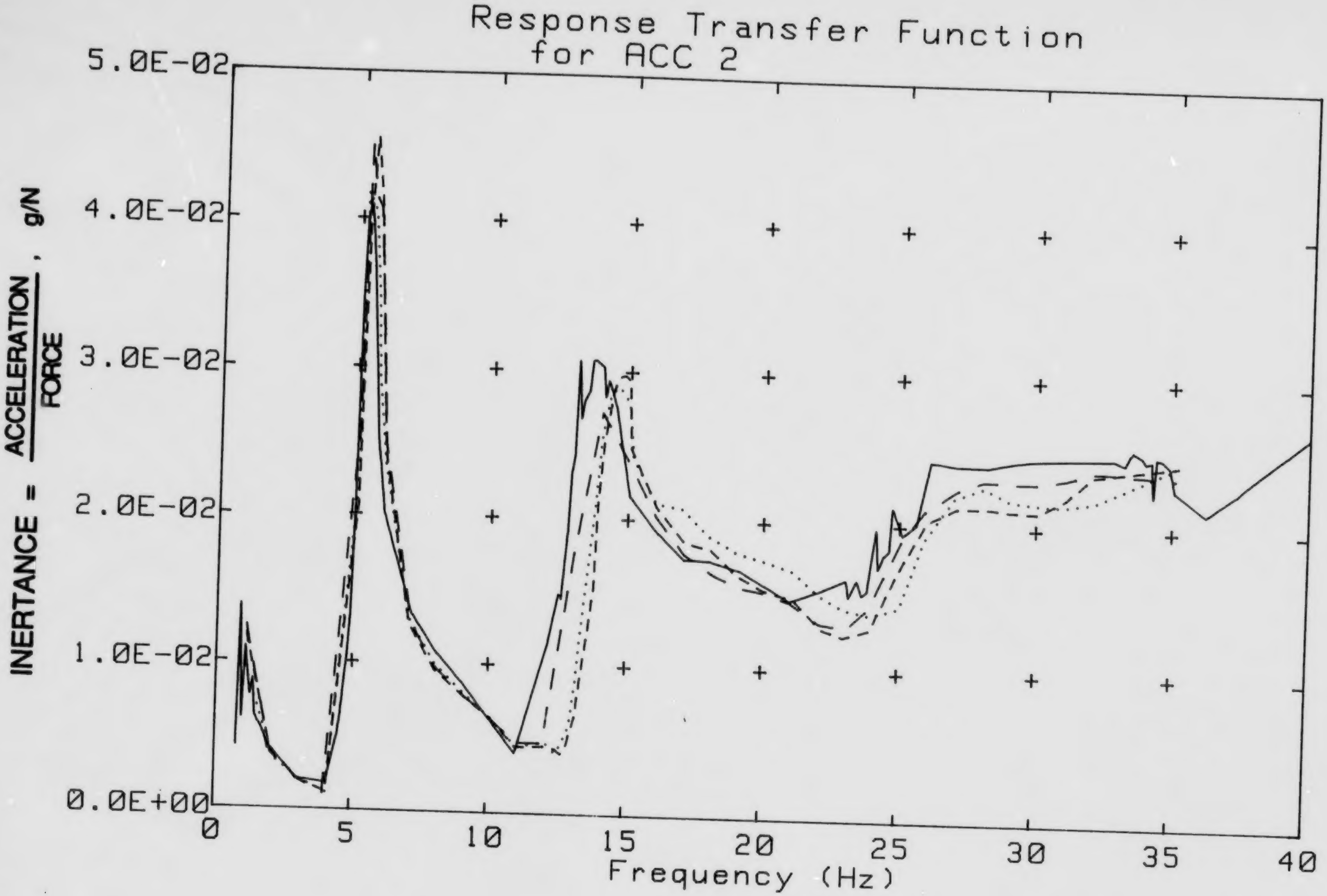
Response Transfer Function
for ACC 2
INERTANCE = ACCELERATION / FORCE , g/N
5.0E-02
4.0E-02
3.0E-02
2.0E-02
1.0E-02
0.0E+00
0
5
10
15
20
25
30
35
40
Frequency (Hz)

Response Transfer Function
for ACC 3

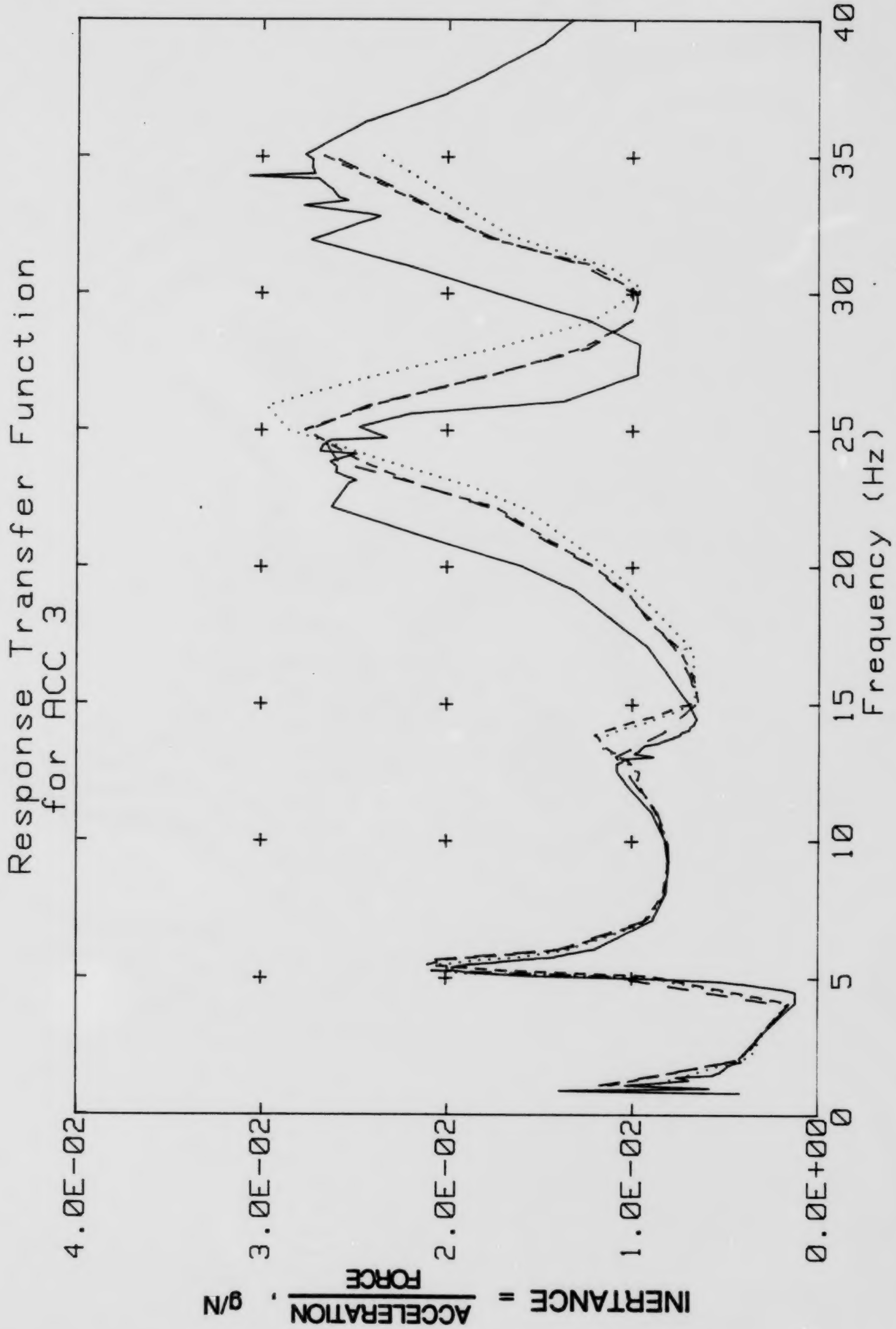

Response Transfer Function
for ACC 4

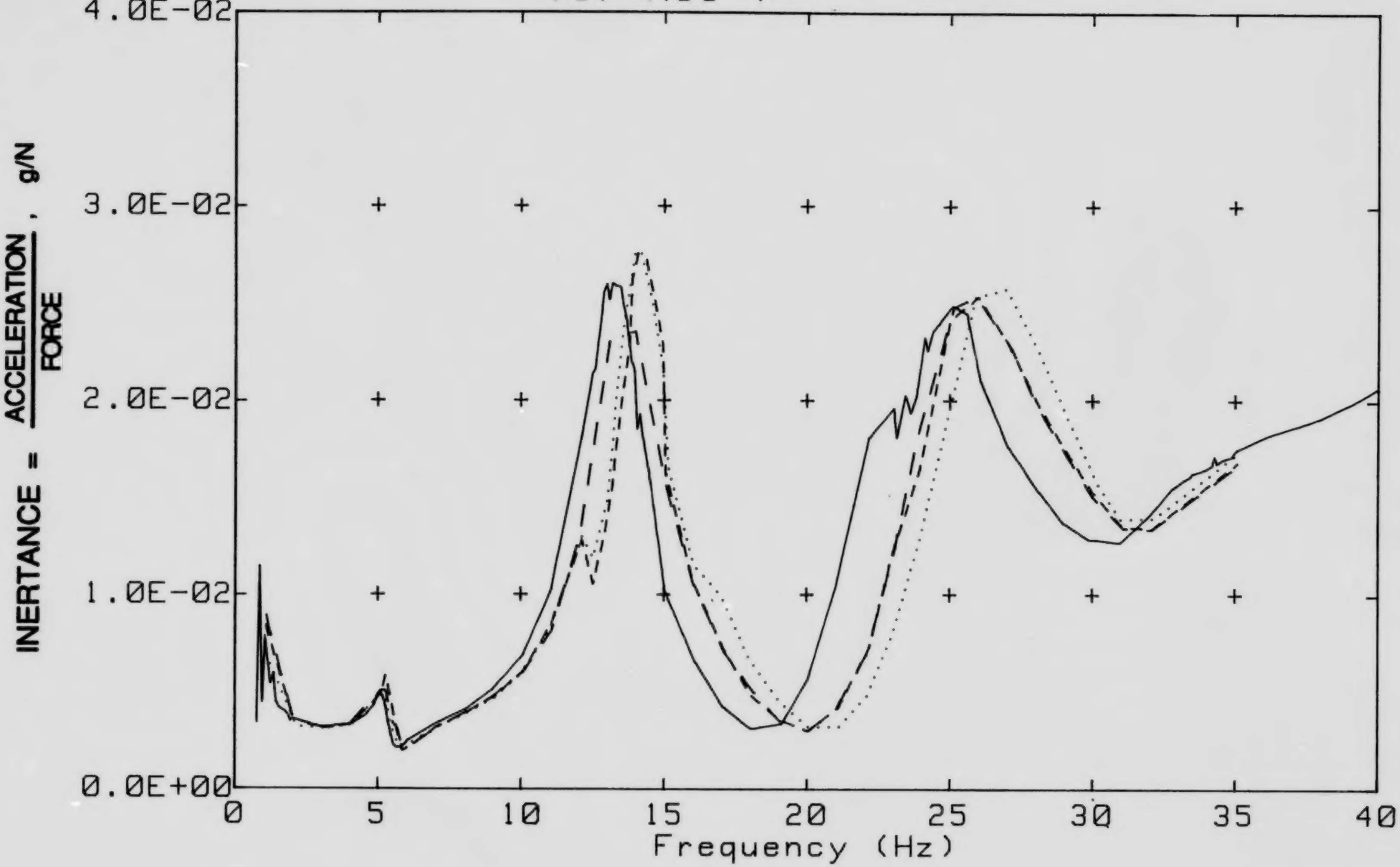

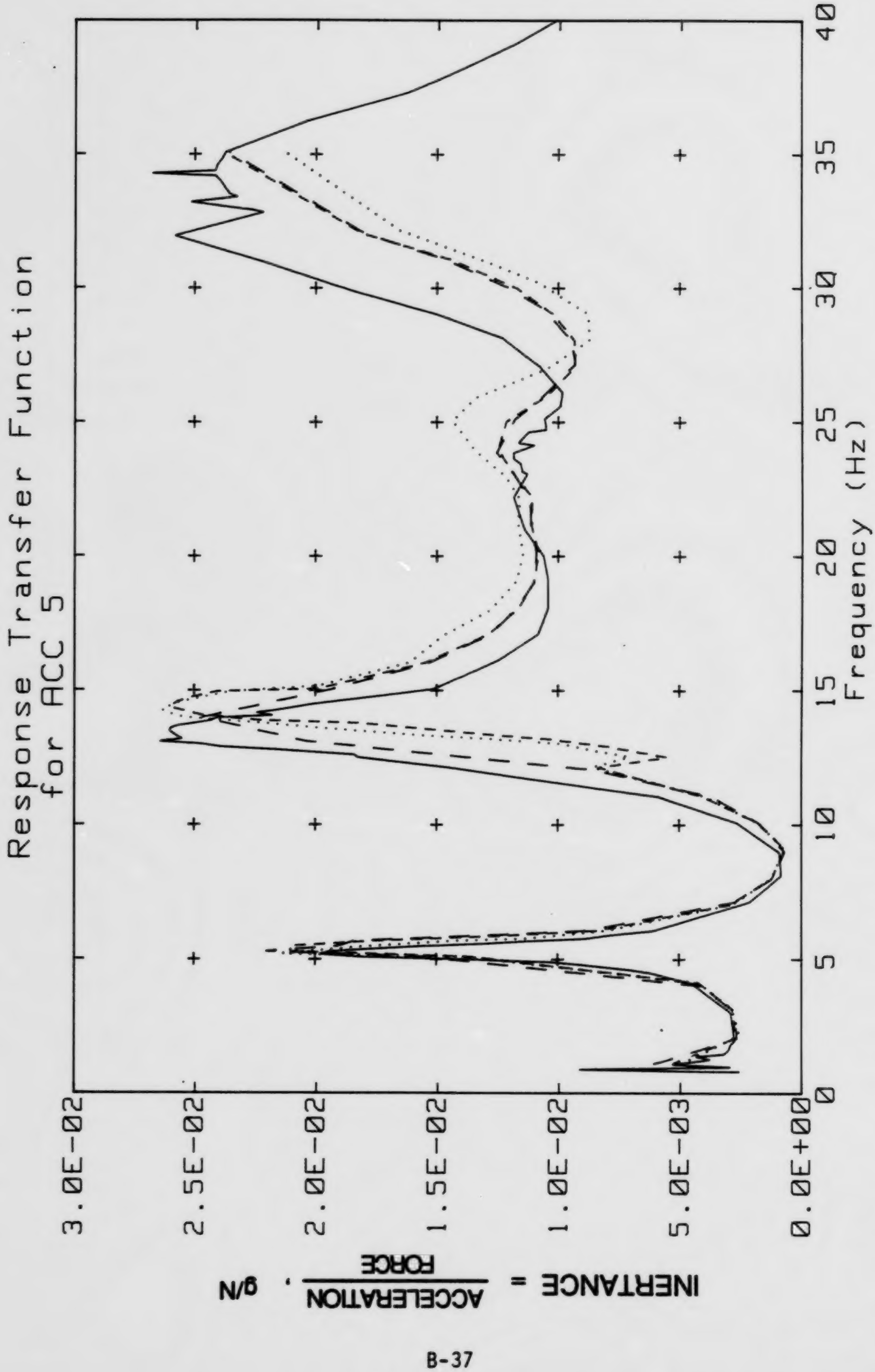Response Transfer Function
for ACC 5
Frequency (Hz)
0
5
10
15
20
25
30
35
40
INERTANCE = ACCELERATION / FORCE, g/N
0.0E+00
5.0E-03
1.0E-02
1.5E-02
2.0E-02
2.5E-02
3.0E-02

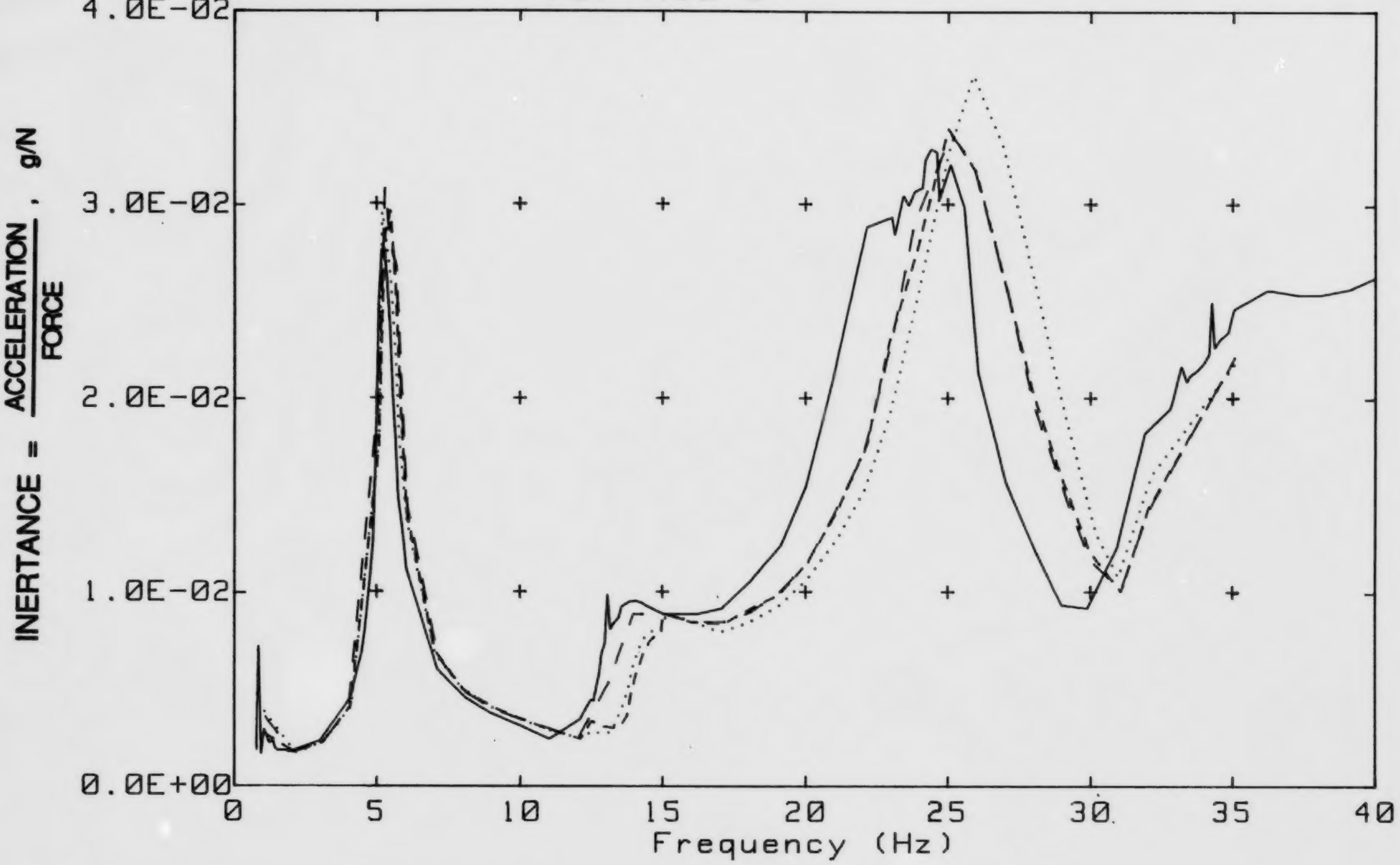

Response Transfer Function
for ACC 6

Response Transfer Function
for ACC 7

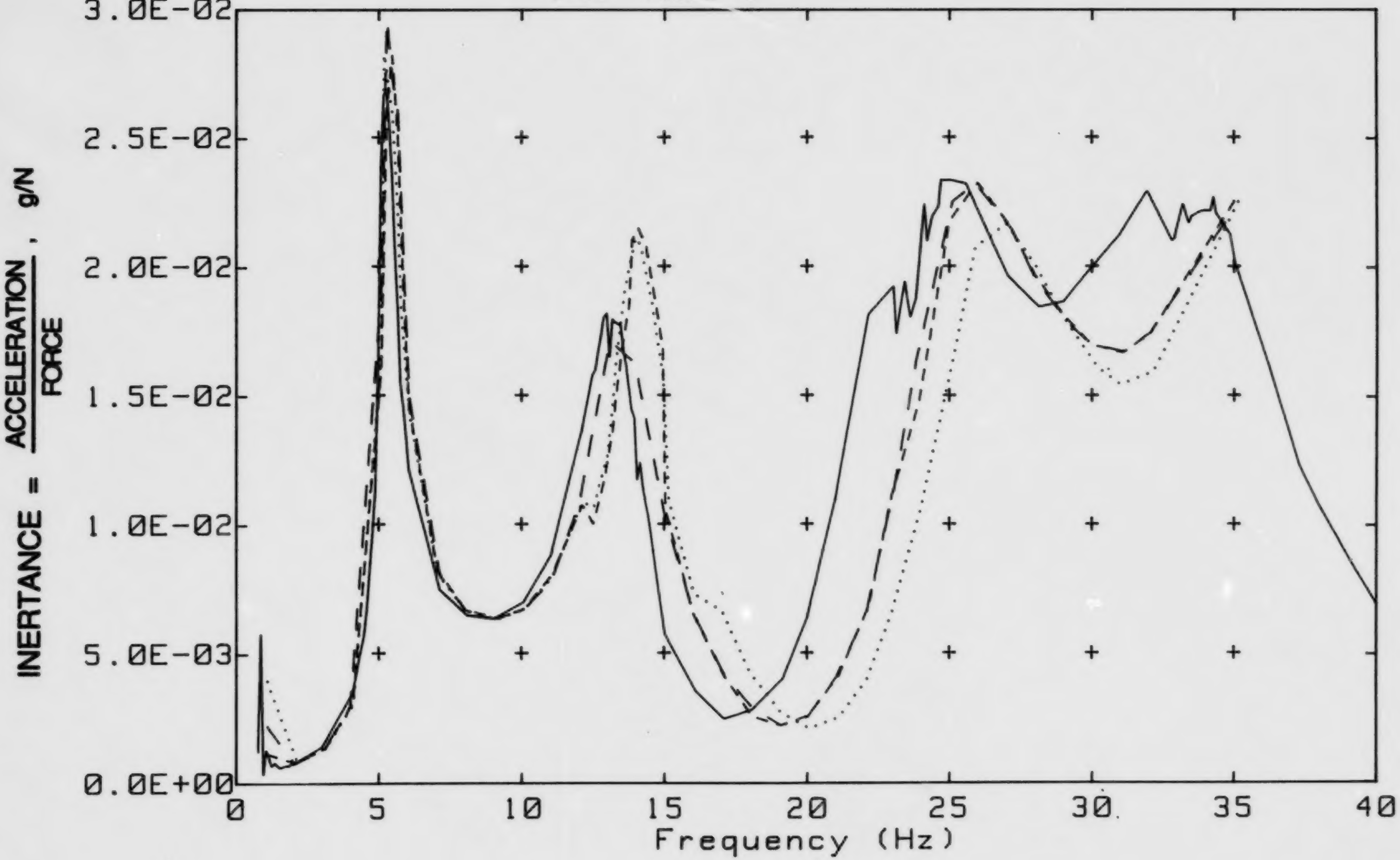

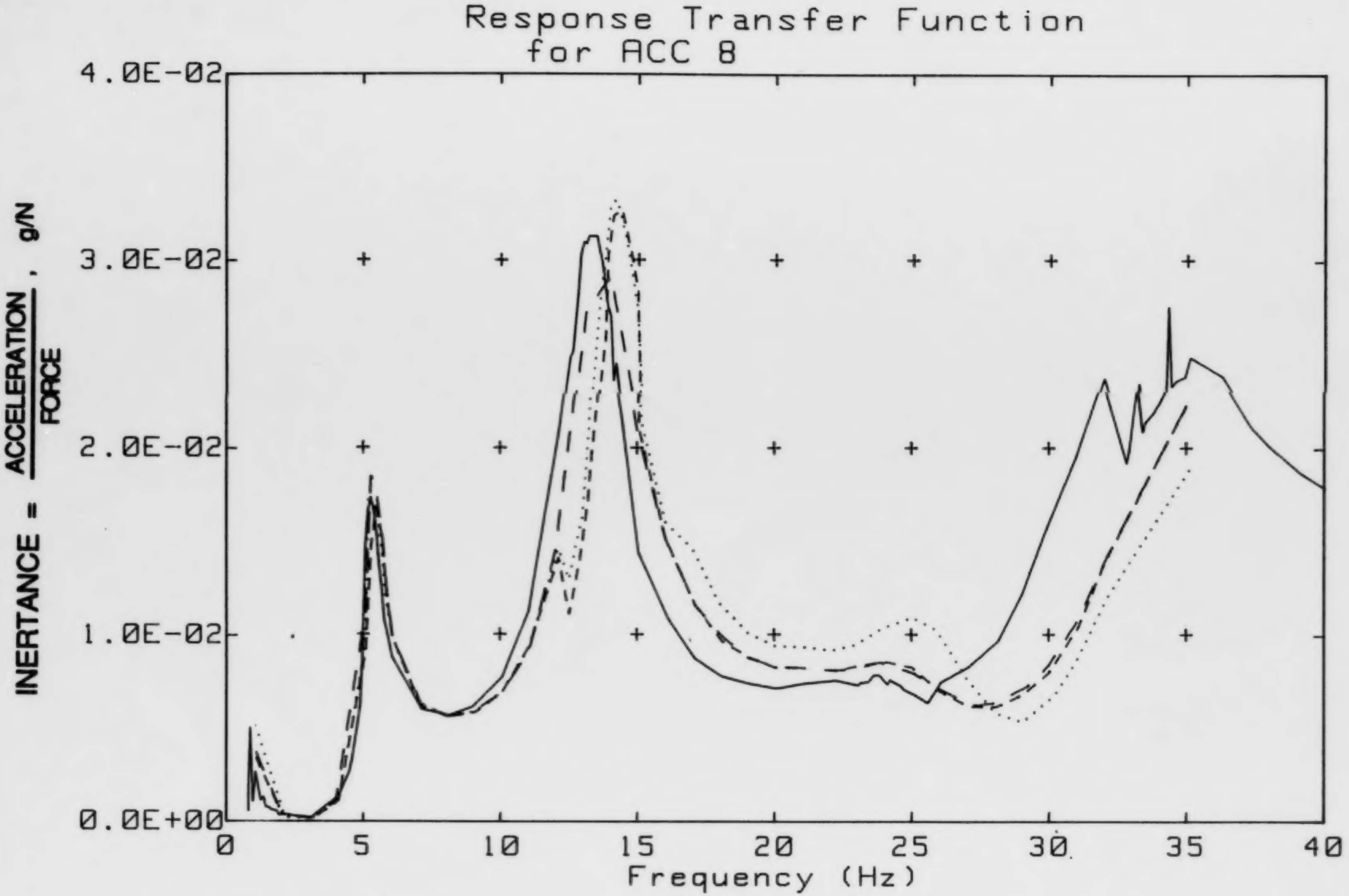
Response Transfer Function
for ACC 8
INERTANCE = ACCELERATION / FORCE , g/N
4.0E-02
3.0E-02
2.0E-02
1.0E-02
0.0E+00
0
5
10
15
20
25
30
35
40
Frequency (Hz)

Response Transfer Function
for ACC 9

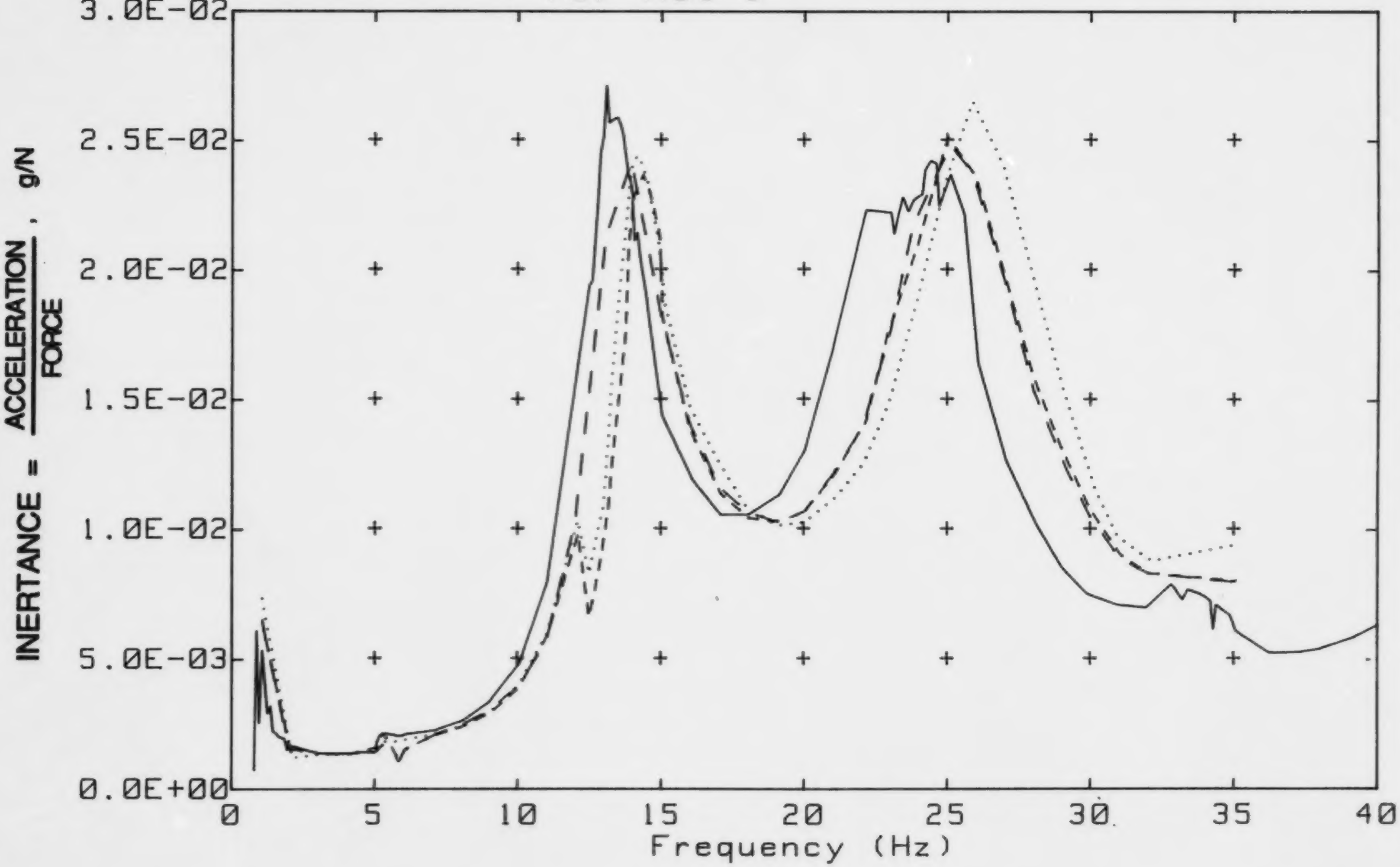

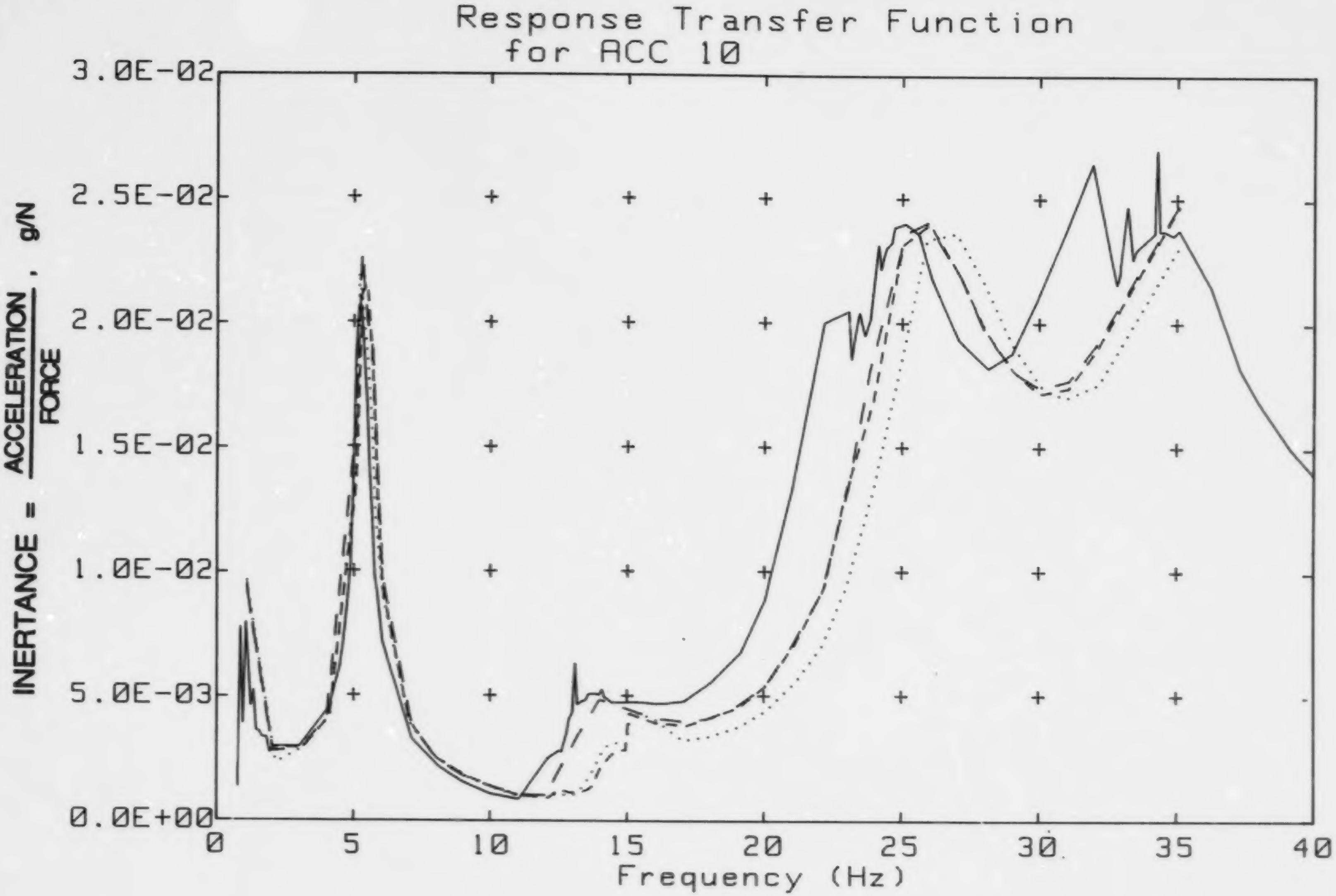
Response Transfer Function for ACC 10

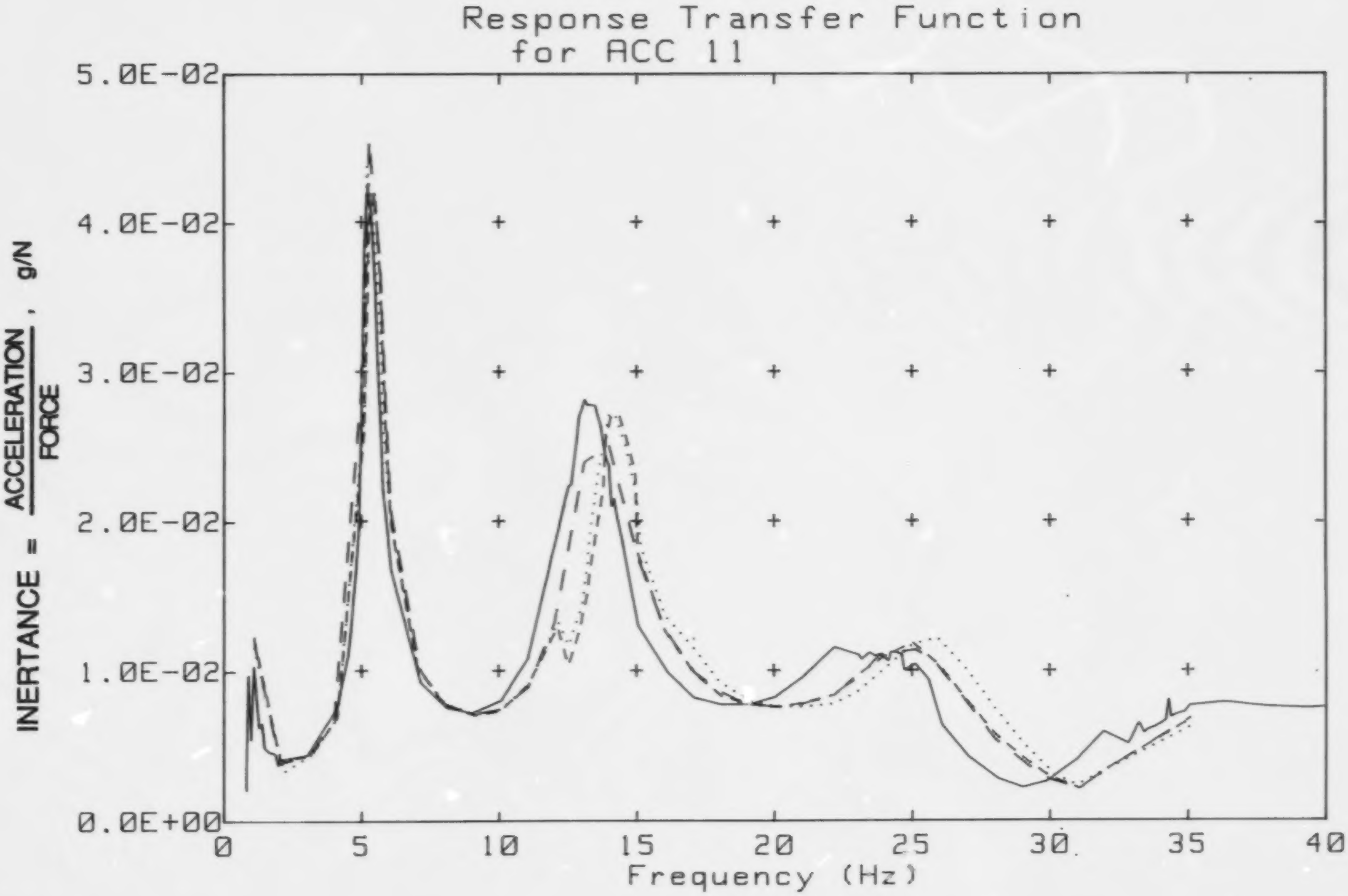

Response Transfer Function
for ACC 11

DRY TEST COMPARISON

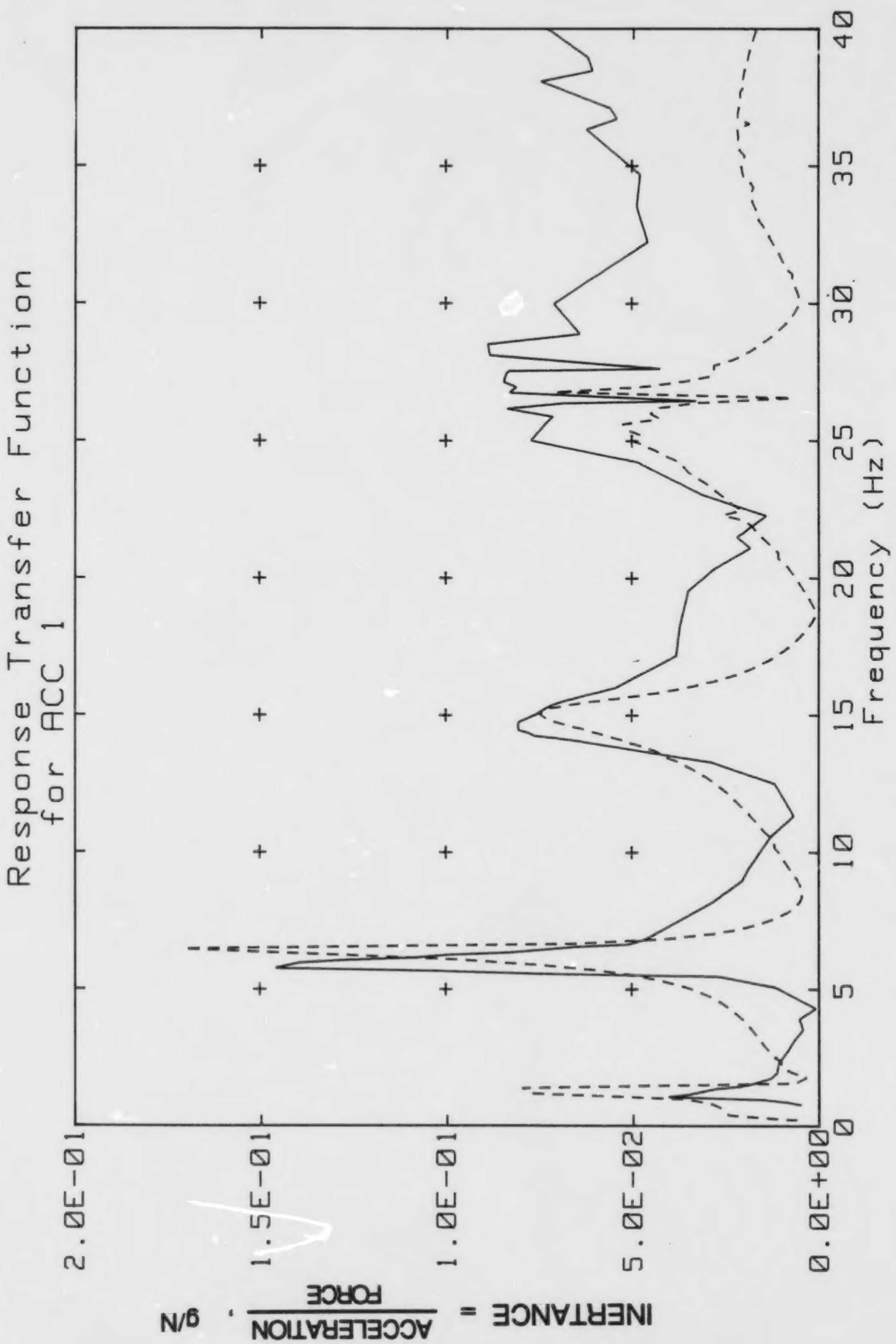
Response Transfer Function
for ACC 1
Frequency (Hz)
0
5
10
15
20
25
30
35
40
0.0E+00
5.0E-02
1.0E-01
1.5E-01
2.0E-01
INERTANCE = ACCELERATION / FORCE , g/N

Response Transfer Function
for ACC 2

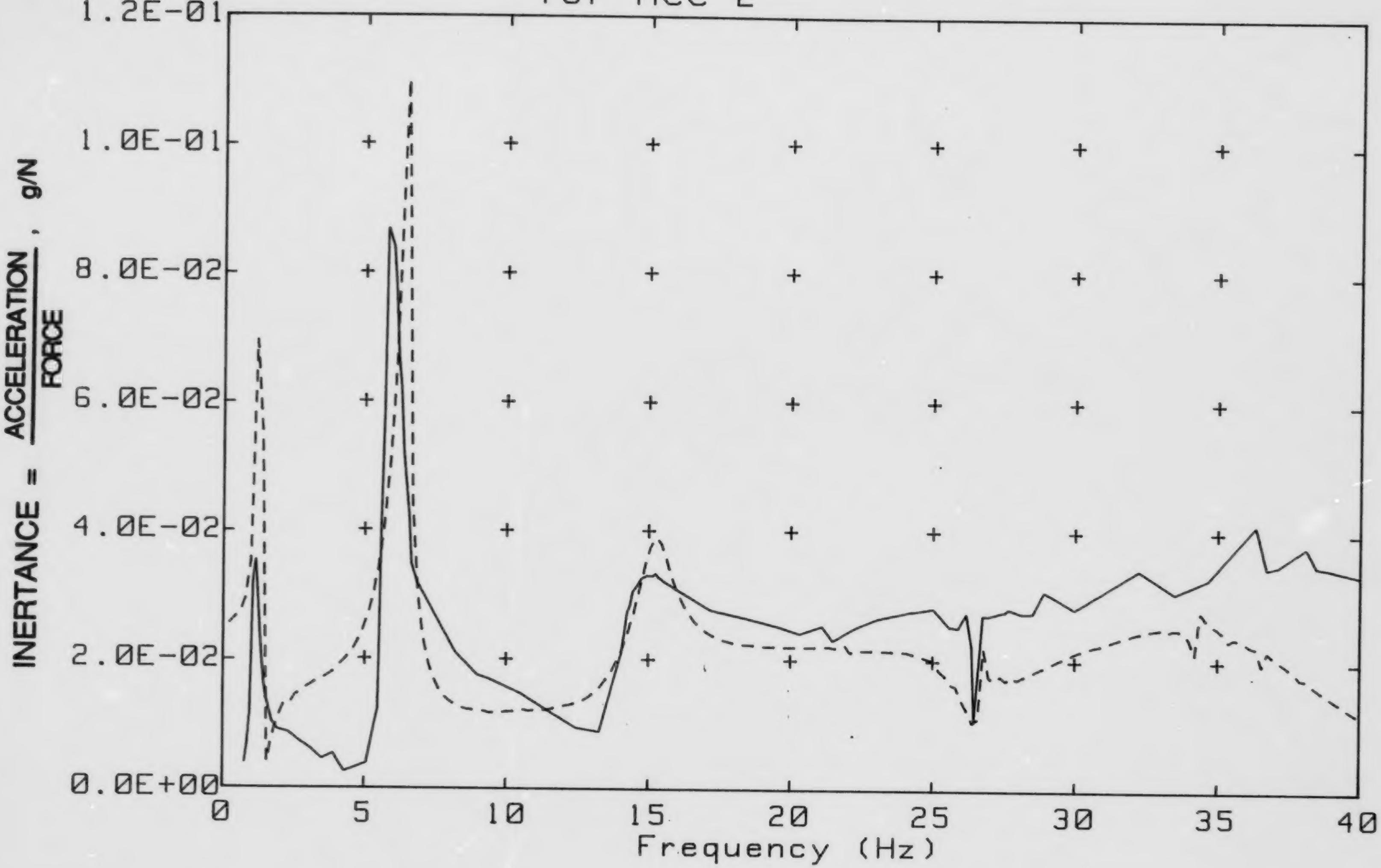

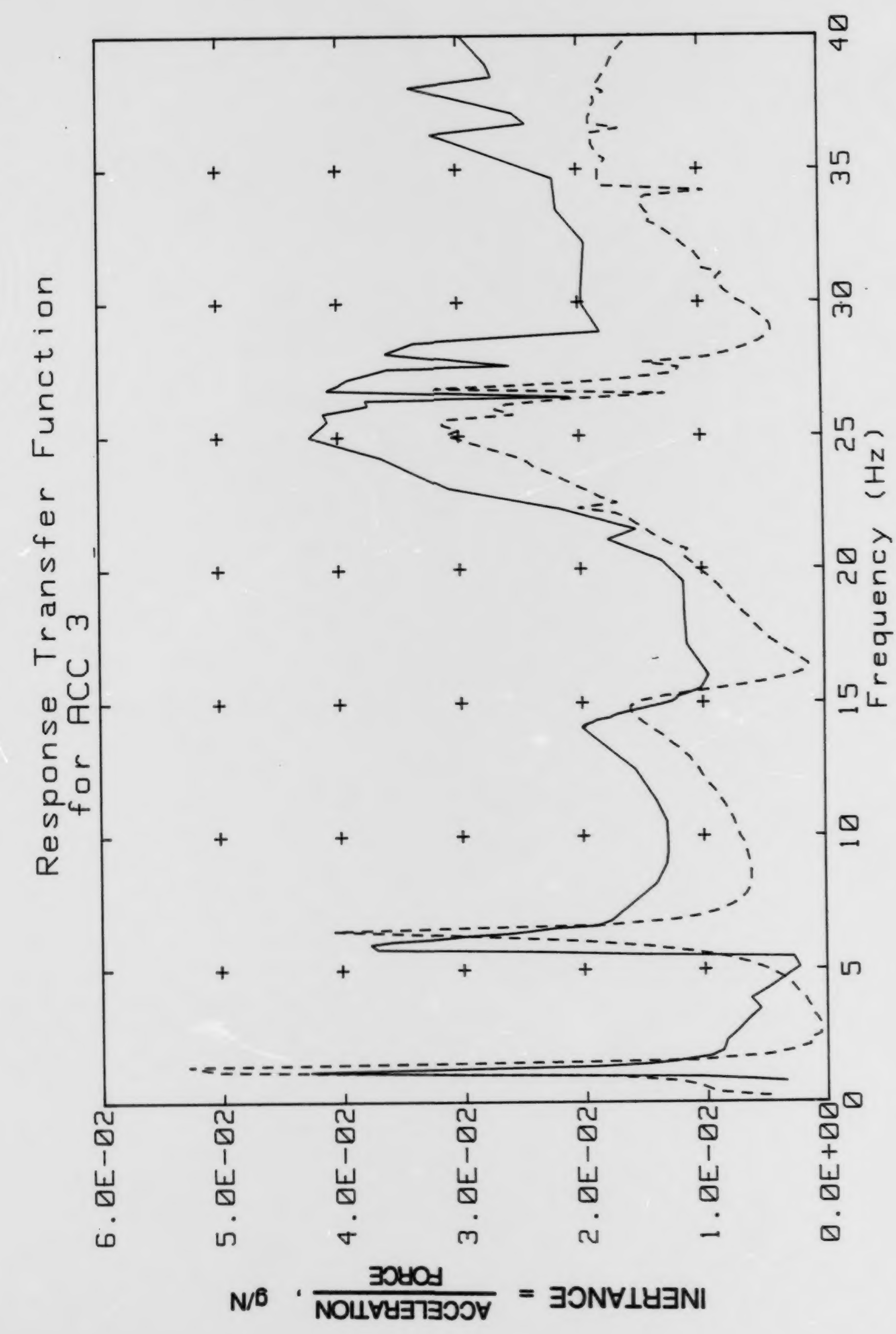
Response Transfer Function for ACC 3

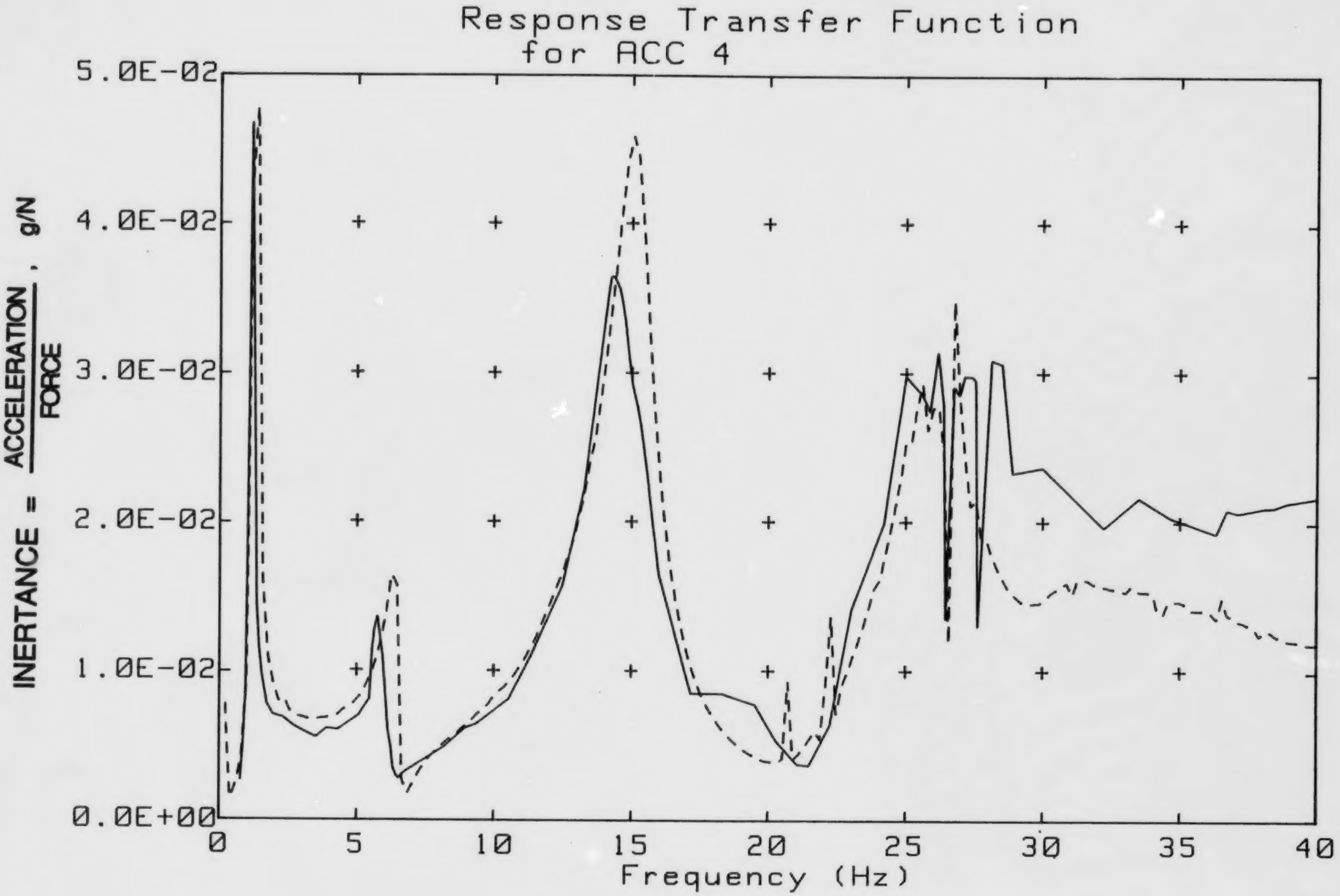
Response Transfer Function
for ACC 4
INERTANCE = ACCELERATION / FORCE , g/N
5.0E-02
4.0E-02
3.0E-02
2.0E-02
1.0E-02
0.0E+00
0
5
10
15
20
25
30
35
40
Frequency (Hz)

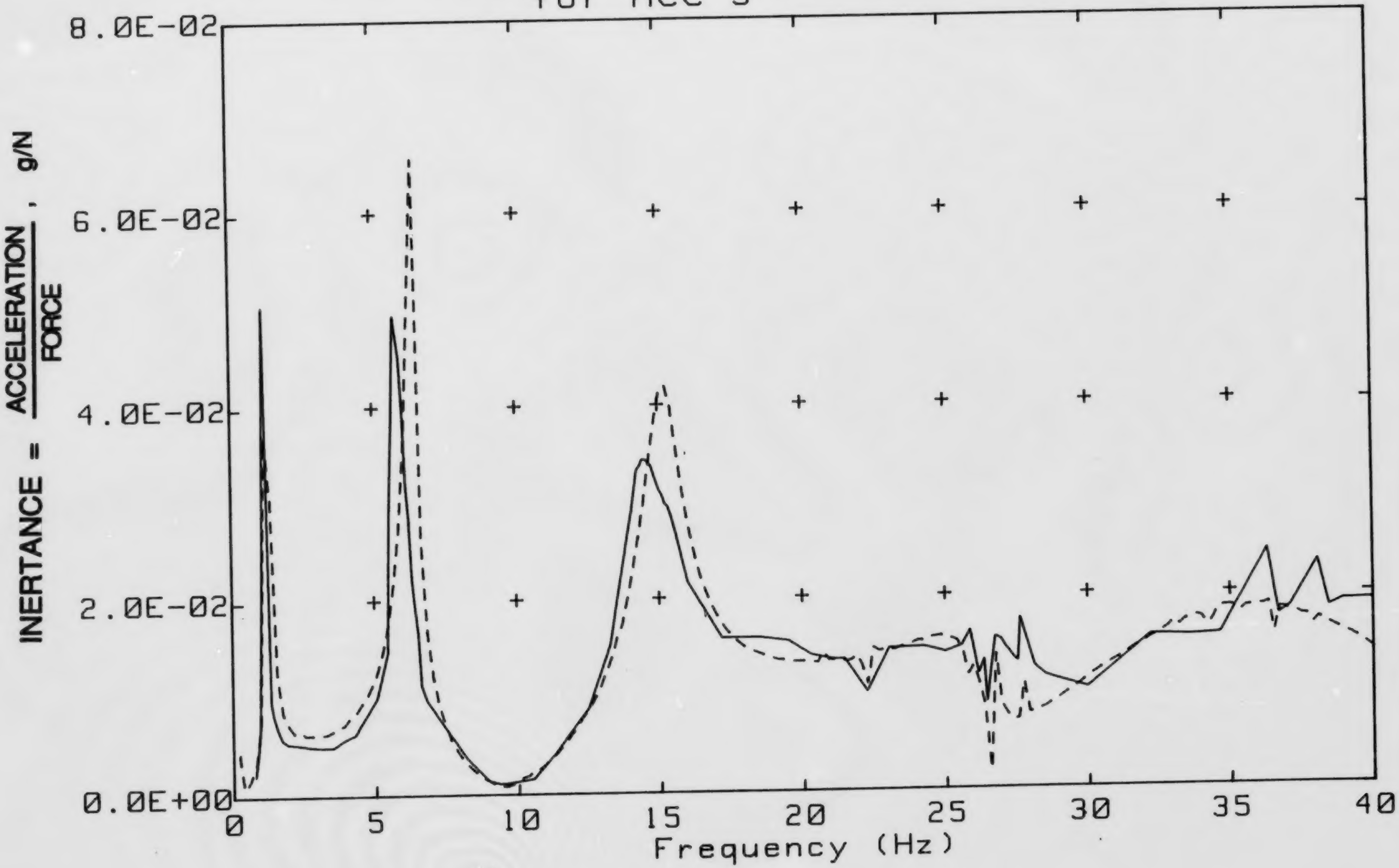

Response Transfer Function
for ACC 5

Response Transfer Function
for ACC 6

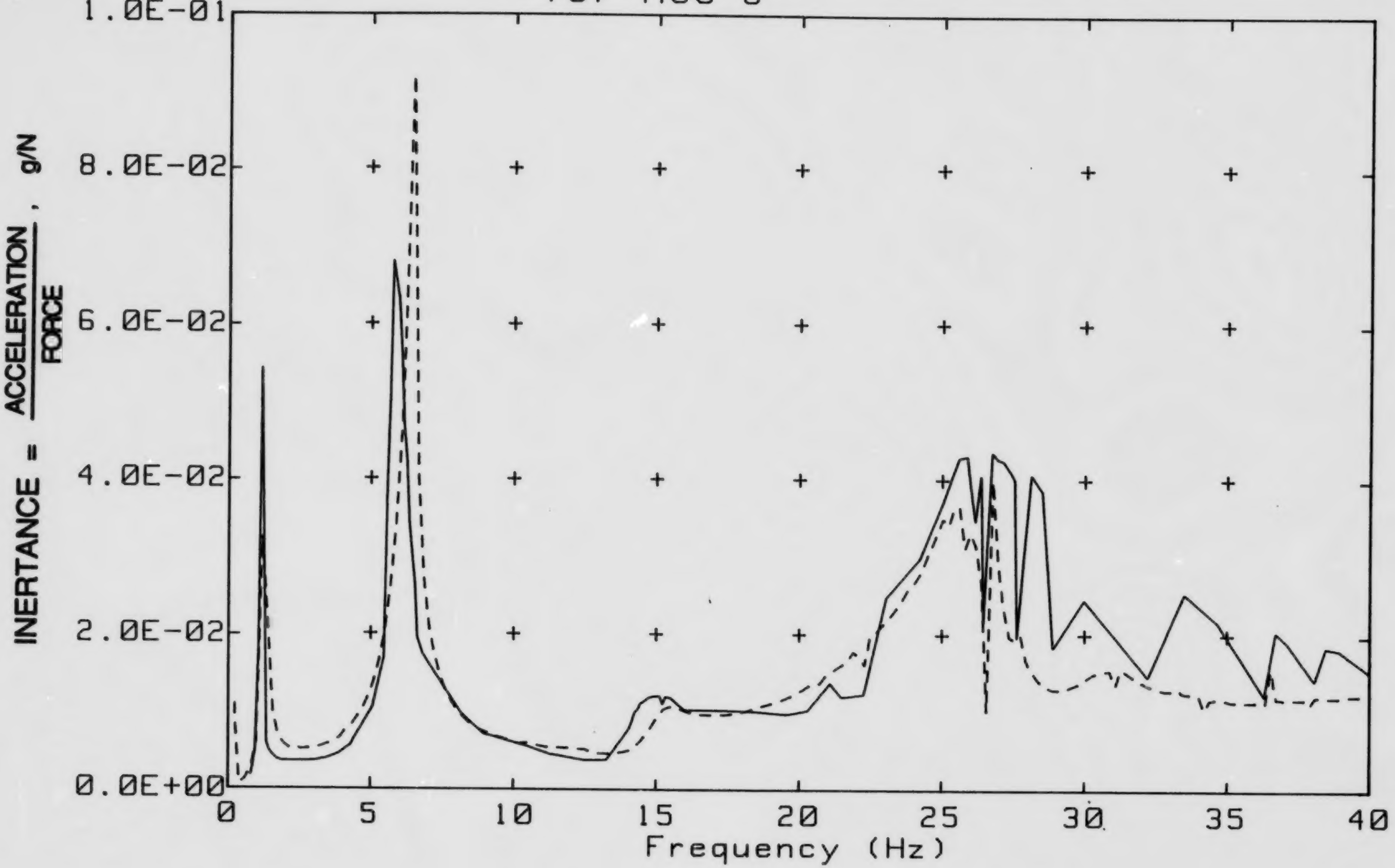

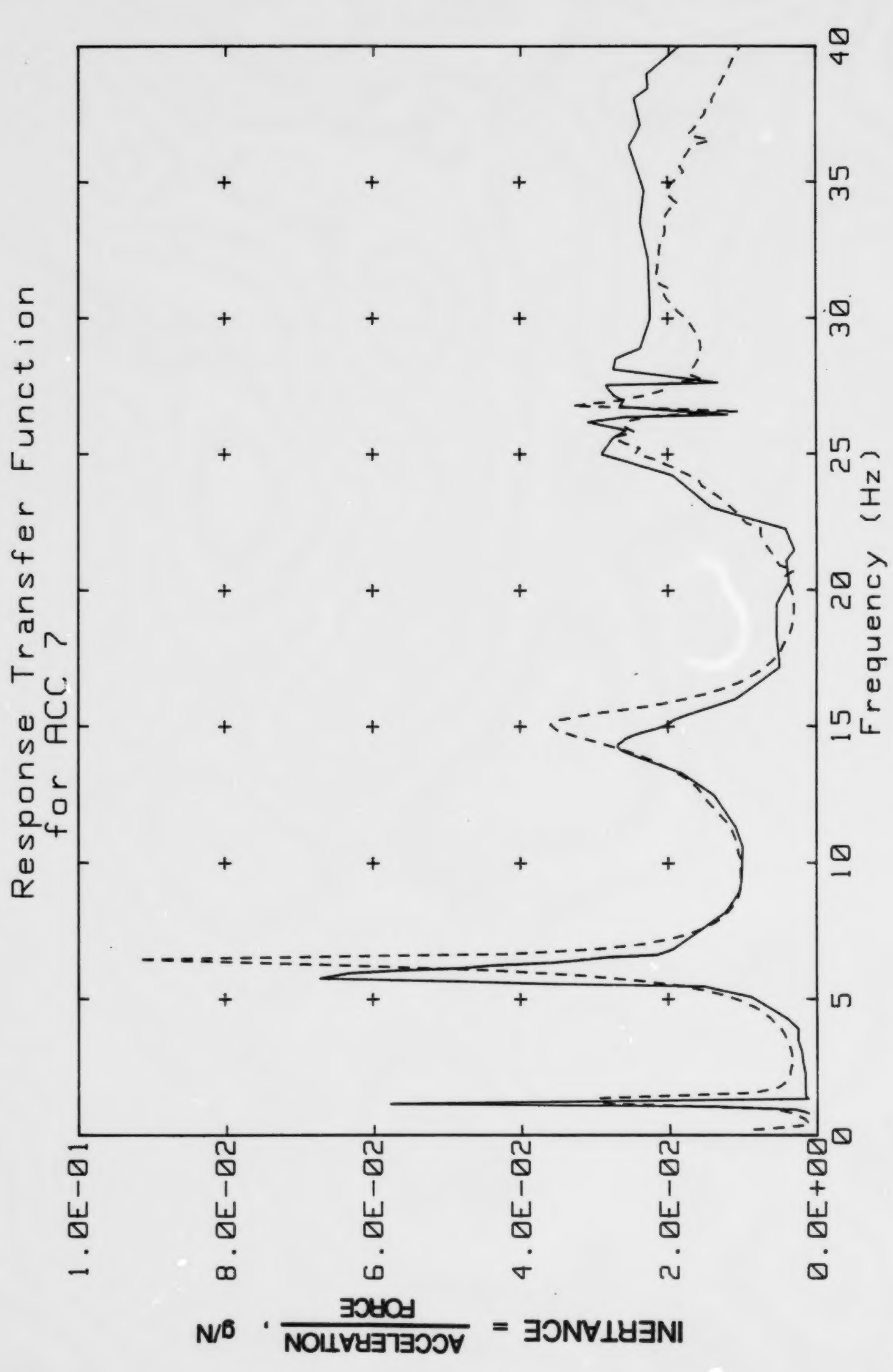
Response Transfer Function
for ACC 7
INERTANCE = ACCELERATION / FORCE , g/N
1.0E-01
8.0E-02
6.0E-02
4.0E-02
2.0E-02
0.0E+00
0
5
10
15
20
25
30
35
40
Frequency (Hz)

Response Transfer Function
for ACC 8

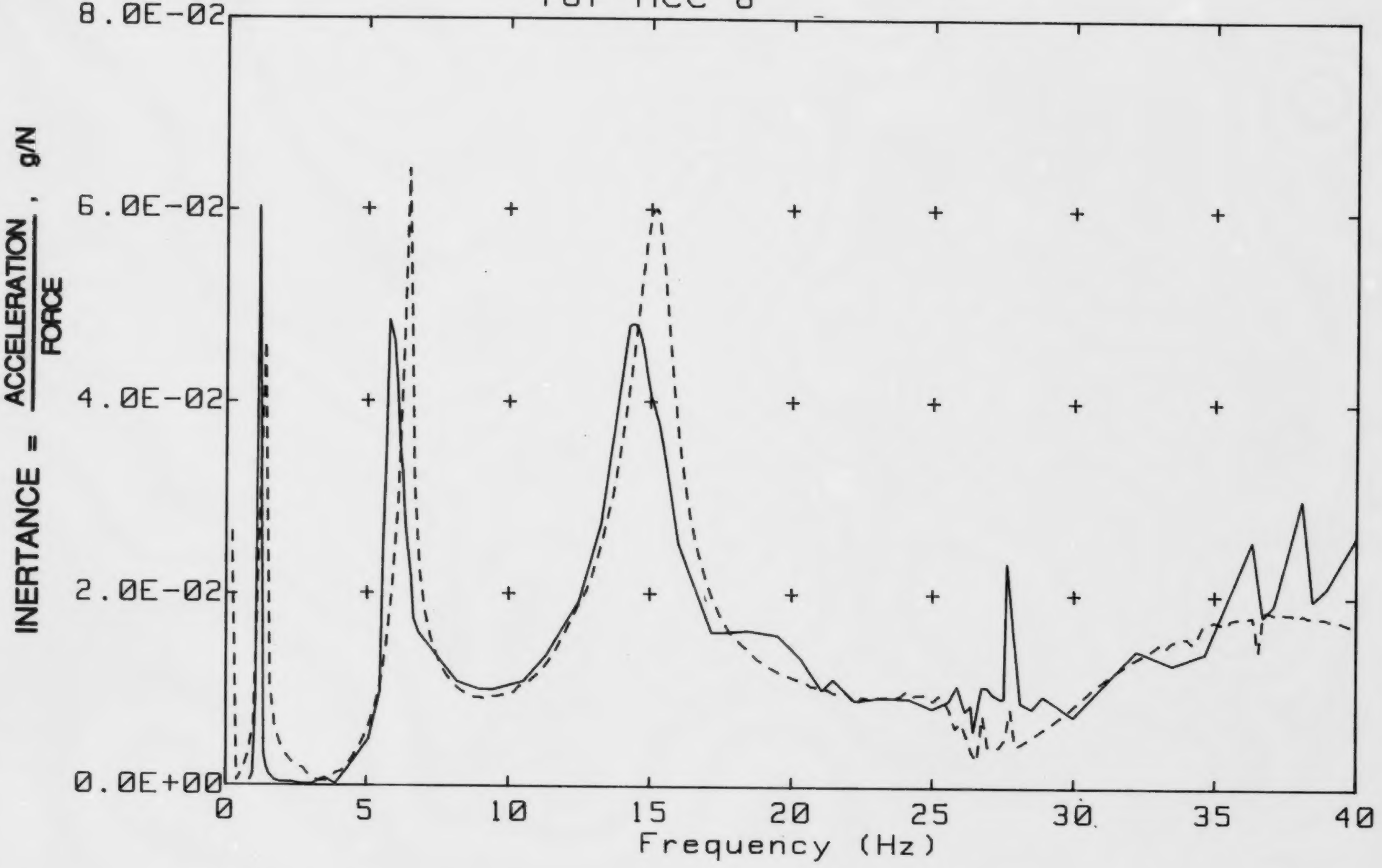

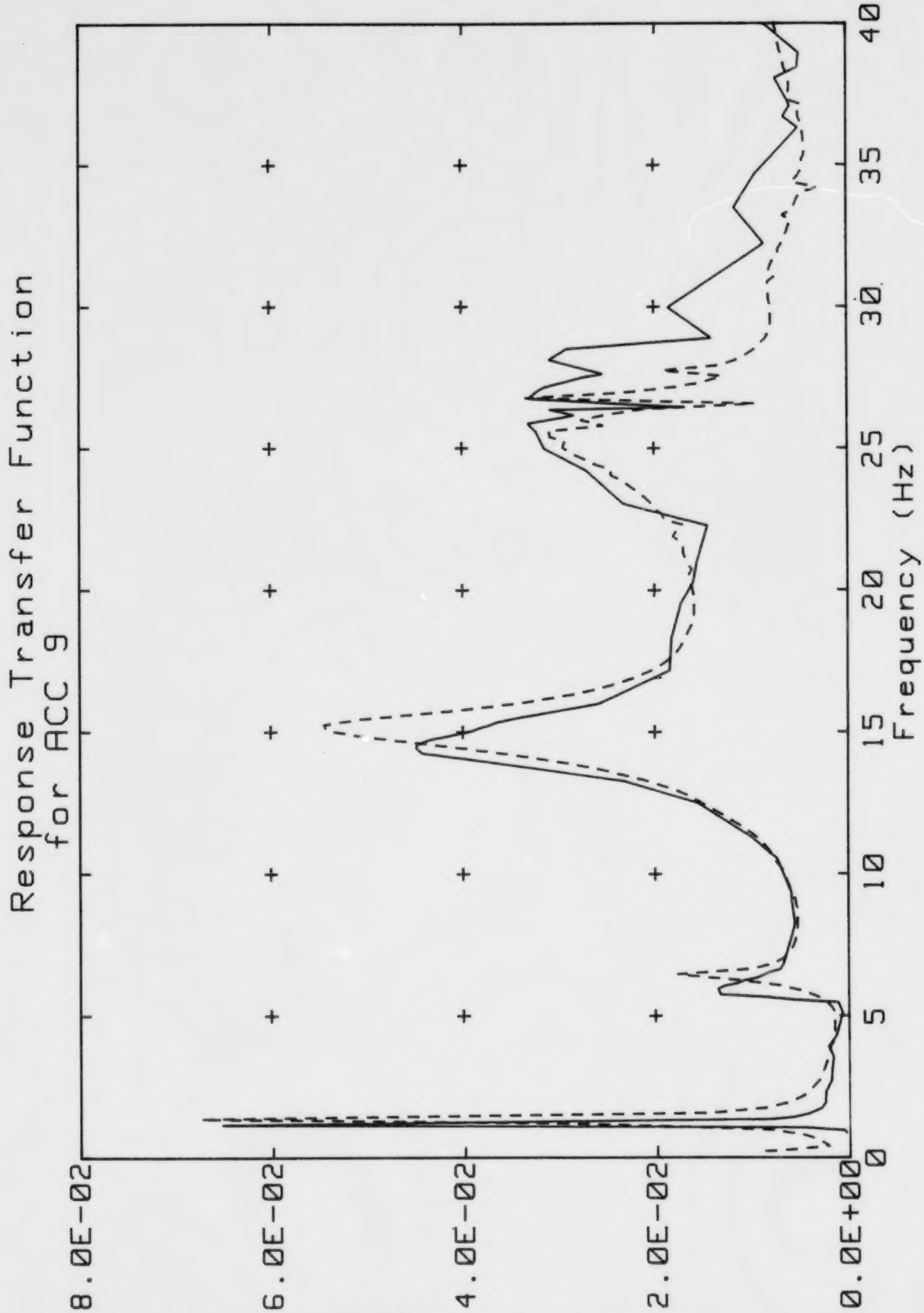Response Transfer Function
for ACC 9
Frequency (Hz)
0
5
10
15
20
25
30
35
40
INERTANCE = ACCELERATION / FORCE , g/N
0.0E+00
2.0E-02
4.0E-02
6.0E-02
8.0E-02

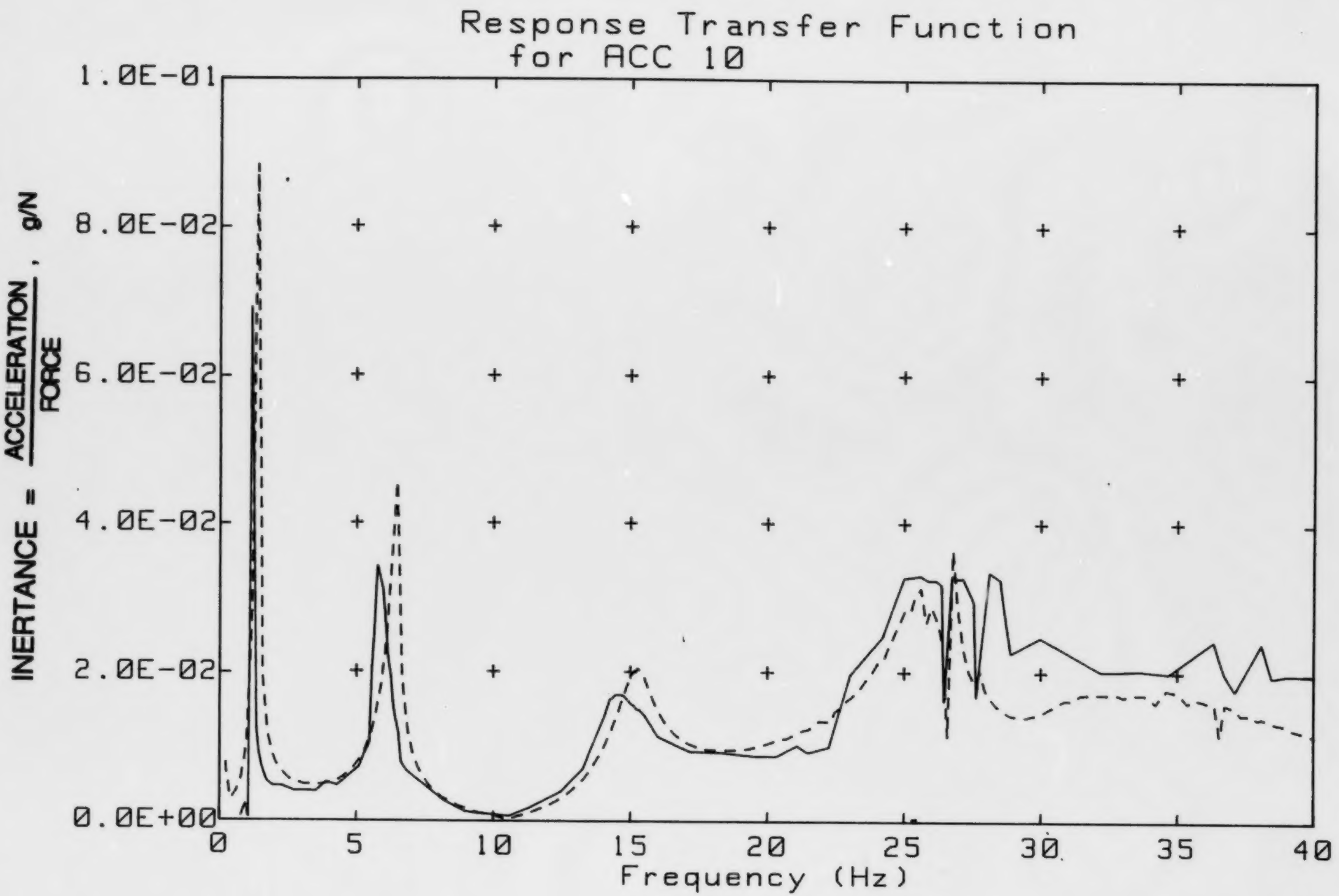
Response Transfer Function
for ACC 10
INERTANCE = ACCELERATION / FORCE , g/N
1.0E-01
8.0E-02
6.0E-02
4.0E-02
2.0E-02
0.0E+00
0
5
10
15
20
25
30
35
40
Frequency (Hz)

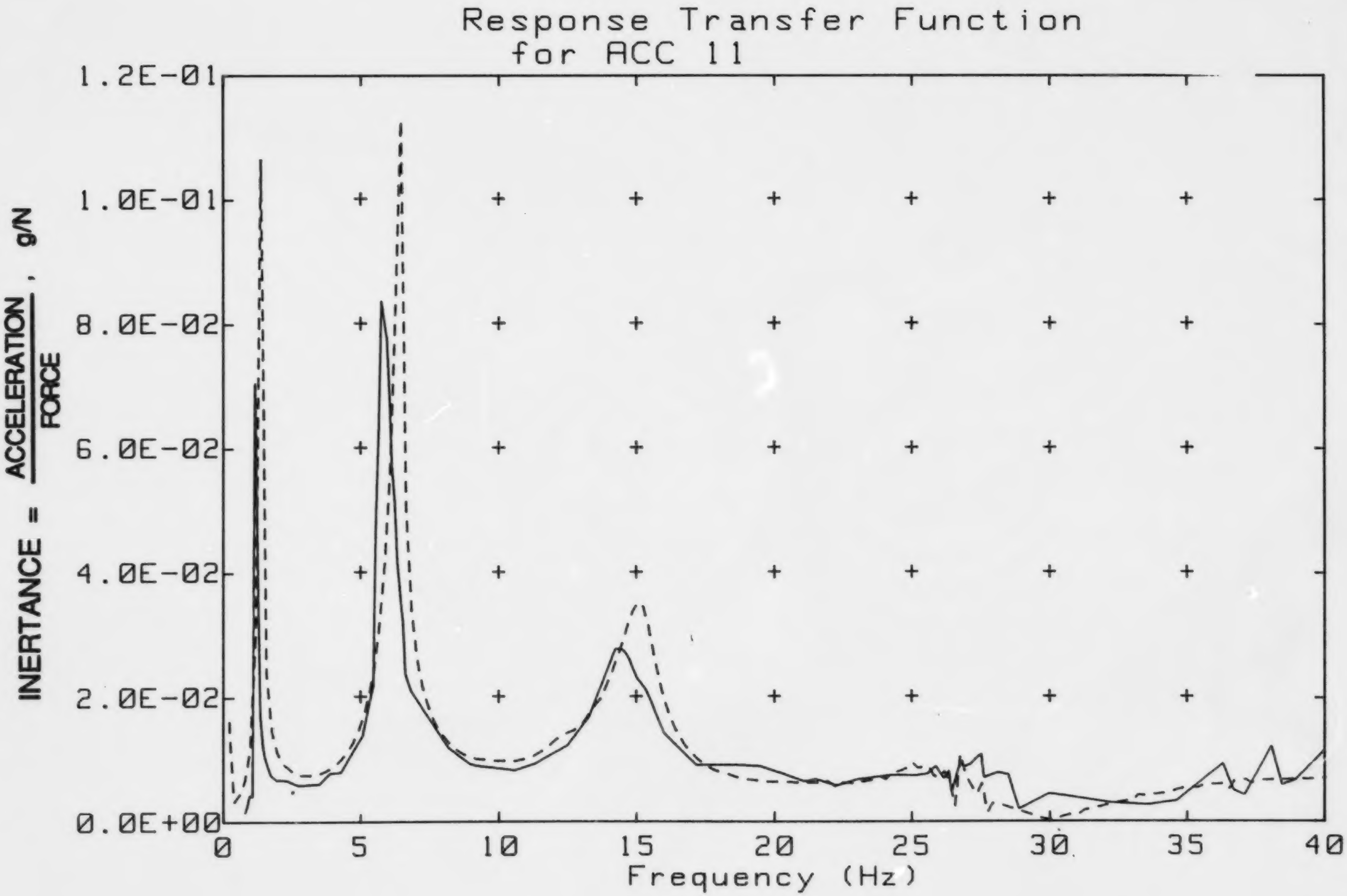
Response Transfer Function
for ACC 11
INERTANCE = ACCELERATION / FORCE , g/N
1.2E-01
1.0E-01
8.0E-02
6.0E-02
4.0E-02
2.0E-02
0.0E+00
0
5
10
15
20
25
30
35
40
Frequency (Hz)

Response Transfer Function
for ACC 12

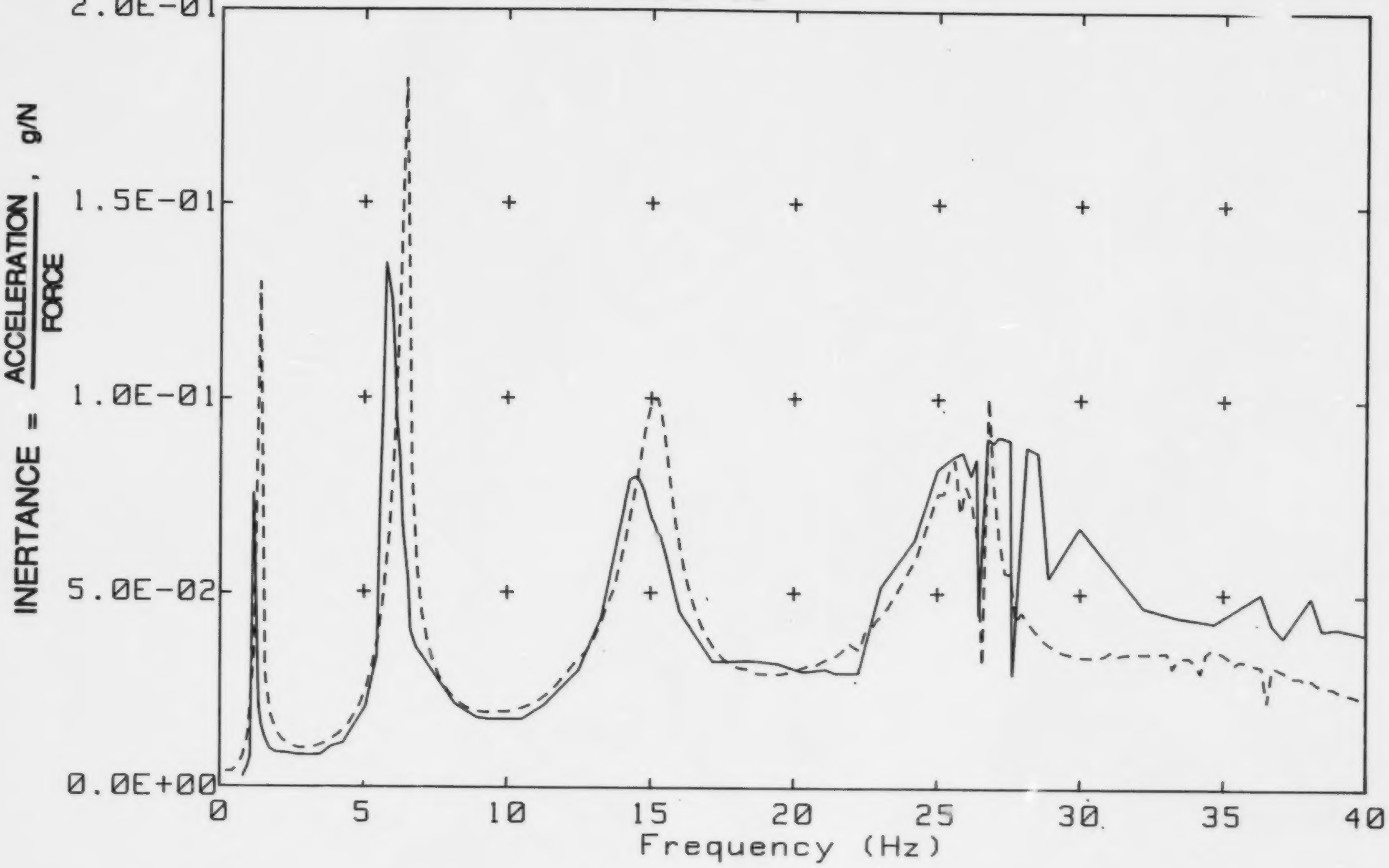

MODE SHAPES FROM THE DRY HAMMER TESTS

MODE SHAPE: 2 FREQ: 6.19 Hz DAMPING: 2.89 %

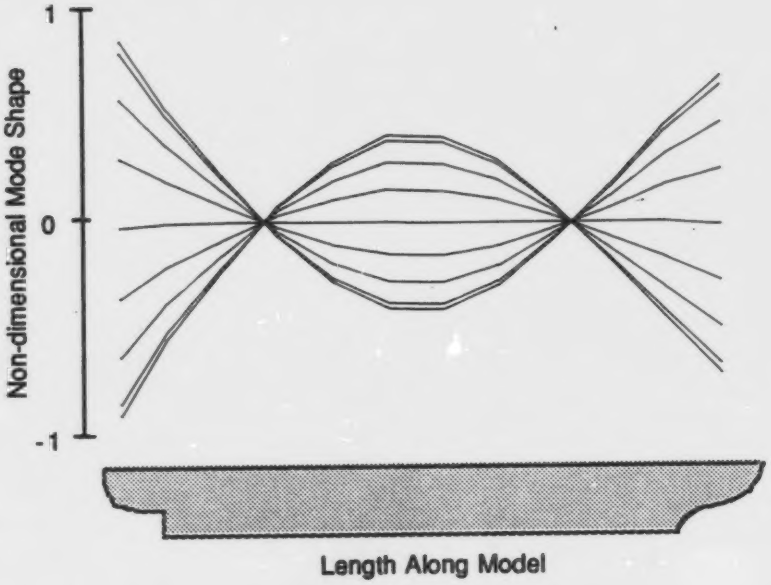

MODE SHAPE: 3 FREQ: 14.94 Hz DAMPING: 4.94 %

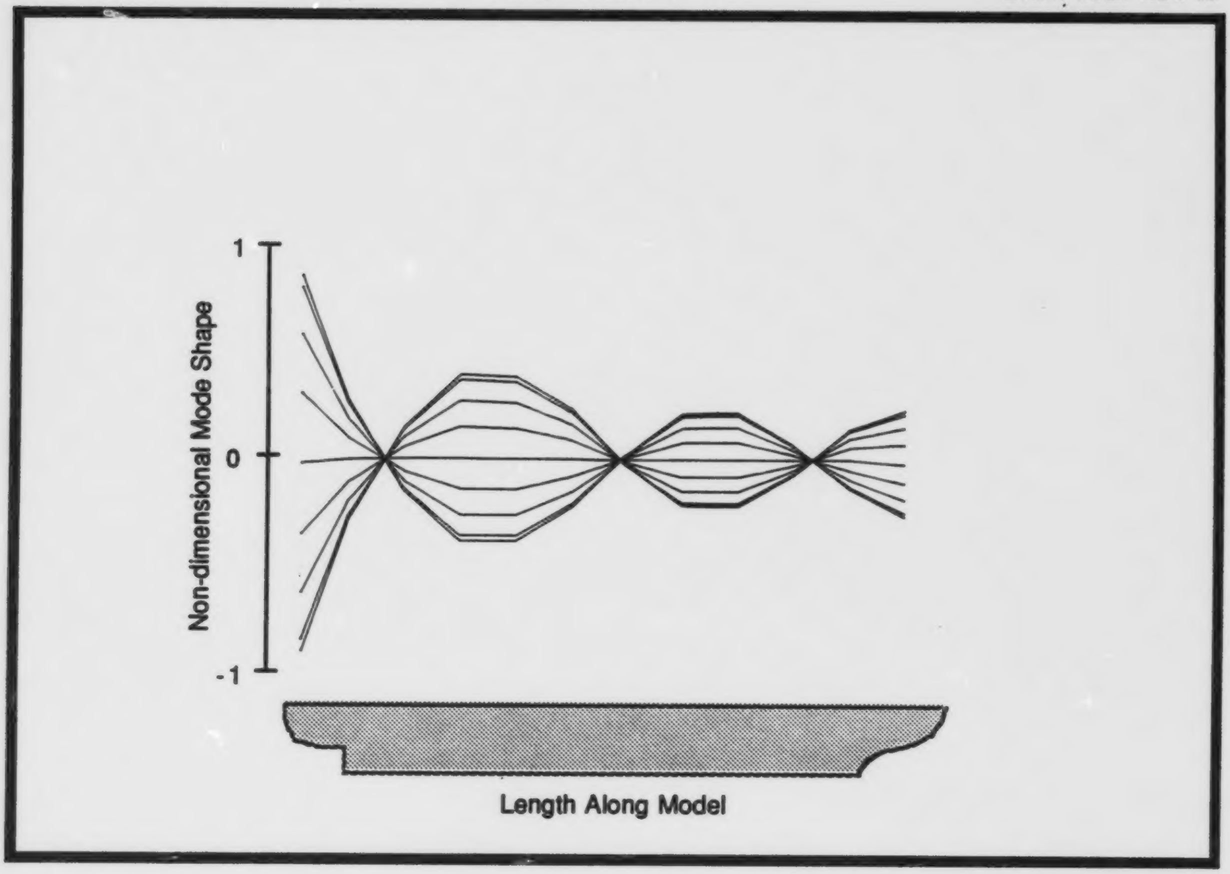

MODE SHAPE: 4 FREQ: 26.14 Hz DAMPING: 3.46 %

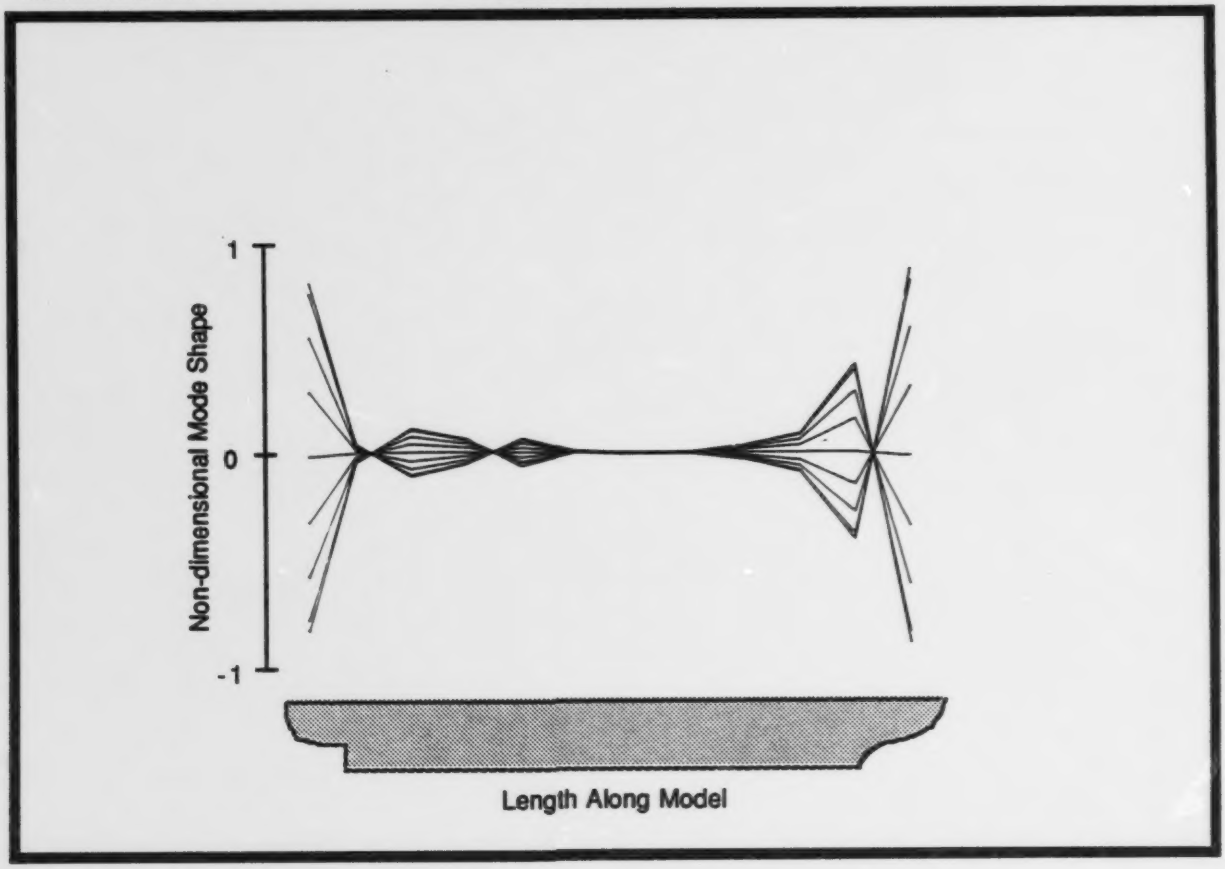

MODE SHAPE: 5 FREQ: 35.25 Hz DAMPING: 8.10 %

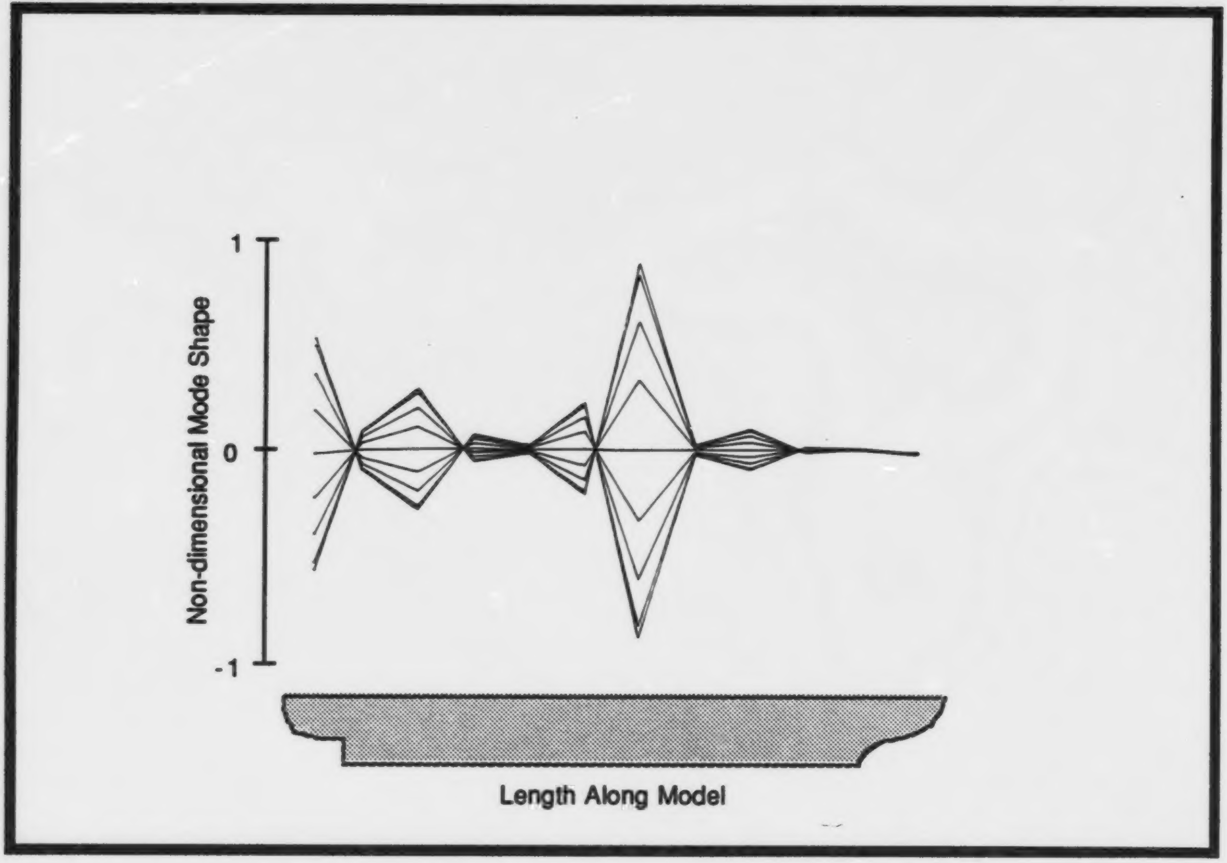

MODE SHAPES FROM THE DRY SHAKER TESTS

MODE SHAPE: 2 FREQ: 5.87 Hz DAMPING: 3.90 %

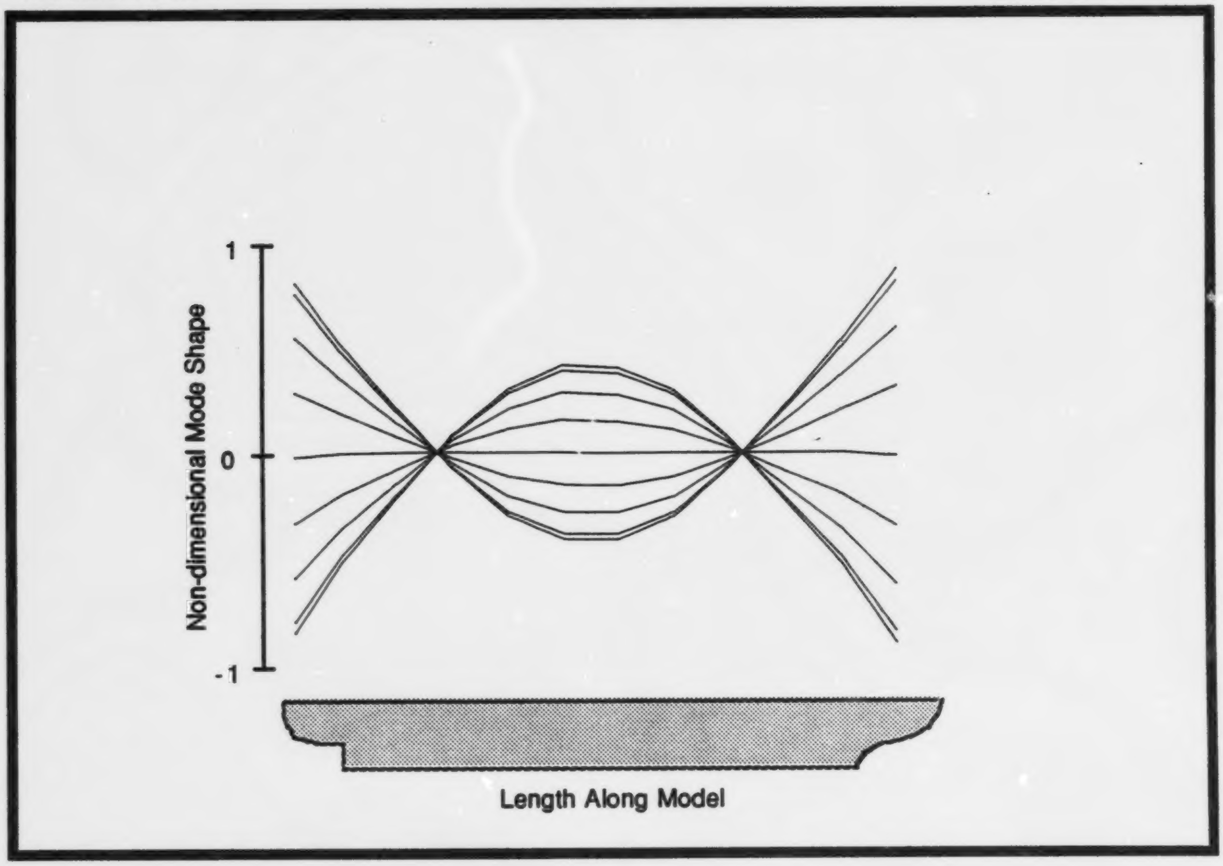

MODE SHAPE: 3 FREQ: 14.46 Hz DAMPING: 5.60 %

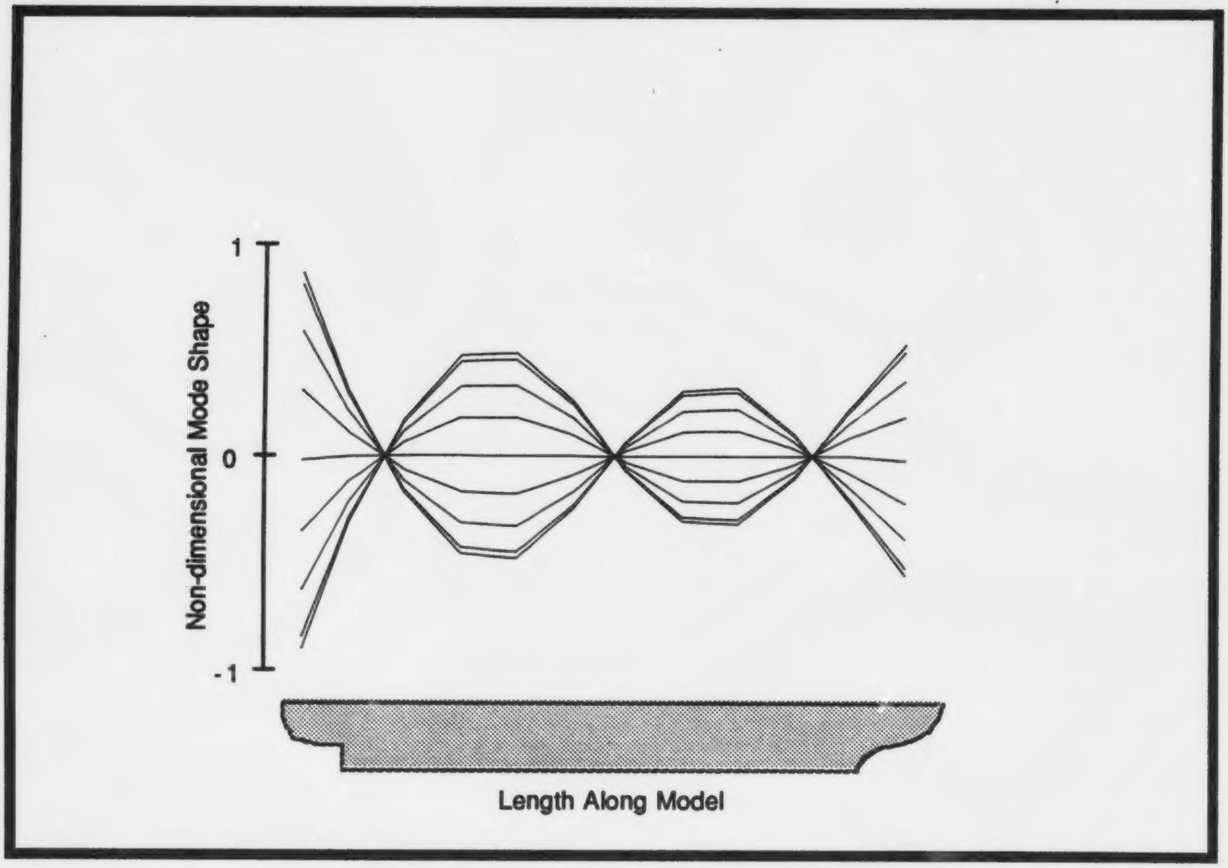

MODE SHAPE: 4 FREQ: 27.69 Hz DAMPING: 5.91 %

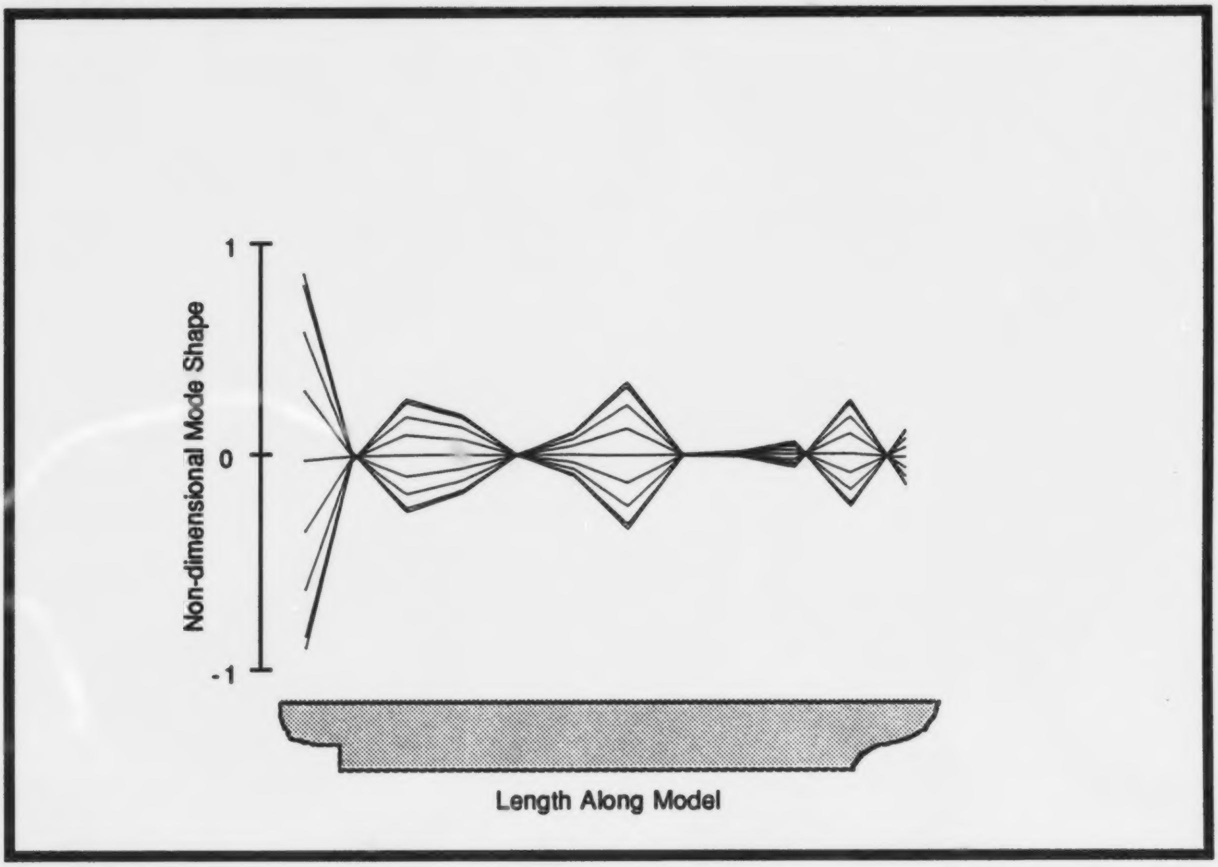

MODE SHAPE: 5 FREQ: 38.96 Hz DAMPING: .19 %

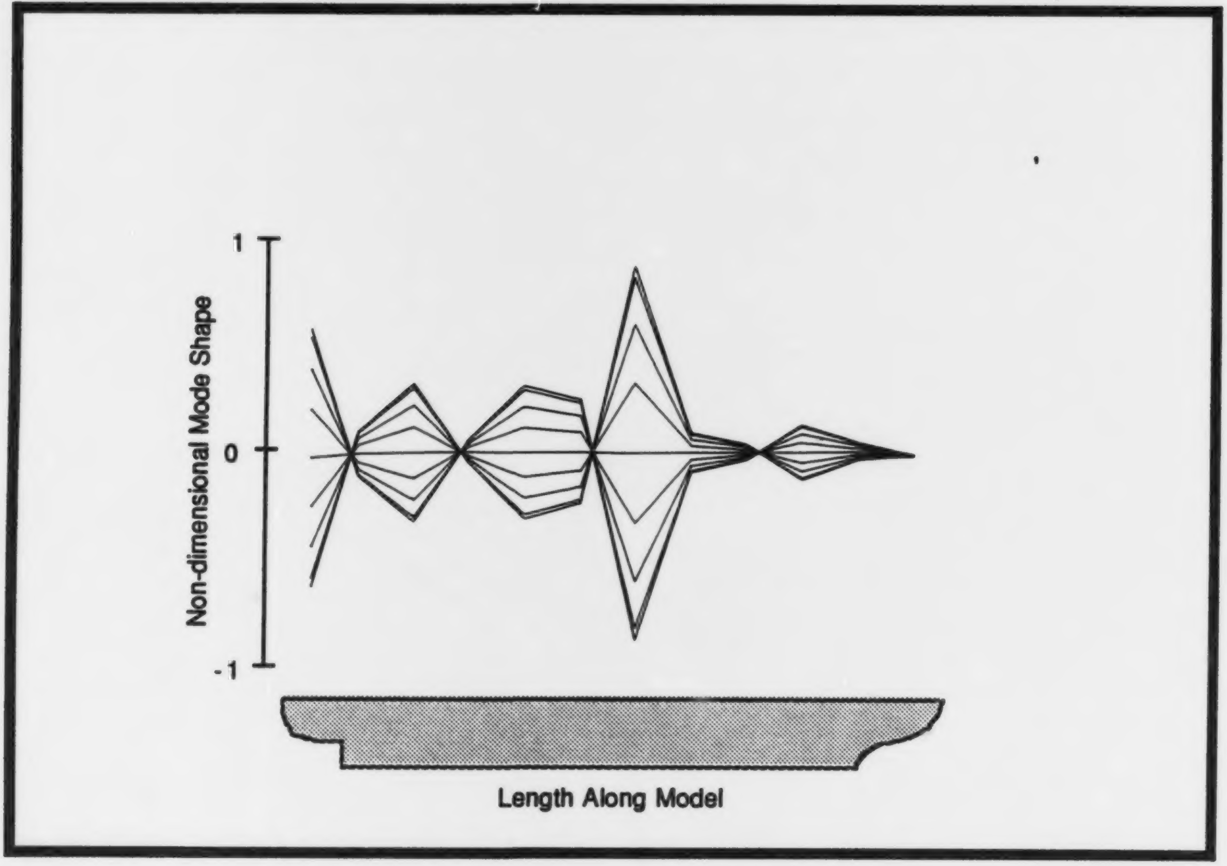

WET TEST COMPARISON

Response Transfer Function
for ACC 1

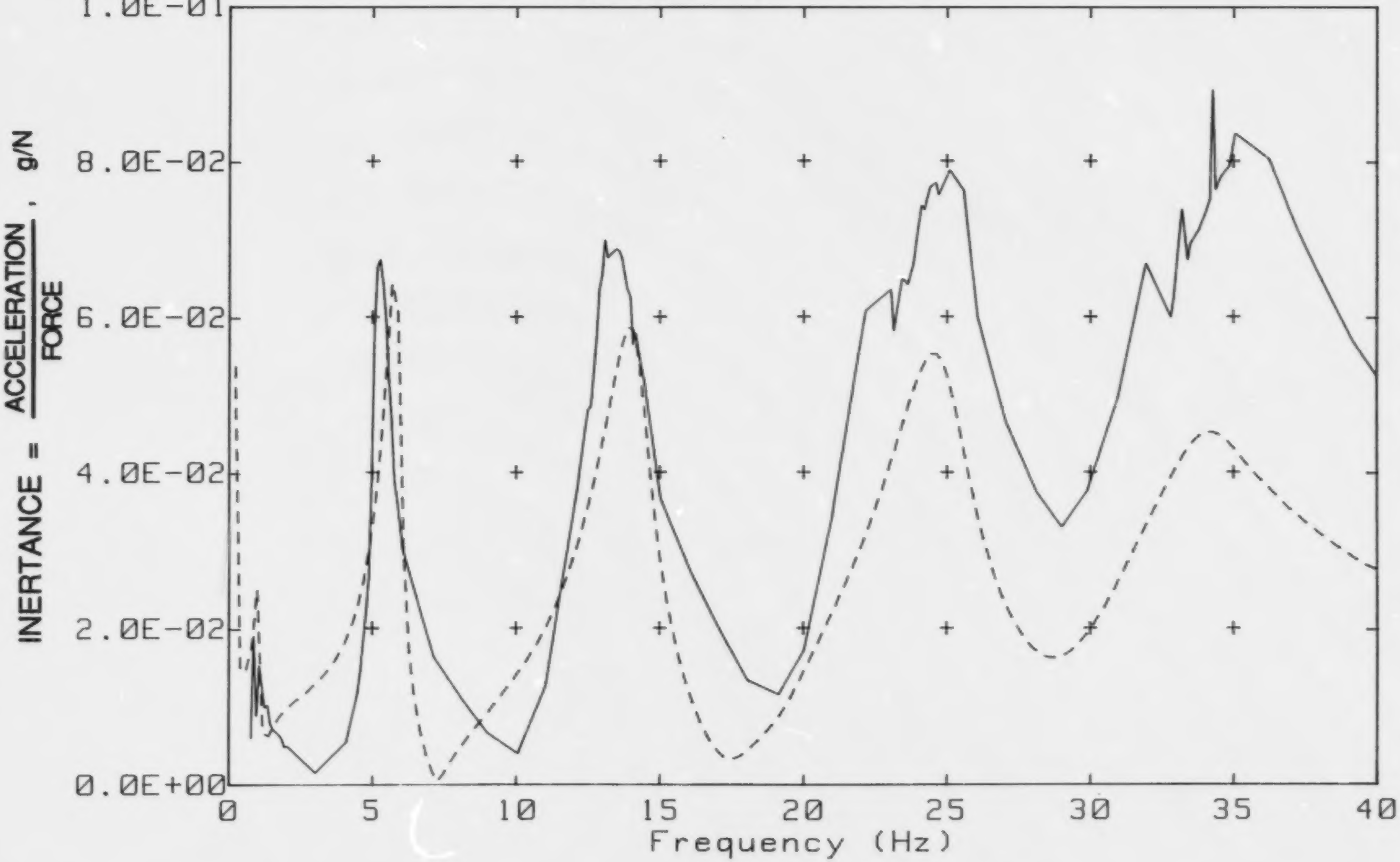

Response Transfer Function
for ACC 2

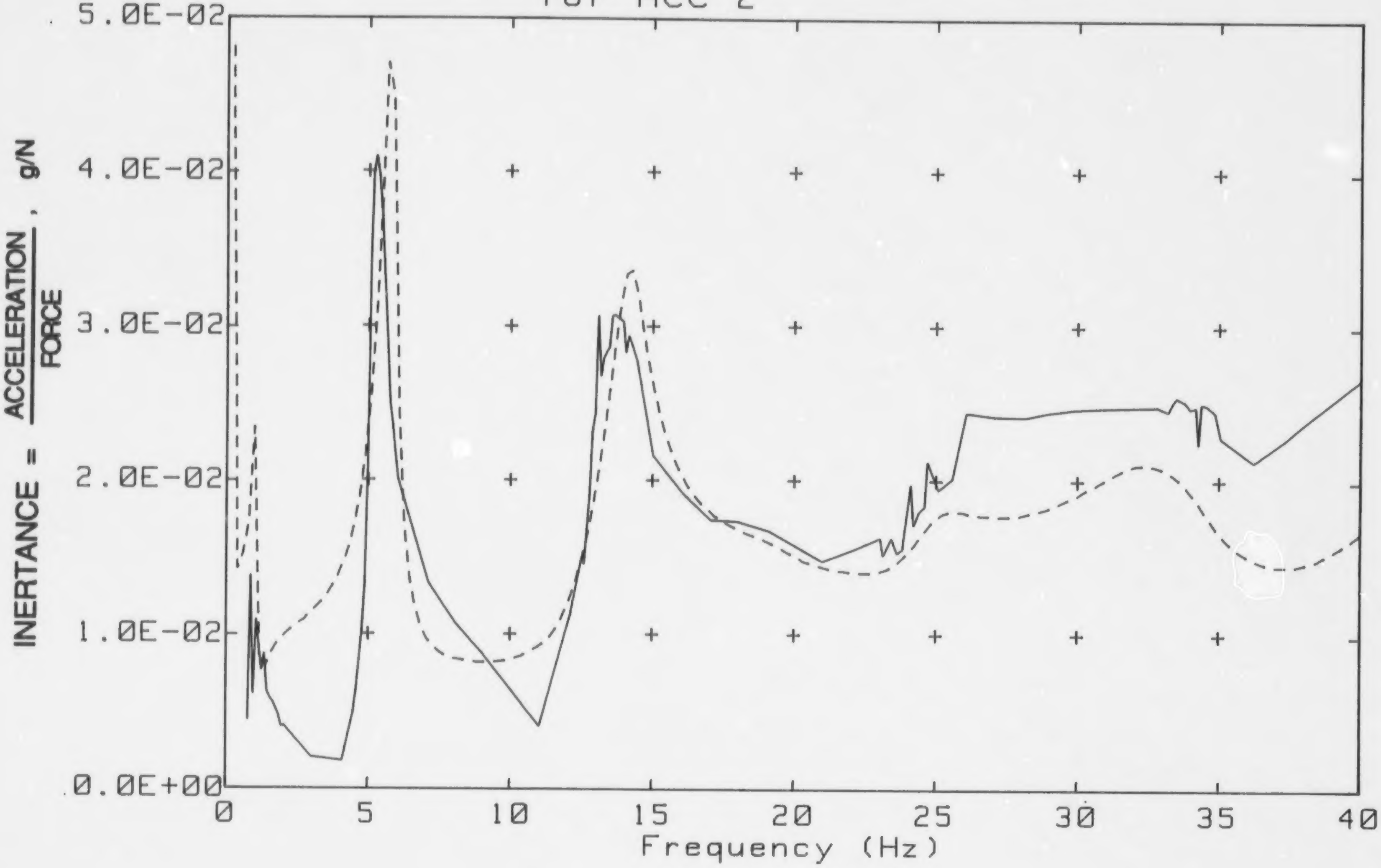

Response Transfer Function
for ACC 3

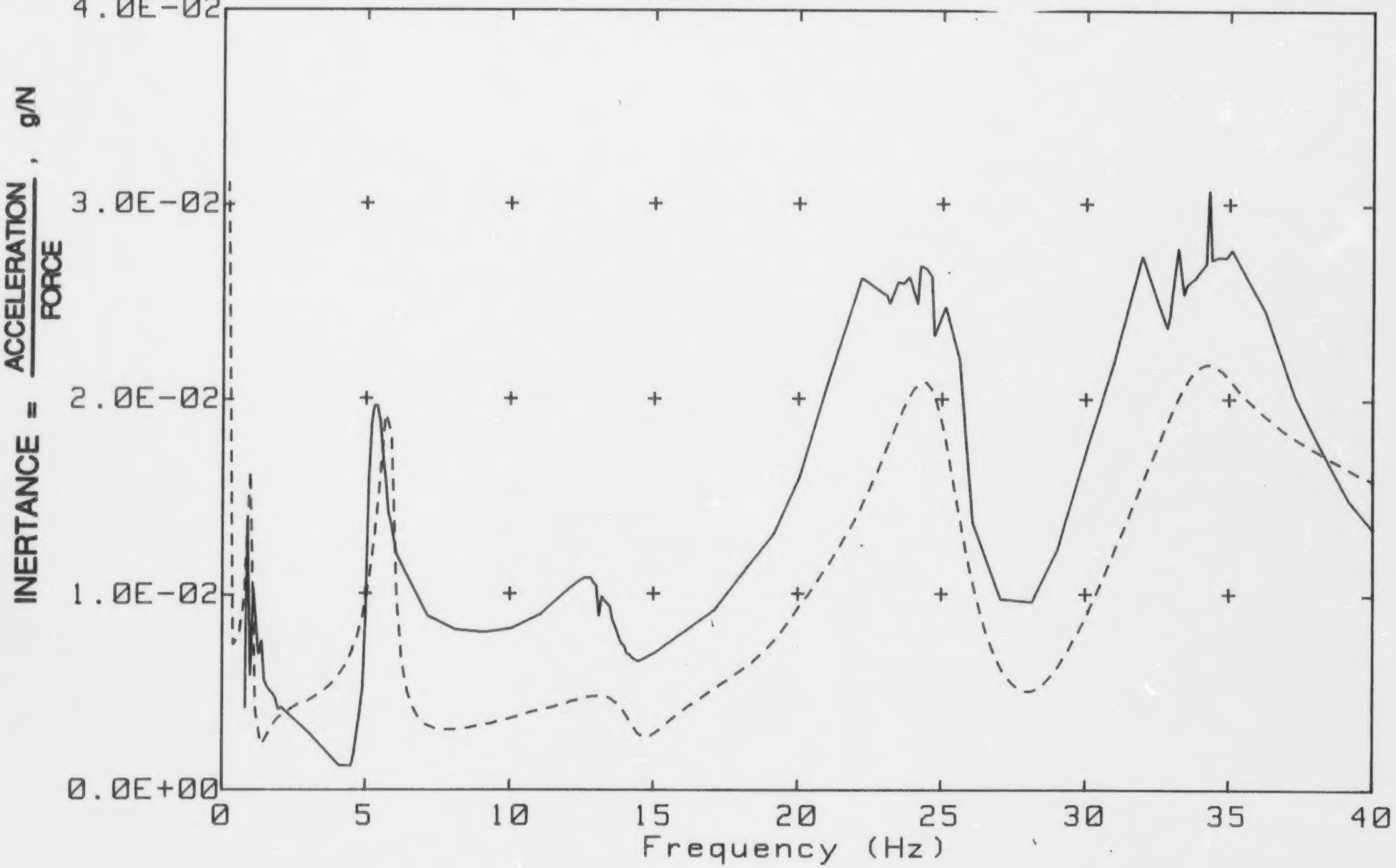

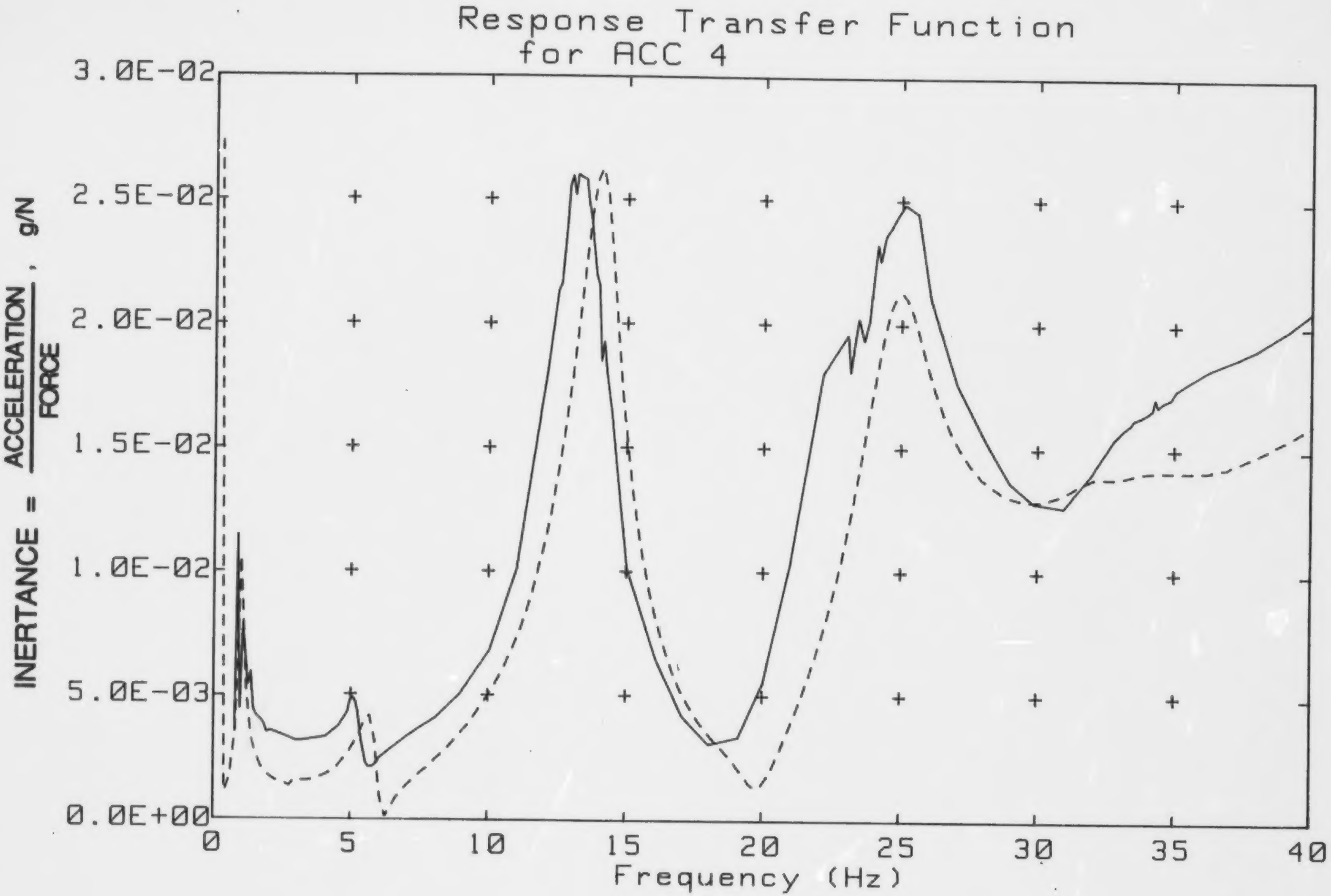
Response Transfer Function
for ACC 4
INERTANCE = ACCELERATION / FORCE , g/N
3.0E-02
2.5E-02
2.0E-02
1.5E-02
1.0E-02
5.0E-03
0.0E+00
0
5
10
15
20
25
30
35
40
Frequency (Hz)

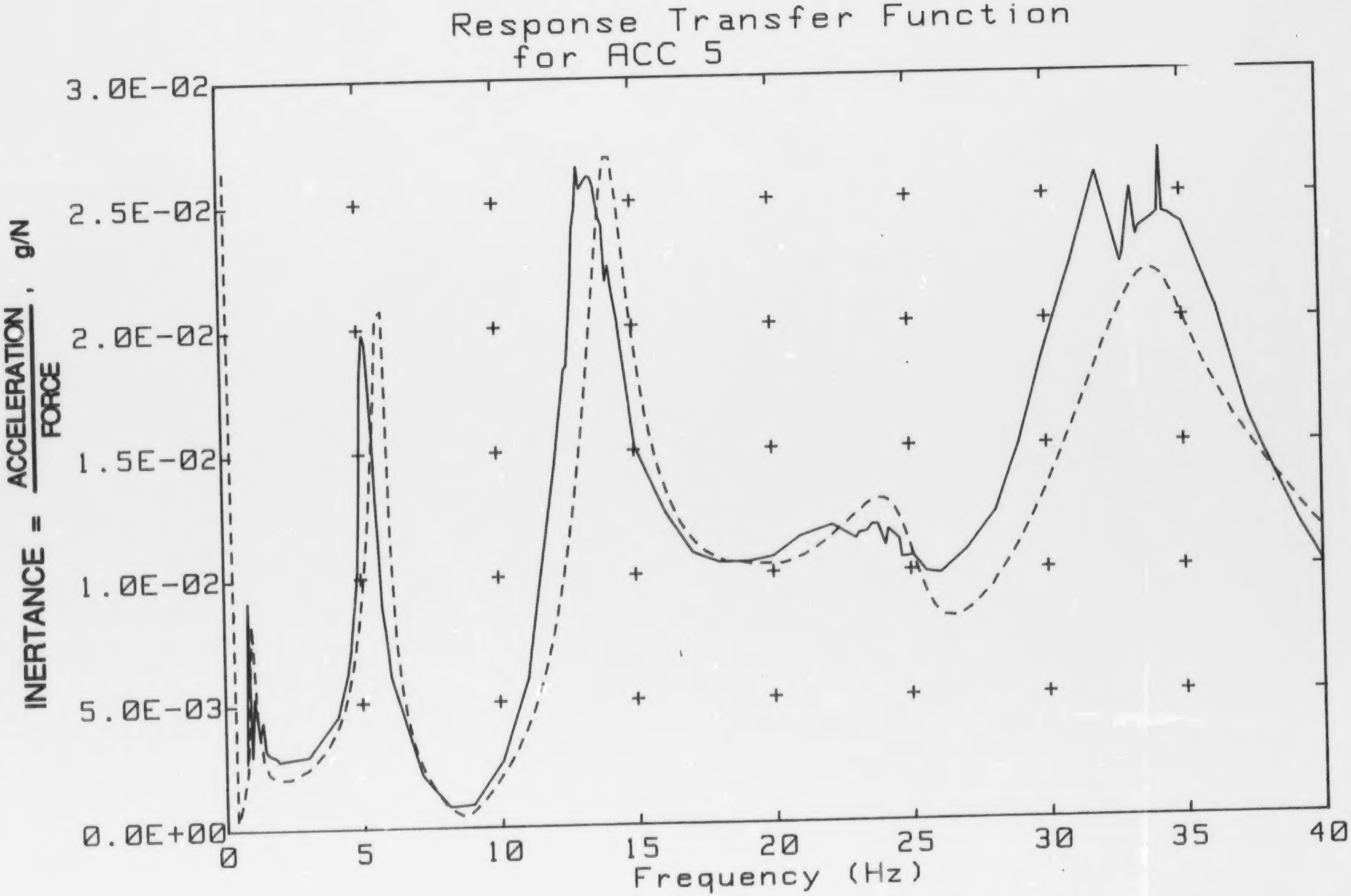
Response Transfer Function
for ACC 5
INERTANCE = ACCELERATION / FORCE , g/N
3.0E-02
2.5E-02
2.0E-02
1.5E-02
1.0E-02
5.0E-03
0.0E+00
0
5
10
15
20
25
30
35
40
Frequency (Hz)

Response Transfer Function
for ACC 6

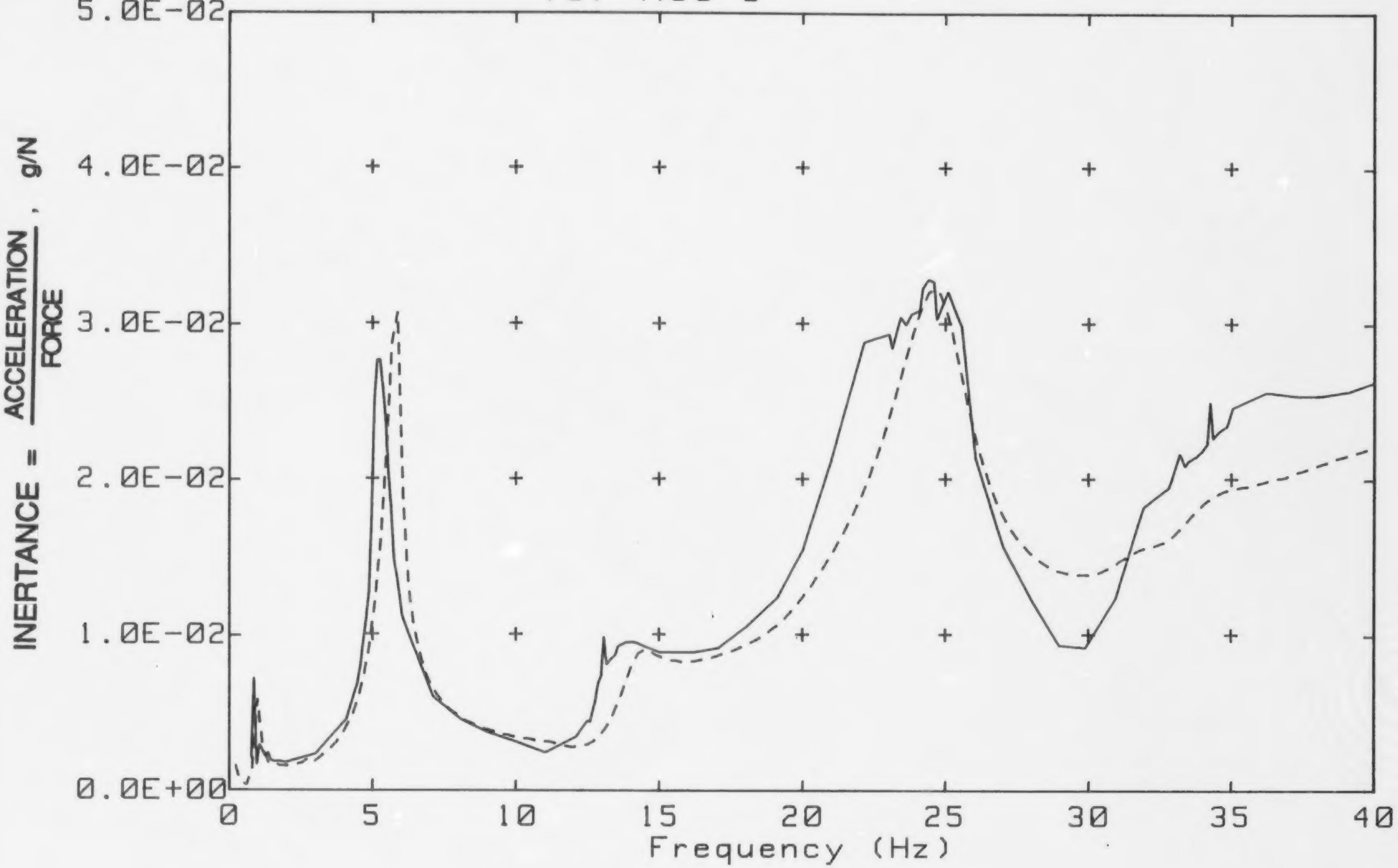

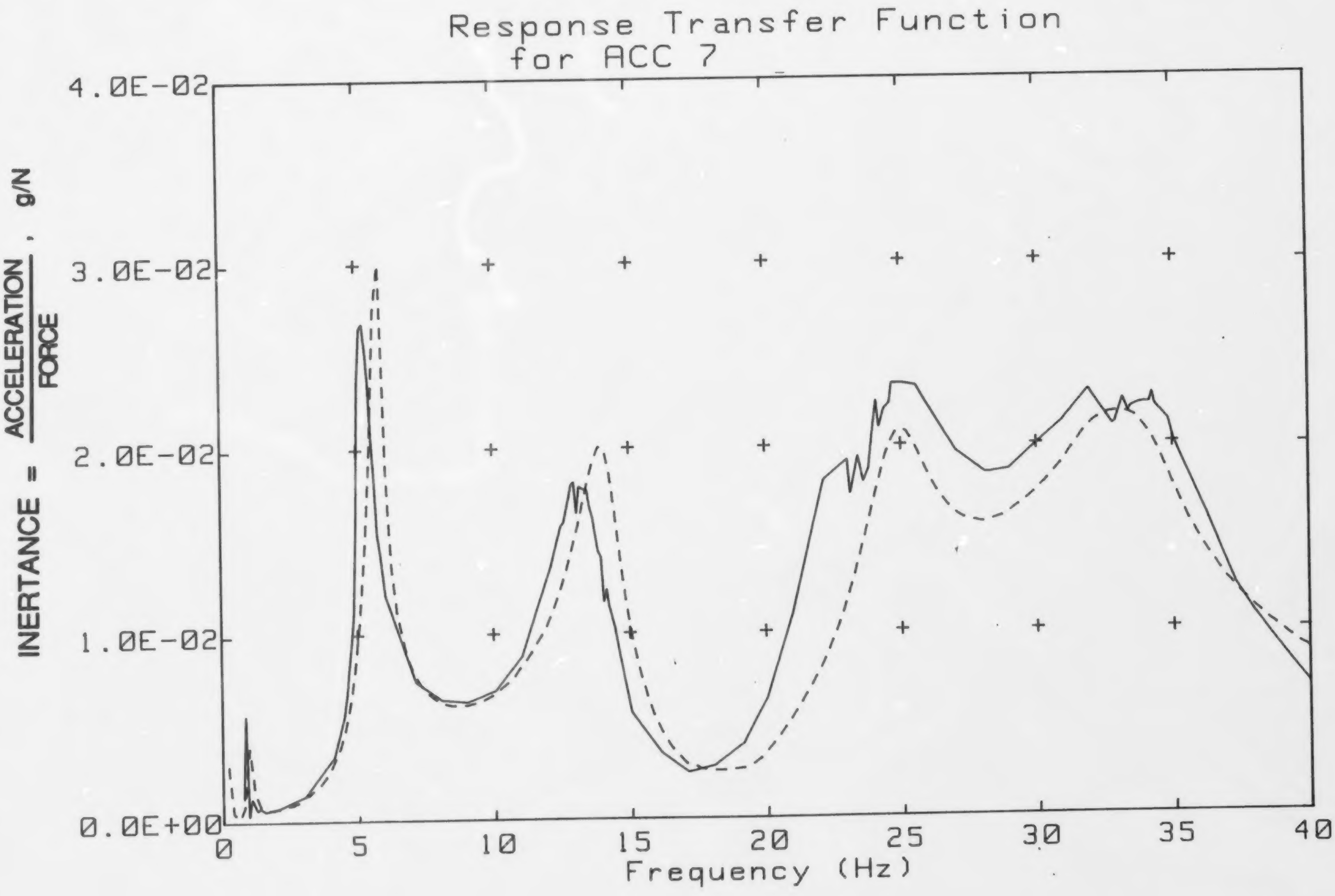
Response Transfer Function
for ACC 7
INERTANCE = ACCELERATION / FORCE , g/N
4.0E-02
3.0E-02
2.0E-02
1.0E-02
0.0E+00
0
5
10
15
20
25
30
35
40
Frequency (Hz)

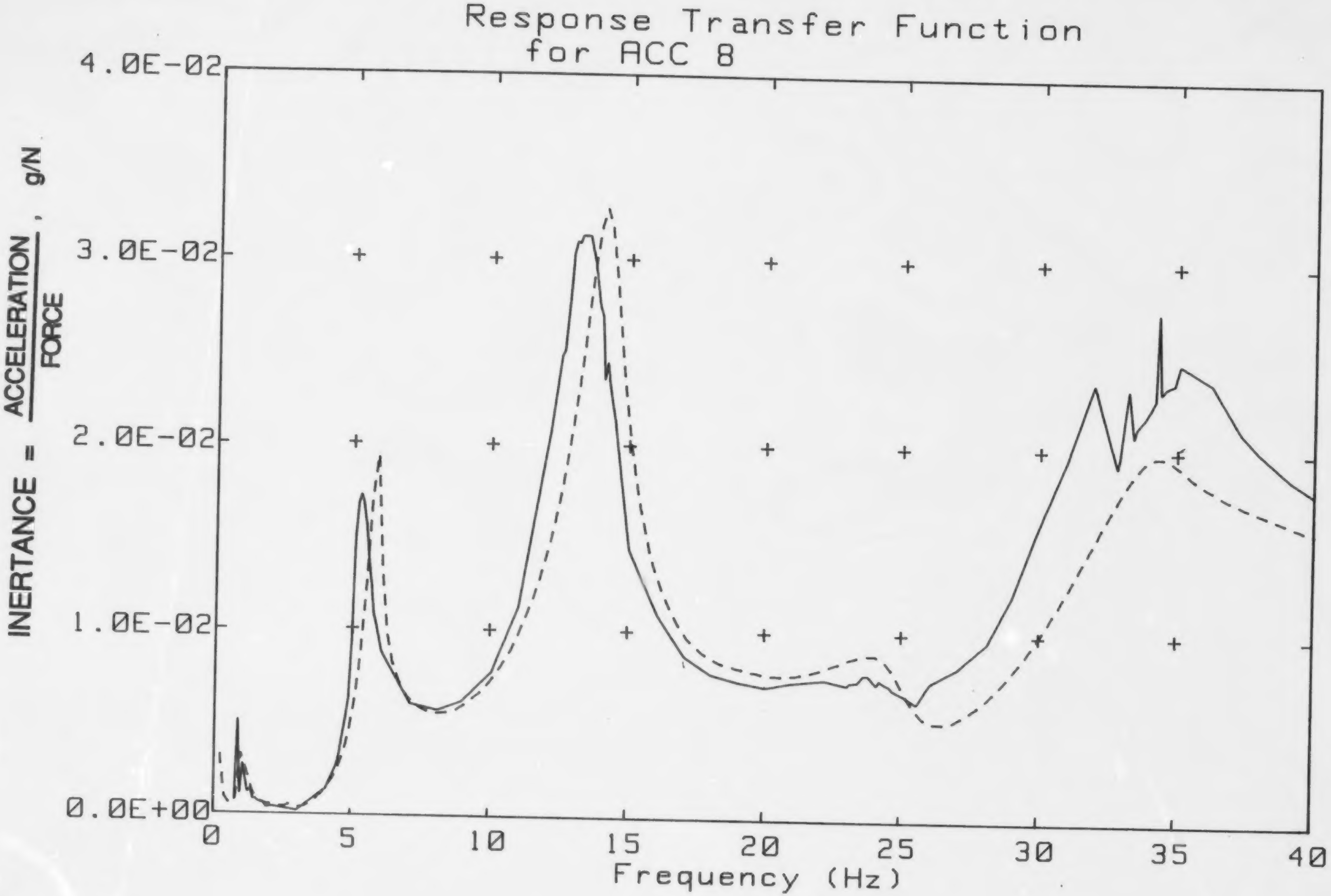
Response Transfer Function
for ACC 8
INERTANCE = ACCELERATION / FORCE , g/N
4.0E-02
3.0E-02
2.0E-02
1.0E-02
0.0E+00
0
5
10
15
20
25
30
35
40
Frequency (Hz)

Response Transfer Function
for ACC 9

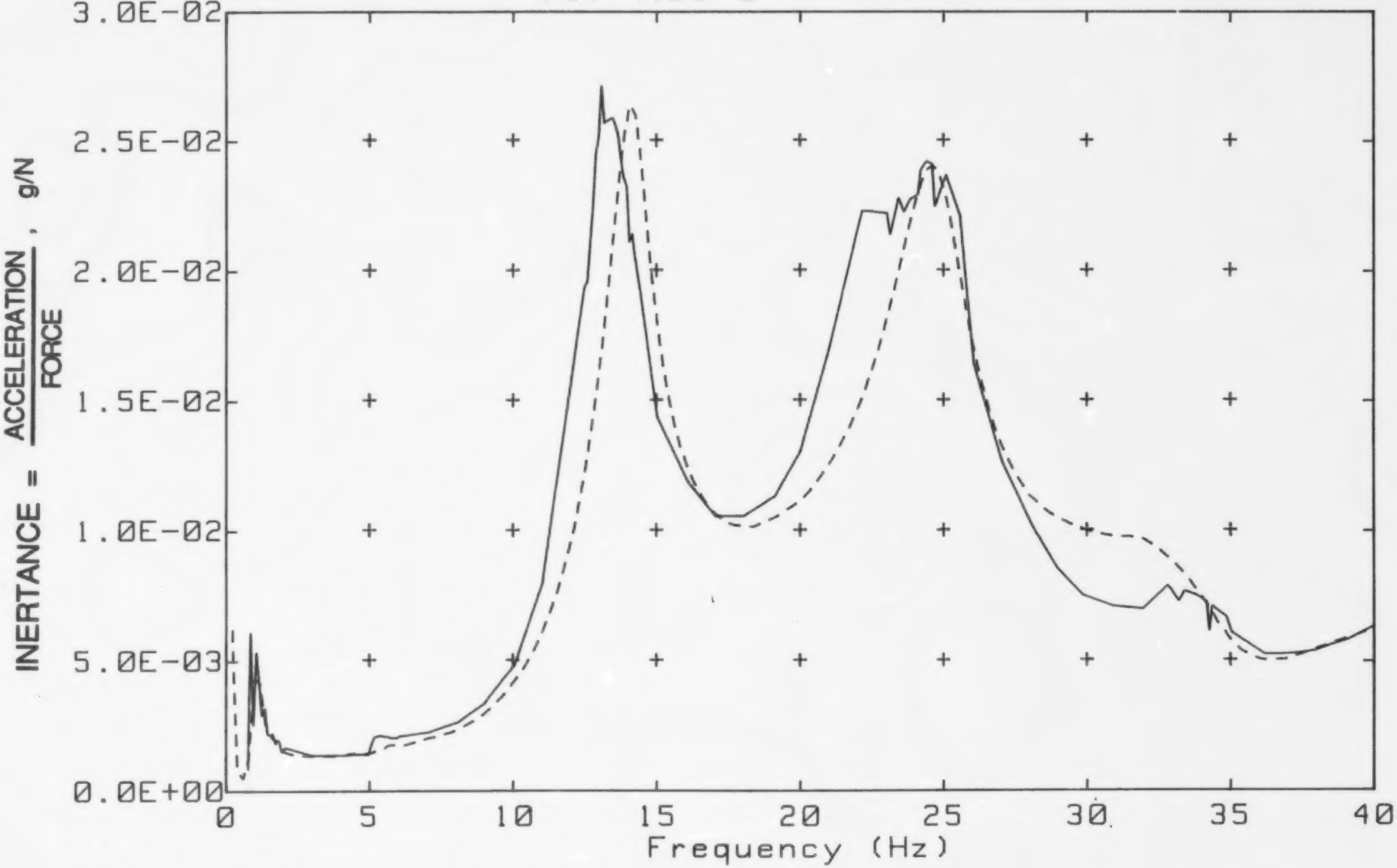

Response Transfer Function
for ACC 10

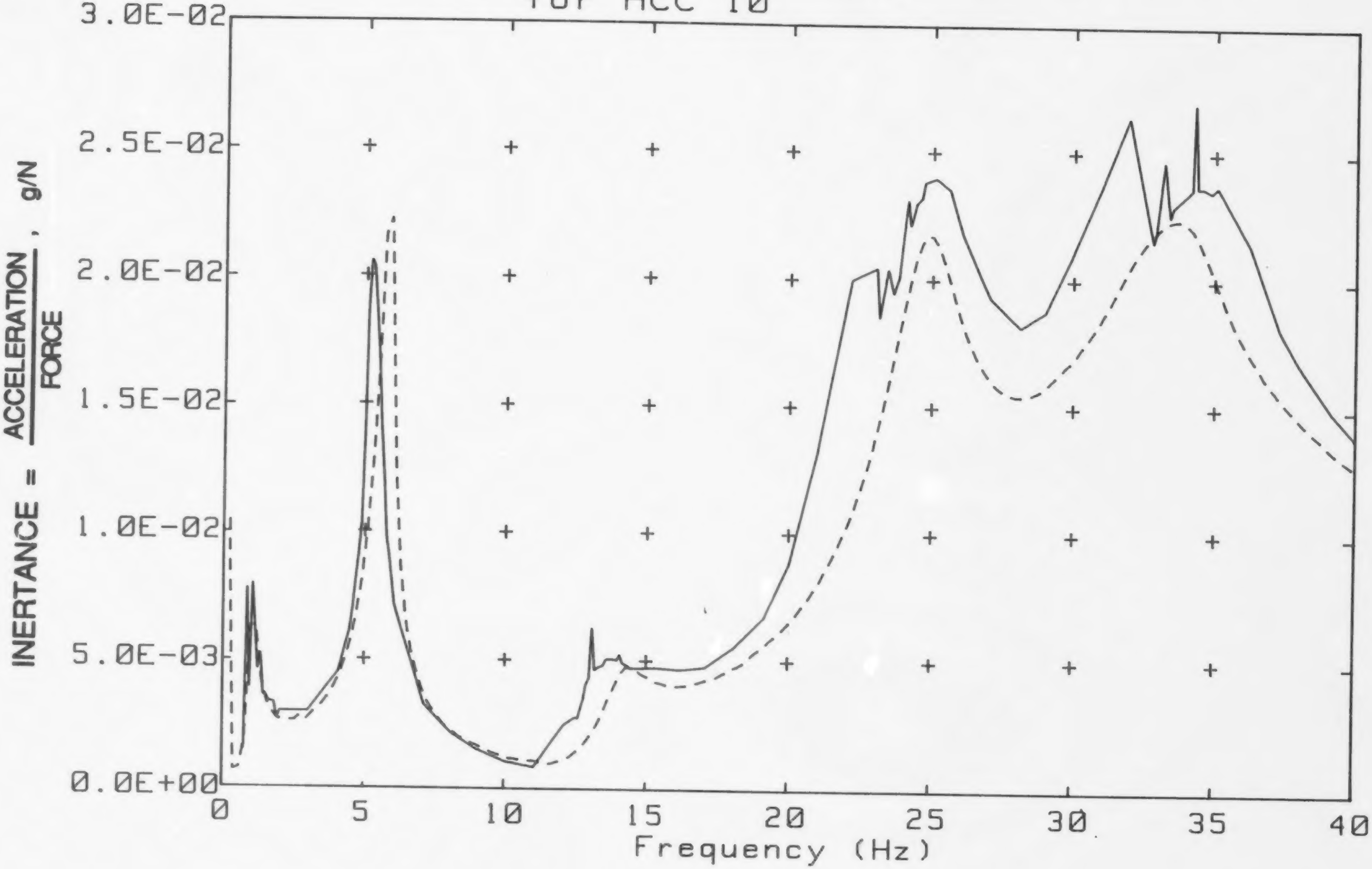

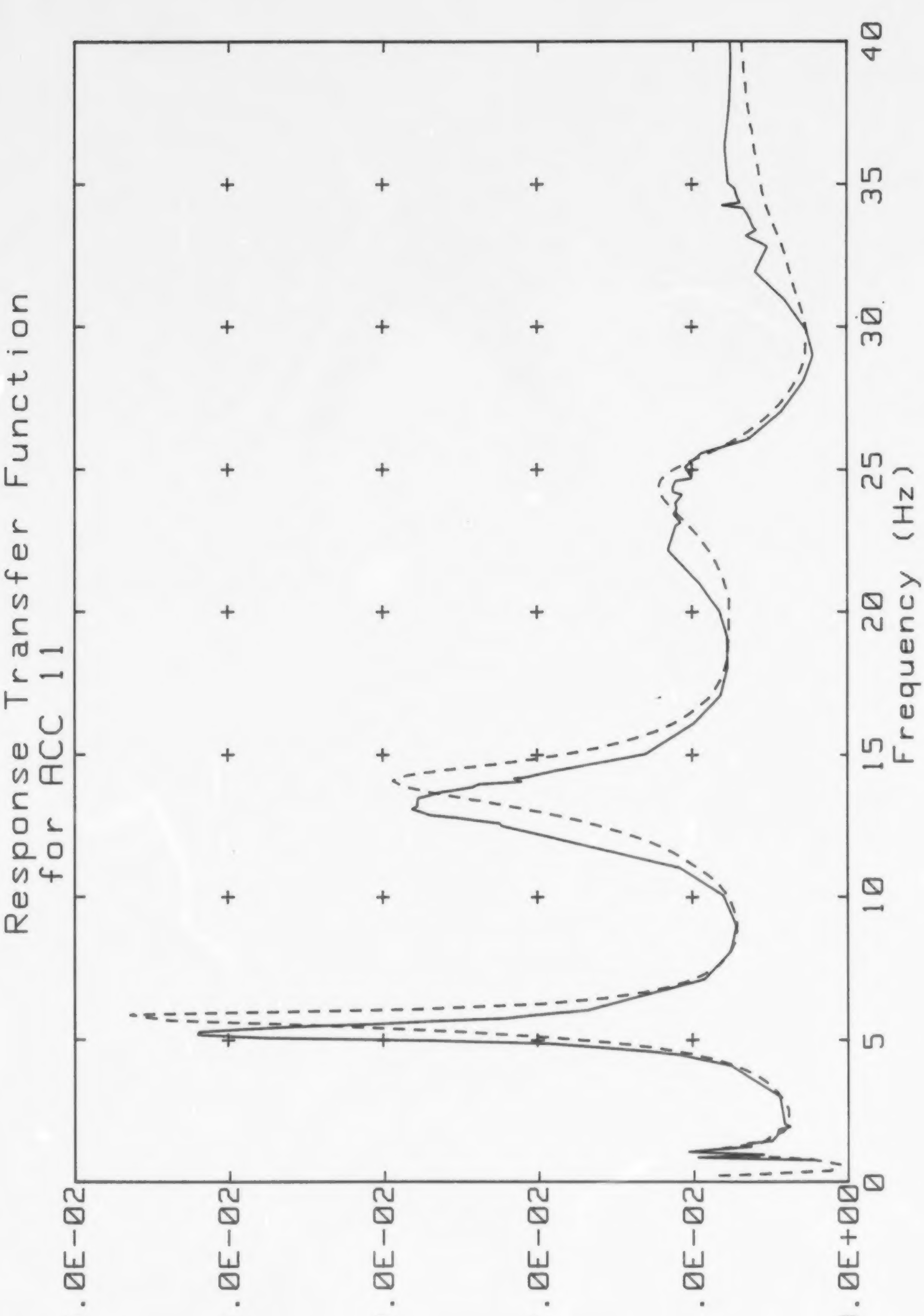

Response Transfer Function for ACC 11

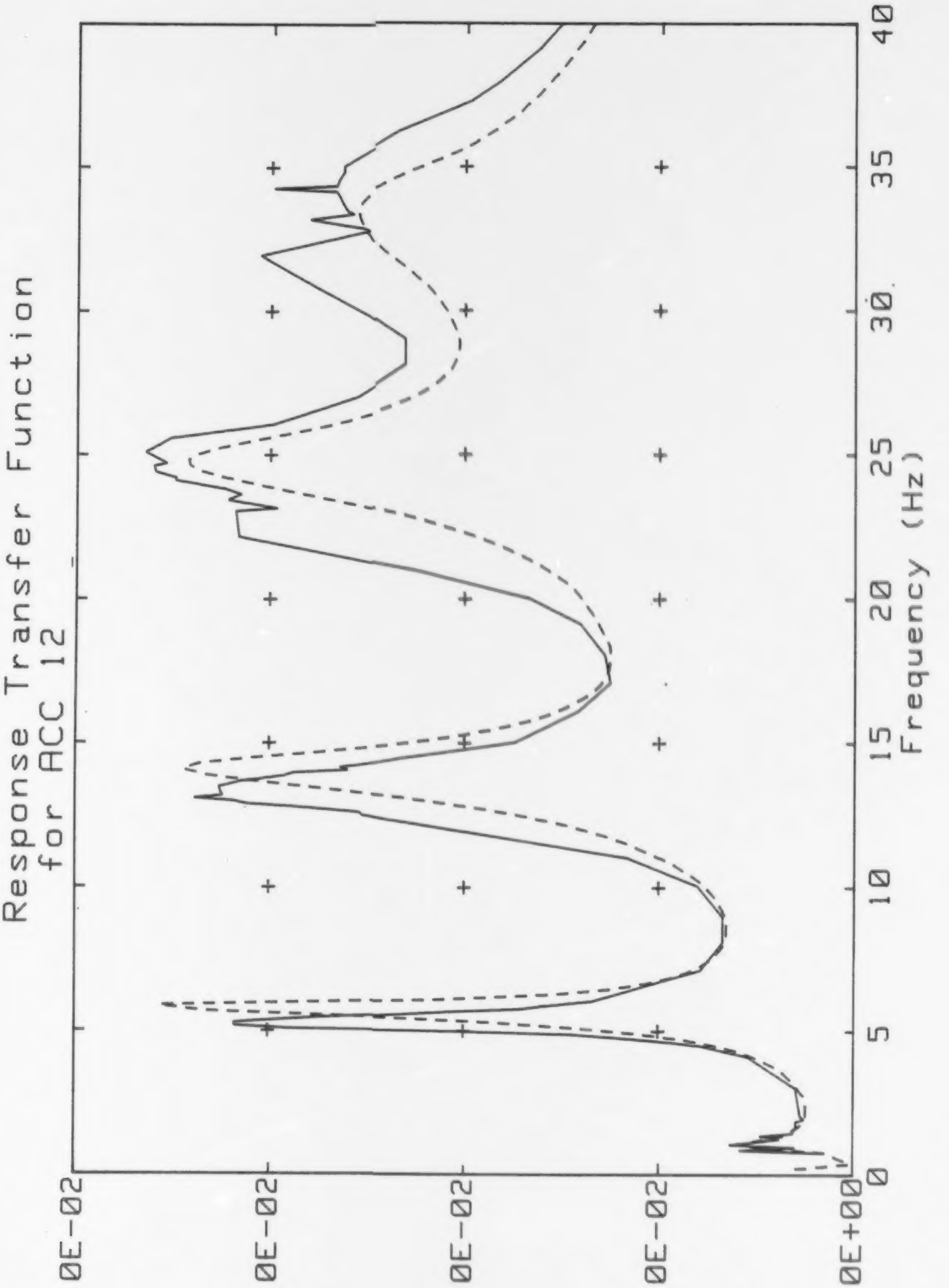
Response Transfer Function
for ACC 12
Frequency (Hz)
INERTANCE = ACCELERATION / FORCE , g/N
8.0E-02
6.0E-02
4.0E-02
2.0E-02
0.0E+00
0
5
10
15
20
25
30
35
40

MODE SHAPES FOR THE DEEP WATER HAMMER TESTS

MODE SHAPE: 2 FREQ: 5.55 Hz DAMPING: 4.80 %

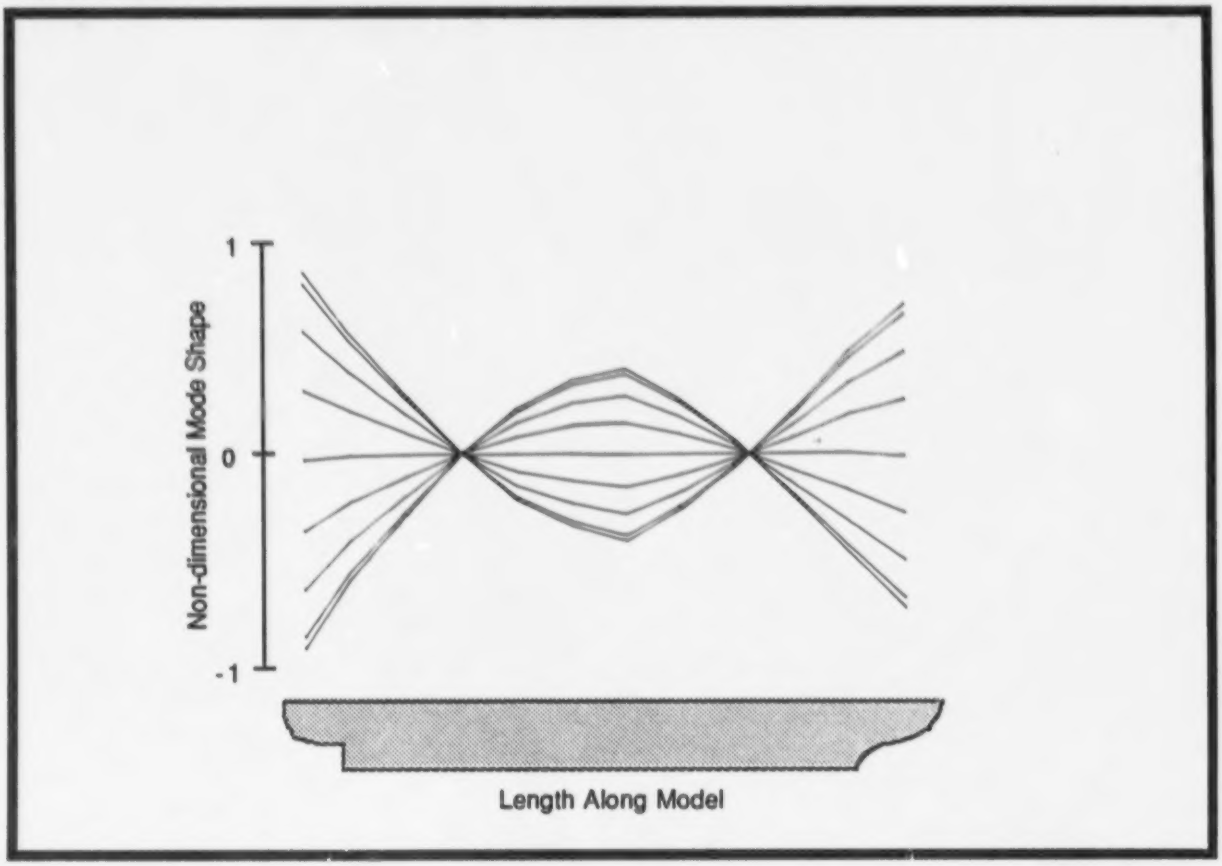

MODE SHAPE: 3 FREQ: 13.82 Hz DAMPING: 6.49 %

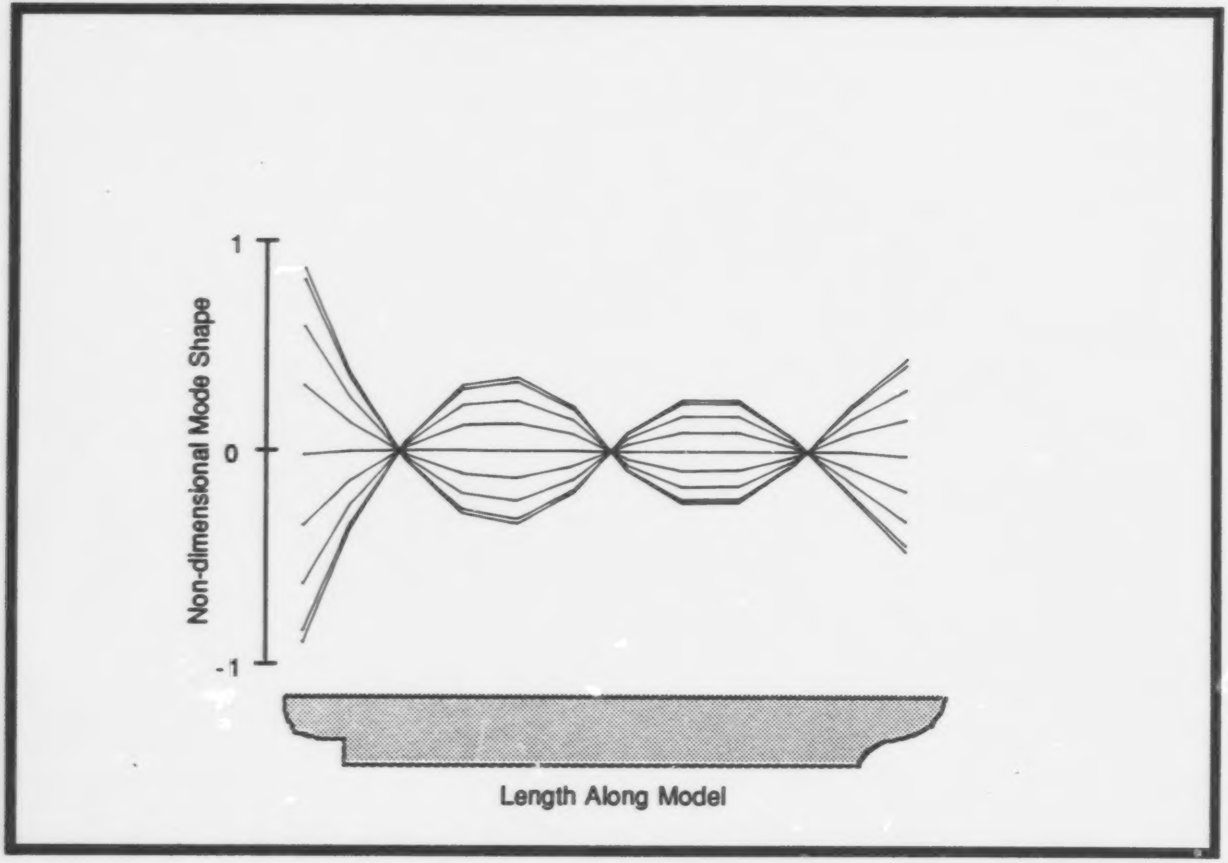

MODE SHAPE: 4 FREQ: 24.47 Hz DAMPING: 6.24 %

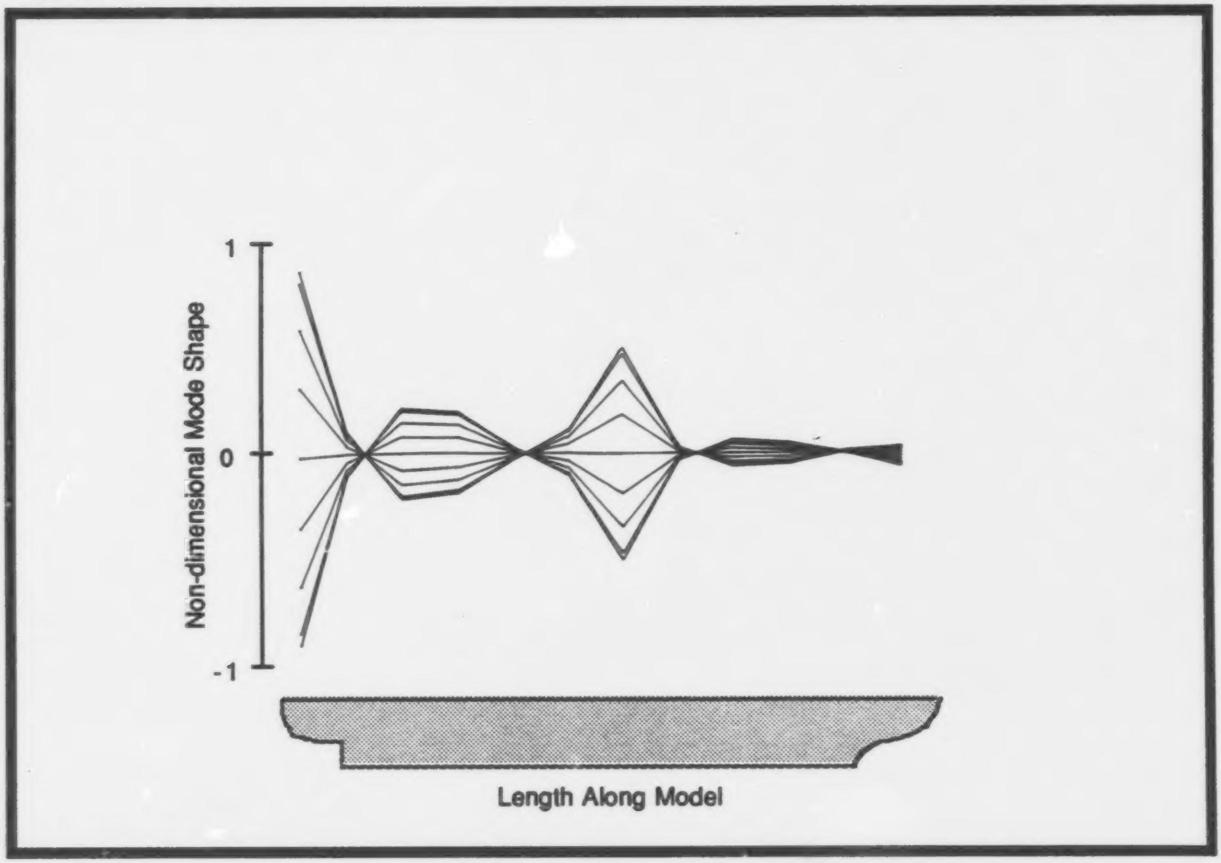

MODE SHAPE: 5 FREQ: 33.48 Hz DAMPING: 7.25 %

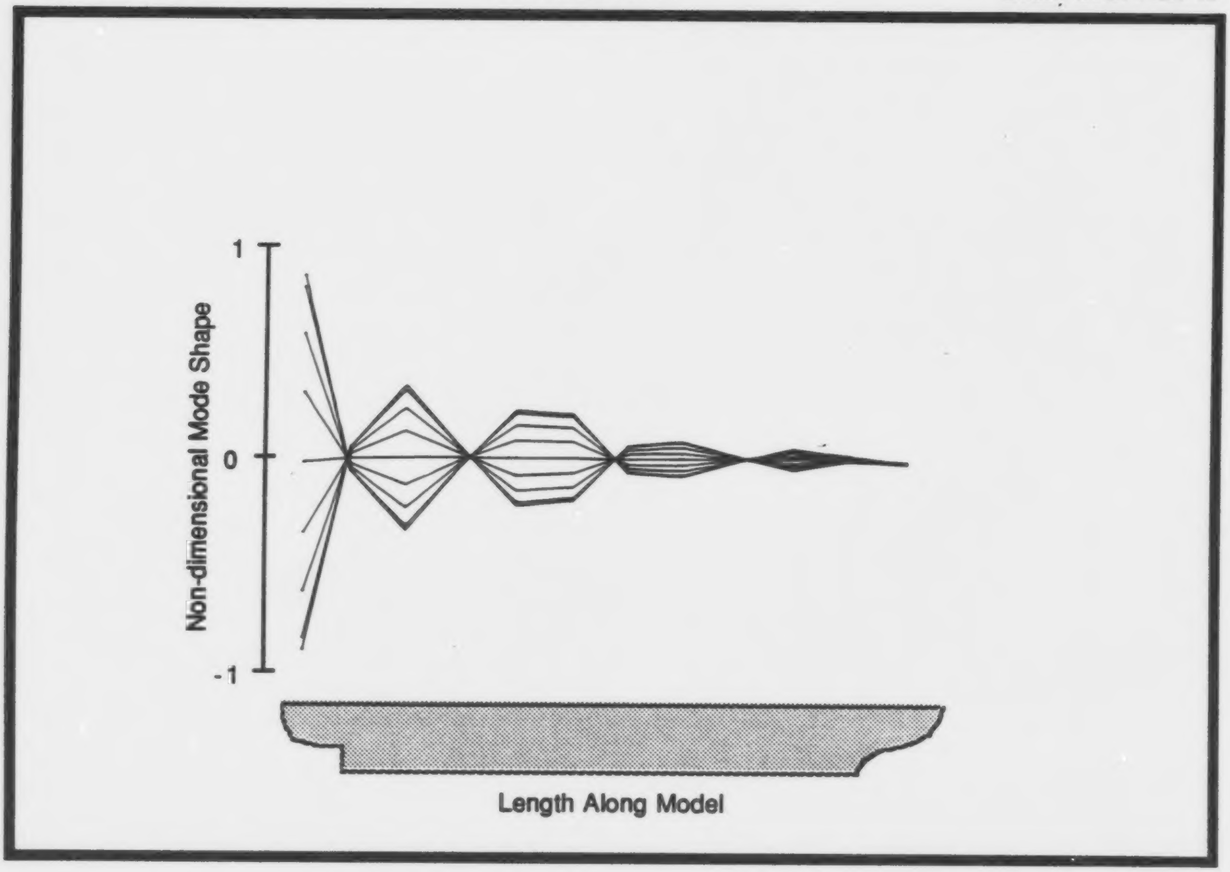

MODE SHAPES FOR THE SHALLOW WATER HAMMER TESTS

MODE SHAPE: 2 FREQ: 5.07 Hz DAMPING: 4.80 %

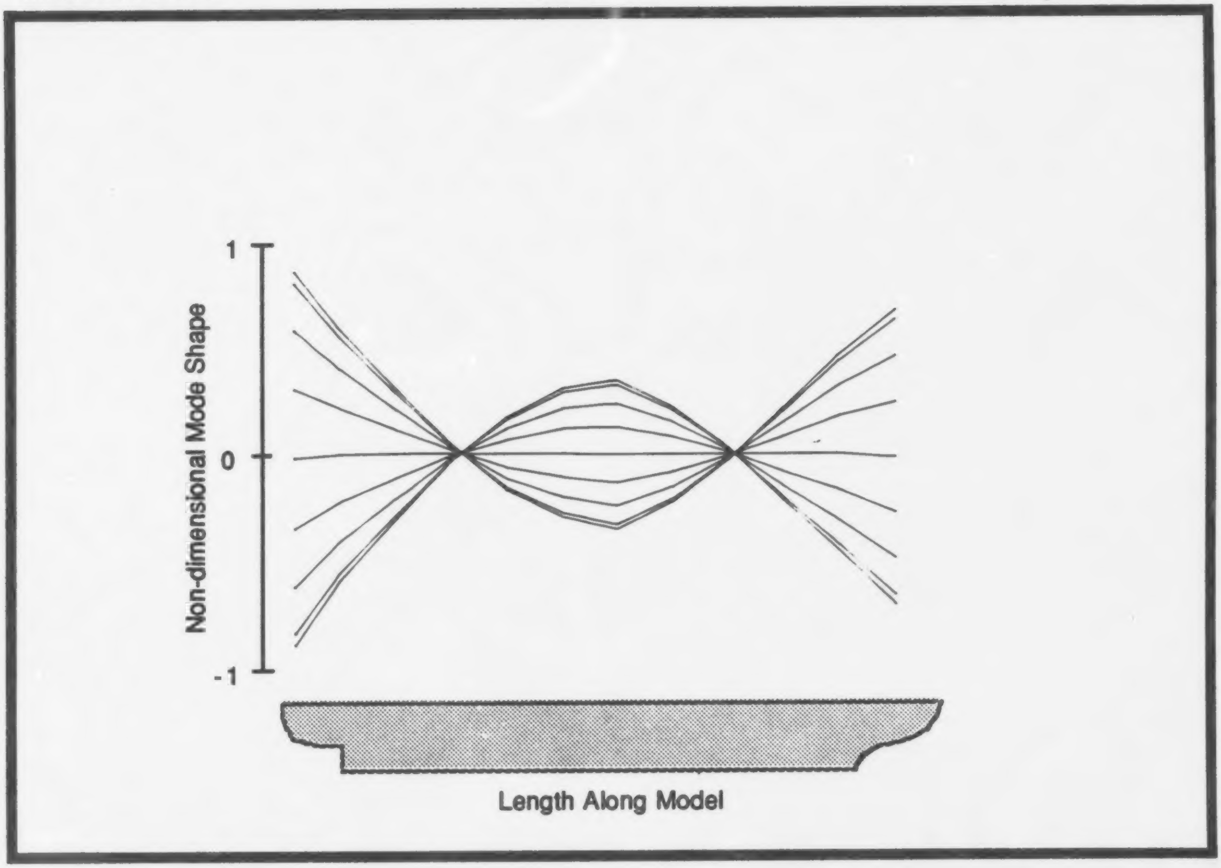

MODE SHAPE: 3 FREQ: 12.63 Hz DAMPING: 5.87 %

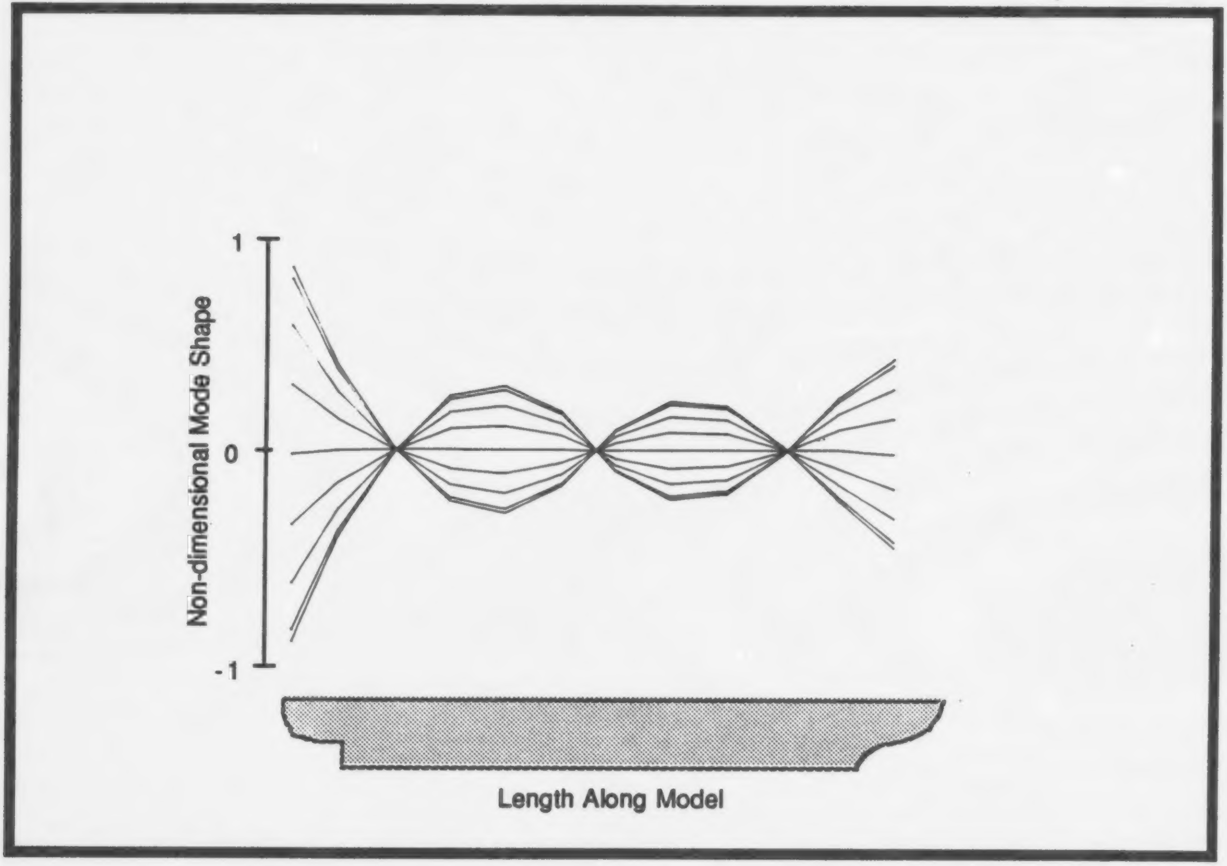

MODE SHAPE: 4 FREQ: 22.70 Hz DAMPING: 5.92 %

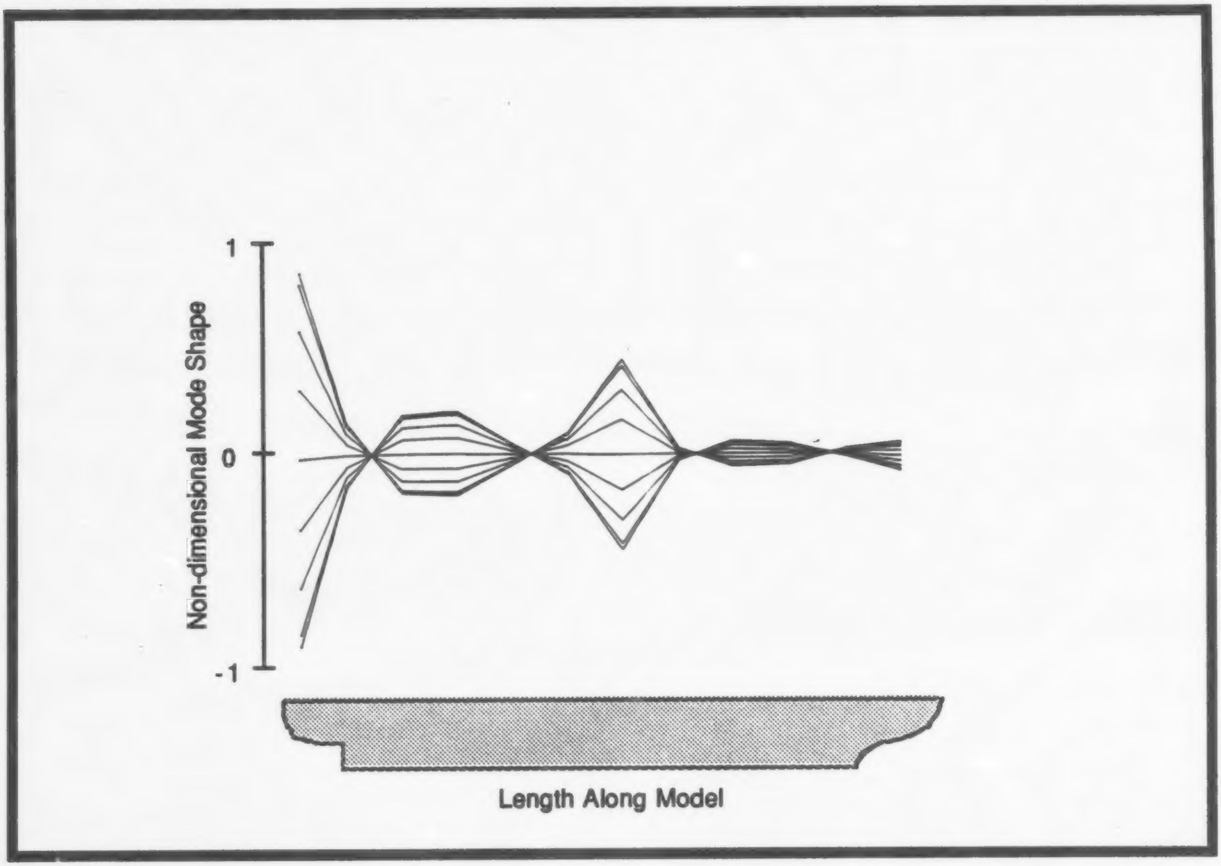

MODE SHAPE: 5 FREQ: 31.79 Hz DAMPING: 5.22 %

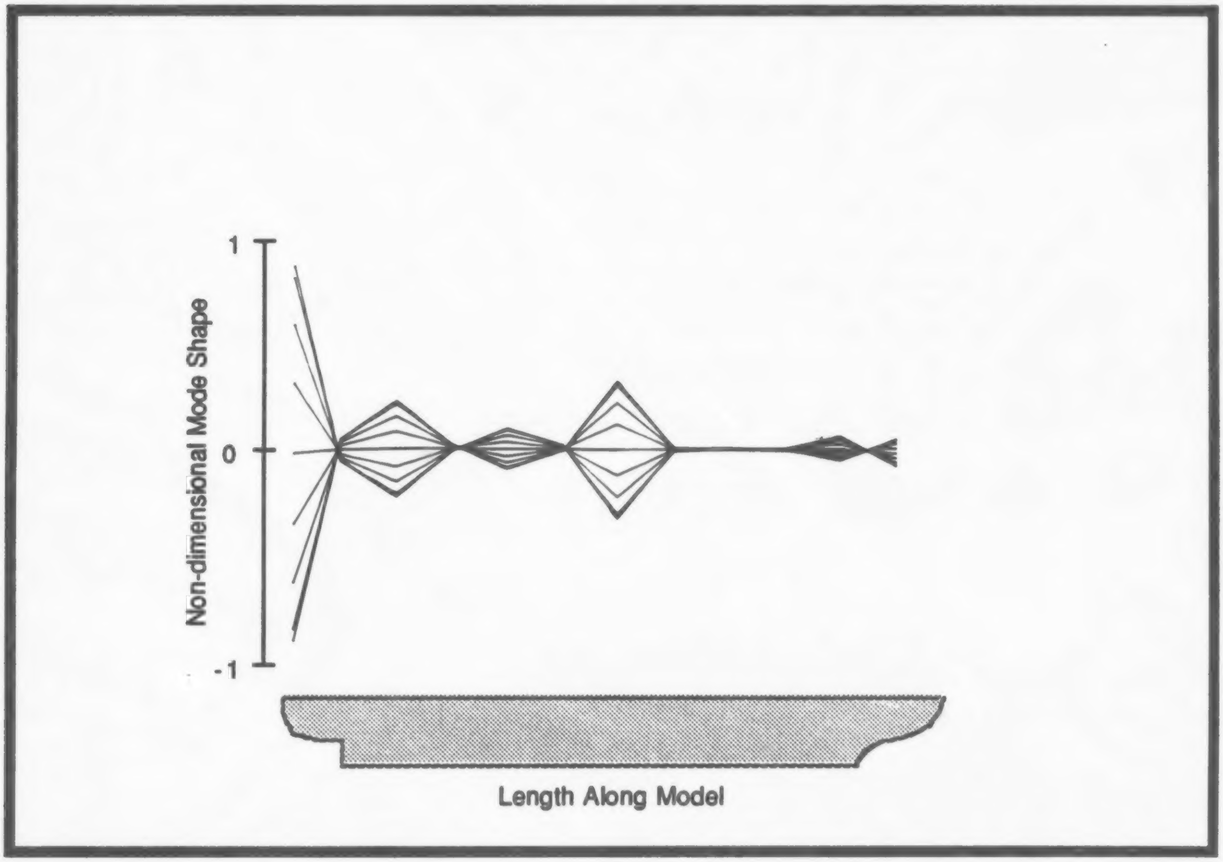

MODE SHAPES FOR THE DEEP WATER SHAKER TESTS

MODE SHAPE: 2 FREQ: 5.22 Hz DAMPING: 5.42 %

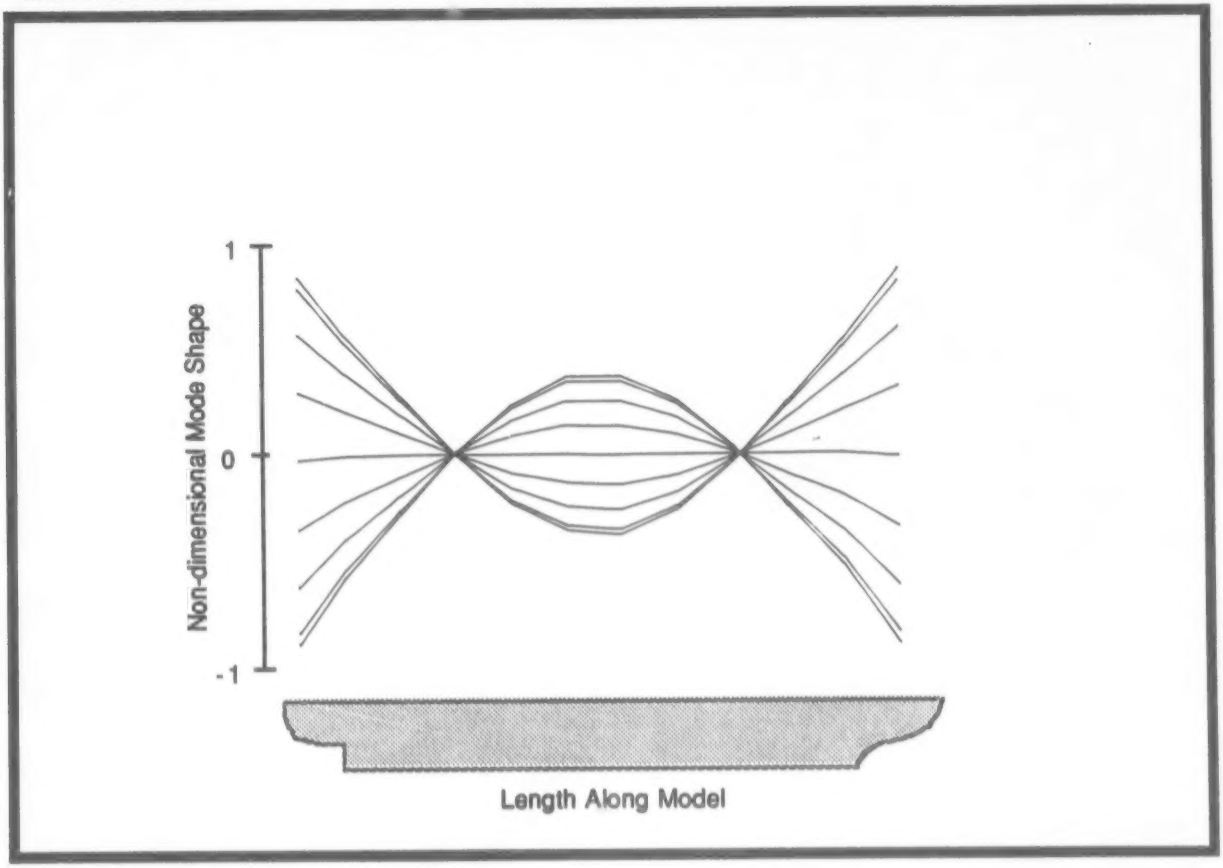

MODE SHAPE: 3 FREQ:13.24 Hz DAMPING: 6.99 %

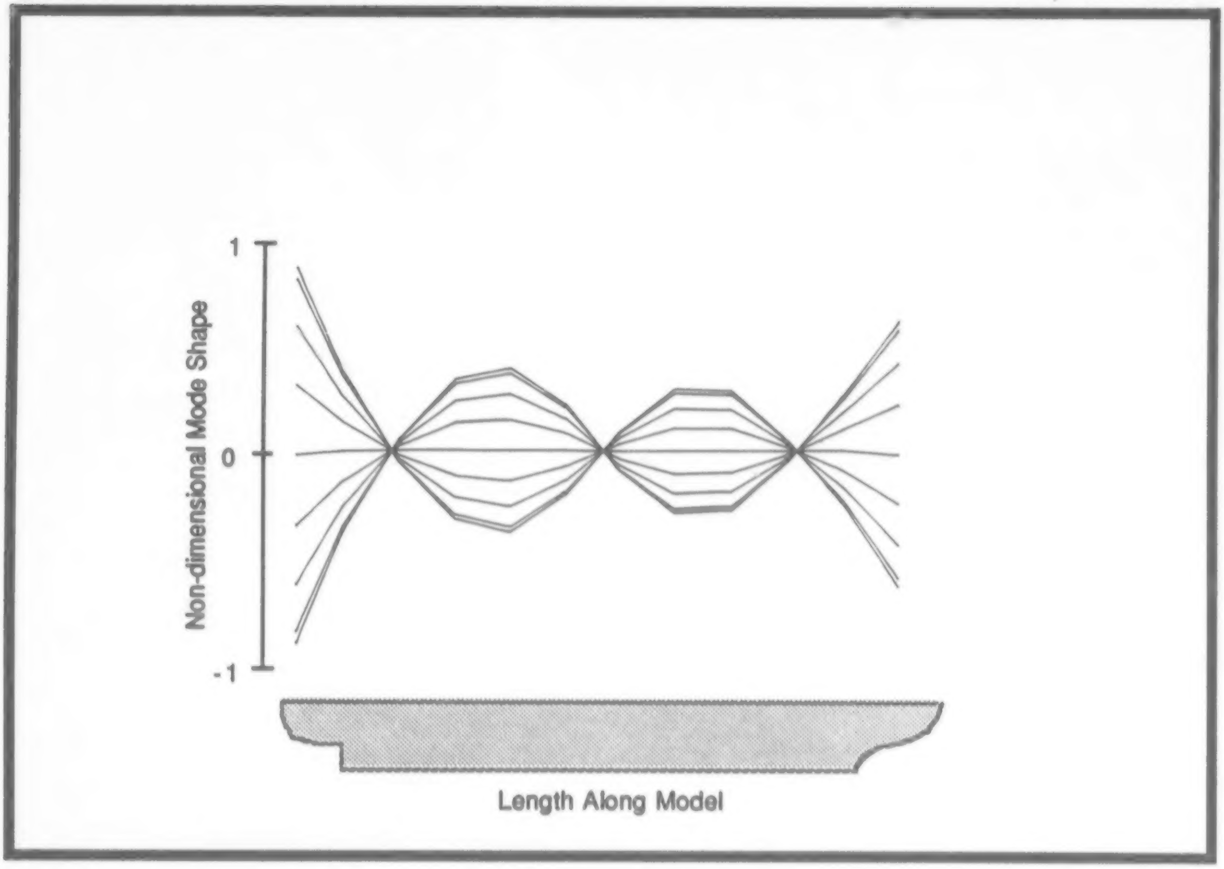

MODE SHAPE: 4 FREQ: 24.88 Hz DAMPING: 7.52 %

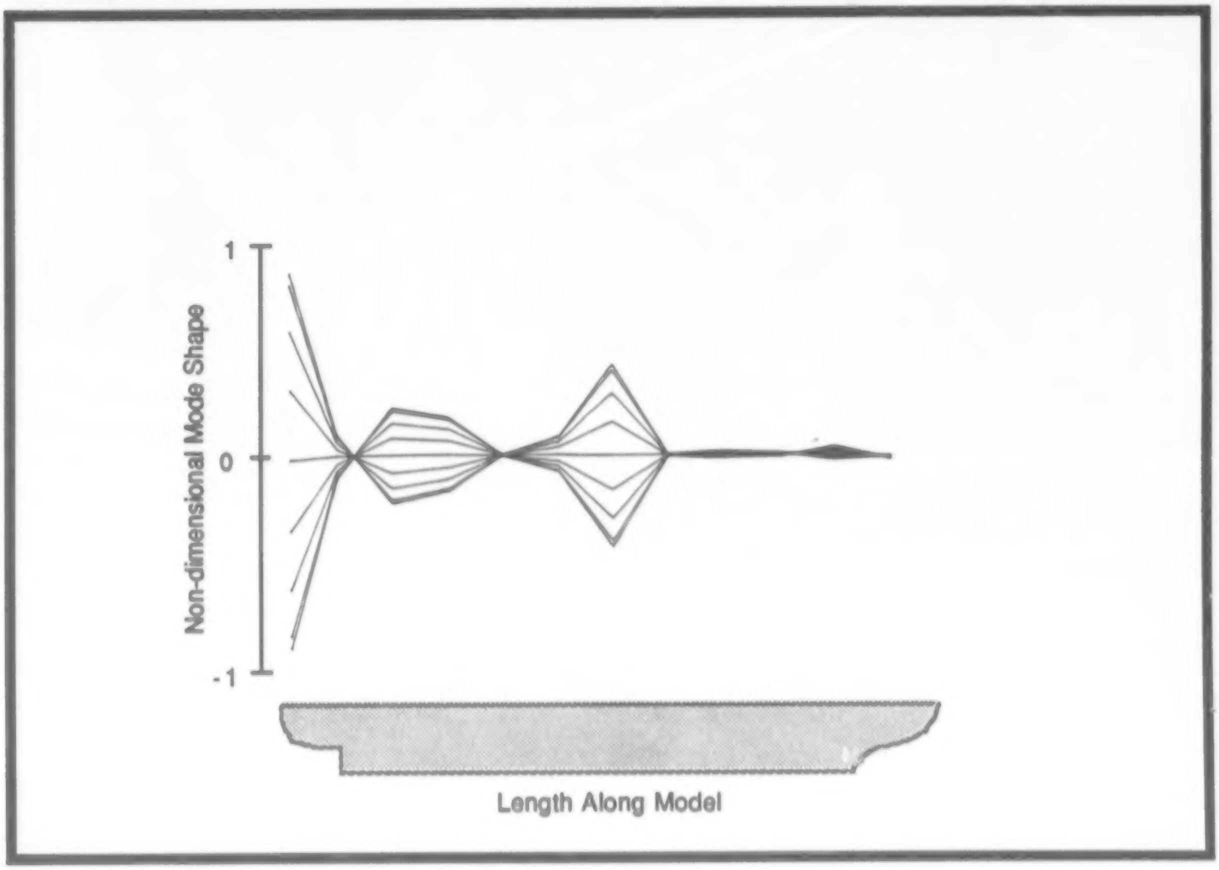

MODE SHAPE: 5 FREQ: 35.23 Hz DAMPING: 7.75 %

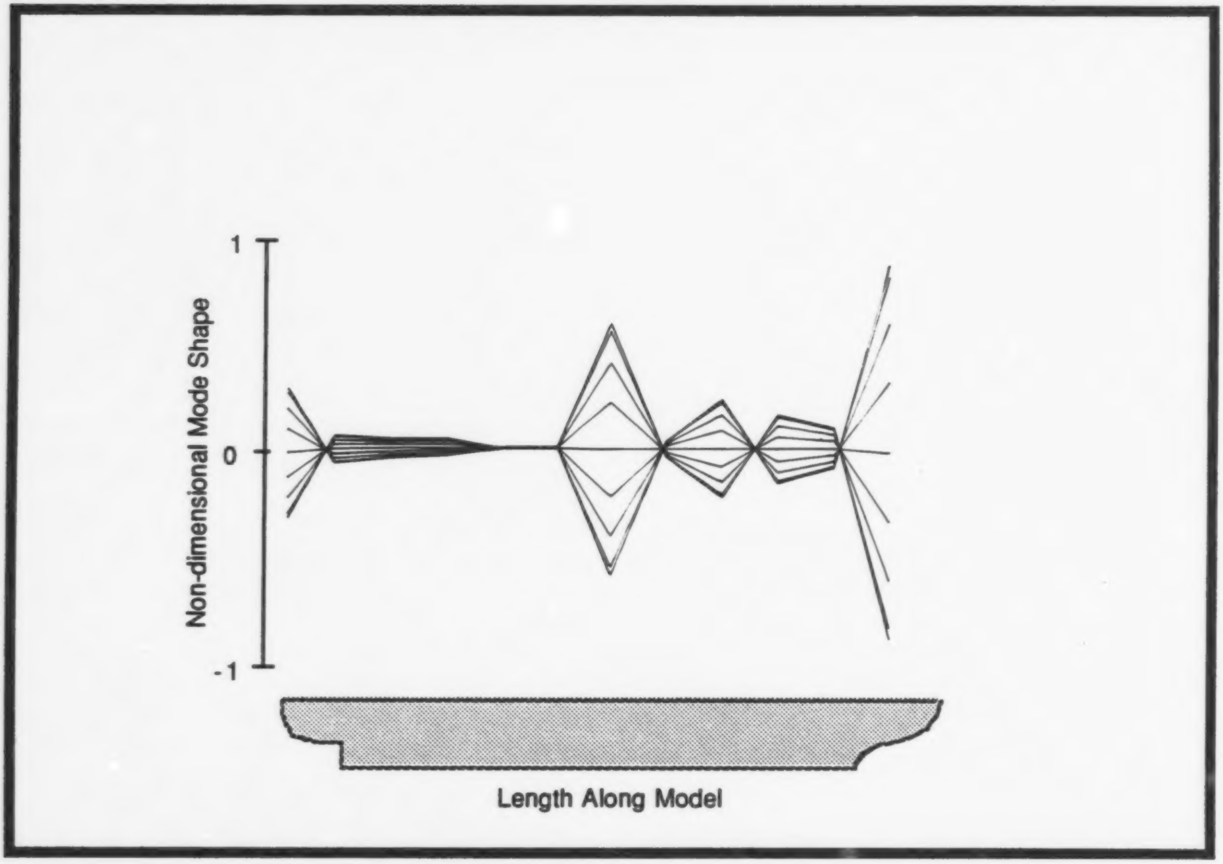

MODE SHAPES FOR THE TOWED SHAKER TESTS

MODE SHAPE: 3 FREQ: 14.31 Hz DAMPING: 5.73 %

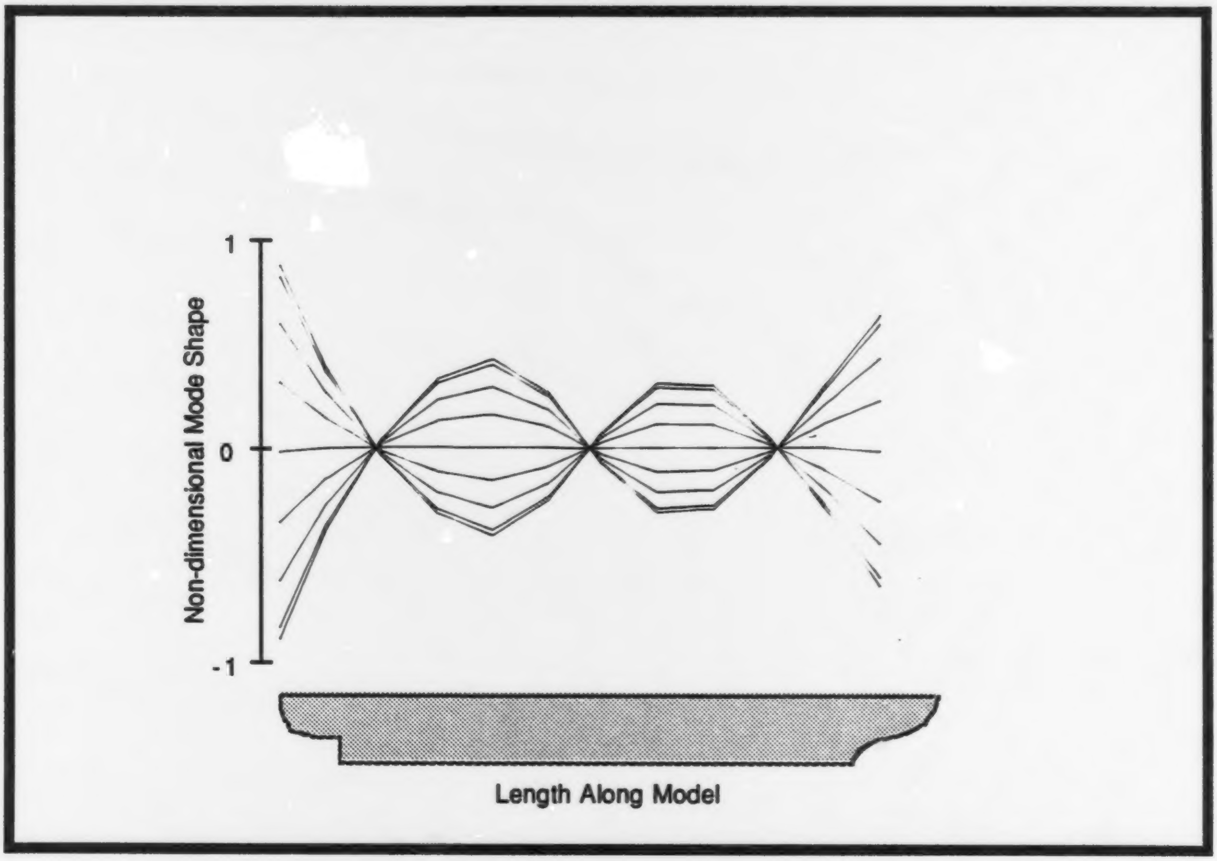

MODE SHAPE: 2 **FREQ: 5.37 Hz** **DAMPING: 6.66 %**

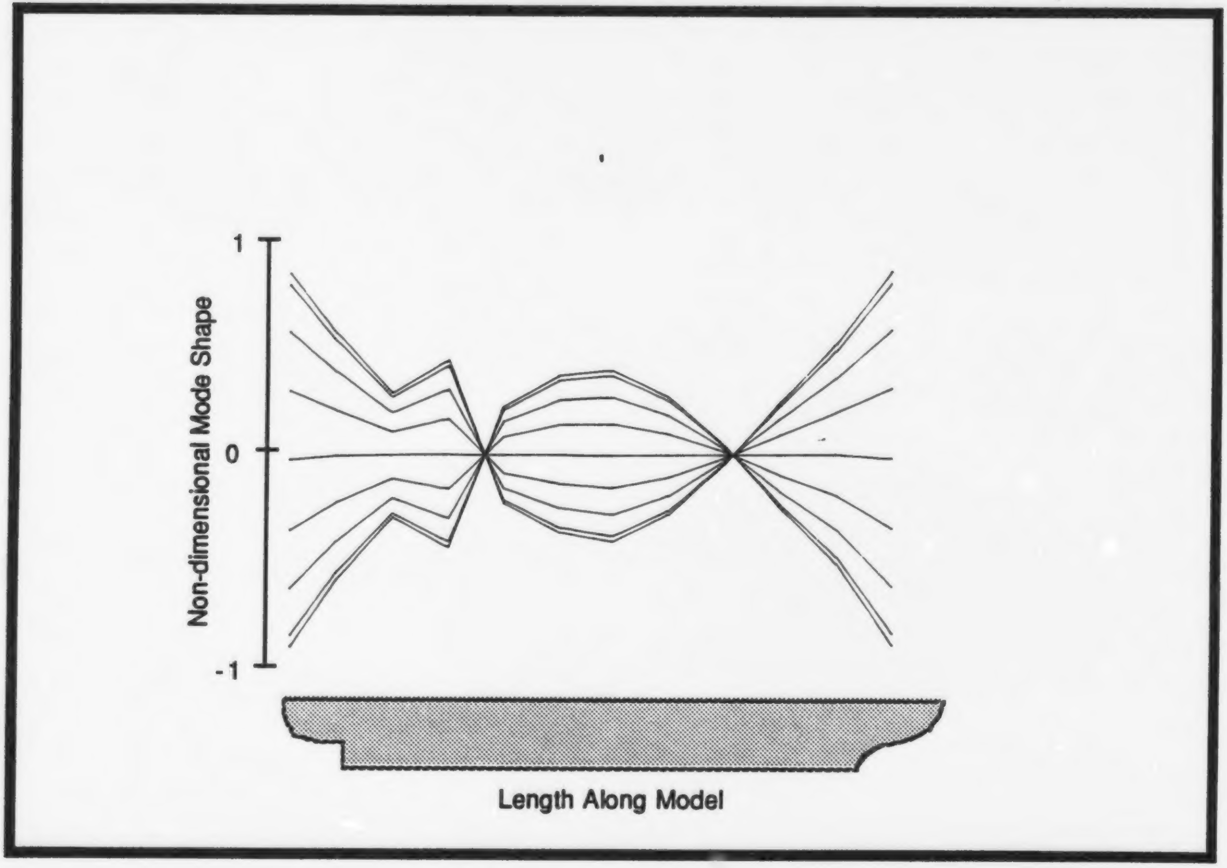

MODE SHAPE: 3 FREQ: 13.55 Hz DAMPING: 9.33 %

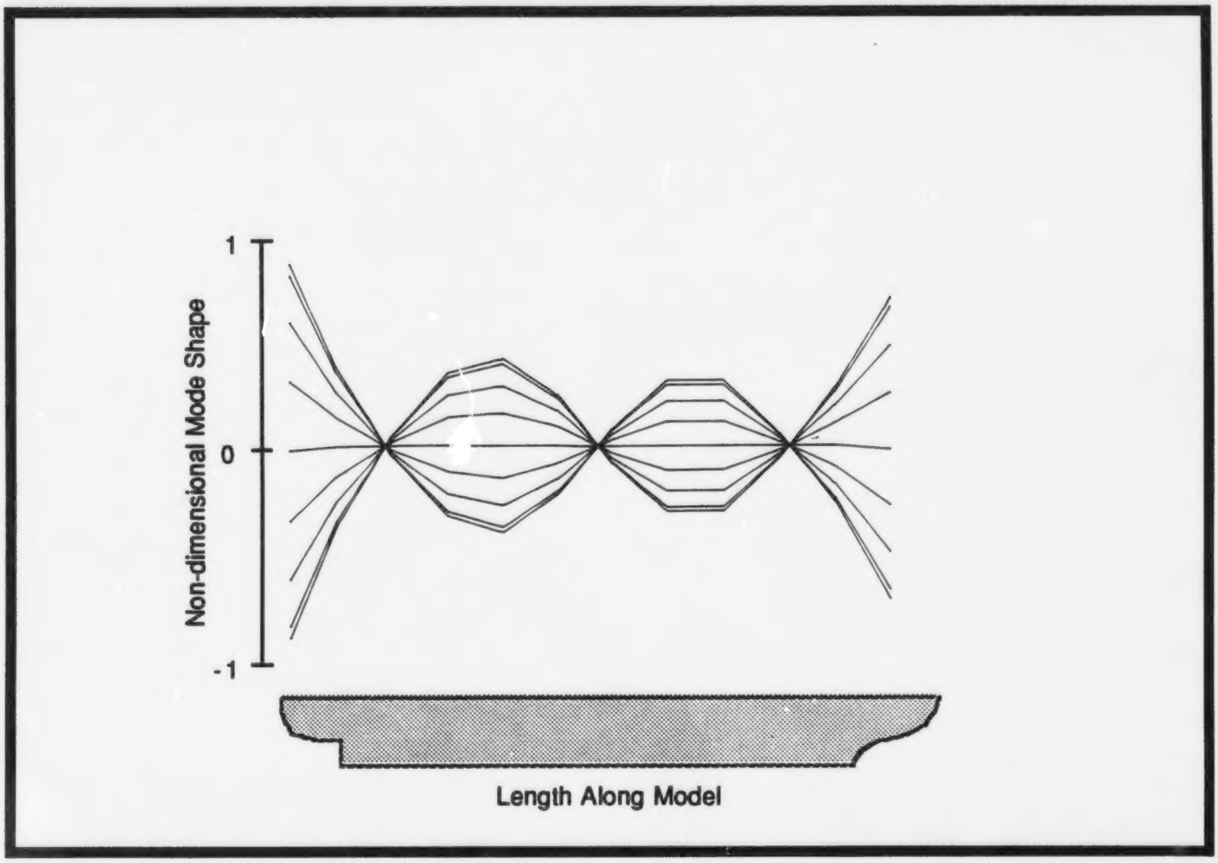

MODE SHAPE: 2 FREQ: 5.31 Hz DAMPING: 5.97 %

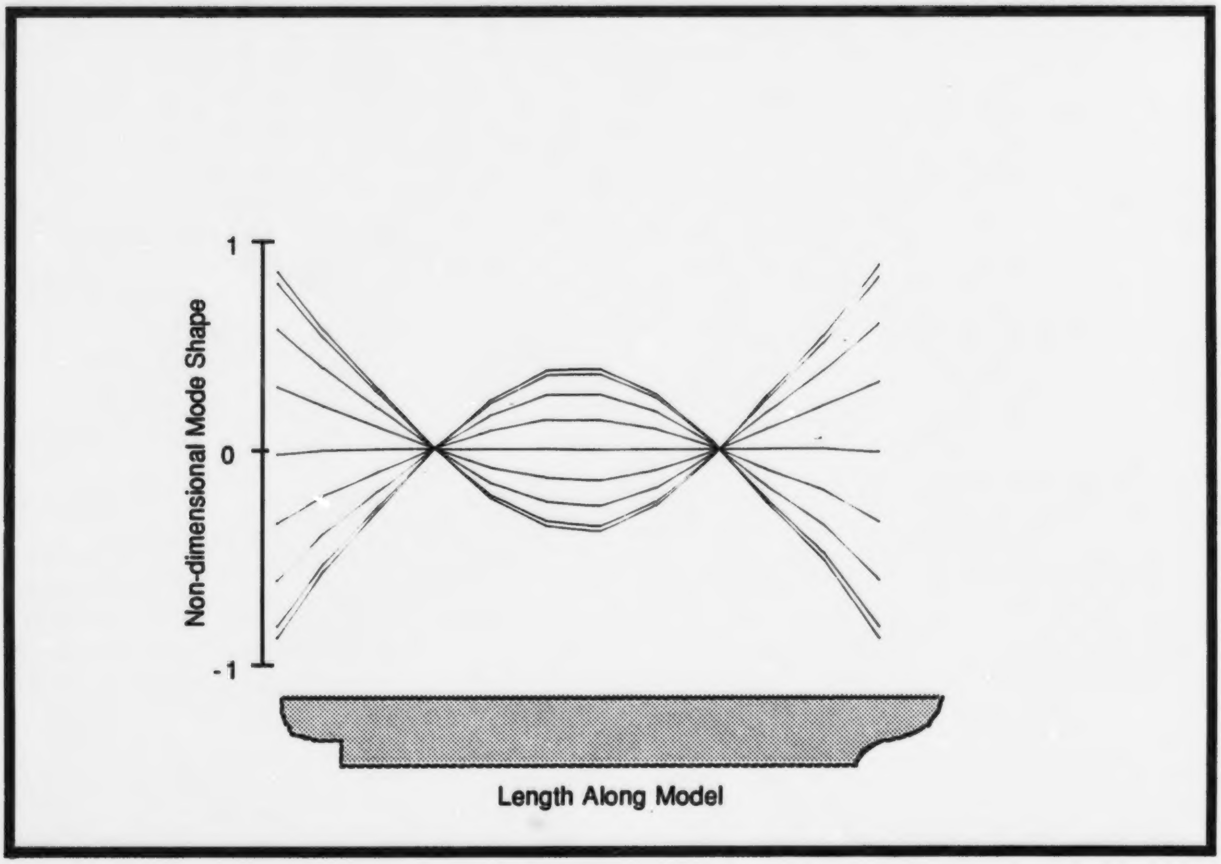

MODE SHAPE: 3 FREQ: 14.15 Hz DAMPING: 6.35 %

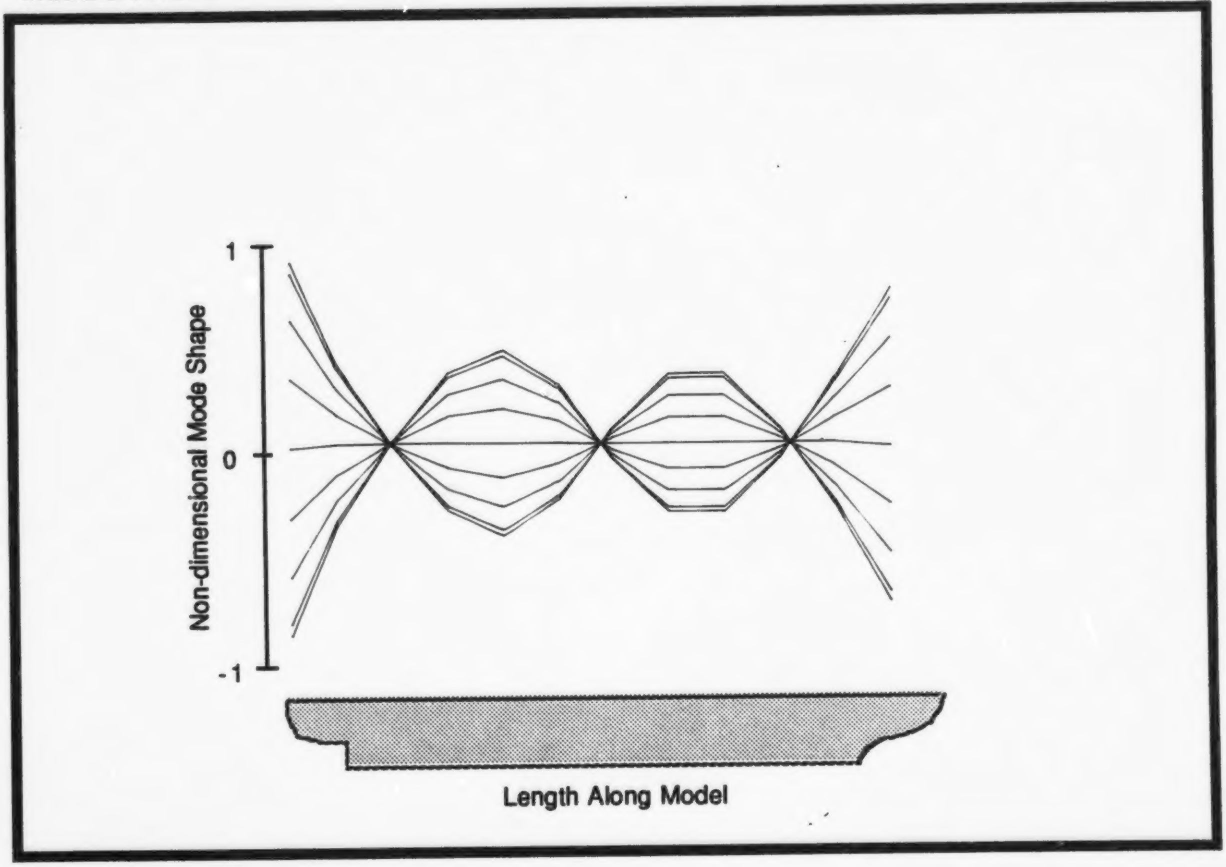

MODE SHAPES IN ICE

MODE SHAPE: 1 FREQ: 1.02 Hz DAMPING: 11.98 %

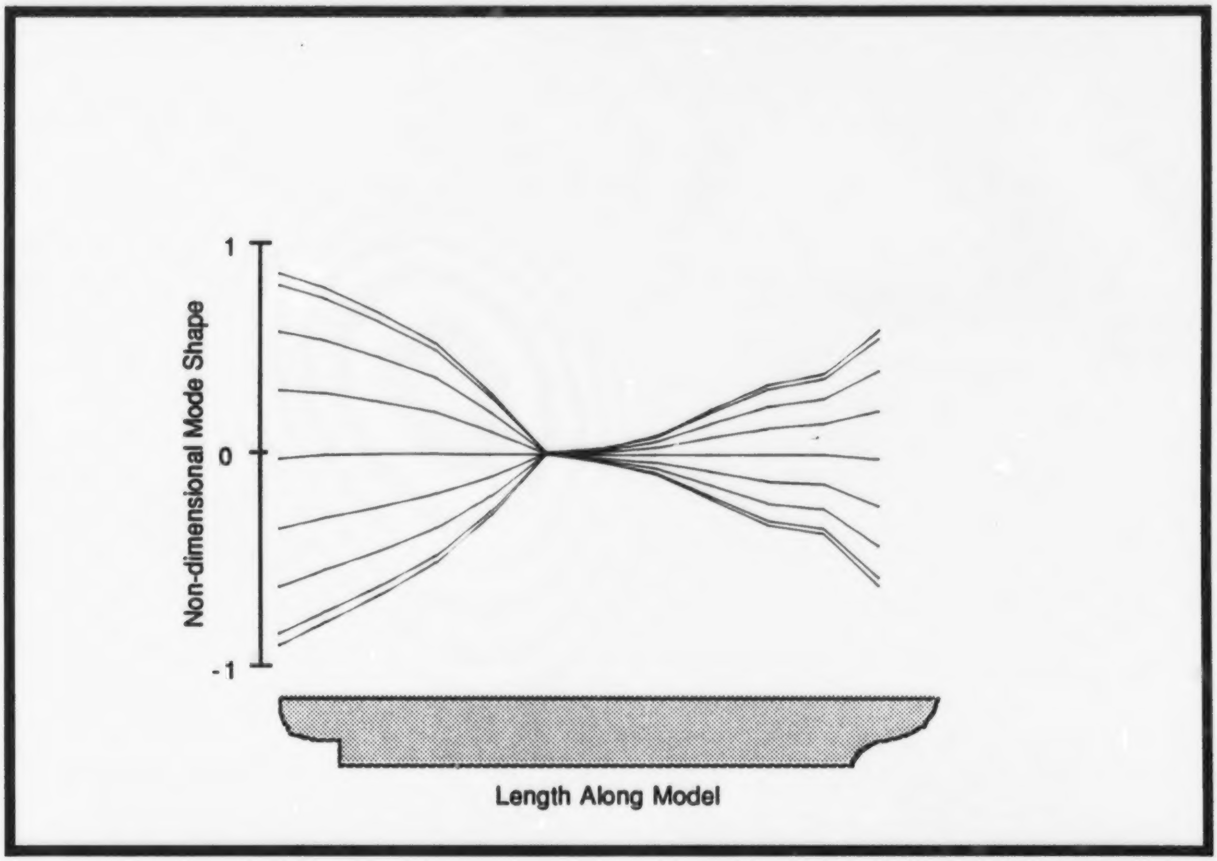

MODE SHAPE: 2 FREQ: 5.36 Hz DAMPING: 5.39 %

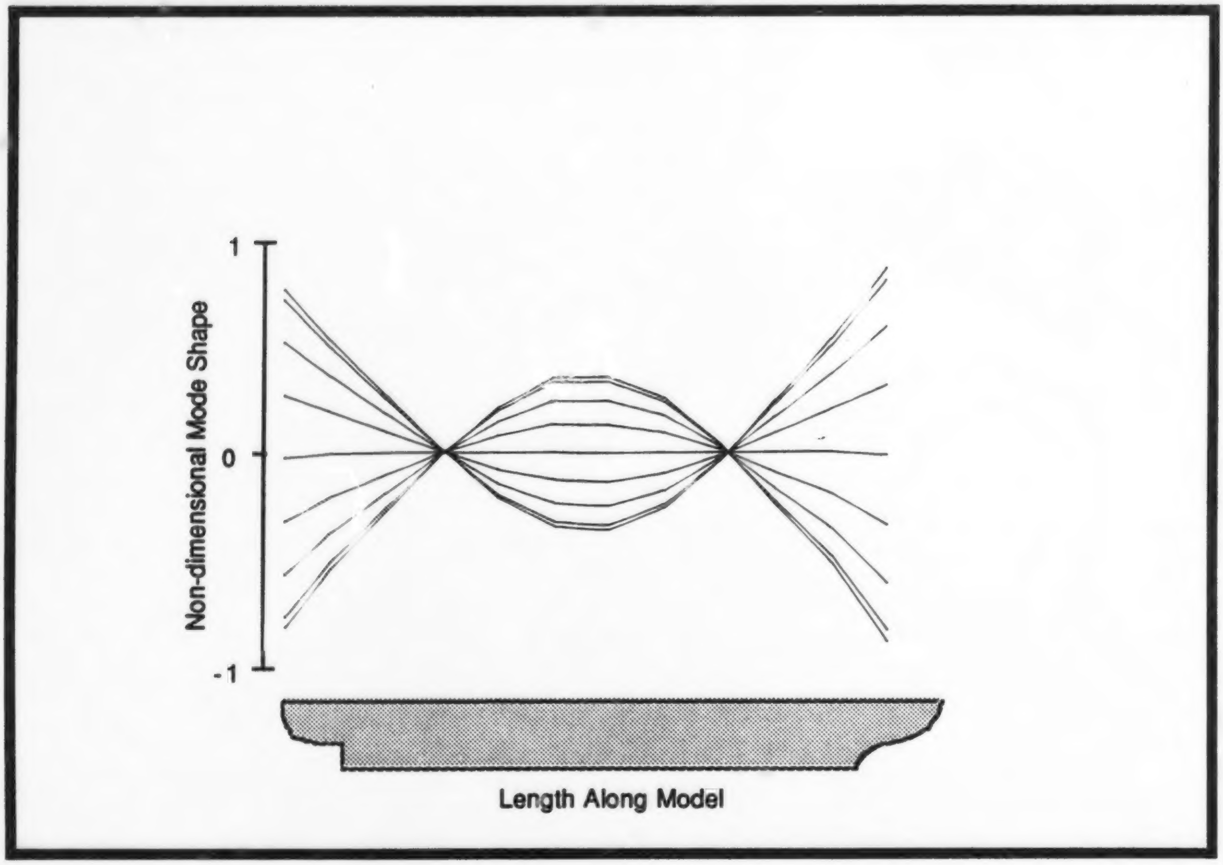

MODE SHAPE: 4 FREQ: 26.08 Hz DAMPING: 6.15 %

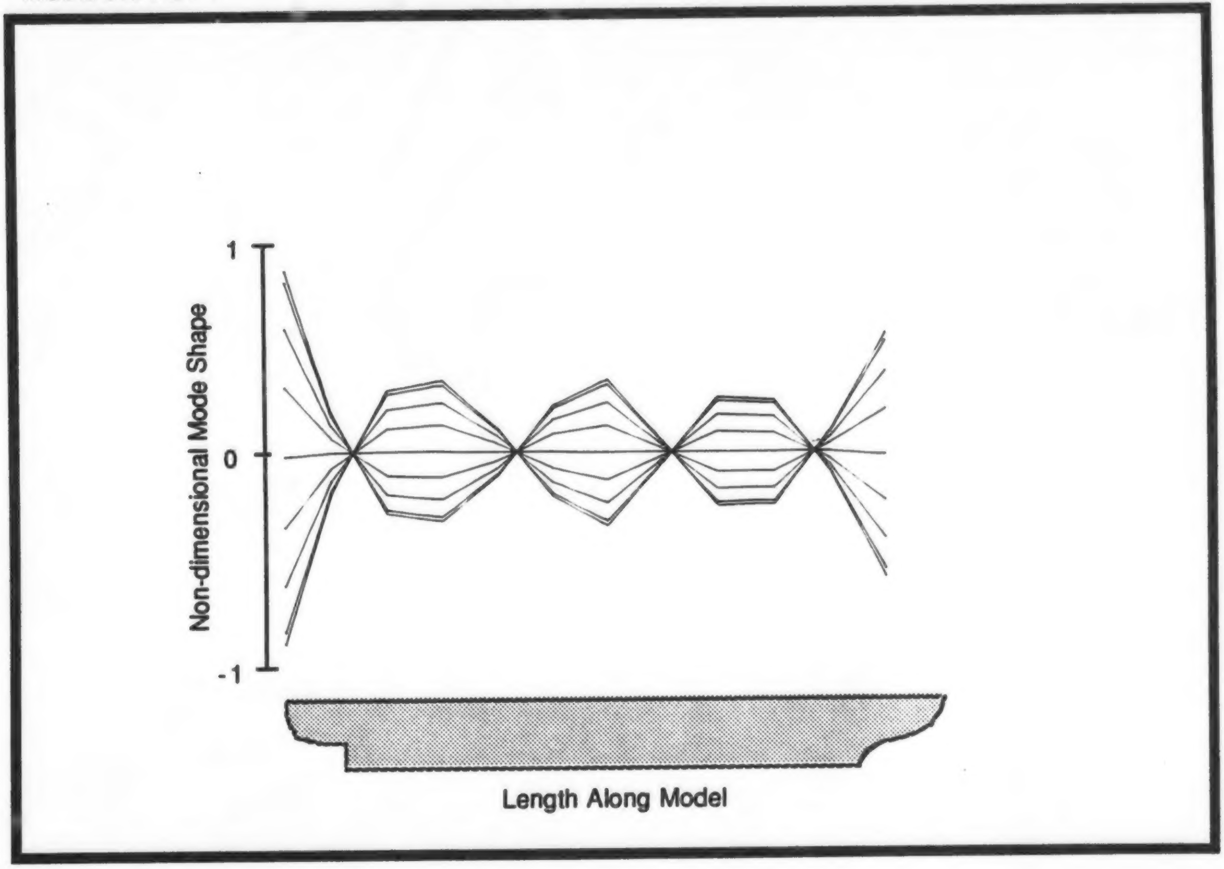

RESPONSE TRANSFER FUNCTION FOR STRUCTURAL FRAME TESTS

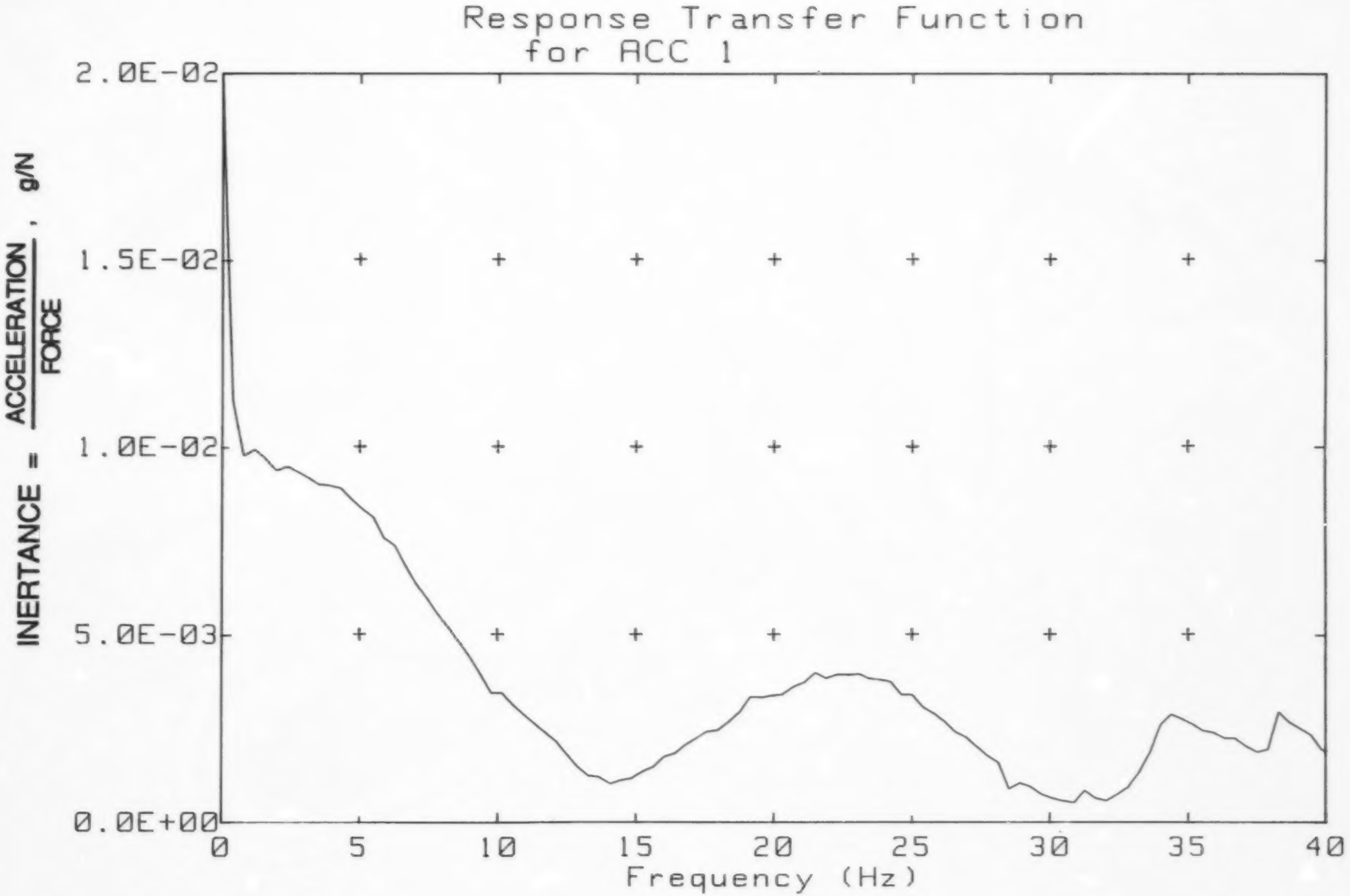
Response Transfer Function
for ACC 1
INERTANCE = ACCELERATION / FORCE , g/N
2.0E-02
1.5E-02
1.0E-02
5.0E-03
0.0E+00
0
5
10
15
20
25
30
35
40
Frequency (Hz)

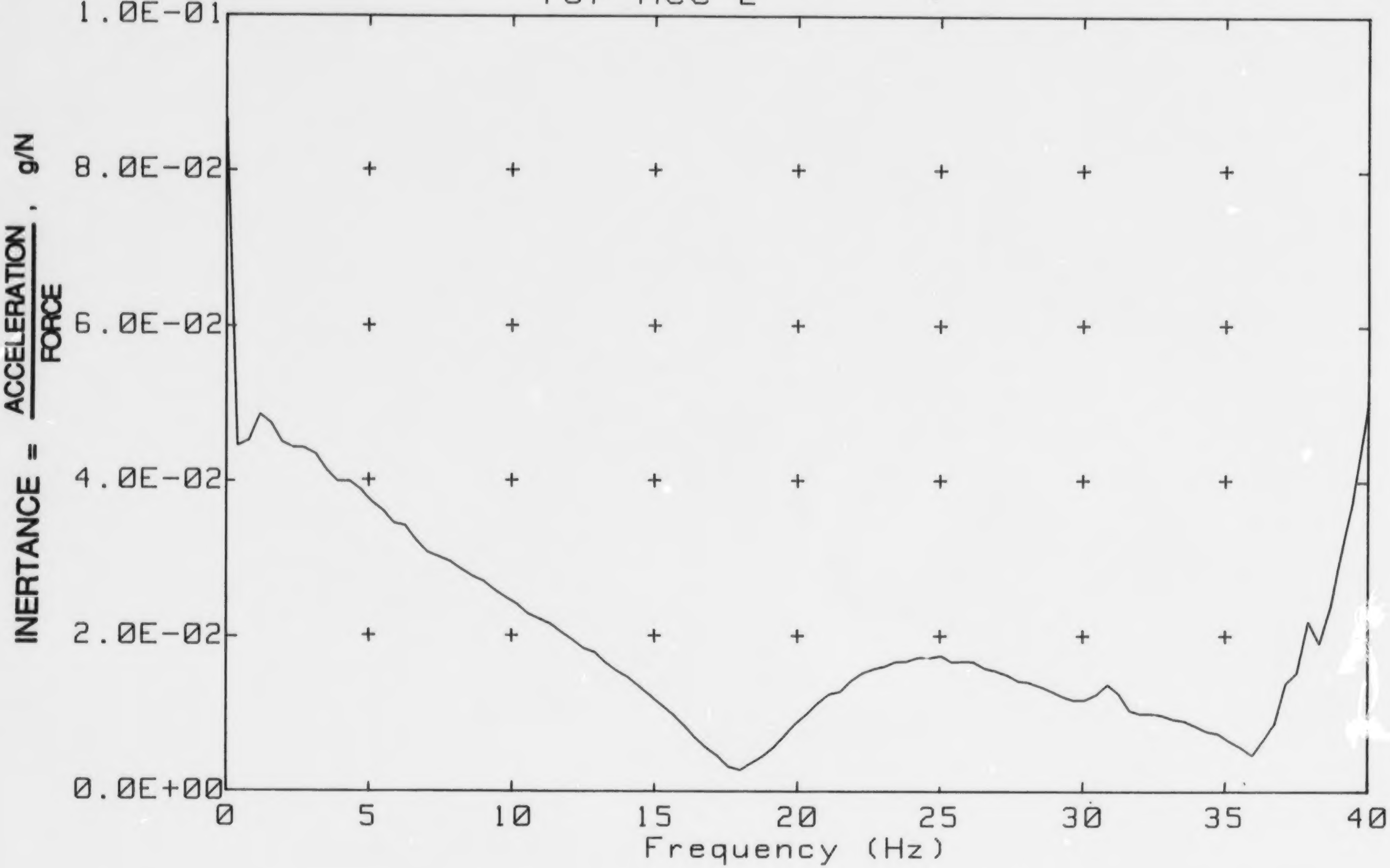

Response Transfer Function
for ACC 2

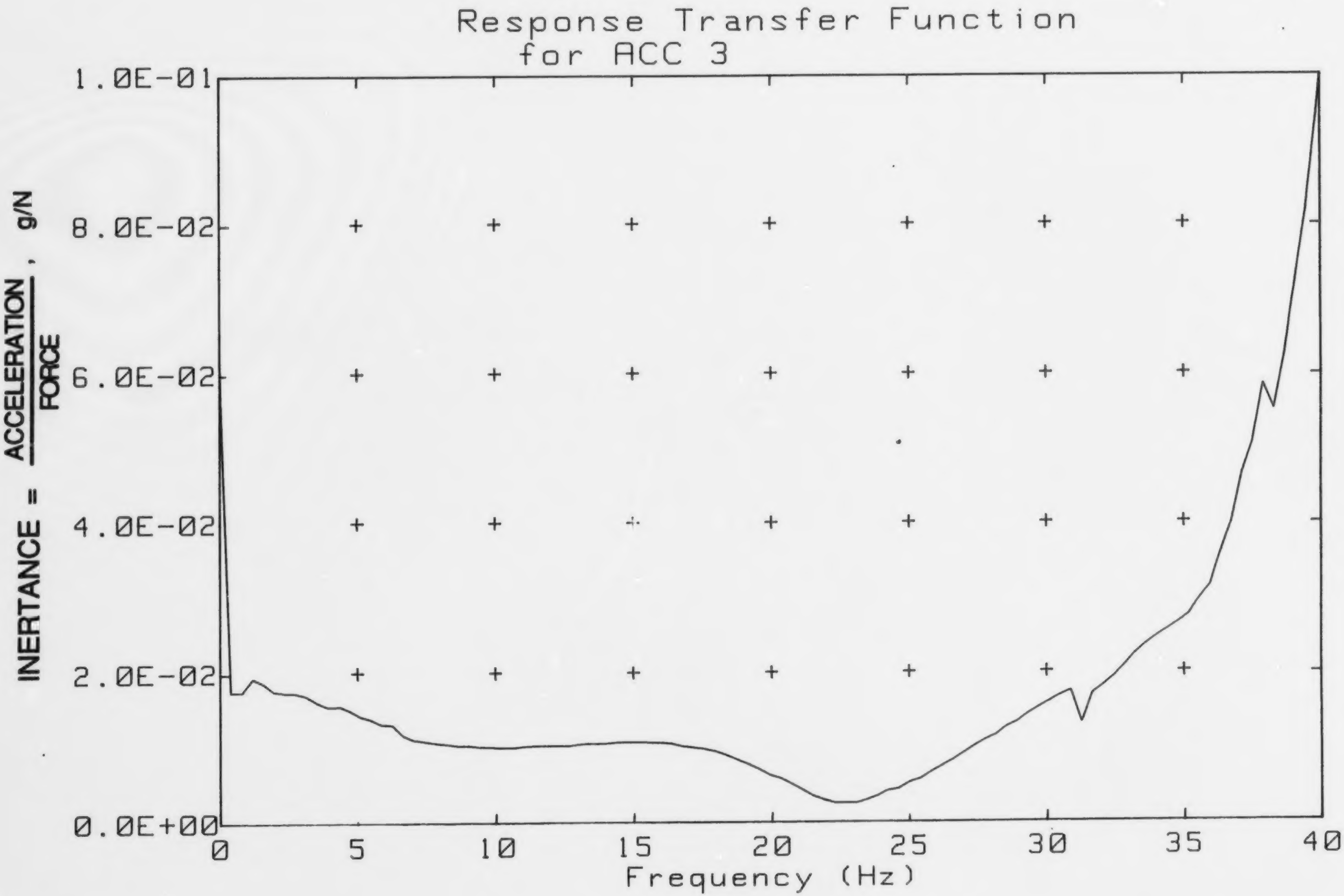

Response Transfer Function
for ACC 3

Response Transfer Function
for ACC 4

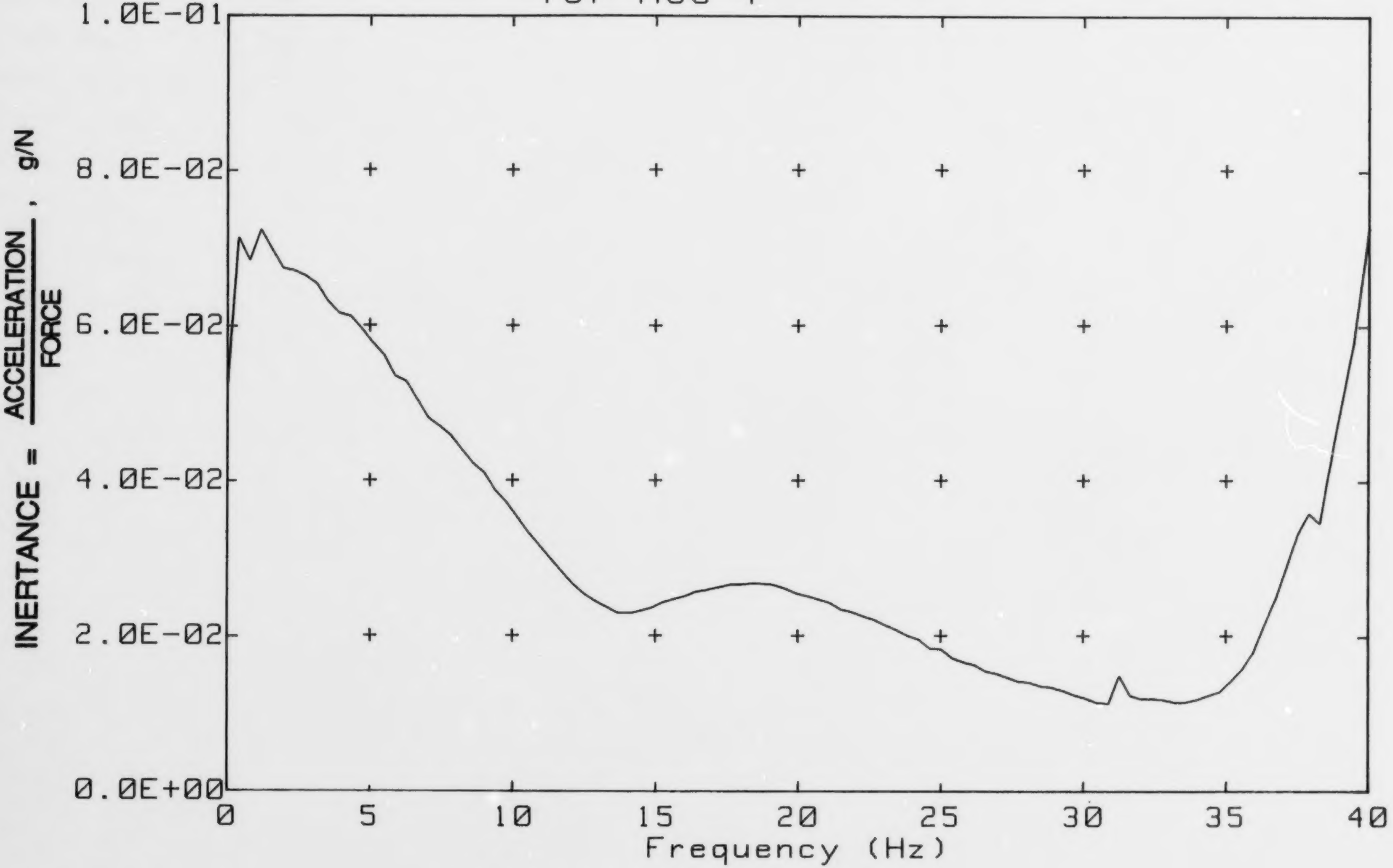

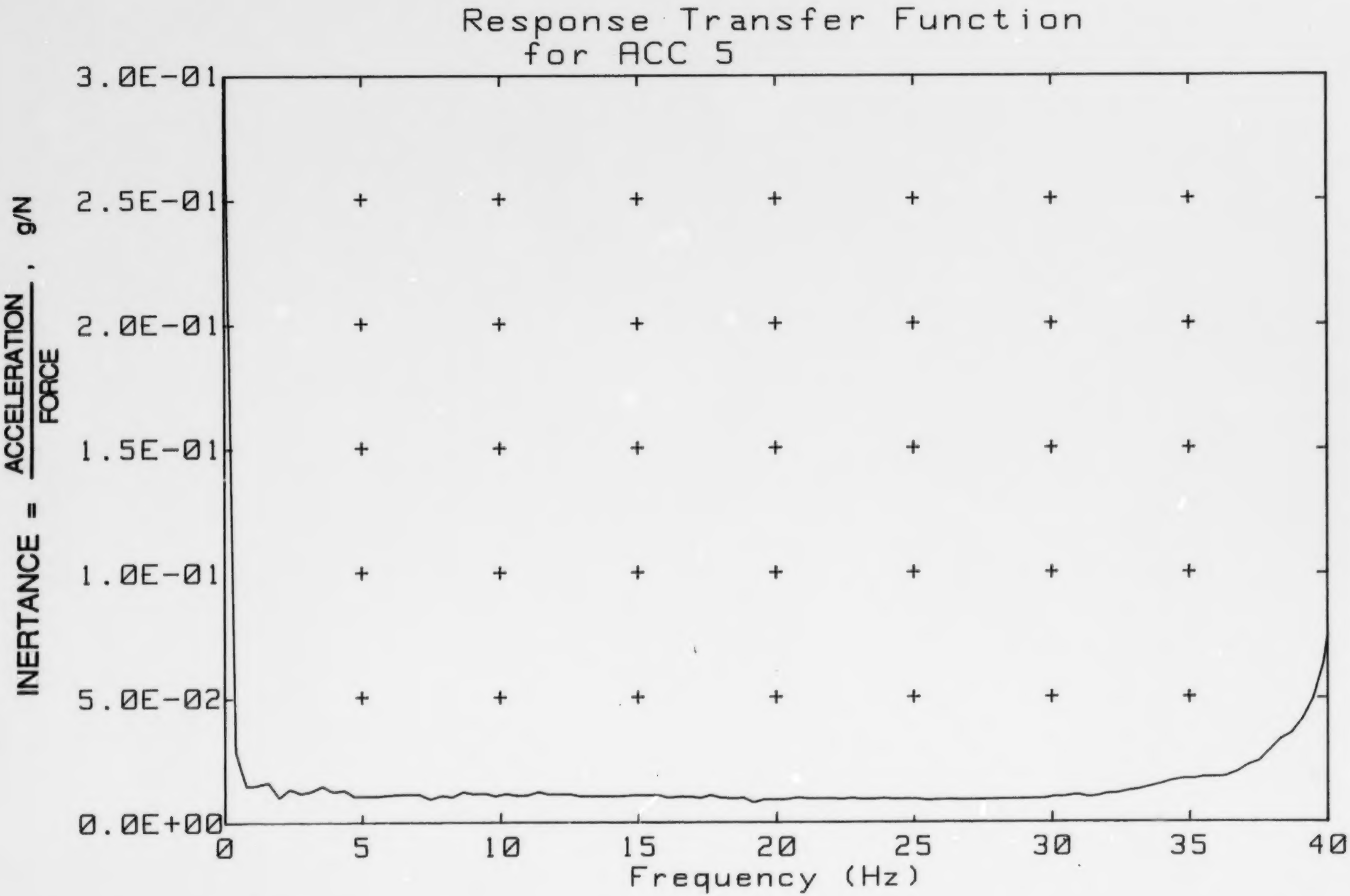
Response Transfer Function
for ACC 5
INERTANCE = ACCELERATION / FORCE , g/N
3.0E-01
2.5E-01
2.0E-01
1.5E-01
1.0E-01
5.0E-02
0.0E+00
0
5
10
15
20
25
30
35
40
Frequency (Hz)

Response Transfer Function
for ACC 6

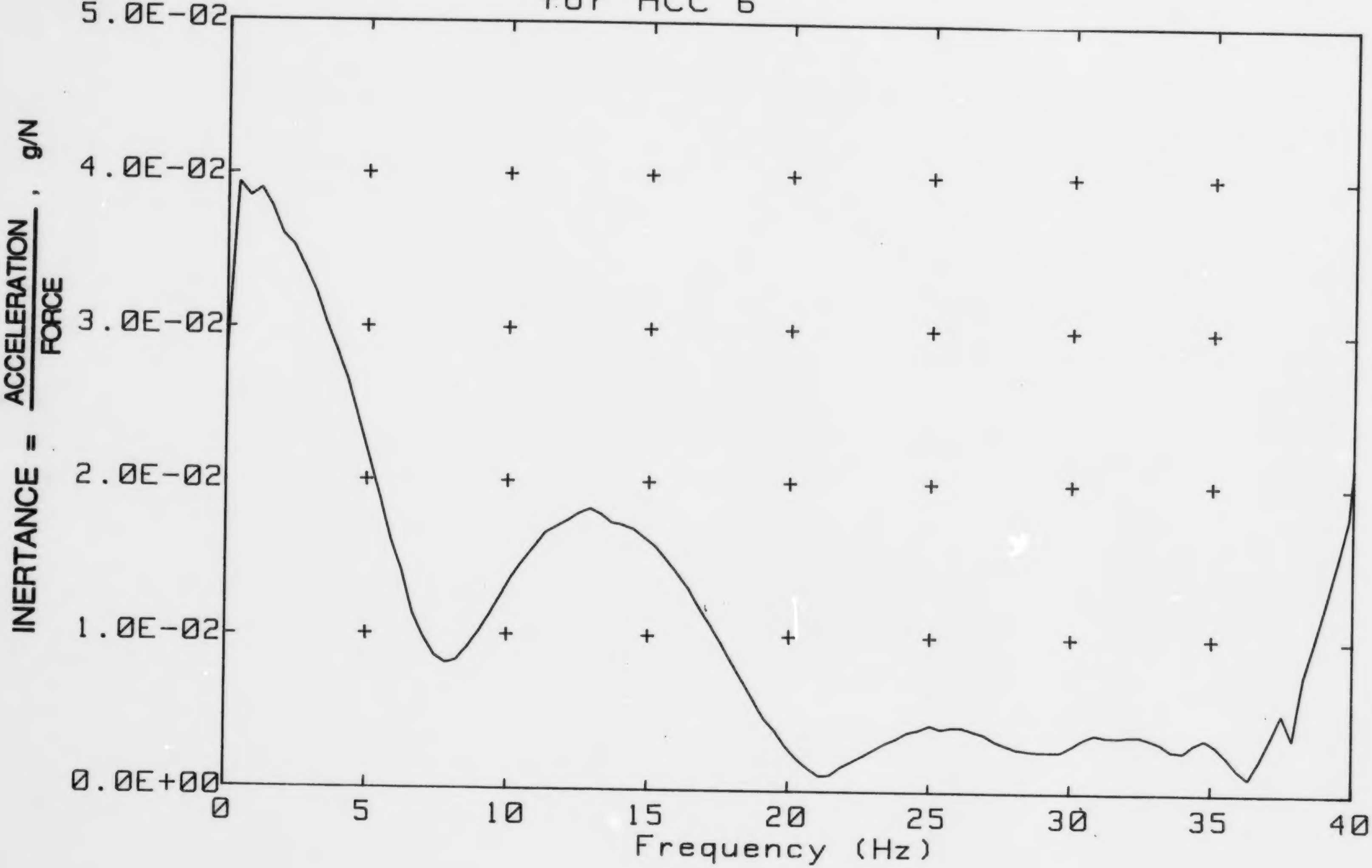

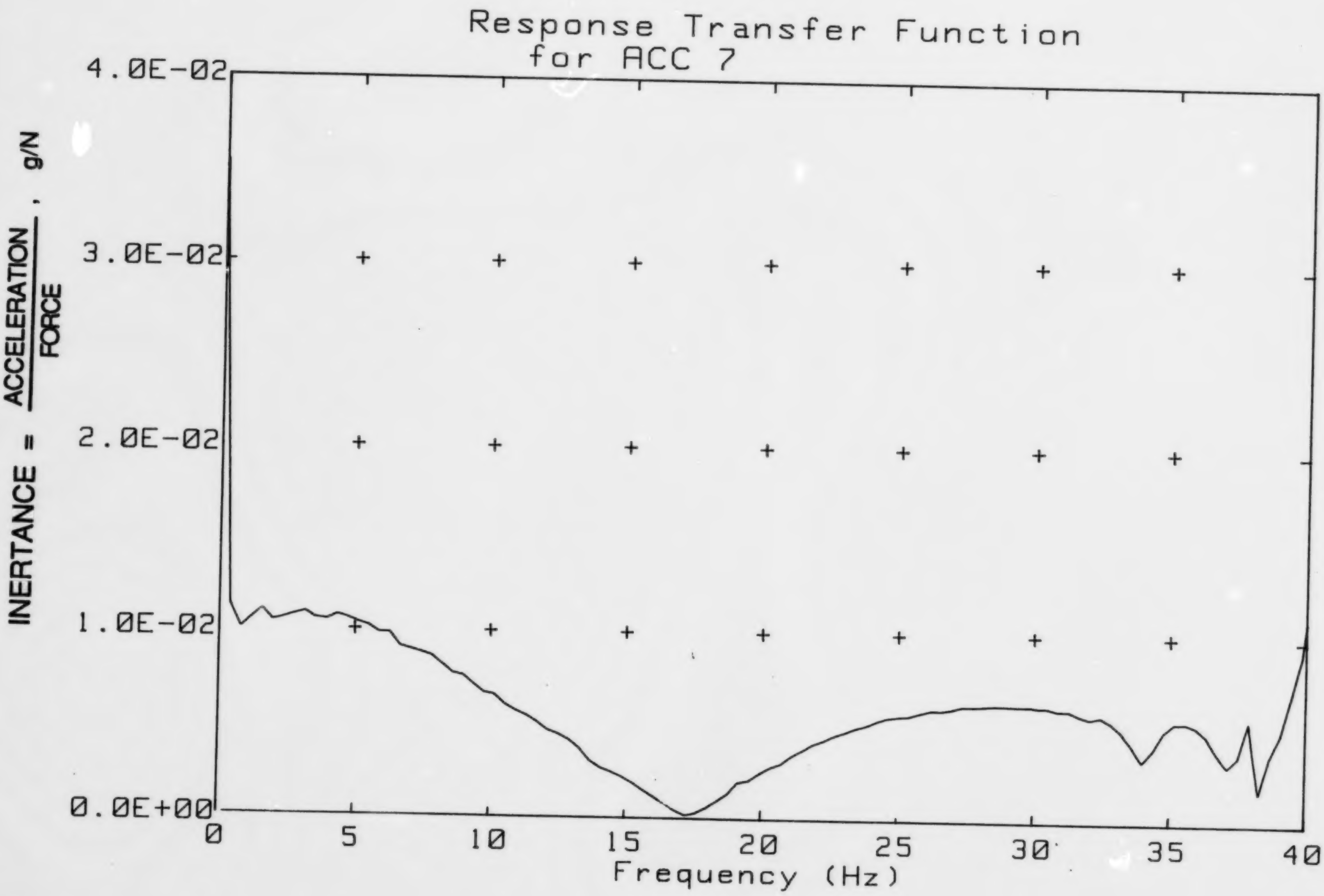

Response Transfer Function for ACC 7

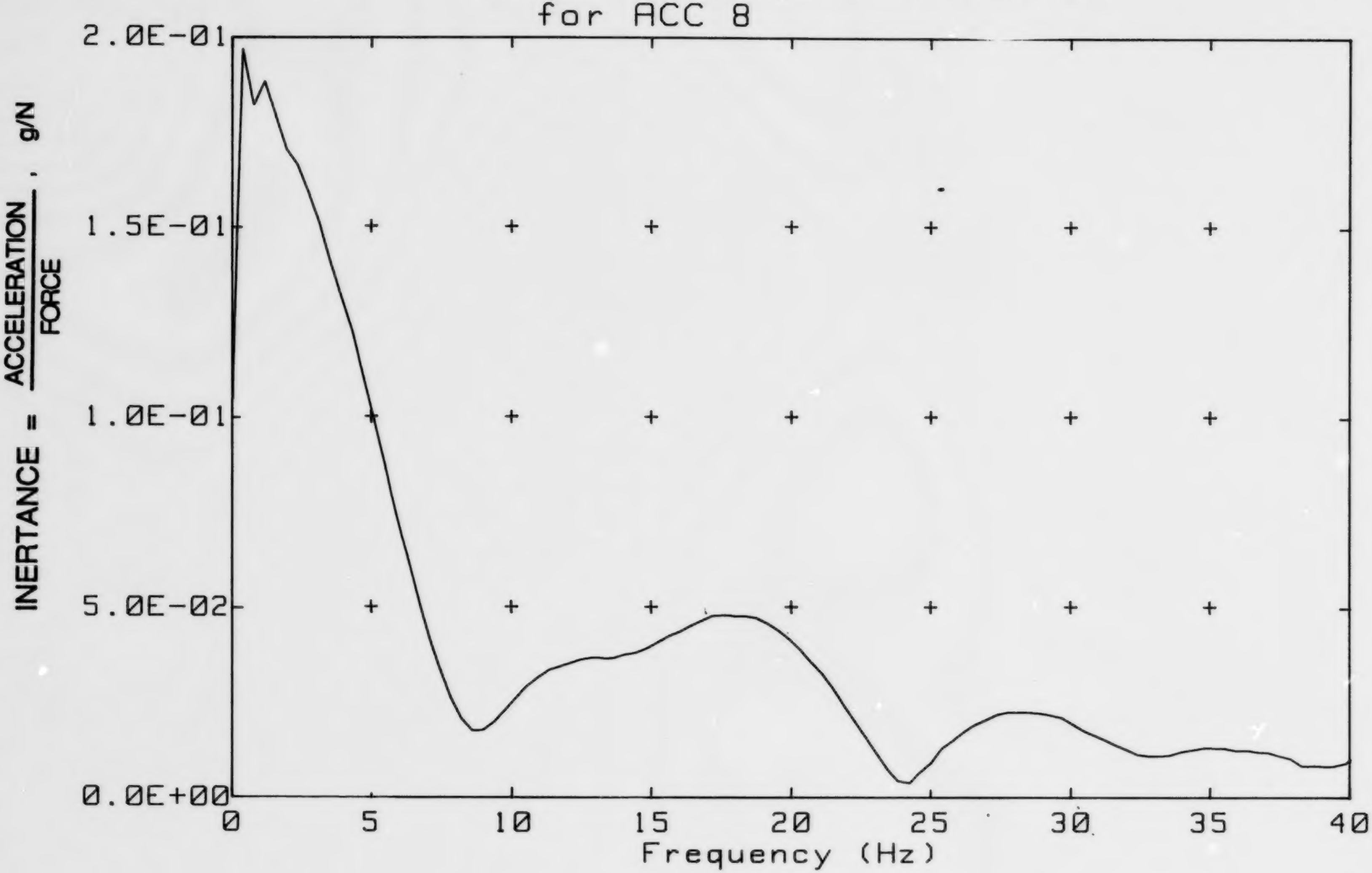

Response Transfer Function for ACC 8

Response Transfer Function
for ACC 9